

PERFORMANCE IMPROVEMENT OF VAPOUR ABSORPTION SYSTEM USING LOOP HEAT PIPES

A

*Thesis Submitted in the Fulfilment of the Requirement for the
Award of the Degree
of*

**DOCTOR OF PHILOSOPHY
IN
MECHANICAL ENGINEERING**

Submitted By:

**ANKIT DWIVEDI
(2k15/PhD/ME/01)**

Under the supervision of
Prof. (Dr.) R. S. MISHRA



**DEPARTMENT OF MECHANICAL ENGINEERING
DELHI TECHNOLOGICAL UNIVERSITY**

(Formerly Delhi College of Engineering)
Bawana Road, Delhi-110042, India

DECLARATION

I, Ankit Dwivedi, hereby declare that the work entitled “**Performance Improvement of Vapour Absorption System Using Loop Heat Pipes**” has been carried out by me under the guidance of Prof. (Dr.) R.S. Mishra, at Delhi Technological University, Delhi.

This dissertation is part of the partial fulfilment of the requirement for the degree of PhD in Thermal Engineering. This is the original work and has not been submitted for any other degree in any other university.

Ankit Dwivedi
2k15/PhD/ME/01

CERTIFICATE

This is to certify that the Ph.D. thesis entitled “**Performance Improvement of Vapour Absorption System Using Loop Heat Pipes**” submitted by Ankit Dwivedi (2k15/PhD/ME/01) for the award of Doctor of Philosophy Degree (Ph.D.) in Mechanical Engineering at Delhi Technological University, Delhi is an authentic work carried out by him under my guidance and supervision.

It is further certified that the work is based on original research and the matter embodied in this thesis has not been submitted to any other university/institute for the award of any degree to the best of our knowledge and belief.

(Prof. (Dr.) R. S. Mishra)
Supervisor

ACKNOWLEDGEMENTS

I am extremely obliged to my Guru & Supervisor, Prof. (Dr.) R.S. Mishra for his exemplary guidance, monitoring and constant encouragement throughout the Ph.D. course. I thank the Almighty for keeping me in the best state of my health & mind and for keeping me driving despite all the odds and injustices in life and for pushing me to every little achievement that I've had till now or will ever have.

I feel eternally grateful to My Parents, My Sister & My Wife for the constant support in my life without which completing such a mammoth task could never have been possible in time.

I am thankful for the support of my friends without whom the research would've been a burden instead of an aspiration.

My existence can best be condensed in this couplet of Mirza Asadullah Baig Khan "Ghalib":

दाम-ए-हर-मौज में है हल्ला-ए-सद-काम-ए-नहंग
देखें क्या गुज़रे है क़तरे पे गुहर होते तक

Daam-e-Har-Mauj Men Hai Halqa-e-Sad-Kaam-e-Nahang

Dekhen Kya Guzre Hai Qatre Pe Guhar Hote Tak

दाम हर मोज़ में है हलफ़ा-ए-सद काम नहंग
दیکھیں کیا گزرے ہے قطرے پہ گہر ہوتے تک

Snares are spread in every wave and a hundred crocodiles in each lure

Will see, till it becomes a pearl, what the drop must endure

**Ankit Dwivedi
2k15/PhD/ME/01**

ABSTRACT

Various industries have waste heat sources owing to the processes being followed for example Power Plants, Food Processing Plants, Solar Plants etc. This waste heat is being utilized in systems utilizing low to medium heat sources such as Vapour Absorption Refrigeration Systems (VARs) (65 – 200+ °C), Ejector Refrigeration Systems (ERS) (80 – 150 + °C), Organic Rankine Cycle (ORC) (~200 °C), etc. These systems generate a huge scope of waste heat recovery, eco-friendly operations and methods of reducing global warming and thermal pollution. The heat recovery has been done using conventional heat exchangers that are bulky and have limited effectiveness.

This research work proposes the waste heat recovery & Intra – cycle heat utilization by a superconductor of heat called Loop Heat Pipe (LHP), which works on the evaporation – condensation principle. The working fluid of the LHP, i.e., Acetone, Methanol, Ethanol, Water etc., is evaporated by the heat influx in the evaporator and the vapour generated is transferred through the porous wicked structure in an insulated line to the Condenser where the vapour gets condensed and rejects the heat and the condensates are transferred back to the evaporator part through insulated lines.

In this investigation of performance improvement of the VARs, intracycle heat exchange has been attempted through the LHP, preheating the mixture before entering the VARs generator and reducing the overall heat input in the generator resulting in a reduction in the irreversibility associated with the conventional heat exchangers & condensers etc. and increasing the overall COP of the system. Moreover, the Feasibility of the VARs combined with the Gas Power Cycle (GPC) through LHP has also been studied comprehensively.

The COP for Single Effect, Half, Effect, Double Effect, Triple Effect & Quadruple Effect Systems have been observed to have increased by 65 %, 60%, 65%, 56-65 % & 41 – 33 % respectively. Amongst the considered systems the refrigeration capacity of the Single Effect, Half, Effect, Double Effect, Triple Effect & Quadruple Effect Systems is 8.6 – 15.1 kW, 360.2 – 528.1 kW, 336 – 370 kW, 134.6 – 274 kW & 207.2 – 395.6 kW at 5°C Evaporator. Moreover, the mass flow rate from the absorber has been kept at 1kg/s for all the systems except single effect systems in which it is 0.05 kg/s. The Component-wise contribution to the overall Irreversibility has been presented to have decreased for the LHP.

Six Eco-friendly refrigerants namely R600, R134a, R290, R152a, R125 & R124 have been used as working fluids for ORC. The combination of Water (LHP H Ex.) & R290 (ORC) is the most suited working fluid among all the 24 Combinations studied. Moreover, the First & Second Law Efficiencies of the System at 1500K Peak GPC Temperature & 65 kPa ORC Condenser Pressure have been recorded as 32% & 80 % respectively with 170 kW net-work output. The irreversibility related to each different component of the lower system has been around 80 kW. The ratio of the mass flow rate of R290 to Water has been around 1.42.

In ERS new eco-friendly refrigerants such as R236ea, R1224yd (Z), R1233zd (E), R245fa, and R365mfc along with R718 have been selected for study as the working fluids. COP & refrigeration capacity of the combined system has been obtained in the range of 0.25-0.28 and 10.35kW-315kW respectively for various combinations of fluids. Based on the eco-friendliness, compactness & industrial viability the system with Water (LHP)-R1224yd (Z) (ERC) has been recommended as the mass flow required for working fluids is the least & utilization of Heat Input Available to ERC is maximum for the operations.

Table of Contents

	Page No.
<i>Declaration</i>	<i>ii</i>
<i>Certificate</i>	<i>iii</i>
<i>Acknowledgements</i>	<i>iv</i>
<i>Abstract</i>	<i>v-vi</i>
<i>Table of Contents</i>	<i>vii-xi</i>
<i>List of Tables</i>	<i>xii</i>
<i>List of Figures</i>	<i>xiii-xxiv</i>
<i>Abbreviations</i>	<i>xxv</i>
Chapter-1	
Introduction	1-44
1.1	Introduction to Heat Pipes 2-23
1.1.1	Operating Principles of Heat Pipes 6-8
1.1.2	Operational Limitations 8-9
1.1.3	Advantages of Heat Pipes 10
1.1.4	Heat Transfer & Temperature Difference in of Heat Pipes 10
1.1.4.1	Heat transfer in the evaporator region 10
1.1.5	Introduction to Loop Heat Pipes (LHP) 11
1.1.6	Operation of Loop Heat Pipes (LHP) 11-12
1.1.7	Properties of Various Loop Heat Pipes Working Fluids 12-14
1.1.8	Advantages of Loop Heat Pipes 14
1.1.9	LHP & Thermodynamics 15
1.1.10	The Conditions for Correct Functioning 16-17
1.1.11	Thermodynamics & Heat Transfer Equations of LHP 17-23
1.2	Introduction to Vapour Absorption Refrigeration System 23-33
1.2.1	Parallels between VCRS & VARS 24
1.2.2	Departures between VCRS & VARS 24-25
1.2.3	Practical VARS 25

1.2.4	Application of Absorption Systems	26
1.2.5	Multi-effect VARS	27-32
1.2.6	Fluid Mixtures of VARS	32
1.3	Introduction to Ejector Refrigeration System	32-35
1.4	Introduction to Organic Rankine Cycle	35-38
1.4.1	Organic Rankine cycle characteristics	36
1.4.2	ORC fluids	37
1.4.3	Commonly used ORC work fluids	37-38
1.5	Introduction to Gas Power Cycle	38-40
1.6	Refrigerants	40-43
1.6.1	Conventional Refrigerants, Applications & Modern Alternatives	41-42
1.6.2	Refrigerants Used in the Analysis	42-43
Chapter-2	Literature Survey	44-86
2.1	Review of the Heat Pipes (HP)	44-61
2.2	Review of Vapour Absorption Refrigeration System (VARS)	62-71
2.3	Review of Ejector Refrigeration Cycle (ERC)	72-79
2.4	Review of Organic Rankine Cycle (ORC)	80-82
2.5	Conclusions of the Literature Survey	83-84
2.6	Identified Gaps in the Literature	85
2.7	Objectives & Scope for the Research Work	86
Chapter-3	Description of Systems	87-111
3.1	Modifications Proposed in the Single-Effect VARS	87-90
3.2	Modifications Proposed in the Half-Effect VARS	90-94
3.3	Modifications Proposed in the Double-Effect VARS	94-97
3.4	Modifications Proposed in the Triple-Effect VARS	98-102
3.5	Modifications Proposed in the Quadruple-Effect VARS	102-106
3.6	Combination ERS with GPC using LHP	107-109

3.7	Combination ORC with GPC using LHP	109-111
Chapter-4	Thermodynamic Modeling & Analysis of Systems	112-193
4.1	Thermodynamic Modeling of Gas Power Cycle (GPC)	113-115
4.2	Modified Single Effect VARS	115-125
4.2.1	Modified Single Effect VARS-I	115-121
4.2.2	Modified Single Effect VARS-II	121-123
4.2.3	Combined GPC & Single Effect VARS	123-125
4.3	Modified Half Effect VARS	126-137
4.3.1	Modified Half Effect VARS-I	126-132
4.3.2	Modified Half Effect VARS-II	132-135
4.3.3	Combined GPC & Half-Effect VARS using LHP	135-137
4.4	Modified Double Effect VARS	138-149
4.4.1	Modified Double Effect VARS-I	138-145
4.4.2	Modified Double Effect VARS-II	145-148
4.4.3	Combined GPC & Double-Effect VARS using LHP	148-149
4.5	Modified Triple Effect VARS	150-166
4.5.1	Modified Triple Effect VARS-I	150-160
4.5.2	Modified Triple Effect VARS-II	160-164
4.5.3	Combined GPC & Triple-Effect VARS using LHP	164-166
4.6	Modified Quadruple Effect VARS	167-187
4.6.1	Modified Quadruple Effect VARS-I	167-179
4.6.2	Modified Quadruple Effect VARS-II	180-185
4.6.3	Combined GPC & Quadruple-Effect VARS using LHP	185-187
4.7	Thermodynamic Modeling of Organic Rankine Cycle (ORC)	188-190
4.8	Thermodynamic Modeling of Ejector Refrigeration Cycle (ERC)	191-193
Chapter-5	Results & Discussions	194-334

5.1	Modified Single Effect VARS	194-195
5.1.1	Single Effect VARS Modification-I	195-201
5.1.2	Single Effect VARS Modification-II	201-208
5.1.3	Combined Single Effect VARS & GPC	208-211
5.2	Modified Half-Effect VARS	212-228
5.2.1	Half-Effect VARS Modification-I	212-218
5.2.2	Half Effect VARS Modification-II	219-226
5.2.3	Combined Half Effect VARS & GPC	226-228
5.3	Modified Double Effect VARS	229-246
5.3.1	Double Effect VARS Modification-I	229-236
5.3.2	Double Effect VARS Modification-II	237-243
5.3.3	Combined Double Effect VARS & GPC	244-246
5.4	Modified Triple Effect VARS	247-264
5.4.1	Triples Effect VARS Modification-I	247-254
5.4.2	Triples Effect VARS Modification-II	255-262
5.4.3	Combined Triple Effect VARS & GPC	262-264
5.5	Modified Quadruple Effect VARS	265-287
5.5.1	Quadruple Effect VARS Modification-I	265-275
5.5.2	Quadruple Effect VARS Modification-II	276-284
5.5.3	Combined Quadruple Effect VARS & GPC	284-287
5.6	Combined ORC & GPC	288-302
5.6.1	Peak Temperature of GPC (T_5) as Input Variable	288-294
5.6.2	Condenser Pressure (P_9) of ORC as Input Variable	294-299
5.6.3	Working Fluid of LHP as Input Variable	299-302
5.7	Combined ERC & GPC	303-320
5.7.1	The Peak Temperature of GPC (T_5)	303-306
5.7.2	The Boiler Pressure of ERS (P_{11})	307-308
5.7.3	Working fluids in the LHP	308-309
5.7.3.1	Acetone	309-311
5.7.3.2	Ethanol	312-314
5.7.3.3	Methanol	315-317
5.7.3.4	Water	318-320

5.8	The Patent- Refrigeration without Condenser-compressor	321-330
5.8.1	Background of the Invention	321-322
5.8.2	Prior Art	322
5.8.3	Brief Description of Drawings	322-323
5.8.4	Refrigeration without Condenser-Compressor	323-325
5.8.5	Conclusions on The Patent	326
5.8.6	The Claims	326-327
5.8.7	Drawings	328-330
5.9	Parameters of Loop Heat Pipes	331-332
5.10	Assumptions for the Analysis	333
5.10.1	Vapour Absorption Refrigeration System	333
5.10.2	Loop Heat Pipes	333
5.10.3	Organic Rankine Cycle	333-334
5.10.4	Ejector Refrigeration System	334
Chapter-6	Conclusions	335-346
6.1	Modified Single Effect LiBr - H ₂ O Vapour Absorption System	335-336
6.2	Modified Half Effect LiBr - H ₂ O Vapour Absorption System	336-338
6.3	Modified Double Effect LiBr - H ₂ O Vapour Absorption System	338-339
6.4	Modified Triple Effect LiBr - H ₂ O Vapour Absorption System	339-341
6.5	Modified Quadruple Effect LiBr - H ₂ O Vapour Absorption System:	341-342
6.6	Combined Organic Rankine Cycle with Gas Power Cycle	343-344
6.7	Combined Ejector Refrigeration Cycle with Gas Power Cycle	344-245
6.8	Scope for Future Research & Development Work	346
	References	347-368
	Publications	369-370

List of Tables

Table	Description	Page No.
1.1	Superheat required to initiate nucleate boiling at atmospheric pressure	12
1.2	Useful ranges of various working fluids	13
1.3	Operating Characteristics Heat Pipes	14
1.4	Useful Properties of the working fluids	37
1.5	Conventional Refrigerants & Modern Alternatives	41
1.6	Refrigerants and useful Properties	43
5.1	Input Data for GPC Analysis	194
5.2	Input Data for Single Effect VARS Analysis	195
5.3	Comparison of Modified Single Effect VARS	207
5.4	Irreversibility in Single Effect Components	208
5.5	Input Parameters for Half Effect VARS Analysis	212
5.6	Comparison with Modified Half Effect VARS	224
5.7	Irreversibility in Half Effect Components	225
5.8	Input Variables for Double Effect VARS Analysis	229
5.9	Comparison of Modified Double Effect VARS	242
5.10	Irreversibility in Double Effect Components	243
5.11	Input Data for Triple Effect VARS Analysis	247
5.12	Comparison of Modified Triple Effect	260
5.13	Irreversibility in Triple Effect Components	261
5.14	Input Variables for Quadruple Effect VARS Analysis	265
5.15	Comparison of Modified Quadruple Effect VARS	282
5.16	Irreversibility in Quadruple Effect Components	283
5.17	Input Variables for ORC Analysis	288
5.18	Input Variables for ERC Analysis	303
5.19	Abbreviations Used in the System-Patent	325
5.20	Parameters of the LHP	331

List of Figures

Figure	Description	Page No.
1.1	Concept of Heat Pipes	3
1.2	Primary Sections of a Heat Pipe	4
1.3	Cross-Section of a Heat Pipe	4
1.4	Loop Heat Pipes	6
1.5	Operational Limitations of Heat Pipes	9
1.6	Cross-Section of Evaporator Section of an LHP	12
1.7	Schematics & Pressure-Temperature Graph of LHP	16
1.8	Comparison Between VCRS & VARS	24
1.9	Schematic of LiBr-H ₂ O VARS	25
1.10	Schematic of Practical VARS	26
1.11	Schematic of Half Effect VARS	28
1.12	Schematic of Single Effect VARS	28
1.13	Schematic of Double Effect (Series) VARS	29
1.14	Schematic of Triple Effect (Series) VARS	30
1.15	Schematic of Quadruple Effect (Series) VARS	31
1.16	Schematic of Standard ERS	33
1.17	P-h diagram of ERC	33
1.18	Model of Ejector and Nozzle	34
1.19	T-s Cycle of ORC	35
1.20	Schematic of ORC	36
1.21	Schematic of Open Cycle Brayton Cycle	39
1.22	Schematic of Closed Cycle Brayton Cycle	39
1.23	Temperature-entropy plot of ideal Brayton Cycle	40
1.24	Temperature-entropy plot of actual Brayton Cycle	40
3.1	Modification-I in Single Effect VARS using LHP	88
3.2	Modification-II in Single Effect VARS using LHP	88
3.3	Modified Single Effect VARS Combined with GPC using LHP	89
3.4	Modification-I in Half Effect VARS using LHP	91
3.5	Modification-II in Half Effect VARS using LHP	92

3.6	Modified Half Effect VARS Combined with GPC using LHP	93
3.7	Modification-I in Double Effect (Series) VARS using LHP	95
3.8	Modification-II in Double Effect (Series) VARS using LHP	96
3.9	Modified Double Effect (Series) VARS Combined with GPC using LHP	97
3.10	Modification-I in Triple Effect (Series) VARS using LHP	99
3.11	Modification-II in Triple Effect (Series) VARS using LHP	100
3.12	Modified Triple Effect (Series) VARS Combined with GPC using LHP	101
3.13	Modification-I in Quadruple Effect (Series) VARS using LHP	103
3.14	Modification-II in Quadruple Effect (Series) VARS using LHP	104
3.15	Modified Quadruple Effect (Series) VARS Combined with GPC using LHP	105
3.16	ERS Combined with GPC using LHP	107
3.16a	The ejector of the ERS	108
3.17	T-s plot of ERS Combined with GPC using LHP	108
3.18	ORC Combined with GPC using LHP	110
3.19	T-s plot of ORC Combined with GPC using LHP	111
3.20	Saturation domes on T-s plot of ORC working fluids	111
4.1	Common Schematic of GPC	113
4.2	Modified Single Effect VARS-I	115
4.3	Modified Single Effect VARS-II	121
4.4	Combined GPC & Single Effect VARS	124
4.5	Modified Half Effect VARS-I	126
4.6	Modified Half Effect VARS-II	133
4.7	Combined GPC & Half Effect VARS	136

4.8	Modified Double Effect VARS-I	138
4.9	Modified Double Effect VARS-I	145
4.10	Combined GPC & Double Effect VARS	148
4.11	Modified Triple Effect VARS-I	150
4.12	Modified Triple Effect VARS-II	160
4.13	Combined GPC & Triple Effect VARS	165
4.14	Modified Quadruple Effect VARS-I	167
4.15	Modified Quadruple Effect VARS-II	180
4.16	Combined GPC & Quadruple Effect VARS	185
4.17	Combined GPC & ORC using LHP	188
4.18	Combined GPC & ERC using LHP	191
5.1	Temperature Variation in Single Effect Modification-I with Generator Temperature	196
5.2	Temperature Variation in Single Effect Modification-I Heat Exchanger with Generator Temperature	196
5.3	Temperature Variation in LHP with Generator Temperature	197
5.4	Heat Interaction in Single Effect Modification-I with Generator Temperature	197
5.5	Heat Interaction in LHP with Generator Temperature	198
5.6	Percentage Irreversibility in Single Effect Modification-I Components with Generator Temperature	199
5.7	Percentage Irreversibility in LHP Components with Generator Temperature	199
5.8	COP & Improved COP with Generator Temperature	200
5.9	Percentage Improvement in COP with Generator Temperature	200
5.10	Mass Flow Rates in Single Effect Modification-I with Generator Temperature	201
5.11	Temperature Variation in Single Effect Modification-II with Generator Temperature	202
5.12	Temperature Variation in LHP-I with Generator Temperature	202

5.13	Temperature Variation in LHP-II with Generator Temperature	203
5.14	Heat Interaction in Single Effect Modification-II with Generator Temperature	204
5.15	Heat Interaction in LHP-II with Generator Temperature	204
5.16	Percentage Irreversibility in Single Effect Modification-II Components with Generator Temperature	205
5.17	Percentage Irreversibility in LHP Components with Generator Temperature	205
5.18	COP & Improved COP with Generator Temperature	206
5.19	Percentage Improvement in COP with Generator Temperature	206
5.20	Temperatures of GPC and Generator Single Effect Modification-II with Mass of Fuel in GPC	209
5.21	Temperatures of LHP-III with Mass of Fuel in GPC	209
5.22	Heat, Exergy & Irreversibility at GPC Exhaust with Mass of Fuel in GPC	210
5.23	Heat, Exergy & Irreversibility at GPC Exhaust with Mass of Fuel in GPC	210
5.24	Number of Single Effect Modification-II Viable with GPC with Mass of Fuel in GPC	211
5.25	Temperature Variation in Half Effect Modification-I with Generator Temperature	213
5.26	Temperature Variation in Half Effect Modification-I Heat Exchanger with Generator Temperature	213
5.27	Temperature Variation in LHP with Generator Temperature	214
5.28	Heat Interaction in Half Effect Modification-I with Generator Temperature	215
5.29	Heat Interaction in LHP with Generator Temperature	215
5.30	Percentage Irreversibility in Half Effect Modification-I Components with Generator Temperature	216
5.31	Percentage Irreversibility in LHP Components with	216

	Generator Temperature	
5.32	COP & Improved COP with Generator Temperature	217
5.33	Percentage Improvement in COP with Generator Temperature	217
5.34	Mass Flow Rates in Half Effect Modification-I High with Generator Temperature	218
5.35	Mass Flow Rates in Half Effect Modification-I Low with Generator Temperature	218
5.36	Temperature Variation in Half Effect Modification-II with Generator Temperature	219
5.37	Temperature Variation in LHP-I with Generator Temperature	220
5.38	Temperature Variation in LHP-II with Generator Temperature	221
5.39	Heat Interaction in Half Effect Modification-II with Generator Temperature	221
5.40	Heat Interaction in LHP-II with Generator Temperature	222
5.41	Percentage Irreversibility in Half Effect Modification-II Components with Generator Temperature	222
5.42	Percentage Irreversibility in LHP Components with Generator Temperature	223
5.43	COP & Improved COP with Generator Temperature	223
5.44	Percentage Improvement in COP with Generator Temperature	224
5.45	Temperatures of GPC and Generator Half Effect Modification-II with Mass of Fuel in GPC	227
5.46	Temperatures of LHP-IV with Mass of Fuel in GPC	227
5.47	Heat, Exergy & Irreversibility at GPC Exhaust with Mass of Fuel in GPC	228
5.48	Heat, Exergy & Irreversibility at GPC Exhaust with Mass of Fuel in GPC	228
5.49	Temperature Variation in Double Effect Modification-I with Generator Temperature	230

5.50	Temperature Variation in Double Effect Modification-I Heat Exchanger-I with Generator Temperature	230
5.51	Temperature Variation in Double Effect Modification-I Heat Exchanger-I with Generator Temperature	231
5.52	Temperature Variation in LHP with Generator Temperature	232
5.53	Heat Interaction in Double Effect Modification-I with Generator Temperature	232
5.54	Heat Interaction in LHP & HEx with Generator Temperature	233
5.55	Percentage Irreversibility in Double Effect Modification-I Components with Generator Temperature	234
5.56	Percentage Irreversibility in LHP Components with Generator Temperature	234
5.57	COP & Improved COP with Generator Temperature	235
5.58	Percentage Improvement in COP with Generator Temperature	235
5.59	Mass Flow Rates in Double Effect Modification-I High with Generator Temperature	236
5.60	Mass Flow Rates in Double Effect Modification-I Low with Generator Temperature	236
5.61	Temperature Variation in Double Effect Modification-II with Generator Temperature	237
5.62	Temperature Variation in LHP-I with Generator Temperature	238
5.63	Temperature Variation in LHP-II with Generator Temperature	238
5.64	Temperature Variation in LHP-III with Generator Temperature	239
5.65	Heat Interaction in Double Effect Modification-II with Generator Temperature	239
5.66	Percentage Irreversibility in Double Effect Modification-II Components with Generator Temperature	240

5.67	Percentage Irreversibility in LHP Components with Generator Temperature	240
5.68	COP & Improved COP with Generator Temperature	241
5.69	Percentage Improvement in COP with Generator Temperature	241
5.70	Temperatures of GPC and Generator Double Effect Modification-II with Mass of Fuel in GPC	244
5.71	Exergy, Irreversibility and Heat Rejected from GPC Exhaust Double Effect Modification-II with Mass of Fuel in GPC	245
5.72	Temperatures of LHP-IV with Mass of Fuel in GPC	245
5.73	Heat, Exergy & Irreversibility at GPC Exhaust with Mass of Fuel in GPC	246
5.74	Temperature Variation in Triple Effect Modification-I with Generator Temperature	248
5.75	Temperature Variation in Triple Effect Modification-I Heat Exchangers with Generator Temperature	249
5.76	Temperature Variation in LHPs with Generator Temperature	249
5.77	Heat Interaction in Triple Effect Modification-I with Generator Temperature	250
5.78	Heat Interaction in LHPs & HEx with Generator Temperature	250
5.79	Percentage Irreversibility in Triple Effect Modification-I Components with Generator Temperature	251
5.80	Percentage Irreversibility in LHP Components with Generator Temperature	251
5.81	COP & Improved COP with Generator Temperature	252
5.82	Percentage Improvement in COP with Generator Temperature	253
5.83	Mass Flow Rates in Triple Effect Modification-I High with Generator Temperature	253

5.84	Mass Flow Rates in Triple Effect Modification-I Med with Generator Temperature	254
5.85	Mass Flow Rates in Triple Effect Modification-I Low with Generator Temperature	254
5.86	Temperature Variation in Triple Effect Modification-II with Generator Temperature	255
5.87	Temperature Variation in LHP-III & V with Generator Temperature	256
5.88	Temperature Variation in LHP-IV with Generator Temperature	256
5.89	Temperature Variation in LHP-II with Generator Temperature	257
5.90	Temperature Variation in LHP-I with Generator Temperature	257
5.91	Heat Interaction in Triple Effect Modification-II with Generator Temperature	258
5.92	Percentage Irreversibility in LHPs Components with Generator Temperature	258
5.93	COP & Improved COP with Generator Temperature	259
5.94	Percentage Improvement in COP with Generator Temperature	259
5.95	Temperatures of GPC and Generator Triple Effect Modification-II with Mass of Fuel in GPC	262
5.96	Temperatures of LHP-VI with Mass of Fuel in GPC	263
5.97	Percentage Irreversibility of LHP-VI with Mass of Fuel in GPC	263
5.98	Exergy, Irreversibility and Heat Rejected from GPC Exhaust Triple Effect Modification-II with Mass of Fuel in GPC	264
5.99	Temperature Variation in Quadruple Effect Modification-I with Generator Temperature	266
5.100	Temperature Variation in Quadruple Effect Modification-I Heat Exchangers I & II with Generator	267

	Temperature	
5.101	Temperature Variation in Quadruple Effect Modification-I Heat Exchangers III & IV with Generator Temperature	267
5.102	Temperature Variation in LHPs with Generator Temperature	268
5.103	Heat Interaction in Quadruple Effect Modification-I with Generator Temperature	269
5.104	Heat Interaction in LHPs & HEx with Generator Temperature	270
5.105	Percentage Irreversibility in Quadruple Effect Modification-I Components with Generator Temperature	271
5.106	Percentage Irreversibility in LHP Components with Generator Temperature	271
5.107	COP & Improved COP with Generator Temperature	272
5.108	Percentage Improvement in COP with Generator Temperature	273
5.109	Mass Flow Rates in Quadruple Effect Modification-I High-II with Generator Temperature	273
5.110	Mass Flow Rates in Quadruple Effect Modification-I High-I with Generator Temperature	274
5.111	Mass Flow Rates in Quadruple Effect Modification-I Medium with Generator Temperature	275
5.112	Mass Flow Rates in Quadruple Effect Modification-I Low with Generator Temperature	275
5.113	Temperature Variation in Quadruple Effect Modification-II with Generator Temperature	276
5.114	Temperature Variation in LHP-III, V & VII with Generator Temperature	277
5.115	Temperature Variation in LHP-IV & VI with Generator Temperature	278
5.116	Temperature Variation in LHP- I & II with Generator Temperature	279

5.117	Heat Interaction in Quadruple Effect Modification-II with Generator Temperature	280
5.118	Percentage Irreversibility in LHP I, II, III & IV Components with Generator Temperature	280
5.119	Percentage Irreversibility in LHP V, VI & VII Components with Generator Temperature	281
5.120	COP & Improved COP with Generator Temperature	281
5.121	Percentage Improvement in COP with Generator Temperature	282
5.122	No. of Feasible Quadruple Effect Modification-II with Mass of Fuel in GPC	285
5.123:	Temperatures of GPC and Generator Quadruple Effect Modification-II with Mass of Fuel in GPC	285
5.124	Temperatures of LHP-VIII with Mass of Fuel in GPC	286
5.125	Percentage Irreversibility of LHP-VIII with Mass of Fuel in GPC	286
5.126	Exergy, Irreversibility and Heat Rejected from GPC Exhaust Quadruple Effect Modification-II with Mass of Fuel in GPC	287
5.127	Irreversibility & Exergy associated with the Condenser of the ORC	289
5. 128	Irreversibility & Exergy associated with the Boiler of the ORC	290
5.129	Irreversibility & Exergy associated with the Evaporator of the LHP	291
5.130	Irreversibility & Exergy associated with the Condenser of the LHP	292
5.131	First & Second Law Efficiencies of the ORC	292
5.132	Net-Work Output of the ORC	293
5.133	Mass Flow Rates in LHP & ORC	294
5.134	Irreversibility & Exergy associated with the Condenser of the ORC	295

5.135	Irreversibility & Exergy associated with the Boiler of the ORC	296
5.136	Irreversibility & Exergy associated with the Evaporator of the LHP	297
5.137	Irreversibility & Exergy associated with the Condenser of the LHP	297
5.138	First & Second Law Efficiency of ORC with Condenser Pressure	298
5.139	Work Output of ORC with P_9	299
5.140	Mass Flow Rates in LHP & ORC with Acetone as LHP Fluid	300
5.141	Mass Flow Rates in LHP & ORC with Ethanol as LHP Fluid	300
5.142	Mass Flow Rates in LHP & ORC with Methanol as LHP Fluid	301
5.143	Mass Flow Rates in LHP & ORC with Water as LHP Fluid	301
5.144	Temperature Profiles of the Components of Combined Cycle with T_5	305
5.145	Refrigeration Capacity of the ERS with T_5	305
5.146	COP of the ERS with T_5	306
5.147	Refrigeration Capacity of the ERS with P_{11}	307
5.148	COP of the ERS with P_{11}	308
5.149	Mass Flow Rate of ERS & LHP with P_{11} for Acetone	309
5.150	Heat Available as Input to ERS & LHP with P_{11} for Acetone	310
5.151	Mass Flow Rate of ERS & LHP with T_5 for Acetone	311
5.152	Heat Available as Input to ERS & LHP with T_5 for Acetone	311
5.153	Mass Flow Rate of ERS & LHP with P_{11} for Ethanol	312
5.154	Heat Available as Input to ERS & LHP with P_{11} for	313

	Ethanol	
5.155	Mass Flow Rate of ERS & LHP with T_5 for Ethanol	314
5.156	Heat Available as Input to ERS & LHP with T_5 for Ethanol	314
5.157	Mass Flow Rate of ERS & LHP with P_{11} for Methanol	315
5.158	Heat Available as Input to ERS & LHP with P_{11} for Methanol	316
5.159	Mass Flow Rate of ERS & LHP with T_5 for Methanol	317
5.160	Heat Available as Input to ERS & LHP with T_5 for Methanol	317
5.161	Mass Flow Rate of ERS & LHP with P_{11} for Water	318
5.162	Heat Available as Input to ERS & LHP with P_{11} for Water	319
5.163	Mass Flow Rate of ERS & LHP with T_5 for Water	320
5.164	Heat Available as Input to ERS & LHP with T_5 for Water	320
Drawing 1	Simple Single Effect System	328
Drawing 2	Mixture Passing Through Condenser of LHP	328
Drawing 3	Simple Single Effect System	329
Drawing 4	A Loop Heat Pipe	329
Drawing 5	Cross-section of Evaporator of Loop Heat Pipe	330

Abbreviations

Parameter	Abbreviation
<i>Specific Enthalpy</i>	<i>h</i>
<i>Specific Entropy</i>	<i>s</i>
<i>Pressure</i>	<i>P</i>
<i>Temperature</i>	<i>T</i>
<i>Mass Flow Rate</i>	<i>ṁ</i>
<i>Dryness Fraction</i>	<i>x</i>
<i>Vapor Compression Refrigeration System</i>	<i>VCRS</i>
<i>Coefficient of Performance</i>	<i>COP</i>
<i>Vapor Absorption Refrigeration System</i>	<i>VARS</i>
<i>Ejector Refrigeration System</i>	<i>ERS</i>
<i>Warming potential</i>	<i>GWP</i>
<i>Ozone Depletion Potential</i>	<i>ODP</i>
<i>Heat Pipes Heat Exchangers</i>	<i>HP-HEx.</i>
<i>Loop Heat Pipes</i>	<i>LHP</i>
<i>Liquid State</i>	<i>l</i>
<i>Vapour State</i>	<i>v</i>
<i>Gaseous State</i>	<i>g</i>
<i>Specific Volume</i>	<i>v</i>
<i>Heat Interaction</i>	<i>Q</i>
<i>Heat Conductance</i>	<i>G</i>
<i>Convective Heat Transfer Coefficient</i>	<i>h</i>
<i>Compensation Chamber</i>	<i>CC</i>
<i>Overall Heat Transfer Coefficient</i>	<i>U</i>
<i>Diameter</i>	<i>d</i>
<i>Thermal Conductivity</i>	<i>k</i>
<i>Length</i>	<i>L</i>

Chapter-1: Introduction

Refrigeration is a need of daily use in the modern era and much advancement has taken place in recent times on modes of refrigeration, processes, components involved, performance improvement & several component designing, the refrigerants, etc. Conventional household refrigeration or air-conditioning systems work on Vapour Compression Refrigeration System (VCRS) requires electrical power and can't be operated in places where electricity supply is not regular or scarce. These systems have the maximum COP of all the practical systems working on low-grade heat for instance waste heat, solar energy, etc.

In addition to the VCRS, there are systems such as the Vapour Absorption Refrigeration System (VARs) or Ejector Refrigeration System (ERS) which can be operated on Heat instead of electricity. This heat may be extracted from industries such as Power Plants, Steel Plants, Food Processing Plants, etc., and utilized as input to these cycles. This waste heat recovery helps in reduction in heat release to the environment which results in Thermal Pollution & Global Warming. Furthermore, these systems normally operate on eco-friendly refrigerants with very nether or no Global Warming potential (GWP) or Ozone Depletion Potential (ODP).

Intra-cycle waste heat recovery can also be attempted in the VARs system which can reduce the overall requirement of heat input and heat rejected in the condenser is reduced. This with help in enhancing the already low COP of even the Single Effect VARs system. Another conventional approach to increasing the COP of VARs is to employ the multi-effect VARs which works at higher pressure and temperature and hence is capable of utilizing higher temperature sources. The intra-cycle waste heat recovery can also be employed in the multi-effect VARs as well for the aforementioned benefits.

Instead of employing a conventional heat exchanger for heat recovery, Loop Heat Pipes (LHP), a superconductor of heat have been proposed which have high effectiveness, flexibility, and high overall heat transfer coefficient when compared to a conventional heat exchanger. This introductory chapter covers the following sections namely based on published literature and texts:

➤ Heat Pipes,

- Vapour Absorption Refrigeration System,
- Ejector Refrigeration System,
- Organic Rankine Cycle,
- Gas Power Cycles and,
- Refrigerants

1.1. Introduction to Heat Pipes [164][165]:

The heat pipe is an outstanding accomplishment of thermal physics and heat transport engineering owing to its exceptional capacity to transport heat for great stretch exclusive of substantial heat losses. The major usage of heat pipes deals with nature conservation and power-saving & fuel economy. Heat pipes' designs have materialized as a valuable and recognized key solution, principally in the large-heat flux operations and in circumstances of inhomogeneous heat fluxes, confined progression of air around the high heat-producing units, and space applications or weight constraints.

The novel initiative of the heat pipe was thought of by Gaugler in 1944 and by Trefethen in 1962. Moreover, Gaugler got the patent of a very low-weight heat transfer apparatus, a very fundamental arrangement of the heat pipe. In 1964, George Grove at the Los Alamos National Laboratory autonomously revived the comparable idea about the space program and its operations and named the heat hauling equipment "heat pipe" and further worked on the development of its functionality.

Heat pipes are two-stage heat transport hardware where components of fluid changing over to fume as well as the other way around move between the evaporator and the condenser with high adequate heat conductivity inferable from which the Heat Pipes Heat Exchangers (HP-HEx.) have a lot lesser sizes than conventional heat exchangers dealing with similar heat flux. In a heat pipe heat can be burned through in the evaporator segment by vanishing the functioning liquids of the heat line and afterward communicated to the condenser area where the fume is permitted to be condensed, and consequently, scattering the heat to the cooling media.

Heat pipes are being used to improve the thermal efficacy in micro-electronics; Thermal energy conservation, aeration, and Air Conditioning (HVAC) systems, temperature control systems for the human body, spacecraft, and nuclear reactor technologies. The heat pipe can be observed as a self-contained arrangement that attains very high thermal conductivity through two-phase fluid flow with capillary movement transferring latent heat of vaporization resulting in the transfer of heat over extended stretches for minute temperature differences.

Heat infused in the evaporator section gets transferred to the functioning liquid through the conduction process, resulting in the vaporization of the functioning liquid at the surface of the capillary wick, which raises the nearby vapour pressure in the evaporator and the resultant vapour streams toward the condenser, henceforth, capitalizing the transmission of latent heat of vaporization. As the heat is removed from the condenser section, the fume is condensed at the surface of the capillary structure. The closed flow of the functioning liquid is kept up with the help of capillary action as well as bulk forces (Fig 1.1).

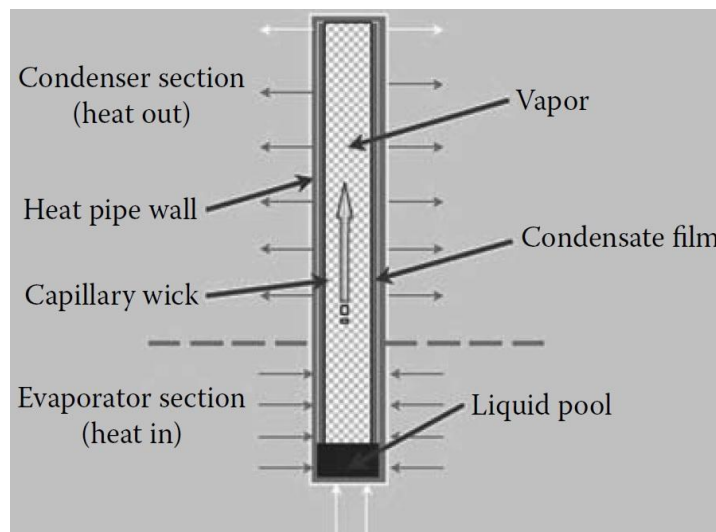


Fig. 1.1: Concept of Heat Pipes [164].

The benefit of heat pipes over other conventional transfer of heat equipment is that they can achieve an extremely high thermal conductivity working in steady-state; hence, they can handle high heat fluxes & transport heat over a comparatively stretched length for a relatively small temperature difference. A heat pipe transports energy by exploiting phase change of the working fluid without external power instead of a large thermal gradient requirement. Moreover, the extent of energy transmitted for a small cross-sectional area through phase change is much bigger

than that by conventional modes of conduction/convection/radiation. Heat pipes can be utilized for a wide range of temperatures selecting a suitable working fluid (Fig. 1.1).

The key segments of a classic heat pipe are shown (Fig. 1.2) longitudinally. External geometrical necessities make this mandatory, to add an adiabatic section to divide the evaporator & condenser. Furthermore, the cross-section of the heat pipe can be seen in Fig. 1.3 exhibiting the container wall, wick structure, & vapour space.

The heat pipe using lithium as the working fluid can transmit an axial flux of 10–20kW/cm² at a temperature of 1500 °C.

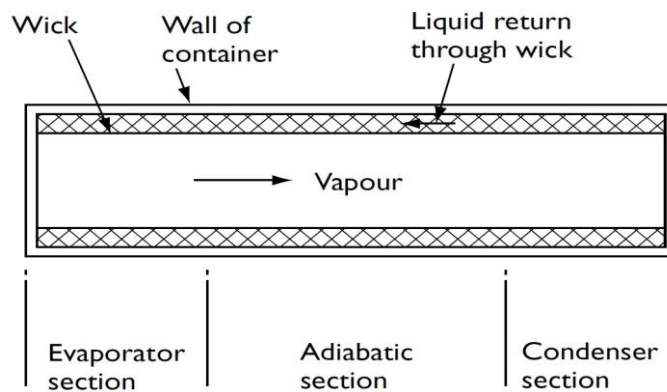


Fig. 1.2: Primary Sections of a Heat Pipe [165].

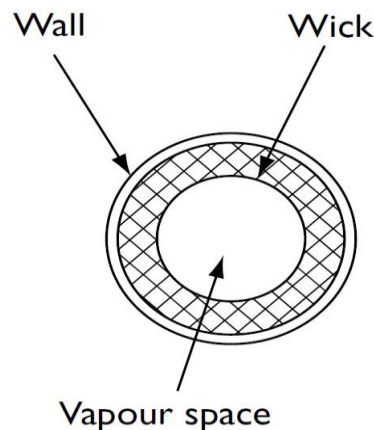


Fig. 1.3: Cross-Section of a Heat Pipe [165].

For numerous functions, the cylindrical geometry heat pipe (Fig. 1.3) has been found fit, however, other geometries can also be adapted to meet particular necessities. The heat pipe can be outlined with the given characteristics:

- i. Having exorbitant actual thermal conductance.
- ii. Operating Capability as a thermal transformer.

- iii. An isothermal surface having a little thermal impedance as the condenser exterior maintains to function at a uniform temperature. At the application of a local, more vapours will condense maintaining the temperature at the pre-specified level. The special heat pipe can also be designed for subsequent characteristics.
- iv. Inconsistent Thermal Impedance sustains the temperature of the heat source at an early invariable level over a broad series of thermal influxes. It is attained to keep the pressure stable in the heat pipe, however, changing condensing area according to the varying thermal input at the same time. A suitable technique for succeeding at this deviation of condensation area is 'gas buffering'. The heat pipe is attached to a storage tank having a larger volume than the heat pipe. The tank is filled with inert gases to contain pressure equivalent to the saturation vapour pressure of working fluids in the heat pipe. Usually, heat pipe vapour pushes inert gas back into the tank and the gas–vapour boundary gets positioned at some point near the condenser surface.
- v. Loop heat pipes (LHP) (Fig. 4) contain an evaporator and condenser, just like conventional heat pipes, however, are dissimilar as they contain vapour and liquid lines connecting Evaporator to Condenser. An exceptional characteristic of LHP is having a compensation chamber and a two-phase reservoir that helps in ascertaining the LHP pressure and temperature, and to retain the supply of working fluid in LHP. LHP can attain very high pumping powers, permitting heat transfer for ranges of several meters.

Heat Pipes also have some functional constraints such as the sonic, the capillary, the entrainment, and the boiling limit. Whenever any of these constraints are faced, the capillary structure can go into a withered situation causing the failure of the heat pipe. Moreover, when liquid metal is employed as a working fluid, startup complexity can occur owing to the possibility of a solid state of the working fluid and low vapour density.

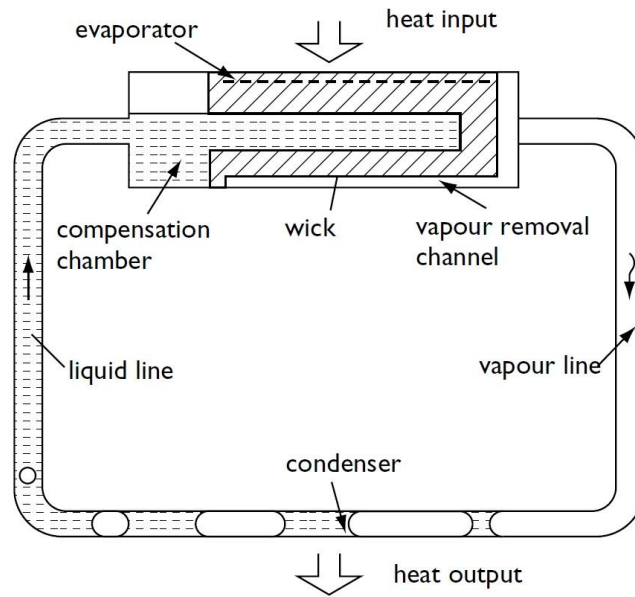


Fig. 1.4: Loop Heat Pipes [165].

1.1.1. Operating Principles of Heat Pipes [164][165]:

The 03 basic units of the heat pipe are namely:

i. The container: The container separates the fluid from the surrounding. Hence, the container must be leak-proof, should retain pressure difference across the walls, and facilitate the heat transmission from and to the functioning fluid of the heat pipe. The choice of material for the container relies on numerous aspects such as:

- Affinity (with fluid & surrounding)
- High Strength-to-weight ratio
- Thermal conductivity
- Construction, which includes welding, machinability, & pliability
- Permeability
- Wettability

A high strength-to-weight quotient is extremely significant for spacecraft functions. The material must be non-porous for avoiding diffusion of vapour n. A high thermal conductivity makes sure of the minimum temperature drop from the heat source to the wick.

ii. Working Fluid: Working Fluid should be appropriate for the working temperature range. For the estimated temperature range, numerous feasible

working fluids may be present, and diverse characteristics need to be investigated to establish the most suitable for the required application. The followings are the foremost requirement:

- Affinity to wick & wall materials
- Excellent thermal stability
- Wettability of wick & wall
- Vapour pressure suitable for temperature range
- High latent heat
- High thermal conductivity
- Low liquid and vapour viscosity
- High surface tension
- Satisfactory freezing or pour point

Moreover, the fluid must be selected based on thermodynamic considerations which are apprehensive about different constraints to heat transport taking place inside the heat pipelines. Furthermore, for heat pipes, greater surface tension is advantageous as it facilitates the heat pipe to function in opposition to gravity and to produce a high capillary rise. Also, fluid needs to wet wick and container for the contact angle to be zero or quite low. Vapour pressure for working temperature variation should be adequately large avoiding large vapour velocities, which results in a massive temperature gradient & instability in the flow.

The latent heat of vaporization should be high as it is advantageous in transporting high heat fluxes with the least fluid flow maintaining small pressure drops. The high thermal conductivity of the working fluid is desirable to reduce the radial temperature gradient & for lessening the chances of boiling in the nucleate phase at the wick or surface of the wall. The impedance of the fluid flow will be low for low vapour and liquid viscosities.

iii. Wick or Capillary Structure: It has a permeable edifice constructed of steel, aluminium, nickel, or copper in various stoma sizes. It is made up of employing metal foams & felts. By changing the pressure on felt during assembling we can shape a variety of stoma sizes. Using detachable metal mandrels, through configuration it can be moulded in felt. Moreover, materials, such as ceramics, have been used extensively having smaller pores. The major drawback of ceramic

is low stiffness and the need for a constant hold up with a metal mesh. Various heat pipes have been effectively made having wicks of carbon fibre showing superior performance.

The main rationale of the wick is for producing capillary pressure which helps in transferring liquid from the condenser to the evaporator and vice-versa, also in dispensing fluid around the evaporator to anywhere where heat is expected to be influx by a heat pipe. Frequently, these two operations need wicks of diverse forms. Hence, the choice of wick relies on numerous factors, many of which are strongly connected to the working fluid properties.

The highest capillary head created by the wick rises declining the stoma size. Wick permeability is enhanced by raising the stoma size. The heat transfer capacity of the heat pipe increases by enhancing the wick thickness. The aggregate thermal impedance of the evaporator is dependent on the thermal conductivity of the HP fluid.

1.1.2. Operational Limitations [164][165]:

There are undeniable limitations that one has to consider for the heat pipe to function appropriately based on the application and the environment. The 05 limitations are the following:

- i. Viscous limit:** At low temperatures, the vapour pressure is also small in lengthy pipes and the influence of viscous forces on the vapour flow may take over the effect of inertial forces. In this state, the motion of the working fluid is restricted, as a result of which, the heat transport gets restricted throughout the heat pipe.
- ii. Sonic limit:** The velocity of the vapour at the outlet of the evaporator may attain the sonic velocity at low vapour pressures. In this case, the evaporator cannot react to an extra decline in the condenser pressure and the vapour flow becomes choked restricting the vapour flow rate.

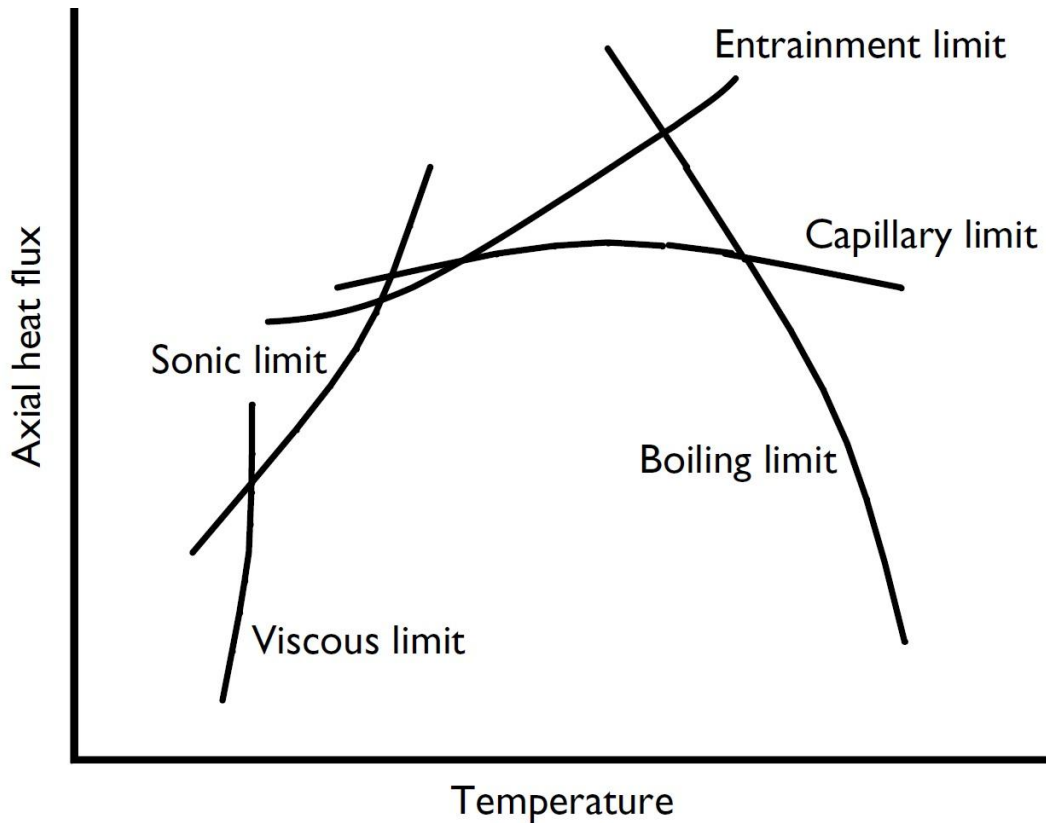


Fig. 1.5: Operational Limitations of Heat Pipes [165].

- iii. **Capillary limit:** The capillary structure is capable to facilitate the movement of working fluid up to a specific extent banking on the permeability of the wick structure and the properties of the working fluid.
- iv. **Entrainment limit:** Vapour flow applies a shear force on the fluid present in the wick, which moves in the reverse direction of the vapour. When this force surpasses the surface tension of the fluid, vapour entrains tiny liquid droplets (Kelvin–Helmholtz instabilities). Entrainment raises the fluid motion; however, the heat doesn't transport throughout the heat pipe. When this capillary force doesn't adapt to the increased flow, drying out of the wick in the evaporator takes place.
- v. **Boiling limit:** Nucleate boiling may occur at high temperatures producing vapour bubbles in the fluid layer. These bubbles can obstruct the stoma and reduce vapour flow. Also, the existence of bubbles reduces the conductivity of the fluid layer restricting the heat transport from the heat pipe shell to the fluid which occurs solely through conduction.

1.1.3. Recognition of Heat Pipes [164]:

The followings are the primary recognition of heat pipes:

- Heat pipes have more extreme heat transportability than other techniques for the same weight and size.
- Heat pipes allow arrangement flexibleness in tract zones with heat sources and heat sinks.
- Heat can be shipped over extensive distances with a paltry temperature drop.
- Capillary pumping in the wick gets produced through a heat transfer and no other power or moving parts are required for pumping condensates.
- Heat pipes can operate decently in a zero-gravity environment.

1.1.4. Heat Transfer & Temperature Difference in Heat Pipes [165]:

Heat transfer with the heat pipe (in & out) occurs by conduction, convection, or radiation modes, as well as, by eddies or by electrons. Temperature drops take place by the mode of conduction across walls of the heat pipe at evaporator and condenser sections. Moreover, a drop in temperature across the wicks occurs in numerous manners. Also, thermal resistance is observed at the two vapour-liquid surfaces and the vapour column.

1.1.4.1. Heat transfer in the evaporator region

A smaller heat flux, conduction, and partially natural convection modes exist for heat transfer through the wick and liquid and the evaporation will take from the liquid surface. With an increase in the heat flux, the working liquid that's in the vicinity of the wall will be converted increasingly into superheated, and the formation of bubbles will take place at the nucleation spots. These bubbles will transfer a fraction of energy latent heat of vaporization and will significantly augment the heat transfer by convection. With an addition in the flux, a censorious state approaches called burnout, at which the wick gets withered and the heat pipe stops functioning.

1.1.5. Introduction to Loop Heat Pipes (LHP) [165]:

To function with the evaporator located higher than the condenser in a gravitational field, the wick must be extended to the whole length of a normal heat pipe. Where the capillary head is in opposite relation to the effectual stoma radius of the wick and is independent of length, hydraulic impedance is directly related to the length of the wick and in opposite relation to the square of the stoma radius. Hence, if the length of a heat pipe functioning in opposition to gravitational force needs to be enlarged, decreasing the pore radius becomes compulsory to facilitate the required capillary head, resulting in a rising pressure drop in liquid. Similarly, the requirement for fluid to stream throughout the wick restricts the whole length of a typical heat pipe.

Loop heat pipes (LHP) (Fig. 1.4) were incorporated to defeat the inbuilt difficulty of using long wick having a tiny pore radius in traditional heat pipes firstly by Gerasimov and Maydanik autonomously in 1972 of the Ural Polytechnic Institute driven by the likely use in space initially considering large heat transfer capacities (0.5–24 kW).

1.1.6. Operation of Loop Heat Pipes (LHP)[165]:

On start-up, fluid is adequate for infilling the condenser as well as the fluid & vapour lines. Moreover, the fluid available in the evaporator section & compensation chamber section is enough for saturating the wick. As the evaporator fluid is subjected to heat in-flux through saddles, it evaporates from the surface of the wick and in the compensation - chamber limited to a low quantity. However, as the wick has substantial thermal impedance, the temperature and pressure in the compensation chamber are lower than in the evaporator. Capillary forces in the wick avert the flow of vapour from the evaporator section to the compensation chamber section. With a rise in the pressure gradient for the evaporator & compensation chamber, fluid moves back from the liquid line & condenser to the compensation chamber.

Performance Improvement of Vapour Absorption System Using Loop Heat Pipes

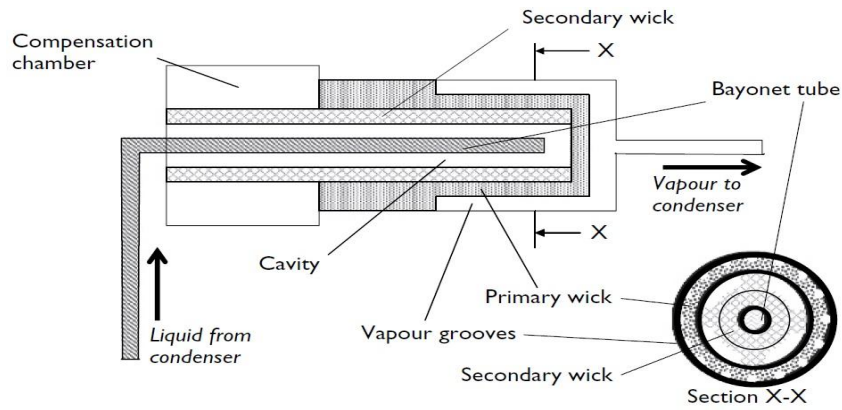


Fig. 1.6: Cross-Section of Evaporator Section of a Loop Heat Pipe [165].

A sectional view of the evaporator is presented in Fig. 1.6. The evaporation occurs on the surface of the wick next to the evaporator wall. Vapour extraction conduits are integrated with the wick or evaporator wall making sure vapour flow from the wick to the vapour line against the least possible pressure drop. The secondary wick is employed to make certain of the consistent liquid availability to the primary wick & for supplying liquid in case transient dry-out occurs.

1.1.7. Properties of Various Loop Heat Pipes Working Fluids (LHP)[165]:

Table 1.1 presents the thermophysical properties of various easily available working fluids/substances for the LHP. It contains Ethanol, Ammonia, and Water for normal low – medium temperature usage, moreover, liquid metals such as Potassium, Sodium & Lithium for extremely high temperatures.

Table 1.1: Superheat required to initiate nucleate boiling at atmospheric pressure [165]

Fluid	Boiling point (K)	Vapour density kg/m³	Latent heat (kJ/kg)	Surface tension (N/m)	ΔT (°C)
Ammonia	239.7	0.3	1 350	0.028	2.0
Ethyl alcohol	338	2.0	840	0.021	0.51
Water	373	0.60	2 258	0.059	0.51
Potassium	1047	0.486	1 938	0.067	8.9
Sodium	1156	0.306	3 913	0.113	26.4
Lithium	1613	0.057	19 700	0.26	44.6

Similarly, Table 1.2 presents the useful operating range of the working fluids which can be used for the temperature ranges of this analysis. It presents the Boiling point and Melting point/solidification temperature of the substances along with the temperature ranges.

Table 1.2: Useful ranges of various operating fluids [165]

Fluid	Melting point (°C)	Boiling point at atmos. press. (°C)	Useful range (°C)
Ammonia	-78	-33	-60 to 100
Pentane	-130	28	-20 to 120
Acetone	-95	57	0 to 120
Methanol	-98	64	10 to 130
Ethanol	-112	78	0 to 130
Heptane	-90	98	0 to 150
Water	0	100	30 to 200
Toluene	-95	110	50 to 200

The following Table 1.3 presents the operating characteristics of the working fluids such as Axial Heat Flux & Radial Heat Flux for the 3 most commonly available fluids Water, Ammonia, Methanol, Etc. Along with the Heat Flux, the table suggests the vessel material which can be used for the working fluids for the LHP.

Table 1.3: Operating Characteristics Heat Pipes [165]

Fluid	Vessel Material	Axial Heat Flux (kW/cm ²)	Radial Heat Flux (kW/cm ²)
Ammonia	Nickel, aluminum, stainless steel	0.295	2.95
Methanol	Copper, nickel, stainless steel	0.45 at 10°C	75.5 at 100°C
Water	Copper, nickel	0.67 at 200°C	146 at 170°C

1.1.8. Advantages of Loop Heat Pipes[165] [164]:

- Large heat flux capacity.
- Capacity to transfer heat over extended space with no restriction of routing of the liquid and vapour lines.
- Capability to function for a series of ‘g’ environments.
- No requirement for wick in the transfer lines (Vapour/Liquid lines).
- Vapour and Liquid streams are separated, hence, no issue of entrainments.
- Can be used for temperature control& management.

The declared benefits emphasize the aptness of the LHP for transferring heat over large distances; nevertheless, the capability to work with high heat fluxes and twisted flow paths makes the application of miniature LHPs eye-catching in the cooling applications of electronic items. Miniaturization produces the problem of not maintaining the essential temperature gap between the evaporating wick and the compensation chamber with the thin wick in a miniature system.

1.1.9. LHP & Thermodynamics [165]:

The thermodynamic cycle of the LHP working under steady-state conditions has been illustrated in Fig. 1.7. State 1 corresponds to the saturated vapour directly above the meniscus on the wick. As the vapour in the evaporator, Vapour passing through the vapour conduits gets superheated by coming in contiguity with the fiery wall of the evaporator, thereafter, goes into the vapour line defining state 2. In the vapour line flow of vapour can be estimated as an isothermal pressure drop to state 3 which is the entrance of the condenser.

Pressure loss in the condenser is usually insignificant and heat transfer is due to condensation of saturated liquid to state 4 and sub-cooling thereafter to state 5. Sub-cooling makes sure no generation vapour in the liquid line returns to the compensation chamber, owing to either the pressure drops in the liquid or heating from the environment.

The liquid then comes into the compensation chamber at state 6 and is then heated to the saturation temperature in the compensation chamber containing saturated liquid at state 7 in equilibrium with the saturated vapour filled in the lingering area of the chamber.

The liquid flowing through the wick reaches state 8. The liquid inside the wick is superheated, however, doesn't get evaporated because of the very tiny pore size and lack of nucleation locations. At the surface, the capillary effect causes the development of menisci at each pore of the wick. The pressure gap across the menisci can be shown as ΔP_c .

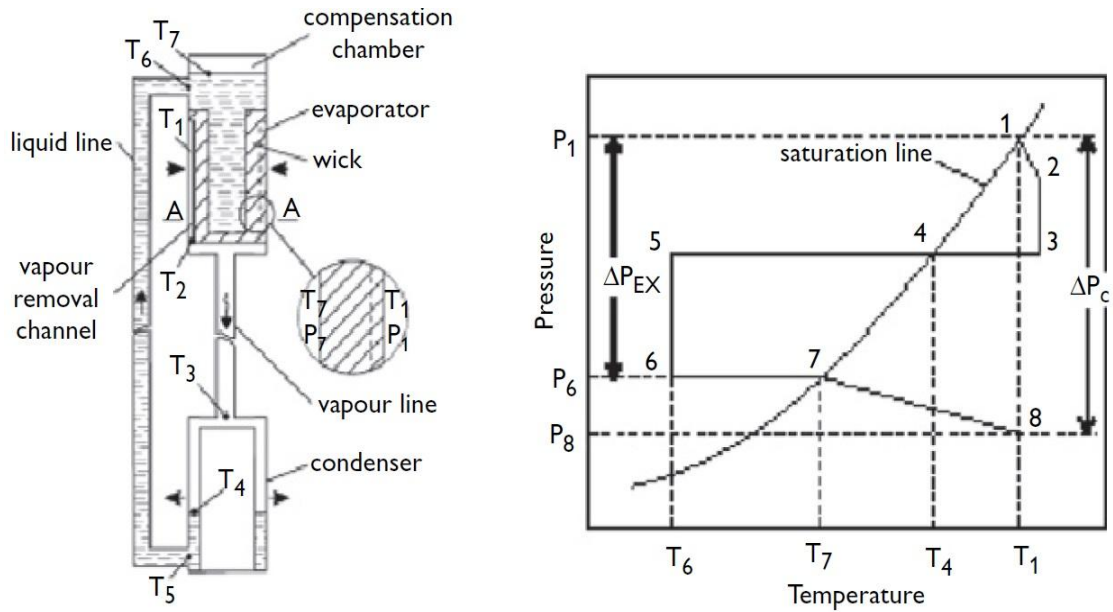


Fig. 1.7: Schematics & Pressure-Temperature Graph of LHP [165].

1.1.10. The Conditions for Correct Functioning [165].

The first condition is that the maximum capillary pumping pressure, $\Delta P_{CM_{max}}$ must be larger than the total pressure loss in LHP having 03 constituents.

- (i) The pressure loss ΔP_1 is essential to re-circulate the fluid from the condenser to the compensation chamber.
- (ii) The pressure loss ΔP_v is essential to make the vapour streams from the evaporator to the condenser.
- (iii) Pressure loss owing to potential head, ΔP_g can be zero, positive or negative, and is dependent on the gradient of the heat pipe. For suitable functioning,

$$\Delta P_{CM_{max}} \geq \Delta P_1 + \Delta P_v + \Delta P_g \tag{1.1}$$

When this condition is not sustained, the evaporator region gets withered and the heat pipe fails to work. The maximum heat flux for which equation 1.1 holds is called the capillary limit which will regulate maximum heat flux over the functioning range.

The second condition is that the pressure loss between the evaporating wick surface and the vapour space in the reservoir, i.e., ΔP_{EX} , matches the change in saturation temperature between states 1 and 7. This liquid gets ousted from the evaporator to

the compensation chamber at start-up. As the temperature variation in LHP is comparatively little, the slope of the $(dP/dT)_{\text{Sat}}$ can be treated constant and the attributes of the LHP must be such that:

$$(dP/dT)_{\text{Sat}} \times \Delta T_{1-7} = \Delta P_{\text{EX}} \quad (1.2)$$

The third prerequisite is that the liquid must be sub-cooled at the exit of the condenser (state 5), adequately to avoid disproportionate flashing in the vapour line.

$$(dP/dT)_{\text{Sat}} \times \Delta T_{4-6} = \Delta P_{5-6} \quad (1.3)$$

1.1.11. Thermodynamics & Heat Transfer Equations of LHP [29]:

As mentioned above the LHP can be apportioned into 07 segments: I. The evaporator along with Compensation Chamber (CC), II. The wick & vapour grooves, III. The vapour line, IV. The superheated section of the condenser, V. The 2-phase segment of the condenser, VI. The sub-cooled part of the condenser; and VII. The liquid line.

I. The Evaporator & Compensation Chamber:

Q_S is the heat transported from the source, at steady-state temperature T_S , via saddle to the outer envelope of the evaporator. Fourier's Law for this heat transfer with Saddle Conductance G_S (W/K) can be given as:

$$Q_S = G_S \times (T_S - T_{\text{Ev-Wall}}) \quad (1.4)$$

Where $T_{\text{Ev-Wall}}$ is the wall temperature of the Evaporator in K.

Q_S are divided into substantial heat transported to the liquid/vapour interface on the outer surface of the wick & the remainder heat leakage between the evaporator and CC walls having thermal conductance k_{HL1} . The Fourier equation for this heat leak Q_{HL1} between the evaporator and CC walls is:

$$Q_{\text{HL1}} = G_{\text{HL1}} \times (T_{\text{Ev-Wall}} - T_{\text{CC-Wall}}) \quad (1.5)$$

Where $T_{\text{CC-Wall}}$ is the temperature of the wall of the compensation chamber.

Similarly, the equation for the heat transferred to the liquid-vapour interface, $Q_{\text{Ev-if}}$, is:

$$Q_{Ev-if} = G_{Ev} \times (T_{Ev-Wall} - T_{Ev-if}) \quad (1.6)$$

Where G_{Ev} is the thermal conductance of the Evaporator & T_{Ev-if} is the Temperature of the Evaporator Liquid/Vapour Interface. G_{Ev} is affected by the type of thermal contact between the wick and evaporator wall and the geometry of the wick as well as by the liquid/vapour interface rescinding deeper into the pores and focussed dry spots where the wick is in contact with the evaporator wall.

The heat at the liquid-vapour interface is further divided as the interface and the fluid in the CC is thermally attached, which results in a second heat leak Q_{HL2} :

$$Q_{HL2} = G_{HL2} \times (T_{Ev-if} - T_{CC-if}) \quad (1.7)$$

Heat transported through the wick Q_{Wi} from the outer surface to the wick core through the metallic structure of the wick and fluid in stoma can be given in the equation

$$Q_{Wi} = (\dot{m} C_{Pl} / ((d_o/d_i)^\eta - 1)) \times (T_{Ev-if} - T_{CC-if}) \quad (1.8)$$

Where η can be given as

$$\eta = \dot{m} C_{Pl} / 2 \times \pi \times k_{eff} \times L_{Wi} \text{ and,} \quad (1.9)$$

$$\text{Effective Thermal Conductivity, } k_{eff} = (k_{max})^n \times (k_{max})^{(1-n)} \quad (1.10)$$

Where, $0.42 < n < 0.5$ and,

$$k_{max} = \varepsilon \times k_f + (1 - \varepsilon) \times k_{wick} \quad (1.11)$$

$$k_{min} = k_f \times k_{wick} / (\varepsilon \times k_{wick} + (1 - \varepsilon) \times k_f) \quad (1.12)$$

Where ε is the porosity of the wick, k_f is the thermal conductivity of the fluid in W/m-K and k_{wick} is the thermal conductivity of the wick material in W/m-K.

The heat required to increase the temperature of the liquid in the compensation chamber can be given as:

$$Q_f = \dot{m} C_{Pl} \times (T_{Ev-if} - T_{CC-if}) \quad (1.13)$$

\dot{m} is the mass flow rate in kg /s, C_{Pl} is the specific heat capacity kJ/kg-K & d_o and d_i are the outer and inner diameter of the evaporator section.

Heat utilized to boil the liquid on the surface of the wick can be given as:

$$Q_{Ev-if} = \dot{m} \times h_{fg} \quad (1.14)$$

Heat interaction between the CC wall and the surrounding can be expressed as:

$$Q_{amb} = G_{amb} \times (T_{amb} - T_{cc-Wall}) \quad (1.15)$$

Where, G_{amb} is Heat Conductance of the Surrounding in W/K, T_{amb} & $T_{cc-Wall}$ are Ambient & CC Wall temperature.

The conductance coefficient of ambient G_{amb} can be shown as

$$G_{amb} = 1.32 \pi L_{CC} d_o ((T_{amb} - T_{cc-Wall}) / d_o)^{0.25} \quad (1.16)$$

The heat transfer between the CC wall and CC fluid is given as:

$$Q_{amb} = G_{CC} \times (T_{cc-Wall} - T_{cc-if}) \quad (1.17)$$

The heating of the sub-cooled liquid can be computed as:

$$Q_{in} = \dot{m} C_{Pl} \times (T_{CC-if} - T_{in}) \quad (1.18)$$

Where T_{CC-if} & T_{in} are the Temperatures at CC interface & CC inlet respectively.

It is also assumed that

$$T_{Ev-Wall} > T_{CC-Wall} > T_{CC-if} > T_{in} > T_{Cond}$$

II. Vapour Grooves:

The highest mass flow rate can be assumed for half-length of the vapour grooves and the pressure drop can be accustomed to the hydraulic diameter of the grooves in the following calculation:

$$\Delta P_{vg} = -f L_{vg} (t+w) \dot{m}^2 / 4n^2 t^3 w^3 \rho_v \quad (1.19)$$

Where f is the friction coefficient, L_{vg} is the length of vapour grooves in m, t & w are the height and width of the vapour grooves in m, \dot{m} is the mass flow rate, n is the number of grooves and ρ_v is the vapour density in kg/m^3 .

The coefficient of friction, f , can be computed as:

$$f = 64/Re \text{ for } Re < 2200 \text{ (Laminar Flow), \&} \quad (1.20)$$

$$f = 0.3164Re^{-0.25} \text{ for } Re > 2200 \text{ (Turbulent Flow)} \quad (1.21)$$

$$\text{Where, Reynolds Number, } Re = 2 \dot{m}/(t+w)\mu_v \quad (1.22)$$

III. Vapour and liquid lines

The temperature change of the fluid in lines is owing to the contact with the environment. The equation for the temperature change, assuming that heat is rejected from the fluid, is:

$$(dT_f/dx) = - (1/ \dot{m}c_p) (UA/L) (T_f - T_{amb}) \quad (1.23)$$

Where L is the length in m, UA/L is the thermal conductance per unit length in W/mK, T_f is the temperature of the fluid. Also,

$$L/UA = 1/h_i\pi d_i + \ln (d_o/d_i)/2\pi k_{wall} + 1/h_o\pi d_o \quad (1.24)$$

Where, h_i & h_o are the convective heat transfer coefficients in W/m^2K for inner & outer surfaces respectively, k_{wall} is the thermal conductivity of the wall of the lines & A is the cross-sectional area of the line.

We know for the convection heat transfer coefficient:

$$h_i = Nu k/d_i, \text{ where, Nusselt Number, } Nu = 0.023 (Re)^{0.8} (Pr)^n \quad (1.25)$$

$$\text{Where, Prandtl Number, } Pr = C_p \mu / k \text{ and exponent } n = 0.4 \quad (1.26)$$

The convective heat transfer coefficient for outer surface of the line is,

$$h_o = 1.32 (T_o - T_{amb}/d_o)^{0.25} \quad (1.27)$$

Where, T_o is the outer surface temperature of the line, and the pressure drop owing to the friction and gravity can be given as:

$$dP_f/dx = -f (8 \dot{m}^2 / \rho_f \pi^2 d_i^5) \pm g \rho_f \sin \phi \quad (1.28)$$

A positive elevation angle ϕ is taken whenever the condenser is elevated above the evaporator and the flow is gravity supported and vice-versa. Furthermore, the sign is taken as positive for the liquid line and negative for the vapour line.

IV. Condenser:

The quality is the ratio of the mass of vapour to the total mass. It varies as a product of condensation:

$$dX/dx = (-1/ \dot{m}h_{gf}) (UA/L) (T_v - T_{\text{heat sink}}) \quad (1.29)$$

Where h_{gf} is the latent heat of fusion.

The hydraulic dia of the liquid film is given by:

$$D_i = 4\delta - 2\delta^2/r_i \quad (1.30)$$

Where δ is Film thickness in m, D_i & r_i are inner dia & radius of the flow channel respectively.

The variation in film thickness is established by the study of the curvature of the interface between the vapour and liquid sections, by the Young-Laplace equation:

$$P_v - P_l = \sigma (1/R_{\text{radial}} + 1/R_{\text{axial}}) \quad (1.31)$$

Where R_{radial} & R_{axial} are the radii of curvature in the radial and axial directions respectively and the axial component can be neglected owing to small changes over a long distance. Hence, the pressure difference resultant from the change in film thickness is:

$$P_v - P_l = (\sigma/ r_i - \delta) (1 + (d\delta/dx)^2)^{-0.5} \quad (1.32)$$

Whereas, equation for the pressure drop in the vapour section can be given as:

$$dP_v/dx = (-2/ r_i - \delta)(\tau_{fr} + \tau_{mt}) - d(\rho_v v_v)/dx \quad (1.33)$$

Where τ_{fr} & τ_{mt} are shear stresses corresponding to friction & momentum transfer in N/m^2 and $\rho_v v_v$ is the mass of the vapour.

The frictional shear stress can be expressed by:

$$\tau_{fr} = \pm 1/8 f \rho_v (v_v - 2 v_l)^2 \quad (1.34)$$

The shear stress due to momentum-transfer is affected by the gap between vapour and liquid velocities and condensation and can be given as:

$$\tau_{mt} = - (dX/dx) (X\dot{m}/2 \pi (r_i - \delta)) (v_v - 2 v_l) \quad (1.35)$$

An empirical correlation projected by Wallis (Carey5) facilitates the film thickness to be estimated using the pressures and quality at a cross-section and is expressed as:

$$\alpha = V_v/V_{tot} = (1+X_{tt}^{0.8})^{-0.378} \quad (1.36)$$

Where X_{tt} is the Lockhart-Martinelli parameter:

$$X_{tt} = (1-X/X)^{0.9} (\rho_v/\rho_l)^{0.5} (\mu_l/\mu_v)^{0.1} \quad (1.37)$$

V. Mass Equation:

Mass Equation can be given as:

$$M_{cc} = M_{ch} - M_{wi} - M_{vg} - M_{vi} - M_{cond} - M_{ll} \quad (1.38)$$

Void Fraction can be given as.

$$\alpha = \rho_l V_{cc} - M_{cc}/(\rho_l - \rho_v) V_{cc} \quad (1.39)$$

VI. Other Important Equations [165]:

Figure of Merit for comparing different working fluids for LHP:

$$MF_h = \rho_l \sigma h_{fg} / \mu_l \quad (1.40)$$

The axial heat flow rate due to the sonic limitation was calculated from the following equation:

$$Q_s = \pi r_p^2 \rho_v h_{fg} \sqrt{\frac{\gamma RT}{2(\gamma+1)}} \quad (1.41)$$

The maximum heat transfer due to the entrainment limit was determined using the equation

$$Q_{Ent} = \pi r_p^2 h_{fg} \sqrt{(2 \pi \rho_v \sigma \cos \phi / \lambda)} \quad (1.42)$$

The maximum heat transfer due to the capillary limit was determined using the equation

$$Q_{Cap} = (MF_h)(A_w k_{hp}/L_{eff}) \{(2/r_p) - (\rho_l g L_{eff} \sin \phi / \sigma)\} \quad (1.43)$$

The degree of superheat to cause nucleation is given by:

$$\Delta T = 3.06 \sigma_l T_{vLHP} / \rho_v h_{fg} \delta \tag{1.44}$$

With reference to mass flow rate of warm and cool air, the heat transfer rates to the evaporator and condenser sections are calculated as follow:

$$q_e = m c_p (T_{e,in} - T_{e,out}) = \rho u A c_p (T_{e,in} - T_{e,out}) \tag{1.45}$$

$$q_c = m c_p (T_{c,in} - T_{c,out}) = \rho u A c_p (T_{c,in} - T_{c,out}) \tag{1.46}$$

$$\text{Heat Transfer Factor, HTF} = 2 M F_h A k_{hp} / r_p \tag{1.47}$$

1.2. Introduction to Vapour Absorption Refrigeration System:

Vapour Absorption Refrigeration Systems (VARs) dissimilar to the vapour compression refrigeration systems (VCRS), require heat to function. These are also referred to as wet absorption systems. Whereas, alike the VCRS, VARs have also been made suitable for commercial usage and are broadly utilized in numerous refrigeration and air conditioning purposes. Because VARs operate on low-grade energy, they are favoured once low-grade energy i.e., waste heat or solar energy is accessible. Traditional absorption systems operate on naturally available refrigerants such as water or ammonia; hence, they are eco-friendly.

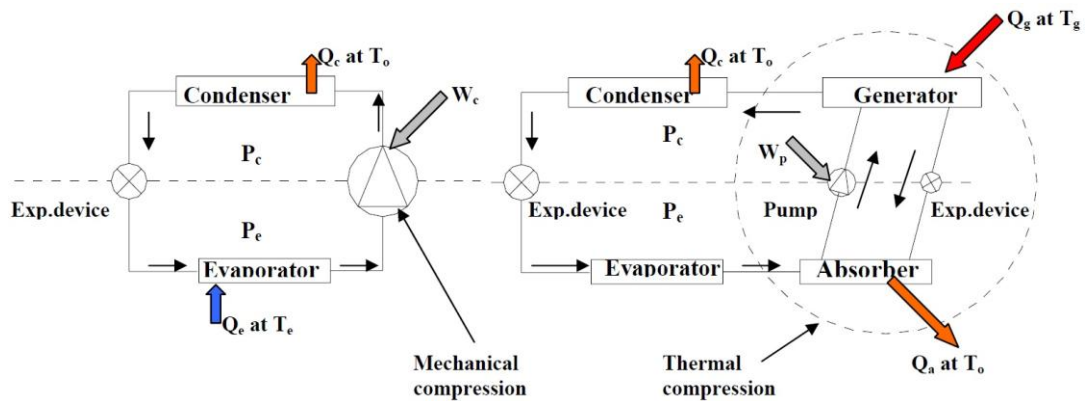


Fig. 1.8: Comparison Between VCRS & VARs [166]

The ordinary VCRS have a condenser, evaporator, throttling valve, & compressor. Refrigerant enters the evaporator as a low-temperature, low-pressure combination of liquid & vapour. Heat is transported to the refrigerant, which makes the liquid refrigerant evaporate. The resultant vapour is then compressed through a compressor, the high temperature; high-pressure vapour from the compressor enters the condenser

where it transmits heat resulting in the saturated liquid refrigerant. The liquid refrigerant flows through the expansion device, to that of the evaporator at low temperature & pressure completing the cycle.

Similar to the VCRS, the refrigerant in VARS moves through the condenser, expansion valve, and evaporator. Nevertheless, the VARS utilizes other refrigerant mixtures and a dissimilar technique of compression, called thermal compression.

VARS substitutes the compressor with a generator and an absorber connected through a Pump & Throttle Valve. Exploiting the analogy of the VCRS, the absorber performs like the suction side of the compressor as it extracts the refrigerant vapour out of the evaporator & mixes it with the absorbent. The pump performs like the compression action as it forces the combination of refrigerant and absorbent up to the Generator/High-Pressure Side of the system. The generator functions as the discharge side of the compressor as it delivers the refrigerant vapour to the condenser. It can be seen as the integration of the Refrigeration cycle consisting of an Evaporator, Expansion Valve & Condenser with a Thermal Compression Cycle consisting of an Absorber, Generator, Solution HEX & Pressure reducing valve.

1.2.1. Parallels between VCRS & VARS:

- The refrigerant flows inside the evaporator to transport heat from one fluid to the other in both systems.
- A machine is used to raise the pressure of the refrigerant and the expansion device to sustain the internal pressure gap to complete the cycle.
- The condenser is used for vapour to condense at high pressure and temperature while throwing out heat to the environment.
- The refrigerant liquid evaporates at low pressure & temperature, soaking up heat from the chiller.

1.2.2. Departures between VCRS & VARS:

- VARS can work on heat (Low-Grade Energy).
- VARS uses a liquid pump which is much simpler and inexpensive taking less work input. The system principally substitutes the work input with heat input.

Performance Improvement of Vapour Absorption System Using Loop Heat Pipes

- VARS works on refrigerants having no environmental hazard, ODP or GWP.
- VARS comprises very few moving parts hence, less noise and vibration, with compact size for huge capacities and needs minute maintenance.
- VARS has low COP and does not reduce considerably at part loads.
- VARS is comparable to a heat engine.

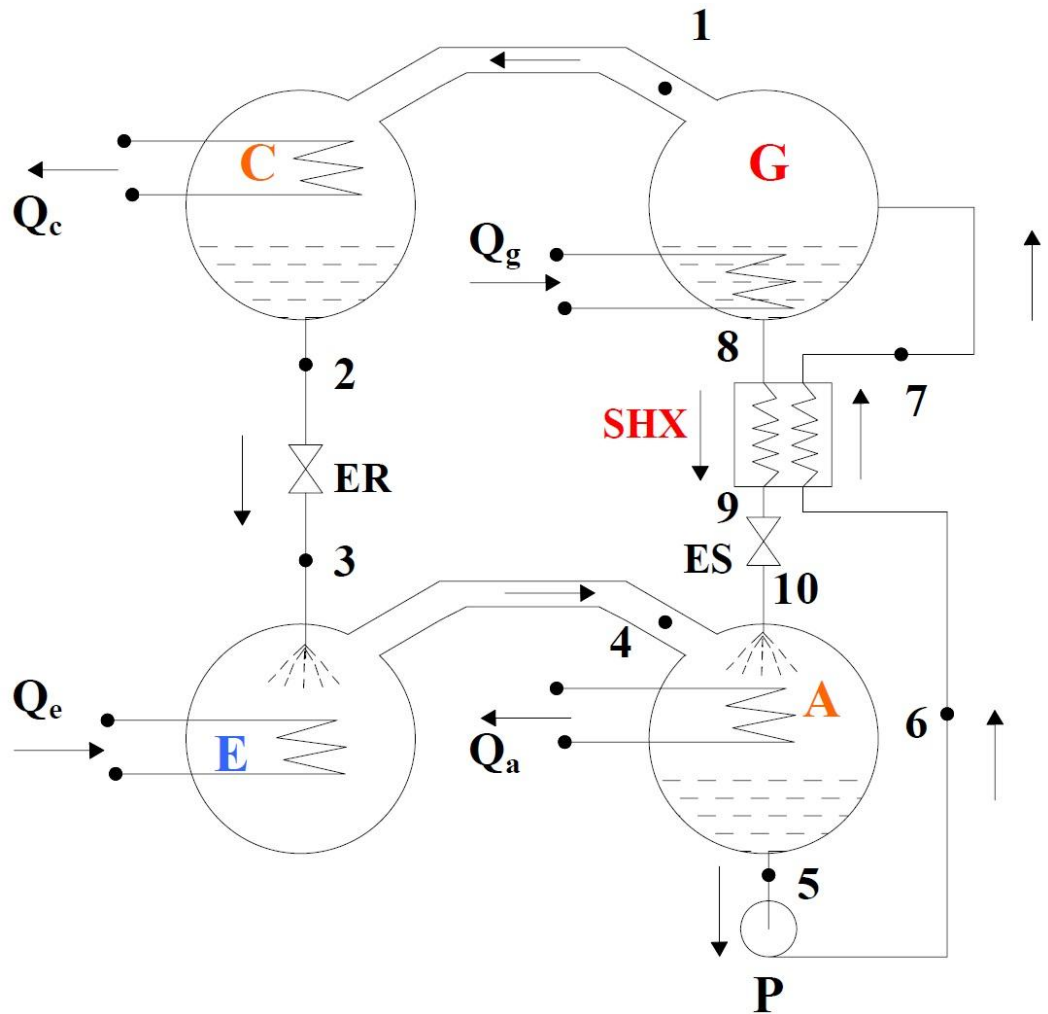


Fig. 1.9: Schematic of LiBr-H₂O VARS [166]

1.2.3. Practical VARS [168]:

A practical VARS (Fig 10) comprises the analyzer, a rectifier, and heat exchangers. The purpose of the analyzer is to eliminate the weak refrigerant moisture from the strong refrigerant.

A rectifier is essentially a small-scale condenser where any traces of absorbent vapour are present in the refrigerant vapour, which is eliminated by condensation.

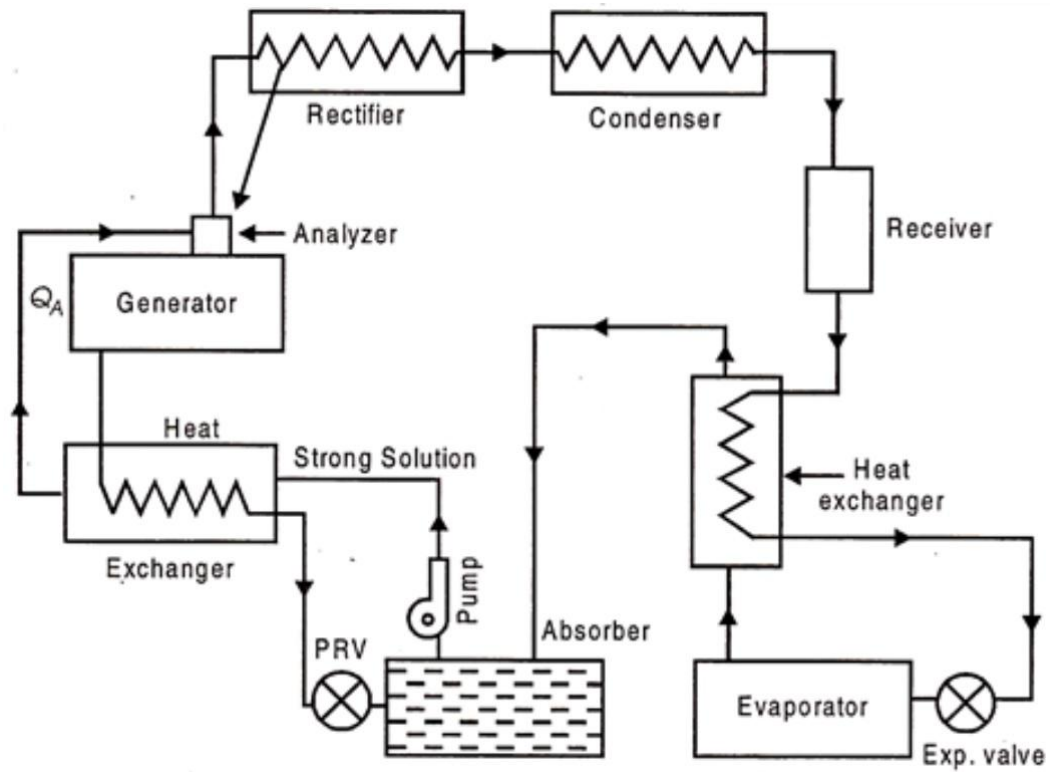


Fig. 1.10: Schematic of Practical VARS [168]

1.2.4. Applications of Absorption Systems:

VARS can employ waste heat which would reject eventually. In terms of energy performance, motor-driven vapour compression chillers will beat absorption chillers every time. The followings are the detailed functions where VARS has a significant benefit over VCRS:

- Services that use a large amount of thermal energy for their procedures generally reject waste heat to the environment.
- Where a concurrent requirement for heat and power is there.
- Where the power supply is not robust, expensive, unreliable, or unavailable.
- For services requiring using a “natural refrigerant and aspirant for LEED certification (Leadership in Energy and Environmental Design.
- Where variable heat sources are available.

1.2.5. Multi-effect VARS

In multi-effect systems, a sequence of generators functioning at gradually dropping pressures is used. Input Heat is provided to the highest stage generator functioning at maximum pressure. The enthalpy from this generator is consumed to produce a few more refrigerant vapours in the lower stage generators and so forth. Hence, this way the input heat to these systems is used proficiently resulting in higher COPs than Conventional VARS or Single Effect VARS. These systems are more complex and need much-elevated heat source temperatures for the peak stage generator.

I. Half-Effect System: The normal half effect VARS contains an evaporator, Low-Pressure & High-Pressure absorbers, Low-Pressure & High-Pressure Generators, Low-Pressure & High-Pressure heat exchangers, a condenser, 2 solution pumps, and 2 solutions, and a refrigerant expansion valve (Fig. 1.9). The condenser and High-Pressure generator function at the highest system pressure. The High-Pressure absorber and Low-Pressure generator work at the same intermediary pressure level while the Low-Pressure absorber and evaporator run at the lowest pressure of the whole system.

The refrigerant vapour after the condenser proceeds to the evaporator through the refrigerant expansion valve. The mixture is running within two separate stages i.e., a Low-Pressure stage and an HP stage between the HP absorber and the HP generator. Compared to a single-stage absorption refrigeration system, there are two additional components viz. HP absorber and LP generator in a half effect system. These are used to concentrate the lithium bromide aqueous solution in the LP stage cycle.

Performance Improvement of Vapour Absorption System Using Loop Heat Pipes

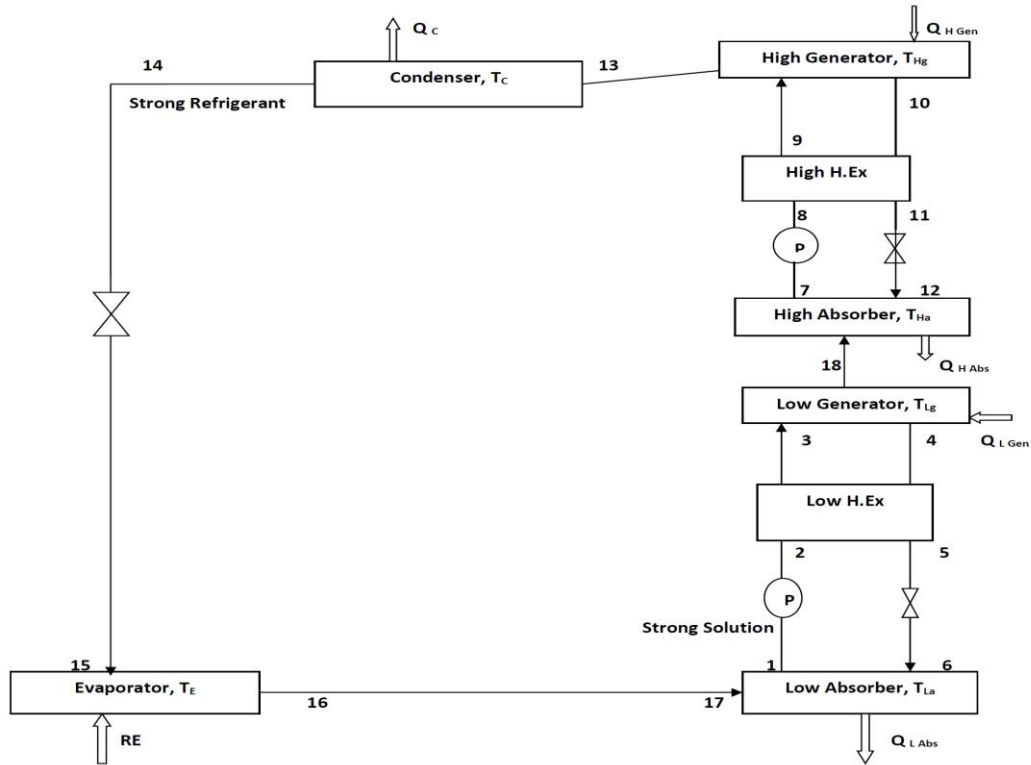


Fig. 1.11: Schematic of Half Effect VARS

II. Single Effect System: It is the conventional system that consists of one Evaporator, Condenser, Generator & Absorber as shown in Fig 1.10. The system works as described in section 1.2.

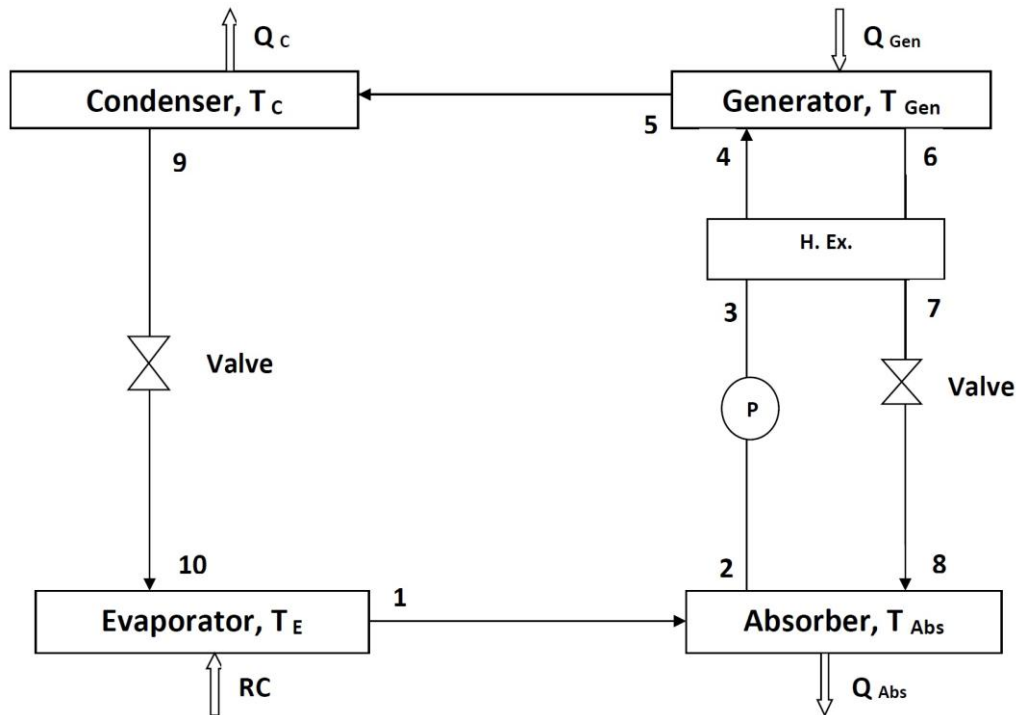


Fig. 1.12: Schematic of Single Effect VARS

III. Double Effect System: A double effect VARS (series) contains 02 generators (High & Low Temperature), 02 condensers, 01 evaporator, 01 absorber, 01 pump, 02 Heat Exchangers for a solution, 02 reducing valves for the solution, and 02 expansion valves for refrigerants as presented in Fig. 1.11. The solution from the absorber is pumped to the high pressure-temperature generator, from where the refrigerant vapour goes into the refrigeration cycle through the High and Low P-T Condenser through the expansion valves. Furthermore, the weak solution after the High P-T generator is passed through a low P-T generator where the remaining refrigerant is also vaporized and let out towards the Low P-T condenser. Hence making the refrigerant available for cooling effect summation of refrigerant from High P-T Condenser & Low P-T Condenser, increasing the efficient use of the refrigerant in the cycle and availability of high-temperature heat input when compared to a conventional VAR.

IV. Triple Effect VARS: The triple effect (series) VARS can be seen in Fig. 1.12. To the Double effect system, another High-temperature Generator & Condenser have been added for the development of the triple effect system. The rest of the cycle works similarly to the double effect system where the refrigerant available at the evaporator for cooling effect is the summation of High, Med Low P-T Condenser being generated in High, Med Low P-T Generator.

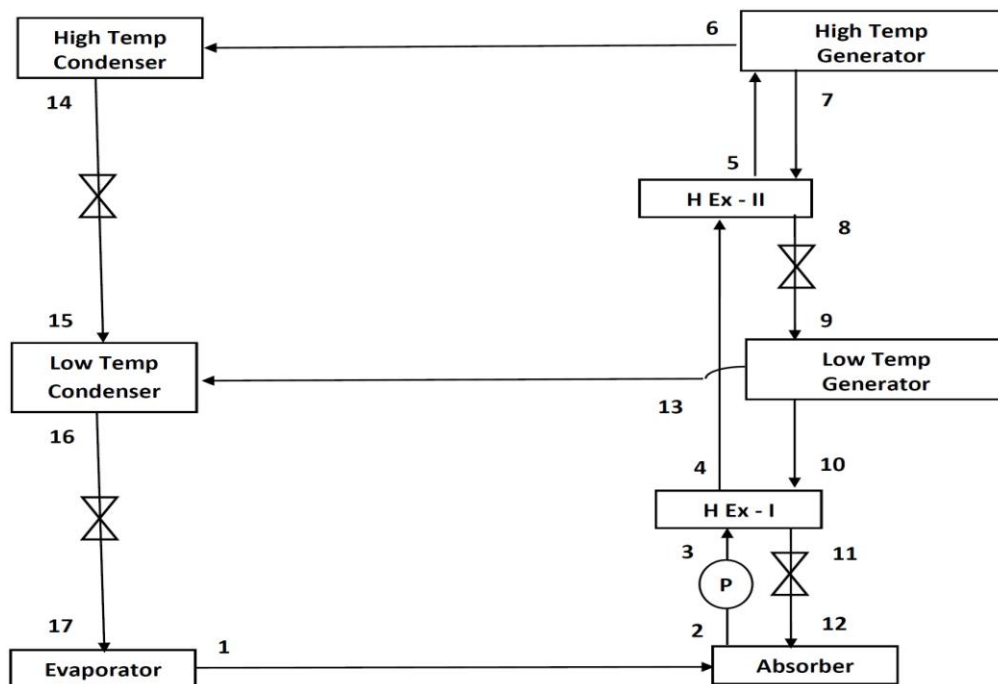


Fig. 1.13: Schematic of Double Effect (Series) VARS

V. Quadruple Effect VARS: Similar to the aforementioned methodology, Quadruple Effect (Series) VARS can be developed by adding another High P-T Generator & Condenser as in Fig. 1.13.

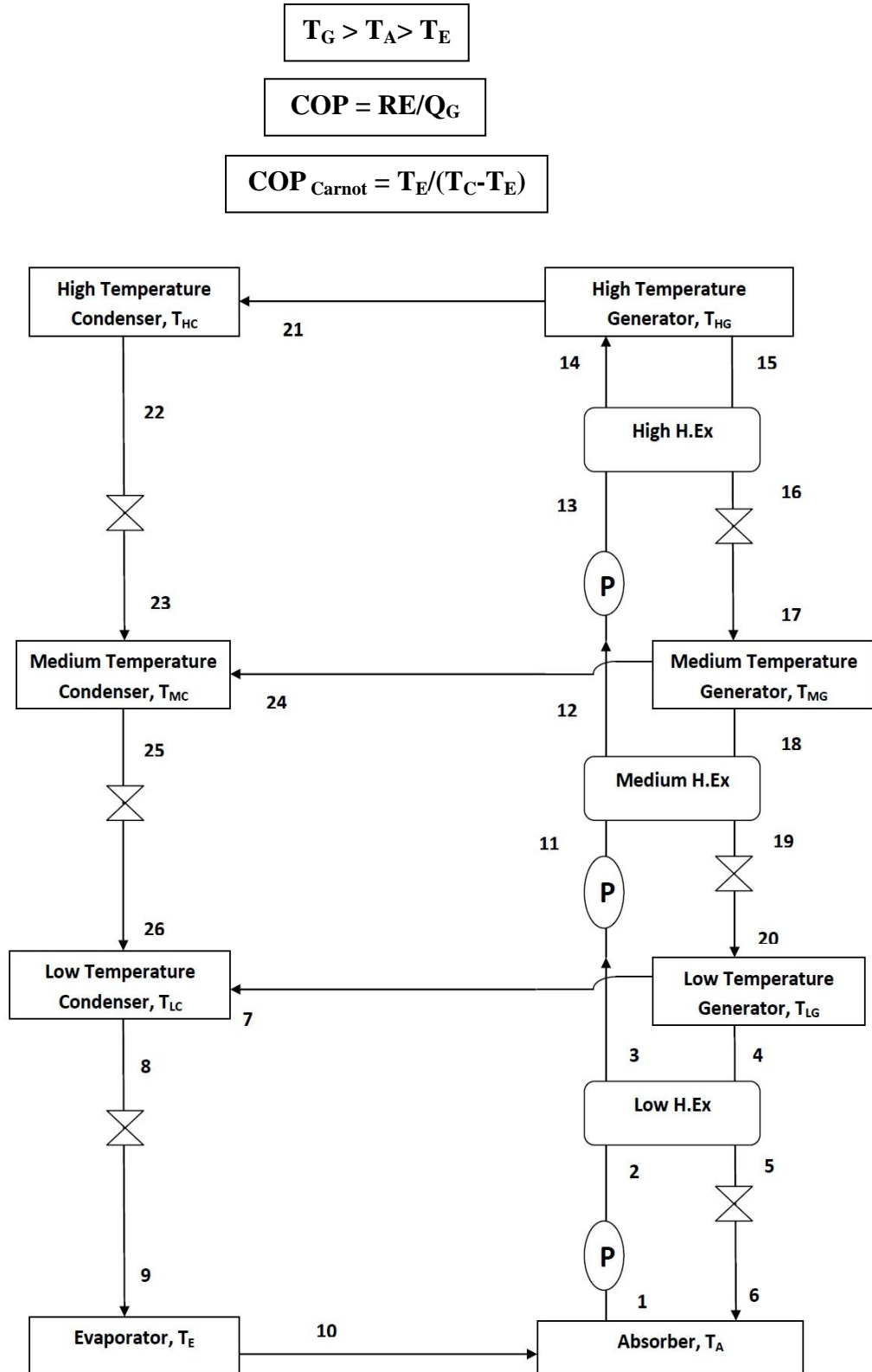


Fig. 1.14: Schematic of Triple Effect (Series) VARS

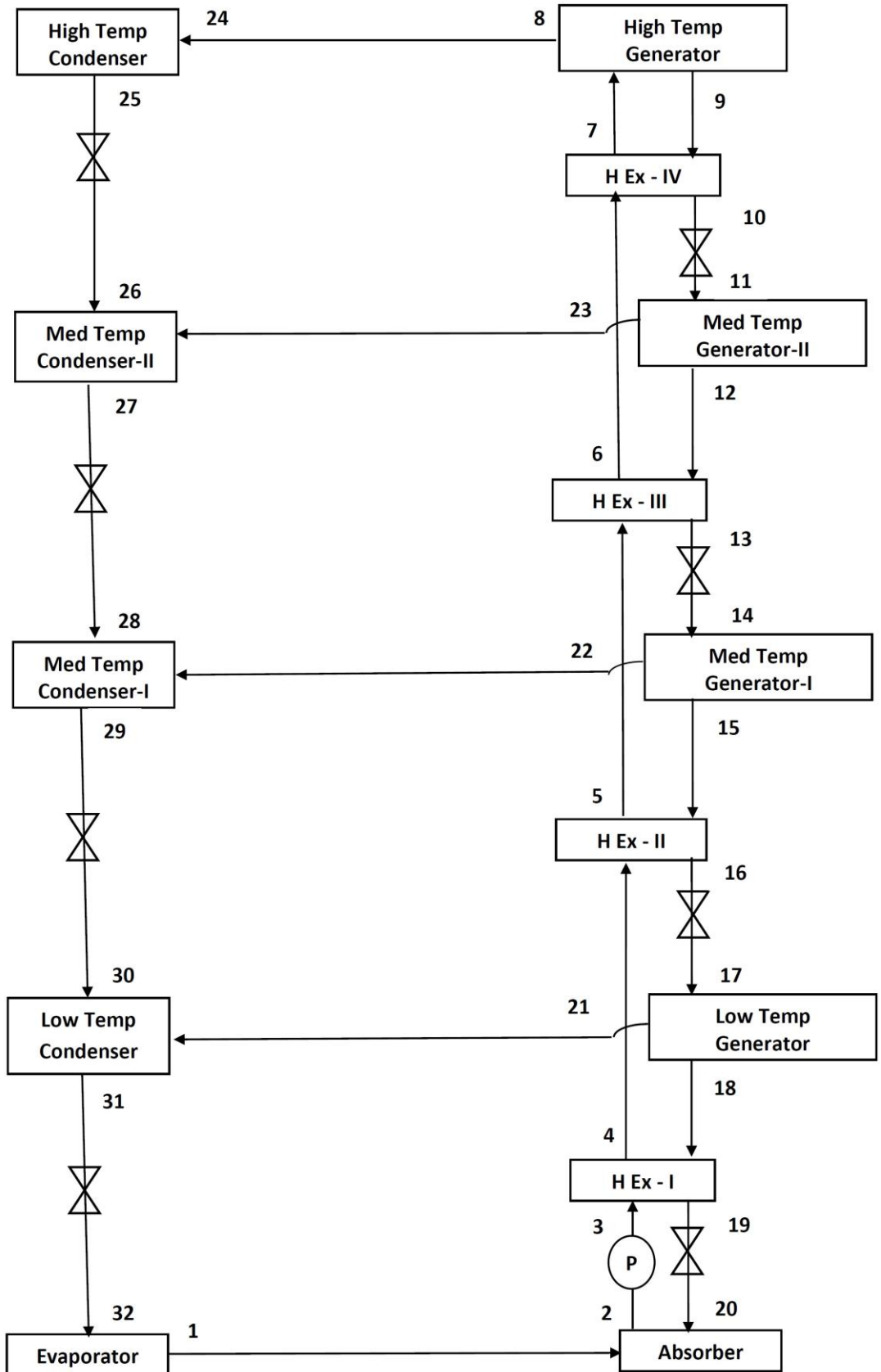


Fig. 1.15: Schematic of Quadruple Effect (Series) VARS

1.2.6. Fluid Mixtures of VARS

Followings are the required properties of the mixtures for VARS are:

- i.** Strong Refrigerant with high solubility with the Absorber (Weak Refrigerant). It should display a negative departure from Raoult's law.
- ii.** A huge distinction in the boiling points of strong refrigerant and absorbent (greater than 200 °C).
- iii.** Low Enthalpy of mixing for high COP.
- iv.** The combination needs to have high thermal conductivity and low viscosity.
- v.** No crystallization or solidification while operating.
- vi.** Safety, chemical stability, non-corrosiveness, low cost, and easy availability.

The most usually exploited refrigerant-absorbent pairs are:

- **Water (Refrigerant)-Lithium Bromide (Absorbent) (H₂O-LiBr):** For above 0°C functions (Air-conditioning).
- **Ammonia (Refrigerant)-Water (Absorbent) (NH₃-H₂O):** For below 0°C functions (Refrigeration).

Moreover, small ammonia-water systems with a third inert gas are employed in a pumpless form of small home refrigerators (triple fluid vapour absorption systems).

1.3. Introduction to Ejector Refrigeration System:

An Ejector refrigeration system (ERS) is a thermal-driven system employed for refrigeration. It has a much lower COP compared to VCRS, however, is simple in design and has no moving components. The ability to generate a cooling effect with available waste heat or solar heat source at or above temperatures of 80 °C. The ERS consists of a Condenser, Pump, Expansion Devices, a Boiler or Generator, an Ejector, a Flash Chamber, and an Evaporator.

Performance Improvement of Vapour Absorption System Using Loop Heat Pipes

The basic ERS consists of two separate cycles, namely the Heat loop and the refrigeration loop. In the heat loop, heat, Q_B , is supplied to the boiler or generator to evaporate the refrigerant at high pressure. The vapour so generated (primary fluid), is expanded in the ejector through a nozzle. The decrease in pressure in the ejector flashes vapour from the flash chamber (secondary fluid). The primary and secondary fluids mix and enter the diffuser. The fluid coming out of the ejector is transported to the condenser for condensation. A part of the liquid coming out of the condenser is pumped to the boiler and the remainder is expanded to the evaporator for refrigeration through an expansion device from where the resulting vapour after generation of refrigeration effect is drawn into the ejector and the cycle continues.

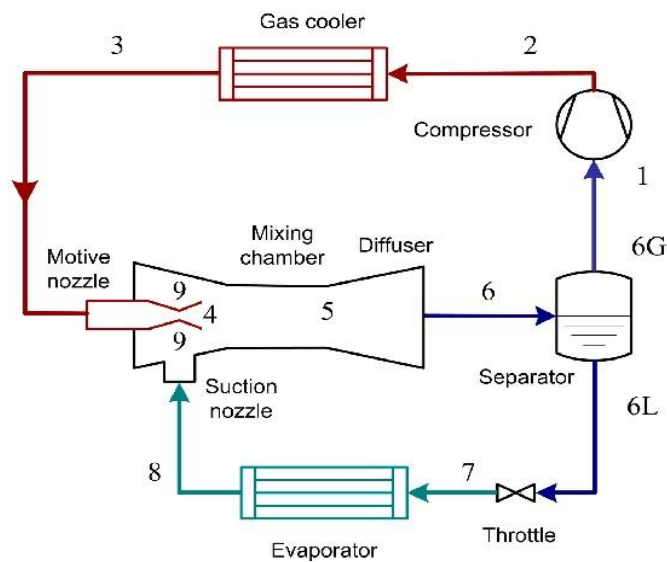


Fig 1.16: Schematic of Standard ERS [171]

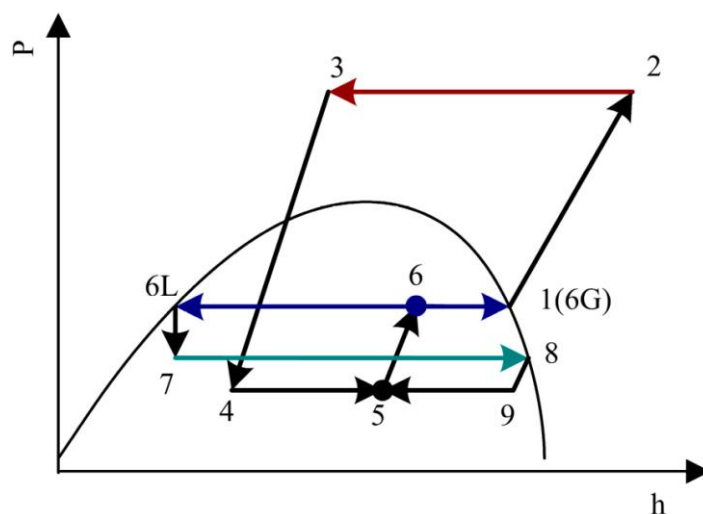


Fig 1.17: P-h diagram of ERC [171]

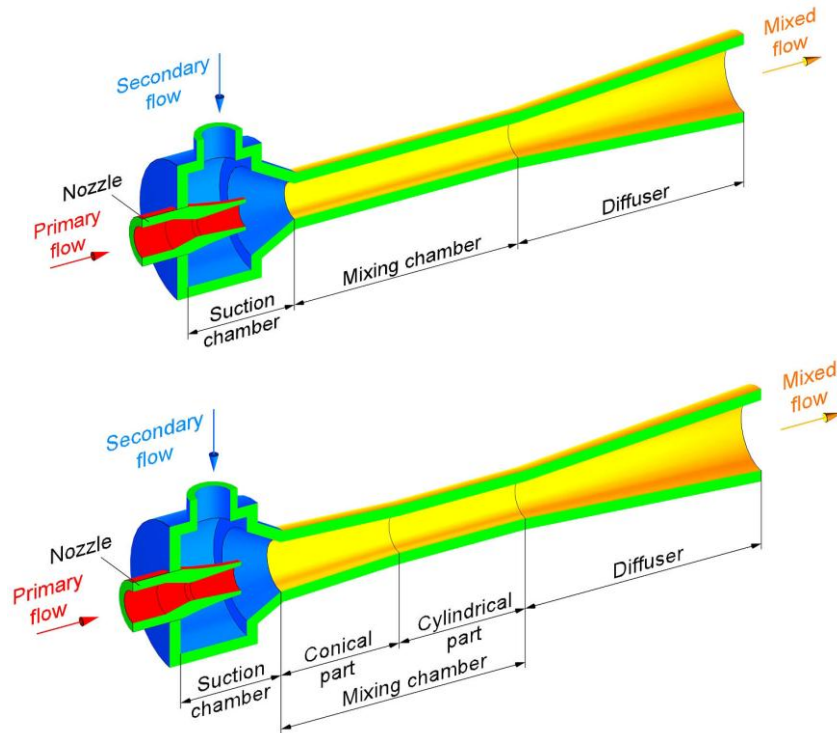


Fig 1.18: Model of Ejector and Nozzle [170]

The ejector has main parts namely a Nozzle for primary/motive vapour flow, and a suction chamber in which secondary vapour is sucked in due to the low pressure generated owing to the expansion of the primary vapour flow. Furthermore, both secondary vapour and primary vapour mix in the mixing chamber, and further expansion in the diffuser chamber increases the pressure.

Applications:

- Relevance in the food sector as waste heat is accessible.
- Food processing factories.
- Tri-generation.

Limitations of Steam Ejector Systems:

- Lower COP, 0.2~0.3, compared to VCRS and others.
- Commercial application data for the technology is not available.
- High-temperature sources are required for efficient operations.
- Low pressure in components such as evaporators and condensers is required.
- Dimensional and weight Constraints.

- Unable to function below 0 °C

Advantages:

- Applications of adequate waste heat or in tri-generation are possible.
- More effectual use of waste heat and improved thermal integration in the food industry.

1.4. Introduction to Organic Rankine Cycle [167]

“Organic Rankine Cycle” (ORC) uses more efficient fluids for heat availability at low-temperature sources (below 300°C) and for low power requirements (a few kW to several MW) primarily owing to the capability to recover low-grade energy. Conventional Rankine Cycle (CRC) requires high temperature-pressure, and hence, high installed power is required to be cost-effective. The ORC proposes a profitable arrangement for small-scale power generation & lower temperature purposes where a Conventional Rankine Plant would be costly.

ORC is analogous to the CRC as evaporation of a high-pressure liquid is expanded to generate mechanical work and the condenser is condensed at the low-pressure vapour and the pump returns the condensed fluid to the high pressure of the evaporator/boiler. The ORC contains components the same as CRC (boiler, work-producing expansion device, condenser, and pump). However, the working fluid has a lower boiling temperature.

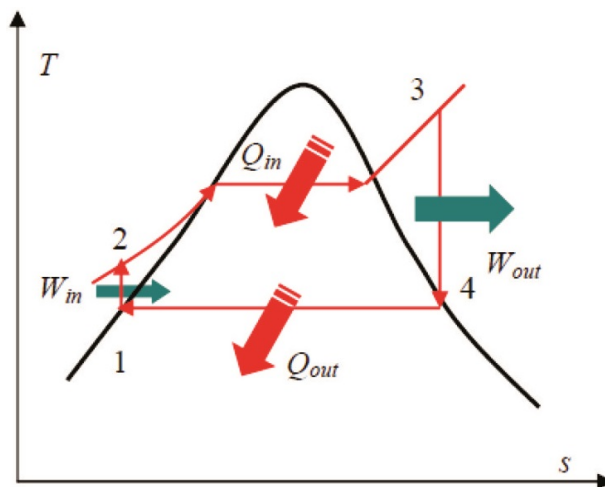


Fig 1.19: T-s Cycle of ORC [167]

Working fluids of the ORC have a large molecular weight and a small boiling point. Also, the critical temperatures and pressures are lower compared to water. For heat sources below 200°C, greater molecular weight fluids can deliver greater efficiencies. The ORC can be used for recovering waste heat which can be utilized through a combined heat and power generation (CHP). The ORC can utilize renewable energy for electricity generation mainly geothermal, biomass, and solar energy sources. The ORC uses single-stage turbines such as screw or scroll expanders.

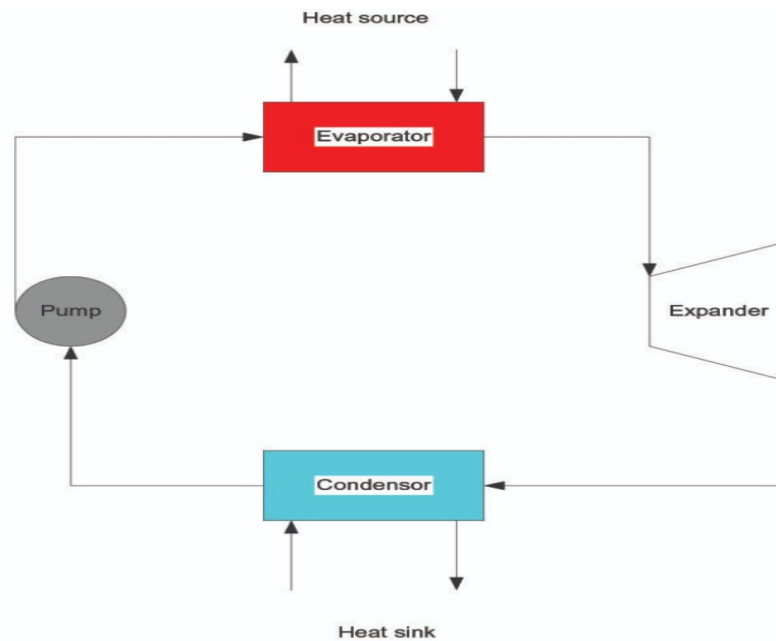


Fig 1.20: Schematic of ORC [167]

1.4.1. Organic Rankine cycle characteristics

Organic working fluids offer attractive properties for operations under low-temperature sources. In comparison with water following are the variations:

- Less Enthalpy of Evaporation,
- Lower saturation evaporation temperature for same pressure of water,
- Higher specific heat capacity owing to high molecular weight,
- The positive slope of the saturated vapour curve.

Owing to this property, superheat is not needed as the expansion process doesn't result in condensation.

1.4.2. ORC fluids

The ORC cycle generally utilizes dry or anisotropic fluids. The benefit of these fluids are as follows:

- Superheating is not required as saturated vapour is found post-expansion.
- Dry fluids generate greater power output at a specified temperature of operation.

ORC systems function in the source temperature range of 100 – 300°C. A new variety of organic fluids has been created to permit the utilization of a wider range of temperatures.

1.4.3. Commonly used ORC work fluids

Following are the most commonly used working fluids for the ORC, amongst all the fluids Silicone oils are the most commercial.

- Toluene
- (Cyclo)-pentane
- Ammonia
- Butane
- Refrigerants
- (R245fa)
- Solkatherm
- Siloxanes (silicone oils)

Table 1.4: Useful Properties of the working fluids

Fluid	Formula/name	T_{Crit} (°C)	P_{Crit} (bar)	Boiling Point (°C)	h_{Evap} (kJ/kg)
Water	H ₂ O	373.9	220.6	100.0	2257.5
Toluene	C ₇ H ₈	318.7	41.1	110.7	365.0
R245fa	C ₃ H ₃ F ₅	154.1	36.4	14.8	195.6
n-pentane	C ₅ H ₁₂	196.6	33.7	36.2	361.8
Cyclopentane	C ₅ H ₁₀	238.6	45.1	49.4	391.7
Solkatherm	Solkatherm	177.6	28.5	35.5	138.1
OMTS	MDM	291.0	14.2	152.7	153.0

For heat temperature sources below 400°C the ORC and for temperature sources greater than 400°C steam is more efficient.

1.5. Introduction to Gas Power Cycle [169]:

The thermodynamic cycles may be generalized into 2 distinct classifications: Power Generating Cycles (Heat Engines) & Heat Pump Cycles. Further, the power generating cycles may be classified as gas power cycles and vapour power cycles (Rankine Cycle). The I C Engines & Gas Turbines follow the different Gas Power Cycles (Diesel, Otto, Dual, Ericson, Atkinson, Brayton, Lenoir, etc.). The 2 main applications of Gas Power Cycles are propulsion and electricity generation.

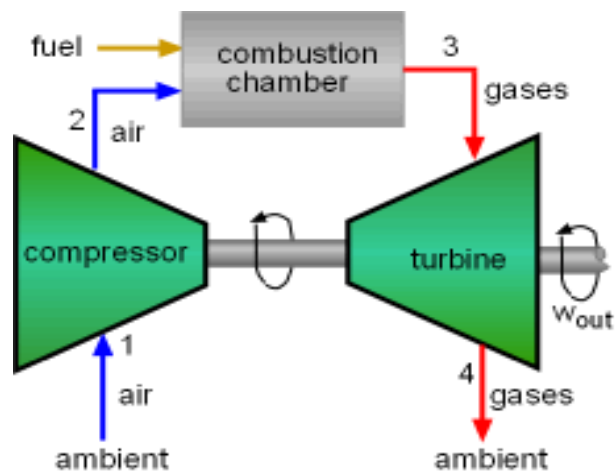


Fig 1.21: Schematic of Open Cycle Brayton Cycle [172]

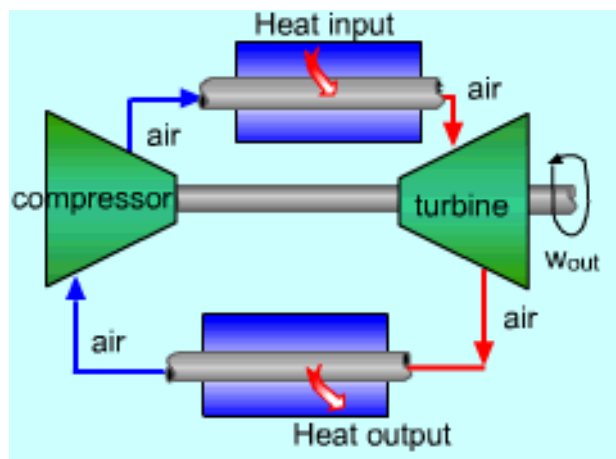


Fig 1.22: Schematic of Closed Cycle Brayton Cycle [172]

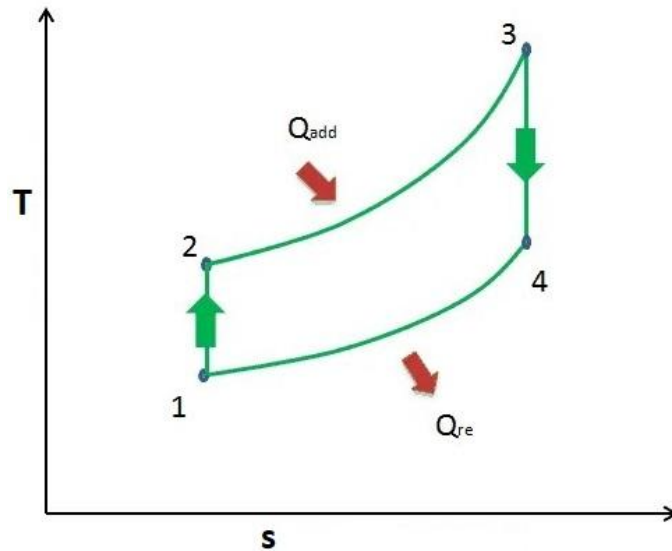


Fig 1.23: Temperature-entropy plot of ideal Brayton Cycle [173]

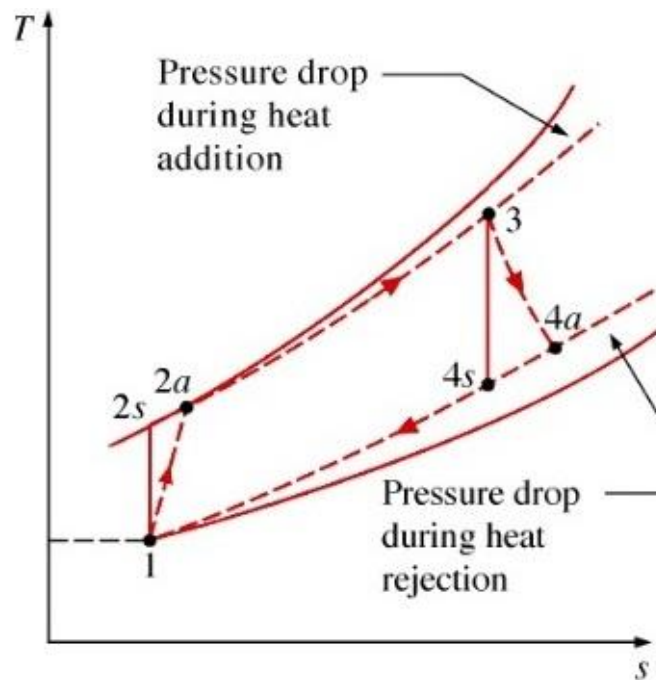


Fig 1.24: Temperature-entropy plot of actual Brayton Cycle [174]

Gas turbines generally function on open cycles (Fig 21), in which,

- A compressor compresses fresh air to a greater temperature and pressure.
- From the compressor air is supplied to the combustion chamber, where an air-fuel mixture at a high A/F ratio is burned at constant pressure resulting in a higher temperature & pressure gas mixture at the entrance of the turbine.
- Further on, the gases are expanded in the turbine to the surrounding pressure to generate mechanical power which can further be converted into electricity.

- Fraction of power generated by the turbine is utilized to run the compressor also nominated as back work ratio.
- As the gases are exhausted from the environment and are not utilized, the cycle becomes open.

The actual gas-turbine cycle is distinctive from the aforementioned cycle as it considers Irreversibilities in separate components (Fig 24). Hence, in the actual cycle, the compressor utilizes more work from the turbine output and the turbine generates less workout. Moreover, there's some pressure loss as well during the isobaric heat addition and rejection in the cycle.

1.6. Refrigerants

Refrigerants are working fluids that work under different pressures and change phases. By this phase change phenomenon, they complete the thermodynamic cycle as prescribed by the Second Law of Thermodynamics. These refrigerants have a few specific thermodynamic properties that make them highly useful for refrigeration purposes such as,

- The high heat of latent heat of vaporization,
- Low specific heat capacity for liquid,
- Large specific heat capacity for vapour,
- High thermal conductivity for both liquid and vapour and
- Low viscosity for both liquid and vapour.

In addition to the thermodynamic properties, environmental properties are also considered such as,

- Low/Zero Ozone Depletion Potential (ODP)
- Low/Zero Global Warming Potential (GWP)
- Non-toxicity

- Non-flammability
- Chemical Stability

Moreover, refrigerants must be easily and economically available.

1.6.1. Conventional Refrigerants, Applications & Modern Alternatives

Table 5 shows the conventional refrigerants, their applications, and the modern alternatives which provide an eco-friendly performance in the long run by replacing the chlorine present in the refrigerant completely with Hydrogen & Fluorine.

Table 1.5: Conventional Refrigerants & Modern Alternatives [166]

Refrigerant	Application	Substitute suggested Retrofit(R)/New (N)
R 11(CFC) NBP = 23.7 °C h_{fg} at NBP=182.5 kJ/kg T_{cr} =197.98 °C Cp/Cv = 1.13 ODP = 1.0 GWP = 3500	<ul style="list-style-type: none"> • Large air conditioning systems • Industrial heat pumps • As foam blowing agent 	R 123 (R,N)
		R 141b (N)
		R 245fa (N)
		n-pentane (R,N)
R 12 (CFC) NBP = -29.8 °C h_{fg} at NBP=165.8 kJ/kg T_{cr} =112.04 °C Cp/Cv = 1.126 ODP = 1.0 GWP = 7300	<ul style="list-style-type: none"> • Domestic refrigerators • Small air conditioners • Water coolers • Small cold storages 	R 22 (R,N)
		R 134a (R,N)
		R 227ea (N)
		R401A, R401B (R,N)
		R411A, R411B (R,N)
R 717 (N)		
R 22 (HCFC) NBP = -40.8 °C h_{fg} at NBP=233.2 kJ/kg T_{cr} =96.02 °C Cp/Cv = 1.166 ODP = 0.05 GWP = 1500	<ul style="list-style-type: none"> • Air conditioning systems • Cold storages 	R 410A, R 410B (N)
		R 417A (R,N)
		R 407C (R,N)
		R 507,R 507A (R,N)
		R 404A (R,N)
R 717 (N)		
R 134a (HFC) NBP = -26.15 °C h_{fg} at NBP=222.5 kJ/kg T_{cr} =101.06 °C Cp/Cv = 1.102	Used as a replacement for R 12 in domestic refrigerators, water coolers, automobile A/Cs, etc	No replacement required * Immiscible in mineral oils * Highly hygroscopic

<p>ODP = 0.0 GWP = 1200</p>		
<p>R 717 (NH₃) NBP = -33.35 °C h_{fg} at NBP=1368.9 kJ/kg T_{cr} =133.0 °C Cp/Cv = 1.31 ODP = 0.0 GWP = 0.0</p>	<ul style="list-style-type: none"> • Cold storages • Ice plants • Food processing • Frozen food cabinets 	<p>No replacement required</p> <ul style="list-style-type: none"> * Toxic and flammable * Incompatible with copper * Highly efficient * Inexpensive and available
<p>744 (CO₂) NBP = -78.4 °C h_{fg} at 40 °C=321.3 kJ/kg T_{cr} =31.1 °C Cp/Cv = 1.3 ODP = 0.0 GWP = 1.0</p>	<ul style="list-style-type: none"> • Cold storages • Air conditioning systems • Simultaneous cooling and heating (Trans-critical cycle) 	<p>No replacement required</p> <ul style="list-style-type: none"> * Very low critical temperature * Eco-friendly * Inexpensive and available
<p>R718 (H₂O) NBP = 100. °C h_{fg} at NBP=2257.9 kJ/kg T_{cr} =374.15 °C Cp/Cv = 1.33 ODP = 0.0 GWP = 1.0</p>	<ul style="list-style-type: none"> • Absorption systems • Steam jet systems 	<p>No replacement required</p> <ul style="list-style-type: none"> * High NBP * High freezing point * Large specific volume * Eco-friendly * Inexpensive and available
<p>R600a (iso-butane) NBP = -11.73 °C h_{fg} at NBP=367.7 kJ/kg T_{cr} =135.0 °C Cp/Cv = 1.086 ODP = 0.0 GWP = 3.0</p>	<ul style="list-style-type: none"> • Replacement for R 12 • Domestic refrigerators • Water coolers 	<p>No replacement required</p> <ul style="list-style-type: none"> * Flammable * Eco-friendly

1.6.2. Refrigerants Used in the Analysis

Table 6 presents the refrigerants used in the analysis performed in the research work for ORC & ERC. It can be noted that the ODP for all the refrigerants is 0 and GWP for most of the refrigerants is low or negligible, which has been the reason for the selection

Table 1.6: Refrigerants and useful Properties

Refrigerant	Critical Temperature, K	ODP	GWP
R236ea	412.4	0	1200
R1224yd(Z)	428.7	0	<1
R1233zd(E)	438.8	0	4.5
R245fa	427	0	1030
R365mfc	460	0	794
R718	674.14	0	0
R124	395.3	0.022	609
R125	339.023	0	3500
R134a	374	0	1200
R152a	386.15	0	124
R290	369.7	0	3
R600	425	0	0

Chapter-2: Literature Survey

Adding on to the introductory chapter, this chapter presents a comprehensive study of published literature & texts. The study has been conducted to understand the systems effectively and to find out the gap & scope for further research investigation. The study has been divided into 7 sections covering the following:

- Heat Pipes (HP) & Loop Heat Pipes (LHP),
- Vapour Absorption Refrigeration Systems (VARs),
- Ejector Jet Refrigeration System (ERS),
- Organic Rankine Power Cycle (ORPC),
- Conclusions of the Literature Review,
- Gaps in the Literature and,
- Objective & Scope of the Research Work

The literature review has been conducted chronologically for each section starting from the oldest to the most recent to develop a basic understanding of the development of the Systems & Technologies.

2.1. Review of the Heat Pipes (HP)

This section presents the review of research works and their outcomes for the Heat Pipes (HP). Varieties of HPs have been studied of which LHP is one. Out of the vast literature available, the HPs & LHPs which have been specifically and especially employed for refrigeration and waste heat recovery purposes have been chosen and presented.

^[1]*Chun et. al. (1999)* analysed domestic solar hot water systems. A chain of tests was studied on diverse systems to obtain the appropriate arrangement of the system for potential commercial use. The heat pipe has a copper tube with the evaporator, adiabatic, and condenser lengths of 1700, 100, & 200 mm respectively. Fins made up of a copper plate were used in the evaporator for increasing solar heat input. Results

were presented for the different working fluids, wicks, & other design aspects connected with the gathering & consumption of solar-based energy.

^[2]*Hussein et. al. (1999)* analyzed various parameters of the momentary thermal conduct of heat pipe which doesn't have a wick and is installed at plate-type solar collectors. The outcomes of the analysis showed that the choice of a plate of the absorber with a large conduction heat transfer rate per unit temperature gap is restricted by pitch distance.

^[3]*Said et. al. [1999]* through experiments investigated 2 categories of heat pipes working on the H₂O. The First was with a cotton wick & another without a wick. The heat pipe was placed at various angles such as 30 °C, 60 °C, and 90 °C with the horizontal. The results found the heat pipe with the cotton wick had a highly substantial performance for the overall coefficient of heat transfer compared with that with no wick. An increase of around 55%, 25%, and 70% for 30 °, 60 °, and 90 ° angles, respectively was evaluated.

^[4]*Khalkhali et. al. (1999)* performed a second law analysis on a developed model of conventional cylindrical heat pipes. It was found that the environment temperature of the condenser & coefficient of convective heat transfer in the evaporator section could be adjusted to decrease entropy generation. Comprehensive parametric analysis was also presented examining the effects of various parameters on entropy generation.

^[5]*Noie-Baghban et. al. (2000)* carried out a study of heat pipes. The design & limitations of heat transfer of heat pipes for 03 categories of wicks & 03 operating fluids had been examined using simulations. The formation of heat pipes had also executed. After the gaining of the suitable heat influx, the air-to-air interface heat pipe was calculated, built, and verified for operating temperature (15-55°C) conditions, for methanol Operating Fluid. The outcomes of the Experiments were very close to results from computer simulation.

^[6]*Smirnov et. al. (2001)* explained and proposed the classification of refrigeration heat pipes (RHPs). The potential of exploiting standard driving forces for the RHP investigation was firmly authenticated. The absorption cycles, ejector & mixed RHP concerning the thermal functioning were contemplated.

^[7]*Mathioulakis et. al. (2002)* studied the novel solar system for generating hot water integrated with a heat pipe. The analysis was theoretical and experimental. A gravity-assisted loop heat pipe without a wick was utilized for transferring heat energy from the collector (HP- Source) to the tank through HEx (HP - Sink). An experiment-based investigation was performed, focussing on the performance of numerous constituents of this novel system. The outcomes showed that this system was satisfactorily efficient. Moreover, a hypothetical model based on the collector was also projected to assess the results of the experiments.

^[8]*Yang et. al. (2003)* deliberated the viability of the use of heat pipes as heat exchangers for heating a large bus through automotive exhaust gases and set up a Practical heat pipe heat exchanger. Experiments were executed to study the heat exchanger. Experimental results showed that the advantages of exhaust gas heating were as per the mathematical outcomes.

^[9]*Ling (2004)* recommended a novel refrigerator and heat pump heat pipe and heat pump which work on jet refrigeration and heat pump cycle. The performance of jet refrigeration and heat pump of the systems are investigated and suggested a technique of thermodynamic performance study.

^[10]*Vasiliev et. al. (2005)* reviewed principally the advances in the heat pipe. It was iterated through the review that heat pipes could easily function as heat exchangers for VAR and VCR heat-pumps, refrigerators with the coefficient of heat exchange in evaporator & condenser around $103\text{--}105 \text{ W/m}^2 \text{ K}$ & resistance to heat exchange around $0.01\text{--}0.03 \text{ K/W}$, hence, resulting into compact size and mass flow requirements.

^[11]*Maydanik (2005)* reviewed two-phase heat-transfer devices widely referred to as Loop heat pipes (LHPs) which work on the capillary effect of the fluid and held leading benefits to standard heat pipes, however, due to the main design and distinct characteristics of the capillary structure, these can transfer heat with high efficiency over long spaces up to quite a few meters at any alignment under gravity, or to numerous tens of meters in a horizontal arrangement. The progress, outcomes of the theoretic examination, and experiments of LHPs were also reviewed and studied.

^[12]Wang *et. al.* (2008) constructed an original double heat pipe type absorber, working on a compound adsorbent of CaCl₂ and expanded graphite improving the adsorption function. Heat pipes were combined with absorbers to solve the issue of corrosion between seawater & steel absorbers under the ammonia-based system improving the heat transfer operation of the absorber. The heat transfer capabilities of heat pipes could take on the demands for adsorption/desorption when the heating/cooling period was 720s & the mass recovery period was 60s. With exhaust gas temperature at 550°C, cooling water temperature at 25°C, and inlet & outlet chilled water was -10 & -15.6°C, respectively; simulations showed that the refrigeration capacity & COP of the system were 5.1kW and 0.38, respectively.

^[13]Launay *et. al.* (2008) conducted a comprehensive review built on the latest experiments and theories to explore the influence of numerous constraints on the LHP operations and the working boundaries were illustrated. The resistance to heat transfer & heat transport capacity is influenced by working fluid, charge ratio, the geometry of the wick, & thermo-physical characteristics. Sink & environmental temperature, evaporator & compensation chamber design, angle of elevation, the existence of non-condensable gases, and decline in pressure down the loop also affect performance.

^[14]Korn (2008) explained the primary operating principles and calculations related to heat pipes.

^[15]Shukla *et. al.* (2008) presented a model for unsteady-state processes of an LHP made up of Stainless Steel/Ammonia. The Fourier equation for a hollow cylinder was computed ascertaining the distribution of temperature in the compensation chamber and the cavity. A 1-D unsteady-state model was formulated as well for ascertaining the temperature of the vapour in the condenser unit.

^[16]Nagano *et. al.* (2008) developed and conducted an all-inclusive test program comprising start-up, power cycle & low power tests. Moreover, estimated, the influence of gravitational field while start-up & heat transportation ability. An investigative model for the loop was established to calculate and estimate steady functioning. Outcomes established the sturdiness of the LHP. The viability of temperature control controlling compensation chamber temperature was verified through experiments.

^[17]*Launay et. al. (2009)* suggested all-purpose calculations for assessing the steady-state operation of an LHP. This novel method of LHP modeling enables the detection of the physical mechanisms affecting functional parameters. Furthermore, the transition heat flux between flexible & set conductance methods could be projected.

^[18]*Hamdan et. al. (2009)* formulated a thermodynamic investigative model to study different parameters that affect LHP. The influence of the length of pipe, dia. of pipe, temperature of condenser, and heat-load were described. As the length of the pipe increases and/or pipe diameter decreases, a higher temperature is attained in the evaporator.

^[19]*Celata et. al. (2010)* illustrated the investigational outcomes for the thermal features of the LHP flat disk evaporator of dia. 50 mm & thickness 13 mm, constructed of stainless steel using water. Examinations were held out at horizontal elevation (orientation) with the evaporator beneath (helpful) and over (adverse) the compensation chamber, which operates on a wide range of heat loads. During the testing of the LHP under single step heat load, the thermal response presented by the loop to achieve steady-state is very long implying a long start-up time. In the evaporator above the compensation chamber (adverse) condition, thermal and hydraulic oscillations were monitored all over the loop having marginal effects on the thermal performance of the LHP. In the helpful formation, no oscillations were detected and the device was capable to transmit a maximum heat load of 75W with a temperature below 150 °C for the evaporator. The thermal resistance i.e., the resistance from the evaporator external surface to the condenser external surface (refrigerant water sink), remained from 3.33 to 50.7 °C/W.

^[20]*Li et. al. (2010)* incorporated comprehensive examination using experiments for copper–water compact Loop Heat Pipe having a square evaporator of 30 mm (L) x 30 mm (W) x 15 mm (H) having a linking tube ID of 5 mm. Two foremost methods, boiling induced start-up & evaporation induced start-up, were projected describing variable start-up conduct for separate heat loads. Eventually, it was understood that the compact LHP could transmit heat loads of over 600W (heat flux more than 100 W/cm²) without evaporator dry-out.

^[21]*Ribeiro et. al. (2010)* examined a novel evaporator design for a small-scale refrigerator supporting current heat pipe expertise being employed in temperature

control for chips. The results from the experiments established that the heat transfer coefficient was susceptible to a greater extent to variation in the refrigerant mass flow than to fluctuations in saturation temperature and rate of heat transfer.

^[22]*Khodabandeh et. al. (2010)* studied the two-phase flow unsteadiness at low and high fluxes for thermo-siphon using R134a as the operating fluid. The heat exchange surface of the evaporator was augmented with copper nano- and micro-porous structures. Moreover, the heat transfer for the improved evaporator was compared to that of a smooth surface evaporator. It was found that the new structure surface reduced the oscillations for the entire range of heat fluxes and increased the heat transfer coefficient.

^[23]*Yeunyongkul et. al. (2010)* examined the use of a closed-loop oscillating heat pipe (CLOHP) as a condenser for VCRS through experiments. The cooling capability got fixed at 3.663 kW and R22 was Working Fluid. The size of the CLOHP condenser was optimized by applying the thermo-economical method and water as the working fluid of the heat pipe delivered the maximum economy. The optimum sized system had a 0.08 m length of evaporator unit, 0.1 m length of condenser segment, an ID of 2.03 mm, and 250 turns. Results showed that COP of condenser for the load of 800 W decreased by around 32.4 %, whereas, pressure fall was lesser than conventional condenser by around 91.2%, moreover, the energy efficiency rating was greater by around 13.4%.

^[24]*Ziapour et. al. (2011)* analyzed diffusion absorption refrigeration heat pipe (DARHP) using NH₃-H₂O cycle along with helium. The second law efficiency was investigated based on performance parameters using computer simulation. The model was authenticated by comparing it with available experimental data. The results showed that best functioning was attained for a rich solution at 0.35 and concentration of weak solution at about 0.1 ammonia mass fraction. Insignificant availability destruction in the evaporator, condenser and dephlegmator was presented. Moreover, as evaporator temperature increases the second law efficiency rises; and it decreases as the thermosyphon temperature increases.

^[25]*Lu et al. (2012)* recommended & examined heat pipe type adsorption refrigerators driven by solar/waste heat. Specific cooling power (SCP) and COP were finalized

through experiments. SCP of the cycle with the mass-heat recovery system is found to be higher than normal cycles employing mass or heat recovery separately.

^[26]*Choi et. al. (2012)* presented a new CPU cooler providing a more efficient heat removal capability from the CPU to a heat sink connected with fins while not attaching any other heat pipes for low noise with a small. Computational fluid dynamics analysis was adopted to exploit a suitable cooling design and the CFD results were verified with experimental results. The novel presented CPU cooling arrangement provided total thermal resistance of 0.11-0.19 °C/W with a low noise level of 21.50-36.3 dBA.

^[27]*Hu et. al. (2013)* conducted an experimental study to understand the effects of interior surfaces on the functioning of grooved heat pipes. The length and OD of the HP for experimentations were 6 and 190 mm respectively. Chemical oxidation treatments were used to alter the wettability of the inner surface of grooved heat pipes along with contact angles. It was established that the creation of an internal surface having positive contact angle inclination along evaporation, adiabatic, and condensation parts caused the thermal resistance to reduce by more than 12% and to enhance by more than 42%.

^[28]*Senthilkumar et. al. (2013)* observed that the finned surfaces have been significantly employed for an increase in natural convective cooling of IC engines, numerous electronics items etc. Rectangular brass fins were chosen in the investigation. Thermocouples were connected around the fins' exterior at even spacing. The evaluation of outside temperature and determining the rate of heat exchange were analyzed on numerous heat loads. The brass surface was covered by carbon nanotubes. The average percentage rise in the rate of heat transfer was demonstrated at about 12% with the nanocoated fins.

^[29]*Page et. al. (2013)* prepared a mathematical model to study the steady-state function of LHP for high heat influx electronics devices. The results obtained from modeling were authenticated by the experimental data of the LHP. The LHP was used against gravity and gravity-assisted inclinations of 5° & 10°. The porous wick selected has 60 % porosity, $6.77 \times 10^{-13} \text{ m}^2$ permeability and an average pore radius of 1 μm and worked on Ammonia. The projected data through operation under constant conductance mode were precise with the experimental results when compared with

theoretical values for the variable conductance mode of operation. The maximum heat loads studied were 60 W, 50 W, and 110 W for horizontal, against-gravitational force, and gravity-assisted functions correspondingly.

^[30]**Baitule et. al. (2013)** directed experimental investigations on the transient and steady-state operation of a two-turn closed-loop PHP. Copper is the capillary tube material of the evaporator and condenser sections with an ID of 2 mm and OD of 3 mm & the total length is 1080 mm. The evaporator and condenser units were 360 mm and 280 mm long, individually. Heat loads in the experiments have been varied from 10 to 100 W stepped up by 10 W. Ethanol, Methanol, Acetone, and Water have been chosen as operational fluids of the PHP and different fill ratios chosen are 0% - 100% stepped up by 20%. Operation parameters of heat pipes have been calculated and are observed enhanced for a 60% fill ratio at several heat inputs.

^[31]**Chiang et. al. (2014)** meticulously examined the composition factors affecting the thermal performance of heat pipes, i.e., wick structures, and working fluids. Moreover, the inflexion fields of the working fluids, and combinations of these factors, were also studied. The assessed materials included micro-grooved, sintered, and wickless heat pipes. Furthermore, magnetic nanofluids having volumetric fractions (vol.) of 0.16%-3.20%, and de-ionized water were taken as working fluids. The results signified that the optimal performance was yielded by the combination of grooved heat pipes and 0.80% vol. of magnetic nanofluids or sintered heat pipes and 0.16% vol. of magnetic nano-fluids. A decrease of around 80 % was observed in the thermal resistance. Moreover, the critical heat flux increased by around 2.7 times in comparison to the general wickless heat pipes which were filled with de-ionized water.

^[32]**Anwar et. al. (2014)** studied the performances of heat pipes working on pure water, and boron nitride/water nanofluids through comprehensive experiments. Average evaporator wall temperature and the overall thermal resistance at diverse nanoparticle mass concentrations (0-3 % for Boron nitride nanofluids), as well as, at the volume filling ratio of 30% were examined and measured up. The evaporator wall temperature and overall thermal resistance were reduced with the use of BN/water nanofluids instead of pure water (i.e., nanofluid with 0 % concentration). Optimal performance was achieved at a concentration of 3 % boron nitride in water

and 100 W power input. The decrease in the evaporator wall temperature and overall thermal resistance of the boron nitride/water nanofluid-filled heat pipe was around 5.660°C (or 8.28%) and 0.1033 °C/W (or 37.80%) which were compared with pure water-filled heat pipe at 00 elevations. Thus, nanoparticles enhanced the thermal performance; moreover, performance was examined by varying the elevation.

^[33]*Chen et. al. (2014)* performed an experimental study on the effects of liquid filling ratios and leakage on the cooling effect of the flat plate heat pipes (FPHPs). The outcomes displayed that the one with the liquid filling ratio of 25% had the best thermal performance, having the dimensions of 150 mm x 50 mm x 2.5 mm for all Al 6061 FPHPs and acetone (99.87% pure) as the working fluid. The resultant maximum heat transfer capacity, least thermal resistance, and highest effective thermal conductivity were about 47 W, 0.254 K/W, and 3150 W/m K, respectively. It was presented that inaccurate vacuum and leakage decrease the aforementioned performance parameters.

^[34]*Alawi et. al. (2014)* performed an overview of available literature corresponding to the current advancements in the area of heat transfer with nano-fluids in heat pipes. Moreover, it presented the means of heat transfer improvement or degradation, the present issues for a variety of heat pipes working on nanofluids, and explored the viable functioning prospects.

^[35]*Nithyanandam et. al. (2014)* performed a study on latent thermal energy storage (LTES) systems embedded with gravity-assisted heat pipes. Transient numerical simulations were prepared & proposed. Moreover, the effect of the design and functional parameters on the dynamic charge and discharge performance of the system was investigated to recognize working ranges that satisfy the U.S. The study explained a design and optimization approach of LTES with embedded gravity-assisted heat pipes (HP-TES) for a concentrating solar power (CSP) plant operation.

^[36]*Khalifa et. al. (2014)* performed a mathematical and experiment-based thermal investigation on the performance of latent heat thermal energy storage (LHTES) systems that use heat pipes (HPs) for solar thermal power generation. The analysis quantified the benefits of using axially situated finned HPs rather than bare HPs in LHTES systems. The advantages of using fins in the HPs could be seen by the improvement of the rate of energy extraction as well as the effectiveness. The results

showed that the extraction of energy increased by 86% and effectiveness increased by 24%.

^[37]*Xu et. al. (2014)* manufactured a Loop Heat Pipe having a flat disk-shaped evaporator with see-through covers to observe the flow motion in various parts of the evaporator section. Moreover, two-layer Cu–Ni composite wicks with a total thickness of all wicks of 5 mm were also projected to weigh against the performance of a copper wick. Bubble accumulation took place on the upper part of the copper-made wick at the start-up. Additionally, the Cu₃Ni₂ wick, which had a 3 mm copper layer placed at the heat source side improved the efficiency of evaporation and the 2 mm thickness of the nickel layer faced the compensation chamber, providing optimized results. The Cu₃Ni₂ wick could start swiftly in about 170 seconds, and the evaporator wall temperature could be maintained under the allowable temperature of 85 °C with the load range from 30 to 120 W.

^[38]*Jiao et. al. (2014)* proposed a simple and rapid numerical model for calculating the non-steady-state start-up. A study of the isothermal features of a heat pipe was also conducted. The vapour temperature variation relationship had been calculated mathematically and the temperature boundary condition had been set. Using FLUENT the various parametric distribution was solved as well. The results exhibited that the time necessary for attaining steady conditions was 450 s, 550 s, and 600 s. Correspondingly, the water bath temperatures were kept at 330 K, 340 K, and 350 K, respectively.

^[39]*Ghajar et. al. (2014)* analyzed the thermal and capillary analysis of a micro loop heat pipe to be used in electronic devices and systems and a model was developed to forecast the heat transfer coefficient in grooved capillary structures. The model using the data of applied heat load calculated the thermal performance, surface temperature of the evaporator, and local & average heat transfer coefficients. The results obtained from the modeling were confirmed by data from the experiment.

^[40]*Jiang et. al. (2014)* projected a 4-step sintering process to construct the sintered wick structure. The results presented that the appropriate sintering temperature for Cu powder of 159µmdia was 950 °C and for Cu powders of 81 and 38 µm was 900 °C, respectively. The wick thickness was found to be 0.45 mm and sintering time

was required as 3 h. The copper powder diameter was taken as 159 μm with a sintering temperature of 950 $^{\circ}\text{C}$.

^[41]*Khalifa et. al. (2015)* proposed a thermal network model for calculating the increase in heat transfer in a high-temperature latent heat storage unit consisting of finned heat pipes to enhance the performance of concentrating solar power plants. The finned heat pipes were used as efficient heat spreaders. The viability of the project was documented by conducting experiments. The results revealed that the performance was considerably enhanced by the addition of finned heat pipes, particularly at the later point of PCM solidification. It was observed that the effectiveness of the twelve-heat pipe configuration was accomplished at 2.4 after 05 hours of the operation. Additionally, an initial system sizing study was performed to approximate the system size necessary for 50 MW output.

^[42]*Ebrahimi et. al. (2015)* through experiments investigated the performance of interconnecting channels for different heat inputs of flat-plate closed-loop pulsating heat pipes (IC-FP-CLPHPs), and the results established that the superior performance of pulsating heat pipes with ICs in comparison with heat pipes without a broad range of heat inputs and filling ratios. It was also observed that the highest efficiency in the performance of IC-FP-CLPHPs took place at a filling ratio of 65%. To study the viability, a mathematical model had been followed on a single-phase liquid to present the role of interconnecting channels to achieve a one-way flow.

^[43] *Paiva et. al. (2015)* projected a new hybrid heat pipe that is associated with the high liquid pumping capacity of sintered metal powder structures. Low liquid pressure drops of diffusion welded wire-plate grooves were also incorporated and studied. Hydrodynamic and thermal models were presented for the models which were adopted to design several hybrid heat pipes and tested the models through an experimental setup. Theoretical models were used to calculate the maximum heat transfer limit and the temperature distribution along the heat pipe. Furthermore, numerous parameters that influenced the performance were investigated.

^[44]*Siedel et. al. (2015)* presented a comprehensive literature review investigating the existing steady-state models of LHPs. The models could be divided into three major categories: mathematical models of the whole system, mathematical models of the evaporator, and methodical models. A synthesis was used to summarize all the

steady-state models. The review exhibited the development of the modeling processes within the past 15 years.

^[45]*Meisel et. al. (2015)* designed heat exchangers based on ceramic heat pipes to be used under a highly abrasive and corrosive environment at temperatures ranging from 800-1200 °C. Heat pipes were gravity-assisted and were based on a multi-layer concept containing sodium as the working fluid. The temperature resistance and functionality of the thermo-siphons could be established through experiments at temperatures up to 1100 °C. The ceramic tubes had an OD of 22 mm and a total length of 770 mm. The axial heat transfer was measured at the still working point with a cold/hot gas temperature of 100 °C/900 °C was 400 W.

^[46]*Spinato et. al. (2015)* studied and reported on experimental flow visualization in a Closed Loop Pulsating Heat Pipe (CLPHP)-using R245fa as a working fluid and operating over a range of conditions. Four discrete flow regimes and their steady thermal oscillation features had been observed and presented.

^[47]*Schamphelire et. al. (2015)* experimented with water/copper heat pipes with a novel wick made up of metal fibers having a small dia of 12 mm and the fiber mesh was compared with other wick structures i.e., screen mesh (145 meshes/ inch) & sintered powder wick. The heat pipes had OD of 6 mm, length of 200 mm, and water was selected to be the working fluid. The heat pipes were tested for a heat input up to 50W & operating temperature of 70 °C and to 160 W and 120 °C for gravity-opposed & gravity-assisted orientations respectively. For gravity-assisted orientation, the screen mesh wick had better performance than fibre and sintered powder wick, owing to superior permeability and enhanced capability to distribute the working fluid over. Whereas, the gravity-opposed orientation, the fibre and screen mesh heat pipe has almost equal results.

^[48]*Sun et. al. (2015)* investigated the feasibility of wall implanted heat pipes (WIHP) in winter. Moreover, the operational hours and heat transfer capability of the south and west WIHPs were calculated and analyzed. The obtained results showed that the south WIHP was operational for more hours, had higher heat transfer capability and more energy-saving rate, utilized in the 93.63% of heating areas. The west WIHP could only be used in specific areas due to the availability of energy. Furthermore, the combination of the west and south WIHPs recommended better performances.

^[49]*Ghanbarpour et. al. (2015)* analyzed the experimental effects of silver nanofluids on the performance of inclined screen mesh heat pipes for cooling operations. Four cylindrical copper heat pipes with two layers of screen mesh were constructed. Distilled water & water-based silver nanofluids having concentrations of 0.25%, 0.5%, and 0.75% based on mass were selected as working fluids. Inclining angles of 0°, 30°, 60°, and 90° were considered for the experimental analysis. Experiments indicated that the performance of heat pipes was enhanced with nanofluids highest at an inclination angle of 60°. Moreover, the thermal resistance decreased with the increase in the concentration of the nano-particles.

^[50]*Tiari et. al. (2015)* executed a mathematical analysis on a high-temperature latent heat energy storage system using finned heat pipes. A model based on transient 3-D finite volume was prepared. The enthalpy-porosity methodology was employed to model the phase change. Diverse arrangements of the heat pipe and quantities were studied. Thermal resistance within the system decreases with the greater number of heat pipes and results in the increase of the rate of the charging process and the reduction in container base wall temperature. Moreover, the natural convection in the charging process provides a better melting rate and decreased base wall temperature.

^[51]*Bai et. al. (2015)* executed an inclusive examination of cryogenic loop heat pipes (CLHPs). A study between 5 different selected CLHPs and ambient LHPs was done. The constraints that affected the performance were investigated, and the strategy to optimize the performance was proposed for engineering applications.

^[52]*Oro et. al. (2015)* presented a heat transfer model to estimate the capillary limit, working temperature, and the essential working fluid through mathematical and experimental investigation. The primary objective was to reduce the temperature of Proton Exchange Membrane (PEM) fuel cells to make sure of the availability of a suitable function in the temperature range of 70–90°C with a small thermal gradient. The system contains a set of stainless-steel flat heat pipes, having a length of 100 mm parallel assembly. Results exhibited that the system could dissipate up to 12 W, conforming to 1.8 W/cm² at the evaporator section.

^[53]*Yan et. al. (2015)* proposed a seasonal cold storage system that used discrete type heat pipes to control the cold energy from the environment in winter automatically, without any consumption of energy. The harnessed cold energy could be stored in

the form of ice in an insulated tank and utilized as chilled water for cooling supply in summer reducing the related electricity consumption costs, operational costs, and greenhouse gas emissions drastically. A quasi-steady two-dimensional numerical model of the system for describing the dynamic performance of ice growth was developed. The model was further verified using the field measurement data from an experiment.

^[54] *Wang et. al. (2015)* proposed a combined cooling system for data centres that is made up of a heat pipe refrigeration cycle and a vapour compression refrigeration cycle. The functioning mode of the system varies with the outside temperature. Primary issues of the integrated system were solved i.e., the combination of the refrigerant and lubricant, the match of heat exchange areas, and the sturdiness of valves. An equilibrium assessment was administered to gauge the system's performance. Experimental data based on thermodynamic analyses showed that the PUE (Power Usage Effectiveness) of data centres using the integrated heat pipe system is often 0.3 less than using the traditional air-cooling systems in cold areas. The energy-saving potential of this system depends on seasonal and regional climate changes.

^[55] *Tian et. al. (2015)* presented an integrated cooling option to enhance the thermal functioning of data centres facing high heat flux. A multi-stage heat pipe was proposed to construct the rack cooled internally, helping eliminate the unwanted mixing of hot and cold air and facilitating uniformed distribution of interior temperature. Water rings of multiple low-temperature sources had been designed to utilize cooling potentials. Energy-efficient switchable and flexible cooling has been proposed. Calculations had been conducted to confirm the effectiveness of this cooling system reducing the cooling cost by around 46% per annum.

^[56] *Hirasawa et. al. (2016)* investigated the thermal functioning of a loop heat pipe having 2 evaporators & 2 condensers employing lumped network model study. Thermosyphon-type vertical loop heat pipe and capillary-pump-type horizontal loop heat pipe were computed against the variation in the heat rate in the evaporators. Results presented that the vapour and liquid flow rates and the thermal conductance of the heat pipe varied appreciably reliant on the distribution ratio of the heating rate. The functioning of the vertical type heat pipe was also studied. The lumped network

model study was deemed to be precise and better for the practical design as the results matched the experimental results.

^[57]*Föste et. al. (2016)* obtained results based on experiments using heat pipes operating at a maximum temperature of 120°C with a high-temperature gradient in the dry-out area working on Butane as a working fluid. This guarantees that the collector performance in the operating range (typically up to 100°C) is not influenced undesirably by the dry-out. Diverse methods to enhance the thermal conductance of heat pipes by boosting the inner surface of the condenser or both, the condenser and the evaporator are evaluated by experiments. Results describe a rise in thermal conductance from 3 W/K (standard geometry) to 23 W/K.

^[58]*Setyawan et. al. (2017)* built a loop heat pipe *that* was made up of capillary wick copper sintered developed by the centrifugal casting process. To eliminate the dry-out a diaphragm pump was added to fast-track the fluid transport from the condenser to the evaporator (*hybrid loop heat pipe, HLHP*), provided with a tank and fitted on the liquid line. The filling ratios (FR) considered for the investigation were 50%, 60%, and 80%. The pump activation would occur with the occurrence of the dry-out by the piezoelectric effect. The results from the experiments showed that the pump could effectively avoid the incidence of dry out, and decreased the temperature of the evaporator from 130°C to 80°C, owing to the distribution of the working fluid between the condenser& the evaporator efficiently. The outcomes showed the best performance at the filling ratio, FR of 60%.

^[59]*Taamneh (2017)* mathematically analyzed the thermal steady and transient study of a basic turbine disk combined with heat pipes for effective cooling. The steady and transient temperature changes with and without heat pipes were explored for numerous parameters. Thermal investigations were achieved by finite element (FE) modeling. In the far-reaching mathematical simulations exhibited with 32 heat pipes, the extreme temperatures at the edge of the disk could be reduced by over 100°C. Moreover, by enhancing the convective heat transfer coefficient of the working fluid of the heat pipes to 10,000 W/m²°C, the maximum temperature can be reduced by over 280 degrees.

^[60]*Hack et. al. (2017)* investigated a heat pipe made up of sintered silicon carbide (SSiC) working on Zinc as a working fluid (Length 1.07m & OD 22mm). The system was tested up to 980°C & 1kW.

^[61]*Lee et. al. (2017)* proposed a numerical model presented for rapid assessment of the maximum heat transfer capacity of tubular r heat pipes with mesh wicks and water as working fluid. The effect of Performance parameters of the heat pipe was studied on the Maximum Heat and it was found that it depends greatly on the evaporation temperature.

^[62]*Yang et. al. (2017)* examined the thermal features of aluminium-ammonia heat pipes having Ω -shaped grooves. The heat pipe was found to have an effective capability of dynamic response. The complete thermal resistance of the heat pipe reduces with the rise in input power, and the resistance is the least when the angle is 60°. With the rise in the liquid filling rate, the maximum heat transfer capability enhances.

^[63]*Nakkaew et. al. (2019)* while investigating a spit-AC integrated with a heat pipe presented that the highest heat transfer rate obtained from the heat pipe set was around 240 W at the air velocity of 5 m/s with a heater surface temperature of 70 °C. The heat pipe set with A-geometry containing 6 heat pipes was claimed to be the best arrangement. However, this arrangement delivered the maximum air-side pressure drop. The best heat pipe set is connected at the exit of the compressor and the refrigeration capacity was 9,000 BTU/hr. The investigational outcomes displayed that the energy efficiency ratios (EER) of the system with heat pipes are slightly higher than those of the conventional system by around 3.11%.

^[64]*Guichet et. al. (2020)* submitted condensation and falling film evaporation/boiling correlations intending to cover adequate information on the falling film dynamic in thermosyphons to facilitate the estimation of heat transfer coefficients.

^[65]*Gai et. al. (2020)* conducted a string of examinations on a loop heat pipe (LHP) having a flat evaporator and a fin-and-tube type condenser. At low heat loads, oscillations in temperature were detected all over the loop, hence, the features of temperature oscillation of the flat LHP at numerous heat loads were studied.

^[66]*Gai et. al. (2020)* observed that the temperature hysteresis of the LHP was associated with the gas-liquid circulation in the compensation chamber (CC), which in turn, was subject to the relations between heat leaking from the evaporator and the reflux of liquid coming from the condenser. The temperature of the evaporator is mounted with the surge in the gas phase in the compensation chamber.

^[67]*Martvoňová et. al. (2020)* enhanced the efficiency of fireplace inserts by preheating the combustion air with flue gases using a heat (closed-loop). The evaporator extracted heat from the flue gas and transfers it to the condenser working on the water as a working fluid increasing the thermal efficiency.

^[68]*Anikivi et. al. (2020)* performed experimental analysis for discrete filling ratio (FR) 40%, 50%, & 60% and various heat loads of 20 W, 40 W, 60 W, 80 W & 100 W. De-Ionized water was used as working fluid for the analysis for copper LHP. Steady and transient states both were estimated. Outcomes displayed for forced water-cooling provision (cooling water temperature 25 °C), the LHP can transmit a maximum heat load of 100 W with the evaporator working at 92°C and thermal resistance 0.5332 °C/W.

^[69]*Rao et. al. (2020)* presented the study of steam condensation using heat pipes. The construction parameter was also studied and construction was presented for Heat Input of approx. 30kW.

^[70]*Mbulu et. al. (2021)* devised and experimentally investigated the heat pipe-based battery thermal management system (BTMS) for high input. L- and I-shaped heat pipes were sandwiched together and supplied 30, 40, 50, and 60 W. The condenser units were water-cooled with a mass flow rate of 0.0167, 0.0333, and 0.05 kg/s. The considered BTMS could provide the highest temperature (T_{max}) below 55 °C, at the maximum power input, and required the temperature difference (ΔT) below 5 °C. It displayed the ability to transmit over 92.18% of the generated heat.

^[71]*Buz et. al. (2021)* proposed a numerical model and computational investigation of dynamic progressions in the loop heat pipe. The calculations exhibited that under particular states in the loop heat pipe there could be auto-oscillations of diverse nature, moreover, techniques for eliminating these auto-oscillations were examined. by regulating the use of a control valve on the additional bypass line which could

also considerably enhance the quality of temperature control and decrease energy utilization.

^[72]*Nemec et. al.* Investigated high-temperature heat pipes to be used in energy conversion functions such as fuel cells, gas turbine re-combustors, and Stirling cycle heat sources. Moreover, further functions comprise heat removal from the reactor and radiator sections. For temperature variations between 500 and 1000 °C, heat pipes can present advantageous features of passive, reliable function, and effective thermal coupling. Extended working life and consistent performance are critical necessities for such uses.

^[73]*Onuma et. al.* recommended a loop heat pipe (LHP) made up of coherent microporous evaporative wick to improve the heat removal with the limited mass constraint of the space system. Furthermore, the design modelled the pressure drop and evaporation rate in the wick comparing it with the calculation of the heat pipe performance using a stochastic wick. The heat pipe performance was projected with the use of evaporation models and the geometric design of the heat pipe has been optimized to attain the highest heat transport per unit mass.

^[74]*Ku et. al.* investigated the temperature oscillation trend using experimental records from a miniature LHP. The working temperature of an LHP acts as related to its working circumstances. The LHP generally attained a steady-state working temperature for given input variables such as heat load or sink temperatures. The operating temperature changed with heat load and/or the sink temperature, ultimately reaching another steady state of operations. Under particular circumstances, the operating temperature never achieved steady-state and remained oscillatory instead.

2.2. Review of Vapour Absorption Refrigeration System (VARs)

Literature available on investigations on Simple VARS & Multi-effect VARS has been studied working on various heat sources such as waste heat, solar heat, etc. The focus has been kept on the articles that employ waste heat recovery in this section.

^[75]**Da-Wen Sun (1996)** performed a comprehensive thermodynamic study of the properties of ammonia-water, ammonia-lithium nitrate, and ammonia-sodium thiocyanate cycles binary fluids and presented polynomial equations. The operational parameters of the systems were studied. It was established that ammonia-lithium nitrate and ammonia-sodium thiocyanate systems were appropriate options for ammonia-water systems. The performance of the ammonia-sodium thiocyanate cycle is a little better than the ammonia-lithium nitrate cycle.

^[76]**Horuz (1998)** studied the Vapour Absorption Refrigeration (VAR) systems and ammonia-water and water-lithium bromide solutions as a working combination. A basic VAR system has been explained and the operating cycle was elaborated. The comparison of the two combinations has been offered for the coefficient of performance (COP), the cooling capacity, and the maximum and minimum system pressures. The water-lithium bromide solution gave better performance.

^[77]**Talbi et al. (2000)** performed an exergy investigation on a single-effect absorption refrigeration cycle working on lithium bromide & water. A design process had been used for the cycle and an optimization consisting of ascertaining the enthalpy, entropy, temperature, mass Flow rate, heat transfer in each unit of the cycle, and coefficient of performance had been executed.

^[78]**Misra et. al. (2003)** used Thermo economic theory for the economic optimization of a single effect water/LiBr vapour absorption refrigeration system to reduce its overall function and amortization cost. A basic cost minimization method is applied to estimate the costs by developing exert economic equations. Eventually, an approximate optimum design arrangement is attained utilizing sequential local optimization.

^[79]**Adewusi et. al (2004)** considered the performance of single and two-stage ammonia-water absorption refrigeration systems (ARSs) and computed the entropy generation of each unit and whole entropy generation of all units along with the

COP. The results exhibited the two-stage system to have a greater S_{tot} and COP and found that the rise in COP is related to a reduction in S_{tot} .

^[80]*Arivazhagan et. al. (2006)* envisaged a prototype of a two-stage half effect vapour absorption refrigeration system having 1 kW refrigeration capacity and working on HFC based working fluids (R134a as refrigerant and DMAC as absorbent) for conducting experiments to ascertain the performance as degassing range, coefficient of performance & second law efficiency. The system can produce evaporating at the lowest temperature of 7 °C with the available generator temperatures of 55 to 75 °C. The degassing range is 40% more in the high absorber than in the low absorber than the high absorber. The optimum generator temperature was 65–70 °C for the corresponding coefficient of performance of 0.36.

^[81]*Gomri et. al. (2008)* executed an exergy analysis of double effect lithium bromide/water absorption refrigeration and presented that the performance of the system is enhanced with the rise in temperature of the low-pressure generator (LPG), however, reduces with the rise in temperature of the high-pressure generator (HPG). The maximum loss of exergy occurred in the absorber and HPG.

^[82]*Khaliq et. al. (2008)* performed exergy analysis and optimized a double-effect vapour absorption refrigeration system working on LiBr–H₂O solution. It was observed that exergy destruction takes place considerably in generators, absorbers, evaporator2, and heat exchangers. Whereas, the exergy destructions in condenser1, evaporator1, throttling valves, and expansion valves were comparatively smaller around 1–5%. COP & ECOP reduced with rise in the temperature of absorber1 and enhanced with the rise in the temperature of generator 1. The total exergy destruction was enhanced appreciably upon a minute rise in the absorber 1 temperature.

^[83]*Gomri (2009)* investigated the single effect and double effect absorption refrigeration systems and submitted when the evaporator temperature changed from 4 °C to 10 °C, the temperature of the condenser and absorber changed from 33 °C to 39 °C and the temperature of the generator (HPG) changed from 60 °C to 190 °C, the highest COP for single effect was around 0.73–0.79 and for double effect around 1.22–1.42. The highest exergetic efficiency for single effect was around 12.5–23.2% and for double effect the around 14.3–25.1%.

^[84]*Kaushik et. al. (2009)* performed energy and exergy analysis of single effect and series flow double effect absorption systems working on water–lithium bromide combination. The study included ascertaining the influences of generator, absorber & evaporator temperatures on the energy and exergy performance. The influence of pressure drop between evaporator & absorber and effectiveness of various heat exchangers were examined. Outcomes of the analysis exhibited that the coefficient of performance of the single effect was around 0.6–0.75 and for the series flow double effect system around 1–1.28.

^[85]*Gebreslassie et. al. (2010)* performed an exergy analysis given only the inevitable exergy destruction for single, double, triple, and half effect absorption cycles working on Water–Lithium bromide and thus obtaining the highest attainable performance under the given operating conditions. The COP enhanced substantially from double effect to triple effect cycles. The maximum exergy destruction takes place in the absorbers and generators, particularly at elevated temperatures of the heat source.

^[86]*Agrawal et. al. (2012)* projected a triple effect refrigeration cycle, in which the absorption cycle was combined with an ejector refrigeration cycle. This new system consisted of the advantages of the absorption cycle, ejector cycle, and low-temperature N₂O refrigerant. The cycle can produce the refrigeration effect of diverse scales at distinct temperatures separately and could work on waste heat. System performance and exergy destruction were evaluated.

^[87]*Farshi et. al. (2014)* performed a thermodynamic comparison of Ammonia/LiNO₃ and ammonia/NaSCN absorption refrigeration cycles as replacements for ammonia/water cycles below 0°C operations. A higher coefficient of performance (COP) with no requirements for purification of the refrigerant vapour was observed. The impact of various operating parameters on performance and the possibility of crystallization was studied. For low generator temperatures, ammonia/LiNO₃ cycles and at high generator temperatures, ammonia/NaSCN displayed better performance.

^[88]*Sachdeva et. al. (2014)* performed an exergy analysis of a vapour absorption refrigeration system working on LiBr-H₂O solution using a modified Gouy-Stodola approach with the prime objective to conclude the performance of the system and different units having major irreversible loss. The results exhibited that the exergy

destruction rate was substantial in absorber and generator followed by evaporator and condenser. The amount of exergy computed by the modified Gouy-Stodola equation varies maximum i.e., 26% in the generator in comparison with the classical Gouy-Stodola method.

^[89]*Rajkumar et. al. (2015)* utilized the waste heat of one condenser to run another low-temperature VAR system. The exergy analysis utilizing a condenser load study was done to exploit condenser heat.

^[90]*Shaikh et. al. (2017)* projected a system working on VCRS & VARS driven by an IC (Internal Combustion) engine. The VCRS worked on R12 whereas LiBr-H₂O was chosen for VARS. The refrigeration system was modelled and a parametric analysis was executed to assess the influences of numerous working constraints on the output.

^[91]*Mishra (2018)* performed the comparative study of 3 cascaded VCRS working on eco-friendly refrigerants namely R1234yf, R134a, R32, R507a, R227ea, R236fa, R245fa & R717 with Single, Double & Triple effect LiBr-H₂O systems. Results showed a 122% & 79.45 % increase in I & II Law Efficiency in the Triple Effect System respectively. Reduction in exergy destruction is 79.45 % & 25.9 % in Triple & Double Effect Respectively.

^[92]*Mishra (2019)* studied the performance of LiBr-H₂O triple effect VARS using multi-cascading VCRS working of eco-friendly refrigerants such as R1234yf (medium cycle, -50°C), R236fa (intermediate cycle, -100°C) & R245fa (ultra-low cycle, -150°C). The enhancement in I law efficiency for single stage cascade, for multi (two stages) cascade VCRS & for multi (three stages) cascade VCRS, is 7.8% 13.45% & 10.15% respectively for all 80°C VARS. Moreover, the enhancement in II law efficiency for single stage cascade, for multi (two stages) cascade VCRS & for multi (three stages) cascade VCRS are 80.8%, 116.5% & 156.2% respectively for all 100 °C of temperature overlapping. Similarly, the percentage decrease in system EDR for single stage cascade, for multi (two stages) cascade VCRS & for multi (three stages) cascade VCRS are 60.51%, 72.85% & 82.55% respectively for all 100 °C temperature overlap with 80 °C of evaporator temperature of VARS.

^[93]*Mishra (2019)* investigated half effect LiBr-H₂O VARS with multistage cascading VCRS working on eco-friendly refrigerants such as R1234yf (medium cycle, -50°C),

R236fa (intermediate cycle, -100°C), R245fa (ultra-low cycle. -150°C), R404a, R600a & R290. A comparative analysis was performed for the various working fluids.

^[94]**Mishra (2019)** analyzed double effect LiBr-H₂O VARS & Multi cascading VCRS working on R1234yf (medium cycle, -50°C), R245fa (intermediate cycle, -100°C), R236fa (ultra-low cycle. -150°C) and observed that overall COP for 123K evaporator temperature working on R236fa was lower than 273K evaporator temperature using 245fa. The percentage enhancement in Overall COP was observed (VCRS) is 15.27% for single-stage cascade VCRS, 24.45% for two-stage cascade VCRS, and 21.03% for three-stage cascade VCRS for all 80°C of VARS evaporator temperature. Similarly, the second law efficiency has been observed to have increased by 79.43 % for single stage cascade VCRS, 113.2 % for two-stage cascade VCRS and 152.2 % for three-stage cascade VCRS for all 10°C of overlap and a percentage decrease in EDR has been analyzed to be 59.21 % for single stage cascade VCRS, 72.03 % for two-stage cascade VCRS and 81.6 % for three-stage cascade VCRS for all 10°C of overlap for 8°C evaporators.

^[95]**Mishra (2020)** investigated LiBr-H₂O single effect VARS cascaded with VCRS using 1234yf (-50°C) and R-245fa (-100°C) & R-236fa (-150°C). The Overall COP for 123K evaporator (R236fa) was found to be lower for 273K evaporator (245fa).

^[96]**Mishra (2020)** evaluated a LiBr-H₂O triple effect VARS cascaded with VCRS using R1234yf , R1224yd(Z),R1234ze(Z), R1243zf, R1225ye(Z), R1233zd(E) , R1234ze(Z) & HFO-1336mzz(z) (-30 to -50°C), R1225ye(Z), R1233zd(E) & R1336mzz(z) (-75 to -95°C) and R1234yf , R1234ze(Z), R1243zf, R1225ye(Z), R1233zd(E) , R1234ze(Z) & HFO-1336mzz(z) (-135 to -150°C). The Overall COP for 123K evaporator (R236fa) was found to be lower for 273K evaporator (245fa).

^[97]**Mishra (2021)** studied the performance of double effect Li/Br-H₂O VARS with 3 cascade VCRS using eco-friendly refrigerants such as R1225ye(Z), R1233zd(E), and R1336mzz(Z) & R1233zd (E). Outcomes displayed that the overall COP of VCARS gets enhanced by 22.6%, while, the COP enhancement of 25.2% is experienced in the absorption segment.

^[98]*Mishra (2021)* performed an analysis of double effect Li/Br-H₂O VARS with 3 cascade VCRS using eco-friendly refrigerants such as R1225ye(Z), R1233zd(E), R1336mzz(Z) & R1233zd (E). It was observed that the performances drop with an increase in condenser & absorber temperatures.

^[99]*Mishra (2021)* analyzed half effect Li/Br-H₂O VARS cascaded with VCRS using eco-friendly refrigerants for ultra-low temperature generation (-75°C in single cascading & -150°C in multi-cascading). It was observed that II Law efficiency is 33.55% (-60°C to -63°C) and for HFO-1336mzz (Z) is 32.51% (-58 °C and -59 °C) and 32.32% using R1225ye (Z) (-57 °C and -58 °C) respectively.

^[100]*Abdulateef et. al. (2019)* developed a computational methodology on MATLAB for the thermodynamic study of the solar absorption refrigeration system and assessed the irreversible losses of components and the total entropy generation (\dot{S}_{tot}) of the system combined. The results exhibited *COP* and \dot{S}_{tot} to be proportional to the temperatures of the generator and evaporator. The *COP* and irreversibility were found to be inversely related to the temperatures of the condenser and absorber. Furthermore, the solar collector contributes the largest to the exergy destruction of the system accompanied by the generator and absorber. The highest losses of solar collectors shoot up to 70% and for generators and absorbers around 6-14%.

^[101]*Hanriot et. al. (2019)* designed and applied a close looped exhaust gas flow control system for Ammonia-water VARS. A succession of examinations was accomplished with variable generator temperatures (180, 200, 240, and 270 °C). It was observed that the system was considered sensitive to generator temperatures, and reasonable performance was only noticed at 200 °C. After 240 min tests, minimum temperatures of -12.5 and -0.6 °C were attained. The highest coefficient of performance (COP) recorded was nearly 0.05.

^[102]*Mohtaram et. al. (2019)* examined the exergy of an absorption refrigeration cycle working on water and lithium-bromide. Numerous elements were investigated in terms of their thermodynamic efficiency. Moreover, exergy efficiency and coefficients of performance (COP) were meticulously studied. It could be noted from the outcomes of the simulations that the highest rate of the destruction of exergy occurs in the absorber (35.87% of the destruction).

^[103]*Alrwashdeh et. al. (2019)* presented an economy-based evaluation between a vapour compression refrigeration system (VCRS) driven by a photovoltaic array and a vapour absorption refrigeration system (VARs) driven by a solar evacuated tube. The evaluation between these two systems was performed founded on a life-cycle cost study including the entire cost of procurement and working across the whole operation duration. The outcomes of the life cycle cost study specified that both systems were cost-effective in the profits over their whole expenses. However, a vapour compression refrigeration system can be preferred over a vapour absorption refrigeration system.

^[104]*Kurtuluş et. al. (2019)* modelled and studied a Vapour Absorption Refrigeration (VAR) system run on exhaust heat from the engine of an intercity bus. The outcomes exhibited that a rough loss of 4,489 kg/year of fuel could be prevented by using the proposed VAR system. The maximum coefficient of performance (COP) of the VAR system was attained as 0.78 and the maximum total exergy destruction for the VAR system was found as 15.25 kW.

^[105]*Sharifi et. al. (2020)* performed a study to develop the functioning of a single-effect Lithium bromide/water absorption cooling system. Generator and Evaporator temperatures were kept varying. The system was augmented to maximize exergetic and energetic efficiencies utilizing a multi-objective–multi-variable Genetic Algorithm. The Group Method of Data Handling neural network method was assumed to originate correlations amongst the design parameters and operational constraints. The system was attached to evacuated tube solar collectors and a comparison was made to an analogous system. The outcomes describe the highest enhancement in energetic and exergetic efficiencies of about 9.1% and 3.0%, respectively. This enhancement is attained by reducing the mean temperature of the generator by 6.2 °C and rising the mean temperature of the evaporator by 1.6 °C.

^[106]*Han et. al. (2020)* projected a LiBr/H₂O absorption refrigeration system based on an enhanced geothermal system (EGS) achieving the cascade operation of geothermal energy. A model was created and substantiated; furthermore, the effect of important parameters was examined. The refrigeration capacity of the system could range beyond 9 MkW with COP above 1.0.

^[107]*Mazyan et. al. (2020)* examined the viability of using low-cost methods to improve the coefficient of performance (COP) of the cooling cycle employed in the liquefaction of natural gas. The influence of mixing the propane refrigerant with ammonia, sulphur dioxide, and carbon dioxide on the functioning and the work input to the compressor was also calculated. It was also revealed that the mixture of ammonia-propane and sulphur dioxide-propane augments the overall COP by 7% and 9%, respectively. The addition of ammonia and sulphur dioxide to the propane refrigerant decreases the overall compressor work by dropping the overall mass flow rate essential. The carbon dioxide-propane reduces the overall COP by 70%. The projected technique needs insignificant capital and running expenses.

^[108]*Toppi et. al. (2020)* observed that in comparison with single effect cycles, the multiple effect cycles permit higher thermal lift however the use of controlled valves is required providing stability and control concerns. The self-adapting concept substitutes the valve with a phase separator. Five new cycle arrangements including the self-adapting concept have been exhibited. Comparative analysis for these cycles has been performed for COP and refrigerating capacity under various conditions. It was observed that the double-lift cycles had COP ranging from 0.35 to 0.20, and around 0.1 more than the triple-lift cycles. Cycles having multiple pumps had more efficiency than single-pump cycles, particularly in high lift conditions. The use of NH_3 – LiNO_3 had a broader working range and higher outcomes at higher thermal lift.

^[109]*Huirem et. al. (2020)* prepared a model of a single-effect LiBr- H_2O vapour absorption refrigeration system of 17.5kW refrigerating capacity. The performance (COP), exergy coefficient of performance (ECOP), total exergy destruction (TED), etc. were estimated. The model calculated the optimum functioning parameters like COP, ECOP, TED, etc. of the system for a function similar to on-farm cooling or transportation packing of fruits and vegetables.

^[110]*Gong et. al. (2021)* examined the capability of ammonia/ionic liquids for a half-effect absorption refrigeration system (ARC). Moreover, the thermodynamic and economic operations have been evaluated between the ammonia/ionic liquid & ammonia/water functioning combination. It was observed that the COP of the ammonia/ionic liquid was better than ammonia/water. Moreover, to attain the

maximum COP an optimum generator temperature was recorded. Eventually, ammonia/[emim][BF₄] was found to be performing best subject to most of the working parameters and were.

^[111]*Ahmed et. al. (2021)* proposed a novel overview of applying nanofluid as external cooling sheathing for the condenser of an air conditioner. Experimental analyses were performed to examine the impact of two types of nanofluids i.e., copper and aluminum oxide nanofluids on the working. The nanofluids were exploited to augment the heat transfer by providing an exterior nanofluid channel around the condenser segment. Both Cu and Al₂O₃ nanofluids were primed in 03 volume fractions of 1%, 2%, and 5% keeping water as the base fluid. The functioning of the air conditioner was estimated by comparison of the coefficient of performance. Experimental outcomes showed that the use of Cu and Al₂O₃ nanofluids produced a substantial improvement in the COP. When volume fraction was boosted, the functioning was found to have augmented. For the maximum volume fraction of 5%, Al₂O₃ nanofluid augmented the COP by a highest of 22.1% whereas copper nanofluid displayed a more substantial improvement of 29.4%.

^[112]*Raut et. al. (2021)* designed a VARS having a refrigeration capacity of 1kW run on hot water available utilizing a solar thermal collector during the Sun and driven by a connected latent heat energy storage system in Sun's absence. The unit had three evacuated tube collectors, latent heat energy storage, and VARS. The sizes of other components were computed by implementing the heat exchanger design method and the relevant equations. The evacuated tube collector of 100 LPD size was adequate for the designed system. Latent heat energy storage of 2.25 kW having charging and discharging 3 hours kW was attached with the system. The system provided a COP of 0.875.

^[113]*Vasilescu et. al.* developed a comprehensive numerical model for the double-effect absorption refrigeration cycle. The model has been verified by accessible data from experiments. The influence of the distribution ratio of the strong solution on the performance of the cycle has been studied. It has been exhibited that the optimum rate of the distribution ratio COP is 0.65.

^[114]*Abdulateef et. al.* proposed a Matlab-based thermodynamic simulation and second-law study of a single-stage solar-driven absorption refrigeration system

working on lithium bromide-water solution under different operating conditions. The results exhibited that a rise in the temperature of the generator transpired into a rise and subsequent reduction in *COP*, whereas, the whole entropy generation of the cycle increased. The *COP* was found to be more susceptible to variations in the functional parameters of the generator and the evaporator.

^[115]*Srikanth et. al.* studied a solar-driven absorption system based on Ammonia-Water Combination and presented that the *COP* of the cycle was minutely reduced by a change in the concentration of ammonia at a constant generator temperature and pressure. The minute reduction in *COP* could be attributed to the increase in the concentration of ammonia enhancing work input requirements. Likewise, with the rise in pressure work input increased at the generator, hence, the *COP* was reduced. The pressure shoots up keeping the concentration of ammonia constant, the enthalpy of the generator increased, consequently, heat input in the generator also increased. Hence, with pressure increase, *COP* gets reduced.

2.3. Review of Ejector Refrigeration Cycle (ERC)

ERC can work on waste heat & low-temperature sources. In this section study of articles on the same has been presented.

^[116]*Nemec et. al. (2006)* focused on the manufacture of the loop heat pipe, thermal visualization of the LHP fluid dynamics, and research. Heat flux transfer by working fluid from the LHP evaporator to the LHP condenser was investigated. The result of the displayed & described the effect of hydrodynamic and thermal processes taking place inside the loop of heat pipe on the heat transport at start-up & during function.

^[117]*Abdulateef et. al. (2009)* conducted a literature review on solar-driven ejector refrigeration systems to understand the operating principles of the ejector. The development history and recent progress showed that solar-driven ejector refrigeration technologies also execute the task of energy and environment preservation.

^[118]*Dahmani et. al. (2010)* described the design parameters of an ejector refrigeration system working on R134a with specified cooling capacity & temperatures the generator, the condenser, and the evaporator are presented for different pressures of the generator. Results exhibited that the COP increases with pressure increase & the heat exchanger pinch decrease.

^[119]*Reddick et. al. (2012)* performed an experimental investigation to ascertain the feasibility of enhancing the energy efficiency of a vapour compression refrigeration system replacing the expansion valve with a two-phase ejector with R134a as the working fluid. The main nozzle of the ejector was prepared with a double throat with a modifiable area for the first throat and a fixed one for the second throat. Experiments exhibited an enhancement of 11% in the coefficient of performance (COP) with the ejector mode in comparison with the conventional mode. A customized ejector refrigeration system with two evaporators was also projected to enhance stability and to addressing the separator effectiveness limitations.

^[120]*Buyadgie et. al. (2012)* performed a theoretical analysis of the ejector cycles and obtained the capability to produce the cooling from +12°C to -40° for the corresponding COP at 0.7 to 0.1 respectively.

^[121]*Untea et. al. (2013)* performed a mathematical energy and exergy study of an ejector refrigeration system working on various fluids namely water, methanol, ammonia, and R134a, operating on the waste heat from the exhaust gas of an IC Engine. Four working fluids are studied. Best performances were achieved for water. The effect of the Generator temperature (T_G), evaporator (T_{Ev}), and condenser (T_{Cd}). Optimal performance was achieved for $T_G = 140^\circ \text{C}$, $T_{Cd} = 30^\circ \text{C}$, $T_{Ev} = 5^\circ \text{C}$ and the COP=0.48 and $\eta_{ex} = 0.085$ were recorded.

^[122]*Pounds et. al. (2013)* performed an experiment-based analysis of an ejector refrigeration system to establish the influence of nozzle size, location of the axial nozzle, temperature of the high-temperature evaporator (120 to 135 °C), condenser temperatures (7-30 °C), and temperature of cooling (5 to 15 °C). A numerical model had been prepared to calculate the COP, following data obtained from the experiments. The experimental results displayed that the ejector refrigeration system could attain a COP of 1.7.

^[123]*Zheng et. al. (2014)* presented a simulation program explaining the performance of solar ejector refrigerant systems for air conditioning residential buildings in which hourly outputs under various functional conditions were examined. Results exhibited that the collector efficiency and the overall coefficient of performance initially increased and declined afterward.

^[124]*Memet et. al. (2015)* performed an investigation is focussing on the influence of generating temperature on the Coefficient of Performance (COP) and the work input to the pump keeping the refrigerating effect (1 kW), the condenser temperature ($t_c = 33^\circ \text{C}$) & the evaporator temperature ($t_e = 3^\circ \text{C}$) & Environment Temperature ($t_o = 23^\circ \text{C}$) fixed. The generator temperature varied ranging from 82 - 92°C, also, the isentropic efficiency of the ejector & pump had been taken 0.90 & 0.75. The Coefficient of Performance & work input to the pump were enhanced with the rise in generator temperature & the best COP was found to be 0.178.

^[125]*Ebadollahi et. al. (2017)* performed a theoretical study of the triple-evaporator ejector refrigeration cycle (TEERC) for achieving efficient cooling, freezing, and ventilation working on 09 suitable fluids i.e., R717, R152a, R134a, R290, cis-2-butene, butane, isobutene, iso-butane, R236fa. The generator was found to have maximum irreversibility followed by an ejector and condenser. The highest and lowest coefficients of performance (COP) were attained for R717 & R236fa at 0.333 & 0.268, respectively and the highest and lowest exergy efficiencies were evaluated for R717 and isobutene at 21.43% & 12/51 %, respectively. The ventilation, cooling, and freezing capacities were achieved for R717 as 11.68 kW, 3.86 kW, & 1.904 kW. It was also found that a rise in temperatures of the evaporators and generator and a reduction in the condenser temperature enhance COP and exergy efficiency.

^[126]*Mishra et. al. (2017)* executed a mathematical thermodynamic study on Ejector Refrigeration Cycle (ERC), working on eco-friendly working (i.e.R-404A, R-410A, R-407C, R-423A, R-500, R-502, and R-507C) to ascertain COP, Second Law Efficiency (η_{II}), Cooling Effect (RE) and Heat Input (Q_{in}) of the ERC varying boiler temperature (T_b), condenser temperature (T_c) and evaporator temperature (T_e). The maximum first Law Efficiency (η_I) was recorded in the range of 1.5-1.8 for R-404A and condenser temperature 328K. At the evaporator temperature of 253K, R-404A provides maximum Second Law Efficiency (η_{II}) 37%. For the complete range of boiler temperature R-410A was having maximum Second Law Efficiency (η_{II}). The cooling effect was recorded at maximum in the range of 200kW to 220kW for R-410A for all the ranges of temperatures. The highest COP was linked with R-404A for all the temperature variations.

^[127]*Seckin (2017)* investigated to establish the functional parameters for an ejector expansion refrigeration cycle (EERC) with R134a as the working fluid. A constant-area two-phase flow ejector at critical mode was simulated to conclude the influence of pressure of condenser (P_{cond}) and pressure of evaporator (P_{evap}) on the ejector expansion factor (EEF) and coefficient of performance (COP). Furthermore, it was proposed to employ the EERC for diverse refrigerating requirements. The two-phase/compressible fluid flow in the ejector was investigated based on the real gas performance of the working fluid.

^[128]**Eh et. al. (2017)** proposed methods to enhance the output of the gas turbine utilizing exergy study of combined Brayton and inverse Brayton cycles with steam injection into the combustion chamber. The influence of the change in working conditions on the output of the gas turbine was studied & the outcomes were compared with the cycle without injection. The investigation displayed that the maximum exergy destruction took place in the combustion chamber. Furthermore, the output was enhanced by 11% in efficiency and 57% in power utilizing steam injection. Steam injection raised the specific fuel consumption and the heat rate.

^[129]**Fang et. al. (2017)** presented a mathematical study of a single-phase supersonic ejector with R134a, hydro-fluoro olefin (HFO) refrigerants R1234yf & R1234ze (E) as working fluids. A comparative study was done regarding the ejector performances under changing working conditions & refrigerant mixture proportions and ejector heat-driven refrigeration cycle (EHDRC). R1234yf provided better performance for drop-in replacement of R134a in a real EHDRC, whereas, the use of R1234ze (E) would require some modifications owing to thermodynamic properties. For the same pressure ratio, the ejector provided a better entrainment ratio with R1234ze(E) and a reduced coefficient of performance (COP) and refrigerating capacity by an average of 4.2% and 26.6%, respectively. Using R1234yf under the same conditions induces a decrease of 5.2% for the entrainment ratio, 9.6% for the COP, and 19.8% for the cooling power on average.

^[130]**Besagni (2018)** discussed the selection of low GWP working fluids for the ejector refrigeration system, utilizing a verified lumped parameter model. The modeling had been done for sub-critic ejector refrigeration systems and some high GWP refrigerants were studied. The effect temperatures of generator, evaporator, and condenser on the ejector performance, for diverse fluids, had been investigated. The outcomes were presented based on the entrainment ratio and coefficient of performance.

^[131]**Reddy (2018)** investigated the ejectors through mathematical examination to optimize functioning factors such as evaporator temperature, condenser temperature, and generator temperature with R245fa as the working fluid. A parametric study was done to assess the result of the geometry of the mixing chamber on the performance of the ejector which has a straight effect on the coefficient of performance cycles.

^[132]*Taleghani et. al. (2019)* executed an exergy analysis of a CO₂ (R744) two-phase ejector utilizing a 1D model keeping a view of single and double choking. Was Results showed that the exergy study and Grassmann efficiency were not suitable standards to estimate the performance of a trans-critical CO₂ ejector.

^[133]*Liu (2019)* investigated a booster-assisted ejector refrigeration system to assess the performance enhancement perspective using conventional and advanced exergy study approaches. The outcomes exhibited that 61.6% of total exergy destruction was attributed to the components. Additionally, 55.5% of the total exergy destruction could be eliminated by enhancing unit efficiencies. The ejector had the maximum enhancement, subsequently the booster and the condenser.

^[134]*Kumar et. al. (2019)* calculated various performance parameters through experiments for six ejectors of diverse geometries. The need for an optimum area ratio of the ejector to attain improved performance was analyzed and it was also observed that a higher value of area ratio provided higher COP for the particular environment. The critical condenser pressure for area ratio 10.08 was 778.9 kPa & 916.72 kPa area ratio 6.451 at the temperature of the generator and evaporator of 80 °C and 15 °C respectively. Further, a shorter length of constant area section was better suited for operations.

^[135]*Zhang et. al. (2019)* proposed a new study on the combined Ejector Refrigeration & Organic Rankine Cycle working on the zeotropic mixture R134a/R123 as a working fluid. The effect of various input parameters on the performance of the combined system and ejector was investigated. It was observed that the entrainment ratio was not responsive to the variation of temperature at the heat source. Exergy examination explained that most of the exergy destruction in the system was related to the ejector, evaporator, & condenser (mainly in the element of ejector up to 50.28%). It was observed that net power decrease is less than power saved by ejector and cooling capacity, moreover, the exergy efficiency of ejector was established, and affecting parameters were investigated. The results displayed that the exergy efficiency of the ejector & COP is inversely related.

^[136]*Shovon et. al. (2019)* mathematically studied the Heat exchanger model within the ejector refrigeration system (ERS) working on R141b as the working fluid based

on the zone model technique able to calculate the outlet temperature. The prepared ejector model was employed to exhibit the changes in the system performance.

^[137]*Suvarnakuta et. al. (2020)* performed an analysis based on computational fluid dynamics (CFD) to examine the output of the steam ejector used in refrigeration systems to increase operational flexibility and COP. A 2 D axisymmetric model of a two-stage ejector (TSE) was developed and its performance was compared to that of the commonly used single-stage ejector. The SST *k*-omega (*k*- ω -sst) model was applied as a turbulence model. In the simulation, the TSE was analyzed using generator temperatures between 100 and 130°C and evaporator temperatures between 0 and 15°C, as in a previous study. The CFD simulation results showed that the TSE provided high entrainment ratios up to 77.2% while showing a marginal decrease in the critical backpressure up to a maximum value of 21.9%. Therefore, it can be concluded that the TSE can significantly benefit refrigeration systems requiring high refrigerating capacity while maintaining a slightly low condensing pressure.

^[138]*Mishra (2020)* presented a comparative study for HFO refrigerants in ejector refrigeration systems other than HFC and HCFC refrigerants.

^[139]*Besagni (2020)* proposed a methodology for screening refrigerants based on the Computational Fluid Dynamic (CFD) Model incorporated into Lumped Parameter Model (LPM). The ejector performances for the various refrigerants were computed by a verified CFD method, while the cycle was modeled by a Lumped Parameter method. For the diverse refrigerants, performance parameters of the systems were computed and the influences of the “*component-scale*” on the “*system-scale*” were studied.

^[140]*Kiseev et. al. (2020)* investigated designs of refrigerating systems based on two-phase loops with control of the flow rate of the liquid. A Model of an ejector-assisted loop heat pipe had been prepared, and the outcomes were compared with the analogous experimental data.

^[141]*Miao et. al. (2020)* projected a small seawater desalination system depending on the phase change to enhance heat transfer utilizing the loop heat pipes. The heat pipe was constructed with a novel spoiler evaporator and an equal-heat plate-fin condenser. The device was best suited for islands, fishing boats, and other remote

areas where power & fresh water sources are scarce. It could also be installed as emergency freshwater equipment for large ships resulting in a reduction in energy and portability.

^[142]*Bencharif et. al. (2020)* performed an experimental and thermodynamic investigation to study the influence of droplet injection on the output of an ejector-based refrigeration cycle prepared for Heating, Ventilation, and Air-Conditioning (HVAC) applications with R245fa as the working fluid. The results exhibited that injection of R245fa droplets at the end of the ejector diffuser glycol temperatures ranging from 20 to 26 °C had a considerable effect on the ejector as well as the complete cycle's performance & the coefficient of performance (COP) was raised by up to 20%.

^[143]*Al-Sayyab et. al. (2021)* investigated a compound PV/T waste heat run ejector-heat pump which utilizes PV/T waste heat for the generator's heat input. Based on the conventional exergy study the compressor has the highest (26%) and the generator shows the smallest (2%) exergy destruction. Through advanced exergy examination, it was found that 59.4% of inefficiencies for the complete system could be eliminated by further optimization. The compressor had the greatest role in the preventable exergy destruction rate (21%), the ejector (18%), and the condenser (8%). The highly developed exergo-economic outcomes established 51% of the costs as unavoidable and the maximum cost associated with the condenser as 30%. Moreover, the evaporator had the maximum exergo-economic feature (94%).

^[144]*Sharma et. al. (2021)* proposed an ejector refrigeration system (ERS) functioning on low-grade energy. The operating parameters and the conventional exergy analysis had been computed for each component of the system. The refrigerant R1234yf having low ODP and GWP was selected to study the exergy investigation and the outcomes exhibited that the highest exergy destruction occurred in the generator afterwards ejector and other components.

^[145]*Li et. al. (2021)* conducted a mathematical analysis to ascertain the performance of the ejector using CFD keeping entrainment ratio, static pressure, and Mach number performance parameters with working fluids R134a, R1234yf, and R1234ze (E) under variable operating temperature conditions. Increasing the generator temperature, increased the entrainment and then decreased subsequently. The rise in

the evaporator temperature weakens the primary-fluid jet expansion. The results exhibited that R1234yf had a higher entrainment ratio than R134a & R1234ze (E).

^[146]*Huang et. al. (2021)* observed that the function mode of LHP was related to the rate of temperature rise in the evaporator during the initial transient performance. The irregular high-temperature rise could be observed for LHP with failure, oscillating, or overshoot mode performance. Hence, it was proposed that the normal mode operation of LHP could be guaranteed from a short transient test in about 80s using stepwise heat load increment, instead of a steady-state test of 1,800s. The proposed test had been applied in the quality inspection of the commercial loop heat pipe in mass production. No breakdown was observed for over 10 years of spans in 30,000 sets of street LED luminaires based on LHP.

^[147]*Verma et. al. (2021)* performed an exergy-based investigation on the Ejector refrigeration system and concluded that the superior quality of the ejector is extra performance-oriented in comparison with the condenser, generator & evaporator.

^[148]*Devarajan et. al. (2021)* investigated to study and enhance the efficiency of ejector refrigeration system built-in with flat-plate collector and Scheffler concentrator. The Scheffler concentrator of 2.7m² and flat-plate collector of 5m² collecting area was connected with the storage tank having 15 l capacity to be the possible substitute of the conventional 1-ton room air conditioner with minimal electricity expense. The results exhibited the possibility of energy-saving potential near 70 to 80% over the conventional system.

^[149]*Vasiliev et. al.* prepared a mathematical methodology corresponding with an electrical analogy (lumped method) for a steady and unsteady mode of operation utilizing a C++ environment. Results of the simulated global model had been compared with the experimental data and were found reasonable for the transient response of the LHP.

2.4. Review of Organic Rankine Cycle (ORC)

Similar to the ERC, ORC also works on low-temperature heat sources & work on waste heat recovery. There has been sufficient work in this field comprehensive review of which has been presented in this section.

^[150]*Borsukiewicz-Gozdur (2013)* studied 18 different organic fluids as working fluids in subcritical ORC plants. The simulation outcomes exhibited that the small critical temperature provides a larger pressure range for the cycle temperature range than higher critical temperatures, which, added to a greater pumping power need. Moreover, the power decrease factor k was presented.

^[151]*Preißinger et. al. (2013)* examined 3 natural and 5 artificial refrigerants for working fluids in a sub- and trans-critical ORC. Moreover, an azeotropic mixture of R227ea/R245fa was investigated under subcritical conditions. It also exhibited the trans-critical ORC to be a capable method to optimize geo power plants. The net power could be augmented by more than 15% in comparison with the standard subcritical cycle. Furthermore, the economic examination specified that trans-critical ORC and zeotropic mixtures result in considerably lesser repayment periods.

^[152]*Lecompte et. al. (2014)* performed a thermo-economic comparative study for the sub-critical cycle, trilateral cycle, and trans-critical cycles and optimized the 3 for waste heat recovery on a temperature variation of 100 °C to 300 °C. The thermodynamic study only provided a minimal performance enhancement for high temperatures. Hence, a thermo-economic study was proposed for low temperatures.

^[153]*Ziviani et. al. (2015)* projected an ORC simulation tool, namely ORC Sim. The program was created utilizing object-oriented programming allowing enhancements and future expansions. 2 cycle arrangements were employed, in form of a conventional ORC and an ORC with liquid-flooded expansion.

^[154]*Wenzel et. al. (2016)* examined the cycle efficiency and the heat exchange area to the evaporator pinch point by constructing a model using heat and mass balance by conducting the variable pinch point from 10 K to 1K. The outcomes displayed that reduction of the pinch point results in less efficient cycles and greater evaporator areas.

^[155]*Amsyari et. al. (2016)* designed a radial turbine for ORC systems working on R-134a utilizing Ansys Vista Radial Turbine Design (Vista RTD). The mass flow rate is 0.7kg/s, the inlet temperature has been taken as 353K, the pressure was 3bar & rotation was 10000 RPM. The outcomes of manual design, and power outputs were 13.818kW & an efficiency of 71.67%. While the simulations attained 16.084kW output power with an efficiency of 80.85%.

^[156]*Alshammari et. al. (2018)* discussed the method of working, mechanical viability, and challenges in the use of turbo-expanders (radial inflow, radial outflow, and axial machines) and volumetric expansion machines (scroll, screw, piston, and vane) for ORC. It was determined that diverse machines were appropriate for a diverse variety of power output from commercial usage. Volumetric machinery was appropriate up to 50 kWe and turbo-machines were appropriate above 50 kWe.

^[157]*Karabarin et. al (2019)* deliberated the design attributes of the Organic Rankine cycle and a computation simulation of the model of a 4 kW unit working on the thermal energy of hot water from the boiler was executed.

^[158]*Liu et. al. (2019)* analyzed the Organic Rankine cycle (ORC) for the temperature variation of 80°C-140°C using R245fa and R600a. It was observed that the rise in heat source temperature increased the optimal inlet temperature of the expander. Evaporator and expander have maximum exergy efficiencies, & with increased heat source temperatures, the expander exergy efficiency remains unaffected and for the condenser, it decreases.

^[159]*Mariani et. al. (2019)* mathematically examined the ORC system as an energy recovery solution for exhaust heat recovery from internal combustion engine (ICE) passenger cars. The engine's working range was made distinct by utilizing engine torque and speed. The ORC recuperated power between 0.5 and 2.5 kW, with an efficiency of 11 to 12% whereas engine efficiency rise varied from 2.5 to 12%. By considering the permanence time in each discretized operating condition the engine efficiency increment resulted slightly higher than 6%.

^[160]*Herath et. al. (2020)* analyzed the feasibility & suitability of various working fluids for the ORC system for they are entirely dependent on the 07 working fluids i.e., R-134a, R-245fa, Benzene, Methanol, Ethanol, Acetone, and Propane (R-290),

working on low-temperature sources solar thermal, geothermal or waste heat recovery. Outcomes displayed that Benzene and Methanol were more efficient and need lesser flow rates per kW comparatively.

^[161]**Bull et. al. (2020)** investigated the ORC system using R-1234yf as the working fluid. Work outputs and thermal efficiency had been computed on numerous functioning pressures. Plate and shell and tube heat exchangers were examined for the units i.e., preheater, evaporator and superheater, precooler, and condenser. Sizing of each unit was done utilizing the suitable correlations for models of single-phase and two-phase fluid and the sizes were optimized. The plate heat exchanger has better performance than the shell and tube based on the overall heat transfer coefficient and area.

^[162]**Touaibi et. al. (2020)** performed an energy analysis for the organic Rankine cycle (ORC) comparing three organic fluids i.e., toluene, R245fa, and R123. A thermodynamic model was established utilizing the EES software to ascertain its output subject to fixed working conditions. The outcomes exhibited that toluene has the best thermal efficiency of the cycle compared to the other fluids at 14.38%.

^[163]**Saadon et. al.** emphasized the various circumstances and arrangements of ORCs. These different arrangements had diverse limitations being measured on an application basis.

2.5. Conclusions of the Literature Survey

The comprehensive review of the literature & texts conducted in the previous sections can be effectively summarized and concluded in the following points:

- 1) HP & LHP can be used for a vast variety of applications from the cooling of micro-processors to the cooling of spacecraft.
- 2) HP & LHPs have been studied for solar cooling or heating, temperature maintenance of spaces, low, medium & high heat fluxes and waste heat recovery, etc.
- 3) Heat Pipes need no external power inputs so are compact and flexible.
- 4) Multi-evaporator LHPs have been studied to be providing better performance over the single evaporator LHP.
- 5) The Wick of the HP enhances the overall heat transfer coefficient when compared to the no wick design.
- 6) The Angle of inclination and gravity has a significant effect on the overall heat transfer capability of HP/LHP.
- 7) The second Law Efficiency of the LHP can be improved by adjusting the surrounding temperature for the condenser and convective heat transfer coefficient in the evaporator.
- 8) A vast range of working fluids can be utilized in the LHP based on the requirement of the applications.
- 9) Heat pipes have low thermal resistance and high heat transfer coefficient owing to the evaporation-condensation heat transfer, leading to compactness.
- 10) The design of the evaporator and compensation chamber, the existence of non-condensable gases and the pressure drops down the loop affect the performance.
- 11) As the length of the pipe increases and/or pipe diameter decreases, a higher temperature is attained in the evaporator.
- 12) As the evaporator temperature increases the second law efficiency increases.

- 13) Fins can be used to enhance the overall heat transfer coefficient of the LHP
- 14) The performance increases with the increase in filling ratio and is maximum for filling ratio of 60%.
- 15) Nano-particles can also be utilized to enhance the HP/LHP.
- 16) Multi-effect VARS systems have better performance and can utilize higher temperature sources.
- 17) VARS systems can work on solar energy, low-grade heat recovery, etc.
- 18) LiBr-H₂O systems have better performance than systems working on NH₃-H₂O systems.
- 19) Sufficient energy is available in the vapour refrigerant leaving the generator which can be utilized for supplying heat at lower temperatures.
- 20) The COP of these VARS systems is considerably lower than VCRS.
- 21) For low generator temperatures, ammonia/LiNO₃ cycles, and at high generator temperatures, ammonia/NaSCN displayed better performance.
- 22) ORC has lower efficiency when compared to the Rankine cycle as it works on lower-temperature heat sources.
- 23) It can work on waste heat, and geothermal heat sources, and can work on eco-friendly refrigerants.
- 24) Similar to ORC, ERC has low COP compared to VARS & VCRS.
- 25) It can work on waste heat, solar heat, etc., and can employ eco-friendly refrigerants such as water.
- 26) It can be noticed that both ORC & ERC if utilized properly, have an inherent eco-friendliness in their functioning.
- 27) These are suitable for industrial setups such as power plants, steel plants, food processing industry, etc. where waste heat is abundant, and the Availability of heat sources can be enhanced for better performance of these systems.

2.6. Identified Gaps in the Literature

Loop heat pipes are being used in Solar Plants, Cooling Electronic devices, Cooling Space Shuttles, etc. In several kinds of research performed they are being used directly to maintain the temperature of several cold storages around the world. It has high heat flux capacity.

The extensive literature & texts available have covered almost all the aspects of the aforementioned systems including thermodynamic analysis, thermo-economic analysis, optimization, etc. However, given the literature review, the following gap in the previously conducted research can be identified to manifest as the basis of the novel presented research work.

- ❖ There are types of VAR systems such as Single Effect, Double Effect, Triple Effect, Quadruple Effect, etc. for which First Law, Second Law, and Economic Analysis have been performed. However, Loop Heat Pipes can be made an integral part of the system and these valuable analyses can be executed on this new system and results can be studied meticulously.
- ❖ Waste heat is released to the environment from the condenser that has never been used within the same system, which can reduce the requirement of heat supply to the generator.
- ❖ Also, the VAR system can be coupled with other systems that may be refrigerating or power generating in which heat is released.
- ❖ The Loop Heat Pipes will make the system compact, and performance optimization can be performed for the various VAR systems.
- ❖ Loop Heat Pipes can be used to extract heat from Power Cycles such as Gas Power Cycles and supplied to ERC and ORC working on Eco-friendly fluids.
- ❖ The study can be performed to develop an Industrial Eco-friendly system absorbing the waste heat and affecting the Global Warming & Thermal Pollution.

2.7. Scope & Objectives for the Research Work

The VAR system uses low-grade energy for its operation, which can be obtained from several cheaply available sources (solar, waste heat, etc). The COP is low and Irreversibility related to heat transfer in the cycle is associated. Using Loop Heat Pipes for intra-cycle heat recovery can increase the COP of the system which will eventually increase the First Law COP, and Second Law COP and will reduce the Irreversibility associated with the operation of a VAR system.

The temperature variation can also be controlled by the use of a heat pipe which will result in the reduction of anergy. The coupling of different cycles will not require complex heat exchangers but Simple LHPs which are available in different heat flux capacities. Studying the literature available on the selected field the objectives of the research work has been decided to be the following:

- ❖ Intra-cycle heat utilization in the VAR system with help of LHP to loop in the waste heat.
- ❖ Thermodynamic analysis of different types VAR systems with LHP for intra-cycle heat transfer e.g., single effect, half effect, etc.
- ❖ Study of the suitability of Heat Pipes for connecting different heat sources with various systems (ERC, ORC).
- ❖ Study of suitable eco-friendly fluids for LHP, ERC & ORC.
- ❖ Study of the suitability of combination of cycles with LHP for Industrial applications.

Chapter-3: Description of Systems

Based on the gaps identified during the literature review and the objectives set for this research work, the Component condenser has been replaced by LHPs. This chapter covers and elaborates on the following systems considered for the research:

- a. Modified Single-Effect VARS
- b. Modified Half-Effect VARS
- c. Modified Double-Effect VARS
- d. Modified Triple-Effect VARS
- e. Modified Quadruple-Effect VARS
- f. Combination of ERC & GPC through LHP
- g. Combination of ORC & GPC through LHP

3.1. Modifications Proposed in the Single-Effect VARS (Ankit Dwivedi, et. al. 2018) ^[183]:

The study begins with the most basic VARS i.e., the Single Effect system (Fig 3.1). This system contains Evaporator, Absorber, Pump, Solution Heat Exchanger, LHP, a Generator, and a refrigerant expansion valve. As mentioned above, in place of the condenser the LHP Evaporator extracts heat from High Pressure-Temperature (P-T) refrigerant vapour coming out of the Generator at state 6. It may be suitably assumed that the vapour refrigerant leaving the generator has a temperature equal to the generator operating temperature. Moreover, the refrigerant leaving the LHP Evaporator is saturated liquid or sub-cooled before entering the refrigerant expander at state 10.

The Low Pressure-Temperature refrigerant liquid goes into the evaporator at state 11 where heat input into the evaporator takes place from the refrigerated area by evaporation of the refrigerant. The vapour refrigerant coming out of the evaporator at state 1 goes into the absorber and mixes with the absorbent. The process inside the

Performance Improvement of Vapour Absorption System Using Loop Heat Pipes

absorber is exothermic and heat is released to the surrounding. This mixture is pumped from state 2 towards the generator.

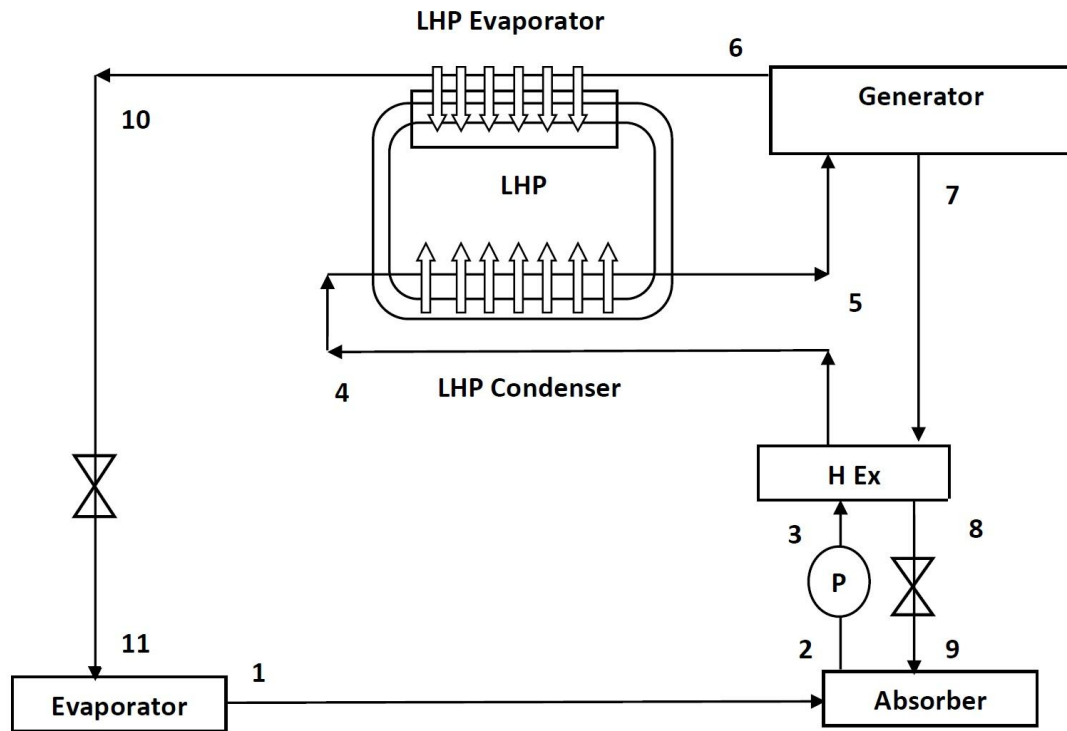


Fig 3.1: Modification-I in Single Effect VARS using LHP [183]

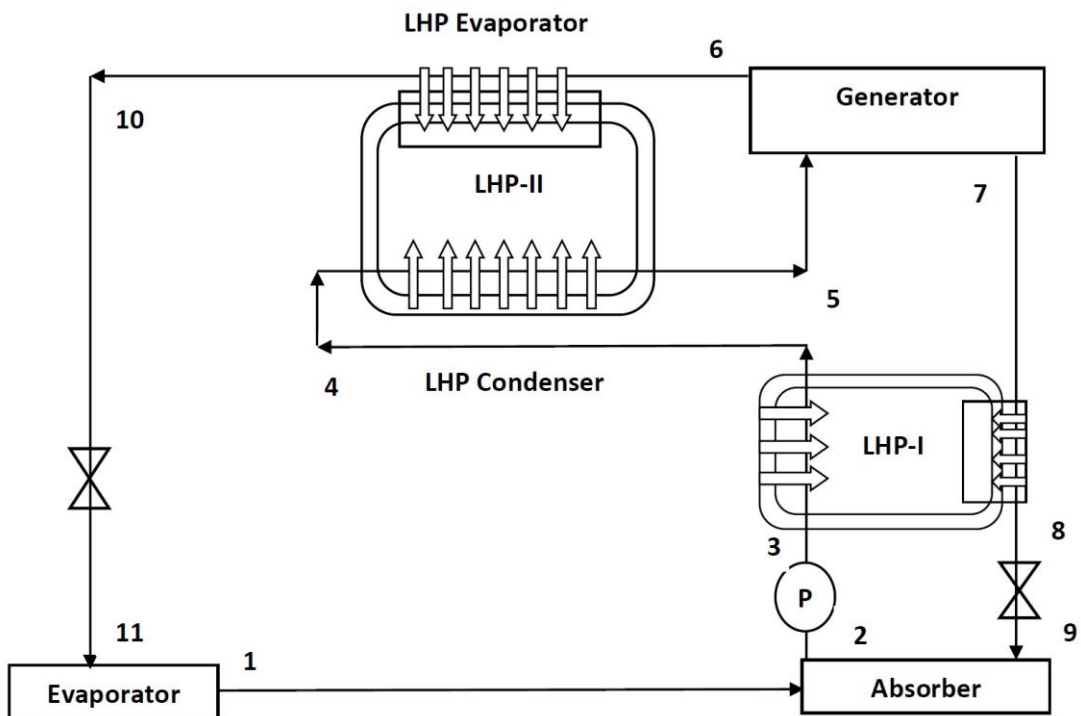


Fig 3.2: Modification-II in Single Effect VARS using LHP

Performance Improvement of Vapour Absorption System Using Loop Heat Pipes

The mixture is pre-heated to state 4 in the Solution Heat Exchanger (HEx) before entering the LHP Condenser Section where the solution is further pre-heated before entering the generator at state 5. In the system shown in Fig 3.1, the preheating before entering the LHP Condenser is done by Heat Exchanger, whereas, in the system shown in Fig 3.2, LHP-I is employed for the same. The heating in the LHP Condenser occurs owing to the condensing LHP Fluid.

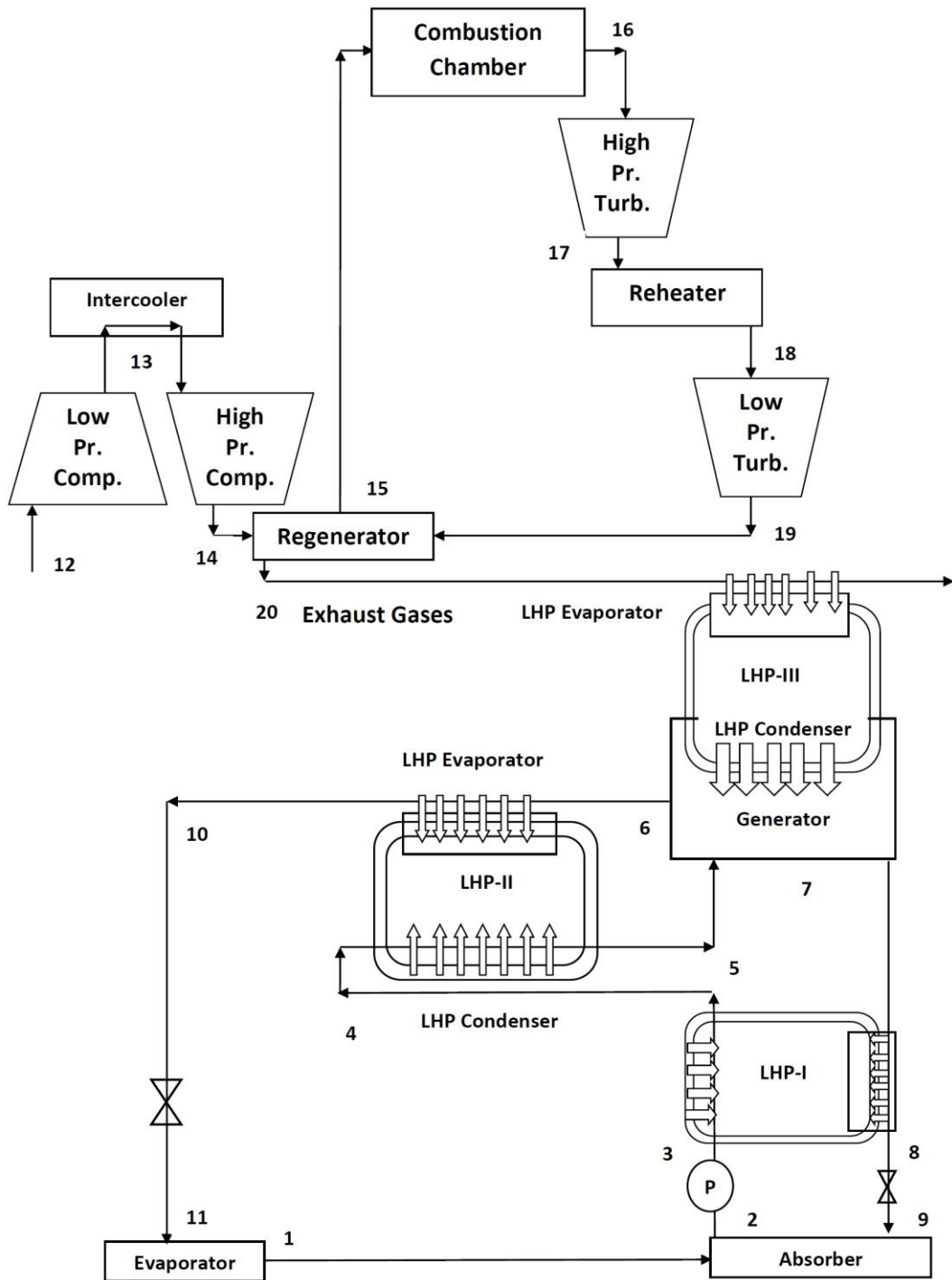


Fig 3.3: Modified Single Effect VARS Combined with GPC using LHP

It can be summarized that on one hand, in the LHP Evaporator section heat transfer occurs between the condensing refrigerant & an evaporating LHP working fluid which renders an extremely high heat transfer rate with practical flexibility and on the other hand in the LHP Condenser the heat transfer occurs between the liquid mixture & condensing LHP working fluid.

The mixture remaining in the generator after the heat addition and subsequent evaporation of the rich refrigerant is throttled back to the absorber after rejecting heat in HEx & LHP-I respectively in Fig 3.1 or Fig 3.2 as the mixture is at high temperature leaving the generator.

Fig 3.3 shows the combined Single Effect VARS & Actual GPC with perfect intercooling, perfect reheating & regenerator. In the GPC as discussed earlier the air is sucked in large amounts and is compressed to the combustion chamber pressure with help of a Low-Pressure & High-Pressure Compressor, for which perfect intercooling is assumed. This compressed air is further preheated before entering the combustion chamber in the regenerator.

Heat is supplied to this preheated compressed air in the combustion chamber by combustion of fuel and the resultant High P-T gas mixture is expanded in a High-P Expander/Turbine at the outlet of the same a reheater is installed to reheat the gas mixture to the initial temperature of High P-T Turbine inlet and is further expanded in Low-P Expander/Turbine. The exhaust from the Low-Pressure Turbine is routed toward the regenerator to utilize the heat in the exhaust. The exhaust from the regenerator is further utilized to operate the Single Effect VARS as the bottom cycle through LHP-III.

The heat extracted from the exhaust by the LHP is transferred to the generator of the VARS through the LHP condenser as the LHP can transmit heat over a large distance.

3.2. Modifications Proposed in the Half-Effect VARS (Ankit Dwivedi, et. al. 2018) [184]:

A half-effect vapour absorption system (Fig 3.4) consists of 2 generators, 2 absorbers, a condenser, an evaporator, 2 pumps, 2 heat exchangers, and 3 throttling valves. The half-effect cycle is a combination of two single-effect absorption cycles each working at different pressure levels. This system has been developed for relatively low-temperature heat source applications than VARS. Also, the COP of the half-effect system is relatively lower because it rejects more heat than a single-effect cycle. The heat from a high-temperature external source transfers to the generators. The absorbers reject heat to the surroundings.

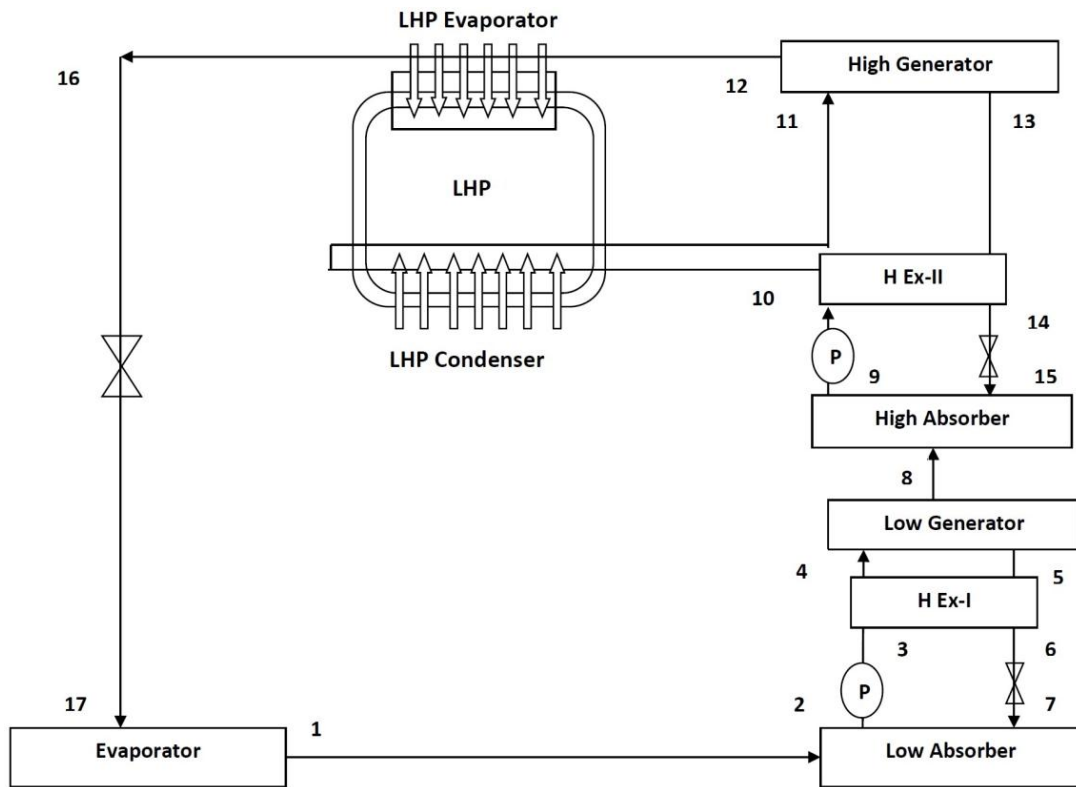


Fig 3.4: Modification-I in Half Effect VARS using LHP [184]

Similar to the modifications in the single-effect VARS in the previous section, the condenser from the Half-effect system has also been replaced by LHP in Fig 3.4. The vapour refrigerant leaving the High P-T generator at state 12 passes through the LHP Evaporator and rejects heat to the LHP Fluid. This Heat Rejection condenses the refrigerant to saturated liquid or sub-cooled at state 16. The evaporated LHP working fluid after absorbing the heat of condensing refrigerant flows towards the LHP

condenser. In Modification –II the heat exchangers have been replaced by LHPs for heat recovery offering a flexible solution.

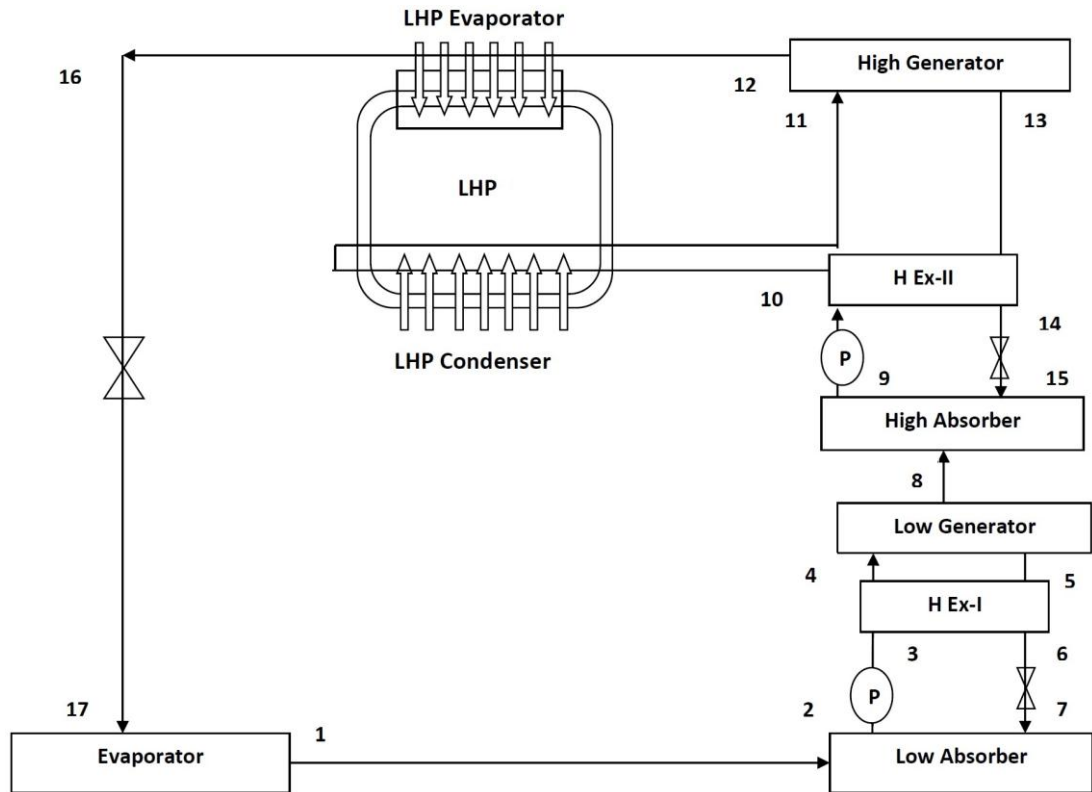


Fig 3.5: Modification-II in Half Effect VARS using LHP

The refrigerant from state 16 is further throttled down to low P-T state 17 where it enters the evaporator. This low P-T refrigerant evaporates in the evaporator producing refrigeration and leaving the evaporator at state 1. This refrigerant then further enters the low-temperature absorber where it mixes with the absorbent at state 2. From where it is passed through a heat exchanger in this modified system in Fig 3.4 & passed through LHP-I in the system in Fig 3.5 for pre-heating and enters the low generator at state 4 respectively. In this generator, heat is supplied and the evaporated refrigerant leaves the generator and enters the high-temperature absorber at state 8 where it further mixes with the absorbent. The remaining high-temperature mixture in the low-temperature absorber is throttled down through the Heat Exchanger-I & LHP-I in modified systems I & II (Fig 3.4 & 3.5) respectively.

Furthermore, the mixture from the High-T absorber is pumped to the generator through HEx-II & LHP in modified system-I and LHP-II & LHP-III in modified

Performance Improvement of Vapour Absorption System Using Loop Heat Pipes

system-II for preheating. The mixture enters the generator at state 11 where it is heated to evaporate the refrigerant.

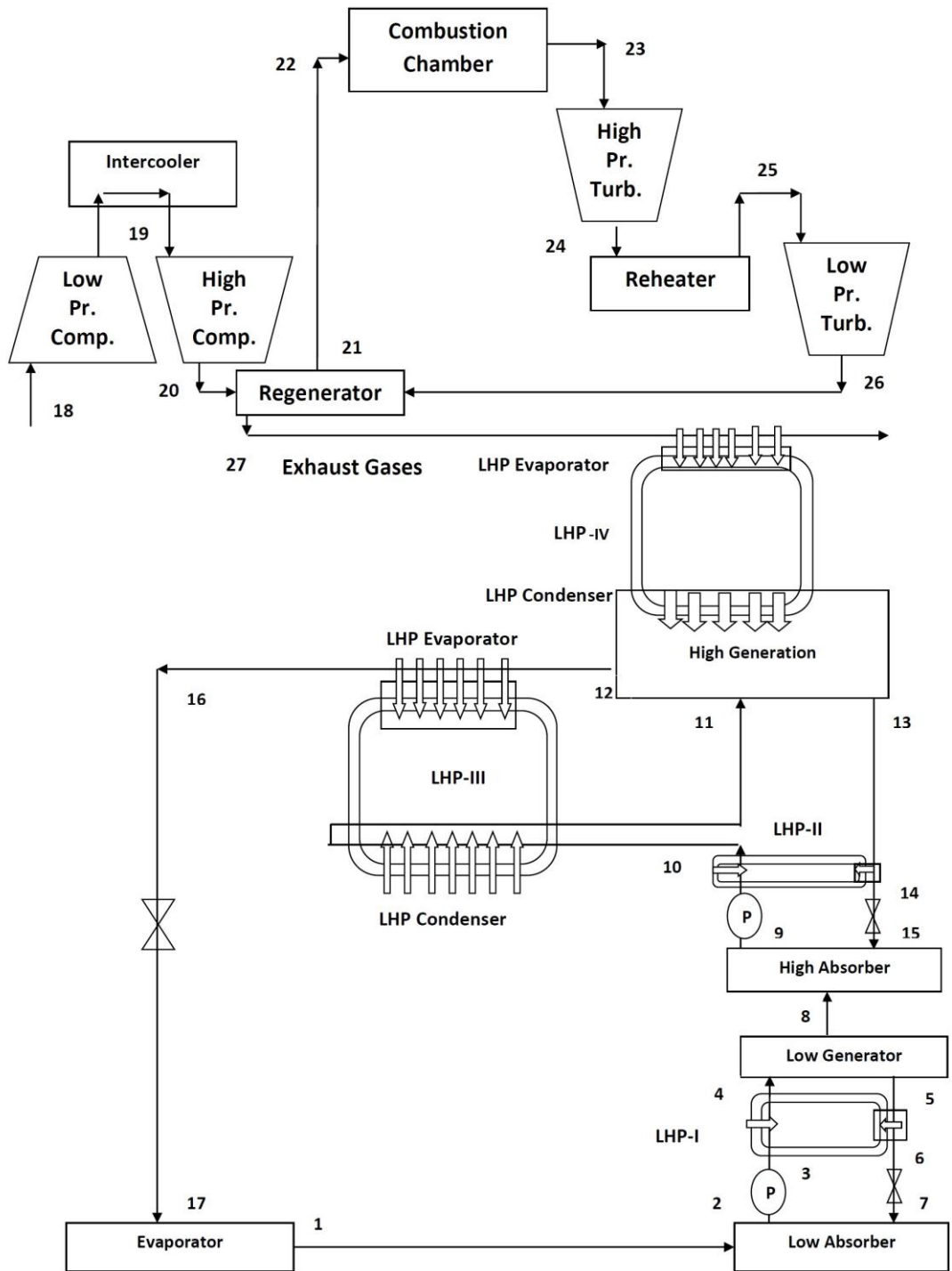


Fig 3.6: Modified Half Effect VARS Combined with GPC using LHP

The refrigerant vapours leave the generator at 12 and the remaining high-temperature mixture coming out of the generator at state 13 & is throttled to state 15 through the HEX-II & LHP-II in the respective modified systems.

Fig 3.6 shows the Modified Half - effect system-II combined with GPC through LHP-IV for accomplishing the efficient & flexible Intra-cycle & inter-cycle heat recovery.

3.3. Modifications Proposed in the Double-Effect VARS (Ankit Dwivedi, et. al. 2018) ^[185].

The half-effect & single-effect VARS are not well suited for the utilization of heat from a source with a temperature higher than a certain temperature as The COP decreases with an increase in temperature beyond a certain point. Hence the requirement of Double Effect VARS is realized by using a high-temperature generator. The basic system has been discussed in Chapter-1, whereas, this section deals with the elaborate discussions of the proposed modifications in the Double-effect VARS in line with the methods proposed for Single-Effect & Half-Effect VARS.

A double effect system is obtained by adding another set of generator-condenser to the single effect VARS. Heat input is only to the Generator at the highest P-T & Intra-cycle heat is utilized to extract a little more refrigerant vapour from the low P-T generator. Similar to the previous sections the Modification-I (Fig 3.7) & Modification-II (Fig 3.8) are different for using Heat Exchangers & LHP for extracting heat from the absorbent returning from the generators. The high P-T condenser has been replaced by LHP for intra-cycle heat recovery.

The primary refrigerant vapour stream at high P-T at state 7 enters the LHP evaporator, condenses while rejecting heat and evaporating LHP working fluid, and exits the LHP Evaporator at state 14 and is throttled to the low P-T condenser where it mixes with secondary refrigerant vapours generated in the low P-T generator. The final mixture thus obtained is then throttled to the evaporator at Low P-T at state 17 where the liquid refrigerant is evaporated generating the refrigeration and comes out at state 1. The vapour refrigerant moves into the absorber and mixes with the absorbent in an exothermic process.

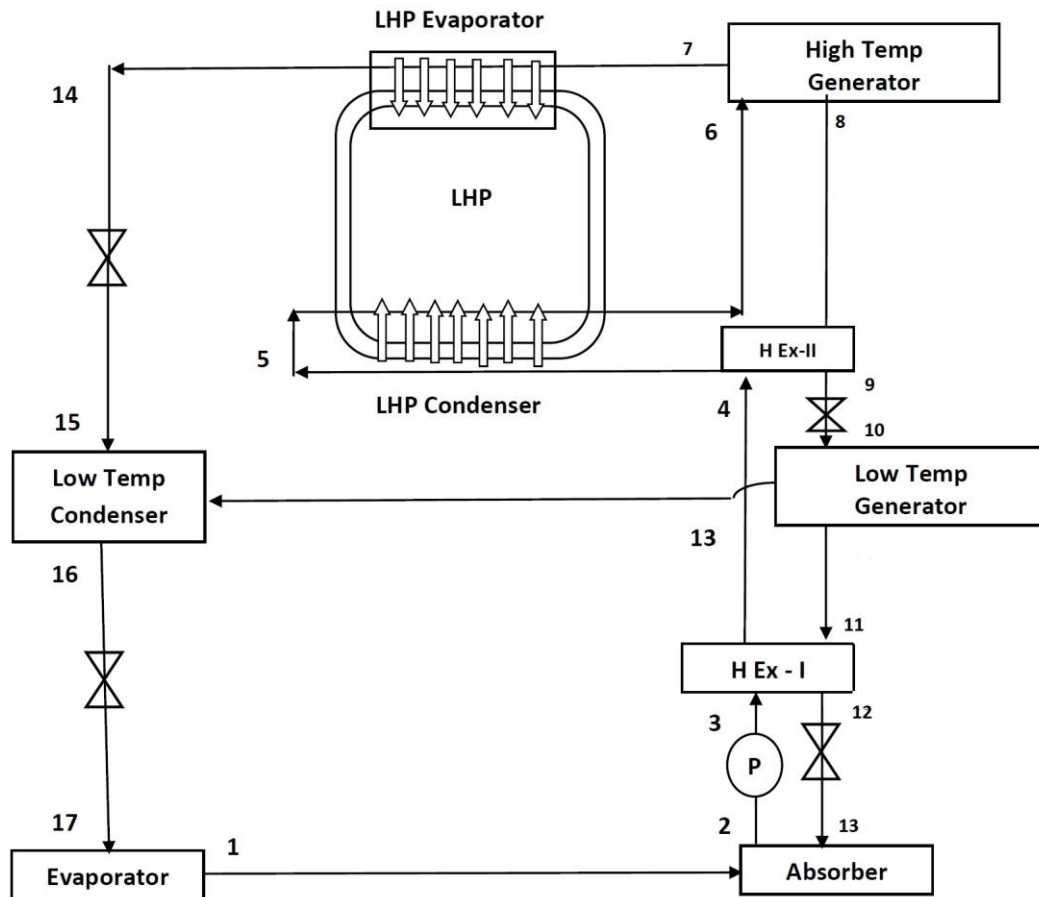


Fig 3.7: Modification-I in Double Effect (Series) VARS using LHP [185]

This mixture is then pumped directly to the High P-T generator through HEx & LHP in the system in Fig 3.7 and LHPs in the system in Fig 3.8 being a series flow system. In the case of a parallel flow system, the mixture is passed through the L-T generator as well. In the High P-T generator the mixture is heated and the primary stream of refrigerant vapour leaves the generator and the remaining high P-T is further throttled down through the low P-T generator, HEx, or LHPs to the absorber at state 13.

In the low P-T generator intra-cycle heat from the condensing refrigerant, heating is done & a secondary stream of vapour refrigerant is generated and is further transferred to the low P-T condenser to mix with the primary stream. This in turn increases the COP, RC & efficiency of heat utilization in the VARS.

Performance Improvement of Vapour Absorption System Using Loop Heat Pipes

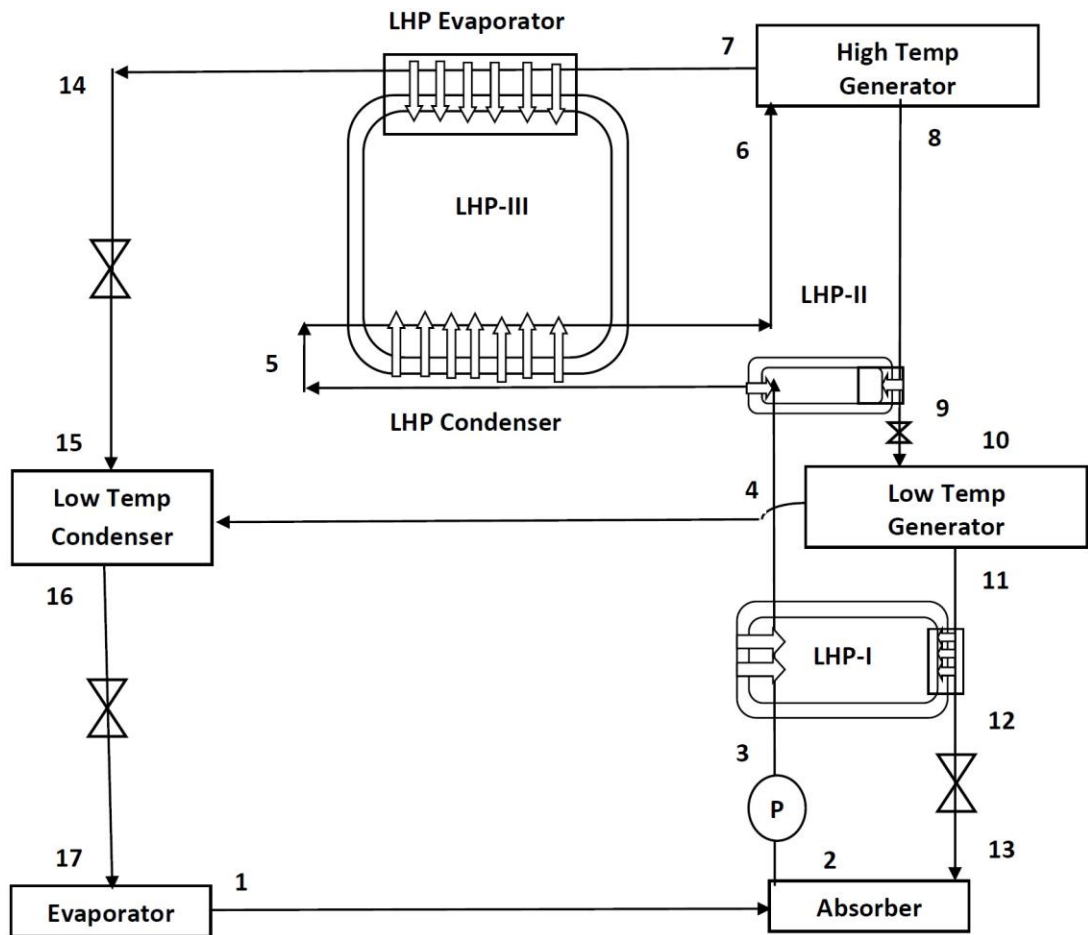


Fig 3.8: Modification-II in Double Effect (Series) VARS using LHP

The modified double-effect system being run on the waste heat recovery from GPC through LHP has been presented in Fig 3.9. The GPC is an intercooling, reheating & regenerating cycle of energy from the exhaust which can be used for evaporating the LHP fluid to become a source of heat for the Bottom VARS.

Performance Improvement of Vapour Absorption System Using Loop Heat Pipes

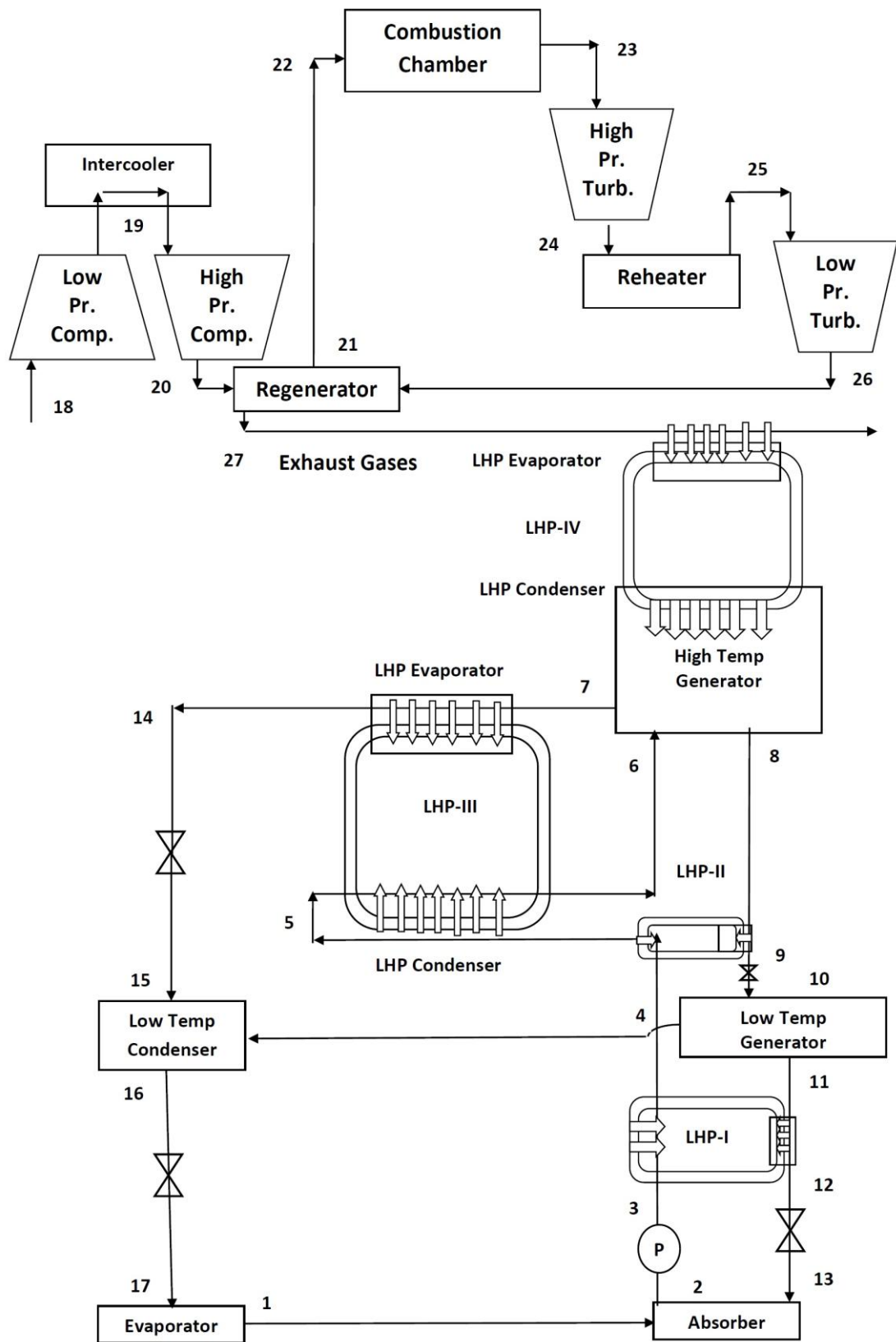


Fig 3.9: Modified Double Effect (Series) VARS Combined with GPC using LHP

3.4. Modifications Proposed in the Triple-Effect VARS (Ankit Dwivedi, et. al. 2018) ^[186].

A triple effect vapour absorption system refrigeration system (VARS) is used when the source temperature is high ($>140-150^{\circ}\text{C}$). The high temperature also corrodes the material of the generator and connecting lines. This VARS system is very useful in utilizing waste heat. The efficiency of the triple effect system is also relatively higher as the operating temperature is very high compared to the aforementioned systems.

The triple effect VARS (series flow) can be obtained by adding another generator-condenser set to the existing double effect VARS. Heat is only added in the highest P-T and the medium & low P-T generators operate on the intracycle heat exchange and some evaporation of refrigerants takes place in both the Medium & Low generators.

Similar to the 3 previous sections in this section well 2 modifications in the triple effect series flow VARS have been proposed in Fig 3.10 & Fig 3.11. The system in Fig 3.10 uses Heat Exchangers for solution heat exchange whereas, the system in Fig3.11 uses LHPs for the same purposes. Moreover, the high & medium P-T condensers have been replaced by LHPs in both Modifications- I & II.

The refrigerant vapour after producing the refrigerating effect exits the evaporator at state 1 and goes into the absorber for absorption in an exothermic process. This mixture from the absorber at state 2 is directly pumped to the high P-T Generator through HEX-LHP or LHP-LHP preheating the mixture before entering the generator at state. As mentioned earlier this preheating is done to reduce the heat requirement in the generator increasing COP.

Upon heat input, in the generator, the refrigerant is evaporated and moves out of the generator, and passes through the LHP evaporator where the condensation of refrigerant takes place. This refrigerant is further throttled down from 20 to 21 where it mixes with the refrigerant liquid coming out of the medium P-T generator.

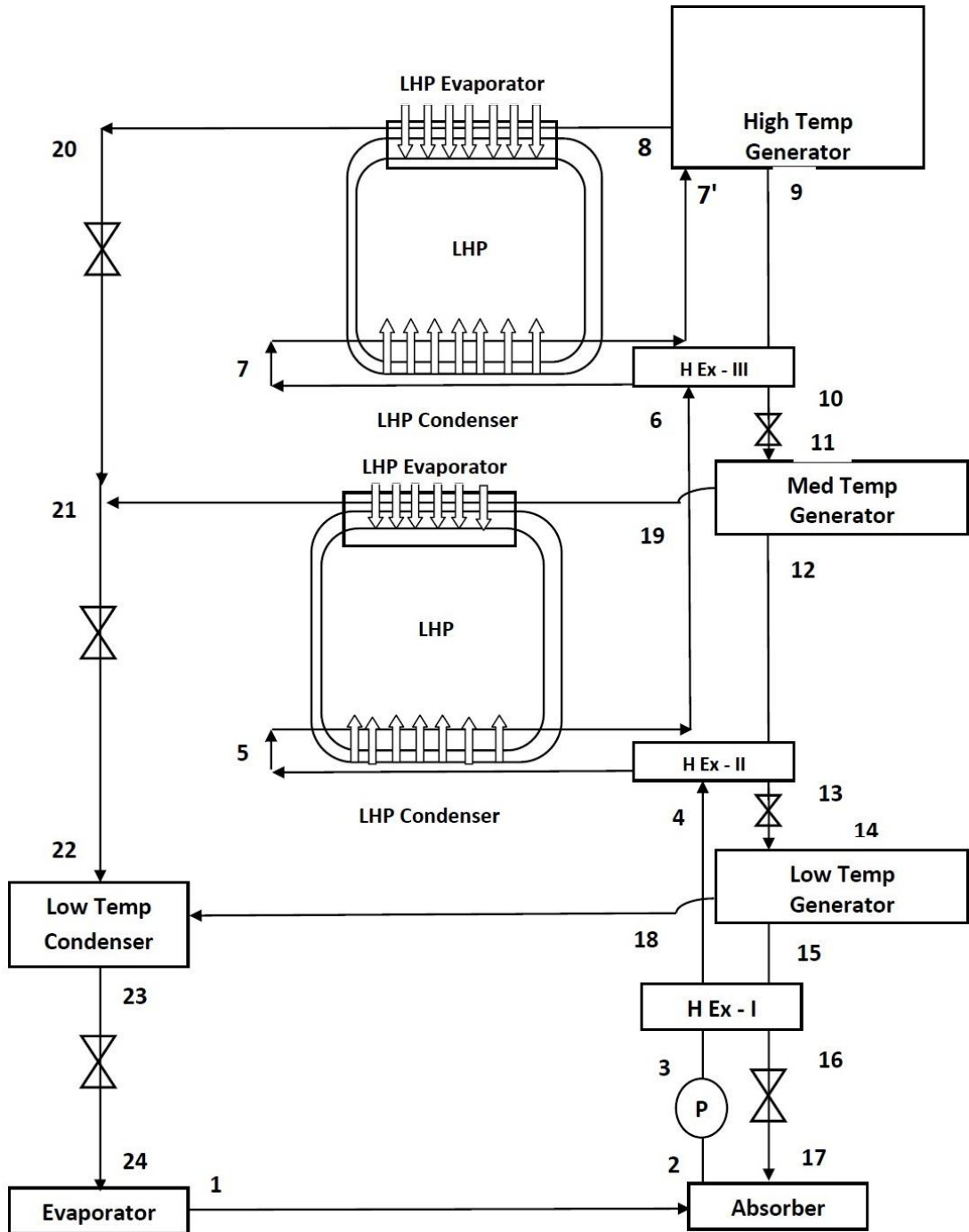


Fig 3.10: Modification-I in Triple Effect (Series) VARS using LHP [186]

This mixture is further throttled to the low P-T condenser to state 22 and mixes with the refrigerant coming out of the Low P-T generator. This final mixture of refrigerants coming out of all the 3 generators is further throttled from state 23 to state 24 which is the entrance of the evaporator.

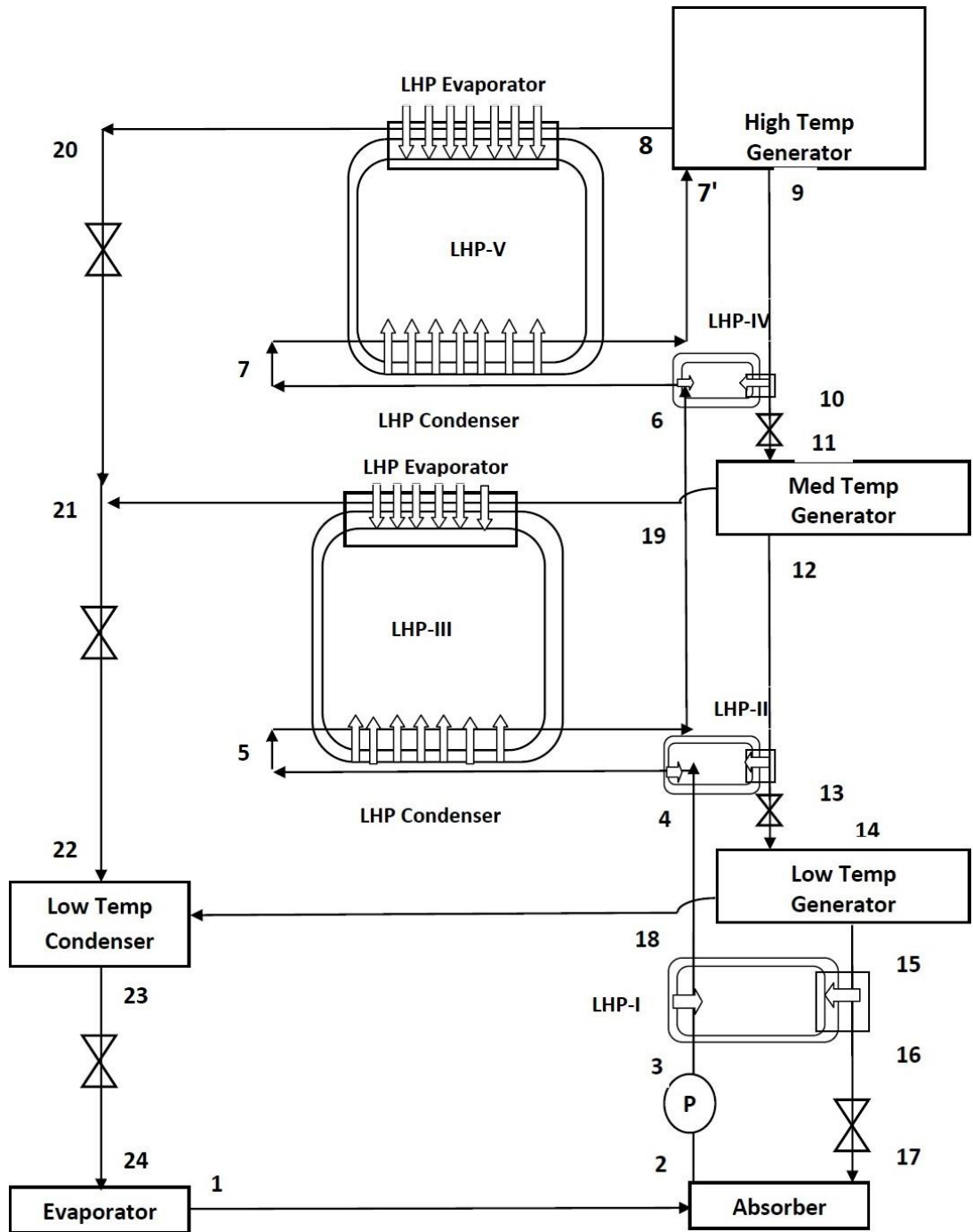


Fig 3.11: Modification-II in Triple Effect (Series) VARS using LHP

The mixture remaining in the high P-T generator is then throttled down to state 11 at the entrance of the medium P-T generator through HEX or LHP where some of the refrigerants evaporate with help of heat from condensing refrigerant in LHP-V and moves out towards the evaporator of LHP-III.

Performance Improvement of Vapour Absorption System Using Loop Heat Pipes

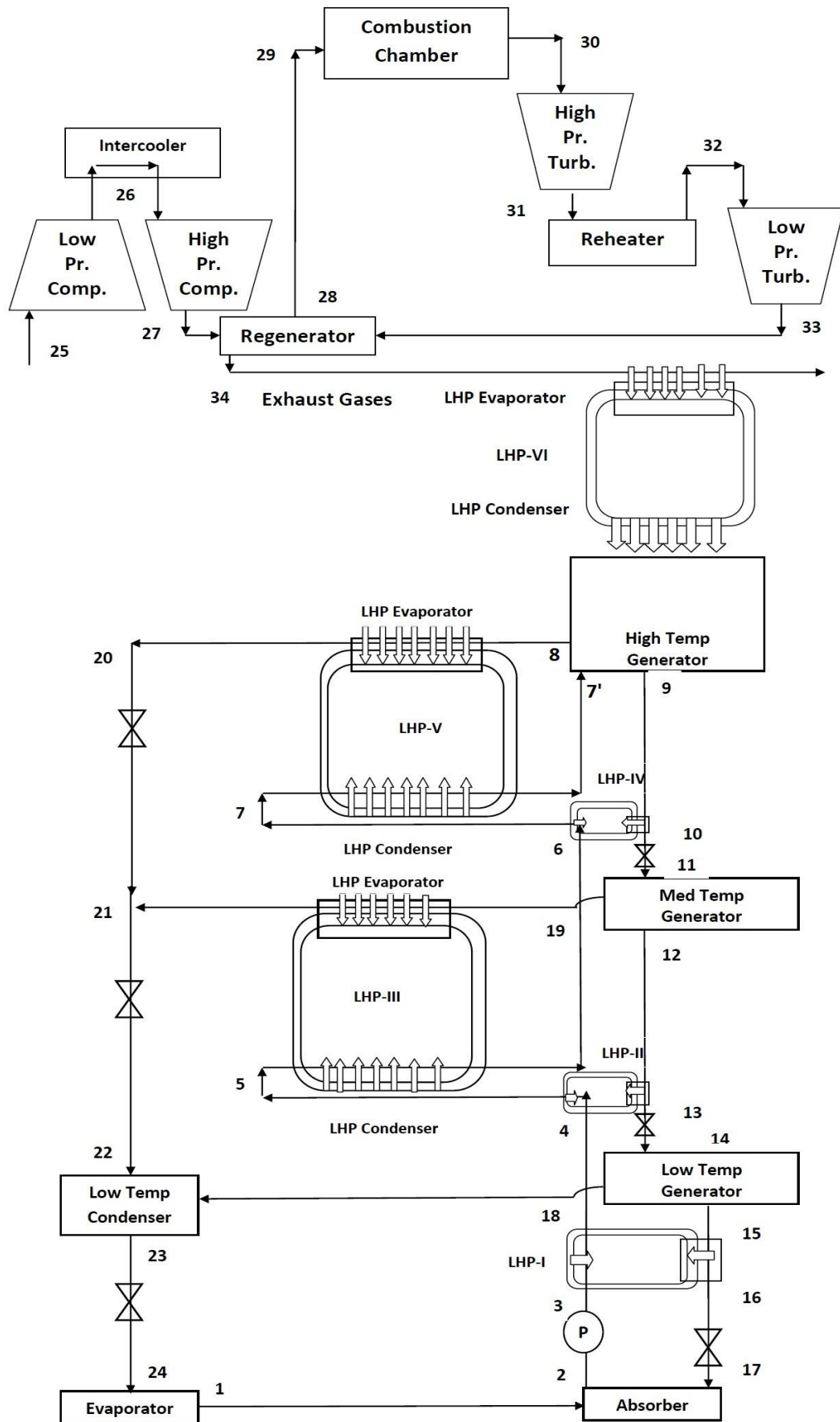


Fig 3.12: Modified Triple Effect (Series) VARS Combined with GPC using LHP

The remaining mixture in the Med P-T generator from state 12 is throttled down to a low P-T generator at the state 14 generators through HEx or LHP. Similar to the med P-T generator in a low P-T generator with intra-cycle heat exchange evaporation of refrigerant takes place and moves out to the low P-T condenser at state 18 where it mixes with the refrigerant from the Medium & High P-T generators. Finally, the remaining mixture in the low P-T generator is throttled from state 15 to the absorber inlet of state 17 through HEx or LHP as shown in Fig 3.10 & 3.11.

Whereas, Fig 3.12 shows the combination of GPC with modified triple effect VARS-II with GPC using LHP

3.5. Modifications Proposed in the Quadruple-Effect VARS:

The modified quadruple effect system -I (Fig 3.13) consists of 01 Evaporator, 04 Generators, 04 Refrigerant Expansion Valves, 04 Pressure Reducing valves, 01 Absorber, 04 Solution Heat Exchanger (HEx), and 03 condensers have been replaced by LHPs, which eliminates the bulkiness of the system and incorporates flexibility. The system is also fit for utilizing High-Temperature Energy sources for Operations.

Whereas, modification-II is obtained by replacing the 04 Solution Heat Exchanger with LHPs (Fig 3.14). Similar to the Double & Triple Effect VARS, heat is only supplied to the highest P-T generator other lower P-T generators operate on the intra-cycle heat exchange & and only a small fraction of refrigerant is evaporated in these generators in comparison to the highest P-T generator.

From the Evaporator at state 1, the refrigerant vapours move into the Absorber where the mixture solution is prepared in an exothermic process. From the absorber the solution from state 2 is pumped directly to the High Pressure- Temperature Generator-II at state 10 through the multiple Heat Exchangers & LHPs for pre-heating in Fig 3.13 & through LHPs in Fig 3.14. This Modified Quadruple VARS in which Med P-T Condenser, High P-T Condenser-I & II have been replaced by LHPs to utilize the intracycle waste heat recovery.

Performance Improvement of Vapour Absorption System Using Loop Heat Pipes

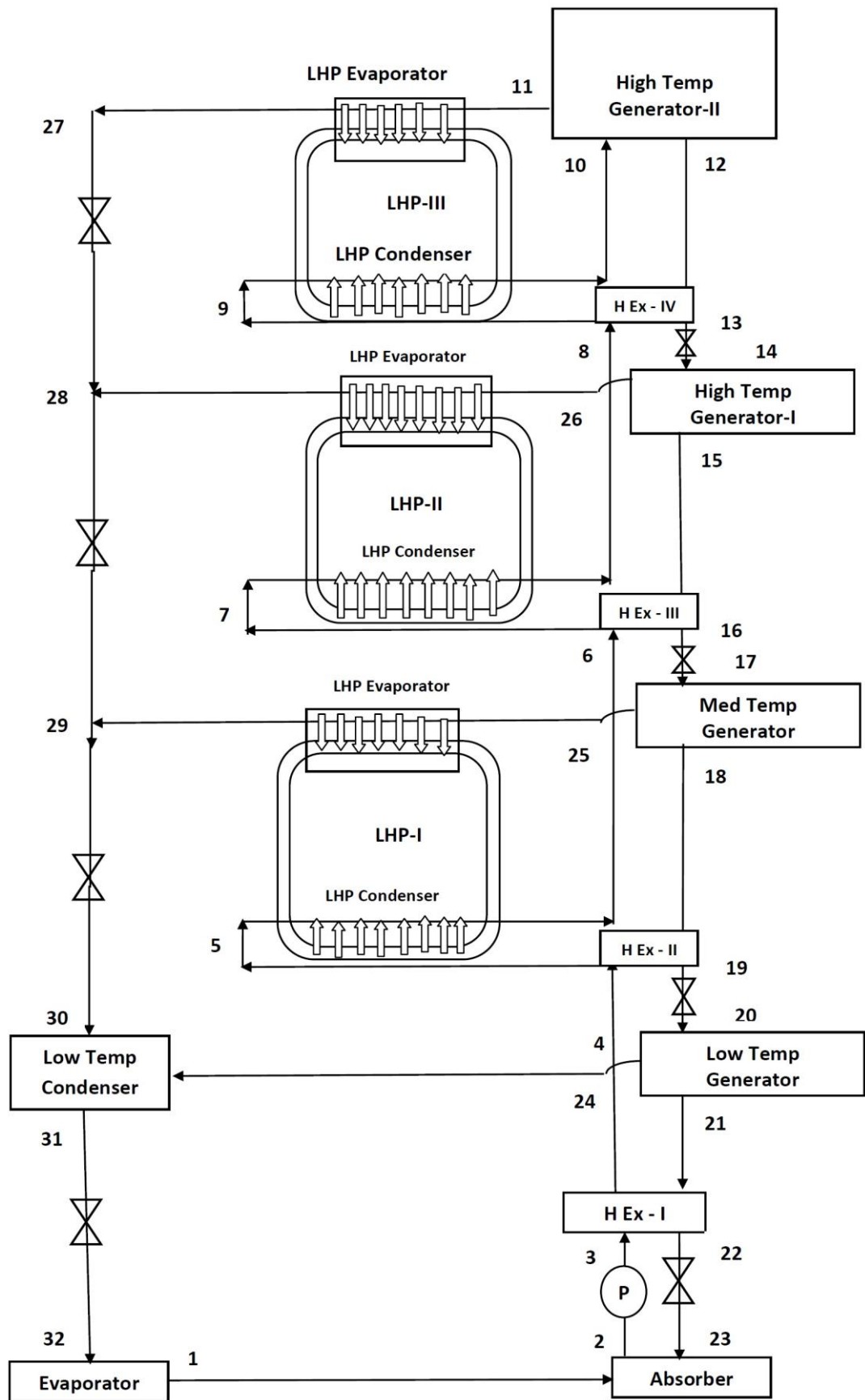


Fig 3.13: Modification-I in Quadruple Effect (Series) VARS using LHP

Performance Improvement of Vapour Absorption System Using Loop Heat Pipes

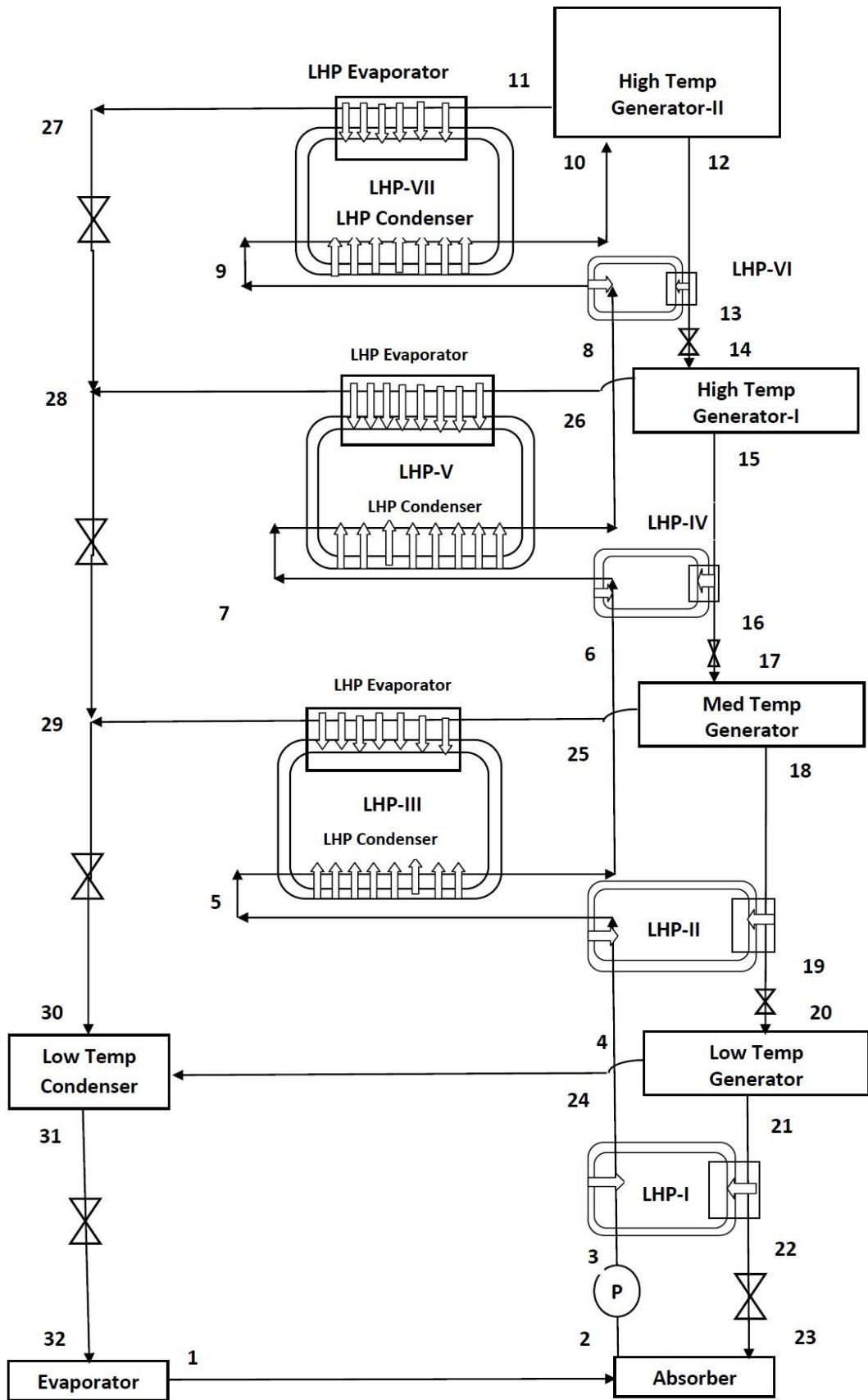


Fig 3.14: Modification-II in Quadruple Effect (Series) VARS using LHP

Performance Improvement of Vapour Absorption System Using Loop Heat Pipes

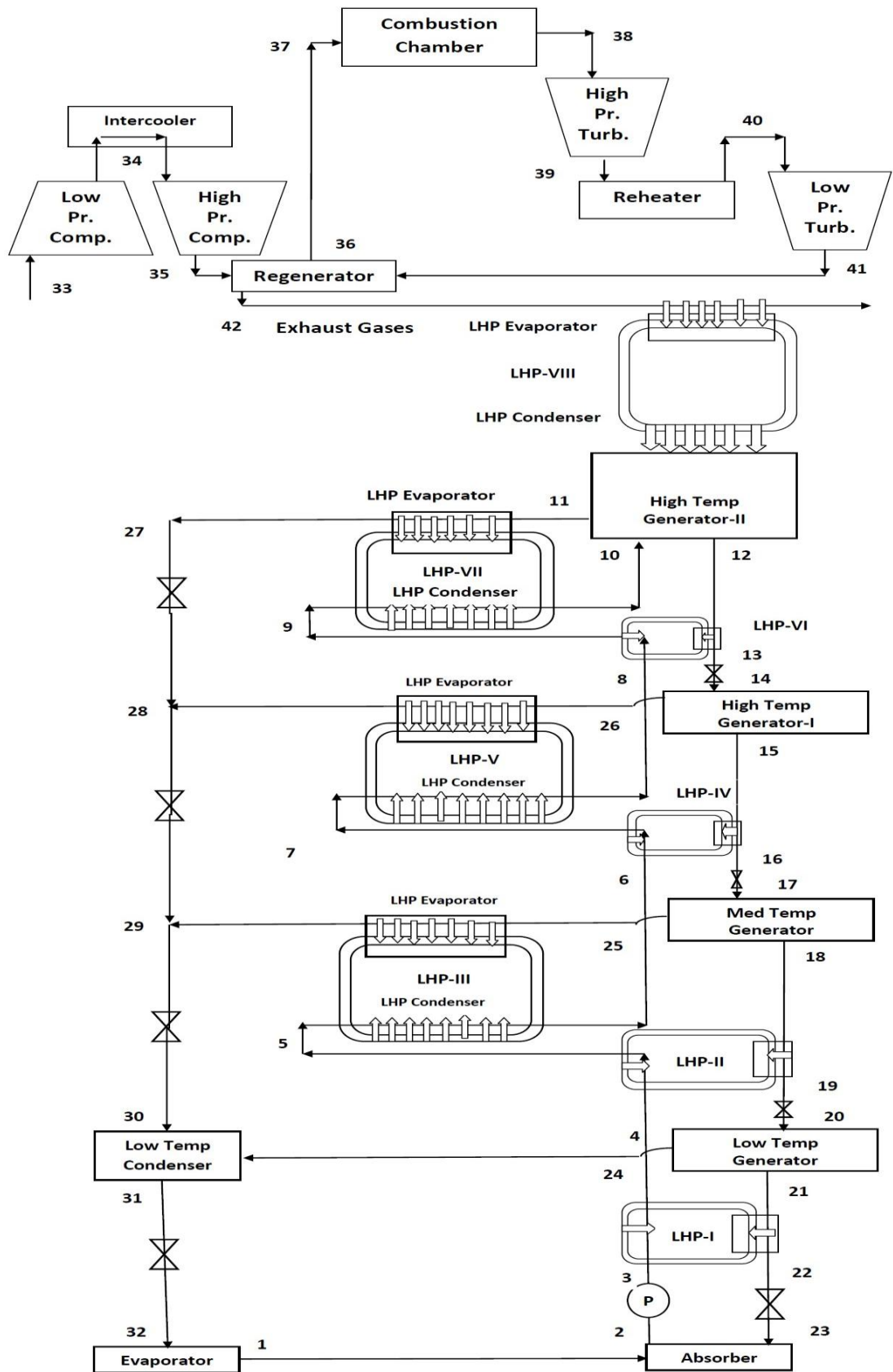


Fig 3.15: Modified Quadruple Effect (Series) VARS Combined with GPC using LHP

From Fig 3.13 & 3.14 it can be seen that in the High P-T generator-II refrigerant having a lesser boiling point temperature is evaporated and is extracted towards the

LHP Evaporator where condensation of the refrigerant vapour takes place and the heat is extracted by the LHP and the heat is transferred to the pre-heating of the mixture at low temperature. The liquid refrigerant which has condensed to saturated or sub-cooled at state 27 is throttled to state 28 where it's mixed with the fraction of vapour evaporated in High P-T generator-I at state 26 after being condensed in the LHP.

Furthermore, this mixture at state 28 is throttled to 29 where it is mixed with vapour coming out of the Med P-T generator at state 25 after being condensed in the LHP. This mixture is further throttled to the low P-T condenser at state 30 where it's mixed with the vapour coming out of the low P-T generator at state 24 after being condensed in the Low P-T Condenser. The final refrigerant quantity coming out of all the 04 generators at state 31 is finally throttled to the entrance of the evaporator at state 32.

The remaining solution in the High P-T generator-II after the evaporation of refrigerant rejects heat in the series of Heat Exchangers in Fig 3.13 & series of LHPs in Fig 3.14. After heat rejection, the mixture at stage 13 is throttled firstly to the High P-T generator-I at state 14, where a fraction of residual refrigerant in the solution is evaporated and sent to LHP for condensation at 26. The remaining mixture repeating the same process from 16 is throttled to Medium P-T generator at 17 where further evaporation of refrigerant fraction is extracted at state 25 and transferred to LHP for condensation. Similar to the previous process the remaining mixture at 19 is throttled to the low P-T generator at state 20 and the vapour generated in this generator is transferred to the Low P-T condenser where it is condensed and is mixed with the refrigerants coming out of other 03 generators.

Finally, the mixture left in the low P-T generator after extracting heat at 22 is throttled to the absorber at 23 completing the compression cycle. Furthermore, Fig 3.15 shows the combination of Modified Quadruple Effect-II with GPC as a heat source through LHP.

3.6. Combination ERS with GPC using LHP (Ankit Dwivedi, et. al. 2021) ^[190]

Fig 3.16 shows GPC combined with ERC using LHP for inter-cycle heat recovery. The GPC is a simple Cycle that doesn't consist of multiple compression or reheat cycles rather only regeneration.

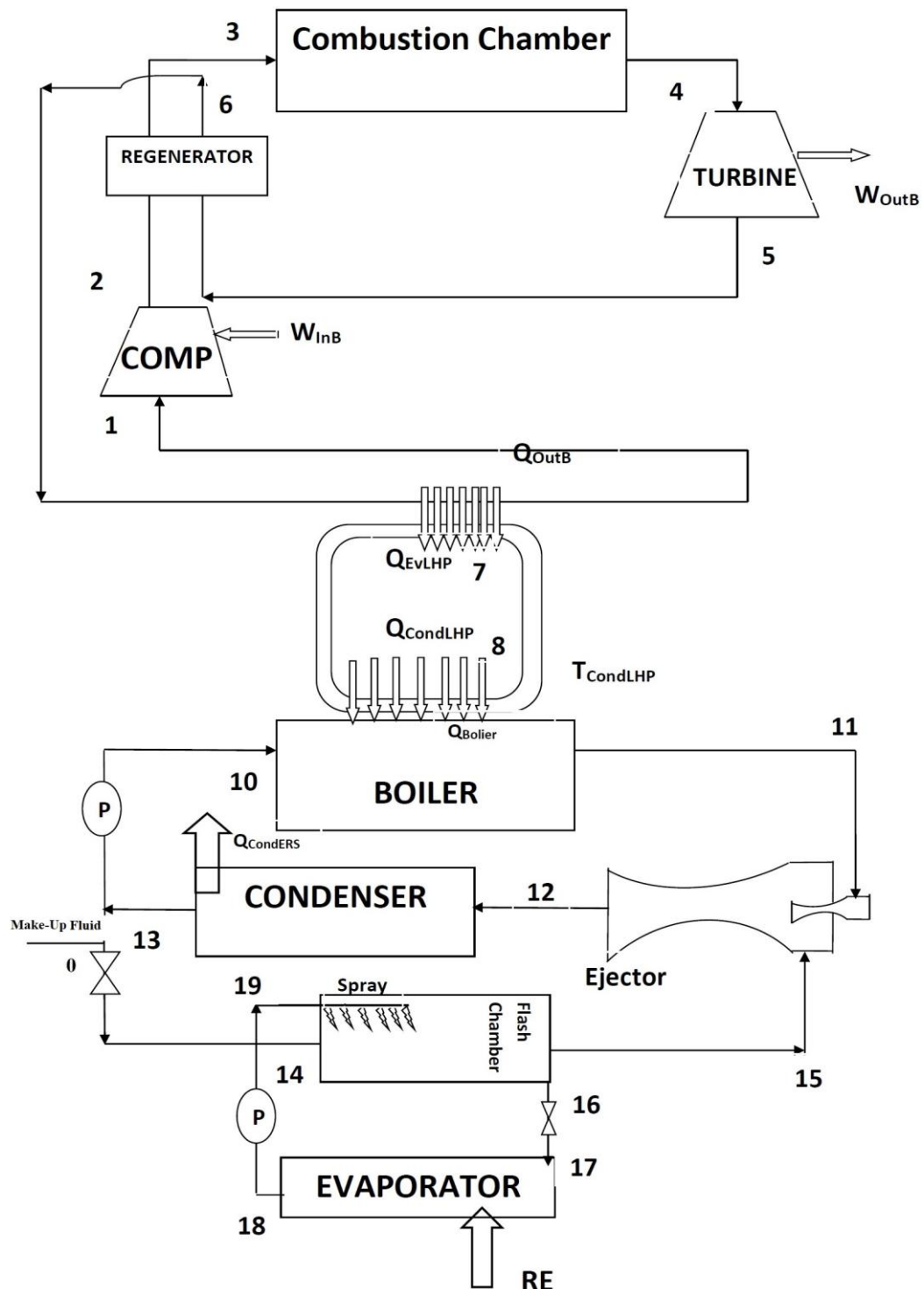


Fig 3.16: ERS Combined with GPC using LHP [190]

The exhaust of the GPC coming out of the regenerator at 8 is passed through the LHP evaporator resulting in the evaporation of the LHP working fluid which is then moved to the LHP condenser to reject the heat into the Boiler/Generator of the ERC and motive vapour is generated at state 13. This motive/primary vapour then expanded through a nozzle into the ejector Fig 3.16a. The sudden expansion of vapour causes a sudden drop of pressure further causing flashing of refrigerant vapour in the flash chamber and the consequent moving of secondary refrigerant into the ejector at state 15.

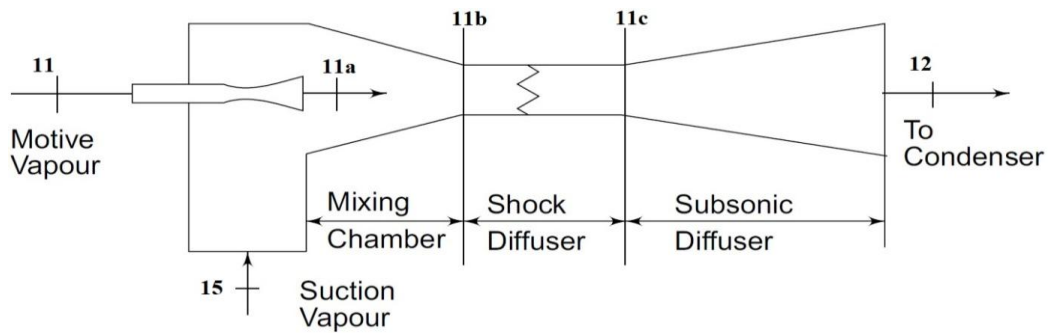


Fig 3.16a: The ejector of the ERS [175]

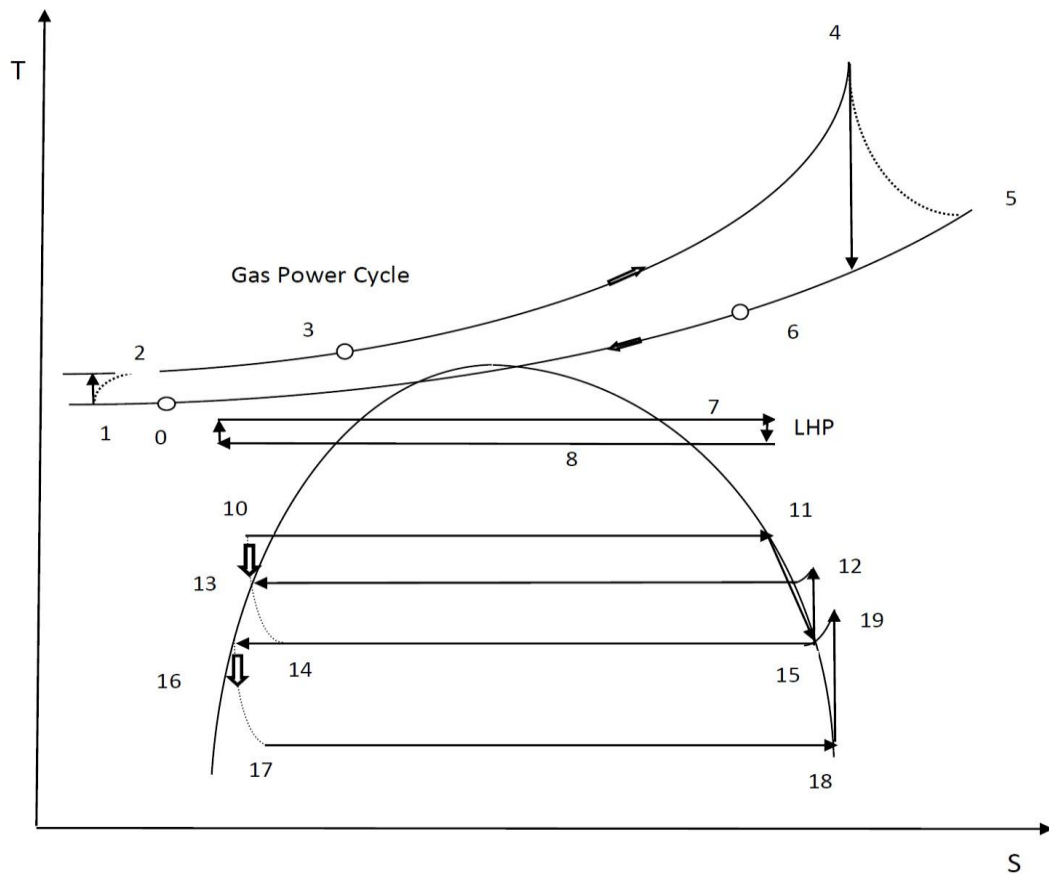


Fig 3.17: T-s plot of ERS Combined with GPC using LHP [186]

Owing to this flashing out in the flash chamber the overall temperature of the refrigerant in the flash chamber falls and this low-temperature refrigerant at state 16 is further throttled down to the low-temperature entrance of the evaporator at state 17, where it is evaporated to produce the refrigeration effect and comes out at 18 and is further compressed/pumped back to the flash chamber at 19.

After mixing the primary and secondary refrigerant vapour in the ejector, it enters the condenser at state 12 and the condensed liquid comes out of the condenser at 13 and is further pumped to the generator/boiled entrance at state 10. Moreover, the making fluid is also supplied to the flash chamber for maintaining the continuity of the cycle as per the requirements.

It can be observed very easily that the ERC is the combination of the Power Cycle & Refrigeration Cycle.

3.7. Combination ORC with GPC using LHP (Ankit Dwivedi, et. al. 2021)^[189] :

This section explains the combination of ORC with GPC using LHP. As mentioned in the chapter the ORC can work on the exhaust heat, geo heat, etc. Hence, a system is being proposed in which a GPC having multi-stage compression and expansion reheating has been combined with the ORC using LHP. Fig. 3.18 presents the schematic of the system in which the exhaust of GPC after the low-pressure turbine enters the LHP evaporator and rejects heat into the LHP working fluid which evaporates and moves to the LHP condenser which is ultimately used to supply the required heat to the Boiler of the ORC.

This heat rejected by the LHP condenser is harnessed in the boiler of ORC to evaporate the ORC working fluid which has been shown in 3 parts Economizer, Evaporator & Superheater from states 10 to 13. First, the heat exchange takes place in the superheater, then in the evaporator, and lastly in the economizer of the Boiler. This superheated vapour is then expanded in the turbine to generate the power output to the state 14.

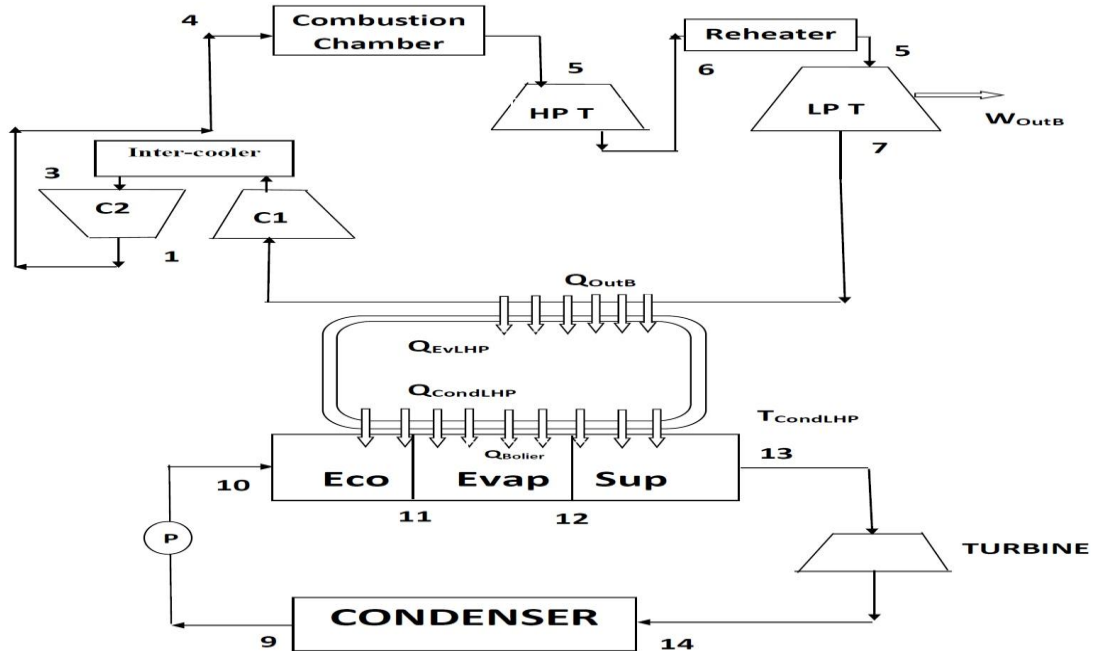


Fig 3.18: ORC Combined with GPC using LHP [189]

From the turbine outlet at state 14, the saturated or super-heated vapour flows into the condenser where heat rejection takes place and the working fluid is condensed to saturated liquid which is further pumped back to the high-pressure side at state 10

where it is heated in the economizer before evaporation. Fig 3.19 shows the T-s plot for the operation of the combined cycle. It is to be mentioned that the saturation dome does not represent the entire refrigerant rather it has been generalized. Realistic domes are presented in Fig 3.20 for certain fluids for a better idea.

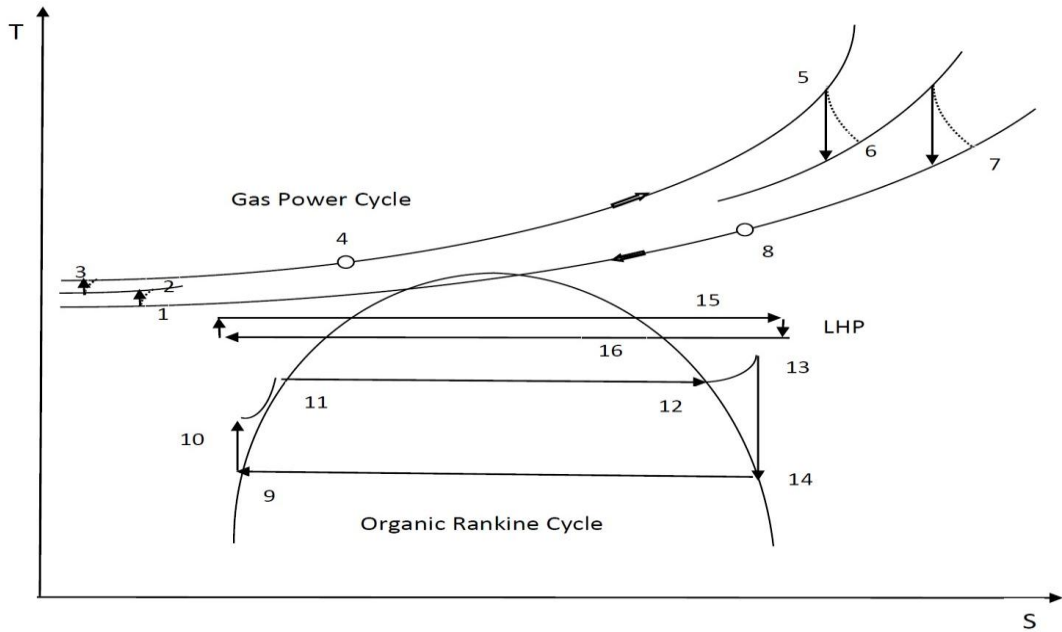


Fig 3.19: T-s plot of ORC Combined with GPC using LHP [185]

It has been assumed that a less minute temperature drop takes during the vapour line & nominal heating takes place in the liquid line of the LHP and the processes are more or less constant temperature. However, in reality, the vapour leaving the LHP Evaporator is superheated & liquid leaving the LHP condenser is sub-cooled as discussed in Chapter -1.

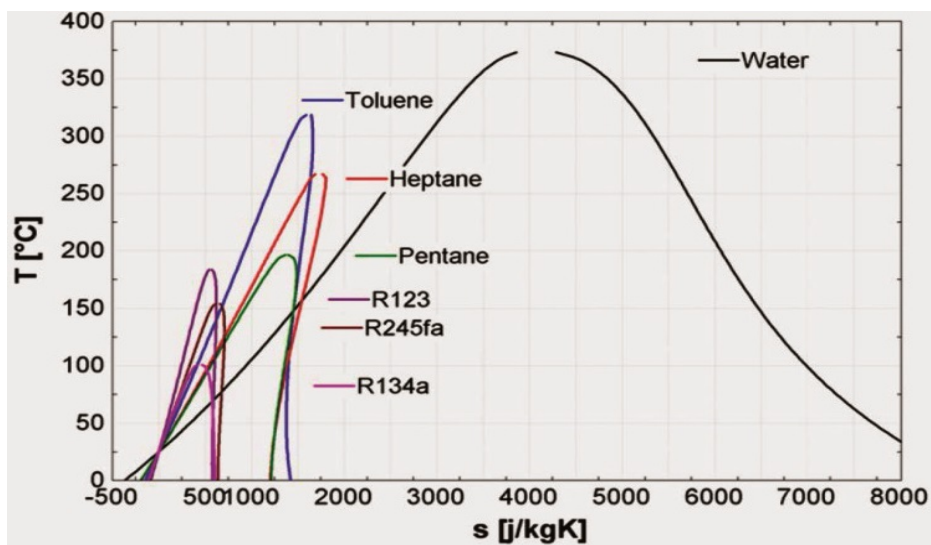


Fig 3.20: Saturation domes on T-s plot of ORC working fluids [167].

Chapter-4: Thermodynamic Modeling & Analysis of the Systems

The basis of all the systems presented in the previous chapter is the intra-cycle or inter-cycle waste heat recovery using LHPs. In the standard VAR systems, several modifications have been introduced by replacing the conventional Heat Exchangers & Condensers with LHPs. Also, GPC & VAR Systems have been combined through LHPs. Similar is the case of GPC & ERC and GPC & ORC.

Thermo-Mathematical Modeling has been achieved based on the various equations and modeling performed in the published literature & texts [164, 165, 166, 175, 176, 177], which have already been covered in Chapters 1 & 2. This Chapter Covers the complete mathematical modeling of all the following systems & iterations mentioned in Chapter-3:

- i. Modified Single Effect VARS**
 - Modification-I
 - Modification-II
 - Combined GPC & Single Effect VARS
- ii. Modified Half Effect VARS**
 - Modification-I
 - Modification-II
 - Combined GPC & Half Effect VARS
- iii. Modified Double Effect VARS**
 - Modification-I
 - Modification-II
 - Combined GPC & Double Effect VARS
- iv. Modified Triple Effect VARS**
 - Modification-I

- Modification-II
 - Combined GPC & Triple Effect VARS
- v. Modified Quadruple Effect VARS
- Modification-I
 - Modification-II
 - Combined GPC & Quadruple Effect VARS
- vi. Combined GPC & ERC
- vii. Combined GPC & ORC

4.1. Thermodynamic Modeling of Gas Power Cycle (GPC)

Figure 4.1 shows the GPC under consideration. To avoid repetition, the regenerative-reheat cycle with multi-compression has been modeled in this section and will be used with minute changes in the notations. Table 4.1 contains the input variable and data fixed for the analysis.

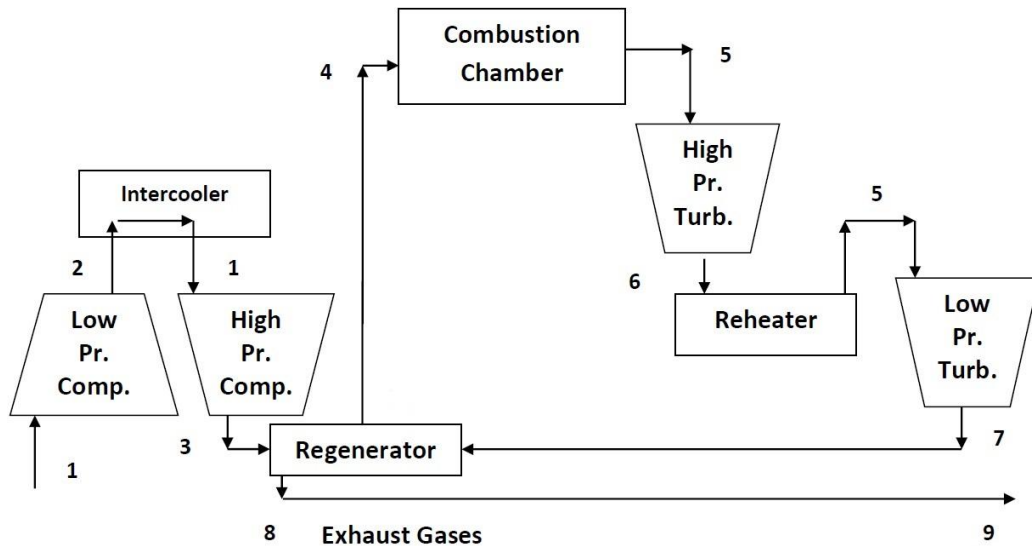


Fig. 4.1: Common Schematic of GPC

Isentropic compression is the work required for the compressor (States 1-2 & 1-3) assuming perfect intercooling i.e., temperature to the entrance of the compressors is

the same. Moreover, reheat is also perfect, hence, the temperature at the entrance of the turbines is the same.

$$T_2/T_1 = r^{(\gamma-1/2\gamma)} = T_5/T_6, \quad (4.1)$$

$$T_2 = T_1 + (T_2 - T_1)/\eta_C = T_3 \text{ \& } T_6 = T_5 - (T_5 - T_6)\eta_T, = T_7 \quad (4.2)$$

Where η_T can be taken as 0.92 & η_C can be taken as 0.86

$$W_{inB} = 2 \times (H_3 - H_1) = 2 \times m_a c_{pa} (T_3 - T_1) \quad (4.3)$$

Isobaric heat addition the net heat added is given by

$$Q_{add} = H_5 - H_4 + H_5 - H_6 = m_a c_{pa} (T_5 - T_4) + (m_a + m_f) c_{pg} (T_5 - T_6) \quad (4.4)$$

Isentropic expansion the work done by turbine is given by

$$W_{outB} = H_5 - H_7 + H_5 - H_6 = \dot{m}_g c_{pg} (T_5 - T_7 + T_5 - T_6) \quad (4.5)$$

$$W_{NetB} = W_{outB} - W_{inB} \quad (4.6)$$

$$\eta_B = W_{NetB} / Q_{add} \quad (4.7)$$

Heat Exchanged in the Regenerator

$$Q_R = H_4 - H_3 = \dot{m}_a c_{pa} (T_4 - T_3) \quad (4.8)$$

$$\text{Where, } T_4 = T_3 + \epsilon_R (T_7 - T_3) \quad (4.9)$$

Heat rejection (in a heat exchanger) at Constant Pressure, can be given by

$$Q_{Rej} = H_8 - H_9 = \dot{m}_g c_{pg} (T_8 - T_1) \quad (4.10)$$

$$\text{Where } T_8 = T_7 - \epsilon_R (T_7 - T_3) \text{ \& } \epsilon_R \text{ can be taken as 0.75} \quad (4.11)$$

Exergy Analysis:

Compressor

Exergy & Irreversibility for Compressor

$$X_{Comp} = m_a (h_1 - h_3) - T_o m_a (s_3 - s_1) \quad (4.12)$$

$$I_{Comp} = T_o m_a (s_3 - s_1) \quad (4.13)$$

$$\text{Where } s_3 - s_1 = c_{Pa} (T_3 - T_1) - R_a \ln(P_3/P_1) \quad (4.14)$$

Regenerator

$$\Delta S_{RH} = S_{Ho} - S_{Hi} \quad (4.15)$$

$$\Delta S_{RC} = S_{Co} - S_{Ci} \quad (4.16)$$

$$X_C = (h_{Co} - h_{Ci}) - T_o (s_{Co} - s_{Ci}) \quad (4.17)$$

$$X_H = (h_{Hi} - h_{Ho}) - T_o (s_{Hi} - s_{Ho}) \quad (4.18)$$

$$I_R = T_o \Delta \dot{S}_o = T_o [\dot{m}_g (s_7 - s_8) - \dot{m}_a (s_4 - s_3)] \quad (4.19)$$

$$\text{Where, } s_7 - s_8 = c_{Pg} \ln(T_7/T_8) \text{ \& } s_4 - s_3 = c_{Pa} \ln(T_4/T_3) \quad (4.20)$$

Combustion Chamber:

$$X_{CC} = Q_{add} - T_o S_{gen} \tag{4.21}$$

$$I_{CC} = T_o S_{gen} \tag{4.22}$$

$$\text{Where, } S_{gen} = \dot{m}_g c_{Pg} \ln(T_5/T_4) - \dot{Q}_{add}/T_{av} \tag{4.23}$$

Turbine:

$$X_T = m_g (h_5 - h_7) - T_o m_g (s_5 - s_7) \tag{4.24}$$

$$I_T = T_o m_g (s_5 - s_7) \tag{4.25}$$

$$\text{Where, } s_5 - s_7 = c_{Pg} (T_5 - T_7) - R_g \ln(P_5/P_7) \tag{4.26}$$

$$I_{TotalORC} = I_{Comp} + I_{CC} + I_R + I_T \tag{4.27}$$

$$\text{Exergetic efficiency} = \frac{W_{net}}{W_{net} + I_{total}} \tag{4.28}$$

4.2. Modified Single Effect VARS

This section deals with the modeling of the 03 systems obtained with the modifications proposed using LHPs.

4.2.1. Modified Single Effect VARS-I (Ankit Dwivedi, et. al. 2018) ^[183]

Fig 4.2 shows the system under consideration which has been elaborately discussed in Chapter-3.

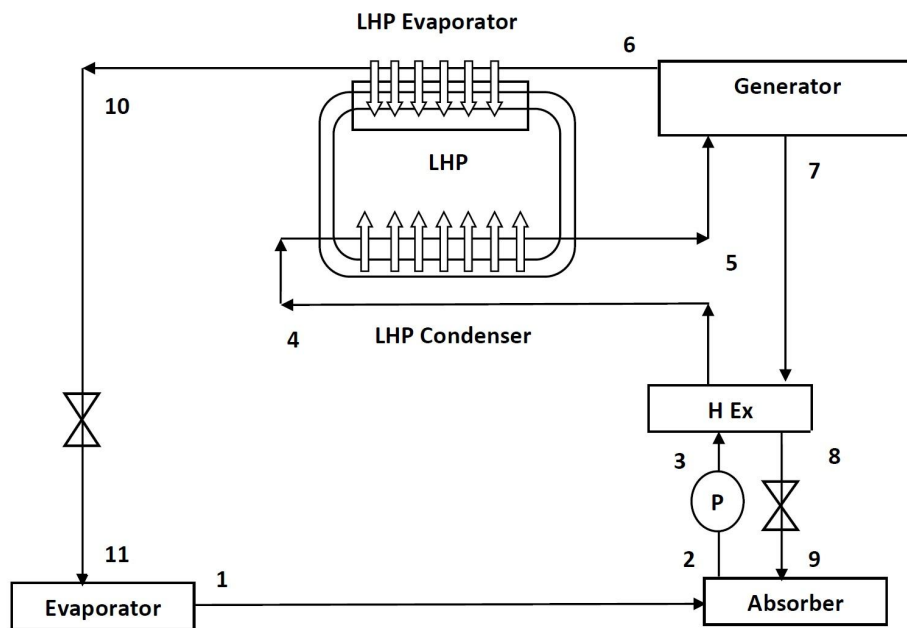


Fig. 4.2: Modified Single Effect VARS-I [183]

This system consists of the following components such as:

- a. Refrigerant Expansion Valve (States 10-11)
- b. Evaporator (States 11-1)
- c. Absorber (States 1-2 & 9-2)
- d. Mixture Pump (States 2-3)
- e. Mixture Heat Exchanger (States 3-4 & 7-8)
- f. LHP Condenser (States 4-5)
- g. Generator (States 5-6 & 5-7)
- h. LHP Evaporator (States 6-10)
- i. Mixture Reducing Valve (States 8-9)

Mass Continuity Equations, m:

$$m_6 = m_{10} = m_{11} = m_1 \quad (4.29)$$

$$m_2 = m_3 = m_4 = m_5 \quad (4.30)$$

$$m_7 = m_8 = m_9 \quad (4.31)$$

$$m_5 = m_6 + m_7 \quad (4.32)$$

Chemical Composition Balance Equations, mζ:

$$m_4 \zeta_4 = m_7 \zeta_7 \quad (4.33)$$

Percentage Absorbent Balance Equation, ζ:

$$\zeta_2 = \zeta_3 = \zeta_4 = \zeta_5 \quad (4.34)$$

$$\zeta_7 = \zeta_8 = \zeta_9 \quad (4.35)$$

$$\text{COP} = \text{RE} / (\text{Q}_G + \text{W}_P) \quad (4.36)$$

Solution Circulation Ratio, F:

$$F = \zeta_4 / (\zeta_7 - \zeta_4) \quad (4.37)$$

- a. Refrigerant Expansion Valve (States 10-11)

The isenthalpic process takes place in the Expansion Valve in which pressure & temperature reduces owing to the fractional flashing out of Condensed Liquid Refrigerant coming out of the LHP, hence the Specific Enthalpy, h & Dryness fraction, x at the exit of the Expansion Valve can be Expressed as,

$$h_{11} = h_{10} \quad (4.38)$$

Where h_{10} is the enthalpy of saturated liquid exiting the LHP Evaporator as x_{10} is 0 for this state.

$$x_{11} = (h_{10} - h_{f11}) / h_{fg11} \quad (4.39)$$

Here h_{f11} is the enthalpy of saturated liquid at pressure of state 11 & h_{fg11} is the enthalpy of evaporation at the pressure of state 11.

b. Evaporator (States 11-1)

The process in the evaporator is the Isobaric Heat Addition in which heat is added to the refrigerant where it gets evaporated called the Refrigerating Effect (RE). The exit of the evaporator is saturated vapour hence the x_1 is 1 for this state. The modeling can be given as:

Energy Analysis:

$$RE = m_1(h_1 - h_{11}) \quad (4.40)$$

Exergy Analysis:

$$X_{Evap} = m_{1'}[(h_{11'} - h_{1'}) - T_O (s_{11'} - s_{1'})] \quad (4.41)$$

Where X_{Evap} is the Exergy of the Evaporator, s is the corresponding specific entropy & T_O is the environment temperature. The states 11' & 1' are the inlet and outlet states of the fluid getting cooled in the evaporator. $m_{1'}$ is the mass flow rate of the fluid.

c. Absorber (States 1-2 & 9-2)

The exothermic mixing process takes place in the absorber in which Q_{Abs} is rejected to the surrounding. Also, after exiting the mixture reducing valve the absorbent enters the absorber. Hence the modeling can be done in the following manner:

Energy Analysis:

$$Q_{Abs} = m_1 h_1 + m_9 h_9 - m_2 h_2 \quad (4.42)$$

Exergy Analysis:

$$X_{Abs} = m_2 [(h_9 - h_2) - T_0 (s_9 - s_2)] \quad (4.43)$$

Where X_{Abs} is the Exergy of the Absorber, s is the corresponding specific entropy & T_0 is the environment temperature and the states 9' & 2' are the inlet and outlet states of the fluid getting heated in the absorber. m_2 is the mass flow rate of the fluid.

d. Mixture Pump (States 2-3)

Mixture pump can be seen as pumping the mixture in a reversible adiabatic compression process of liquid, the Work input in the Pump can be given as W_p :

$$W_p = m_2 v_2 (dP) \quad (4.44)$$

Where v_2 is the specific volume of the mixture and dP is the pressure raised by the pump.

Also, Specific Enthalpy at the Exit of the Pump can be given as:

$$h_3 = m_2 h_2 + W_p \quad (4.45)$$

e. Mixture Heat Exchanger (States 3-4 & 7-8)

The mixture Heat exchanger is used to exchange heat between the low-temperature mixture at state 3 and the high-temperature absorbent at state 7 the process is isobaric heat exchange and can be modeled as the followings:

Energy Analysis:

$$\text{Effectiveness of Heat Exchanger, } \epsilon_{H-EX} = (T_7 - T_8) / (T_7 - T_3) \quad (4.46)$$

$$\text{Heat Exchange in the Heat Exchanger, } Q_{H-EX} = m_4 (h_4 - h_3) = m_7 (h_7 - h_8) \quad (4.47)$$

$$\text{Specific Heat Capacity for Hot Fluid, } c_{Hot} = (h_7 - h_8) / (T_7 - T_8) \quad (4.48)$$

$$\text{Specific Heat Capacity for Cold Fluid, } c_{Cold} = (h_4 - h_3) / (T_4 - T_3) \quad (4.49)$$

Exergy Analysis:

$$X_{H-Ex} = m_3[(h_3-h_4) - T_O (s_3-s_4)] \quad (4.50)$$

Where X_{H-Ex} is the Exergy of the Heat Exchanger, s is the corresponding specific entropy & T_O is the environment temperature.

f. LHP Condenser (States 4-5)

The detailed modeling of the LHP has been presented in Chapter-1, Section 1.1.9, and from Eq. 1.1 to Eq. 1.47. The heat transfer to the mixture at stage 04 in the LHP Condenser is the heat exchange between a condensing fluid and a liquid mixture, which can be modeled as:

Energy Analysis:

$$\text{Heat Input to the Mixture, } Q_{InMix} = m_5(h_5-h_4) \quad (4.51)$$

Heat Rejected by the Condensing Fluid in LHP,

$$Q_{LHPCond} = m_{LHP} (h_{fgLHPCond} + c_F \Delta T_{Sub}) \quad (4.52)$$

Where $h_{fgLHPCond}$ is the latent heat of condensation in the LHP Condenser, c_F is the specific heat capacity, m_{LHP} is the mass flow in the LHP & ΔT_{Sub} is the degree of subcooling in the LHP condenser for the LHP working fluid.

$$\text{Effectiveness of the LHP Condenser, } \epsilon_{LHPCond} = (T_5-T_4) / (T_{InLHPCond}-T_4) \quad (4.53)$$

Where $T_{InLHPCond}$ is the Input Temperature of the LHP Condenser.

Exergy Analysis:

$$X_{LHPCond} = m_3[(h_4-h_5) - T_O (s_4-s_5)] \quad (4.54)$$

Where $X_{LHPCond}$ is the Exergy of the Heat Exchanger, s is the corresponding specific entropy & T_O is the environment temperature.

g. Generator (States 5-6 & 5-7)

Heat is added to the mixture in the generator. This heat Q_G can be expressed as:

Energy Analysis:

$$Q_G = h_6m_6 + h_7m_7 - h_5m_5 \quad (4.55)$$

Exergy Analysis:

$$X_G = m_{6'}[(h_{6'} - h_{7'}) - T_O (s_{6'} - s_{7'})] \quad (4.56)$$

Where X_G is the Exergy of the Generator, s is the corresponding specific entropy & T_O is the environment temperature and the states 6' & 7' are the inlet and outlet states of the fluid supplying heat to the generator. $M_{6'}$ is the mass flow rate of the fluid.

h. LHP Evaporator (States 6-10)

Heat exchange in the LHP Evaporator takes place between Condensing Refrigerant & Evaporating LHP Working Fluid. It has to be mentioned that the temperature of the evaporator is ascertained by the Condensation Temperature of the Refrigerant. Also, there's a very minute temperature drop in the LHP. In addition to the LHP Modeling explained in Chapter-1, the heat transfer can be modeled as:

Energy Analysis:

$$\text{Heat Rejected by the Condensing Refrigerant, } Q_{\text{CondR}} = m_6(h_6 - h_{10}) \quad (4.57)$$

Heat Absorbed by the LHP Working Fluid in the LHP Evaporator,

$$Q_{\text{LHPEvap}} = m_{\text{LHP}}(h_{\text{fgLHPEvap}} + c_F \Delta T_{\text{Sup}}) \quad (4.58)$$

Where $h_{\text{fgLHPEvap}}$ is the latent heat of evaporation in the LHP Evaporator, c_F is the specific heat capacity, m_{LHP} is the mass flow in the LHP & ΔT_{Sup} is the degree of superheat in the LHP evaporator for the LHP working fluid.

Also, the maximum heat capacity of an LHP Evaporator has been given based on Sonic, Entrainment & Capillary Limits in Eq 1.41 to 1.43. Out of these, the lowest value has been chosen.

Exergy Analysis:

$$X_{\text{LHPEvap}} = m_6[(h_6 - h_{10}) - T_O (s_6 - s_{10})] \quad (4.59)$$

Where X_{LHPEvap} is the Exergy of the LHP Evaporator, s is the corresponding specific entropy & T_O is the environment temperature.

i. Mixture Reducing Valve (States 8-9)

The isenthalpic process takes place in the Mixture Reducing Valve in which pressure & temperature reduces for the absorbent coming out of the Heat Exchanger, hence the Specific Enthalpy, h can be expressed as,

$$h_8 = h_9 \tag{4.60}$$

4.2.2. Modified Single Effect VARS-II

Fig 4.3 shows the system under consideration which has been elaborately discussed in Chapter-3. As it has been suggested in the previous chapter that modification-II is obtained by replacing the mixture heat exchanger with LHP. Hence, there are 02 sets of LHPs (LHP-I & LHP-II) in the system being used for the intra-cycle Heat Transfer.

Consequently, state 4 i.e., the inlet of the LHP-II, and state 8 i.e., the inlet to the mixture reducing valve will be modified owing to the different effectiveness of the LHP-I.

The modeling of this system has been achieved by replacing the HEx equations with LHP Equations in the previous section:

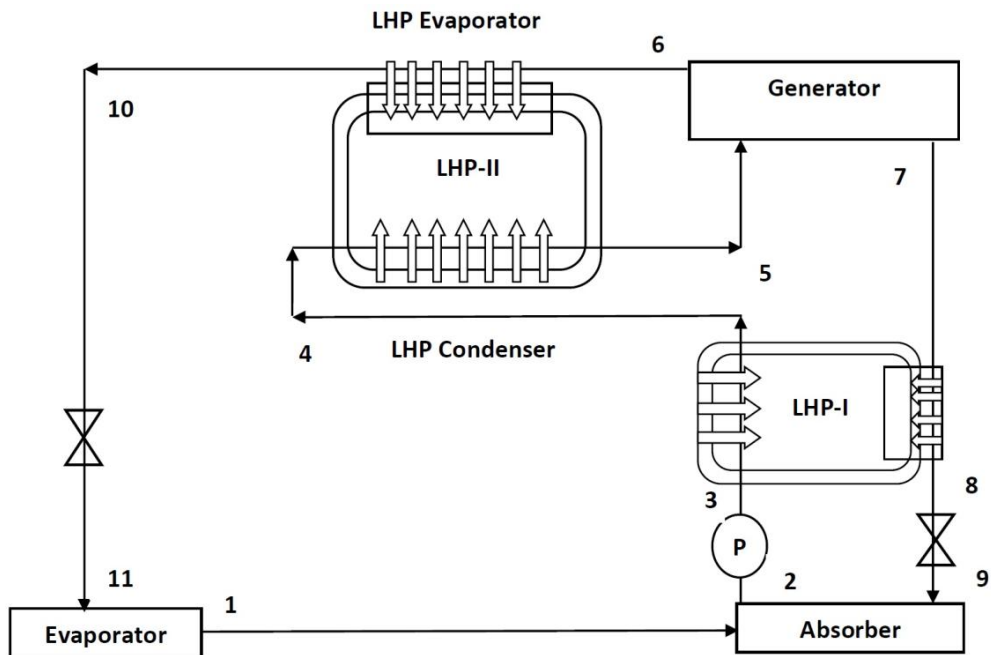


Fig. 4.3: Modified Single Effect VARS-II

e. LHP-I for the Mixture Heat Exchange (States 3-4 & 7-8)

Similar to the LHP-I, the heat is absorbed in the LHP Evaporator (States 7-8) & Rejected in the LHP Condenser (States 3-4) of LHP-I.

- **LHP-I Condenser**

Energy Analysis:

Heat Input to the Mixture, $Q_{InMixI} = m_3(h_4-h_3)$ (4.61)

Heat Rejected by the Condensing Fluid in LHP,

$$Q_{LHPICond} = m_{LHPI} (h_{fgLHPICond} + c_F \Delta T_{SubI})$$
 (4.62)

Where $h_{fgLHPICond}$ is the latent heat of condensation in the LHP-I Condenser, c_F is the specific heat capacity, m_{LHPI} is the mass flow in the LHP-I & ΔT_{SubI} is the degree of subcooling in LHP-I condenser for the LHP-I working fluid.

Effectiveness of the LHP-I Condenser, $\epsilon_{LHPICond} = (T_4-T_3) / (T_{InLHPICond}-T_3)$ (4.63)

Where $T_{InLHPICond}$ is the Input Temperature of the LHP-I Condenser.

Exergy Analysis:

$$X_{LHPICond} = m_3[(h_3-h_4) - T_O (s_3-s_4)]$$
 (4.64)

Where $X_{LHPICond}$ is the Exergy of the LHP-I, s is the corresponding specific entropy & T_O is the environment temperature.

- **LHP-I Evaporator**

Energy Analysis:

Heat Rejected by the Absorbent, $Q_{RejI} = m_7(h_7 - h_8)$ (4.65)

Heat Absorbed by the LHP-I Working Fluid in the LHP-I Evaporator,

$$Q_{LHPIEvap} = m_{LHPI} (h_{fgLHPIEvap} + c_F \Delta T_{SupI})$$
 (4.66)

Where $h_{fgLHPIEvap}$ is the latent heat of evaporation in the LHP-I Evaporator, c_F is the specific heat capacity, m_{LHPI} is the mass flow in the LHP-I & ΔT_{SupI} is the degree of superheat in the LHP-I evaporator for the LHP-I working fluid.

Also, the maximum heat capacity of an LHP Evaporator has been given based on Sonic, Entrainment & Capillary Limits in Eq 1.41 to 1.43. Out of these, the lowest value has been chosen.

Exergy Analysis:

$$X_{\text{LHP-IEvap}} = m_7[(h_7-h_8) - T_O (s_7-s_8)] \quad (4.67)$$

Where $X_{\text{LHP-IEvap}}$ is the Exergy of the LHP-I Evaporator, s is the corresponding specific entropy & T_O is the environment temperature.

4.2.3. Combined GPC & Single Effect VARS

Fig 4.4 shows the combination of GPC & Single Effect VARS using LHP. To obtain the modeling of this system the GPC has been added to the Modified VARS-II through an LHP (LHP-III). Hence, the GPC & the LHP-III are added in the following point to the Modification-II. To avoid repetition, the regenerative -reheat cycle with multi-compression has been modeled in this section and will be used with minute changes in the notations.

j. Gas Power Cycle (State 12-21)

k. LHP-III

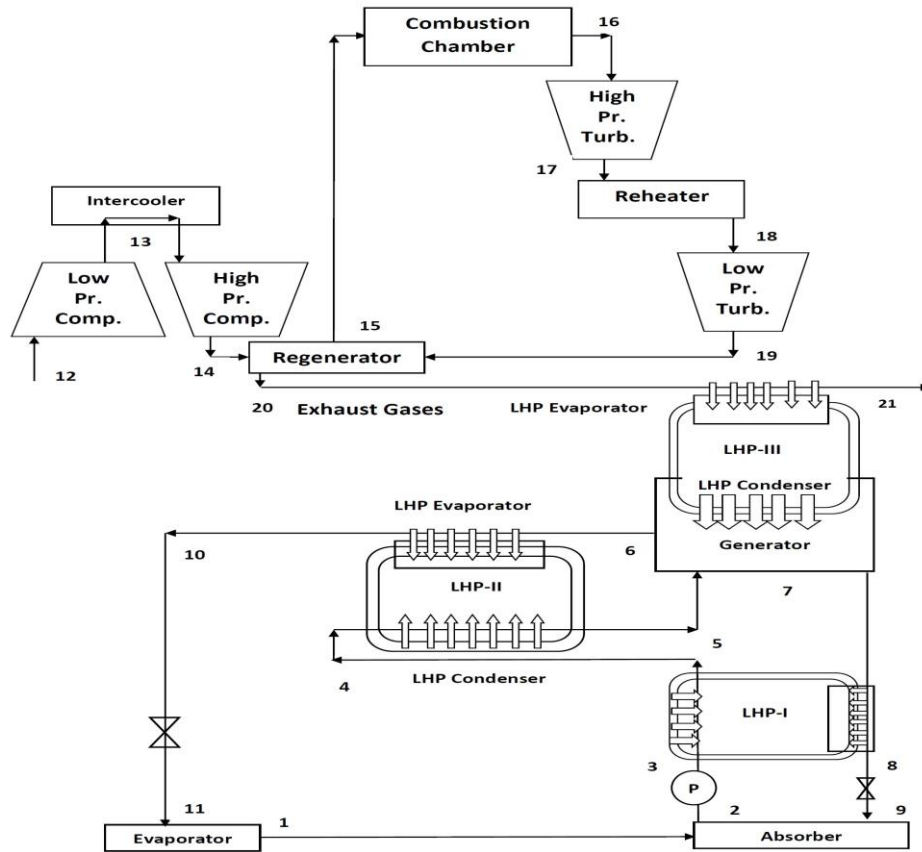


Fig. 4.4: Combined GPC & Single Effect VARS

j. Gas Power Cycle (State 12-21)

In this system, the entrance to the GPC is at state 12 and the exhaust leaves the regenerator at state 20 & leaves the LHP-III Evaporator at state 21. Also, the temperature in state 16 & state 18 is the same. The heat input to the LHP-III, $Q_{InLHPIII}$ can be calculated as:

$$Q_{InLHPIII} = \dot{m}_g c_{pg} (T_{20} - T_{21}) \tag{4.68}$$

k. LHP-III

The heat rejected at the exhaust of GPC is harnessed by the LHP-III Evaporator and transferred to the VARS Generator through LHP-III Condensers.

• LHP-III Evaporator

Energy Analysis:

$$Q_{InLHPIII} = \dot{m}_g c_{pg} (T_{20} - T_{21}) \tag{4.69}$$

Heat Absorbed by the LHP-III Working Fluid in the LHP-III Evaporator,

$$Q_{LHP\text{III}Evap} = m_{LHP\text{III}} (h_{fgLHP\text{III}Evap} + c_F \Delta T_{Sup\text{III}}) \quad (4.70)$$

Where $h_{fgLHP\text{III}Evap}$ is the latent heat of evaporation in the LHP-III Evaporator, c_F is the specific heat capacity, $m_{LHP\text{III}}$ is the mass flow in the LHP-III & $\Delta T_{Sup\text{III}}$ is the degree of superheat in the LHP-III evaporator for the LHP-III working fluid.

Also, the maximum heat capacity of an LHP Evaporator has been given based on Sonic, Entrainment & Capillary Limits in Eq 1.41 to 1.43. Out of these, the lowest value has been chosen.

Exergy Analysis:

$$X_{LHP\text{III}Evap} = m_g [(h_{20} - h_{21}) - T_O (s_{20} - s_{21})] \quad (4.71)$$

Where $X_{LHP\text{III}Evap}$ is the Exergy of the LHP-III Evaporator, s is the corresponding specific entropy & T_O is the environment temperature.

• **LHP-III Condenser**

Energy Analysis:

$$\text{Heat Input to the Generator, } Q_{InGenerator} = h_6 m_6 + h_7 m_7 - h_5 m_5 \quad (4.72)$$

Heat Rejected by the Condensing Fluid in LHP into the Generator,

$$Q_{LHP\text{III}Cond} = m_{LHP\text{III}} (h_{fgLHP\text{III}Cond} + c_F \Delta T_{Sub\text{III}}) \quad (4.73)$$

Where $h_{fgLHP\text{III}Cond}$ is the latent heat of condensation in the LHP-III Condenser, c_F is the specific heat capacity, $m_{LHP\text{III}}$ is the mass flow in the LHP-III & $\Delta T_{Sub\text{III}}$ is the degree of subcooling in the LHP-III condenser for the LHP-III working fluid.

4.3. Modified Half Effect VARS

This section deals with the modeling of the 03 Half Effect Systems Obtained with the modifications proposed using LHPs.

4.3.1. Modified Half Effect VARS-I (Ankit Dwivedi, et. al. 2018) [184]

Fig 4.5 shows the Modified Half Effect VARS-I which has been elaborately discussed in Chapter-3. Similar to the previous section we will attempt the Thermo-Mathematical Modeling of this system for the following components.

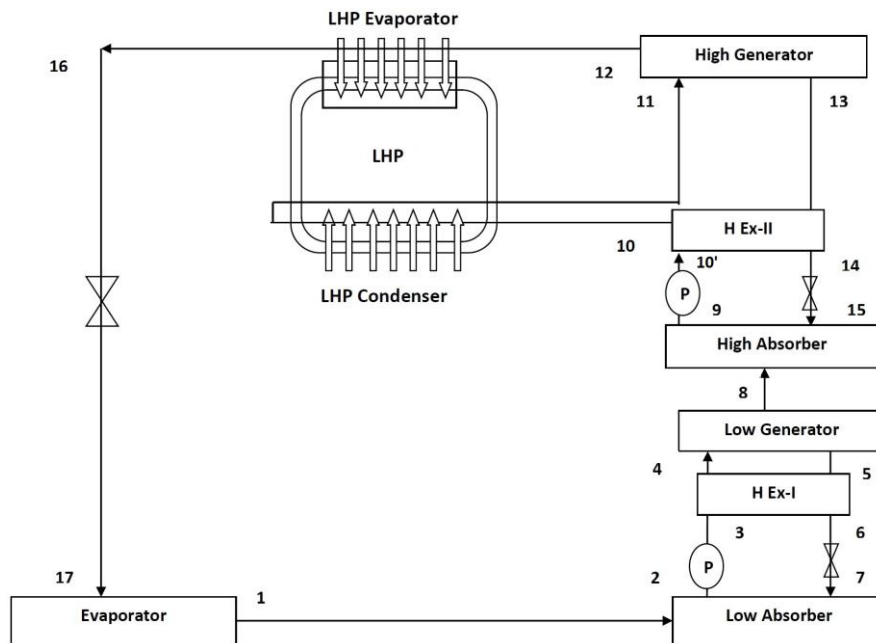


Fig. 4.5: Modified Half Effect VARS-I [184]

- a. Refrigerant Expansion Valve (States 16-17)
- b. Evaporator (States 17-1)
- c. Low Temp. Absorber (States 1-2 & 7-2) and High Temp. Absorber (States 8-9 & 15-9)
- d. Mixture Pump-I & II (States 2-3) and (9-10')
- e. Mixture Heat Exchange-I (States 3-4 & 7-8) & HEx-II (States 10'-10 & 13-14)
- f. LHP Condenser (States 10-11)

g. Low Generator (States 4-8 & 4-5) & High Generator (States 11-12 & 11-13)

h. LHP Evaporator (States 12-16)

i. Mixture Reducing Valve- I & II (States 6-7 & 14-15)

Mass Continuity Equations, m:

$$m_{12} = m_{16} = m_{17} = m_1 \quad (4.74)$$

$$m_2 = m_3 = m_4 \quad (4.75)$$

$$m_7 = m_6 = m_5 \quad (4.76)$$

$$m_{11} = m_{10} = m_9 \quad (4.77)$$

$$m_{13} = m_{14} = m_{15} \quad (4.78)$$

$$m_{11} = m_{12} + m_{13} \quad (4.79)$$

$$m_4 = m_8 + m_5 \quad (4.80)$$

Chemical Composition Balance Equations, m ζ :

$$m_4 \zeta_4 = m_5 \zeta_5 \quad (4.81)$$

$$m_{11} \zeta_{11} = m_{13} \zeta_{13} \quad (4.82)$$

Percentage Absorbent Balance Equation, ζ :

$$\zeta_2 = \zeta_3 = \zeta_4 \quad (4.83)$$

$$\zeta_7 = \zeta_6 = \zeta_5 \quad (4.84)$$

$$\zeta_9 = \zeta_{10} = \zeta_{11} \quad (4.85)$$

$$\zeta_{13} = \zeta_{14} = \zeta_{15} \quad (4.85a)$$

$$COP = RE / (Q_{GH-T} + W_P) \quad (4.86)$$

Solution Circulation Ratio, F:

$$F = \zeta_4 / (\zeta_5 - \zeta_4) \quad (4.87)$$

$$F = \zeta_{11} / (\zeta_{13} - \zeta_{11}) \quad (4.88)$$

a. Refrigerant Expansion Valve (States 16-17)

Expansion Valve can be Expressed as,

$$h_{16} = h_{17} \quad (4.89)$$

Where h_{16} is the enthalpy of saturated liquid exiting the LHP Evaporator as x_{16} is 0 for this state.

$$x_{17} = (h_{16} - h_{f17}) / h_{fg17} \quad (4.90)$$

Here h_{f17} is the enthalpy of saturated liquid at pressure of state 17 & h_{fg17} is the enthalpy of evaporation at the pressure of state 17.

b. Evaporator (States 17-1)

The modeling can be given as:

Energy Analysis:

$$RE = m_1(h_1 - h_{17}) \quad (4.91)$$

Exergy Analysis:

$$X_{Evap} = m_1 \cdot [(h_{17'} - h_{1'}) - T_O (s_{17'} - s_{1'})] \quad (4.92)$$

Where X_{Evap} is the Exergy of the Evaporator, s is the corresponding specific entropy & T_O is the environment temperature. The states 17' & 1' are the inlet and outlet states of the fluid getting cooled in the evaporator. m_1 is the mass flow rate of the fluid.

c. Low Temp. Absorber (States 1-2 & 7-2) and High Temp. Absorber (States 8-9 & 15-9)

The modeling can be done for Heat Rejected in Low-Temperature Absorber Q_{AbsL-T} & High-Temperature Absorber Q_{AbsH-T} in the following manner:

Energy Analysis:

$$Q_{AbsL-T} = m_1 h_1 + m_7 h_7 - m_2 h_2 \quad (4.93)$$

$$Q_{AbsH-T} = m_8 h_8 + m_{15} h_{15} - m_9 h_9 \quad (4.94)$$

Exergy Analysis:

$$X_{\text{AbsL-T}} = m_2 [(h_{7'} - h_{2'}) - T_O (s_{7'} - s_{2'})] \quad (4.95)$$

$$X_{\text{AbsH-T}} = m_9 [(h_{15'} - h_{9'}) - T_O (s_{15'} - s_{9'})] \quad (4.96)$$

Where $X_{\text{AbsL-T}}$ & $X_{\text{AbsH-T}}$ are the Exergy of the Low-T & High-T Absorber, s is the corresponding specific entropy & T_O is the environment temperature and the states 7' & 2' are the inlet and outlet states of the fluid getting heated in the Low-T absorber and 15' & 9' are the inlet and outlet states of the fluid getting heated in the High-T absorber. m_2 is the mass flow rate of the fluid.

d. Mixture Pump-I & II (States 2-3) and (9-10')

The Work input in the Pumps can be given as $W_{\text{P-I}}$ & $W_{\text{P-II}}$:

$$W_{\text{P-I}} = m_2 v_2 (dP) \quad (4.97)$$

$$W_{\text{P-II}} = m_9 v_9 (dP) \quad (4.98)$$

Where v_2 & v_9 are the specific volumes of the mixture and dP is the pressure raised by the pump.

Also, Specific Enthalpy at the Exit of the Pumps can be given as:

$$h_3 = m_2 h_2 + W_{\text{P-I}} \quad (4.99)$$

$$h_{10'} = m_9 h_9 + W_{\text{P-II}} \quad (4.100)$$

e. Mixture Heat Exchange-I (States 3-4 & 7-8) & HEx-II (States 10'-10 & 13-14)

It can be modeled as the followings:

Energy Analysis for HEx-I:

$$\text{Effectiveness of Heat Exchanger, } \epsilon_{\text{H-EX-I}} = (T_5 - T_6) / (T_5 - T_3) \quad (4.101)$$

$$\text{Heat Exchange in the Heat Exchanger, } Q_{\text{H-EX-I}} = m_4 (h_4 - h_3) = m_5 (h_5 - h_6) \quad (4.102)$$

$$\text{Specific Heat Capacity for Hot Fluid, } c_{\text{Hot-I}} = (h_5 - h_6) / (T_5 - T_6) \quad (4.103)$$

$$\text{Specific Heat Capacity for Cold Fluid, } c_{\text{Cold-I}} = (h_4 - h_3) / (T_4 - T_3) \quad (4.104)$$

Exergy Analysis for HEx-I:

$$X_{H-Ex-I} = m_3[(h_3-h_4) - T_O (s_3-s_4)] \quad (4.105)$$

Where X_{H-Ex-I} is the Exergy of the Heat Exchanger-I, s is the corresponding specific entropy & T_O is the environment temperature.

Energy Analysis for HEx-II:

$$\text{Effectiveness of Heat Exchanger, } \varepsilon_{H-Ex-II} = (T_{13}-T_{14}) / (T_{13}-T_{10'}) \quad (4.106)$$

Heat Exchange in the Heat Exchanger,

$$Q_{H-Ex-II} = m_9(h_{10} - h_{10'}) = m_{13}(h_{13} - h_{14}) \quad (4.107)$$

$$\text{Specific Heat Capacity for Hot Fluid, } c_{Hot-II} = (h_{13} - h_{14}) / (T_{13}-T_{14}) \quad (4.108)$$

$$\text{Specific Heat Capacity for Cold Fluid, } c_{Cold-II} = (h_{10} - h_{10'}) / (T_{10}-T_{10'}) \quad (4.109)$$

Exergy Analysis for HEx-II:

$$X_{H-Ex-II} = m_9[(h_{10'}-h_{10}) - T_O (s_{10'}-s_{10})] \quad (4.110)$$

Where $X_{H-Ex-II}$ is the Exergy of the Heat Exchanger-II, s is the corresponding specific entropy & T_O is the environment temperature.

f. LHP Condenser (States 10-11)

It can be modeled as:

Energy Analysis:

$$\text{Heat Input to the Mixture, } Q_{InMix} = m_{10}(h_{11}-h_{10}) \quad (4.111)$$

Heat Rejected by the Condensing Fluid in LHP,

$$Q_{LHPCond} = m_{LHP} (h_{fgLHPCond} + c_F \Delta T_{Sub}) \quad (4.112)$$

Where $h_{fgLHPCond}$ is the latent heat of condensation in the LHP Condenser, c_F is the specific heat capacity, m_{LHP} is the mass flow in the LHP & ΔT_{Sub} is the degree of subcooling in the LHP condenser for the LHP working fluid.

Effectiveness of the LHP Condenser,

$$\varepsilon_{\text{LHPCond}} = (T_{11} - T_{10}) / (T_{\text{InLHPCond}} - T_{10}) \quad (4.113)$$

Where $T_{\text{InLHPCond}}$ is the Input Temperature of the LHP Condenser.

Exergy Analysis:

$$X_{\text{LHPCond}} = m_{10}[(h_{10} - h_{11}) - T_O (s_{10} - s_{11})] \quad (4.114)$$

Where X_{LHPCond} is the Exergy of the Heat Exchanger, s is the corresponding specific entropy & T_O is the environment temperature.

g. Low Generator (States 4-8 & 4-5) & High Generator (States 11-12 & 11-13)

Heat is added to the mixture in the generator. This heat input to the High-Temperature Generator $Q_{\text{GH-T}}$ & Low-Temperature Generator $Q_{\text{GL-T}}$ can be expressed as:

Energy Analysis, High-Temperature Generator:

$$Q_{\text{GH-T}} = h_{13}m_{13} + h_{12}m_{12} - h_{11}m_{11} \quad (4.115)$$

Exergy Analysis, High Temperature Generator:

$$X_{\text{GH-T}} = m_{12}'[(h_{12}' - h_{13}') - T_O (s_{12}' - s_{13}')] \quad (4.116)$$

Where $X_{\text{GH-T}}$ is the Exergy of the High-T Generator, s is the corresponding specific entropy & T_O is the environment temperature and the states 12' & 13' are the inlet and outlet states of the fluid supplying heat to the generator. M_{12}' is the mass flow rate of the fluid.

Energy Analysis, Low Temperature Generator:

$$Q_{\text{GL-T}} = h_8m_8 + h_5m_5 - h_4m_4 \quad (4.117)$$

Exergy Analysis, Low Temperature Generator:

$$X_{\text{GL-T}} = m_8'[(h_8' - h_5') - T_O (s_8' - s_5')] \quad (4.118)$$

Where $X_{\text{GL-T}}$ is the Exergy of the Low-T Generator, s is the corresponding specific entropy & T_O is the environment temperature and the states 8' & 5' are the inlet and outlet states of the fluid supplying heat to the generator. m_8' is the mass flow rate of the fluid.

h. LHP Evaporator (States 12-16)

It can be modeled as:

Energy Analysis:

Heat Rejected by the Condensing Refrigerant,

$$Q_{\text{CondR}} = m_{12}(h_{12} - h_{16}) \quad (4.119)$$

Heat Absorbed by the LHP Working Fluid in the LHP Evaporator,

$$Q_{\text{LHPEvap}} = m_{\text{LHP}} (h_{\text{fgLHPEvap}} + c_F \Delta T_{\text{Sup}}) \quad (4.120)$$

Where $h_{\text{fgLHPEvap}}$ is the latent heat of evaporation in the LHP Evaporator, c_F is the specific heat capacity, m_{LHP} is the mass flow in the LHP & ΔT_{Sup} is the degree of superheat in the LHP evaporator for the LHP working fluid.

Exergy Analysis:

$$X_{\text{LHPEvap}} = m_{12}[(h_{12}-h_{16}) - T_O (s_{12}-s_{16})] \quad (4.121)$$

Where X_{LHPEvap} is the Exergy of the LHP Evaporator, s is the corresponding specific entropy & T_O is the environment temperature.

i. Mixture Reducing Valve- I & II (States 6-7 & 14-15)

Modeling can be done as:

$$h_6 = h_7 \quad (4.122)$$

$$h_{14} = h_{15} \quad (4.123)$$

4.3.2. Modified Half Effect VARS-II

In this modification as discussed earlier Heat Exchangers have been replaced by LHP-I & LHP-II which can be shown in Fig 4.5. The modeling of this system can be achieved by replacing the modeling of Heat Exchangers with LHP in the previous section.

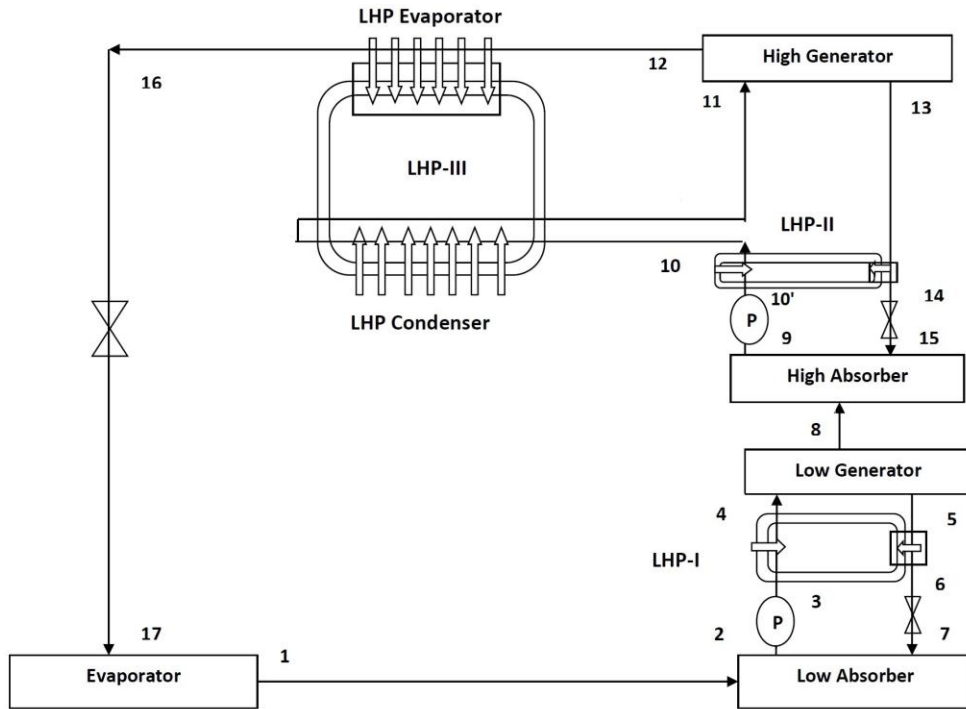


Fig 4.6. Modified Half Effect VARS-II

e. Mixture Heat Exchange-I (States 3-4 & 7-8) & HEx-II (States 10'-10 & 13-14)

The heat is absorbed in the LHP Evaporator (States 5-6) & Rejected in the LHP Condenser (States 3-4) of LHP-I. Moreover, the heat is absorbed in the LHP Evaporator (States 13-14) & Rejected in the LHP Condenser (States 10'-10) of LHP-II.

• LHP-I Condenser

Energy Analysis:

$$\text{Heat Input to the Mixture, } Q_{\text{InMixI}} = m_3(h_4-h_3) \tag{4.124}$$

Heat Rejected by the Condensing Fluid in LHP,

$$Q_{\text{LHPICond}} = m_{\text{LHPI}} (h_{\text{fgLHPICond}} + c_F \Delta T_{\text{SubI}}) \tag{4.125}$$

Where $h_{\text{fgLHPICond}}$ is the latent heat of condensation in the LHP-I Condenser, c_F is the specific heat capacity, m_{LHPI} is the mass flow in the LHP-I & ΔT_{SubI} is the degree of subcooling in LHP-I condenser for the LHP-I working fluid.

$$\text{Effectiveness of the LHP-I Condenser, } \varepsilon_{\text{LHPICond}} = (T_4-T_3) / (T_{\text{InLHPICond}}-T_3) \tag{4.126}$$

Where $T_{\text{InLHPICond}}$ is the Input Temperature of the LHP-I Condenser.

Exergy Analysis:

$$X_{\text{LHPICond}} = m_3[(h_3 - h_4) - T_0 (s_3 - s_4)] \quad (4.127)$$

Where X_{LHPICond} is the Exergy of the LHP-I, s is the corresponding specific entropy & T_0 is the environment temperature.

• **LHP-I Evaporator**

Energy Analysis:

$$\text{Heat Rejected by the Absorbent, } Q_{\text{RejI}} = m_5(h_5 - h_6) \quad (4.128)$$

Heat Absorbed by the LHP-I Working Fluid in the LHP-I Evaporator,

$$Q_{\text{LHPIEvap}} = m_{\text{LHPI}} (h_{\text{fgLHPIEvap}} + c_F \Delta T_{\text{SupI}}) \quad (4.129)$$

Where $h_{\text{fgLHPIEvap}}$ is the latent heat of evaporation in the LHP-I Evaporator, c_F is the specific heat capacity, m_{LHPI} is the mass flow in the LHP-I & ΔT_{SupI} is the degree of superheat in the LHP-I evaporator for the LHP-I working fluid.

Exergy Analysis:

$$X_{\text{LHPIEvap}} = m_5[(h_5 - h_6) - T_0 (s_5 - s_6)] \quad (4.130)$$

Where X_{LHPIEvap} is the Exergy of the LHP-I Evaporator, s is the corresponding specific entropy & T_0 is the environment temperature.

• **LHP-II Condenser**

Energy Analysis:

$$\text{Heat Input to the Mixture, } Q_{\text{InMixII}} = m_{10}(h_{10} - h_{10}') \quad (4.131)$$

Heat Rejected by the Condensing Fluid in LHP,

$$Q_{\text{LHPICond}} = m_{\text{LHPII}} (h_{\text{fgLHPICond}} + c_F \Delta T_{\text{SubII}}) \quad (4.132)$$

Where $h_{\text{fgLHPICond}}$ is the latent heat of condensation in the LHP-II Condenser, c_F is the specific heat capacity, m_{LHPII} is the mass flow in the LHP-II & ΔT_{SubII} is the degree of subcooling in the LHP-II condenser for the LHP-II working fluid.

Effectiveness of the LHP-II Condenser,

$$\epsilon_{\text{LHP-II Cond}} = (T_{10} - T_{10}') / (T_{\text{InLHP-II Cond}} - T_{10}') \quad (4.133)$$

Where $T_{\text{InLHP-II Cond}}$ is the Input Temperature of the LHP-II Condenser.

Exergy Analysis:

$$X_{\text{LHP-II Cond}} = m_{10}[(h_{10}' - h_{10}) - T_O (s_{10}' - s_{10})] \quad (4.134)$$

Where $X_{\text{LHP-II Cond}}$ is the Exergy of the LHP-II, s is the corresponding specific entropy & T_O is the environment temperature.

• **LHP-II Evaporator**

Energy Analysis:

$$\text{Heat Rejected by the Absorbent, } Q_{\text{RejII}} = m_{13}(h_{13} - h_{14}) \quad (4.135)$$

Heat Absorbed by the LHP-II Working Fluid in the LHP-II Evaporator,

$$Q_{\text{LHP-II Evap}} = m_{\text{LHP-II}} (h_{\text{fgLHP-II Evap}} + c_F \Delta T_{\text{SupII}}) \quad (4.136)$$

Where $h_{\text{fgLHP-II Evap}}$ is the latent heat of evaporation in the LHP-II Evaporator, c_F is the specific heat capacity, $m_{\text{LHP-II}}$ is the mass flow in the LHP-II & ΔT_{SupII} is the degree of superheat in the LHP-II evaporator for the LHP-II working fluid.

Exergy Analysis:

$$X_{\text{LHP-II Evap}} = m_{13}[(h_{13} - h_{14}) - T_O (s_{13} - s_{14})] \quad (4.137)$$

Where $X_{\text{LHP-II Evap}}$ is the Exergy of the LHP-II Evaporator, s is the corresponding specific entropy & T_O is the environment temperature.

4.3.3. Combined GPC & Half-Effect VARS using LHP

The Modified Half Effect VARS-II has been combined with the Reheating-Regenerative & Multi-compression system through LHP-IV as shown in Fig 4.7.

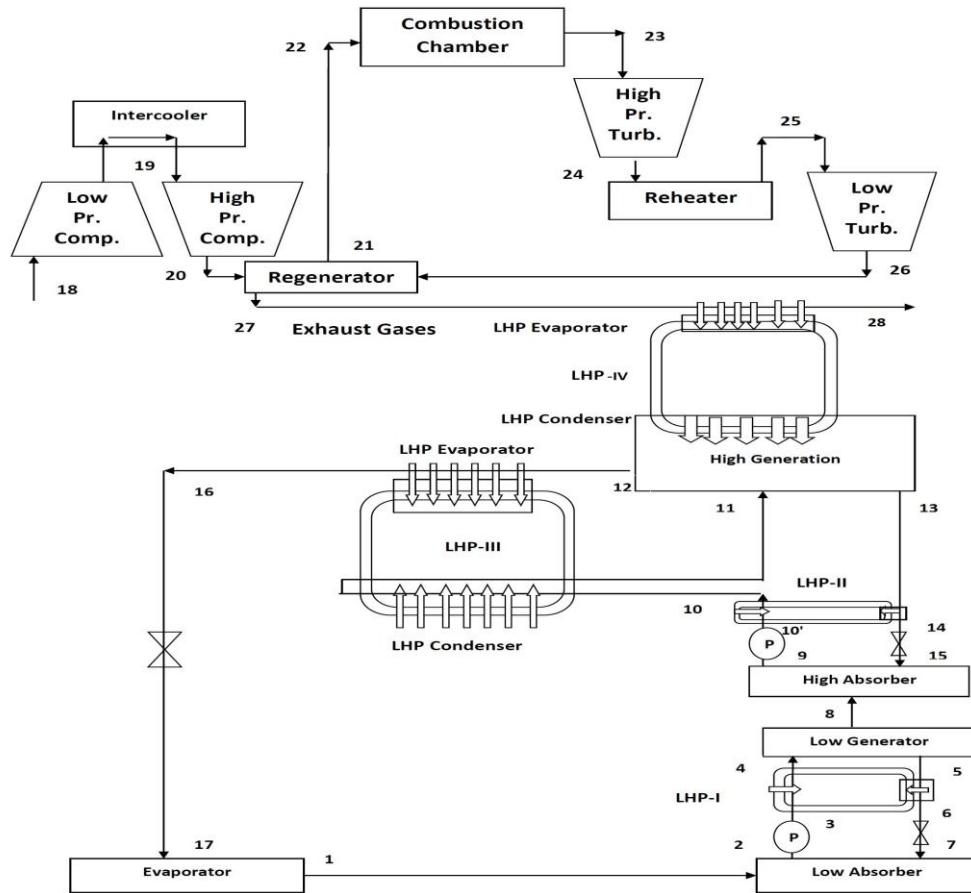


Fig. 4.7: Combined GPC & Half Effect VARS

The inlet to the GPC is at state 18 & the exit of and the exhaust leaves the LHP-IV Evaporator at 28. In addition to the modeling of the GPC presented in section 4.1. Also, the temperature in state 23 & state 25 is the same. The LHP-IV has been modeled similar to the previous section:

j. Gas Power Cycle (State 12-21)

The heat input to the LHP-IV, $Q_{InLHP-IV}$ can be calculated as:

$$Q_{InLHP-IV} = \dot{m}_g c_{pg} (T_{27} - T_{28}) \tag{4.138}$$

k. LHP-IV

The heat rejected at the exhaust of GPC is harnessed by the LHP-IV Evaporator and transferred to the VARS Generator through LHP-IV Condensers.

• LHP-IV Evaporator

Energy Analysis:

$$Q_{\text{InLHP-IV}} = \dot{m}_g c_{pg} (T_{27} - T_{28}) \quad (4.139)$$

Heat Absorbed by the LHP-IV Working Fluid in the LHP-IV Evaporator,

$$Q_{\text{LHP-IV Evap}} = \dot{m}_{\text{LHP-IV}} (h_{fg\text{LHP-IV Evap}} + c_F \Delta T_{\text{SupIV}}) \quad (4.140)$$

Where $h_{fg\text{LHP-IV Evap}}$ is the latent heat of evaporation in the LHP-IV Evaporator, c_F is the specific heat capacity, $\dot{m}_{\text{LHP-IV}}$ is the mass flow in the LHP-IV & ΔT_{SupIV} is the degree of superheat in the LHP-IV evaporator for the LHP-IV working fluid.

Exergy Analysis:

$$X_{\text{LHP-IV Evap}} = \dot{m}_g [(h_{27} - h_{28}) - T_0 (s_{27} - s_{28})] \quad (4.141)$$

Where $X_{\text{LHP-IV Evap}}$ is the Exergy of the LHP-IV Evaporator, s is the corresponding specific entropy & T_0 is the environment temperature.

• **LHP-II Condenser**

Energy Analysis:

Heat Input to the Generator,

$$Q_{\text{InGenerator}} = h_{12} \dot{m}_{12} + h_{13} \dot{m}_{13} - h_{11} \dot{m}_{11} \quad (4.142)$$

Heat Rejected by the Condensing Fluid in LHP into the Generator,

$$Q_{\text{LHP-IV Cond}} = \dot{m}_{\text{LHP-IV}} (h_{fg\text{LHP-IV Cond}} + c_F \Delta T_{\text{SubIV}}) \quad (4.143)$$

Where $h_{fg\text{LHP-IV Cond}}$ is the latent heat of condensation in the LHP-IV Condenser, c_F is the specific heat capacity, $\dot{m}_{\text{LHP-IV}}$ is the mass flow in the LHP-IV & ΔT_{SubIV} is the degree of subcooling in the LHP-IV condenser for the LHP-IV working fluid.

4.4. Modified Double Effect VARS

This section deals with the modeling of the 03 systems obtained with the modifications proposed using LHPs.

4.4.1. Modified Double Effect VARS-I (Ankit Dwivedi, et. al. 2018) ^[180]

Fig 4.8 shows the system under consideration which has been elaborately discussed in Chapter-3.

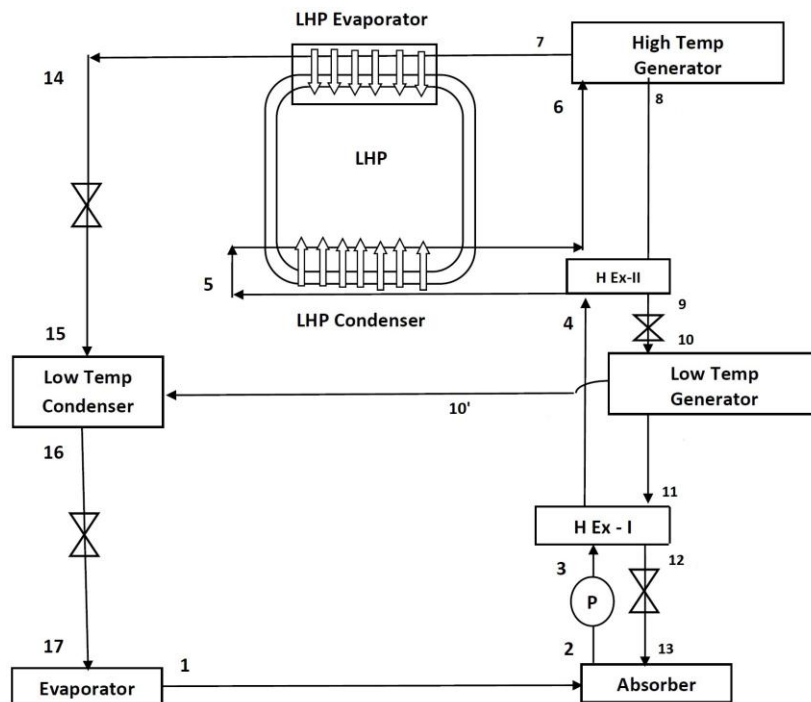


Fig 4.8. Modified Double Effect VARS-I [180]

- a. Refrigerant Expansion Valves I & II (States 14-15 & 16-17)
- b. Evaporator (States 17-1)
- c. Absorber (States 1-2 & 13-2)
- d. Mixture Pump (States 2-3)
- e. Mixture Heat Exchange-I (States 3-4 & 11-12) & HEx-II (States 4-5 & 8-9)
- f. LHP Condenser (States 5-6)
- g. Low Generator (States 10-11 & 10-13) & High Generator (States 6-7 & 6-8)

- h.** LHP Evaporator (States 7-14)
- i.** Mixture Reducing Valve- I & II (States 12-13 & 9-10)
- j.** Low Temperature Condenser (States 15-16 & 10'-16)

Mass Continuity Equations, m:

$$m_7 = m_{14} = m_{15} \quad (4.144)$$

$$m_{16} = m_{17} = m_1 \quad (4.145)$$

$$m_2 = m_3 = m_4 = m_5 = m_6 \quad (4.146)$$

$$m_8 = m_{10} = m_9 \quad (4.147)$$

$$m_{11} = m_{12} = m_{13} \quad (4.148)$$

$$m_{10} = m_{10'} + m_{11} \quad (4.149)$$

$$m_6 = m_7 + m_8 \quad (4.150)$$

$$m_{16} = m_{15} + m_{10'} \quad (4.151)$$

Chemical Composition Balance Equations, m ζ :

$$m_6 \zeta_6 = m_8 \zeta_8 \quad (4.152)$$

$$m_{10} \zeta_{10} = m_{11} \zeta_{11} \quad (4.153)$$

Percentage Absorbent Balance Equation, ζ :

$$\zeta_2 = \zeta_3 = \zeta_4 = \zeta_6 = \zeta_5 \quad (4.154)$$

$$\zeta_8 = \zeta_9 = \zeta_{10} \quad (4.155)$$

$$\zeta_{13} = \zeta_{12} = \zeta_{11} \quad (4.156)$$

$$COP = RE / (Q_{GH-T} + W_P) \quad (4.157)$$

Solution Circulation Ratio, F:

$$F = \zeta_6 / (\zeta_8 - \zeta_6) \quad (4.158)$$

$$F = \zeta_{10} / (\zeta_{11} - \zeta_{10}) \quad (4.159)$$

a. Refrigerant Expansion Valves I & II (States 14-15 & 16-17)

Expansion Valve-I can be expressed as,

$$h_{14} = h_{15} \quad (4.160)$$

Where h_{14} is the enthalpy of saturated liquid exiting the LHP Evaporator as x_{14} is 0 for this state.

$$x_{17} = (h_{16} - h_{f17}) / h_{fg17} \quad (4.161)$$

Here h_{f17} is the enthalpy of saturated liquid at pressure of state 17 & h_{fg17} is the enthalpy of evaporation at the pressure of state 17.

Moreover, Expansion Valve-II can be expressed as,

$$h_{16} = h_{17} \quad (4.162)$$

Where h_{16} is the enthalpy of saturated liquid exiting the Low-T condenser as x_{16} is 0 for this state.

$$x_{17} = (h_{16} - h_{f17}) / h_{fg17} \quad (4.163)$$

Here h_{f17} is the enthalpy of saturated liquid at pressure of state 17 & h_{fg17} is the enthalpy of evaporation at the pressure of state 17.

b. Evaporator (States 17-1)

The modeling can be given as:

Energy Analysis:

$$RE = m_1 (h_1 - h_{17}) \quad (4.164)$$

Exergy Analysis:

$$X_{Evap} = m_{1'} [(h_{17'} - h_{1'}) - T_0 (s_{17'} - s_{1'})] \quad (4.165)$$

Where X_{Evap} is the Exergy of the Evaporator, s is the corresponding specific entropy & T_0 is the environment temperature. The states 17' & 1' are the inlet and outlet states of the fluid getting cooled in the evaporator. $m_{1'}$ is the mass flow rate of the fluid.

c. Absorber (States 1-2 & 13-2)

The modeling can be done for Heat Rejected in Absorber Q_{Abs} .

Energy Analysis:

$$Q_{Abs} = m_1 h_1 + m_{13} h_{13} - m_2 h_2 \quad (4.166)$$

Exergy Analysis:

$$X_{Abs} = m_2' [(h_{13}' - h_2') - T_O (s_{13}' - s_2')] \quad (4.167)$$

Where X_{Abs} the Exergy of Absorber, s is the corresponding specific entropy & T_O is the environment temperature and the states 13' & 2' are the inlet and outlet states of the fluid getting heated in the absorber. m_2' is the mass flow rate of the fluid.

d. Mixture Pump (States 2-3)

The Work input in the Pumps can be given as W_P :

$$W_P = m_2 v_2 (dP) \quad (4.168)$$

Where v_2 is the specific volume of the mixture and dP is the pressure raised by the pump.

Also, Specific Enthalpy at the Exit of the Pumps can be given as:

$$h_3 = m_2 h_2 + W_P \quad (4.169)$$

e. HEx-I (States 3-4 & 11-12) & HEx-II (States 4-5 & 8-9)

It can be modeled as the followings:

Energy Analysis for HEx-I:

$$\text{Effectiveness of Heat Exchanger, } \epsilon_{H-Ex-I} = (T_{11} - T_{12}) / (T_{11} - T_3) \quad (4.170)$$

Heat Exchange in the Heat Exchanger,

$$Q_{H-Ex-I} = m_4 (h_4 - h_3) = m_{11} (h_{11} - h_{12}) \quad (4.171)$$

$$\text{Specific Heat Capacity for Hot Fluid, } c_{Hot-I} = (h_{11} - h_{12}) / (T_{11} - T_{12}) \quad (4.172)$$

$$\text{Specific Heat Capacity for Cold Fluid, } c_{Cold-I} = (h_4 - h_3) / (T_4 - T_3) \quad (4.173)$$

Exergy Analysis for HEx-I:

$$X_{H-Ex-I} = m_3[(h_3-h_4) - T_O (s_3-s_4)] \quad (4.174)$$

Where X_{H-Ex-I} is the Exergy of the Heat Exchanger-I, s is the corresponding specific entropy & T_O is the environment temperature.

Energy Analysis for HEx-II:

$$\text{Effectiveness of Heat Exchanger, } \varepsilon_{H-Ex-II} = (T_8-T_9) / (T_8-T_4) \quad (4.175)$$

Heat Exchange in the Heat Exchanger,

$$Q_{H-Ex-II} = m_4(h_5 - h_4) = m_8(h_8 - h_9) \quad (4.176)$$

$$\text{Specific Heat Capacity for Hot Fluid, } c_{Hot-II} = (h_8 - h_9) / (T_8-T_9) \quad (4.178)$$

$$\text{Specific Heat Capacity for Cold Fluid, } c_{Cold-II} = (h_4 - h_5) / (T_4-T_5) \quad (4.179)$$

Exergy Analysis for HEx-II:

$$X_{H-Ex-II} = m_4[(h_4-h_5) - T_O (s_4-s_5)] \quad (4.180)$$

Where $X_{H-Ex-II}$ is the Exergy of the Heat Exchanger-II, s is the corresponding specific entropy & T_O is the environment temperature.

f. LHP Condenser (States 5-6)

It can be modeled as:

Energy Analysis:

$$\text{Heat Input to the Mixture, } Q_{InMix} = m_5(h_6-h_5) \quad (4.181)$$

Heat Rejected by the Condensing Fluid in LHP,

$$Q_{LHPCond} = m_{LHP} (h_{fgLHPCond} + c_F \Delta T_{Sub}) \quad (4.182)$$

Where $h_{fgLHPCond}$ is the latent heat of condensation in the LHP Condenser, c_F is the specific heat capacity, m_{LHP} is the mass flow in the LHP & ΔT_{Sub} is the degree of subcooling in the LHP condenser for the LHP working fluid.

Effectiveness of the LHP Condenser,

$$\varepsilon_{\text{LHPCond}} = (T_6 - T_5) / (T_{\text{InLHPCond}} - T_5) \quad (4.183)$$

Where $T_{\text{InLHPCond}}$ is the Input Temperature of the LHP Condenser.

Exergy Analysis:

$$X_{\text{LHPCond}} = m_5[(h_5 - h_6) - T_0 (s_5 - s_6)] \quad (4.184)$$

Where X_{LHPCond} is the Exergy of the Heat Exchanger, s is the corresponding specific entropy & T_0 is the environment temperature.

g. Low Generator (States 10-10' & 10-11) & High Generator (States 6-7 & 6-8)

Heat is added to the mixture in the generator. This heat input to the High-Temperature Generator $Q_{\text{GH-T}}$ & Low-Temperature Generator $Q_{\text{GL-T}}$ can be expressed as:

Energy Analysis, High-Temperature Generator:

$$Q_{\text{GH-T}} = h_7 m_7 + h_8 m_8 - h_6 m_6 \quad (4.185)$$

Exergy Analysis, High Temperature Generator:

$$X_{\text{GH-T}} = m_7[(h_7 - h_8) - T_0 (s_7 - s_8)] \quad (4.186)$$

Where $X_{\text{GH-T}}$ is the Exergy of the High-T Generator, s is the corresponding specific entropy & T_0 is the environment temperature and the states 7' & 8' are the inlet and outlet states of the fluid supplying heat to the generator. M_7 is the mass flow rate of the fluid.

Energy Analysis, Low Temperature Generator:

$$Q_{\text{GL-T}} = h_{10'} m_{10'} + h_{10} m_{10} - h_{11} m_{11} \quad (4.187)$$

Exergy Analysis, Low Temperature Generator:

$$X_{\text{GL-T}} = m_{11'} [(h_{11'} - h_{12'}) - T_0 (s_{11'} - s_{12'})] \quad (4.188)$$

Where $X_{\text{GL-T}}$ is the Exergy of the Low-T Generator, s is the corresponding specific entropy & T_0 is the environment temperature and the states 11' & 12' are the inlet and outlet states of the fluid supplying heat to the generator. $m_{11'}$ is the mass flow rate of the fluid.

h. LHP Evaporator (States 7-14)

It can be modeled as:

Energy Analysis:

Heat Rejected by the Condensing Refrigerant,

$$Q_{\text{CondR}} = m_{17} (h_{12} - h_{14}) \quad (4.189)$$

Heat Absorbed by the LHP Working Fluid in the LHP Evaporator,

$$Q_{\text{LHPEvap}} = m_{\text{LHP}} (h_{\text{fgLHPEvap}} + c_F \Delta T_{\text{Sup}}) \quad (4.190)$$

Where $h_{\text{fgLHPEvap}}$ is the latent heat of evaporation in the LHP Evaporator, c_F is the specific heat capacity, m_{LHP} is the mass flow in the LHP & ΔT_{Sup} is the degree of superheat in the LHP evaporator for the LHP working fluid.

Exergy Analysis:

$$X_{\text{LHPEvap}} = m_7 [(h_7 - h_{14}) - T_0 (s_7 - s_{14})] \quad (4.191)$$

Where X_{LHPEvap} is the Exergy of the LHP Evaporator, s is the corresponding specific entropy & T_0 is the environment temperature.

i. Mixture Reducing Valve- I & II (States 12-13 & 9-10)

Modeling can be done as:

$$h_{12} = h_{13} \quad (4.192)$$

$$h_9 = h_{10} \quad (4.193)$$

j. Low Temperature Condenser (States 15-16 & 10'-16)

The Low-T Condenser deals with the liquid refrigerant coming out of the LHP & Refrigerant Expansion Valve-I and mixes it with the liquid refrigerant obtained after condensing the vapour coming out of the Low-T Generator. The heat rejected from the low-T Condenser can be modeled as:

Energy Analysis:

$$Q_{\text{L-Cond}} = m_{10'} h_{10'} + m_{15} h_{15} - m_{16} h_{16} \quad (4.194)$$

Exergy Analysis:

$$X_{L-Cond} = m_{15'} [(h_{15'} - h_{16'}) - T_O (s_{15'} - s_{16'})] \tag{4.195}$$

Where X_{L-Cond} is the Exergy of the Low-Temperature Condenser, s is the corresponding specific entropy & T_O is the environment temperature. The states 15' & 16' are the inlet and outlet states of the fluid getting cooled in the Condenser. $m_{15'}$ is the mass flow rate of the fluid.

4.4.2. Modified Double Effect VARS-II

The modified system has been shown in Fig 4.9 in which it has been proposed that the Heat Exchangers of Modified System-I are replaced with LHP-I & LHP-II.

Hence, similar to the previous systems LHP-I & LHP-II can be modeled with the following methodology. The heat is absorbed in the LHP Evaporator (States 5-6) & Rejected in the LHP Condenser (States 3-4) of LHP-I. Moreover, the heat is absorbed in the LHP Evaporator (States 13-14) & Rejected in the LHP Condenser (States 10'-10) of LHP-II.

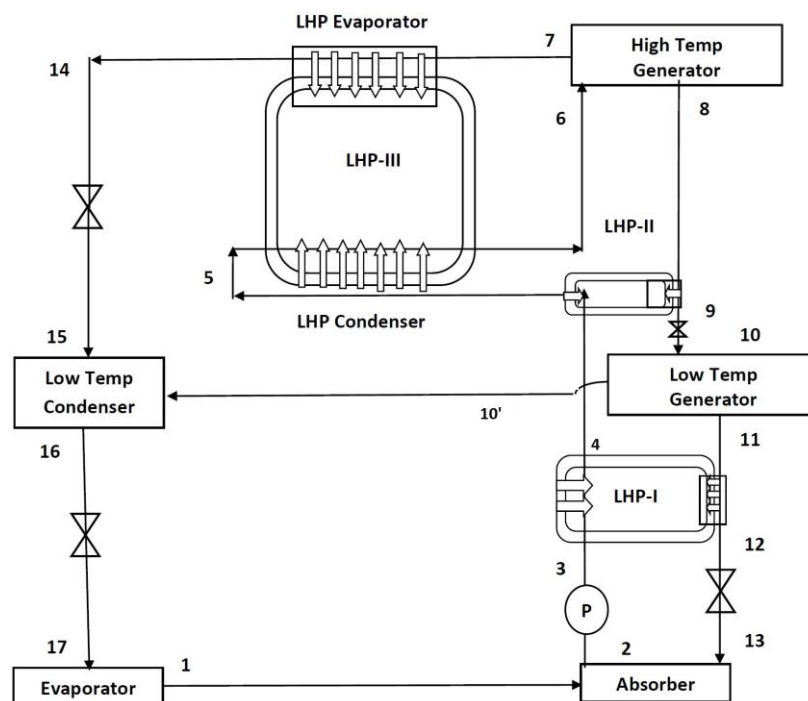


Fig 4.9. Modified Double Effect VARS-I

e. LHP-I (States 3-4 & 11-12) & LHP-II (States 4-5 & 8-9)

- **LHP-I Condenser**

Energy Analysis:

$$\text{Heat Input to the Mixture, } Q_{\text{InMixI}} = m_3(h_4 - h_3) \quad (4.196)$$

Heat Rejected by the Condensing Fluid in LHP,

$$Q_{\text{LHPICond}} = m_{\text{LHPI}} (h_{\text{fgLHPICond}} + c_F \Delta T_{\text{SubI}}) \quad (4.197)$$

Where $h_{\text{fgLHPICond}}$ is the latent heat of condensation in the LHP-I Condenser, c_F is the specific heat capacity, m_{LHPI} is the mass flow in the LHP-I & ΔT_{SubI} is the degree of subcooling in the LHP-I condenser for the LHP-I working fluid.

$$\text{Effectiveness of the LHP-I Condenser, } \varepsilon_{\text{LHPICond}} = (T_4 - T_3) / (T_{\text{InLHPICond}} - T_3) \quad (4.198)$$

Where $T_{\text{InLHPICond}}$ is the Input Temperature of the LHP-I Condenser.

Exergy Analysis:

$$X_{\text{LHPICond}} = m_3[(h_3 - h_4) - T_O (s_3 - s_4)] \quad (4.199)$$

Where X_{LHPICond} is the Exergy of the LHP-I, s is the corresponding specific entropy & T_O is the environment temperature.

- **LHP-I Evaporator**

Energy Analysis:

$$\text{Heat Rejected by the Absorbent, } Q_{\text{RejI}} = m_{11}(h_{11} - h_{12}) \quad (4.200)$$

Heat Absorbed by the LHP-I Working Fluid in the LHP-I Evaporator,

$$Q_{\text{LHPIEvap}} = m_{\text{LHPI}} (h_{\text{fgLHPIEvap}} + c_F \Delta T_{\text{SupI}}) \quad (4.201)$$

Where $h_{\text{fgLHPIEvap}}$ is the latent heat of evaporation in the LHP-I Evaporator, c_F is the specific heat capacity, m_{LHPI} is the mass flow in the LHP-I & ΔT_{SupI} is the degree of superheat in the LHP-I evaporator for the LHP-I working fluid.

Exergy Analysis:

$$X_{\text{LHPIEvap}} = m_{11}[(h_{11} - h_{12}) - T_O (s_{11} - s_{12})] \quad (4.130)$$

Where $X_{LHP\text{IEvap}}$ is the Exergy of the LHP-I Evaporator, s is the corresponding specific entropy & T_O is the environment temperature.

• **LHP-II Condenser**

Energy Analysis:

$$\text{Heat Input to the Mixture, } Q_{\text{InMixII}} = m_4(h_5-h_4) \quad (4.202)$$

Heat Rejected by the Condensing Fluid in LHP,

$$Q_{LHP\text{IICond}} = m_{LHP\text{II}} (h_{fgLHP\text{IICond}} + c_F \Delta T_{\text{SubII}}) \quad (4.203)$$

Where $h_{fgLHP\text{IICond}}$ is the latent heat of condensation in the LHP-II Condenser, c_F is the specific heat capacity, $m_{LHP\text{II}}$ is the mass flow in the LHP-II & ΔT_{SubII} is the degree of subcooling in the LHP-II condenser for the LHP-II working fluid.

Effectiveness of the LHP-II Condenser,

$$\epsilon_{LHP\text{IICond}} = (T_5 - T_4) / (T_{\text{InLHP\text{IICond}}} - T_4) \quad (4.204)$$

Where $T_{\text{InLHP\text{IICond}}}$ is the Input Temperature of the LHP-II Condenser.

Exergy Analysis:

$$X_{LHP\text{IICond}} = m_4[(h_4-h_5) - T_O (s_4-s_5)] \quad (4.205)$$

Where $X_{LHP\text{IICond}}$ is the Exergy of the LHP-II, s is the corresponding specific entropy & T_O is the environment temperature.

• **LHP-II Evaporator**

Energy Analysis:

$$\text{Heat Rejected by the Absorbent, } Q_{\text{RejII}} = m_8(h_8 - h_9) \quad (4.206)$$

Heat Absorbed by the LHP-II Working Fluid in the LHP-II Evaporator,

$$Q_{LHP\text{IIEvap}} = m_{LHP\text{II}} (h_{fgLHP\text{IIEvap}} + c_F \Delta T_{\text{SupII}}) \quad (4.207)$$

Where $h_{fgLHP\text{IIEvap}}$ is the latent heat of evaporation in the LHP-II Evaporator, c_F is the specific heat capacity, $m_{LHP\text{II}}$ is the mass flow in the LHP-II & ΔT_{SupII} is the degree of superheat in the LHP-II evaporator for the LHP-II working fluid.

Exergy Analysis:

$$X_{LHP\text{IIEvap}} = m_8[(h_8-h_9) - T_0 (s_8-s_9)] \tag{4.208}$$

Where $X_{LHP\text{IIEvap}}$ is the Exergy of the LHP-II Evaporator, s is the corresponding specific entropy & T_0 is the environment temperature.

4.4.3. Combined GPC & Double-Effect VARS using LHP

The Modified Double Effect VARS-II has been combined with the Reheating-Regenerative & Multi-compression system through LHP-IV as shown in Fig 4.7. The inlet to the GPC is at state 18 & the exit of the exhaust leaves the LHP-IV Evaporator at 28.

In addition to the modeling of the GPC presented in section 4.1. Also, the temperature in state 23 & state 25 is the same. The LHP-IV has been modeled similar to the previous section:

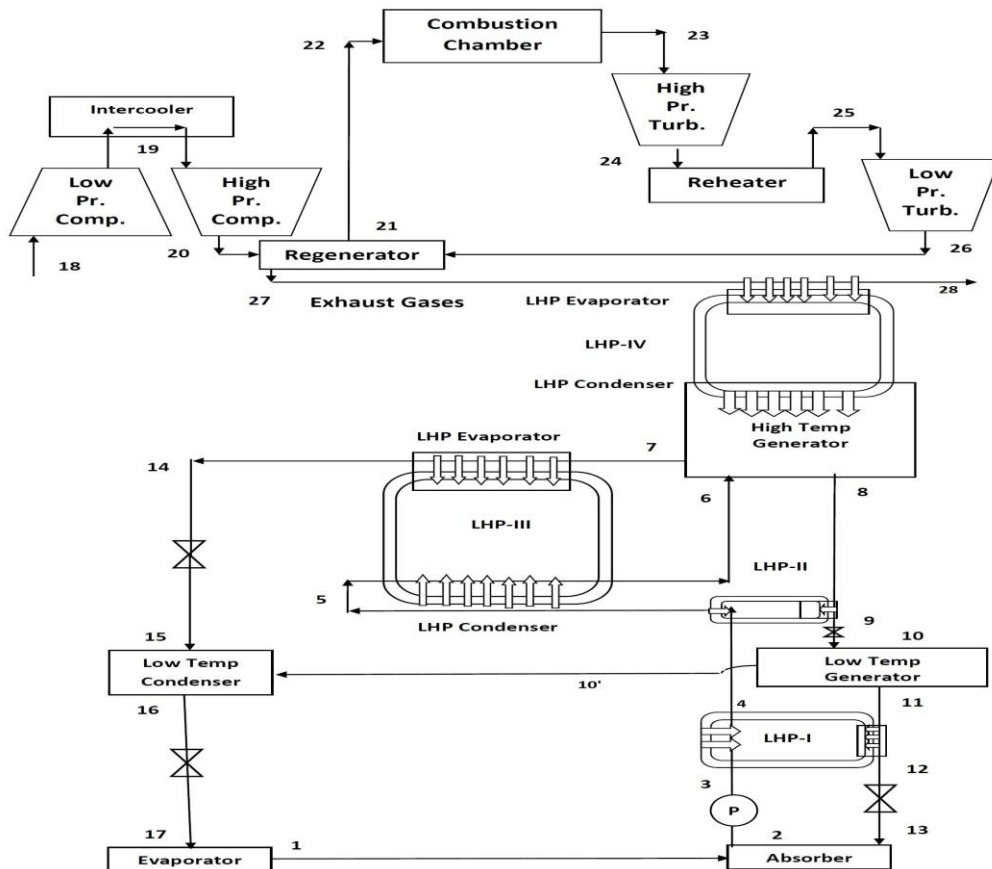


Fig. 4.10: Combined GPC & Double Effect VARS

k. Gas Power Cycle (State 18-28)

The heat input to the LHP-IV, $Q_{InLHP-IV}$ can be calculated as:

$$Q_{InLHP-IV} = \dot{m}_g c_{pg} (T_{27} - T_{28}) \quad (4.209)$$

l. LHP-IV

The heat rejected at the exhaust of GPC is harnessed by the LHP-IV Evaporator and transferred to the VARS Generator through LHP-IV Condensers.

• **LHP-IV Evaporator**

Energy Analysis:

$$Q_{InLHP-IV} = \dot{m}_g c_{pg} (T_{27} - T_{28}) \quad (4.210)$$

Heat Absorbed by the LHP-IV Working Fluid in the LHP-IV Evaporator,

$$Q_{LHP-IV\,Evap} = \dot{m}_{LHP-IV} (h_{fgLHP-IV\,Evap} + c_F \Delta T_{SupIV}) \quad (4.211)$$

Where $h_{fgLHP-IV\,Evap}$ is the latent heat of evaporation in the LHP-IV Evaporator, c_F is the specific heat capacity, \dot{m}_{LHP-IV} is the mass flow in the LHP-IV & ΔT_{SupIV} is the degree of superheat in the LHP-IV evaporator for the LHP-IV working fluid.

Exergy Analysis:

$$X_{LHP-IV\,Evap} = \dot{m}_g [(h_{27} - h_{28}) - T_O (s_{27} - s_{28})] \quad (4.212)$$

Where $X_{LHP-IV\,Evap}$ is the Exergy of the LHP-IV Evaporator, s is the corresponding specific entropy & T_O is the environment temperature.

• **LHP-IV Condenser**

Energy Analysis:

Heat Input to the Generator,

$$Q_{InGenerator} = h_7 \dot{m}_7 + h_8 \dot{m}_8 - h_6 \dot{m}_6 \quad (4.213)$$

Heat Rejected by the Condensing Fluid in LHP into the Generator,

$$Q_{LHP-IV\,Cond} = \dot{m}_{LHP-IV} (h_{fgLHP-IV\,Cond} + c_F \Delta T_{SubIV}) \quad (4.214)$$

Where $h_{fgLHP-IVCond}$ is the latent heat of condensation in the LHP-IV Condenser, c_F is the specific heat capacity, m_{LHP-IV} is the mass flow in the LHP-IV & ΔT_{SubIV} is the degree of subcooling in the LHP-IV condenser for the LHP-IV working fluid.

4.5. Modified Triple Effect VARS

This section deals with the modeling of the 03 systems obtained with the modifications proposed in the Triple Effect VARS using LHPs.

4.5.1. Modified Triple Effect VARS-I (Ankit Dwivedi, et. al. 2018) [186]

Fig 4.11 shows the system under consideration which has been elaborately discussed in Chapter-3.

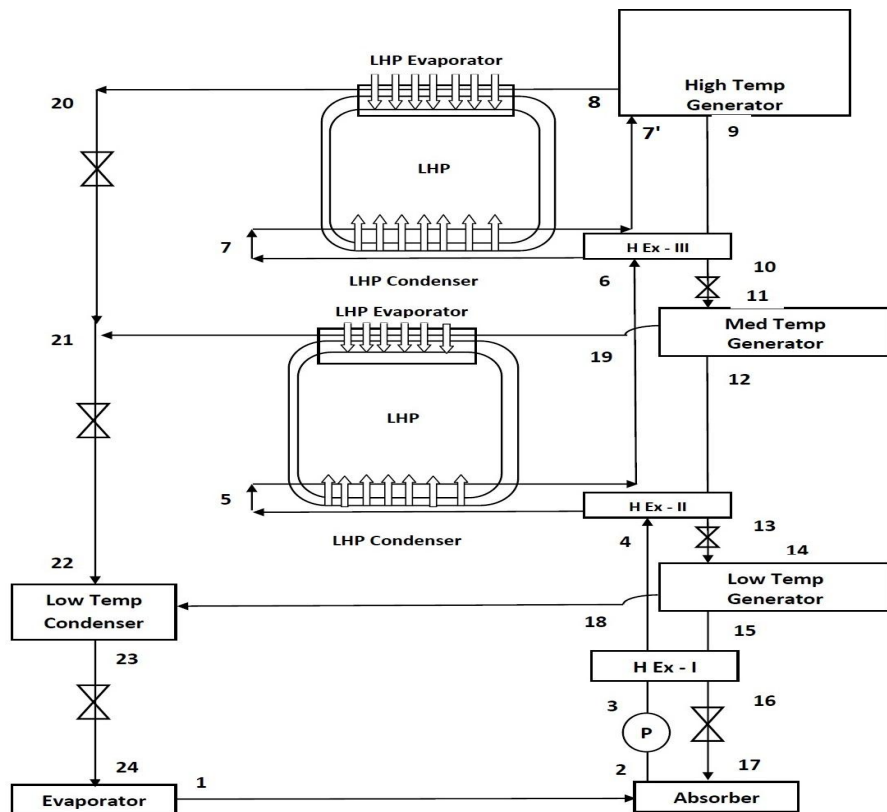


Fig 4.11. Modified Triple Effect VARS-I [186]

- a. Refrigerant Expansion Valves I, II & III (States 20-21, 21-17 & 23-24)
- b. Evaporator (States 24-1)
- c. Absorber (States 1-2 & 17-2)

- d. Mixture Pump (States 2-3)
- e. Mixture Heat Exchange-I, II & III (States 3-4 & 15-16, States 4-5 & 12-13 and States 6-7 & 9-10)
- f. LHP I & II Condenser (States 5-6 & 7-7')
- g. Low, Med & High-T Generator (States 14-15 & 14-18, States 11-12 & 11-19 and States 7'-8 & 7'-9)
- h. LHP I & II Evaporator (States 19-21 & 8-20)
- i. Mixture Reducing Valve- I, II & III (States 10-11, 13-14, & 16-17)
- j. Low Temperature Condenser (States 22-23 & 18-23)

Mass Continuity Equations, m:

$$m_8 = m_{20} \quad (4.215)$$

$$m_{21} = m_{22} \quad (4.216)$$

$$m_{23} = m_{24} = m_1 \quad (4.217)$$

$$m_2 = m_3 = m_4 = m_5 = m_6 = m_7 = m_{7'} \quad (4.218)$$

$$m_{11} = m_{10} = m_9 \quad (4.219)$$

$$m_{14} = m_{12} = m_{13} \quad (4.220)$$

$$m_{15} = m_{16} = m_{17} \quad (4.221)$$

$$m_{21} = m_{20} + m_{19} \quad (4.222)$$

$$m_{23} = m_{22} + m_{18} \quad (4.223)$$

$$m_{7'} = m_8 + m_9 \quad (4.224)$$

$$m_{11} = m_{12} + m_{19} \quad (4.225)$$

$$m_{14} = m_{15} + m_{18} \quad (4.226)$$

Chemical Composition Balance Equations, m ζ :

$$m_{7'}\zeta_7 = m_9 \zeta_9 \quad (4.227)$$

$$m_{11}\zeta_{11} = m_{12} \zeta_{12} \quad (4.229)$$

$$m_{14}\zeta_{14} = m_{15} \zeta_{15} \quad (4.230)$$

Percentage Absorbent Balance Equation, ζ :

$$\zeta_2 = \zeta_3 = \zeta_4 = \zeta_6 = \zeta_5 = \zeta_7 \quad (4.232)$$

$$\zeta_{15} = \zeta_{16} = \zeta_{17} \quad (4.233)$$

$$\zeta_8 = \zeta_9 = \zeta_{10} \quad (4.234)$$

$$\zeta_{13} = \zeta_{12} = \zeta_{14} \quad (4.235)$$

$$\text{COP} = \text{RE} / (\text{Q}_{\text{GH-T}} + \text{W}_\text{P}) \quad (4.236)$$

Solution Circulation Ratio, F:

$$F = \zeta_7 / (\zeta_9 - \zeta_7) \quad (4.237)$$

$$F = \zeta_{11} / (\zeta_{12} - \zeta_{11}) \quad (4.238)$$

$$F = \zeta_{14} / (\zeta_{15} - \zeta_{14}) \quad (4.239)$$

a. Refrigerant Expansion Valves I, II & III (States 20-21, 21-17 & 23-24)

Expansion Valve-I can be expressed as,

$$h_{20} = h_{21'} \quad (4.240)$$

Where h_{20} is the enthalpy of saturated liquid exiting the LHP Evaporator as x_{20} is 0 for this state. Moreover, State 21' is the state after the Expansion Valve-I.

$$x_{21'} = (h_{20} - h_{f21'}) / h_{fg21'} \quad (4.241)$$

$$m_{21}h_{21} = m_{21'}h_{21'} + m_{19'}h_{19'} \quad (4.242)$$

Here $h_{f21'}$ is the enthalpy of saturated liquid at pressure of state 21' & $h_{fg21'}$ is the enthalpy of evaporation at the pressure of state 21' and state 19' is the state of condensate out of the LHP-II.

Moreover, Expansion Valve-II can be expressed as,

$$h_{21} = h_{22} \quad (4.243)$$

Where h_{22} is the enthalpy at the exit of Valve-II.

$$X_{22} = (h_{21} - h_{f22}) / h_{fg22} \quad (4.244)$$

Here h_{22} is the enthalpy of saturated liquid at pressure of state 22 & h_{fg22} is the enthalpy of evaporation at the pressure of state 22.

Moreover, Expansion Valve-III can be expressed as,

$$h_{23} = h_{24} \quad (4.245)$$

Where h_{23} is the enthalpy of saturated liquid exiting the Low-T condenser as x_{16} is 0 for this state.

$$X_{24} = (h_{23} - h_{f24}) / h_{fg24} \quad (4.246)$$

Here h_{f24} is the enthalpy of saturated liquid at pressure of state 24 & h_{fg24} is the enthalpy of evaporation at the pressure of state 24.

b. Evaporator (States 24-1)

The modeling can be given as:

Energy Analysis:

$$RE = m_{24} (h_1 - h_{24}) \quad (4.247)$$

Exergy Analysis:

$$X_{Evap} = m_{1'} [(h_{24'} - h_{1'}) - T_O (s_{24'} - s_{1'})] \quad (4.248)$$

Where X_{Evap} is the Exergy of the Evaporator, s is the corresponding specific entropy & T_O is the environment temperature. The states 24' & 1' are the inlet and outlet states of the fluid getting cooled in the evaporator. $m_{1'}$ is the mass flow rate of the fluid.

c. Absorber (States 1-2 & 17-2)

The modeling can be done for Heat Rejected in Absorber Q_{Abs} .

Energy Analysis:

$$Q_{Abs} = m_1 h_1 + m_{17} h_{17} - m_2 h_2 \quad (4.249)$$

Exergy Analysis:

$$X_{Abs} = m_2 [(h_{17'} - h_{2'}) - T_O (s_{17'} - s_{2'})] \quad (4.250)$$

Where X_{Abs} the Exergy of Absorber, s is the corresponding specific entropy & T_O is the environment temperature and the states $17'$ & $2'$ are the inlet and outlet states of the fluid getting heated in the absorber. m_2 is the mass flow rate of the fluid.

d. Mixture Pump (States 2-3)

The Work input in the Pumps can be given as W_P :

$$W_P = m_2 v_2 (dP) \quad (4.251)$$

Where v_2 is the specific volume of the mixture and dP is the pressure raised by the pump.

Also, Specific Enthalpy at the Exit of the Pumps can be given as:

$$h_3 = m_2 h_2 + W_P \quad (4.252)$$

e. Mixture Heat Exchange-I, II & III (States 3-4 & 15-16, States 4-5 & 12-13 and States 6-7 & 9-10)

It can be modeled as the followings:

Energy Analysis for HEx-I:

$$\text{Effectiveness of Heat Exchanger, } \epsilon_{H-Ex-I} = (T_{15} - T_{16}) / (T_{15} - T_3) \quad (4.253)$$

Heat Exchange in the Heat Exchanger,

$$Q_{H-Ex-I} = m_4 (h_4 - h_3) = m_{15} (h_{15} - h_{16}) \quad (4.254)$$

$$\text{Specific Heat Capacity for Hot Fluid, } c_{Hot-I} = (h_{15} - h_{16}) / (T_{15} - T_{16}) \quad (4.255)$$

$$\text{Specific Heat Capacity for Cold Fluid, } c_{Cold-I} = (h_4 - h_3) / (T_4 - T_3) \quad (4.256)$$

Exergy Analysis for HEx-I:

$$X_{H-Ex-I} = m_3 [(h_3 - h_4) - T_O (s_3 - s_4)] \quad (4.257)$$

Where X_{H-Ex-I} is the Exergy of the Heat Exchanger-I, s is the corresponding specific entropy & T_O is the environment temperature.

Energy Analysis for HEx-II:

$$\text{Effectiveness of Heat Exchanger, } \varepsilon_{H-Ex-II} = (T_{12}-T_{13}) / (T_{12}-T_4) \quad (4.258)$$

Heat Exchange in the Heat Exchanger,

$$Q_{H-Ex-II} = m_4(h_5 - h_4) = m_{12}(h_{12} - h_{13}) \quad (4.259)$$

$$\text{Specific Heat Capacity for Hot Fluid, } c_{Hot-II} = (h_{12} - h_{13}) / (T_{12}-T_{13}) \quad (4.260)$$

$$\text{Specific Heat Capacity for Cold Fluid, } c_{Cold-II} = (h_4 - h_5) / (T_4-T_5) \quad (4.261)$$

Exergy Analysis for HEx-II:

$$X_{H-Ex-II} = m_4[(h_4-h_5) - T_O (s_4-s_5)] \quad (4.262)$$

Where $X_{H-Ex-II}$ is the Exergy of the Heat Exchanger-II, s is the corresponding specific entropy & T_O is the environment temperature.

Energy Analysis for HEx-III:

$$\text{Effectiveness of Heat Exchanger, } \varepsilon_{H-Ex-III} = (T_9-T_{10}) / (T_9-T_6) \quad (4.263)$$

Heat Exchange in the Heat Exchanger,

$$Q_{H-Ex-III} = m_6(h_7 - h_6) = m_9(h_9 - h_{10}) \quad (4.264)$$

$$\text{Specific Heat Capacity for Hot Fluid, } c_{Hot-III} = (h_9 - h_{10}) / (T_9-T_{10}) \quad (4.265)$$

Specific Heat Capacity for Cold Fluid,

$$c_{Cold-III} = (h_7 - h_6) / (T_7-T_6) \quad (4.266)$$

Exergy Analysis for HEx-III:

$$X_{H-Ex-III} = m_6[(h_6-h_7) - T_O (s_6-s_7)] \quad (4.267)$$

Where $X_{H-Ex-III}$ is the Exergy of the Heat Exchanger-III, s is the corresponding specific entropy & T_O is the environment temperature.

f. LHP I & II Condenser (States 5-6 & 7-7')

Modeling for LHP-I

Energy Analysis:

$$\text{Heat Input to the Mixture, } Q_{\text{InMixI}} = m_5(h_6-h_5) \quad (4.268)$$

Heat Rejected by the Condensing Fluid in LHP-I,

$$Q_{\text{LHPICond}} = m_{\text{LHPI}} (h_{\text{fgLHPICond}} + c_F \Delta T_{\text{SubI}}) \quad (4.269)$$

Where $h_{\text{fgLHPICond}}$ is the latent heat of condensation in the LHP-I Condenser, c_F is the specific heat capacity, m_{LHPI} is the mass flow in the LHP-I & ΔT_{SubI} is the degree of subcooling in LHP-I condenser for the LHP-I working fluid.

Effectiveness of the LHP-I Condenser,

$$\epsilon_{\text{LHPICond}} = (T_6 - T_5) / (T_{\text{InLHPICond}} - T_5) \quad (4.270)$$

Where $T_{\text{InLHPICond}}$ is the Input Temperature of the LHP-II Condenser.

Exergy Analysis:

$$X_{\text{LHPICond}} = m_5[(h_5-h_6) - T_0 (s_5-s_6)] \quad (4.271)$$

Where X_{LHPICond} is the Exergy of the Heat Exchanger, s is the corresponding specific entropy & T_0 is the environment temperature.

Modeling for LHP-II

Energy Analysis:

$$\text{Heat Input to the Mixture, } Q_{\text{InMixII}} = m_7(h_7-h_7) \quad (4.272)$$

Heat Rejected by the Condensing Fluid in LHP-II,

$$Q_{\text{LHPICond}} = m_{\text{LHPII}} (h_{\text{fgLHPICond}} + c_F \Delta T_{\text{SubII}}) \quad (4.273)$$

Where $h_{\text{fgLHPICond}}$ is the latent heat of condensation in the LHP-II Condenser, c_F is the specific heat capacity, m_{LHPII} is the mass flow in the LHP-II & ΔT_{SubII} is the degree of subcooling in the LHP-II condenser for the LHP-II working fluid.

Effectiveness of the LHP-II Condenser,

$$\varepsilon_{\text{LHP-Cond}} = (T_{7'} - T_7) / (T_{\text{InLHP-Cond}} - T_7) \quad (4.274)$$

Where $T_{\text{InLHP-Cond}}$ is the Input Temperature of the LHP-II Condenser.

Exergy Analysis:

$$X_{\text{LHP-Cond}} = m_7[(h_7 - h_{7'}) - T_0 (s_7 - s_{7'})] \quad (4.275)$$

Where $X_{\text{LHP-Cond}}$ is the Exergy of the Heat Exchanger, s is the corresponding specific entropy & T_0 is the environment temperature.

g. Low, Med & High-T Generator (States 14-15 & 14-18, States 11-12 & 11-19 and States 7'-8 & 7'-9)

Heat is added to the mixture in the generator. This heat input to the High-Temperature Generator $Q_{\text{GH-T}}$, Medium Temperature Generator, $Q_{\text{GM-T}}$ & Low-Temperature Generator $Q_{\text{GL-T}}$ can be expressed as:

Energy Analysis, High-Temperature Generator:

$$Q_{\text{GH-T}} = h_8 m_8 + h_9 m_9 - h_{7'} m_{7'} \quad (4.276)$$

Exergy Analysis, High Temperature Generator:

$$X_{\text{GH-T}} = m_{8'}[(h_{8'} - h_{9'}) - T_0 (s_{8'} - s_{9'})] \quad (4.277)$$

Where $X_{\text{GH-T}}$ is the Exergy of the High-T Generator, s is the corresponding specific entropy & T_0 is the environment temperature and the states 8' & 9' are the inlet and outlet states of the fluid supplying heat to the generator. $m_{8'}$ is the mass flow rate of the fluid.

Energy Analysis, Medium Temperature Generator:

$$Q_{\text{GM-T}} = h_{19} m_{19} + h_{12} m_{12} - h_{11} m_{11} \quad (4.278)$$

Exergy Analysis, Medium Temperature Generator:

$$X_{\text{GM-T}} = m_{11'}[(h_{11'} - h_{12'}) - T_0 (s_{11'} - s_{12'})] \quad (4.279)$$

Where $X_{\text{GM-T}}$ is the Exergy of the Med-T Generator, s is the corresponding specific entropy & T_0 is the environment temperature and the states 11' & 12' are the inlet

and outlet states of the fluid supplying heat to the generator. $m_{11'}$ is the mass flow rate of the fluid.

Energy Analysis, Low Temperature Generator:

$$Q_{GL-T} = h_{15}m_{15} + h_{18}m_{18} - h_{14}m_{14} \quad (4.280)$$

Exergy Analysis, Low Temperature Generator:

$$X_{GL-T} = m_{14'} [(h_{14'} - h_{15'}) - T_O (s_{14'} - s_{15'})] \quad (4.281)$$

Where X_{GL-T} is the Exergy of the Low-T Generator, s is the corresponding specific entropy & T_O is the environment temperature and the states 14' & 15' are the inlet and outlet states of the fluid supplying heat to the generator. $m_{14'}$ is the mass flow rate of the fluid.

h. LHP I & II Evaporator (States 19-21 & 8-20)

LHP-I can be modeled as:

Energy Analysis:

Heat Rejected by the Condensing Refrigerant,

$$Q_{CondRI} = m_{19} (h_{19} - h_{19'}) \quad (4.282)$$

Heat Absorbed by the LHP Working Fluid in the LHP Evaporator,

$$Q_{LHPIEvap} = m_{LHPI} (h_{fgLHPIEvap} + c_F \Delta T_{SupI}) \quad (4.283)$$

Where $h_{fgLHPIEvap}$ is the latent heat of evaporation in the LHP Evaporator, c_F is the specific heat capacity, m_{LHPI} is the mass flow in the LHP-I & ΔT_{SupI} is the degree of superheat in the LHP evaporator for the LHP-I working fluid. State 19' is the exit of the LHP-I Evaporator.

Exergy Analysis:

$$X_{LHPIEvap} = m_{19} [(h_{19} - h_{19'}) - T_O (s_{19} - s_{19'})] \quad (4.284)$$

Where $X_{LHPIEvap}$ is the Exergy of the LHP Evaporator, s is the corresponding specific entropy & T_O is the environment temperature.

LHP-II can be modeled as:

Energy Analysis:

Heat Rejected by the Condensing Refrigerant,

$$Q_{\text{CondRII}} = m_8 (h_8 - h_{20}) \quad (4.285)$$

Heat Absorbed by the LHP Working Fluid in the LHP Evaporator,

$$Q_{\text{LHP IIEvap}} = m_{\text{LHP II}} (h_{\text{fgLHP IIEvap}} + c_F \Delta T_{\text{Sup II}}) \quad (4.286)$$

Where $h_{\text{fgLHP IIEvap}}$ is the latent heat of evaporation in the LHP-II Evaporator, c_F is the specific heat capacity, $m_{\text{LHP II}}$ is the mass flow in the LHP & $\Delta T_{\text{Sup II}}$ is the degree of superheat in the LHP evaporator for the LHP-II working fluid.

Exergy Analysis:

$$X_{\text{LHP IIEvap}} = m_7 [(h_7 - h_{14}) - T_O (s_7 - s_{14})] \quad (4.287)$$

Where $X_{\text{LHP IIEvap}}$ is the Exergy of the LHP-II Evaporator, s is the corresponding specific entropy & T_O is the environment temperature.

i. Mixture Reducing Valve- I, II & III (States 10-11, 13-14 & 16-17)

Modeling can be done as:

$$h_{10} = h_{11} \quad (4.288)$$

$$h_{13} = h_{14} \quad (4.289)$$

$$h_{16} = h_{17} \quad (4.290)$$

j. Low Temperature Condenser (States 22-23 & 18-23)

The Low-T Condenser deals with the liquid refrigerant coming out of the LHP-I & II and Refrigerant Expansion Valve-I & II and mixes it with the liquid refrigerant obtained after condensing the vapour coming out of the Low-T Generator. The heat rejected from the low-T Condenser can be modeled as:

Energy Analysis:

$$Q_{\text{L-Cond}} = m_{18}h_{18} + m_{22}h_{22} - m_{23}h_{23} \quad (4.291)$$

Exergy Analysis:

$$X_{L-Cond} = m_{22'} [(h_{22'} - h_{23'}) - T_O (s_{22'} - s_{23'})] \tag{4.292}$$

Where X_{L-Cond} is the Exergy of the Low-Temperature Condenser, s is the corresponding specific entropy & T_O is the environment temperature. The states 22' & 23' are the inlet and outlet states of the fluid getting cooled in the condenser. $m_{22'}$ is the mass flow rate of the fluid.

4.5.2. Modified Triple Effect VARS-II

The modified system has been shown in Fig 4.12 in which it has been proposed that the Heat Exchangers of Modified System-I are replaced with LHP-I, LHP-II & LHP-IV.

Hence, similar to the previous systems LHP-I & LHP-II have been nominated in LHP-III & LHP-V respectively. LHP-I, LHP-II & LHP-IV can be modeled with the following methodology.

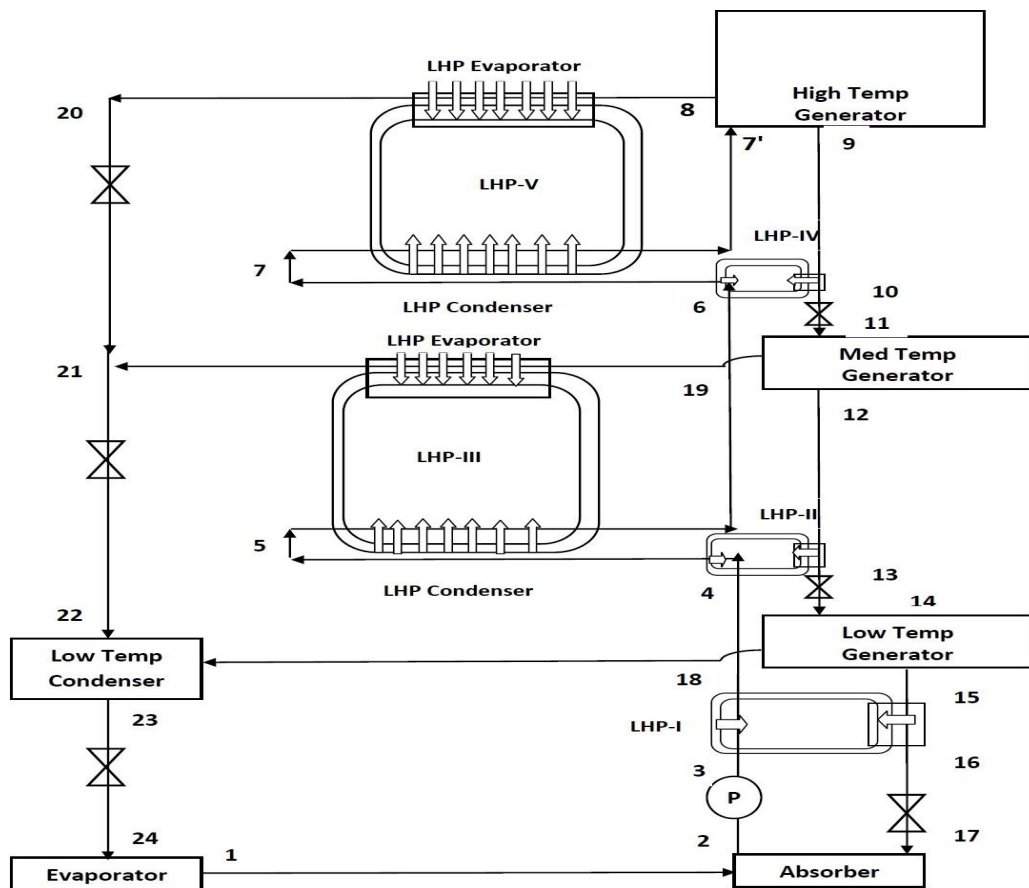


Fig 4.12. Modified Triple Effect VARS-II

e. LHP-I, II & IV (States 3-4 & 15-16, States 4-5 & 12-13 and States 6-7 & 9-10)

• LHP-I Condenser

Energy Analysis:

$$\text{Heat Input to the Mixture, } Q_{\text{InMixI}} = m_3 (h_4 - h_3) \quad (4.293)$$

Heat Rejected by the Condensing Fluid in LHP,

$$Q_{\text{LHPICond}} = m_{\text{LHPI}} (h_{\text{fgLHPICond}} + c_F \Delta T_{\text{SubI}}) \quad (4.294)$$

Where $h_{\text{fgLHPICond}}$ is the latent heat of condensation in the LHP-I Condenser, c_F is the specific heat capacity, m_{LHPI} is the mass flow in the LHP-I & ΔT_{SubI} is the degree of subcooling in LHP-I condenser for the LHP-I working fluid.

$$\text{Effectiveness of the LHP-I Condenser, } \varepsilon_{\text{LHPICond}} = (T_4 - T_3) / (T_{\text{InLHPICond}} - T_3) \quad (4.295)$$

Where $T_{\text{InLHPICond}}$ is the Input Temperature of the LHP-I Condenser.

Exergy Analysis:

$$X_{\text{LHPICond}} = m_3 [(h_3 - h_4) - T_0 (s_3 - s_4)] \quad (4.296)$$

Where X_{LHPICond} is the Exergy of the LHP-I, s is the corresponding specific entropy & T_0 is the environment temperature.

• LHP-I Evaporator

Energy Analysis:

$$\text{Heat Rejected by the Absorbent, } Q_{\text{RejI}} = m_{11} (h_{11} - h_{12}) \quad (4.297)$$

Heat Absorbed by the LHP-I Working Fluid in the LHP-I Evaporator,

$$Q_{\text{LHPIEvap}} = m_{\text{LHPI}} (h_{\text{fgLHPIEvap}} + c_F \Delta T_{\text{SupI}}) \quad (4.298)$$

Where $h_{\text{fgLHPIEvap}}$ is the latent heat of evaporation in the LHP-I Evaporator, c_F is the specific heat capacity, m_{LHPI} is the mass flow in the LHP-I & ΔT_{SupI} is the degree of superheat in the LHP-I evaporator for the LHP-I working fluid.

Exergy Analysis:

$$X_{\text{LHP-IEvap}} = m_{11}[(h_{11}-h_{12}) - T_O (s_{11}-s_{12})] \quad (4.299)$$

Where $X_{\text{LHP-IEvap}}$ is the Exergy of the LHP-I Evaporator, s is the corresponding specific entropy & T_O is the environment temperature.

- **LHP-II Condenser**

Energy Analysis:

$$\text{Heat Input to the Mixture, } Q_{\text{InMixII}} = m_4(h_5-h_4) \quad (4.300)$$

Heat Rejected by the Condensing Fluid in LHP,

$$Q_{\text{LHP-II Cond}} = m_{\text{LHP-II}} (h_{\text{fgLHP-II Cond}} + c_F \Delta T_{\text{SubII}}) \quad (4.301)$$

Where $h_{\text{fgLHP-II Cond}}$ is the latent heat of condensation in the LHP-II Condenser, c_F is the specific heat capacity, $m_{\text{LHP-II}}$ is the mass flow in the LHP-II & ΔT_{SubII} is the degree of subcooling in the LHP-II condenser for the LHP-II working fluid.

Effectiveness of the LHP-II Condenser,

$$\epsilon_{\text{LHP-II Cond}} = (T_5 - T_4) / (T_{\text{InLHP-II Cond}} - T_4) \quad (4.302)$$

Where $T_{\text{InLHP-II Cond}}$ is the Input Temperature of the LHP-II Condenser.

Exergy Analysis:

$$X_{\text{LHP-II Cond}} = m_4[(h_4-h_5) - T_O (s_4-s_5)] \quad (4.303)$$

Where $X_{\text{LHP-II Cond}}$ is the Exergy of the LHP-II, s is the corresponding specific entropy & T_O is the environment temperature.

- **LHP-II Evaporator**

Energy Analysis:

$$\text{Heat Rejected by the Absorbent, } Q_{\text{RejII}} = m_{12}(h_{12} - h_{13}) \quad (4.303)$$

Heat Absorbed by the LHP-II Working Fluid in the LHP-II Evaporator,

$$Q_{\text{LHP-II Evap}} = m_{\text{LHP-II}} (h_{\text{fgLHP-II Evap}} + c_F \Delta T_{\text{SupII}}) \quad (4.304)$$

Where $h_{fgLHP\text{IIEvap}}$ is the latent heat of evaporation in the LHP-II Evaporator, c_F is the specific heat capacity, $m_{LHP\text{II}}$ is the mass flow in the LHP-II & ΔT_{SupII} is the degree of superheat in the LHP-II evaporator for the LHP-II working fluid.

Exergy Analysis:

$$X_{LHP\text{IIEvap}} = m_{12}[(h_{12}-h_{13}) - T_O (s_{12}-s_{13})] \quad (4.305)$$

Where $X_{LHP\text{IIEvap}}$ is the Exergy of the LHP-II Evaporator, s is the corresponding specific entropy & T_O is the environment temperature.

• **LHP-IV Condenser**

Energy Analysis:

$$\text{Heat Input to the Mixture, } Q_{\text{InMixIV}} = m_6(h_7-h_6) \quad (4.306)$$

Heat Rejected by the Condensing Fluid in LHP,

$$Q_{LHP\text{IVCond}} = m_{LHP\text{IV}} (h_{fgLHP\text{IVCond}} + c_F \Delta T_{\text{SubIV}}) \quad (4.307)$$

Where $h_{fgLHP\text{IVCond}}$ is the latent heat of condensation in the LHP-IV Condenser, c_F is the specific heat capacity, $m_{LHP\text{IV}}$ is the mass flow in the LHP-IV & ΔT_{SubIV} is the degree of subcooling in the LHP-IV condenser for the LHP-IV working fluid.

Effectiveness of the LHP-IV Condenser,

$$\epsilon_{LHP\text{IVCond}} = (T_7-T_6) / (T_{\text{InLHP\text{IVCond}}}-T_6) \quad (4.308)$$

Where $T_{\text{InLHP\text{IVCond}}}$ is the Input Temperature of the LHP-IV Condenser.

Exergy Analysis:

$$X_{LHP\text{IVCond}} = m_6[(h_6-h_7) - T_O (s_6-s_7)] \quad (4.309)$$

Where $X_{LHP\text{IVCond}}$ is the Exergy of the LHP-IV, s is the corresponding specific entropy & T_O is the environment temperature.

• **LHP-IV Evaporator**

Energy Analysis:

$$\text{Heat Rejected by the Absorbent, } Q_{\text{RejIV}} = m_9(h_9 - h_{10}) \quad (4.310)$$

Heat Absorbed by the LHP-IV Working Fluid in the LHP-IV Evaporator,

$$Q_{\text{LHP-IV Evap}} = m_{\text{LHP-IV}} (h_{\text{fgLHP-IV Evap}} + c_F \Delta T_{\text{SupIV}}) \quad (4.311)$$

Where $h_{\text{fgLHP-IV Evap}}$ is the latent heat of evaporation in the LHP-IV Evaporator, c_F is the specific heat capacity, $m_{\text{LHP-IV}}$ is the mass flow in the LHP-IV & ΔT_{SupIV} is the degree of superheat in the LHP-IV evaporator for the LHP-IV working fluid.

Exergy Analysis:

$$X_{\text{LHP-IV Evap}} = m_9 [(h_9 - h_{10}) - T_0 (s_9 - s_{10})] \quad (4.312)$$

Where $X_{\text{LHP-IV Evap}}$ is the Exergy of the LHP-IV Evaporator, s is the corresponding specific entropy & T_0 is the environment temperature.

4.5.3. Combined GPC & Triple-Effect VARS using LHP

The Modified Triple Effect VARS-II has been combined with the Reheating-Regenerative & Multi-compression system through LHP-VI as shown in Fig 4.13. The inlet to the GPC is at state 25 & the exit of the exhaust leaves the LHP-VI Evaporator at 35.

In addition to the modeling of the GPC presented in section 4.1. Also, the temperature at state 30 & state 32 is the same. The LHP-VI has been modeled similar to the previous section:

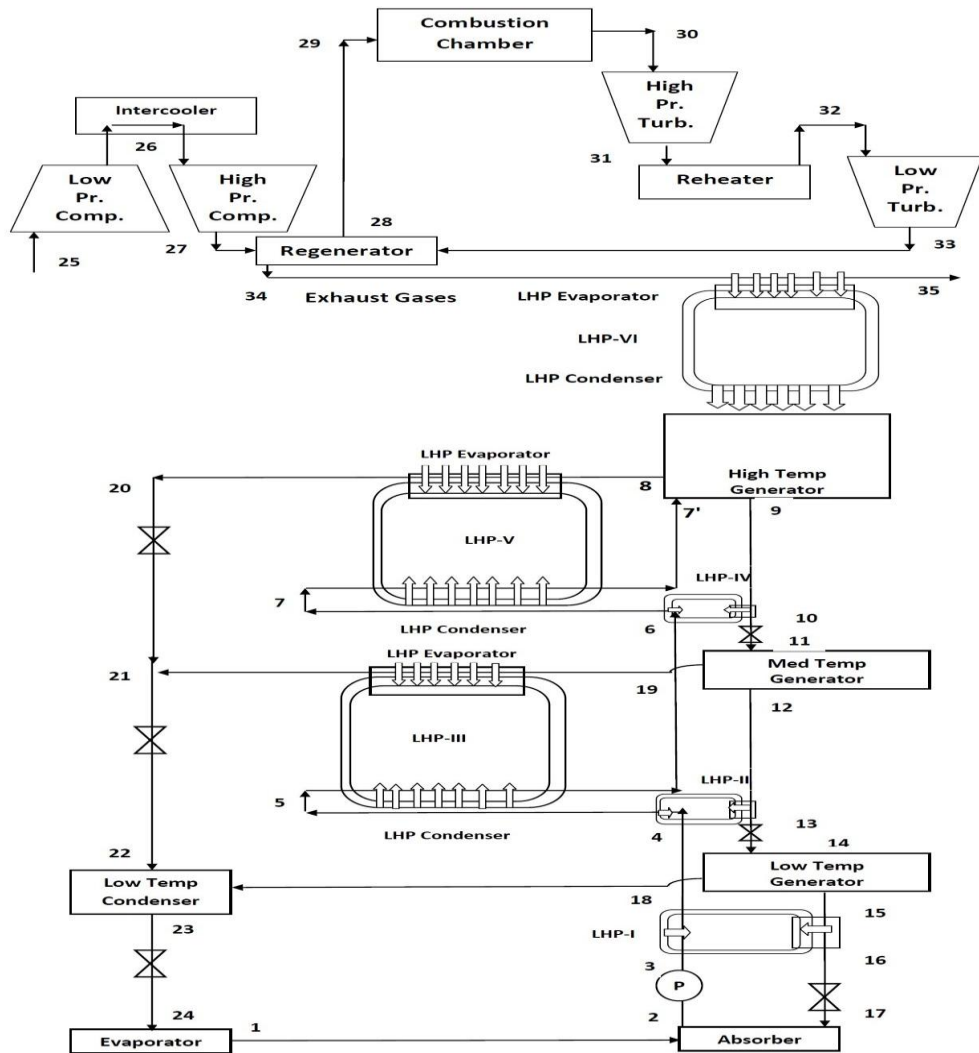


Fig. 4.13: Combined GPC & Triple Effect VARS

k. Gas Power Cycle (State 12-21)

The heat input to the LHP-VI, $Q_{InLHPVI}$ can be calculated as:

$$Q_{InLHPVI} = \dot{m}_g c_{pg} (T_{34} - T_{35}) \tag{4.313}$$

l. LHP-VI

The heat rejected at the exhaust of GPC is harnessed by the LHP-VI Evaporator and transferred to the VARS Generator through LHP-VI Condensers.

• LHP-VI Evaporator

Energy Analysis:

$$Q_{InLHPVI} = \dot{m}_g c_{pg} (T_{34} - T_{35}) \tag{4.314}$$

Heat Absorbed by the LHP-VI Working Fluid in the LHP-VI Evaporator,

$$Q_{\text{LHPVIEvap}} = m_{\text{LHPVI}} (h_{\text{fgLHPVIEvap}} + c_F \Delta T_{\text{SupVI}}) \quad (4.315)$$

Where $h_{\text{fgLHPVIEvap}}$ is the latent heat of evaporation in the LHP-VI Evaporator, c_F is the specific heat capacity, m_{LHPVI} is the mass flow in the LHP-VI & ΔT_{SupVI} is the degree of superheat in the LHP-VI evaporator for the LHP-VI working fluid.

Exergy Analysis:

$$X_{\text{LHPVIEvap}} = m_g [(h_{34} - h_{35}) - T_O (s_{34} - s_{35})] \quad (4.316)$$

Where $X_{\text{LHPVIEvap}}$ is the Exergy of the LHP-VI Evaporator, s is the corresponding specific entropy & T_O is the environment temperature.

• **LHP-VI Condenser**

Energy Analysis:

Heat Input to the Generator,

$$Q_{\text{InGenerator}} = h_9 m_9 + h_8 m_8 - h_7 \cdot m_7 \quad (4.317)$$

Heat Rejected by the Condensing Fluid in LHP into the Generator,

$$Q_{\text{LHPVICond}} = m_{\text{LHPVI}} (h_{\text{fgLHPVICond}} + c_F \Delta T_{\text{SubVI}}) \quad (4.318)$$

Where $h_{\text{fgLHPVICond}}$ is the latent heat of condensation in the LHP-VI Condenser, c_F is the specific heat capacity, m_{LHPVI} is the mass flow in the LHP-VI & ΔT_{SubVI} is the degree of subcooling in the LHP-VI condenser for the LHP-VI working fluid.

4.6. Modified Quadruple Effect VARS

This section deals with the modeling of the 03 systems obtained with the modifications proposed in the Quadruple Effect VARS using LHPs.

4.6.1. Modified Quadruple Effect VARS-I

Fig 4.14 shows the system under consideration which has been elaborately discussed in Chapter-3.

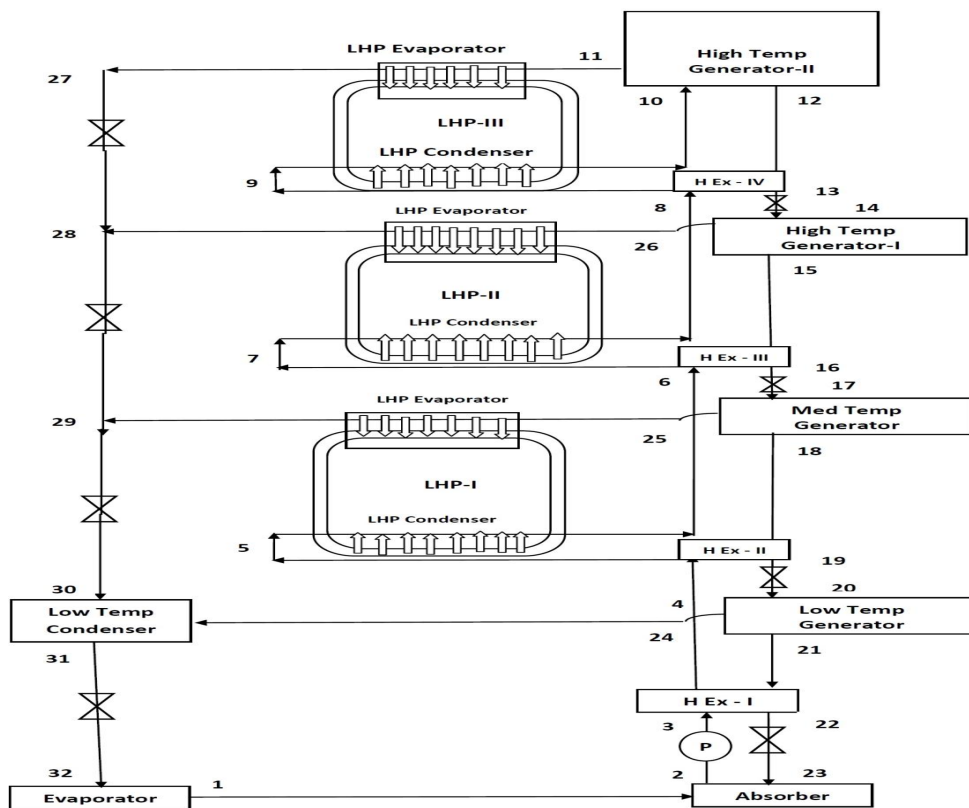


Fig 4.14. Modified Quadruple Effect VARS-I

- a. Refrigerant Expansion Valves I, II, III & IV (States 27-28, 28-29, 29-30 & 31-32)
- b. Evaporator (States 32-1)
- c. Absorber (States 1-2 & 23-2)
- d. Mixture Pump-I (States 2-3)

- e. Mixture Heat Exchange-I, II, III & IV (States 3-4 & 21-22, States 4-5 & 18-19, States 6-7 & 15-16 and States 8-9 & 12-13)
- f. LHP I, II & III Condenser (States 5-6, 7-8 & 9-10)
- g. Low, Med, High-T Generator-I & II (States 20-21 & 20-24, States 17-18 & 17-25, States 14-15 & 14-26 and States 10-12 & 10-11)
- h. LHP I, II & III Evaporator (States 25-29, 26-28 & 11-27)
- i. Mixture Reducing Valve- I, II, III & IV (States 13-14, 16-17, 19-20 & 22-23)
- j. Low Temperature Condenser (States 24-31 & 30-31)

Mass Continuity Equations, m:

$$m_{11} = m_{27} \tag{4.319}$$

$$m_{29} = m_{30} \tag{4.320}$$

$$m_{31} = m_{32} = m_1 \tag{4.321}$$

$$m_2 = m_3 = m_4 = m_5 = m_6 = m_8 = m_9 = m_{10} \tag{4.322}$$

$$m_{18} = m_{19} = m_{20} \tag{4.323}$$

$$m_{14} = m_{12} = m_{13} \tag{4.324}$$

$$m_{15} = m_{16} = m_{17} \tag{4.325}$$

$$m_{21} = m_{22} = m_{23} \tag{4.326}$$

$$m_{29} = m_{28} + m_{25} \tag{4.327}$$

$$m_{28} = m_{27} + m_{11} \tag{4.328}$$

$$m_{31} = m_{30} + m_{24} \tag{4.329}$$

$$m_{10} = m_{11} + m_{12} \tag{4.330}$$

$$m_{14} = m_{15} + m_{26} \tag{4.331}$$

$$m_{17} = m_{18} + m_{15} \tag{4.332}$$

$$m_{20} = m_{21} + m_{24} \tag{4.333}$$

Chemical Composition Balance Equations, $m\zeta$:

$$m_{10}\zeta_{10} = m_{12} \zeta_{12} \quad (4.334)$$

$$m_{14}\zeta_{14} = m_{15} \zeta_{15} \quad (4.335)$$

$$m_{17}\zeta_{17} = m_{18}\zeta_{18} \quad (4.336)$$

$$m_{20}\zeta_{20} = m_{21} \zeta_{21} \quad (4.337)$$

Percentage Absorbent Balance Equation, ζ :

$$\zeta_2 = \zeta_3 = \zeta_4 = \zeta_6 = \zeta_5 = \zeta_7 = \zeta_8 = \zeta_9 = \zeta_{10} \quad (4.338)$$

$$\zeta_{15} = \zeta_{16} = \zeta_{17} \quad (4.339)$$

$$\zeta_{18} = \zeta_{19} = \zeta_{20} \quad (4.340)$$

$$\zeta_{13} = \zeta_{12} = \zeta_{14} \quad (4.341)$$

$$\zeta_{21} = \zeta_{22} = \zeta_{23} \quad (4.342)$$

$$COP = RE / (Q_{GH-T-II} + W_P) \quad (4.343)$$

Solution Circulation Ratio, F :

$$F = \zeta_{10} / (\zeta_{12} - \zeta_{10}) \quad (4.344)$$

$$F = \zeta_{14} / (\zeta_{15} - \zeta_{14}) \quad (4.345)$$

$$F = \zeta_{17} / (\zeta_{18} - \zeta_{17}) \quad (4.346)$$

$$F = \zeta_{20} / (\zeta_{21} - \zeta_{20}) \quad (4.347)$$

a. Refrigerant Expansion Valves I, II, III & IV (States 27-28, 28-29, 29-30 & 31-32)

Expansion Valve-I can be expressed as,

$$h_{27} = h_{27'} \quad (4.348)$$

Where h_{27} is the enthalpy of saturated liquid exiting the LHP Evaporator as x_{27} is 0 for this state. Moreover, State 27' is the state after the Expansion Valve-I.

$$x_{27'} = (h_{27} - h_{f27'}) / h_{fg27'} \quad (4.349)$$

$$m_{28}h_{28} = m_{27}h_{27'} + m_{26}h_{26'} \quad (4.350)$$

Here $h_{f27'}$ is the enthalpy of saturated liquid at pressure of state 27' & $h_{fg27'}$ is the enthalpy of evaporation at the pressure of state 27' and state 26' is the condensate at exit of the LHP-II.

Moreover, Expansion Valve-II can be expressed as,

$$h_{28} = h_{28'} \quad (4.351)$$

Where h_{22} is the enthalpy at the exit of Valve-II.

$$X_{28'} = (h_{28} - h_{f28'}) / h_{fg28'} \quad (4.352)$$

$$m_{29}h_{29} = m_{28}h_{28'} + m_{25}h_{25'} \quad (4.353)$$

Here $h_{28'}$ is the enthalpy of saturated liquid at pressure of state 28' & $h_{fg28'}$ is the enthalpy of evaporation at the pressure of state 28' and state 25' is the condensate at exit of the LHP-I.

Moreover, Expansion Valve-III can be expressed as,

$$h_{30} = h_{29} \quad (4.354)$$

Where h_{23} is the enthalpy of saturated liquid exiting the Low-T condenser as x_{16} is 0 for this state.

$$x_{30} = (h_{29} - h_{f30}) / h_{fg30} \quad (4.355)$$

Here h_{f30} is the enthalpy of saturated liquid at a pressure of state 30 & h_{fg30} is the enthalpy of evaporation at the pressure of state 30.

Moreover, Expansion Valve-IV can be expressed as,

$$h_{31} = h_{32} \quad (4.356)$$

Where h_{23} is the enthalpy of saturated liquid exiting the Low-T condenser as x_{16} is 0 for this state.

$$x_{32} = (h_{31} - h_{f32}) / h_{fg32} \quad (4.357)$$

Here h_{f32} is the enthalpy of saturated liquid at a pressure of state 32 & h_{fg32} is the enthalpy of evaporation at the pressure of state 32.

b. Evaporator (States 32-1)

The modeling can be performed as:

Energy Analysis:

$$RE = m_{32} (h_1 - h_{32}) \quad (4.358)$$

Exergy Analysis:

$$X_{Evap} = m_{1'} [(h_{32'} - h_{1'}) - T_O (s_{32'} - s_{1'})] \quad (4.359)$$

Where X_{Evap} is the Exergy of the Evaporator, s is the corresponding specific entropy & T_O is the environment temperature. The states 32' & 1' are the inlet and outlet states of the fluid getting cooled in the evaporator. $m_{1'}$ is the mass flow rate of the fluid.

c. Absorber (States 1-2 & 23-2)

The modeling can be done for Heat Rejected in Absorber Q_{Abs} .

Energy Analysis:

$$Q_{Abs} = m_1 h_1 + m_{23} h_{23} - m_2 h_2 \quad (4.360)$$

Exergy Analysis:

$$X_{Abs} = m_{2'} [(h_{23'} - h_{2'}) - T_O (s_{23'} - s_{2'})] \quad (4.361)$$

Where X_{Abs} the Exergy of Absorber, s is the corresponding specific entropy & T_O is the environment temperature and the states 23' & 2' are the inlet and outlet states of the fluid getting heated in the absorber. $m_{2'}$ is the mass flow rate of the fluid.

d. Mixture Pump (States 2-3)

The Work input in the Pumps can be given as W_P :

$$W_P = m_2 v_2 (dP) \quad (4.362)$$

Where v_2 is the specific volume of the mixture and dP is the pressure raised by the pump.

Also, Specific Enthalpy at the Exit of the Pumps can be given as:

$$h_3 = m_2 h_2 + W_p \quad (4.363)$$

e. Mixture Heat Exchange-I, II, III & IV (States 3-4 & 21-22, States 4-5 & 18-19, States 6-7 & 15-16 and States 8-9 & 12-13)

It can be modeled as the followings:

Energy Analysis for HEx-I:

$$\text{Effectiveness of Heat Exchanger, } \varepsilon_{H-Ex-I} = (T_{21} - T_{22}) / (T_{21} - T_3) \quad (4.364)$$

Heat Exchange in the Heat Exchanger,

$$Q_{H-Ex-I} = m_4(h_4 - h_3) = m_{21}(h_{21} - h_{22}) \quad (4.365)$$

$$\text{Specific Heat Capacity for Hot Fluid, } c_{Hot-I} = (h_{21} - h_{22}) / (T_{21} - T_{22}) \quad (4.366)$$

$$\text{Specific Heat Capacity for Cold Fluid, } c_{Cold-I} = (h_4 - h_3) / (T_4 - T_3) \quad (4.367)$$

Exergy Analysis for HEx-I:

$$X_{H-Ex-I} = m_3[(h_3 - h_4) - T_0(s_3 - s_4)] \quad (4.368)$$

Where X_{H-Ex-I} is the Exergy of the Heat Exchanger-I, s is the corresponding specific entropy & T_0 is the environment temperature.

Energy Analysis for HEx-II:

$$\text{Effectiveness of Heat Exchanger, } \varepsilon_{H-Ex-II} = (T_{18} - T_{19}) / (T_{18} - T_4) \quad (4.369)$$

Heat Exchange in the Heat Exchanger,

$$Q_{H-Ex-II} = m_4(h_5 - h_4) = m_{18}(h_{18} - h_{19}) \quad (4.370)$$

$$\text{Specific Heat Capacity for Hot Fluid, } c_{Hot-II} = (h_{18} - h_{19}) / (T_{18} - T_{19}) \quad (4.371)$$

$$\text{Specific Heat Capacity for Cold Fluid, } c_{Cold-II} = (h_4 - h_5) / (T_4 - T_5) \quad (4.372)$$

Exergy Analysis for HEx-II:

$$X_{H-Ex-II} = m_4[(h_4-h_5) - T_O (s_4-s_5)] \quad (4.373)$$

Where $X_{H-Ex-II}$ is the Exergy of the Heat Exchanger-II, s is the corresponding specific entropy & T_O is the environment temperature.

Energy Analysis for HEx-III:

$$\text{Effectiveness of Heat Exchanger, } \varepsilon_{H-Ex-III} = (T_{15}-T_{16}) / (T_{15}-T_6) \quad (4.374)$$

Heat Exchange in the Heat Exchanger,

$$Q_{H-Ex-III} = m_6(h_7 - h_6) = m_{15}(h_{15} - h_{16}) \quad (4.375)$$

$$\text{Specific Heat Capacity for Hot Fluid, } c_{Hot-III} = (h_{15} - h_{16}) / (T_{15}-T_{16}) \quad (4.376)$$

Specific Heat Capacity for Cold Fluid,

$$c_{Cold-III} = (h_7 - h_6) / (T_7-T_6) \quad (4.377)$$

Exergy Analysis for HEx-III:

$$X_{H-Ex-III} = m_6[(h_6-h_7) - T_O (s_6-s_7)] \quad (4.378)$$

Where $X_{H-Ex-III}$ is the Exergy of the Heat Exchanger-III, s is the corresponding specific entropy & T_O is the environment temperature.

Energy Analysis for HEx-IV:

$$\text{Effectiveness of Heat Exchanger, } \varepsilon_{H-Ex-IV} = (T_{12}-T_{13}) / (T_{12}-T_{13}) \quad (4.379)$$

Heat Exchange in the Heat Exchanger,

$$Q_{H-Ex-IV} = m_8(h_9 - h_8) = m_{12}(h_{12} - h_{13}) \quad (4.380)$$

$$\text{Specific Heat Capacity for Hot Fluid, } c_{Hot-IV} = (h_{12} - h_{13}) / (T_{12}-T_{13}) \quad (4.381)$$

Specific Heat Capacity for Cold Fluid,

$$c_{Cold-IV} = (h_9 - h_8) / (T_9-T_8) \quad (4.382)$$

Exergy Analysis for HEx-IV:

$$X_{H-Ex-IV} = m_8[(h_8-h_9) - T_O (s_8-s_9)] \quad (4.383)$$

Where $X_{H-Ex-IV}$ is the Exergy of the Heat Exchanger-IV, s is the corresponding specific entropy & T_O is the environment temperature.

f. LHP I, II & III Condenser (States 5-6, 7-8 & 9-10)

Modeling for LHP-I

Energy Analysis:

$$\text{Heat Input to the Mixture, } Q_{InMixI} = m_5(h_6-h_5) \quad (4.384)$$

Heat Rejected by the Condensing Fluid in LHP-I,

$$Q_{LHPICond} = m_{LHPI} (h_{fgLHPICond} + c_F \Delta T_{SubI}) \quad (4.385)$$

Where $h_{fgLHPICond}$ is the latent heat of condensation in the LHP-I Condenser, c_F is the specific heat capacity, m_{LHPI} is the mass flow in the LHP-I & ΔT_{SubI} is the degree of subcooling in LHP-I condenser for the LHP-I working fluid.

Effectiveness of the LHP-I Condenser,

$$\epsilon_{LHPICond} = (T_6 - T_5) / (T_{InLHPICond} - T_5) \quad (4.386)$$

Where $T_{InLHPICond}$ is the Input Temperature of the LHP-I Condenser.

Exergy Analysis:

$$X_{LHPICond} = m_5 [(h_5 - h_6) - T_O (s_5 - s_6)] \quad (4.387)$$

Where $X_{LHPICond}$ is the Exergy of the Heat Exchanger, s is the corresponding specific entropy & T_O is the environment temperature.

Modeling for LHP-II

Energy Analysis:

$$\text{Heat Input to the Mixture, } Q_{InMixII} = m_7(h_8-h_7) \quad (4.388)$$

Heat Rejected by the Condensing Fluid in LHP-II,

$$Q_{LHPICond} = m_{LHPII} (h_{fgLHPICond} + c_F \Delta T_{SubII}) \quad (4.389)$$

Where $h_{fgLHP-II\text{Cond}}$ is the latent heat of condensation in the LHP-II Condenser, c_F is the specific heat capacity, m_{LHP-II} is the mass flow in the LHP-II & ΔT_{SubII} is the degree of subcooling in the LHP-II condenser for the LHP-II working fluid.

Effectiveness of the LHP-II Condenser,

$$\epsilon_{LHP-II\text{Cond}} = (T_8 - T_7) / (T_{\text{InLHP-II\text{Cond}}} - T_7) \quad (4.390)$$

Where $T_{\text{InLHP-II\text{Cond}}}$ is the Input Temperature of the LHP-II Condenser.

Exergy Analysis:

$$X_{LHP-II\text{Cond}} = m_7[(h_7 - h_8) - T_O (s_7 - s_8)] \quad (4.391)$$

Where $X_{LHP-II\text{Cond}}$ is the Exergy of the Heat Exchanger, s is the corresponding specific entropy & T_O is the environment temperature.

Modeling for LHP-III

Energy Analysis:

$$\text{Heat Input to the Mixture, } Q_{\text{InMixIII}} = m_9(h_{10} - h_9) \quad (4.392)$$

Heat Rejected by the Condensing Fluid in LHP-III,

$$Q_{LHP-III\text{Cond}} = m_{LHP-III} (h_{fgLHP-III\text{Cond}} + c_F \Delta T_{\text{SubIII}}) \quad (4.393)$$

Where $h_{fgLHP-III\text{Cond}}$ is the latent heat of condensation in the LHP-III Condenser, c_F is the specific heat capacity, $m_{LHP-III}$ is the mass flow in the LHP-III & ΔT_{SubIII} is the degree of subcooling in the LHP-III condenser for the LHP-III working fluid.

Effectiveness of the LHP-III Condenser,

$$\epsilon_{LHP-III\text{Cond}} = (T_{10} - T_9) / (T_{\text{InLHP-III\text{Cond}}} - T_9) \quad (4.394)$$

Where $T_{\text{InLHP-III\text{Cond}}}$ is the Input Temperature of the LHP-III Condenser.

Exergy Analysis:

$$X_{LHP-III\text{Cond}} = m_9[(h_9 - h_{10}) - T_O (s_9 - s_{10})] \quad (4.395)$$

Where $X_{LHP-III\text{Cond}}$ is the Exergy of the Heat Exchanger, s is the corresponding specific entropy & T_O is the environment temperature.

g. Low, Med, High-T Generator-I & II (States 20-21 & 20-24, States 17-18 & 17-25, States 14-15 & 14-26 and States 10-12 & 10-11)

Heat is added to the mixture in the generator. This heat input to the High-Temperature Generator- I & II, Q_{GH-T-I} & $Q_{GH-T-II}$, Medium Temperature Generator, Q_{GM-T} & Low-Temperature Generator Q_{GL-T} can be expressed as:

Energy Analysis, High-Temperature Generator-II:

$$Q_{GH-T-II} = h_{11}m_{11} + h_{12}m_{12} - h_{10}m_{10} \quad (4.396)$$

Exergy Analysis, High Temperature Generator-II:

$$X_{GH-T-II} = m_{11}'[(h_{11}' - h_{12}') - T_O (s_{11}' - s_{12}')] \quad (4.397)$$

Where $X_{GH-T-II}$ is the Exergy of the High-T Generator-II, s is the corresponding specific entropy & T_O is the environment temperature and the states 11' & 12' are the inlet and outlet states of the fluid supplying heat to the generator. M_{11}' is the mass flow rate of the fluid.

Energy Analysis, High Temperature Generator-I:

$$Q_{GH-T-I} = h_{26}m_{26} + h_{15}m_{15} - h_{14}m_{14} \quad (4.398)$$

Exergy Analysis, High Temperature Generator-I:

$$X_{GH-T-I} = m_{14}'[(h_{14}' - h_{15}') - T_O (s_{14}' - s_{15}')] \quad (4.399)$$

Where X_{GH-T-I} is the Exergy of the High-T Generator-I, s is the corresponding specific entropy & T_O is the environment temperature and the states 14' & 15' are the inlet and outlet states of the fluid supplying heat to the generator. m_{14}' is the mass flow rate of the fluid.

Energy Analysis, Medium Temperature Generator:

$$Q_{GM-T} = h_{25}m_{25} + h_{18}m_{18} - h_{17}m_{17} \quad (4.400)$$

Exergy Analysis, Medium Temperature Generator:

$$X_{GM-T} = m_{17}'[(h_{17}' - h_{18}') - T_O (s_{17}' - s_{18}')] \quad (4.401)$$

Where X_{GM-T} is the Exergy of the Med-T Generator, s is the corresponding specific entropy & T_O is the environment temperature and the states 17' & 18' are the inlet and outlet states of the fluid supplying heat to the generator. $m_{17'}$ is the mass flow rate of the fluid.

Energy Analysis, Low Temperature Generator:

$$Q_{GL-T} = h_{21}m_{21} + h_{24}m_{24} - h_{20}m_{20} \quad (4.402)$$

Exergy Analysis, Low Temperature Generator:

$$X_{GL-T} = m_{20'} [(h_{20'} - h_{21'}) - T_O (s_{20'} - s_{21'})] \quad (4.403)$$

Where X_{GL-T} is the Exergy of the Low-T Generator, s is the corresponding specific entropy & T_O is the environment temperature and the states 20' & 21' are the inlet and outlet states of the fluid supplying heat to the generator. $m_{20'}$ is the mass flow rate of the fluid.

h. LHP I, II & III Evaporator (States 25-29, 26-28 & 11-27)

LHP-I can be modeled as:

Energy Analysis:

Heat Rejected by the Condensing Refrigerant,

$$Q_{CondRI} = m_{25} (h_{25} - h_{25'}) \quad (4.404)$$

Heat Absorbed by the LHP Working Fluid in the LHP Evaporator,

$$Q_{LHPIEvap} = m_{LHPI} (h_{fgLHPIEvap} + c_F \Delta T_{SupI}) \quad (4.405)$$

Where $h_{fgLHPIEvap}$ is the latent heat of evaporation in the LHP Evaporator, c_F is the specific heat capacity, m_{LHPI} is the mass flow in the LHP-I & ΔT_{SupI} is the degree of superheat in the LHP evaporator for the LHP-I working fluid. State 25' is the exit of the LHP-I Evaporator.

Exergy Analysis:

$$X_{LHPIEvap} = m_{25} [(h_{25} - h_{25'}) - T_O (s_{25} - s_{25'})] \quad (4.406)$$

Where $X_{LHP\text{IEvap}}$ is the Exergy of the LHP-I Evaporator, s is the corresponding specific entropy & T_O is the environment temperature.

LHP-II can be modeled as:

Energy Analysis:

Heat Rejected by the Condensing Refrigerant,

$$Q_{\text{CondRII}} = m_{26} (h_{26} - h_{26'}) \quad (4.407)$$

Heat Absorbed by the LHP Working Fluid in the LHP Evaporator,

$$Q_{\text{LHP\text{IEvap}}} = m_{\text{LHP\text{II}}} (h_{\text{fgLHP\text{IEvap}}} + c_F \Delta T_{\text{Sup\text{II}}}) \quad (4.408)$$

Where $h_{\text{fgLHP\text{IEvap}}}$ is the latent heat of evaporation in the LHP-II Evaporator, c_F is the specific heat capacity, $m_{\text{LHP\text{II}}}$ is the mass flow in the LHP & $\Delta T_{\text{Sup\text{II}}}$ is the degree of superheat in the LHP evaporator for the LHP-II working fluid.

Exergy Analysis:

$$X_{\text{LHP\text{IEvap}}} = m_{26} [(h_{26} - h_{26'}) - T_O (s_{26} - s_{26'})] \quad (4.409)$$

Where $X_{\text{LHP\text{IEvap}}}$ is the Exergy of the LHP-II Evaporator, s is the corresponding specific entropy & T_O is the environment temperature.

LHP-III can be modeled as:

Energy Analysis:

Heat Rejected by the Condensing Refrigerant,

$$Q_{\text{CondRIII}} = m_{11} (h_{11} - h_{27}) \quad (4.410)$$

Heat Absorbed by the LHP Working Fluid in the LHP Evaporator,

$$Q_{\text{LHP\text{IEvap}}} = m_{\text{LHP\text{III}}} (h_{\text{fgLHP\text{IEvap}}} + c_F \Delta T_{\text{Sup\text{III}}}) \quad (4.411)$$

Where $h_{\text{fgLHP\text{IEvap}}}$ is the latent heat of evaporation in the LHP-III Evaporator, c_F is the specific heat capacity, $m_{\text{LHP\text{III}}}$ is the mass flow in the LHP & $\Delta T_{\text{Sup\text{III}}}$ is the degree of superheat in the LHP evaporator for the LHP-III working fluid.

Exergy Analysis:

$$X_{LHP\text{III}Evap} = m_{11}[(h_{11}-h_{27}) - T_O (s_{11}-s_{27})] \quad (4.412)$$

Where $X_{LHP\text{III}Evap}$ is the Exergy of the LHP-III Evaporator, s is the corresponding specific entropy & T_O is the environment temperature.

i. Mixture Reducing Valve- I, II, III & IV (States 13-14, 16-17, 19-20 & 22-23)

Modeling can be done as:

$$h_{22} = h_{23} \quad (4.413)$$

$$h_{13} = h_{14} \quad (4.414)$$

$$h_{16} = h_{17} \quad (4.415)$$

$$h_{19} = h_{20} \quad (4.416)$$

j. Low Temperature Condenser (States 24-31 & 30-31)

The Low-T Condenser deals with the liquid refrigerant coming out of the LHP-I, II & III and Refrigerant Expansion Valve-I, II & III and mixes it with the liquid refrigerant obtained after condensing the vapour coming out of the Low-T Generator. The heat rejected from the low-T Condenser can be modeled as:

Energy Analysis:

$$Q_{L-Cond} = m_{24}h_{24} + m_{30}h_{30} - m_{31}h_{31} \quad (4.417)$$

Exergy Analysis:

$$X_{L-Cond} = m_{30'} [(h_{30'}-h_{31'}) - T_O (s_{30'}-s_{31'})] \quad (4.418)$$

Where X_{L-Cond} is the Exergy of the Low-Temperature Condenser, s is the corresponding specific entropy & T_O is the environment temperature. The states 30' & 31' are the inlet and outlet states of the fluid getting cooled in the condenser. $m_{30'}$ is the mass flow rate of the fluid.

4.6.2. Modified Quadruple Effect VARS-II

The modified system has been shown in Fig 4.15 in which it has been proposed that the 04 Heat Exchangers of Modified System-I are replaced with LHP-I, LHP-II, LHP-IV & LHP-VI.

Hence, similar to the previous systems LHP-I, LHP-II & LHP-III have been nominated in LHP-III, LHP-V & LHP-VII respectively. LHP-I, LHP-II, LHP-IV & LHP-VI can be modeled with the following methodology.

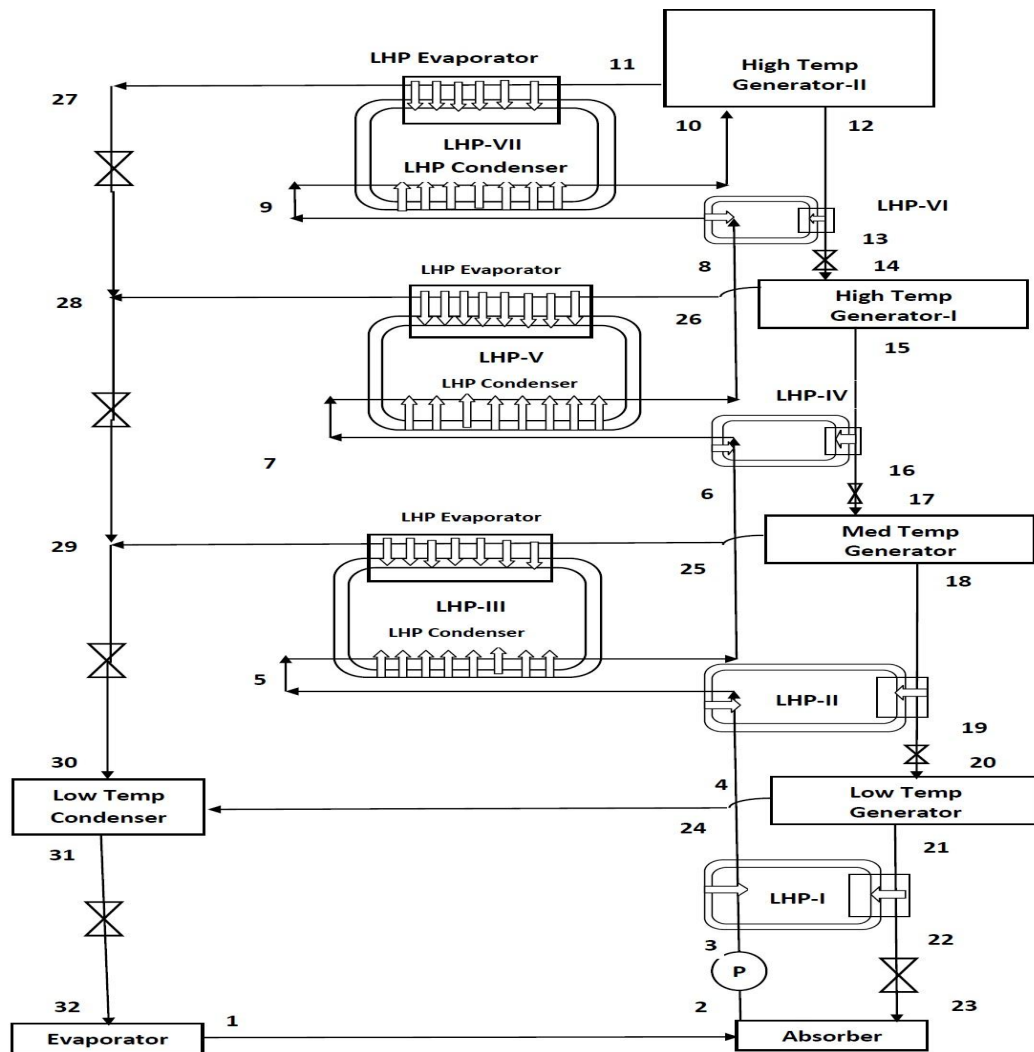


Fig 4.15. Modified Quadruple Effect VARS-II

e. LHP I, II, IV & VI (States 3-4 & 21-22, States 4-5 & 18-19, States 6-7 & 15-16 and States 8-9 & 12-13)

- LHP-I Condenser

Energy Analysis:

$$\text{Heat Input to the Mixture, } Q_{\text{InMixI}} = m_3(h_4-h_3) \quad (4.419)$$

Heat Rejected by the Condensing Fluid in LHP,

$$Q_{\text{LHPICond}} = m_{\text{LHPI}} (h_{\text{fgLHPICond}} + c_F \Delta T_{\text{SubI}}) \quad (4.420)$$

Where $h_{\text{fgLHPICond}}$ is the latent heat of condensation in the LHP-I Condenser, c_F is the specific heat capacity, m_{LHPI} is the mass flow in the LHP-I & ΔT_{SubI} is the degree of subcooling in LHP-I condenser for the LHP-I working fluid.

$$\text{Effectiveness of the LHP-I Condenser, } \varepsilon_{\text{LHPICond}} = (T_4 - T_3) / (T_{\text{InLHPICond}} - T_3) \quad (4.421)$$

Where $T_{\text{InLHPICond}}$ is the Input Temperature of the LHP-I Condenser.

Exergy Analysis:

$$X_{\text{LHPICond}} = m_3[(h_3-h_4) - T_O (s_3-s_4)] \quad (4.422)$$

Where X_{LHPICond} is the Exergy of the LHP-I, s is the corresponding specific entropy & T_O is the environment temperature.

• **LHP-I Evaporator**

Energy Analysis:

$$\text{Heat Rejected by the Absorbent, } Q_{\text{RejI}} = m_{21}(h_{21} - h_{22}) \quad (4.423)$$

Heat Absorbed by the LHP-I Working Fluid in the LHP-I Evaporator,

$$Q_{\text{LHPIEvap}} = m_{\text{LHPI}} (h_{\text{fgLHPIEvap}} + c_F \Delta T_{\text{SupI}}) \quad (4.424)$$

Where $h_{\text{fgLHPIEvap}}$ is the latent heat of evaporation in the LHP-I Evaporator, c_F is the specific heat capacity, m_{LHPI} is the mass flow in the LHP-I & ΔT_{SupI} is the degree of superheat in the LHP-I evaporator for the LHP-I working fluid.

Exergy Analysis:

$$X_{\text{LHPIEvap}} = m_{21}[(h_{21}-h_{22}) - T_O (s_{21}-s_{22})] \quad (4.425)$$

Where X_{LHPIEvap} is the Exergy of the LHP-I Evaporator, s is the corresponding specific entropy & T_O is the environment temperature.

• **LHP-II Condenser**

Energy Analysis:

$$\text{Heat Input to the Mixture, } Q_{\text{InMixII}} = m_4(h_5 - h_4) \quad (4.426)$$

Heat Rejected by the Condensing Fluid in LHP,

$$Q_{\text{LHP-II Cond}} = m_{\text{LHP-II}} (h_{\text{fgLHP-II Cond}} + c_F \Delta T_{\text{SubII}}) \quad (4.427)$$

Where $h_{\text{fgLHP-II Cond}}$ is the latent heat of condensation in the LHP-II Condenser, c_F is the specific heat capacity, $m_{\text{LHP-II}}$ is the mass flow in the LHP-II & ΔT_{SubII} is the degree of subcooling in the LHP-II condenser for the LHP-II working fluid.

Effectiveness of the LHP-II Condenser,

$$\epsilon_{\text{LHP-II Cond}} = (T_5 - T_4) / (T_{\text{InLHP-II Cond}} - T_4) \quad (4.428)$$

Where $T_{\text{InLHP-II Cond}}$ is the Input Temperature of the LHP-II Condenser.

Exergy Analysis:

$$X_{\text{LHP-II Cond}} = m_4[(h_4 - h_5) - T_O (s_4 - s_5)] \quad (4.429)$$

Where $X_{\text{LHP-II Cond}}$ is the Exergy of the LHP-II, s is the corresponding specific entropy & T_O is the environment temperature.

• **LHP-II Evaporator**

Energy Analysis:

$$\text{Heat Rejected by the Absorbent, } Q_{\text{RejII}} = m_{18}(h_{18} - h_{19}) \quad (4.430)$$

Heat Absorbed by the LHP-II Working Fluid in the LHP-II Evaporator,

$$Q_{\text{LHP-II Evap}} = m_{\text{LHP-II}} (h_{\text{fgLHP-II Evap}} + c_F \Delta T_{\text{SupII}}) \quad (4.431)$$

Where $h_{\text{fgLHP-II Evap}}$ is the latent heat of evaporation in the LHP-II Evaporator, c_F is the specific heat capacity, $m_{\text{LHP-II}}$ is the mass flow in the LHP-II & ΔT_{SupII} is the degree of superheat in the LHP-II evaporator for the LHP-II working fluid.

Exergy Analysis:

$$X_{\text{LHP-II Evap}} = m_{12}[(h_{12}-h_{13}) - T_O (s_{12}-s_{13})] \quad (4.432)$$

Where $X_{\text{LHP-II Evap}}$ is the Exergy of the LHP-II Evaporator, s is the corresponding specific entropy & T_O is the environment temperature.

- **LHP-IV Condenser**

Energy Analysis:

$$\text{Heat Input to the Mixture, } Q_{\text{InMixIV}} = m_6(h_7-h_6) \quad (4.433)$$

Heat Rejected by the Condensing Fluid in LHP,

$$Q_{\text{LHP-IV Cond}} = m_{\text{LHP-IV}} (h_{\text{fgLHP-IV Cond}} + c_F \Delta T_{\text{SubIV}}) \quad (4.434)$$

Where $h_{\text{fgLHP-IV Cond}}$ is the latent heat of condensation in the LHP-IV Condenser, c_F is the specific heat capacity, $m_{\text{LHP-IV}}$ is the mass flow in the LHP-IV & ΔT_{SubIV} is the degree of subcooling in the LHP-IV condenser for the LHP-IV working fluid.

Effectiveness of the LHP-IV Condenser,

$$\epsilon_{\text{LHP-IV Cond}} = (T_7 - T_6) / (T_{\text{InLHP-IV Cond}} - T_6) \quad (4.435)$$

Where $T_{\text{InLHP-IV Cond}}$ is the Input Temperature of the LHP-IV Condenser.

Exergy Analysis:

$$X_{\text{LHP-IV Cond}} = m_6[(h_6-h_7) - T_O (s_6-s_7)] \quad (4.436)$$

Where $X_{\text{LHP-IV Cond}}$ is the Exergy of the LHP-IV, s is the corresponding specific entropy & T_O is the environment temperature.

- **LHP-IV Evaporator**

Energy Analysis:

$$\text{Heat Rejected by the Absorbent, } Q_{\text{RejIV}} = m_9(h_9 - h_{10}) \quad (4.437)$$

Heat Absorbed by the LHP-IV Working Fluid in the LHP-IV Evaporator,

$$Q_{\text{LHP-IV Evap}} = m_{\text{LHP-IV}} (h_{\text{fgLHP-IV Evap}} + c_F \Delta T_{\text{SupIV}}) \quad (4.438)$$

Where $h_{fgLHPIVEvap}$ is the latent heat of evaporation in the LHP-IV Evaporator, c_F is the specific heat capacity, m_{LHPIV} is the mass flow in the LHP-IV & ΔT_{SupIV} is the degree of superheat in the LHP-IV evaporator for the LHP-IV working fluid.

Exergy Analysis:

$$X_{LHPIVEvap} = m_{15}[(h_{15}-h_{16}) - T_O (s_{15}-s_{16})] \quad (4.439)$$

Where $X_{LHPIVEvap}$ is the Exergy of the LHP-IV Evaporator, s is the corresponding specific entropy & T_O is the environment temperature.

• **LHP-VI Condenser**

Energy Analysis:

$$\text{Heat Input to the Mixture, } Q_{InMixVI} = m_8(h_9-h_8) \quad (4.440)$$

Heat Rejected by the Condensing Fluid in LHP,

$$Q_{LHPVICond} = m_{LHPVI} (h_{fgLHPVICond} + c_F \Delta T_{SubVI}) \quad (4.441)$$

Where $h_{fgLHPVICond}$ is the latent heat of condensation in the LHP-VI Condenser, c_F is the specific heat capacity, m_{LHPVI} is the mass flow in the LHP-VI & ΔT_{SubVI} is the degree of subcooling in the LHP-VI condenser for the LHP-VI working fluid.

Effectiveness of the LHP-VI Condenser,

$$\epsilon_{LHPVICond} = (T_9 - T_8) / (T_{InLHPVICond} - T_8) \quad (4.442)$$

Where $T_{InLHPVICond}$ is the Input Temperature of the LHP-VI Condenser.

Exergy Analysis:

$$X_{LHPVICond} = m_8[(h_8-h_9) - T_O (s_8-s_9)] \quad (4.443)$$

Where $X_{LHPVICond}$ is the Exergy of the LHP-VI, s is the corresponding specific entropy & T_O is the environment temperature.

• **LHP-VI Evaporator**

Energy Analysis:

$$\text{Heat Rejected by the Absorbent, } Q_{RejVI} = m_{12}(h_{12} - h_{13}) \quad (4.444)$$

Heat Absorbed by the LHP-VI Working Fluid in the LHP-VI Evaporator,

$$Q_{\text{LHPVIEvap}} = m_{\text{LHPVI}} (h_{\text{fgLHPVIEvap}} + c_F \Delta T_{\text{SupVI}}) \quad (4.445)$$

Where $h_{\text{fgLHPVIEvap}}$ is the latent heat of evaporation in the LHP-VI Evaporator, c_F is the specific heat capacity, m_{LHPVI} is the mass flow in the LHP-VI & ΔT_{SupVI} is the degree of superheat in the LHP-VI evaporator for the LHP-VI working fluid.

Exergy Analysis:

$$X_{\text{LHPVIEvap}} = m_{12} [(h_{12} - h_{13}) - T_O (s_{12} - s_{13})] \quad (4.446)$$

Where $X_{\text{LHPVIEvap}}$ is the Exergy of the LHP-VI Evaporator, s is the corresponding specific entropy & T_O is the environment temperature.

4.6.3. Combined GPC & Quadruple-Effect VARS using LHP

The Modified Quadruple Effect VARS-II has been combined with the Reheating-Regenerative & Multi-compression system through LHP-VIII as shown in Fig 4.16. The inlet to the GPC is at state 42 & the exit of the exhaust leaves the LHP-VIII Evaporator at 43.

Also, the temperature at state 38 & state 40 is the same. The LHP-VIII has been modeled similar to the previous section:

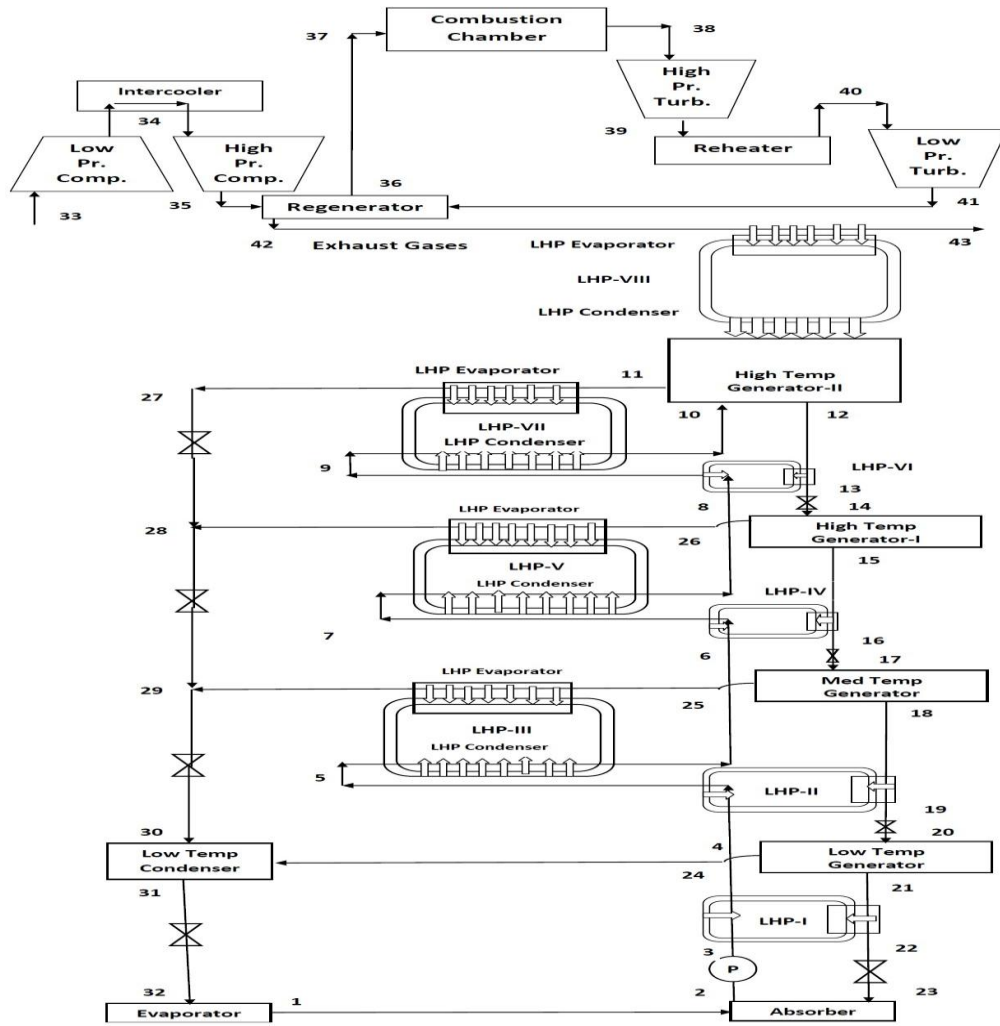


Fig 4.16. Combined GPC & Quadruple Effect VARS

k. Gas Power Cycle (State 12-21)

The heat input to the LHP-VIII, $Q_{InLHPVIII}$ can be calculated as:

$$Q_{InLHPVIII} = \dot{m}_g c_{pg} (T_{42} - T_{43}) \quad (4.447)$$

l. LHP-VIII

The heat rejected at the exhaust of GPC is harnessed by the LHP-VIII Evaporator and transferred to the VARS Generator through LHP-VIII Condensers.

• LHP-VIII Evaporator

Energy Analysis:

$$Q_{InLHPVI} = \dot{m}_g c_{pg} (T_{42} - T_{43}) \quad (4.448)$$

Heat Absorbed by the LHP-VIII Working Fluid in the LHP-VIII Evaporator,

$$Q_{LHPVIII\text{Evap}} = m_{LHPVIII} (h_{fgLHPVIII\text{Evap}} + c_F \Delta T_{\text{SupVIII}}) \quad (4.449)$$

Where $h_{fgLHPVIII\text{Evap}}$ is the latent heat of evaporation in the LHP-VIII Evaporator, c_F is the specific heat capacity, $m_{LHPVIII}$ is the mass flow in the LHP-VIII & $\Delta T_{\text{SupVIII}}$ is the degree of superheat in the LHP-VIII evaporator for the LHP-VIII working fluid.

Exergy Analysis:

$$X_{LHPVIII\text{Evap}} = m_g [(h_{42} - h_{43}) - T_O (s_{42} - s_{43})] \quad (4.450)$$

Where $X_{LHPVIII\text{Evap}}$ is the Exergy of the LHP-VIII Evaporator, s is the corresponding specific entropy & T_O is the environment temperature.

• **LHP-VIII Condenser**

Energy Analysis:

Heat Input to the Generator,

$$Q_{\text{InGenerator}} = h_{11}m_{11} + h_{12}m_{12} - h_9m_9 \quad (4.451)$$

Heat Rejected by the Condensing Fluid in LHP into the Generator,

$$Q_{LHPVIII\text{Cond}} = m_{LHPVIII} (h_{fgLHPVIII\text{Cond}} + c_F \Delta T_{\text{SubVIII}}) \quad (4.452)$$

Where $h_{fgLHPVIII\text{Cond}}$ is the latent heat of condensation in the LHP-VIII Condenser, c_F is the specific heat capacity, $m_{LHPVIII}$ is the mass flow in the LHP-VIII & $\Delta T_{\text{SubVIII}}$ is the degree of subcooling in the LHP-VIII condenser for the LHP-VIII working fluid.

4.7. Thermodynamic Modeling of Organic Rankine Cycle (ORC) (Ankit Dwivedi, et. al. 2021) [189]

The ORC and GPC have been combined with LHP which utilizes the exhaust gas from the GPC to supply to the ORC for operations. The GPC has been modeled comprehensively in section 4.1 of this chapter. In this system in Fig 4.17, the GPC doesn't have the regenerator hence that section from the GPC modeling can be eliminated. The inlet to the LHP Evaporator is 7 and the exit from the LHP evaporator is 8. Hence, Heat Rejected by the GPC into the LHP Evaporator may be given as

$$\text{Hence, } Q_{\text{RejGPC}} = \dot{m}_g c_{pg} (T_7 - T_8) \tag{4.447}$$

Moreover, the Availability, X_{RejGPC} of this heat can be given as:

$$X_{\text{RejGPC}} = \dot{m}_g c_{pg} (T_7 - T_8) - T_O (s_7 - s_8) \tag{4.448}$$

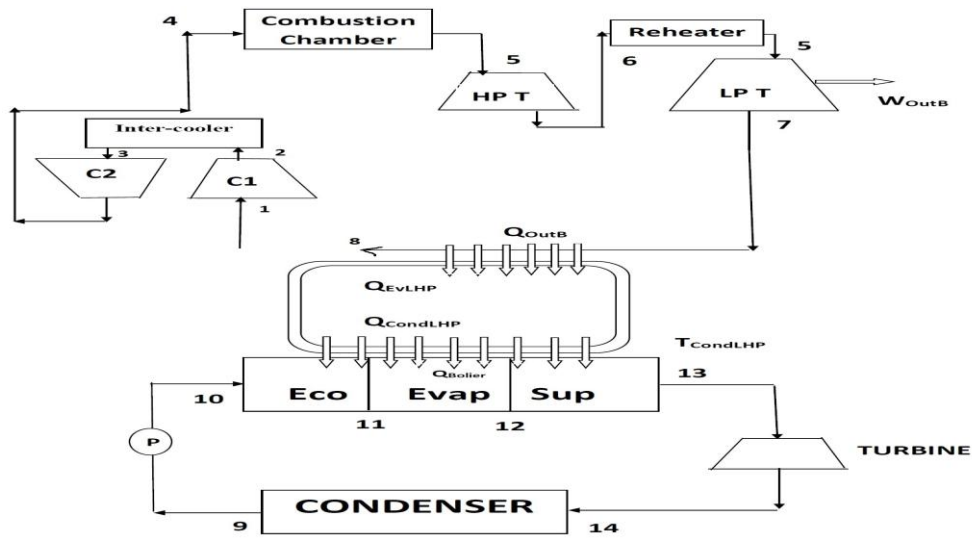


Fig 4.17: Combined GPC & ORC using LHP [189]

• LHP Evaporator

Energy Analysis:

$$Q_{\text{InLHP}} = \dot{m}_g c_{pg} (T_7 - T_8) \tag{4.449}$$

Heat Absorbed by the LHP Working Fluid in the LHP Evaporator,

$$Q_{\text{LHPEvap}} = m_{\text{LHP}} (h_{\text{fgLHPEvap}} + c_F \Delta T_{\text{Sup}}) \tag{4.450}$$

Where $h_{fgLHPEvap}$ is the latent heat of evaporation in the LHP Evaporator, c_F is the specific heat capacity, m_{LHP} is the mass flow in the LHP & ΔT_{Sup} is the degree of superheat in the LHP evaporator for the LHP working fluid.

Exergy Analysis:

$$X_{LHPEvap} = m_g[(h_7-h_8) - T_O (s_7-s_8)] \quad (4.451)$$

Where $X_{LHPEvap}$ is the Exergy of the LHP Evaporator, s is the corresponding specific entropy & T_O is the environment temperature.

• **LHP Condenser**

Energy Analysis:

$$Q_{LHPCond} = m_{LHP} (h_{fgLHPCond} + c_F \Delta T_{Sub}) \quad (4.452)$$

Where $h_{fgLHPCond}$ is the latent heat of condensation in the LHP Condenser, c_F is the specific heat capacity, m_{LHP} is the mass flow in the LHP & ΔT_{Sub} is the degree of subcooling in the LHP condenser for the LHP working fluid.

• **ORC**

The power absorbed by the pump is estimated by equation

$$W_{inR} = (h_{10}-h_9) \quad (4.453)$$

$$\eta_p = (h_{10s}-h_9)/(h_{10}-h_9) \quad (4.454)$$

$$Q_{BoilR} = (h_{13}-h_{10}) \quad (4.455)$$

$$(h_{13} - h_{10}) = c_{pR}(T_{in}-T_{pp}) \quad (4.456)$$

The useful work output can be estimated by equation.

$$W_{outR} = (h_{13}-h_{14}) \quad (4.457)$$

$$Q_{ConR} = (h_{14}-h_9) \quad (4.458)$$

Where Q_{ConR} is the rejected in the condenser area (kW)

Thermal efficiency can be given as:

$$\eta_{Th} = (W_{outR} - W_{inP}) / Q_{BoilR} \quad (4.459)$$

Exergy destruction in pump can be given as:

$$I_{pump} = T_o (s_9 - s_{10}) \quad (4.460)$$

$T_{H-ORC} = (T_{in} + T_{pp})/2$, the energy destruction in evaporator can be estimated by equation.

$$I_{evp} = T_o [(s_{13} - s_{10}) - (h_{13} - h_{10} / T_{H-ORC})] \quad (4.461)$$

Where;

I_{evp} is the exergy destruction rate in the evaporator (kW), s_{13} is specific entropy at boiler outlet kJ/kgK)

Exergy destruction in turbine can be given as:

$$I_{Turb} = T_o (s_{14} - s_{13}) \quad (4.462)$$

I_{Turb} is the exergy destruction rate in the turbine (kW), s_{14} is specific entropy at turbine outlet (kJ/kgK)

Exergy destruction in the condenser

$T_{L-ORC} = (T_{ci} + T_{co})/2$ can be used to estimate the exergy destruction in the condenser. The equation gives the exergy destruction in the condenser.

$$I_{con} = \dot{m}_R \times T_o [(s_9 - s_{14}) - (h_9 - h_{14} / T_L)] \quad (4.463)$$

I_{con} refers to the exergy destruction rate in condenser (kW)

The system's total energy destruction can be calculated by combining equations

$$I_{TotalORC} = I_{Pump} + I_{Evap} + I_{Turb} + I_{Con} \quad (4.464)$$

This gives:

$$I_{Total} = T_o \times \left[\frac{h_{13} - h_{10}}{T_{H-ORC}} - \frac{h_9 - h_{14}}{T_{L-ORC}} \right] \quad (4.465)$$

$$\text{Exergetic efficiency} = \frac{W_{net}}{W_{net} + I_{total}} \quad (4.466)$$

4.8. Thermodynamic Modeling of Ejector Refrigeration Cycle (ERC) (Ankit Dwivedi, et. al. 2021) [190]

Similar to the ORC, the ERC has also been combined with the GPC using LHP. In this system the GPC doesn't have multi compression or expansion rather it has a regenerator. The Entry of the Exhaust gases to the LHP Evaporator Occurs at 7 & exits at 8.

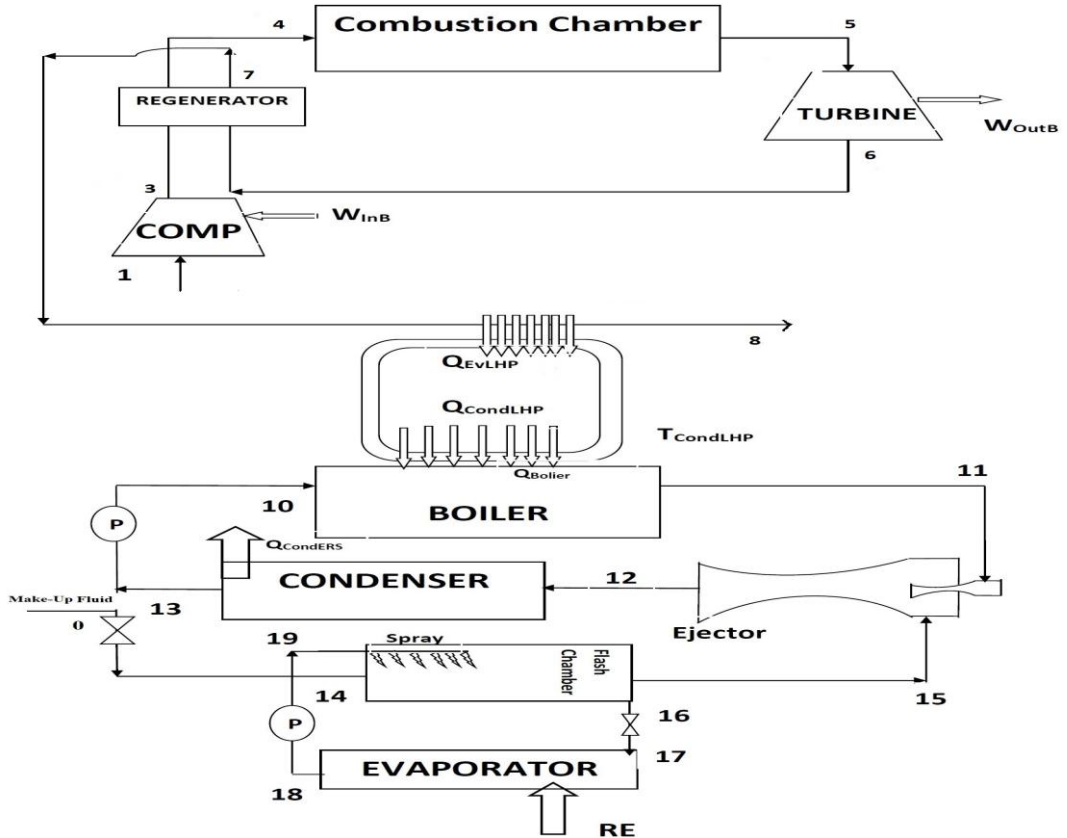


Fig 4.18: Combined GPC & ERC using LHP [190]

Hence, Heat Rejected by the GPC into the LHP Evaporator may be given as:

$$\text{Hence, } Q_{\text{RejGPC}} = \dot{m}_g c_{pg} (T_7 - T_8) \tag{4.467}$$

Moreover, the Availability, X_{RejGPC} of this heat can be given as:

$$X_{\text{RejGPC}} = \dot{m}_g c_{pg} (T_7 - T_8) - T_0 (s_7 - s_8) \tag{4.468}$$

• LHP Evaporator

Energy Analysis:

$$Q_{\text{InLHP}} = \dot{m}_g c_{pg} (T_7 - T_8) \quad (4.469)$$

Heat Absorbed by the LHP Working Fluid in the LHP Evaporator,

$$Q_{\text{LHPEvap}} = m_{\text{LHP}} (h_{\text{fgLHPEvap}} + c_F \Delta T_{\text{Sup}}) \quad (4.470)$$

Where $h_{\text{fgLHPEvap}}$ is the latent heat of evaporation in the LHP Evaporator, c_F is the specific heat capacity, m_{LHP} is the mass flow in the LHP & ΔT_{Sup} is the degree of superheat in the LHP evaporator for the LHP working fluid.

Exergy Analysis:

$$X_{\text{LHPEvap}} = m_g [(h_6 - h_6') - T_O (s_6 - s_6')] \quad (4.471)$$

Where X_{LHPEvap} is the Exergy of the LHP Evaporator, s is the corresponding specific entropy & T_O is the environment temperature.

• **LHP Condenser**

Energy Analysis:

$$Q_{\text{LHPCond}} = m_{\text{LHP}} (h_{\text{fgLHPCond}} + c_F \Delta T_{\text{Sub}}) \quad (4.472)$$

Where $h_{\text{fgLHPCond}}$ is the latent heat of condensation in the LHP Condenser, c_F is the specific heat capacity, m_{LHP} is the mass flow in the LHP & ΔT_{Sub} is the degree of subcooling in the LHP condenser for the LHP working fluid.

• **ERC**

The Jet Velocity at the exit of the Nozzle,

$$C_{11a} = \sqrt{2\eta_N (h_{11} - h_{12})}, \text{ where } \eta_N \text{ is nozzle efficiency } 0.85. \quad (4.473)$$

$$\text{Continuity Equation at the Mixing Section } m_{11} + m_{15} = m_{11bc}, \quad (4.474)$$

Where; point 11_{bc} shows the throat right before the shock.

Momentum Equation at the Mixing Section

$$(m_{11} + m_{15}) C_{11b} = m_{11} C_{11a} - m_{15} C_{15} \quad (4.475)$$

Velocity & Mass Flow at the Suction of vapour from flash chamber m_{15} & C_{15} are considered to be negligible.

$$m_{11bc}C_{11b} = m_{11} C_{11a} \quad (4.476)$$

Energy Equation of Mixing Process

$$m_{11}h_{11} = m_{11bc} (h_{11b} + c_{11a}^2/2) \quad (4.477)$$

Continuity Equation for Shock Diffuser Section

$$m_{11bc} = C_{11b} A/v_{11b} = C_{11c}A/v_{11c}, \text{ where } v \text{ is the specific volume.} \quad (4.478)$$

Momentum equation at shock diffuser section:

$$(p_{11c} - p_{11b}) A = (C_{11b} - C_{11c}) m_{11bc} \quad (4.479)$$

Energy equation at shock diffuser section:

$$h_{11b} + C_{11b}^2 / 2 = h_{11c} + C_{11c}^2 / 2 \quad (4.480)$$

Energy equation at shock diffuser section:

$$h_{12} - h_{11c} = C_{11c}^2 / 2 = h_{12s} - h_{11c} / \eta_D, \text{ where } \eta_D = 0.8 \text{ is the diffuser efficiency} \quad (4.481)$$

Neglecting the shock waves,

$$\eta_E m_{11} C_{12}^2 / 2 = m_{11bc} C_{11bc}^2 / 2, \text{ where } \eta_E = 0.65 \text{ is the entrainment efficiency} \quad (4.482)$$

$$\text{Mass Ratio, } m_R = m_{11}/m_{15} = h_{12s} - h_{11bc} / [\eta_N \eta_D \eta_E (h_{11} - h_{11bc}) - (h_{12s} - h_{11bc})] \quad (4.483)$$

$$\eta_N \eta_D \eta_E = \text{Overall Efficiency of Ejector, } \eta_O \quad (4.484)$$

$$\text{Refrigeration Effect, } RE = h_{18} - h_{17} \quad (4.485)$$

$$\text{Heat Supplied, } Q_{\text{Sup}} = h_{11} - h_{10} \quad (4.486)$$

$$\text{COP} = RE/Q_{\text{Sup}} \quad (4.487)$$

Chapter-5: Results & Discussions

The mathematical modeling presented in Chapter-4 has been analyzed using Engineering Equation Solver. The results obtained have been discussed in this chapter. This chapter consists of the following sections:

- i.** Modified Single Effect VARS
- ii.** Modified Half Effect VARS
- iii.** Modified Double Effect VARS
- iv.** Modified Triple Effect VARS
- v.** Modified Quadruple Effect VARS
- vi.** Combined ORC & GPC
- vii.** Combined ERC & GPC
- viii.** The Patent

5.1. Modified Single Effect VARS

This section presents the results obtained from the Modeling of the systems shown in Fig 4.2, 4.3 & 4.4. Table 5.1 shows the input data for the analysis of the GPC shown in Fig 4.1 & the parameters in Table 5.2 presents the data of the Single Effect VARS.

Table 5.1: Input Data for GPC Analysis

Sl. No.	Input Parameters	Data
1.	Pressure Ratio, r	6
2.	Peak Temperature, T_5	1500K
3.	Turbine Efficiency, η_T	0.92
4.	Compressor Efficiency, η_C	0.86
5.	Working Fluid	Air & Gas Mixture
6.	Regenerator Effectiveness, ϵ_R	0.75
7.	Air Flow	1 kg/s
8.	CV of Fuel	43MJ

The analysis has been performed keeping the Generator Temperature T_G as the primary input parameters. Heat Interactions in the LHP & VARS, Temperature

variations in LHP & VARS, Mass Flow Rates within the VARS, % Irreversibility of Components, COP, and Improved COP have been presented in this section for Modification-I, Modification-II & Combined Single Effect VARS.

Table 5.2: Input Data for Single Effect VARS Analysis

Sl. No.	Input Parameters	Data
1.	Peak Temperature, T_G	100 °C
2.	Evaporator Temperature, T_{Evap}	5 °C
3.	Working Fluid	LiBr-H ₂ O
4.	Heat Exchanger Effectiveness, ϵ_{H-Ex}	0.5-0.7
5.	Condenser Temperature, T_C	35 °C
6.	Mass Flow rate after absorber, m_2	0.05 kg/s
7.	Ambient Temperature	25°C

5.1.1. Single Effect VARS Modification-I (Ankit Dwivedi, et. al. 2018) ^[183]

The study has been performed by varying the Generator Temperature from 100-110 °C to obtain the various aforementioned performance parameters. The focus has been kept on the COP, Temperature Variations & Heat Available for Intra-cycle recovery. Fraction Irreversibility associated with the various components of the system have also been studied.

Fig 5.1 shows the temperature variation in the Mod VARS-I with Generator Temperature. For this study Exit Temperature of the Absorbent from the Generator, Inlet Temperature of the Mixture to the Generator After being Preheated in the LHP & Evaporator Temperature have been presented. The Absorbent Temperature is observed to be varying from 90-100 °C, and the Mixture Temperature entering the Generator can be obtained as 70-80 °C. The evaporator temperature is kept at 5 °C for the study.

Fig 5.2 presents the Inlet and Outlet temperatures of the Mixture coming out of the pump & Absorbent returning from the generator for the Mixture Heat Exchanger.

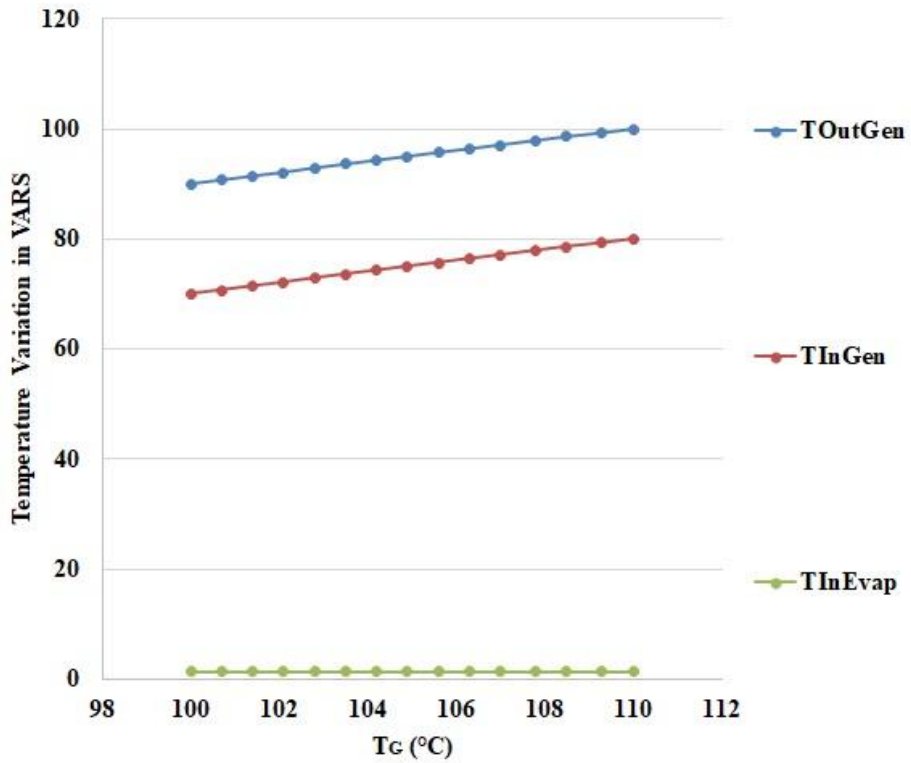


Fig 5.1: Temperature Variation in Single Effect Modification-I with Generator Temperature

The mixture enters the HEx at 35 °C and exits at 65.6-66.9 °C, whereas the Absorbent enters the HEx at 90-100 °C and exits at 54.8 – 58.4 °C with an average effectiveness of 55-60 % owing to high-temperature gaps from the Fig 5.2.

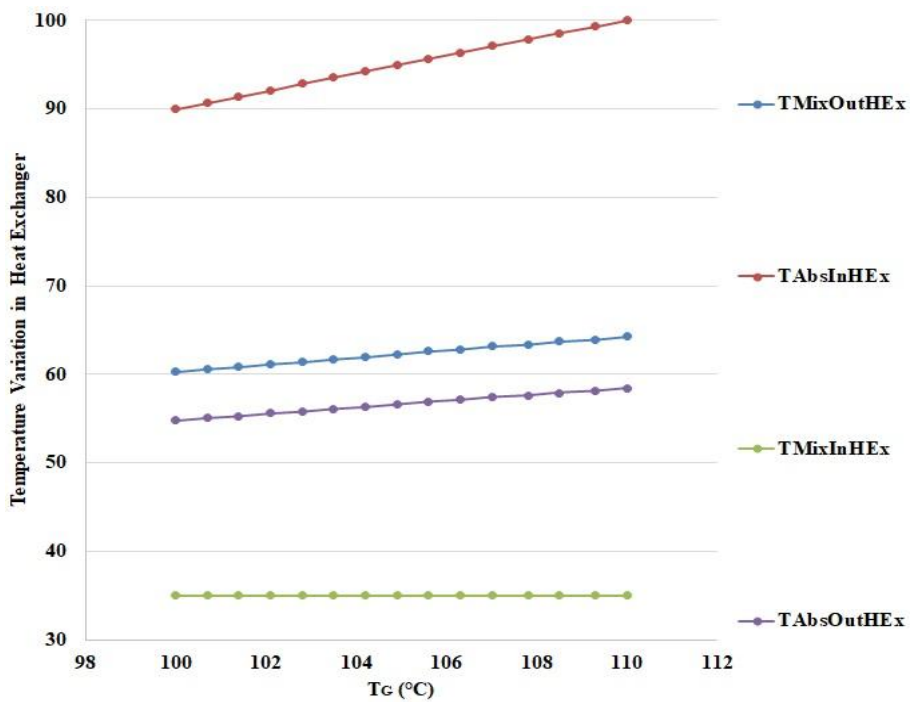


Fig 5.2: Temperature Variation in Single Effect Modification-I Heat Exchanger with Generator Temperature

Similarly, Fig 5.3 presents the Temperature variation within the LHP replacing the Condenser. The LHP Evaporator Temperature is dependent on the Refrigerant Temperature leaving the Generator and varies approximately from 80-90 °C, whereas, the inlet refrigerant temperature to the LHP Evaporator can be studied to be varying approximately from 85-90 °C. The Temperature difference for the heat temperature has been kept at 5 °C.

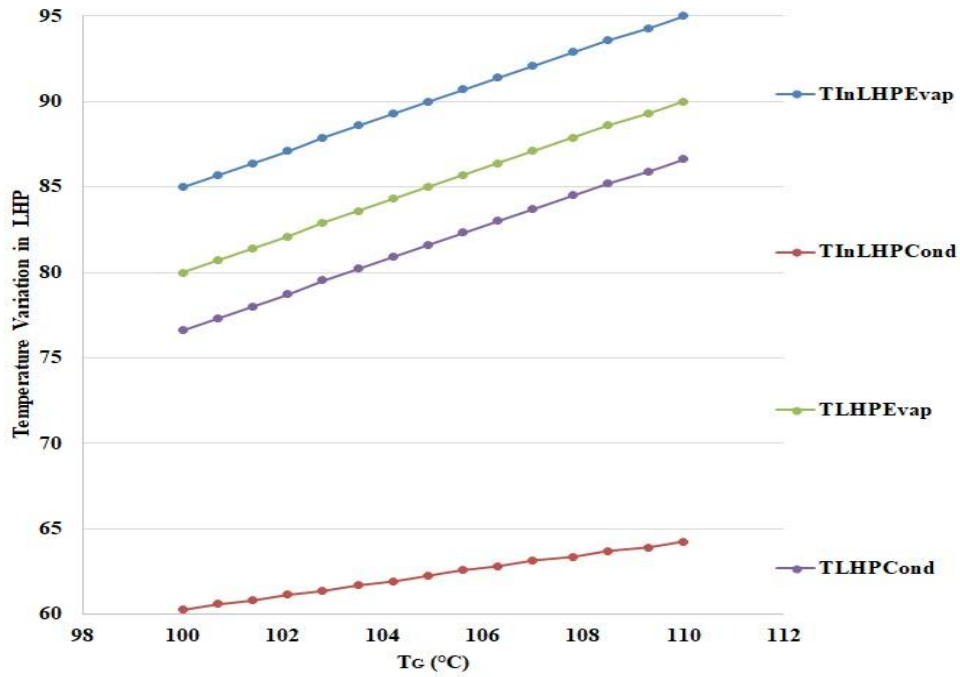


Fig 5.3: Temperature Variation in LHP with Generator Temperature

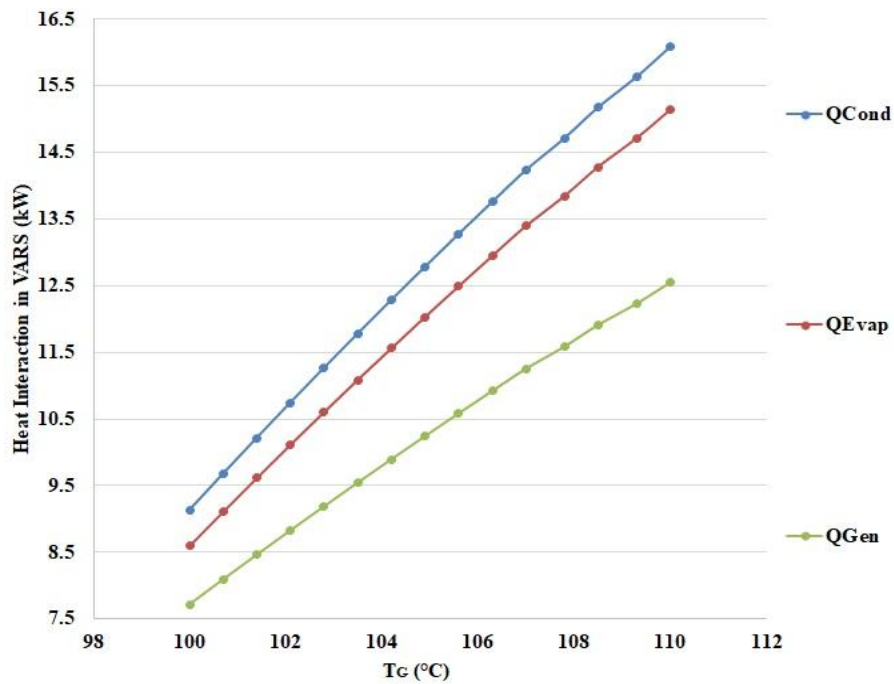


Fig 5.4: Heat Interaction in Single Effect Modification-I with Generator Temperature

Furthermore, it can be seen from the Fig. 5.3 that the LHP Condenser can sustain a Temperature as high as approximately 80-90 °C, and the mixture temperature entering the LHP Condenser for Heat Exchange is 60.2 – 64.2 °C which can be heated up to approximately 70-80 °C or even more reducing the overall requirement of Heat to be added inside the Generator.

The Heat interaction in the VARS can be observed in Fig 5.4. The Heat interaction in the evaporator has been calculated as 8.6 – 15.1 kW, whereas, the unmodified original VARS requires heat input as 12.2 – 20.5 kW ^[176], also the heat rejected in the Condenser is 9.1 – 16 kW. The modification brings down the requirement of heat input to the generator and the Heat Input is 7.7 – 12.5 kW.

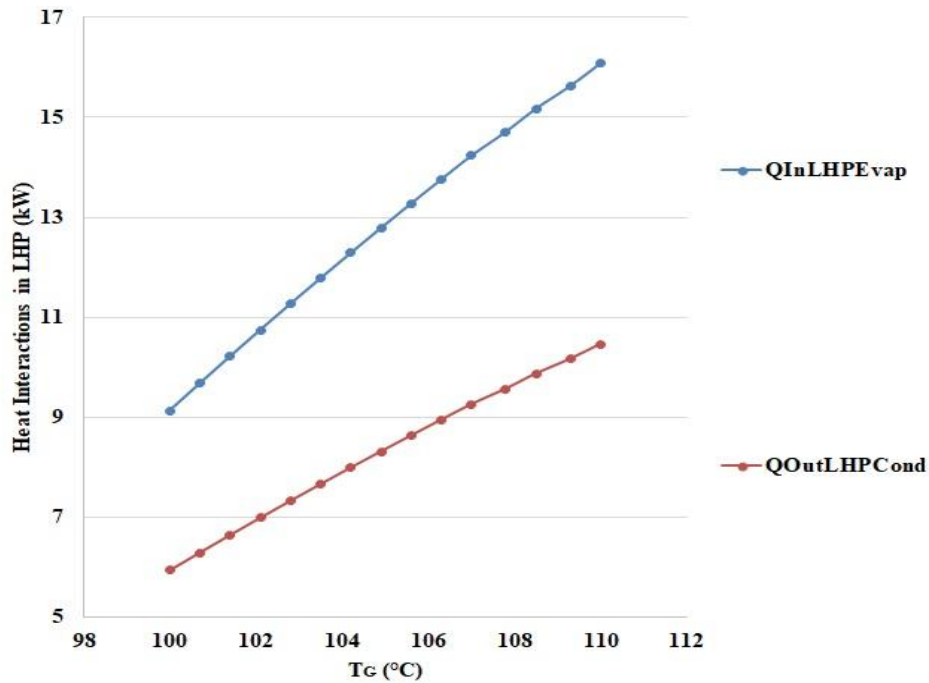


Fig 5.5: Heat Interaction in LHP with Generator Temperature

From Fig 5.5 the heat available for absorbing at LHP Evaporator has been calculated as 9.13 – 16.1 kW and the Heat Available at the LHP Condenser is seen to be 5.9 – 10.4 kW. Similarly, Fig 5.4 shows the Heat Interactions within the VARS.

Fig 5.6 shows the Percentage of Component - wise Irreversibility for the VARS, where, the Evaporator Contributes approximately 8.92 %, the Generator Contributes up to 39.34 %, the Condenser Contributes up to 15.83 %, the Absorber up to 27.9 %, and the heat exchanger up to 5.28 % of the irreversibility of the system. Originally, the Irreversibility decreases with the rising temperature; however, for simplicity, the

component-wise percentage Irreversibility contribution towards the overall system has been more or less invariable.

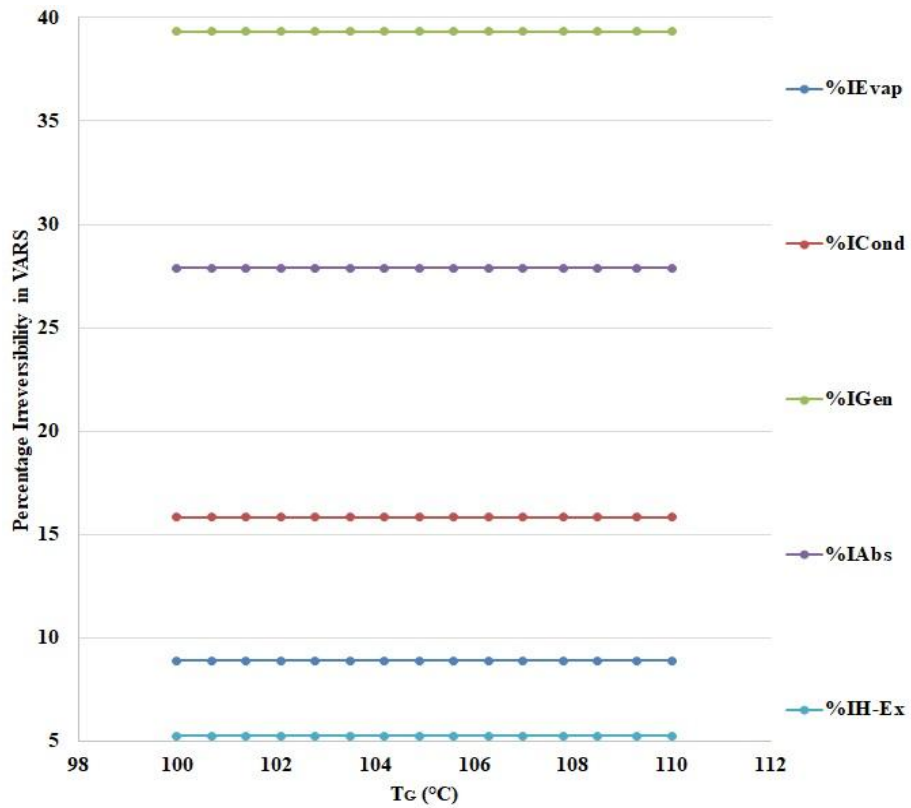


Fig 5.6: Percentage Irreversibility in Single Effect Modification-I Components with Generator Temperature

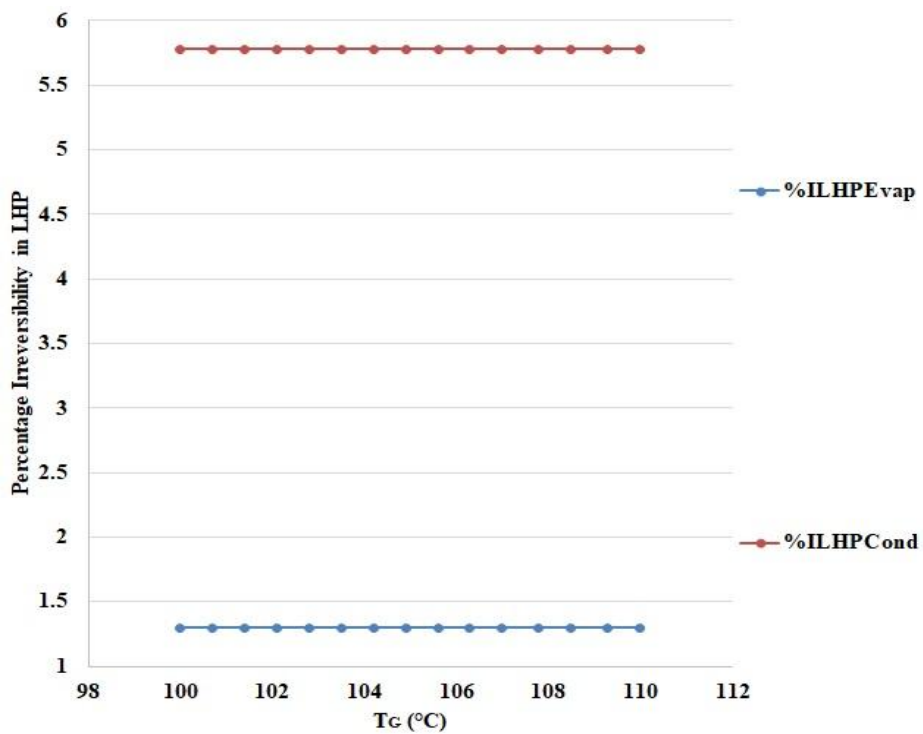


Fig 5.7: Percentage Irreversibility in LHP Components with Generator Temperature

Performance Improvement of Vapour Absorption System Using Loop Heat Pipes

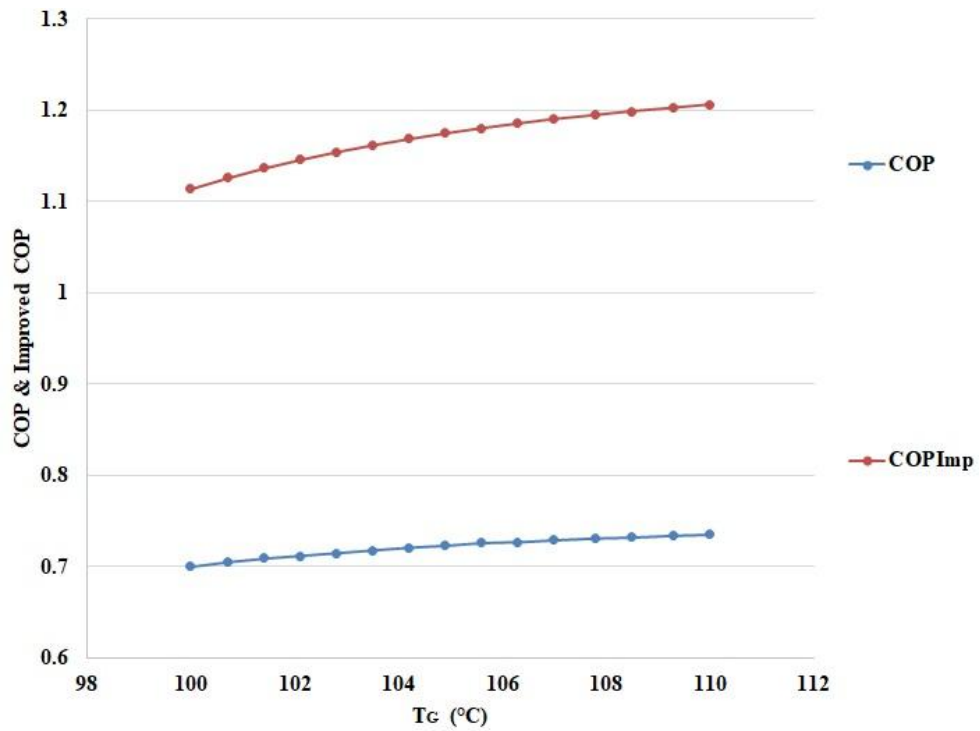


Fig 5.8: COP & Improved COP with Generator Temperature

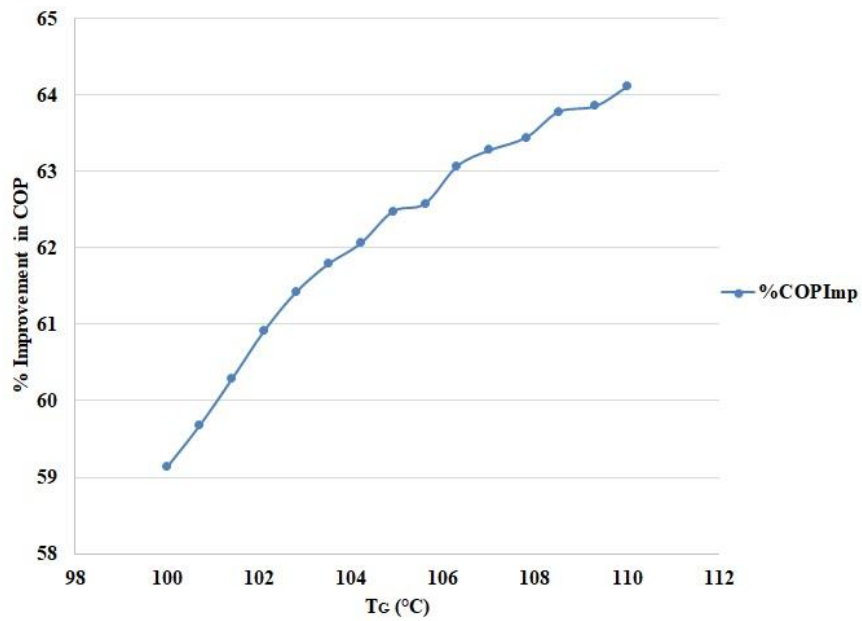


Fig 5.9: Percentage Improvement in COP with Generator Temperature

Fig 5.7 shows that the LHP Evaporator Contributes approximately 1.2 % & the LHP Condenser Contributes approximately up to 5.78 % of the irreversibility, which is lower than the Condenser.

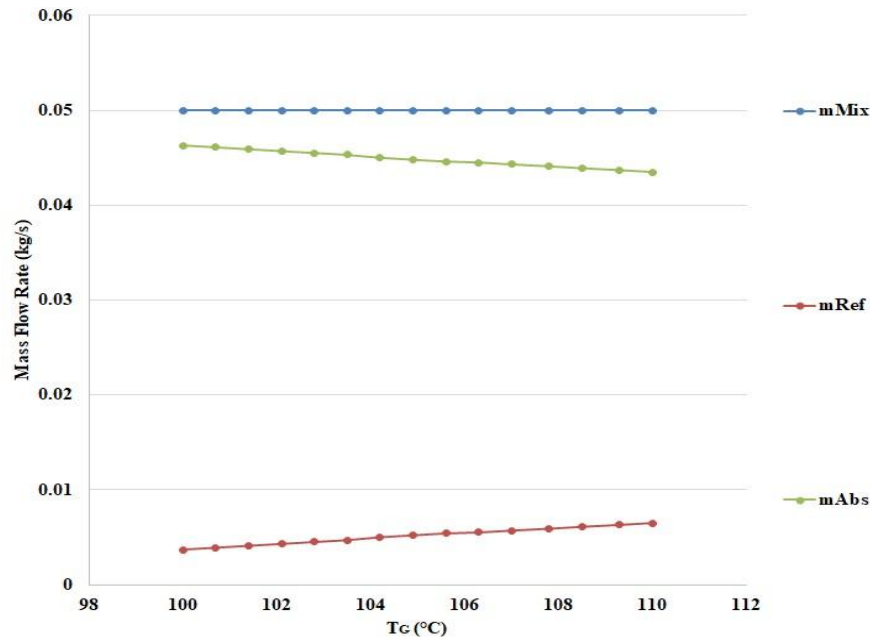


Fig 5.10: Mass Flow Rates in Single Effect Modification-I with Generator Temperature

It can be seen that the Original COP of the Single Effect VARS System varies from 0.7-0.735 [176], whereas, the VARS Modification-I has the COP variation from approx. 1.1-1.2 from Fig 5.8. The Percentage increase can be seen to vary from 60-64 % approximately. Fig 5.9 shows the mass flow rate in the VARS system with the unit mass flow of the mixture to the Generator. Mass Flow Rate of Refrigerant 0.0037 – 0.0065 kg/s , Absorbent 0.0463 – 0.0435 kg/s & Mixture 0.05 kg/s.

5.1.2. Single Effect VARS Modification-II

The modification-II has been obtained by the replacement of the Mixture HEx by the LHP (LHP-I) and the LHP replacing the condenser has been termed as LHP-II for this system. As a result of the replacement of the HEx, the overall Heat transfer effectiveness improves and the results reflect in the improvement of COP & reduction in the Irreversibility Associated.

Performance Improvement of Vapour Absorption System Using Loop Heat Pipes

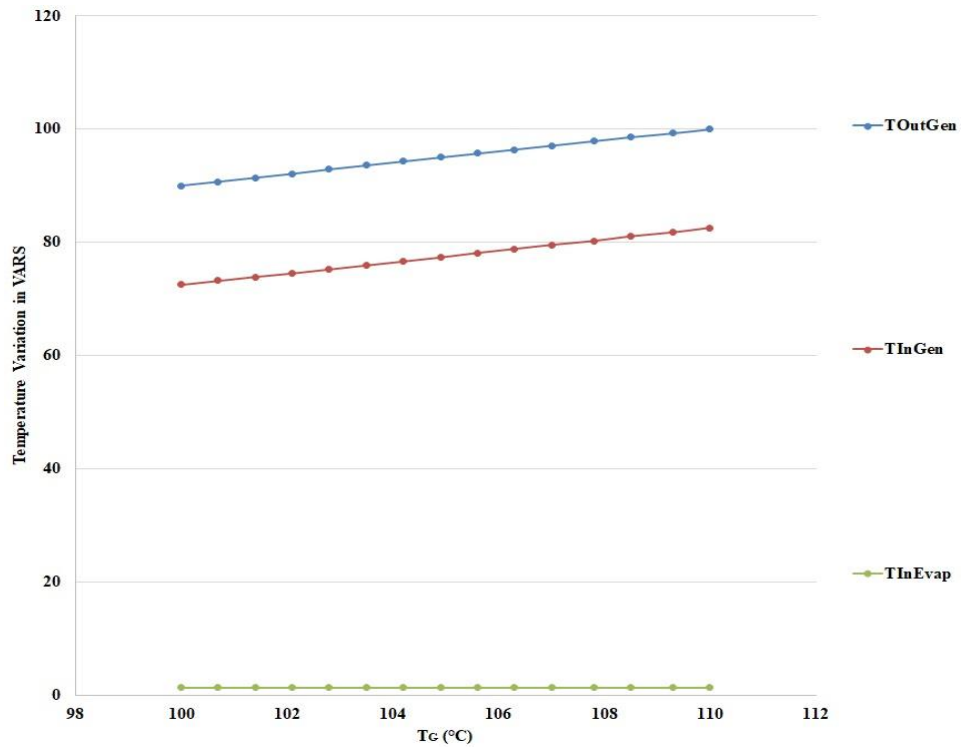


Fig 5.11: Temperature Variation in Single Effect Modification-II with Generator Temperature

Fig 5.11 shows the temperature variation in the VARS components. It can be seen that the temperature of the mixture at the inlet is approximately 72.5-82.5 $^{\circ}\text{C}$ which is higher than the Modification-I as the heat interaction in the LHP-I is more than the HEX.

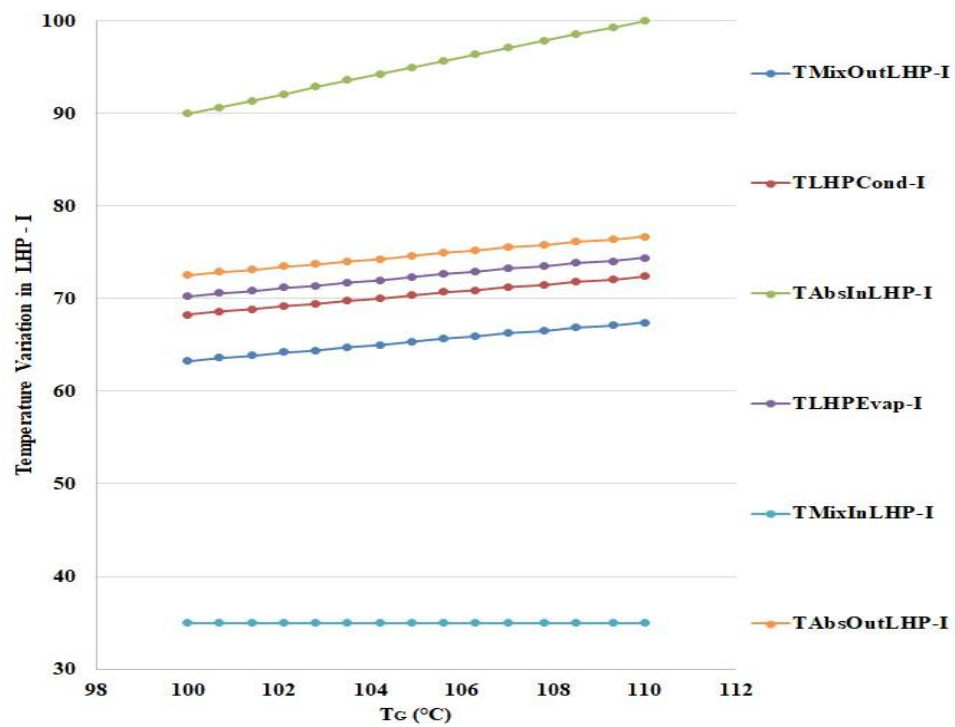


Fig 5.12: Temperature Variation in LHP-I with Generator Temperature

On the other hand, Fig 5.12 shows the Temperature Variation in the LHP-I. It can be seen that the LHP Evaporator and Condenser Temperatures are obtained as approximately 85-95 °C & 80.15-90.2 °C respectively. The Inlet and Outlet temperatures of the High Temperature Absorbent to the LHP - I Evaporator are 90-100°C & 72 – 76 °C respectively. Whereas, the Inlet and Outlet temperatures of the Mixture to the LHP - I Condenser are 35°C & 63.2 – 67.4 °C which is higher than the HEx. Hence, the overall heat exchange increases, and the corresponding requirement of Heat to the Generator reduce and increase the COP further for the Modification-II.

Similarly, Fig 5.13 shows the temperature variation of the LHP-I which is only different for the inlet and outlet temperature of the Mixture.

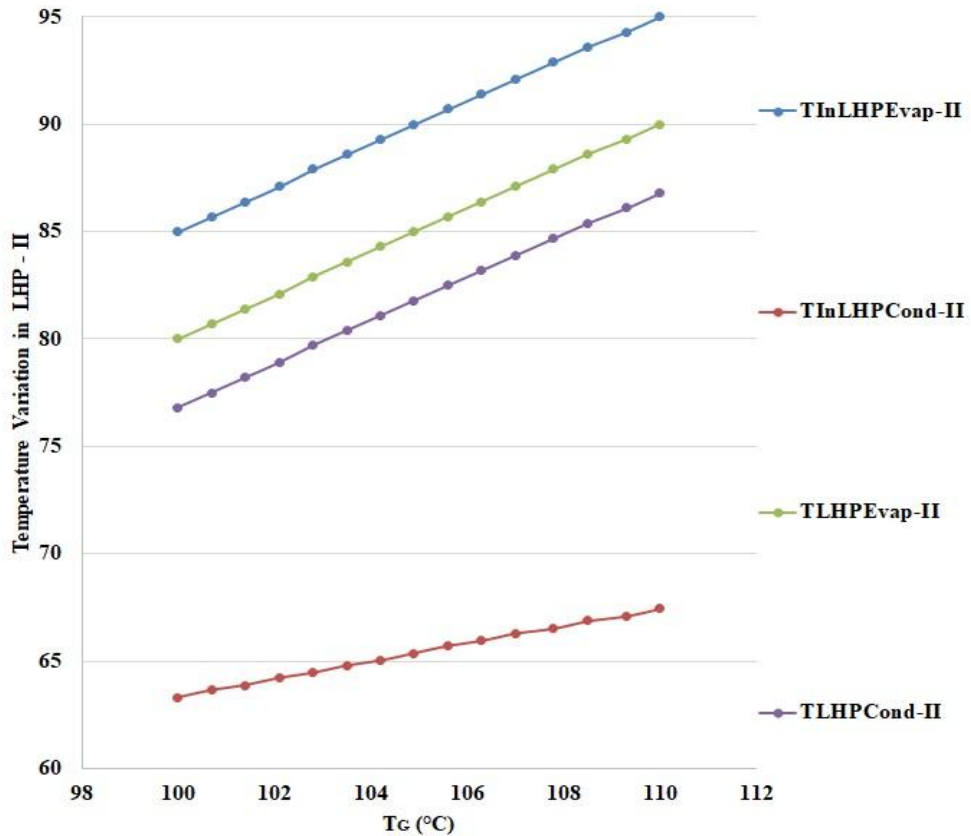


Fig 5.13: Temperature Variation in LHP-II with Generator Temperature

Fig 5.14 shows the Heat Exchange in the VARS in which the requirement in the generator is less than that of the Modification-I. The Heat required in Mod – II is 7.2 – 11.7 kW.

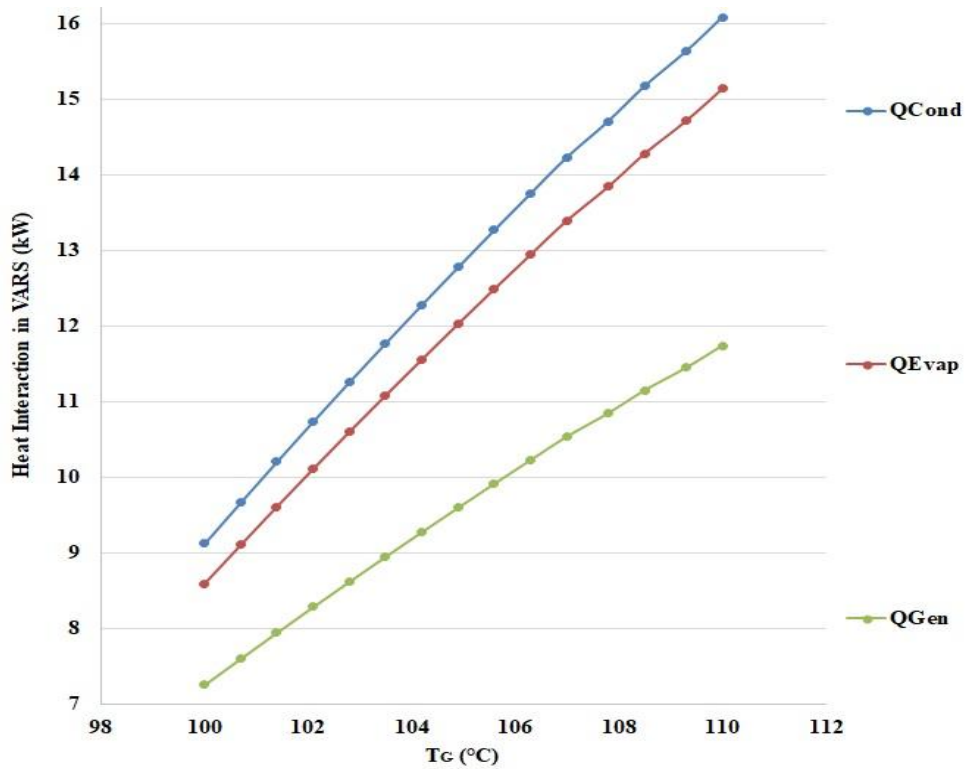


Fig 5.14: Heat Interaction in Single Effect Modification-II with Generator Temperature

The Heat input at the LHP-II can be seen in Fig 5.15 to be 9.13-16 kW at the Evaporator and 5.9 – 10.45 kW at the Condenser.

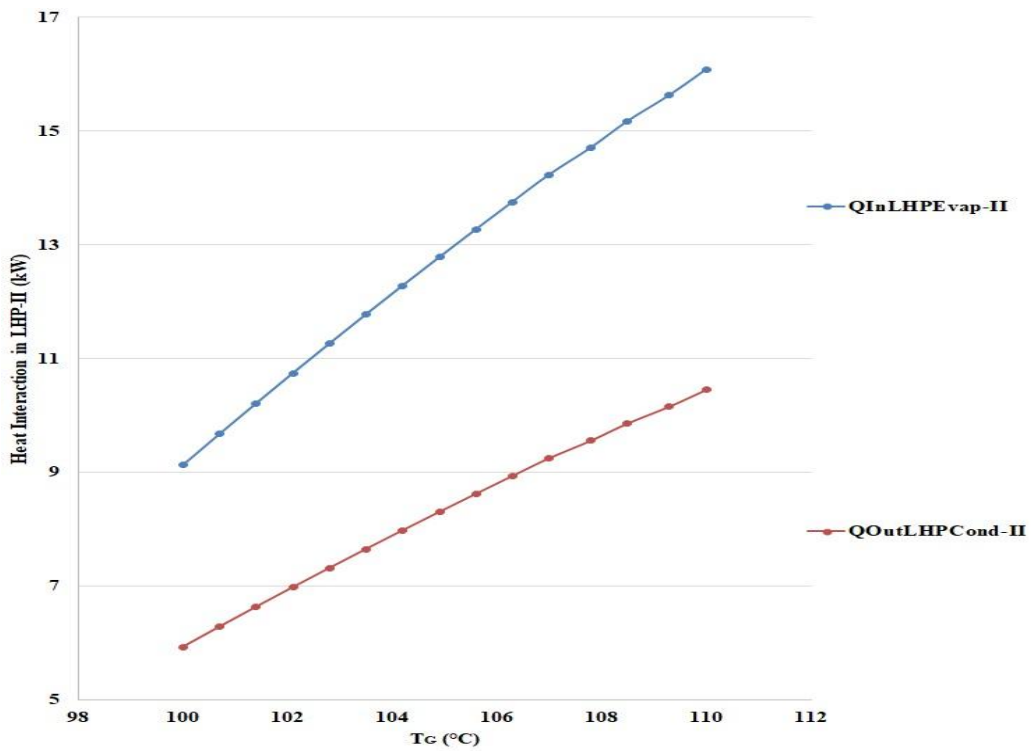


Fig 5.15: Heat Interaction in LHP-II with Generator Temperature

Performance Improvement of Vapour Absorption System Using Loop Heat Pipes

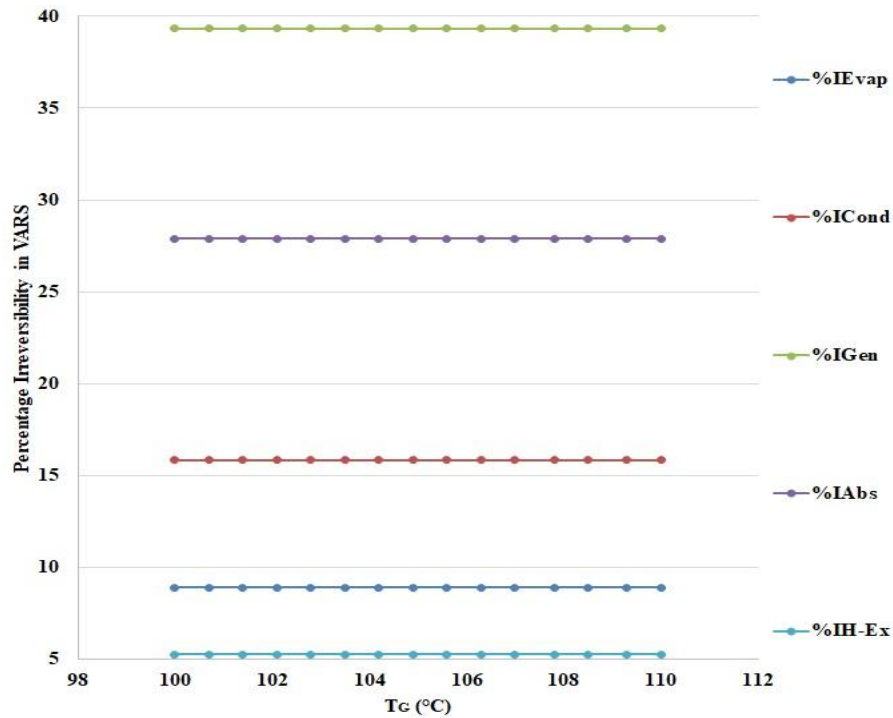


Fig 5.16: Percentage Irreversibility in Single Effect Modification-II Components with Generator Temperature

Fig 5.17 shows the percentage Irreversibility contribution of the LHP-I & LHP-II. The Evaporators of LHP-I & II contribute approximately 1.3 & 1.7 % of the system respectively, whereas, the Condensers of LHP- I & II contribute approximately 2.7 & 5.78 % of the system respectively.

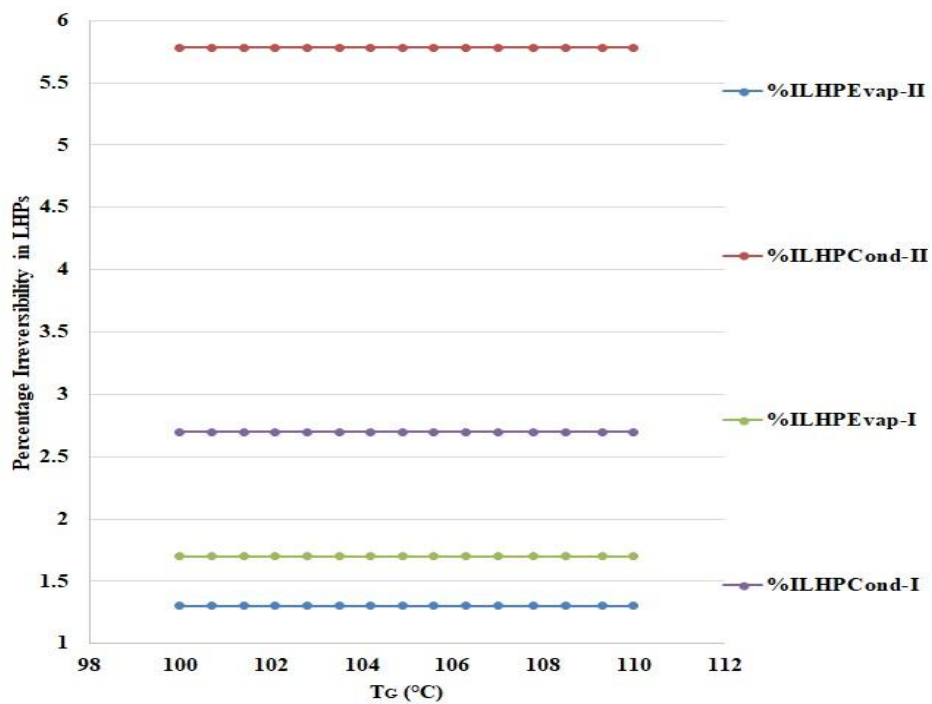


Fig 5.17: Percentage Irreversibility in LHP Components with Generator Temperature

Performance Improvement of Vapour Absorption System Using Loop Heat Pipes

Furthermore, the COP for Modification-II has been obtained to be 1.18-1.28 which is on an average 6-7 % increase in the COP for the Modification-I as shown in Fig 5.18 & 5.19.

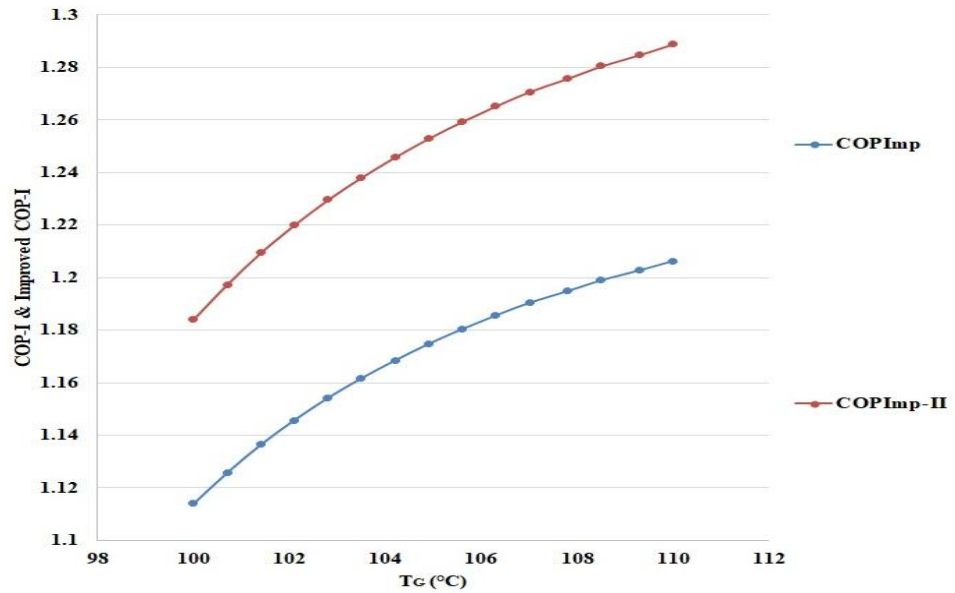


Fig 5.18: COP & Improved COP with Generator Temperature

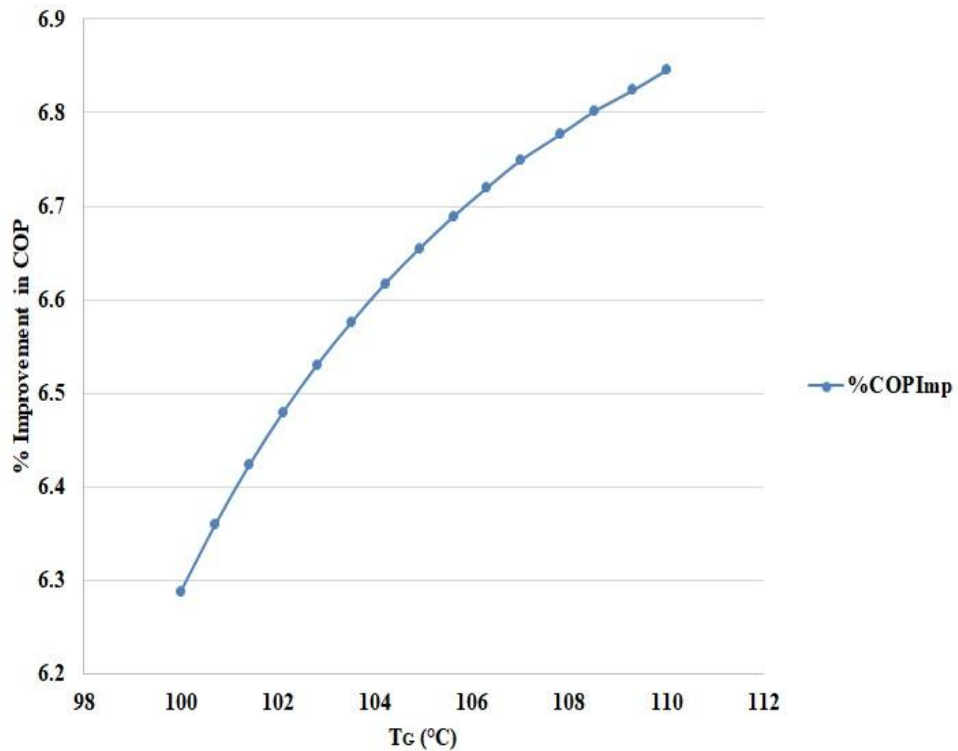


Fig 5.19: Percentage Improvement in COP with Generator Temperature

Table 5.3 present the comparison between the Texts, Published Work & Proposed modification based on the various parameter performance parameters. The results have been well within the permissible limits.

Table 5.3: Comparison of Modified Single Effect VARS

Parameters	Herold et. al. (2016) ^[176]	Modi et. al. (2017) ^[178]	Proposed Work	
			Modification-I	Modification-II
Mass Flow Rate of Mixture from Absorbent (kg/s)	0.05	9.035	0.05	0.05
Mass Flow Rate of Refrigerant in Evaporator (kg/s)	0.0037	1	0.0037	0.0037
Generator Temperature (°C)	100	87.8	100	100
Evaporator Temperature (°C)	5	7.2	5	5
Absorber Temperature	35	37.8	35	35
Q _{Evap} (kW)	8.6	2355	8.6	8.6
Q _{Cond} (kW)	9.131	2506	9.131	9.131
Q _{Gen} (kW)	12.7	3093	7.7	7.25
COP	0.761	0.761	1.11	1.18
η_{II} (%)	22.85	24	36.37	38.66

Table 5.4 present a similar comparative study of the Published work & proposed work based on the Component-wise Irreversibility & Percentage Irreversibility Contribution to the system as a whole at 100 °C.

Table 5.4: Irreversibility in Single Effect Components

Parameters/ Irreversibility	Modi et. al. (2017) ^[178]		Proposed Work			
	kW	%	Modification-I		Modification-II	
			kW	%	kW	%
I _{Evap}	0.07	9.17	0.163	8.92	0.163	8.92
I _{Gen}	0.31	40.43	0.72	39.34	0.72	39.34
I _{Cond}	0.1247	16.27	-	-	-	-
I _{HEx}	0.041	5.43	0.096	5.28	-	-
I _{Abs}	0.219	28.67	0.51	27.9	0.51	27.9
LHP-I	-	-	-	-	0.0326	4.4
LHP-II	-	-	0.129	7.08	0.129	7.08
Refrigeration Capacity (RC) (kW)	3.5		8.8			
Total Irreversibility	0.76		1.62		1.55	

5.1.3. Combined Single Effect VARS & GPC

This section presents the performance parameters of the combined Single Effect VARS & GPC through LHP (LHP-III) with variation in the Mass of Fuel Required to run the GPC & Consequently the VARS. Fig 5.20 shows the Peak, Exhaust & Generator Temperature. The Mass of Fuel can be seen to vary from 0.016 to 0.021 kg/s for the GPC. The Consequent Peak Temperature obtained in the GPC is 927-

1227 °C. The exhaust temperature of the GPC is found to be 299.6 – 360.4 °C, whereas, the generator works at around 100-110 °C for this system. This provides an opportunity of having a higher effect VARS to be used for the study.

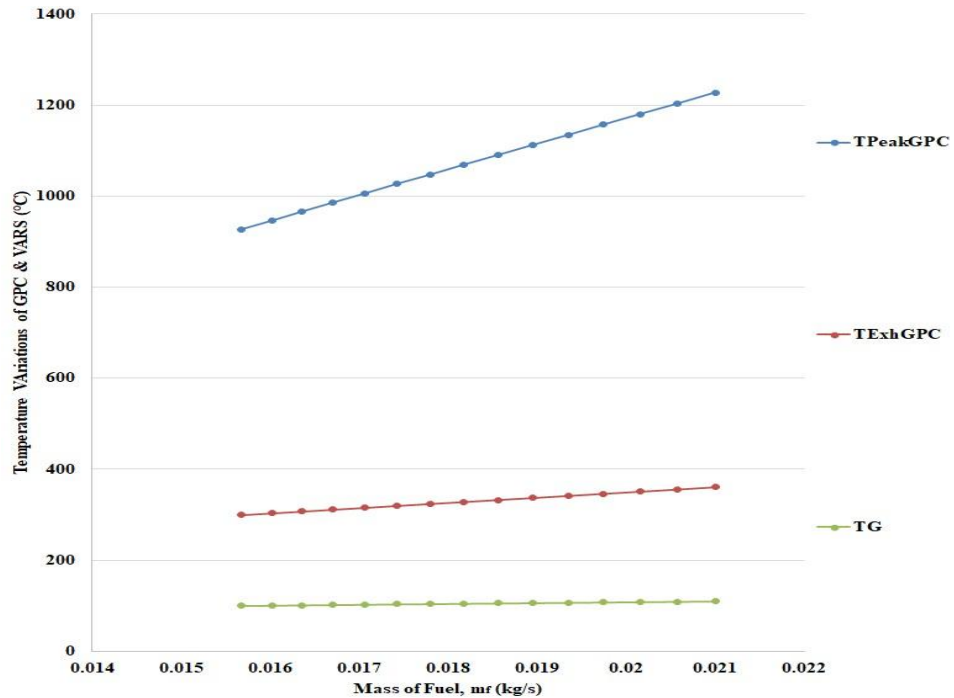


Fig 5.20: Temperatures of GPC and Generator Single Effect Modification-II with Mass of Fuel in GPC

Similarly, the temperature of the LHP-III Condenser which becomes the interface for the heat transfer to the generator is 288-348 °C approximately as shown in Fig. 5.21.

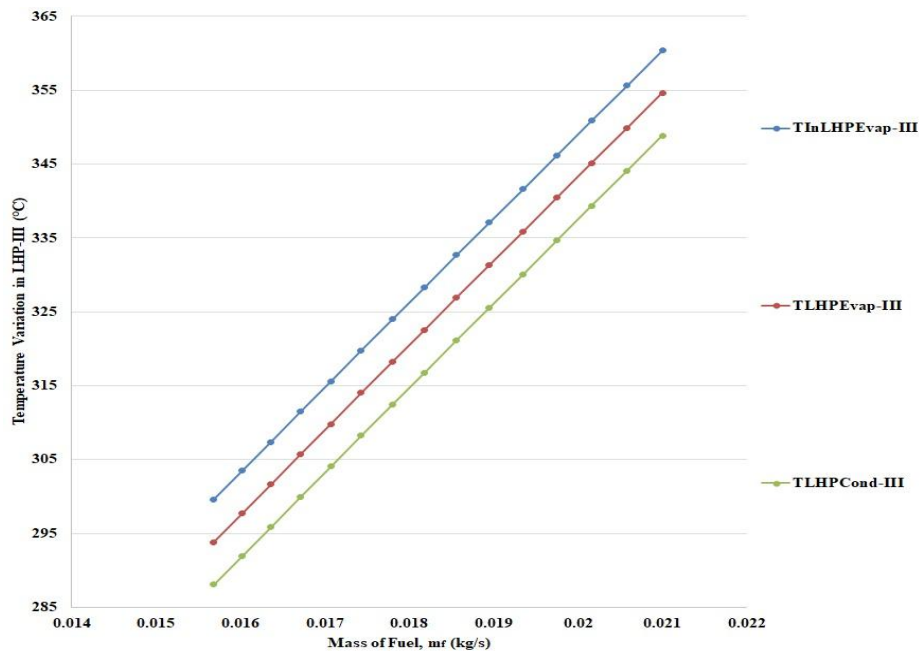


Fig 5.21: Temperatures of LHP-III with Mass of Fuel in GPC

Performance Improvement of Vapour Absorption System Using Loop Heat Pipes

Similarly, the Heat Content, Exergy & Irreversibility of the Exhaust gases have been presented in Fig 5.22. The heat content is 187.4-251.4 kW; the Exergy can be obtained as 75.38-109.9 kW and the Irreversibility 112.1-141.5 kW.

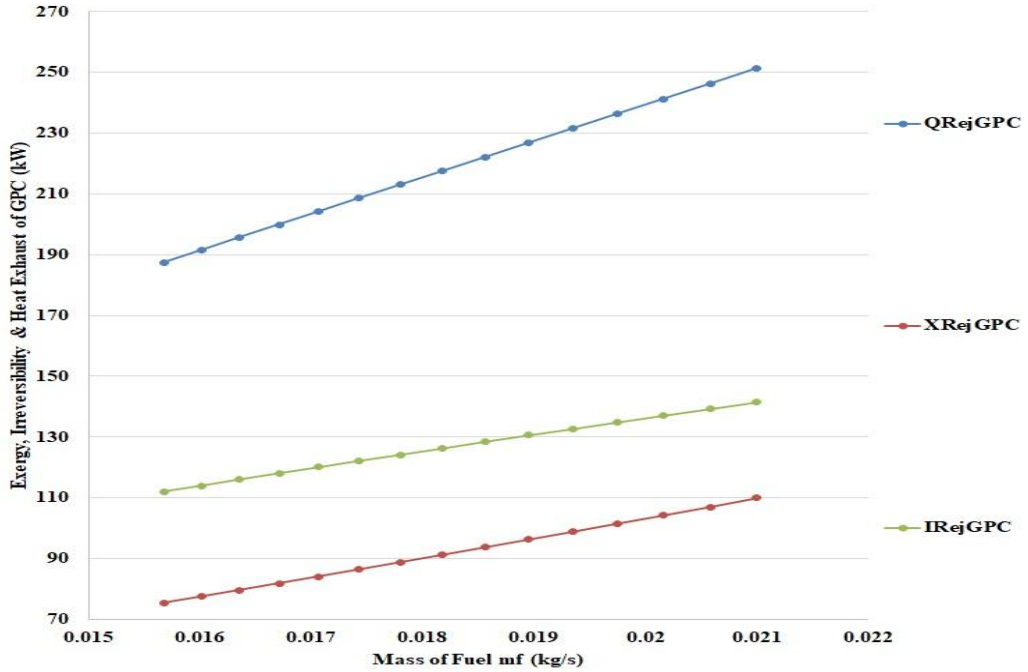


Fig 5.22: Heat, Exergy & Irreversibility at GPC Exhaust with Mass of Fuel in GPC

Fig 5.23 shows the Percentage Irreversibility related to the LHP-III evaporator to be 4.35% & the condenser to be 12.4 %.

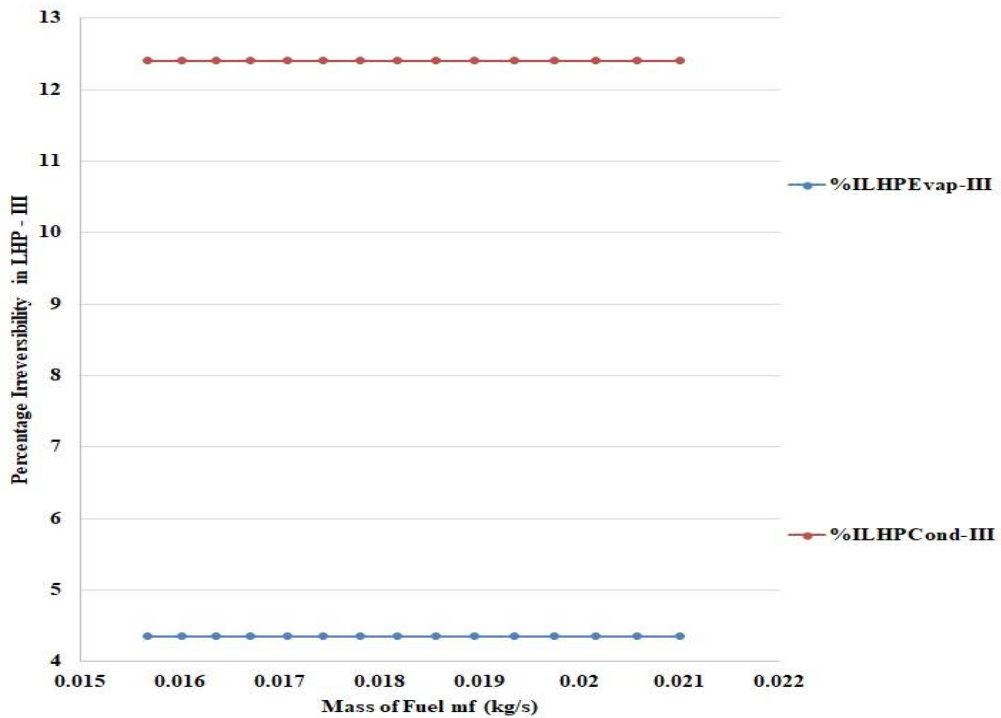


Fig 5.23: Heat, Exergy & Irreversibility at GPC Exhaust with Mass of Fuel in GPC

Fig 5.24 shows the viable number of the VARS system under consideration that can be run by this GPC in a combined system. Around 8-10 Single Effect VARS Modification-II can be operated with the GPC under the presented parameters.

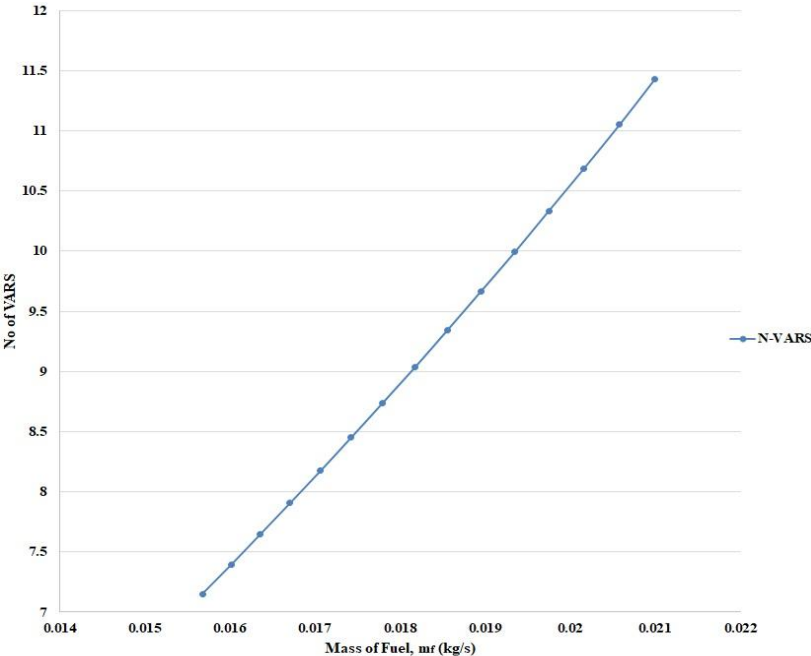


Fig 5.24: Number of Single Effect Modification-II Viable with GPC with Mass of Fuel in GPC

5.2. Modified Half-Effect VARS (Ankit Dwivedi, et. al. 2018) ^[184]

This section presents the results obtained from the analysis performed for the Half-Effect Systems under consideration. Table 5.5 Presents the Input Parameters taken for the analysis. The Generator temperature has been varied from 65-75 °C to obtain the basic heat performance parameters such as mass flow rates, COP, Irreversibility, Temperature & Heat Interaction Variation, etc for the 2 modifications. The Modification-II system is also combined with the GPC (Table 5.1) for which the results have been presented as well.

Table 5.5: Input Parameters for Half Effect VARS Analysis

Sl. No.	Input Parameters	Data
1.	Peak Temperature, T_G	65 °C
2.	Evaporator Temperature, T_{Evap}	5 °C
3.	Working Fluid	LiBr-H ₂ O
4.	Heat Exchanger Effectiveness, ϵ_{H-Ex}	0.5-0.7
5.	Condenser Temperature, T_C	35 °C
6.	Mass Flow rate after absorber, m_2	1
7.	Absorber Temperature, T_{Abs}	35 °C
8.	Low Generator Temperature, T_{G-L}	65°C

5.2.1. Half-Effect VARS Modification-I

This section presents the analysis by Modification-I in the Half Effect VARS by LHP employing Intra-cycle Heat Exchange. Fig 5.25 presents the temperature variation in the VARS. It can be observed that the Mixture Temperature Entering the Generator is approximately 47.8 - 57.8 °C, the Temperature of Refrigerant Vapour Leaving the Generator is approximately 59.7- 69.7 °C, the Temperature of Absorbent Leaving the Generator 62 – 72 °C and the Evaporator temperature has been kept at 5 °C. The Mixture temperature entering both the generators of the unmodified system was 40.5 – 43.5 °C

Similarly, Fig 5.26 shows the temperature variation in the Heat Exchanger. It can be examined that the Absorbent enters the HEx at approximately 62-72 °C and leave the

Performance Improvement of Vapour Absorption System Using Loop Heat Pipes

HEX at approximately 55– 58.4 °C. Moreover, the Mixture is pumped into the HEX at 35 °C and leaves the HEX at 40.5 - 43.5 °C.

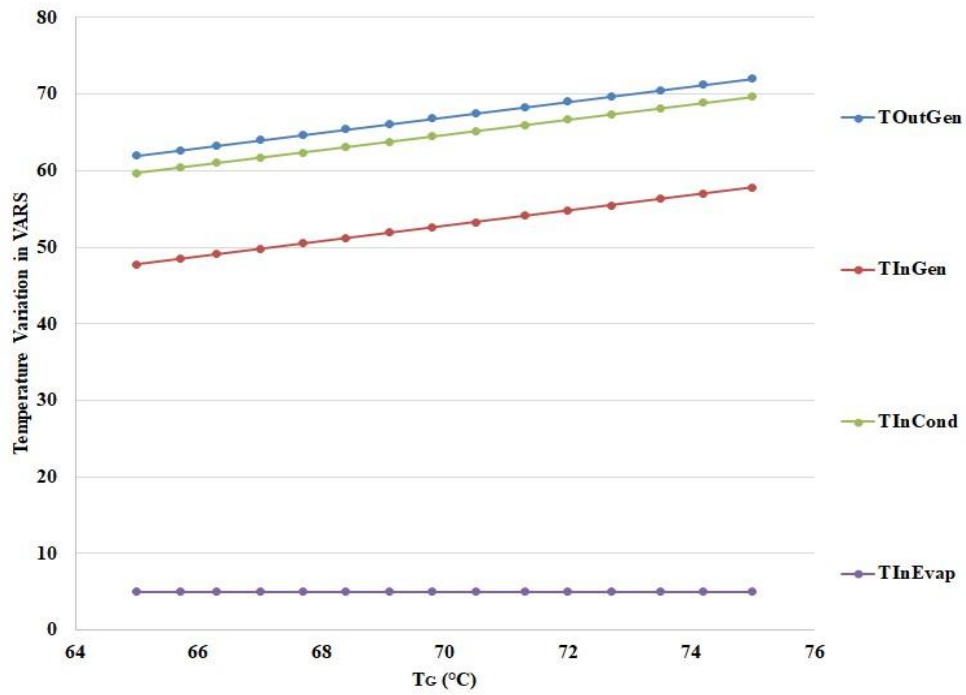


Fig 5.25: Temperature Variation in Half Effect Modification-I with Generator Temperature

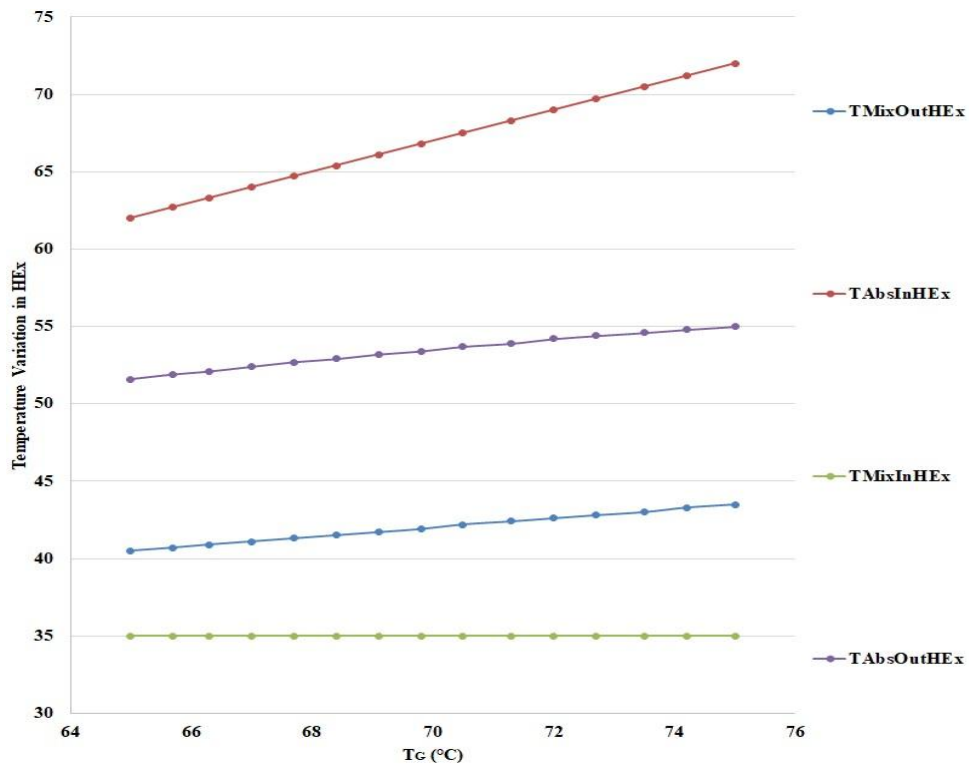


Fig 5.26: Temperature Variation in Half Effect Modification-I Heat Exchanger with Generator Temperature

Fig 5.27 examines the temperatures that are being observed in the LHP being used in this system. It can be seen that the Temperature of the Fluid entering the LHP is approximately 59.7- 69.7 °C for heat rejection to the LHP Evaporator. It is the same as the Refrigerant Vapour Leaving Generator. Consequently, the Evaporator of the LHP has a temperature of approximately 54.4 – 64.7 °C keeping the temperature Gap of 5 °C for heat exchange. Furthermore, the Temperature obtained in the condenser is approximately 51.8 - 61.8 °C. The heated mixture leaves at a temperature of around 47.8 - 57.8 °C. It is to be mentioned that the results are presented for both the Generators & the Heat Absorbed from the Condensing Vapour Refrigerants are supplied in a combined manner to the Mixtures, preheating to increase the overall performance and reducing the Heat Requirements. The COP of the Half Effect System is dependent on the Heat Input to the Low & High Generators, unlike Double, Triple or Quadruple Effect Systems.

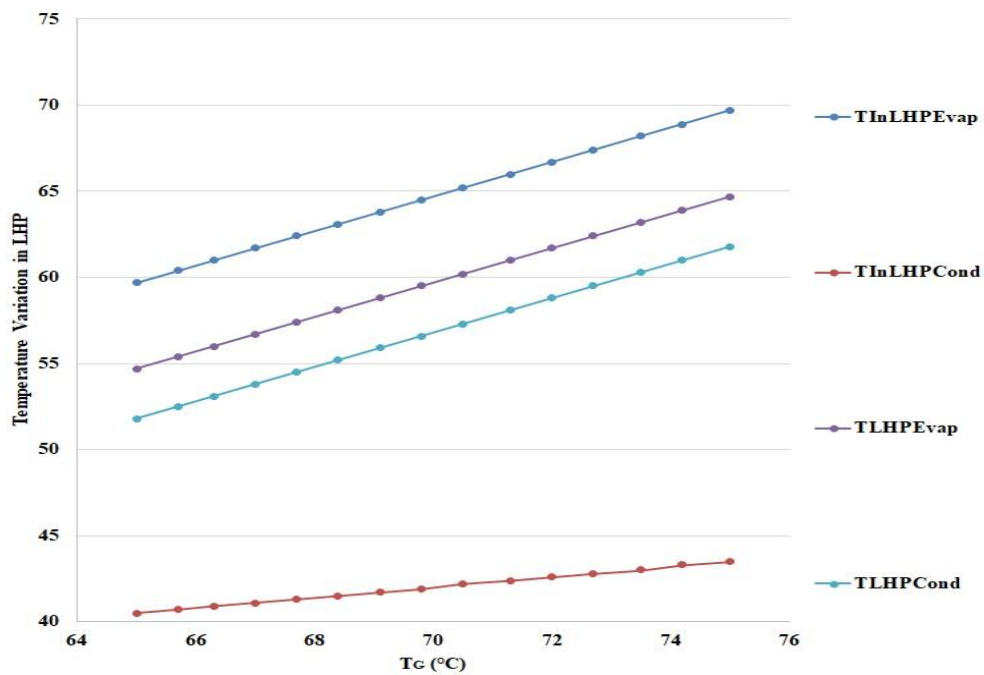


Fig 5.27: Temperature Variation in LHP with Generator Temperature

Fig 5.28 shows the Heat Exchange in the VARS. It can be noticed that the Heat Interaction in the High & Low Generators are approximately 332 - 478 kW & 236 – 337 kW respectively, whereas, the Heat extracted in the Evaporator is approximately 360- 528 kW. The heat available for the LHP Evaporator is approximately 375-550 kW. The Heat Input to the Original System for High & Low generators was 435.56 – 630 kW & 339.9 – 488.9 kW ^[176] respectively.

Performance Improvement of Vapour Absorption System Using Loop Heat Pipes

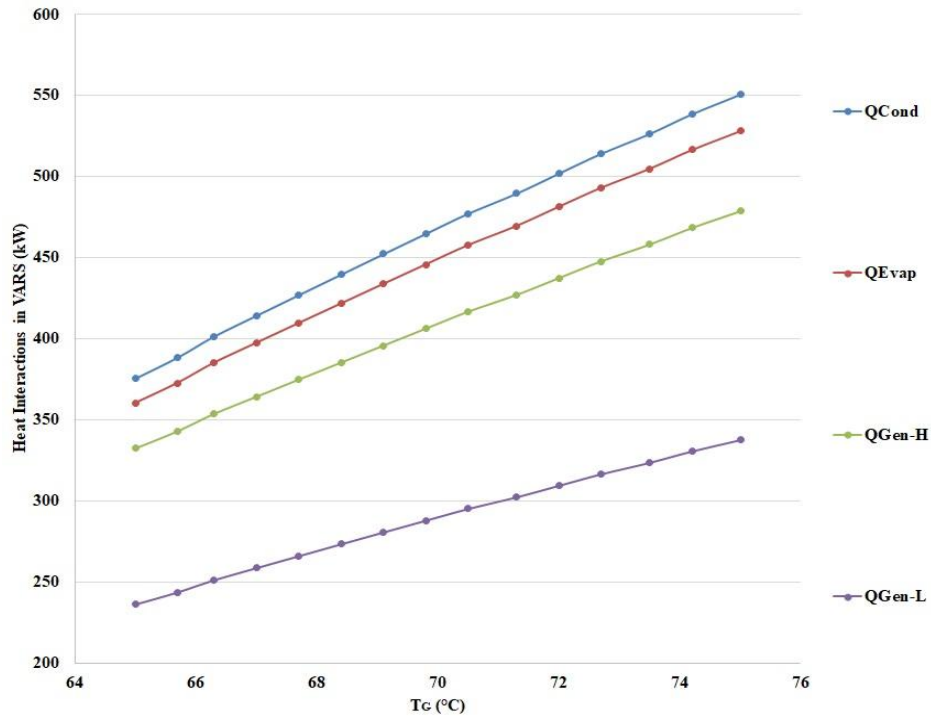


Fig 5.28: Heat Interaction in Half Effect Modification-I with Generator Temperature

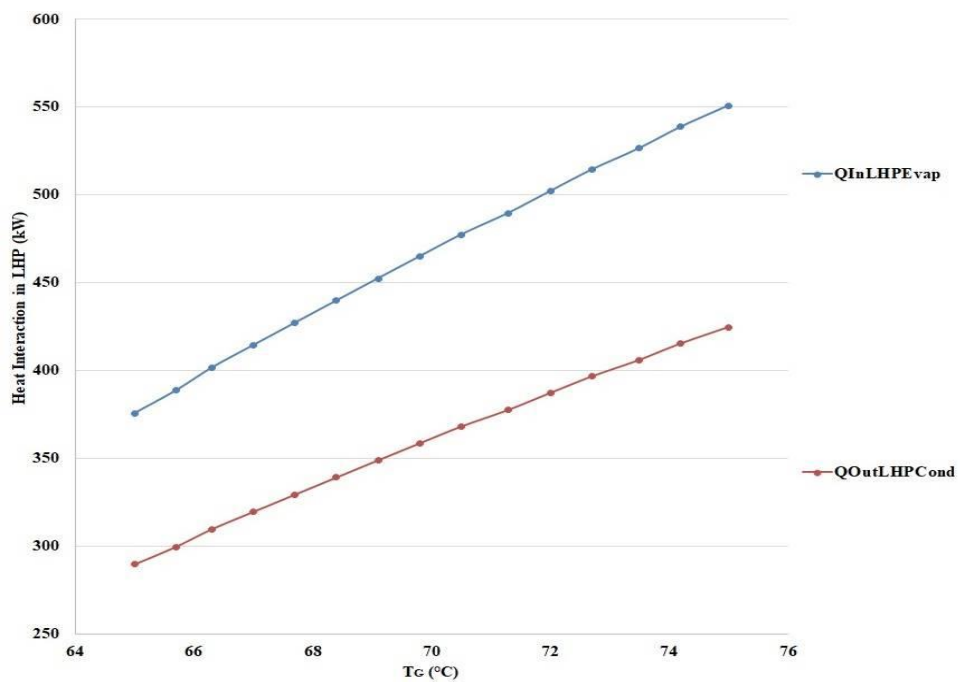


Fig 5.29: Heat Interaction in LHP with Generator Temperature

Fig 5.29 shows the heat exchange for the LHP. It can be shown that the Heat Input to the LHP Evaporator is approximately 375 – 550 kW as mentioned earlier. However, the heat transfer available for the LHP Condenser is approximately 290 – 424 kW.

Performance Improvement of Vapour Absorption System Using Loop Heat Pipes

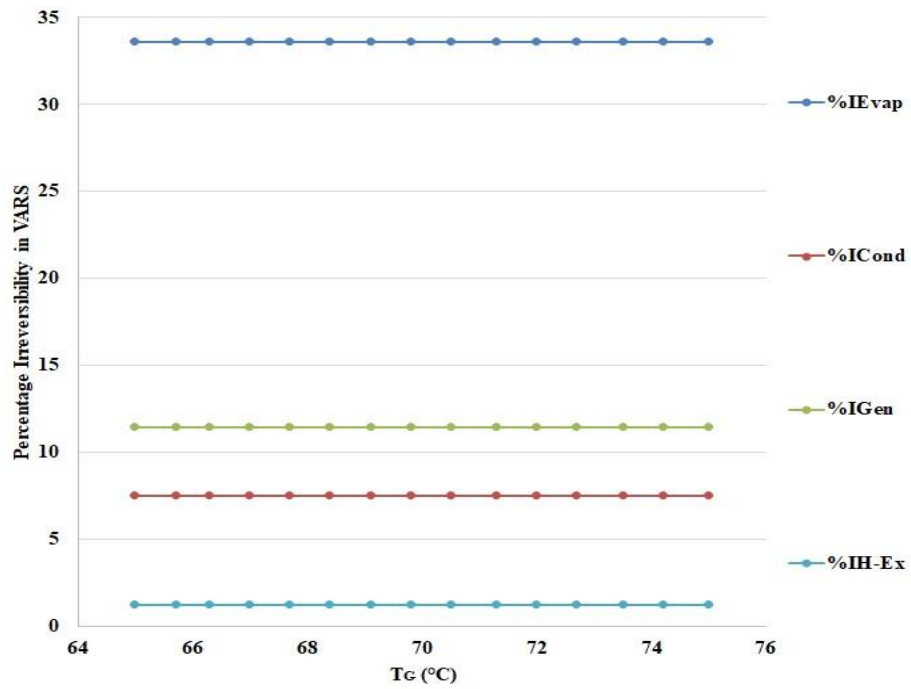


Fig 5.30: Percentage Irreversibility in Half Effect Modification-I Components with Generator Temperature

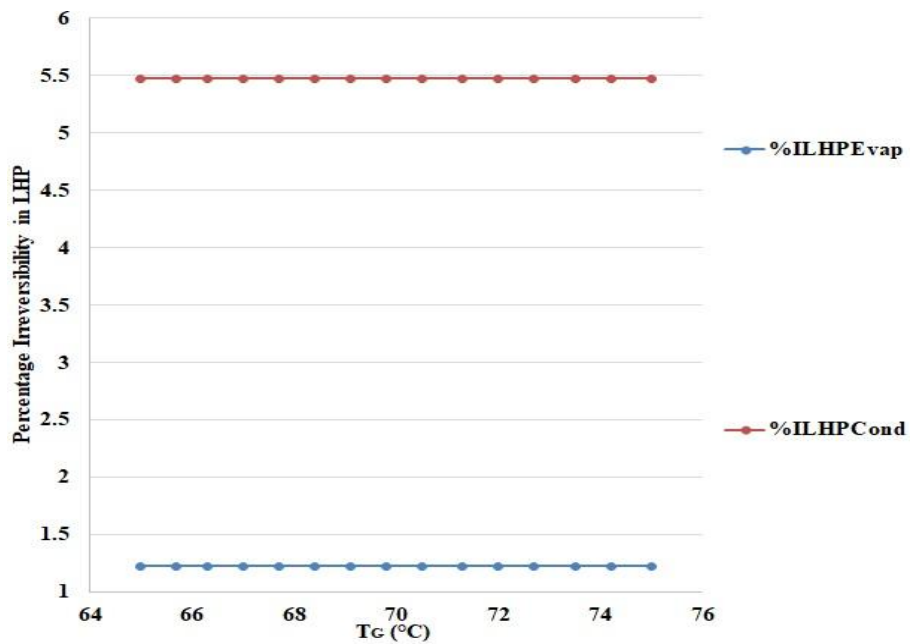


Fig 5.31: Percentage Irreversibility in LHP Components with Generator Temperature

The percentage Irreversibility associated with the Components of the VARS. It can be seen that the Evaporator, and Condenser (replaced by LHP). Generators (I & II) & Heat Exchangers contribute to the overall Irreversibility by 33.6 %, 7.5 %, 11.45 % & 1.25 % respectively.

Performance Improvement of Vapour Absorption System Using Loop Heat Pipes

Furthermore, the Irreversibility of the LHP replacing the condenser has been 1.23 % & 5.4 % for the LHP Evaporator & Condenser respectively as shown in Fig 5.

Fig 5.32 shows the Comparison of COP Obtained for the Modification-I over the original Half-Effect System ^[176]. It can be seen that the Improved COP is near 0.63 whereas the original COP is near 0.4. The Overall Improvement can be seen as around 60% in Fig 5.31.

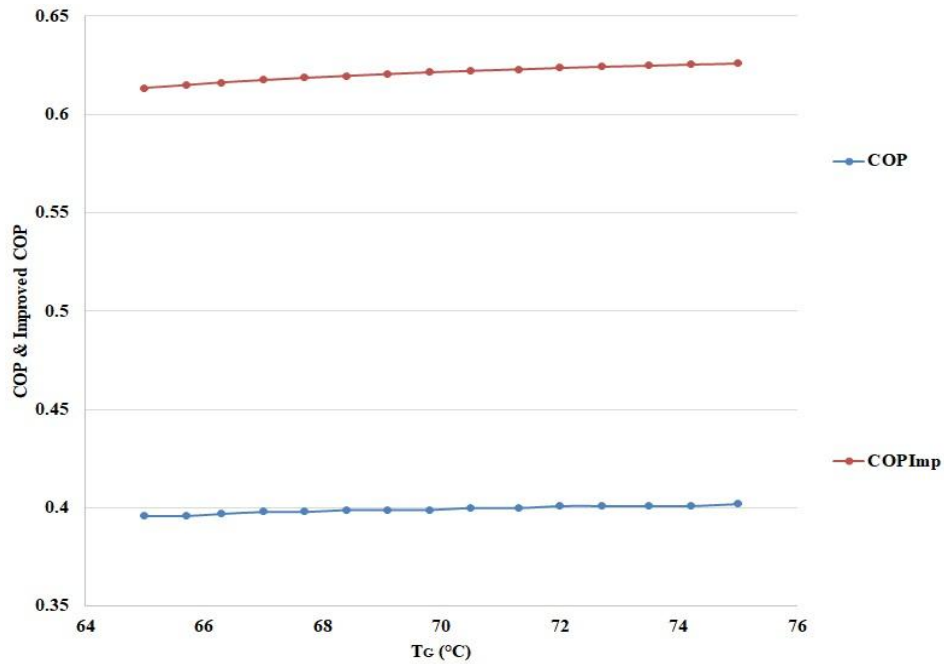


Fig 5.32: COP & Improved COP with Generator Temperature

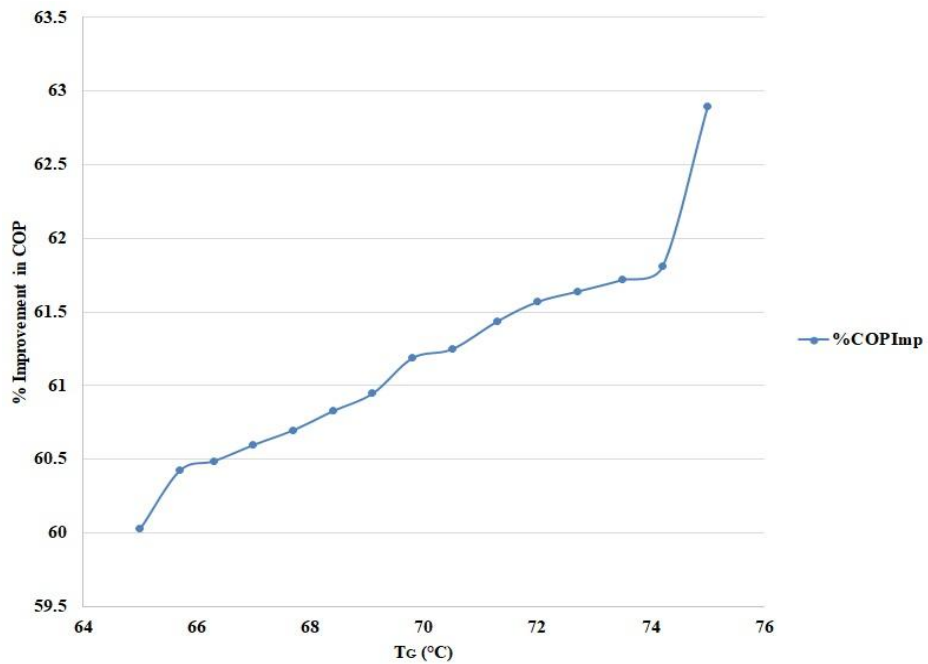


Fig 5.33: Percentage Improvement in COP with Generator Temperature

Performance Improvement of Vapour Absorption System Using Loop Heat Pipes

Figs. 5.34 & 5.35 show the mass flow rates of Refrigerant, Mixture & the Absorbent at Low & High stages. The mass flow of the Mixture in both stages has been taken as 1 kg/s and the calculation has been done accordingly. Refrigerant & Absorbent mass flow rates for low stage were found to be 0.12-0.18 kg/s & 0.87 – 0.81 kg/s respectively. Furthermore, Refrigerant & Absorbent mass flow rates for high stage were found to be 0.15-0.22 kg/s & 0.84 – 0.77 kg/s respectively

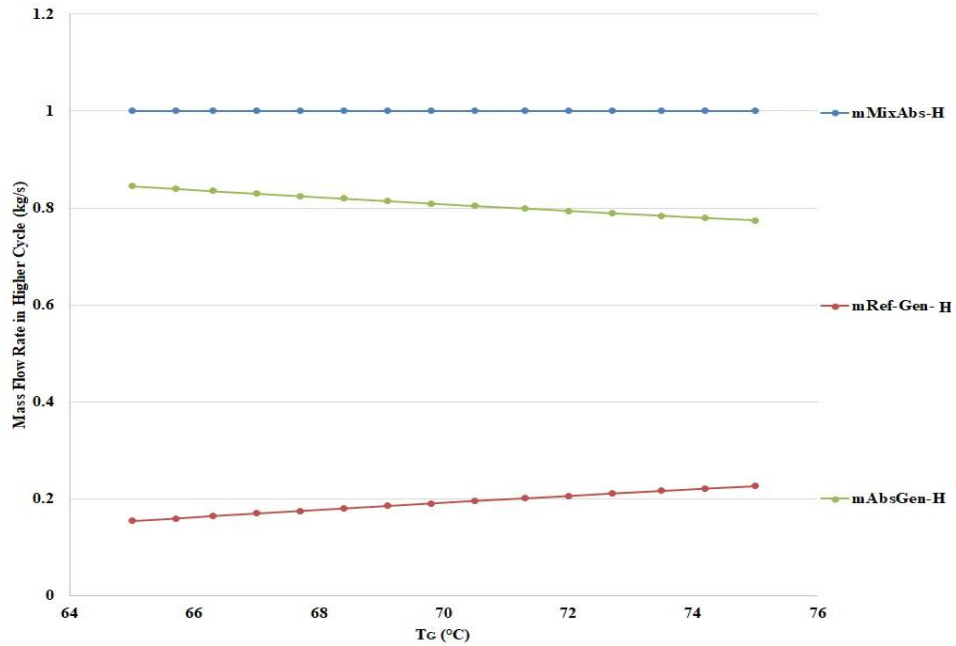


Fig 5.34: Mass Flow Rates in Half Effect Modification-I High with Generator Temperature

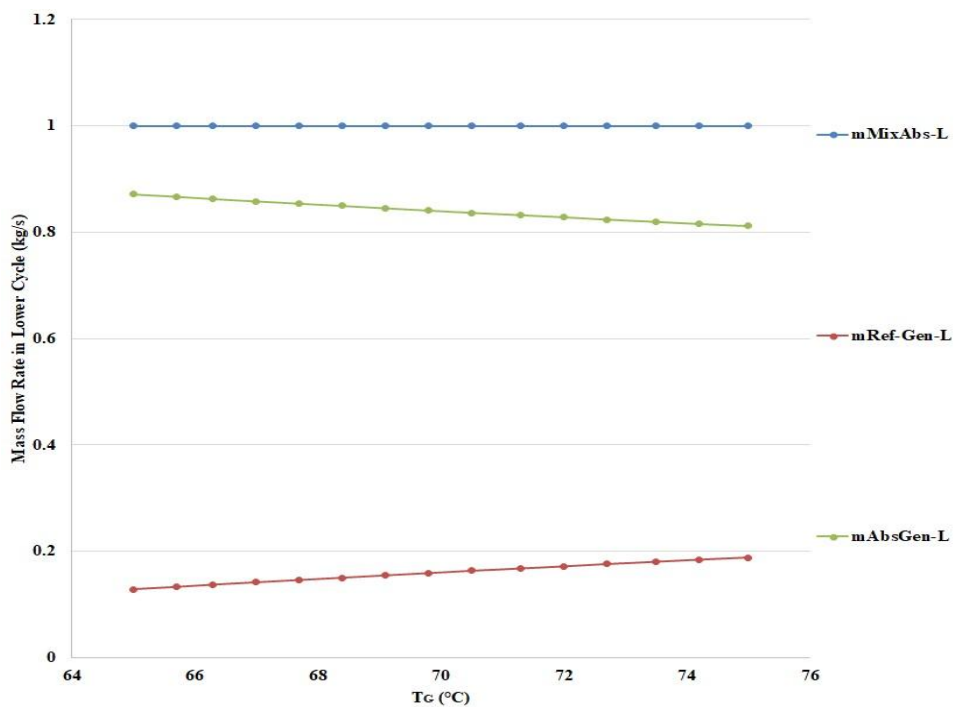


Fig 5.35: Mass Flow Rates in Half Effect Modification-I Low with Generator Temperature

5.2.2. Half Effect VARS Modification-II

Furthermore, the HEX of the Modification- I have been replaced by the LHPs. HEX-I has been replaced by LHP-I, HEX-II has been replaced by LHP-II and the LHP of the Modification-I has been re-nominated as LHP-III, which forms the Modification-II. This section covers the analysis of Modification-II. Fig 5.36 presents the Temperature variation of the VARS. It can be observed that the Mixture Temperature Entering the Generator increases and is approximately 51.1 - 59.1 °C owing to the application of LHP in place of the HEX.

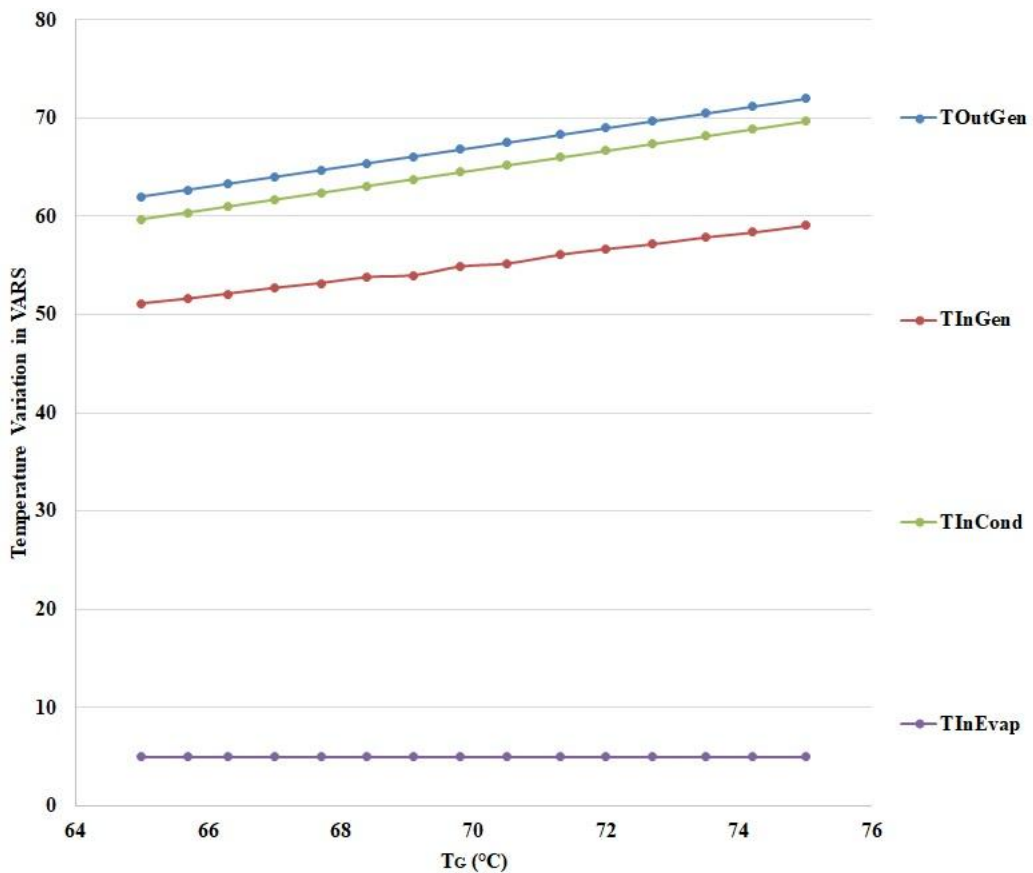


Fig 5.36: Temperature Variation in Half Effect Modification-II with Generator Temperature

Similarly, Fig 5.37 shows the temperature variation in the LHP-I & II. It can be examined that the Absorbent enters the LHPs at approximately 62-72 °C and leave the HEX at approximately 51.6 – 55 °C. Moreover, the Mixture is pumped into the HEX at 35 °C and leaves the LHP at 49.21 - 57.21 °C. It can be observed that the LHPs have better thermal performance when compared to the HEX. The Temperature of the LHP Evaporator & Condenser are near 57-67 °C & 54.3 - 64.3 °C etc.

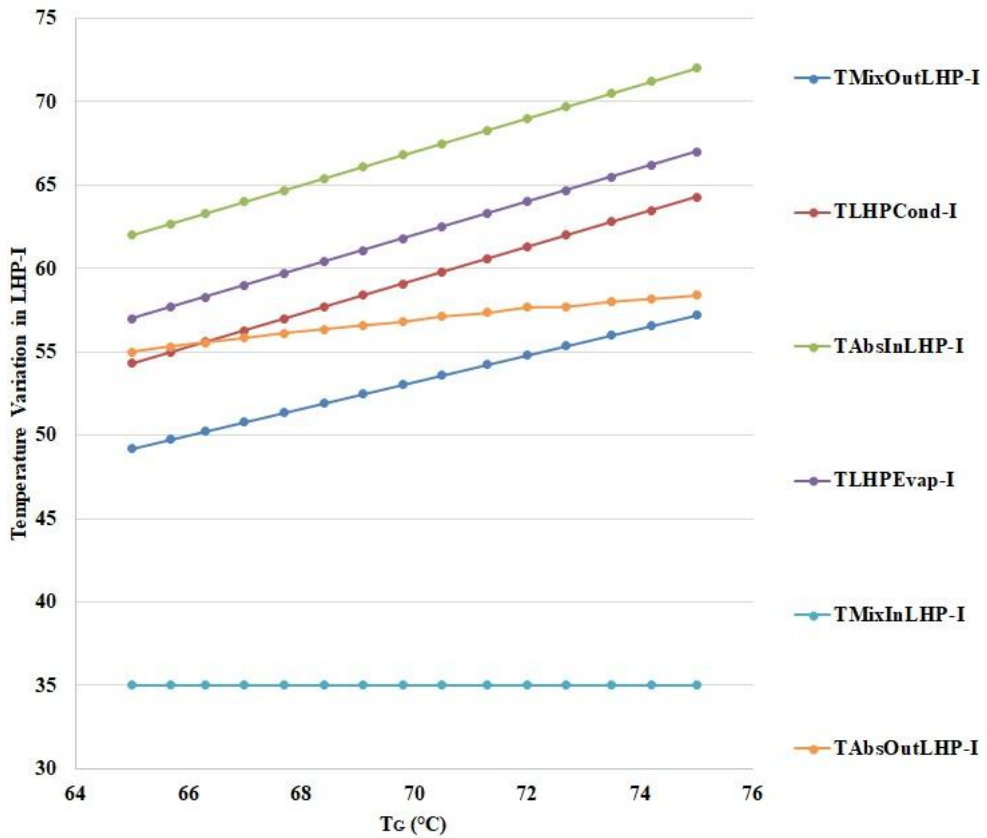


Fig 5.37: Temperature Variation in LHP-I with Generator Temperature

Fig 5.38 examines the temperatures in the LHP-III being used in this system. The heated mixture leaves the LHP Condenser at a temperature of around 51.1 – 59.1 °C more than Modification-I. Other temperatures obtained are similar to Modification-I. Similarly, the heat interaction in the LHP-III is the same in the Modification-II to the Modification-III for Fig 5.40.

On the other hand, Fig 5.39 exhibits the Heat Interaction in the VARS and it can be observed that owing to the LHP-I, II & III combined, the Heat Input Required in the Low & High Generators are 217.3 – 310 kW & 313.5-451 kW respectively. The heat requirement in the Generators is reduced hence the COP can be seen to have further increased.

Performance Improvement of Vapour Absorption System Using Loop Heat Pipes

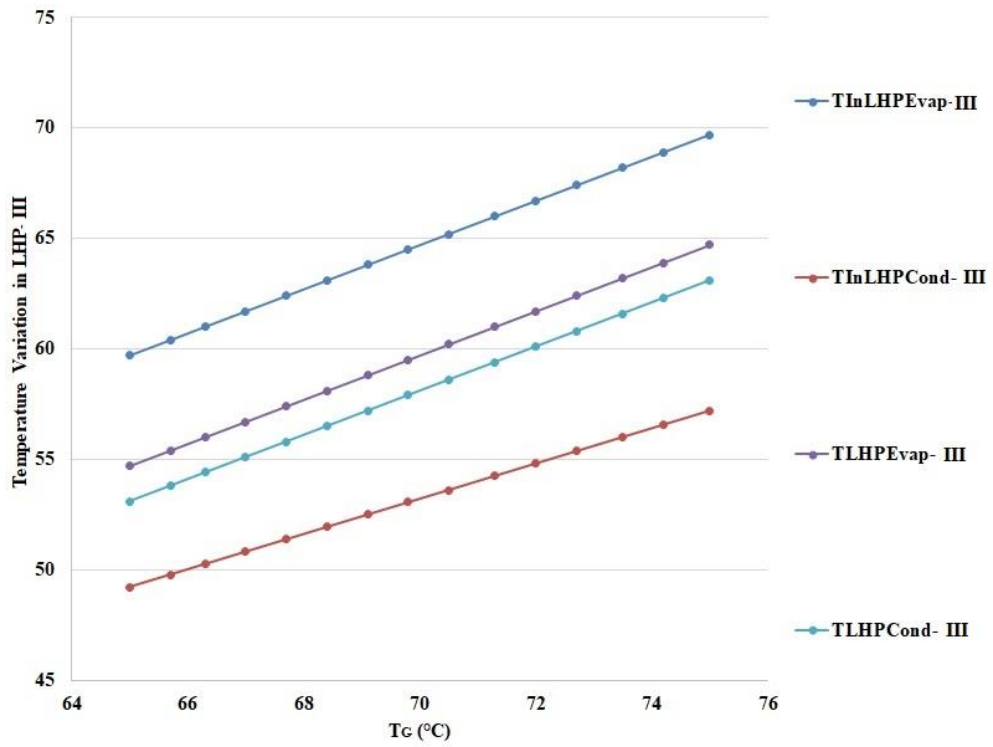


Fig 5.38: Temperature Variation in LHP-III with Generator Temperature

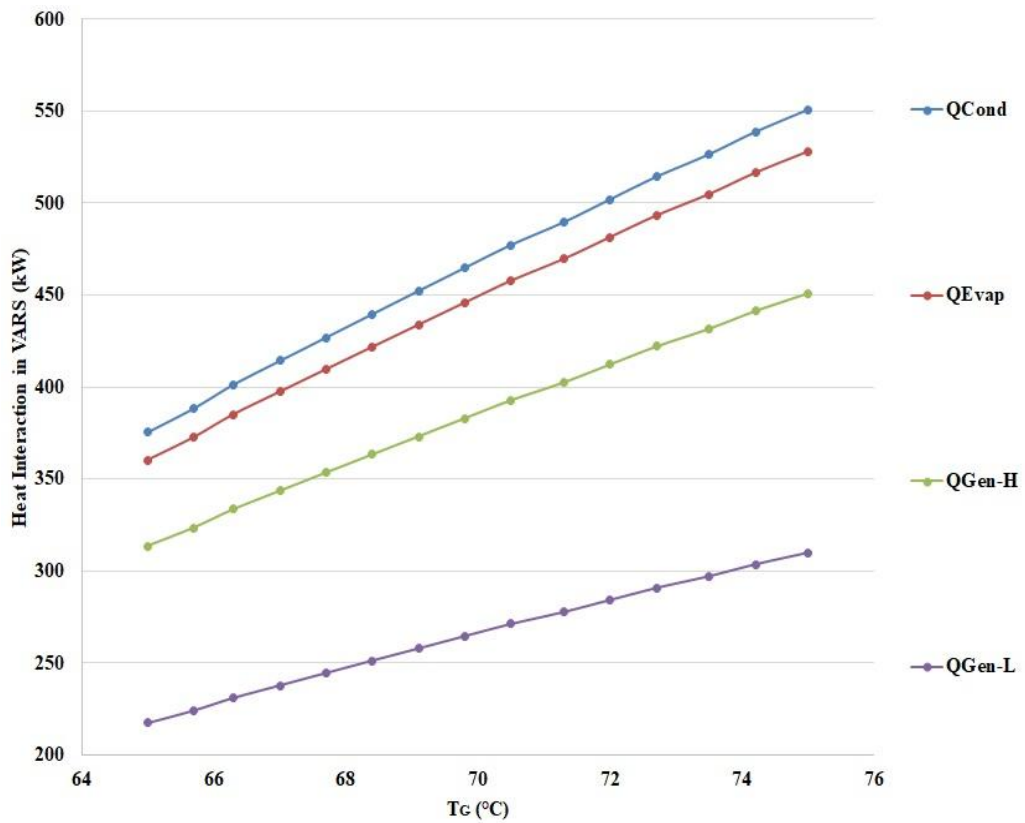


Fig 5.39: Heat Interaction in Half Effect Modification-II with Generator Temperature

Performance Improvement of Vapour Absorption System Using Loop Heat Pipes

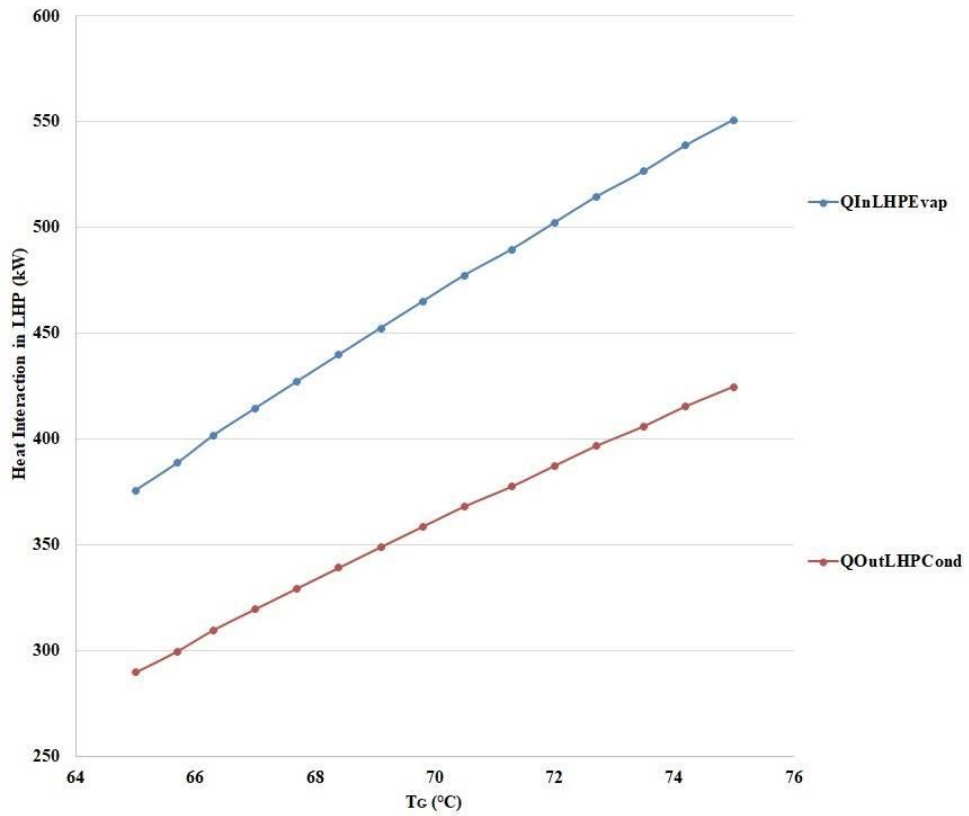


Fig 5.40: Heat Interaction in LHP-II with Generator Temperature

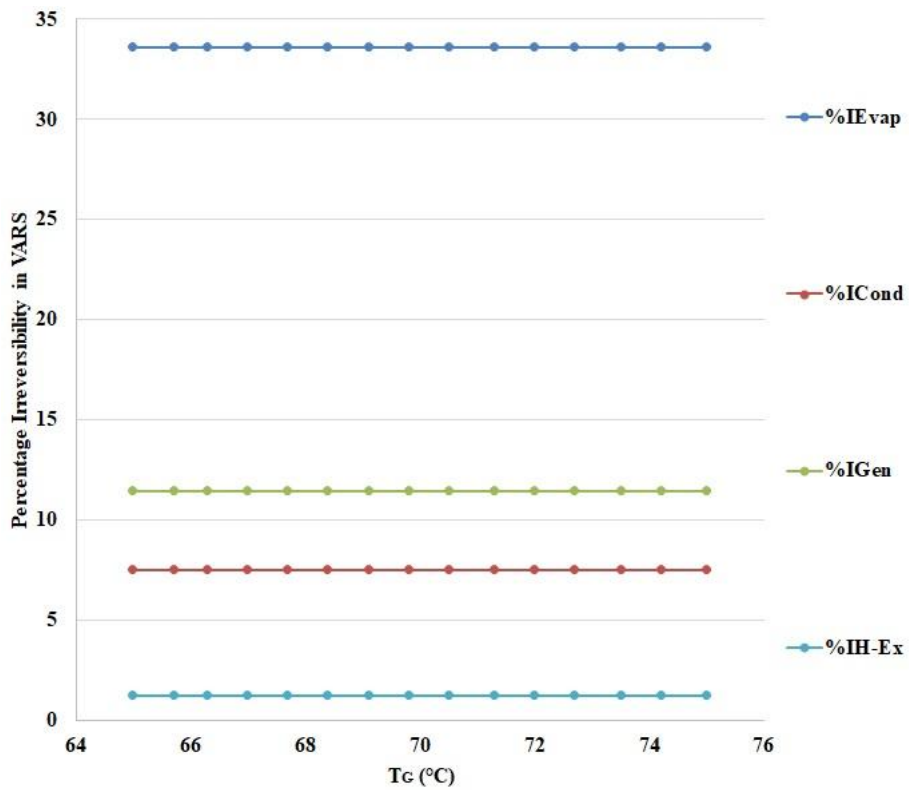


Fig 5.41: Percentage Irreversibility in Half Effect Modification-II Components with Generator Temperature

Performance Improvement of Vapour Absorption System Using Loop Heat Pipes

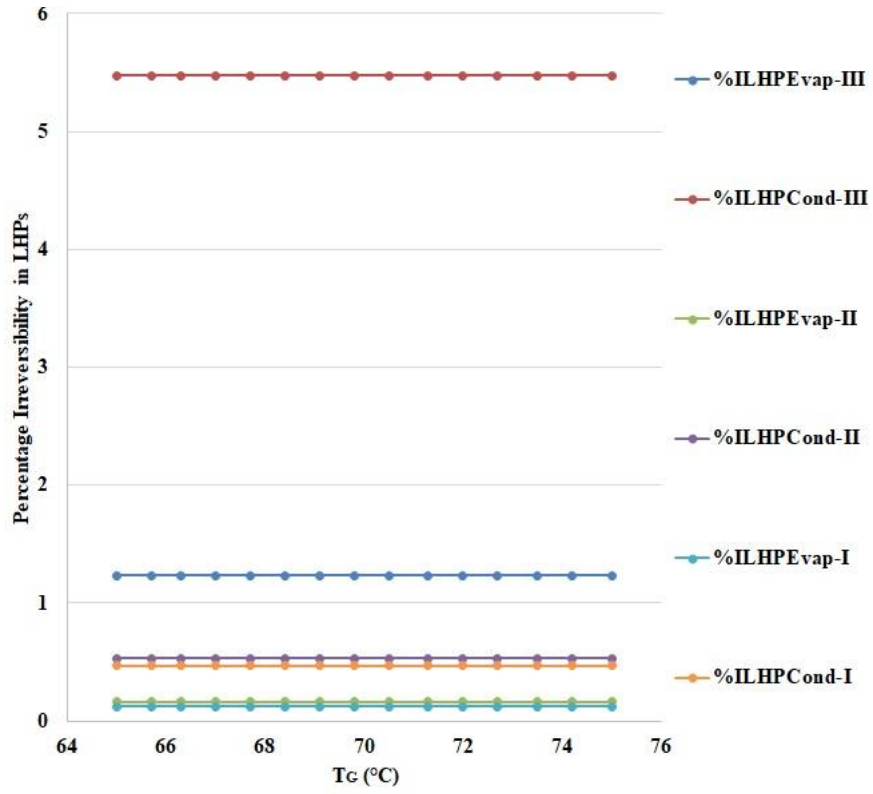


Fig 5.42: Percentage Irreversibility in LHP Components with Generator Temperature

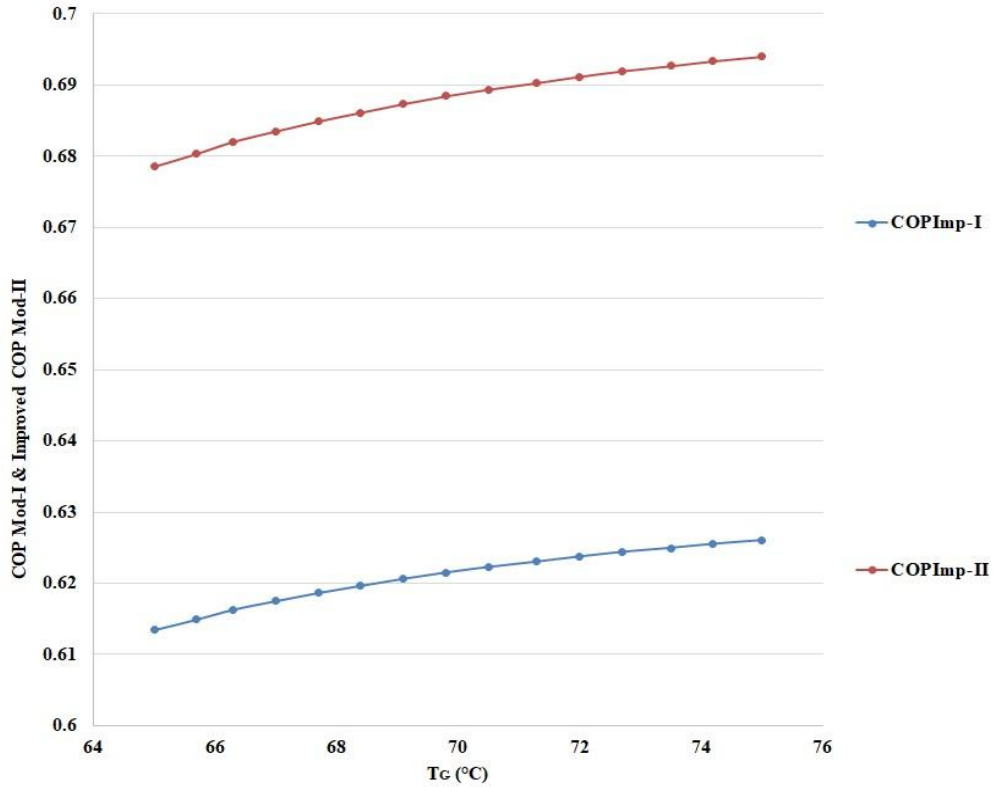


Fig 5.43: COP & Improved COP with Generator Temperature

Fig 5.41 shows that the component-wise Irreversibility of Modification – II is negligibly different from Modification – I. The percentage Irreversibility of LHP – I, II & III has been shown in Fig 5.42. The LHP I, II & III Evaporator and Condenser are 0.12 %, 0.16 % & 1.23 % and 0.467 %, 0.53 % & 5.47 % respectively.

Fig 5.43 shows the Comparison of the COP obtained for Modification-I & Modification-II. It can be observed that the COP of Modification-I is around 0.63, whereas, the COP for Modification-II is around 0.68. The overall Percentage rise in the COP for Modification-II is around 10% as shown in Fig 5.44.

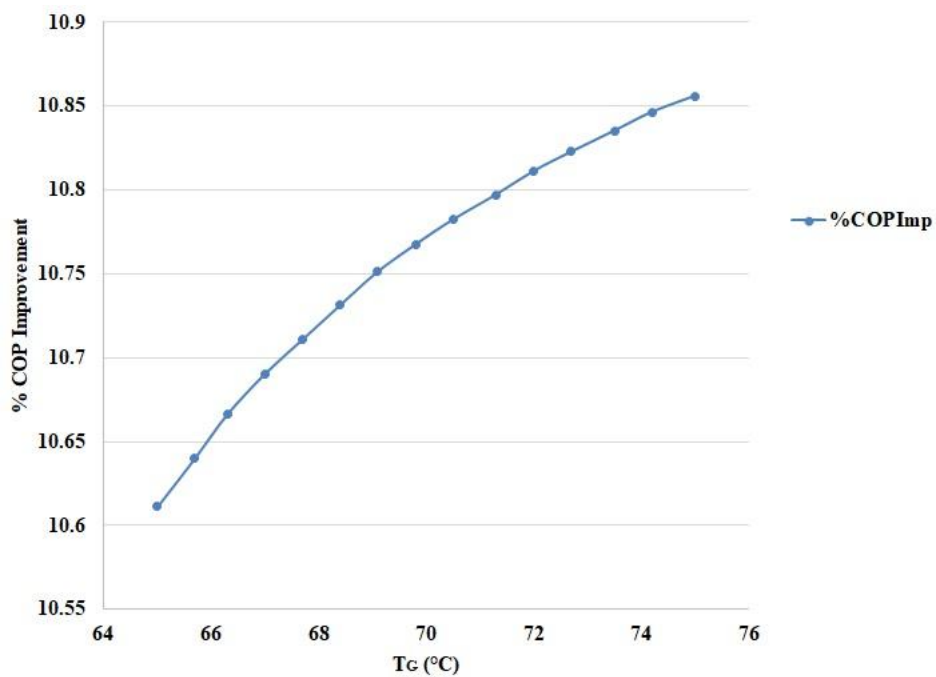


Fig 5.44: Percentage Improvement in COP with Generator Temperature

Table 5.6 comprises the comparison parameters of Text, Published Literature & the results obtained for the proposed work. It can be seen that the parameters are satisfying the performance parameters aptly.

Table 5.6: Comparison with Modified Half Effect VARS

Parameters	Herold et. al. (2016) [176]	Karaali et. al. (2016) [181]	Proposed Work	
			Modification-I	Modification-II
Mass Flow Rate of Mixture from	1	2.13	1	1

Absorbent (kg/s)				
Mass Flow Rate of Refrigerant in Evaporator (kg/s)	0.128	0.1	0.128	0.128
Generator Temperature (°C)	65	50	65	65
Evaporator Temperature (°C)	5	7	5	5
Absorber Temperature	35	32	35	35
Q_{Evap} (kW)	360.2	238	360.2	360.2
Q_{Cond} (kW)	375.52	246	375.52	375.52
Q_{Gen-I} (kW)	339.3714	269.7	236.103	217.327
Q_{Gen-II} (kW)	435.56	253.8	332.292	313.516
COP	0.396	0.45	0.63371	0.67854
η_{II} (%)	24.07	37.37	38.52	41.25

Table 5.7 tabulates the comparison of performance parameters of the Published Literature & Proposed work based on the Component -wise Irreversibility & Percentage Irreversibility at 65 °C.

Table 5.7: Irreversibility in Half Effect Components

Parameters/ Irreversibility	Karaali et. al. (2016) ^[181]		Proposed Work			
	kW	%	Modification-I		Modification-II	
			kW	%	kW	%
I_{Evap}	31.6	40	40.68	33.6	40.68	33.6

I_{Gen}	-	-	13.86	11.45	13.86	11.45
I_{Cond}	0.1247	8	-	-	-	-
I_{HEX}	-	-	1.51	1.25	-	-
I_{Abs}	41.3	52	54.11	44.7	54.11	44.7
LHP-I	-	-	-	-	0.71	0.59
LHP-II	-	-	-	-	0.843	0.696
LHP-III	-	-	8.1	6.7	8.1	6.7
Refrigeration Capacity (RC) (kW)	238		360.2			
Total Irreversibility (kW)	80		118.3		118.3	

5.2.3. Combined Half Effect VARS & GPC

The Half Effect Modification-II has been combined with the GPC as mentioned in Table 5.1 through an LHP nominated as LHP-IV. As mentioned earlier, this LHP is used to extract heat from the Exhaust of GPC to transfer to the VARS. The results have been presented for the Mass of Fuel required to run the GPC. Fig 5.45 it can be seen that the Peak GPC Temperature varies from 927-1227 °C. The Exhaust Temperature that can be observed is 299 – 360 °C, whereas, the generator of Modification-II works in the range of 65-75°C which is a huge gap. This Gap in temperature and availability of Exhaust Heat in abundance suggests that a series of multi-effect systems can be run from the same heat source.

Performance Improvement of Vapour Absorption System Using Loop Heat Pipes

Fig 5.46 presents the temperature variation in the LHP-IV. It can be observed that the Temperature of the LHP Evaporator is directly related to the Exhaust Temperature. Moreover, the LHP-IV Evaporator Temperature is 293 – 355 °C. The Corresponding LHP-IV condenser Temperature is 288 – 348 °C.

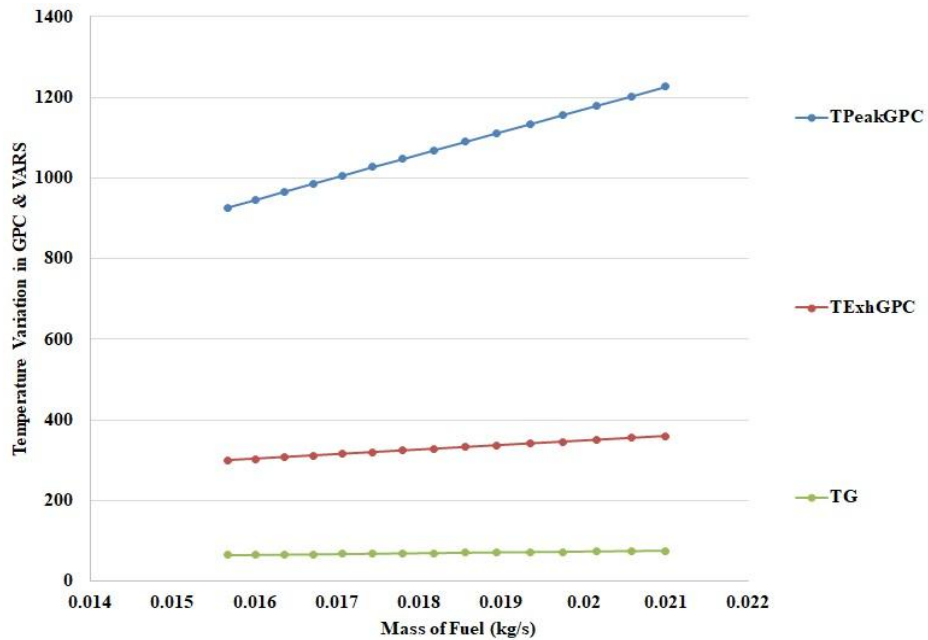


Fig 5.45: Temperatures of GPC and Generator Half Effect Modification-II with Mass of Fuel in GPC

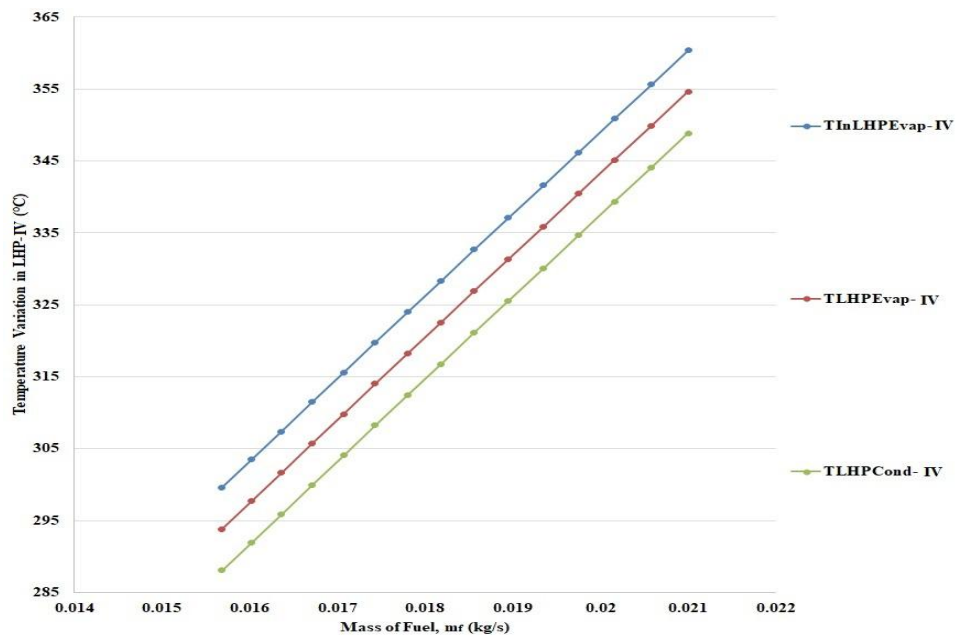


Fig 5.46: Temperatures of LHP-IV with Mass of Fuel in GPC

Fig 5.47 presents the Heat Rejected by the GPC and the Corresponding Exergy & Irreversibility. It can be seen that the Heat Rejected and Associated Exergy and

Performance Improvement of Vapour Absorption System Using Loop Heat Pipes

Irreversibility with the exhaust gas are 219.8 – 283.7 kW, 82.7 – 117.2 kW & 137 – 166.5 kW respectively.

Furthermore, Fig 5.47 presents the Percentage contribution to the Irreversibility by the LHP – IV. The LHP Evaporator & Condenser contribute by 4.23 % & 12.15% respectively.

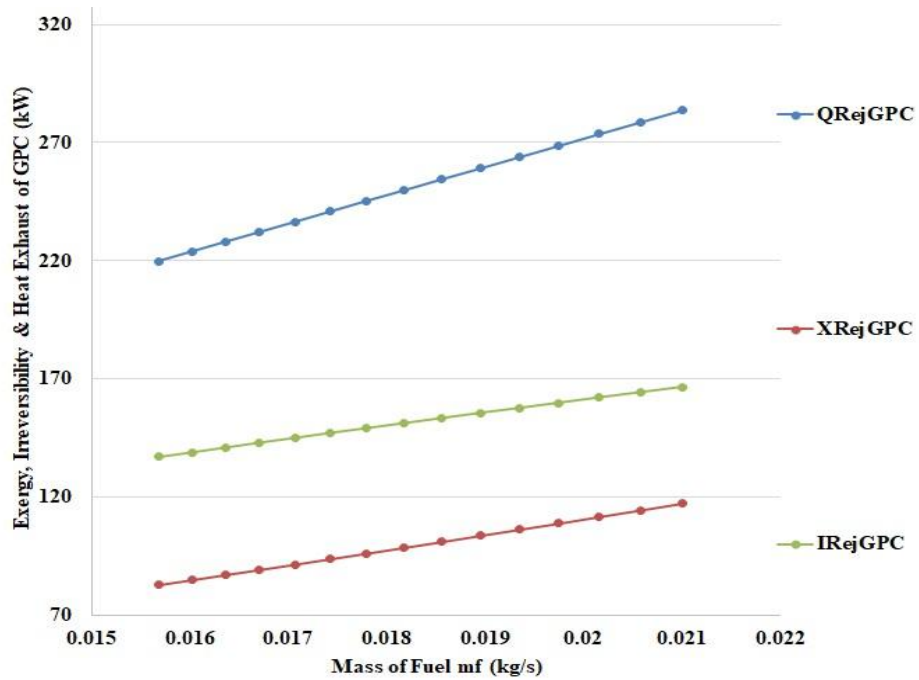


Fig 5.47: Heat, Exergy & Irreversibility at GPC Exhaust with Mass of Fuel in GPC

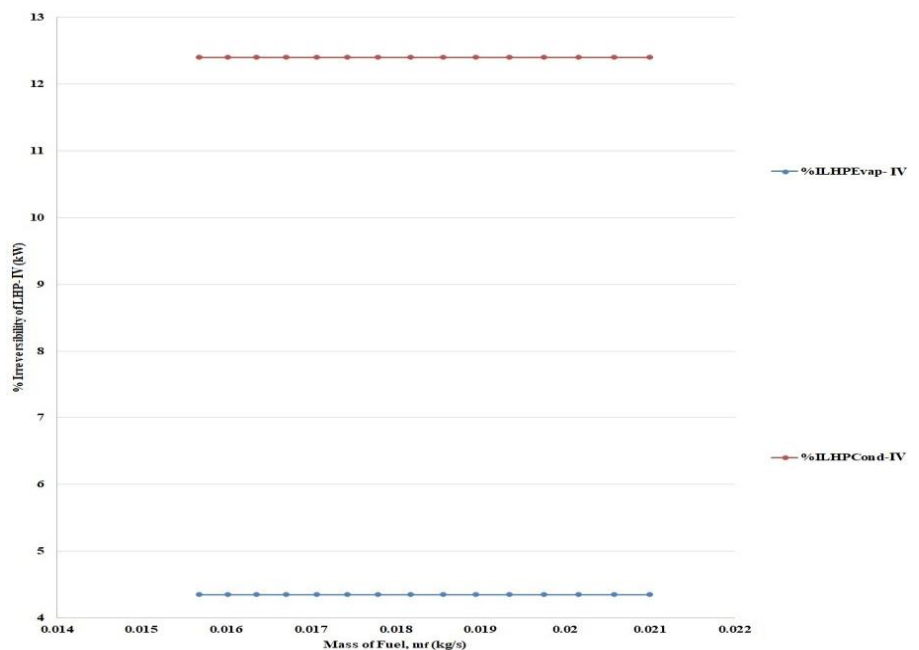


Fig 5.48: Heat, Exergy & Irreversibility at GPC Exhaust with Mass of Fuel in GPC

5.3. Modified Double Effect VARS

The second effect of VARS as discussed earlier is employed to employ a Higher Temperature Heat Source when compared to the Single Effect System. In this system, the generator temperature has been kept variable from 140-150 °C to obtain the corresponding performance parameters in line with the previous performance parameters. Table 5.8 comprises the Input variables of Double effect VARS Modeling has been done for the following components:

Table 5.8: Input Variables for Double Effect VARS Analysis

Sl. No.	Input Parameters	Data
1.	Peak Temperature, T_G	140 °C
2.	Evaporator Temperature, T_{Evap}	5 °C
3.	Working Fluid	LiBr-H ₂ O
4.	Heat Exchanger Effectiveness, ϵ_{H-Ex}	0.5-0.7
5.	Condenser Temperature, T_{C-L}	30 °C
6.	Mass Flow rate after absorber, m_2	1 kg/s

5.3.1. Double Effect VARS Modification-I (Ankit Dwivedi, et. al. 2018) ^[185]

This section presents the comprehensive analysis of the Modification-I to the Double Effect VARS. Fig 5.59 presents the overall temperature variation in Modification-I at various important points. The temperature of the mixture entering the High-Temperature Generator is approximated as 107 – 114 °C. The vapour of refrigerant leaving the High Generator has a temperature of 131-138 °C, whereas, the vapour refrigerant leaving the Low Generator has a temperature of 56 - 58 °C. The evaporator temperature varies from 5.71 – to 5 °C. The temperature of absorbent leaving the High Generator & Entering the Low Generator is 137-146 °C & 66.3 - 69.5 °C. The Mixture temperature entering the high generator of the unmodified system was 95– 102 °C.

Performance Improvement of Vapour Absorption System Using Loop Heat Pipes

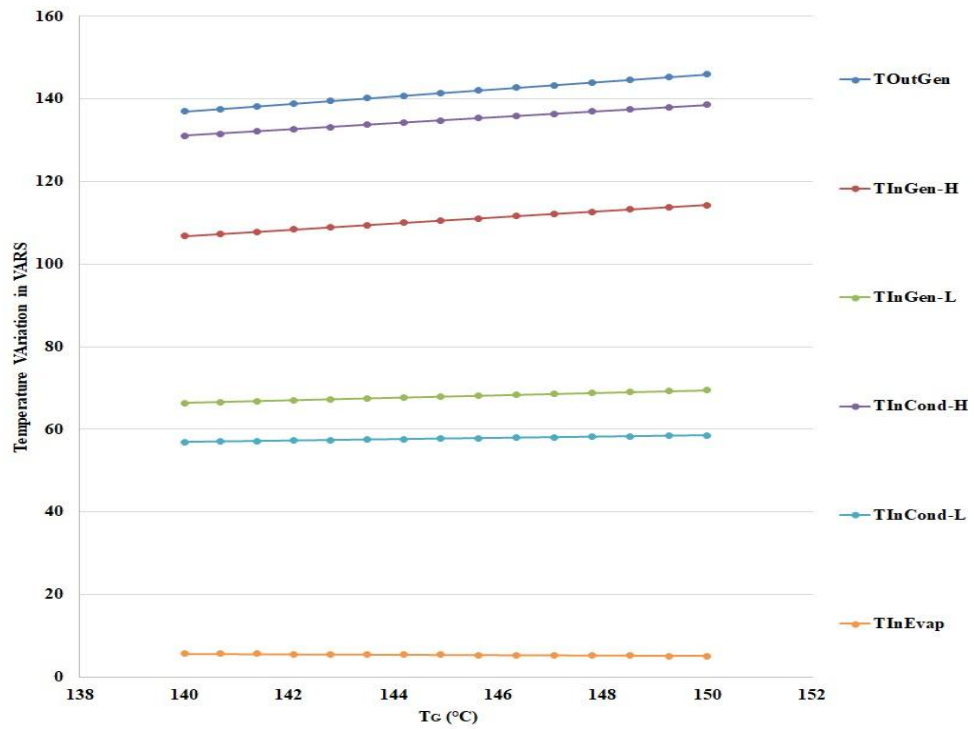


Fig 5.49: Temperature Variation in Double Effect Modification-I with Generator Temperature

Similarly, Fig 5.50 presents the temperature variation in the HEx-I, where, the mixture enters the HEx-I at 30 °C and leaves at 48-49 °C. Similarly, the Absorbent leaving the Low Generator enters HEx-I at 73-78 °C and leaves at 52 – 54 °C.

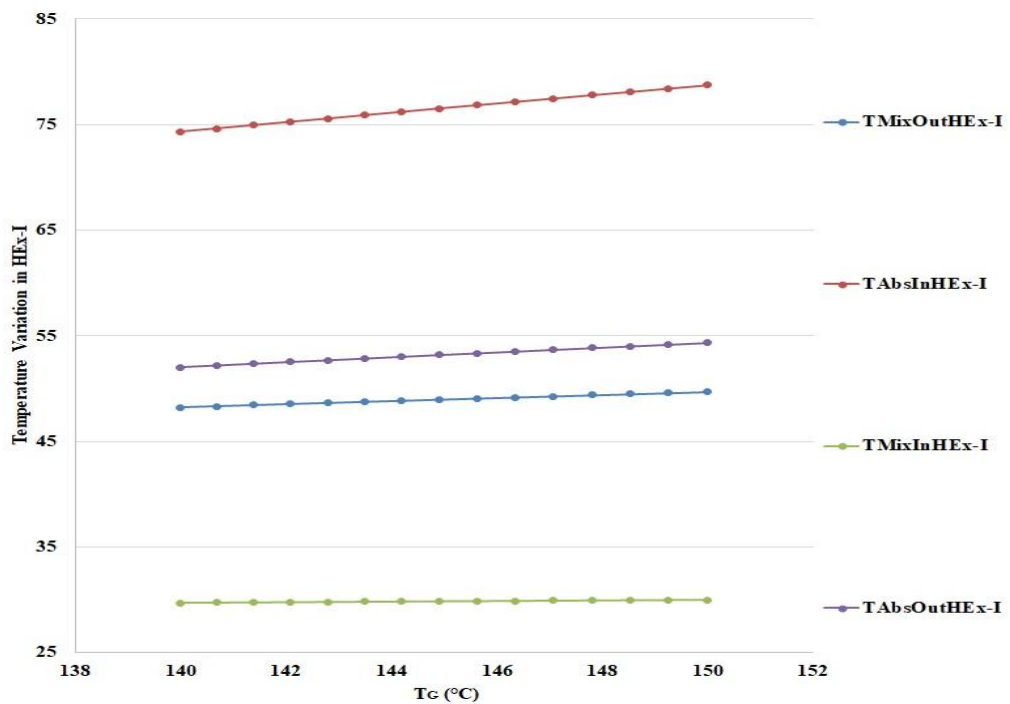


Fig 5.50: Temperature Variation in Double Effect Modification-I Heat Exchanger-I with Generator Temperature

Fig 5.51 presents a similar analysis for HEx-II, in which, the mixture leaving the HEx enters at 48 – 49 °C and leaves at 84 - 88 °C, and enters the LHP for further heat exchange. The absorbent leaving the High Generator enters HEx-II at 136-145 °C and leaves at 84 – 88 °C. Furthermore, Fig 5.52 explains the temperature variations experienced in the LHP. It can be observed that the Refrigerant Vapour enters the LHP Evaporator at 131 – 138 °C, consequently, the LHP evaporator temperature has been observed as 126-133 °C, keeping a difference of 5 °C for heat exchange during evaporation of LHP Fluid. The temperature of the LHP Condenser obtained is 122 – 130 °C. The Mixture enters the LHP Condenser at 84 – 88 °C. It can be mentioned that the temperature for heat transfer and temperature difference of mixture & LHP condenser for heat exchange is more suitable in double effect in VARS than single & half effect systems.

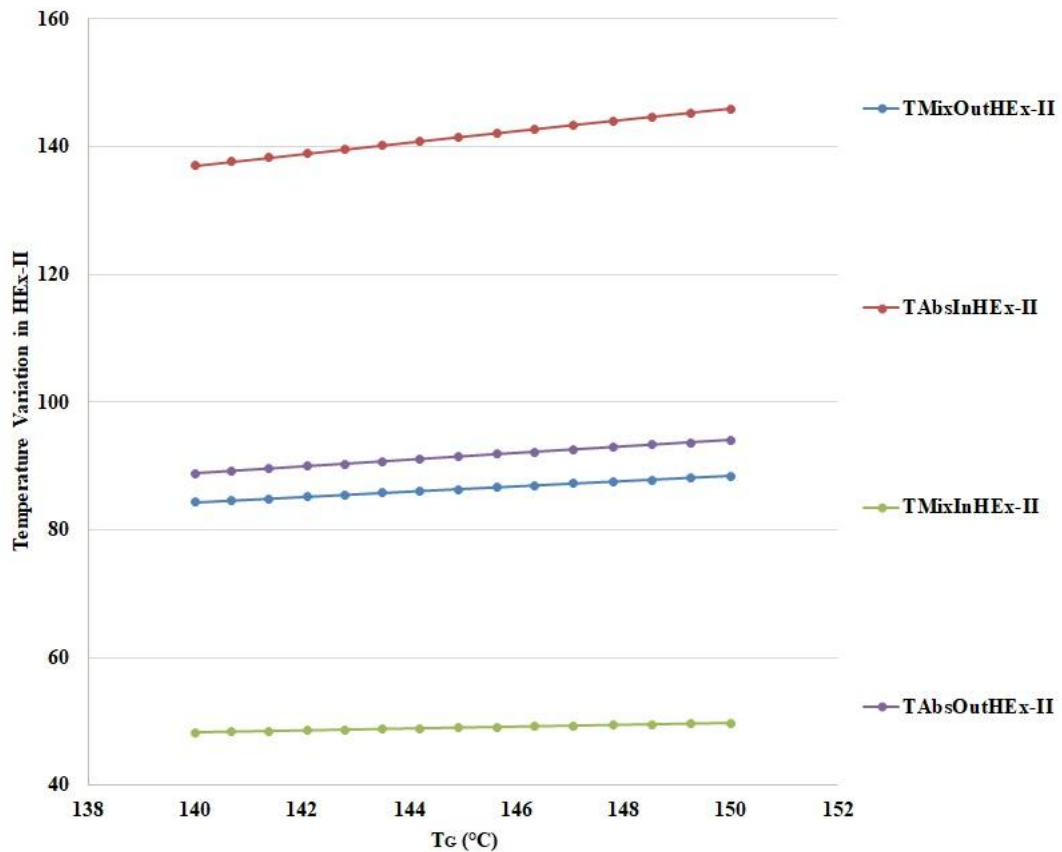


Fig 5.51: Temperature Variation in Double Effect Modification-I Heat Exchanger-I with Generator Temperature

Performance Improvement of Vapour Absorption System Using Loop Heat Pipes

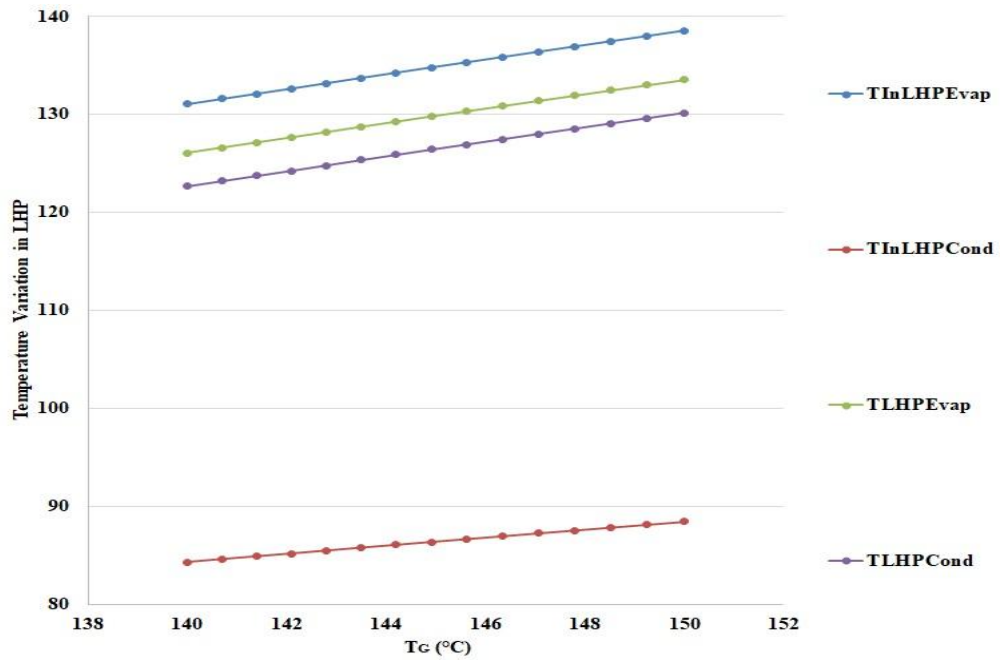


Fig 5.52: Temperature Variation in LHP with Generator Temperature

Fig 5.53 shows the heat interactions in the VARS components. The Heat Interaction in the Evaporator is 336 – 370 kW, whereas, in the High Generator it is 161 – 179 kW, which has been reduced owing to the heat recovery by the LHP employed. The heat interaction in the Low Generator is 163 – 180 kW which can be easily supplied from the Heat Extracted in the LHP. The Heat Input to the Original System High & Low Generator was 268 – 297 kW & 163 – 181 kW respectively ^[176].

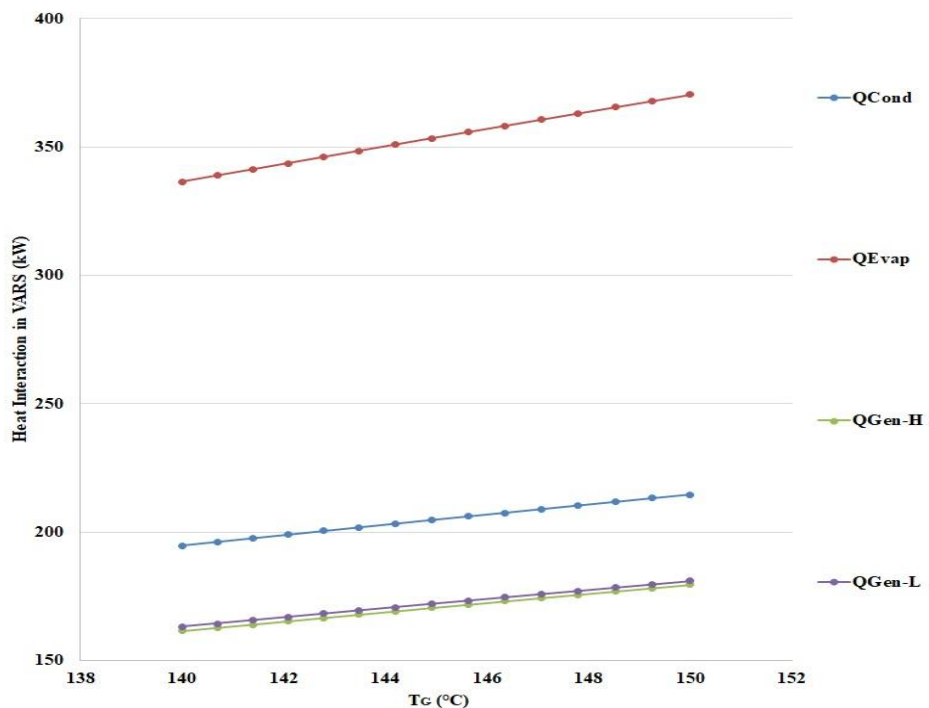


Fig 5.53: Heat Interaction in Double Effect Modification-I with Generator Temperature

Fig 5.54 presents the heat interaction within the LHP, HEX-I & II. It can be seen that the input heat to the LHP Evaporator is the heat of the refrigerant vapour leaving the generator i.e., 194 – 214 kW, and the heat available at the LHP condenser is 155 – 171 kW. Heat Interaction in the HEX -I & II are 31 – 49 kW & 77 – 82 kW respectively.

Fig 5.55 shows the Percentage Irreversibility Contribution by the VARS Components. The Evaporator contributes to around 12.4% of Irreversibility, whereas, the High & Low Generators Contribute to 17.1 & 3.8 %. The Condenser has the lowest of 5.8 % Irreversibility contribution. The HEX-I & II have irreversibility contributions of around 8.5 % & 15.7 % respectively. It can be stated although the Irreversibility of the components owing to the increase of the temperature is decreasing slightly, for simplicity of the presentation the percentage contribution has been taken constantly over the range of Generator Temperature.

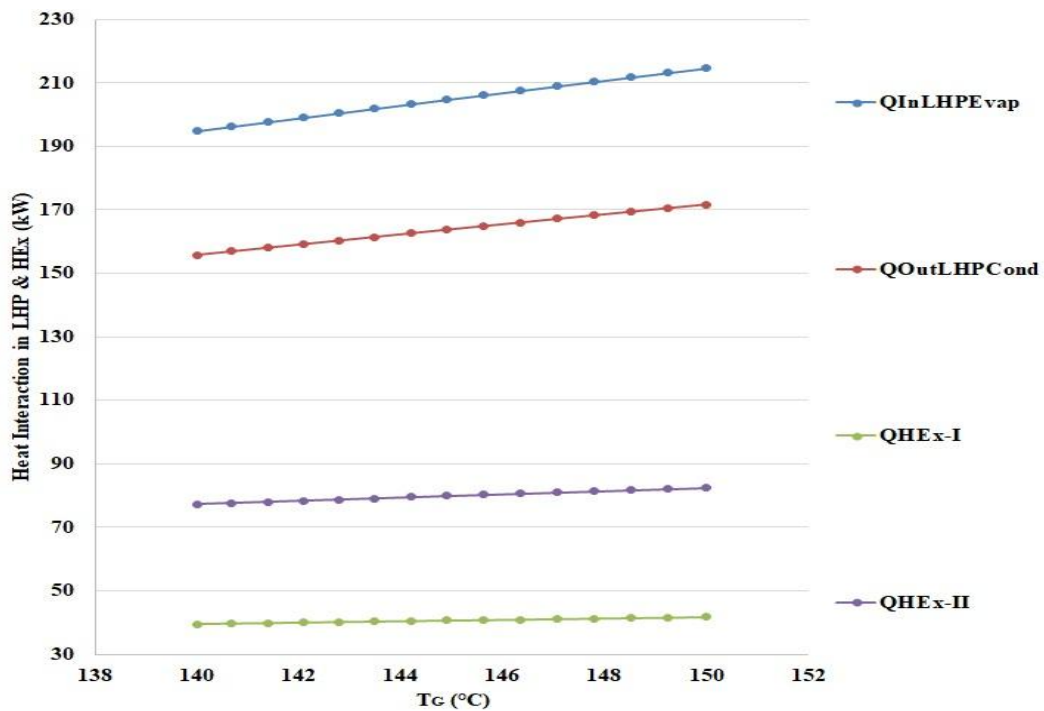


Fig 5.54: Heat Interaction in LHP & HEX with Generator Temperature

Performance Improvement of Vapour Absorption System Using Loop Heat Pipes

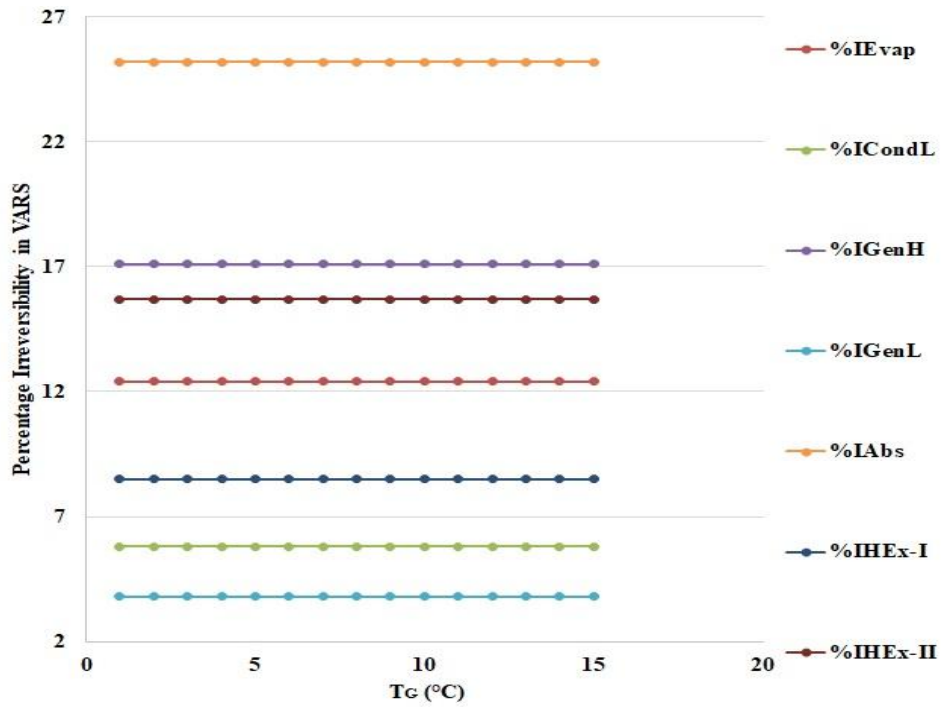


Fig 5.55: Percentage Irreversibility in Double Effect Modification-I Components with Generator Temperature

Similarly, the LHP Evaporator & Condenser contribute 1.34 % & 2.89 % to the overall Irreversibility as shown in Fig 5.56.

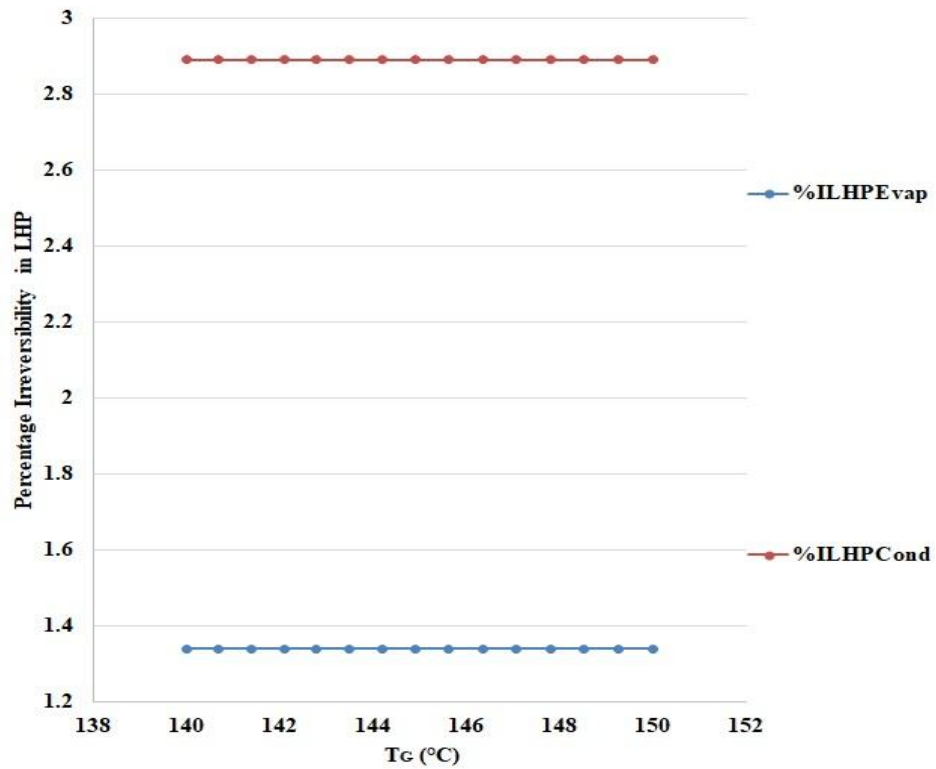


Fig 5.56: Percentage Irreversibility in LHP Components with Generator Temperature

Fig 5.57 presents the COP improvement to the original COP obtained from the second effect system. It can be seen the Improved COP is 2.08 – 2.06, whereas, the original COP of the system was 1.25 - 1.24 ^[176]. It can be seen the COP shows a decreasing trend which presents the fact the range of Double effect Generator Temperature is around 130 – 140 °C, beyond which increasing temperature may not present favourable results. It can further be presented in Fig 5.58 that the percentage improvement in COP is around 65 %.

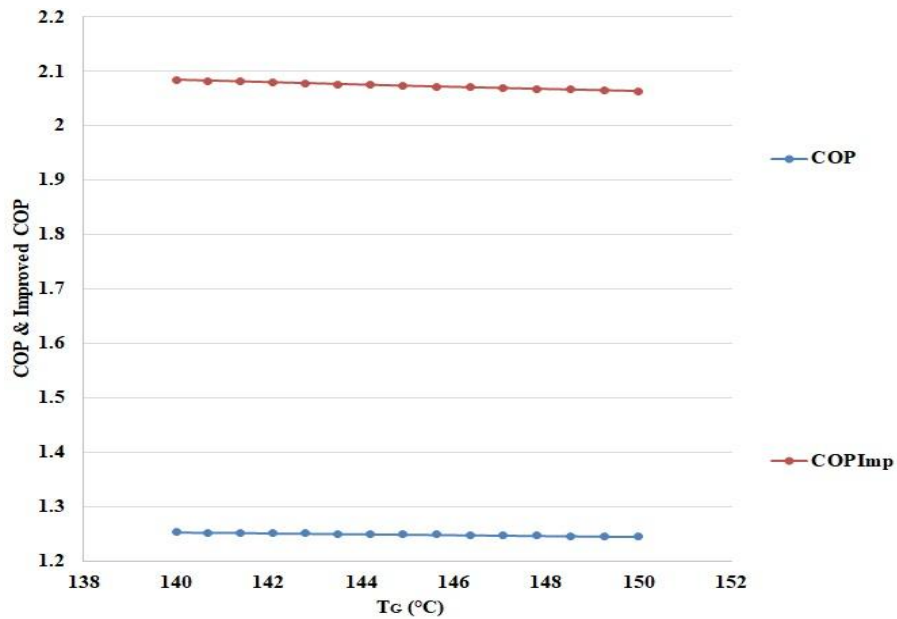


Fig 5.57: COP & Improved COP with Generator Temperature

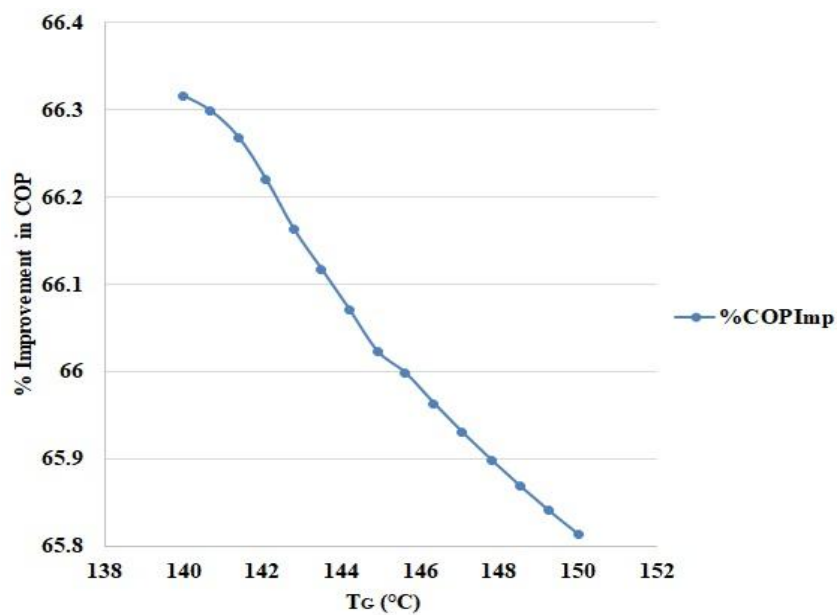


Fig 5.58: Percentage Improvement in COP with Generator Temperature

Fig 5.59 presents the mass flow rate in various components in the high cycle of the VARS. The mass flow rate of refrigerant vapour in the LHP Evaporator is 0.069 – 0.076 kg/s, whereas, the mass flow rate of the mixture in the LHP Condenser is 1 kg/s. The mass flow rate of absorbent in leaving a high generator is 0.931 – 0.923 kg/s and 0.859 – 0.845 kg/s in the low generator. The mass of refrigerant vapour leaving the low generator is 0.072 – 0.078 kg/s. Hence, the total mass flow of refrigerant in the evaporator is 0.141- 0.155 kg/s for Refrigeration which can be seen in Fig 5.60.

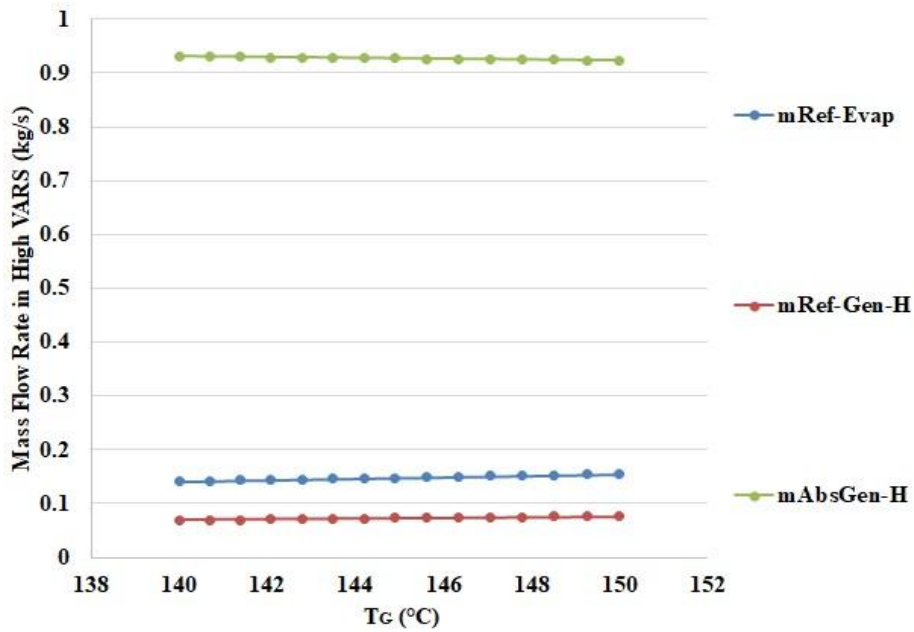


Fig 5.59: Mass Flow Rates in Double Effect Modification-I High with Generator Temperature

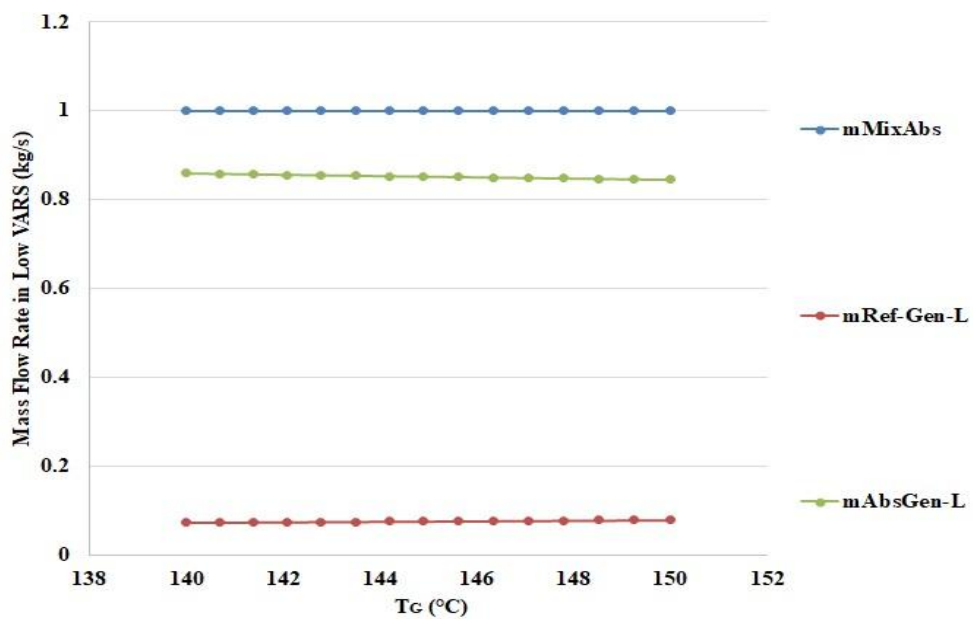


Fig 5.60: Mass Flow Rates in Double Effect Modification-I Low with Generator Temperature

5.3.2. Double Effect VARS Modification-II

The 2 HEx have been replaced by the LHP-I & II to obtain Modification-II and the designation of LHP of Modification-I has been kept as LHP-III. The performance analysis of Modification-II has been presented similar to Modification-I in this section. Fig 5.61 presents the Temperature Experienced in the VARS. In comparison with the Modification-I, the Mixture temperature entering the high generator and absorbent temperature entering the low generator are 118 – 125 °C & 56 – 58 °C respectively.

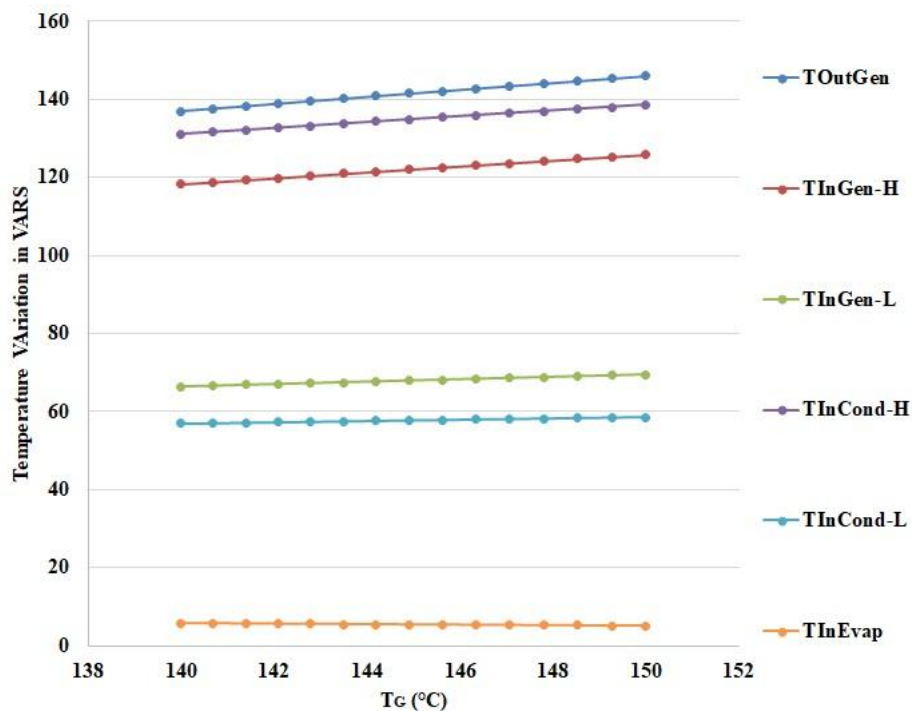


Fig 5.61: Temperature Variation in Double Effect Modification-II with Generator Temperature

Similarly, Fig 5.62 presents temperature variation in the LHP-I, where the absorbent is entering & leaving the LHP Evaporator at 74 – 78 °C & 47 – 49 °C respectively. Consequently, the LHP-I Evaporator & Condenser temperature attained 69 – 73 °C & 65 – 70 °C respectively. The mixture temperature leaving the LHP Condenser is 56-60°C. Similarly, from Fig 5.63 for the LHP-I the where the absorbent enters & leaves the LHP Evaporator at 137 – 146 °C & 83 – 88 °C respectively making the LHP-I Evaporator & Condenser temperature attained 132 – 142 °C & 127 – 136 °C respectively. The mixture temperature leaving the LHP-II is 108 - 117 °C. Furthermore, it can be seen from Fig 5.64, that the temperature of the mixture entering the High Generator is 118 – 125 °C.

Performance Improvement of Vapour Absorption System Using Loop Heat Pipes

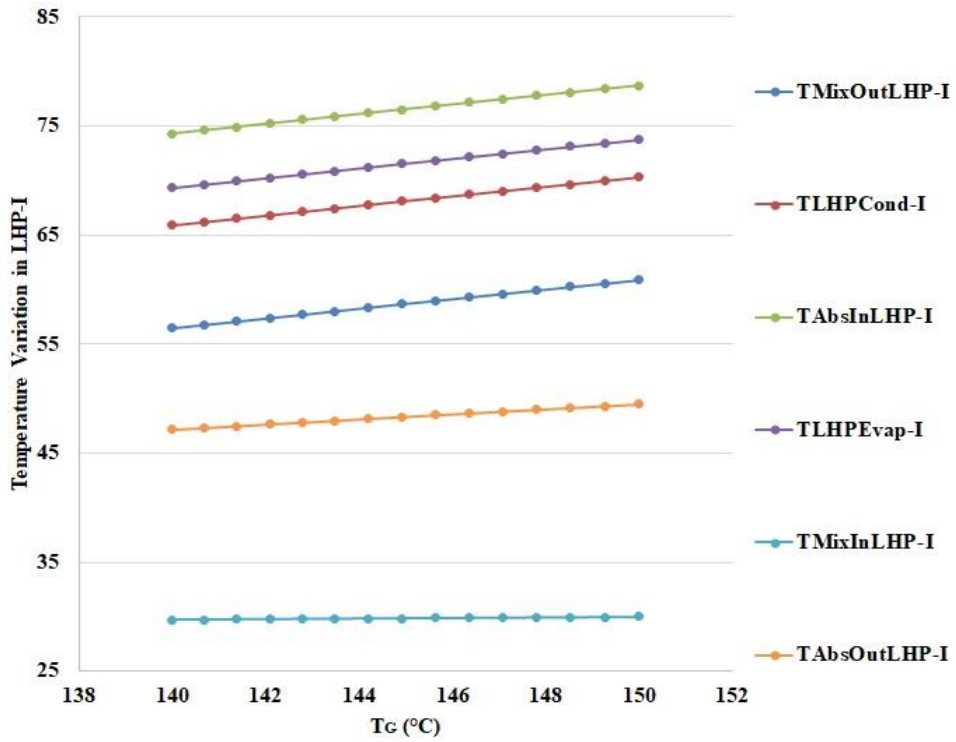


Fig 5.62: Temperature Variation in LHP-I with Generator Temperature

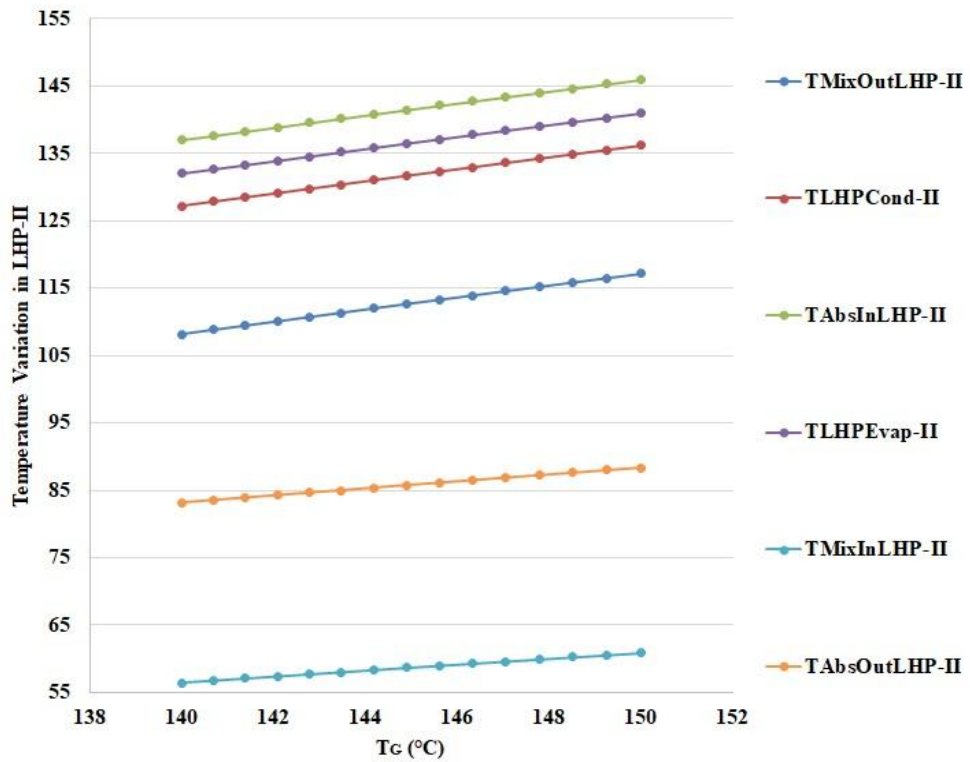


Fig 5.63: Temperature Variation in LHP-II with Generator Temperature

Fig 5.65 presents the heat interaction within the VARS, it can be seen that heat input requirements in High & Low Generators have been reduced by the application of the

LHPs. The new heat requirements in Low & High Generators are 163 – 180 kW & 142 – 158 kW.

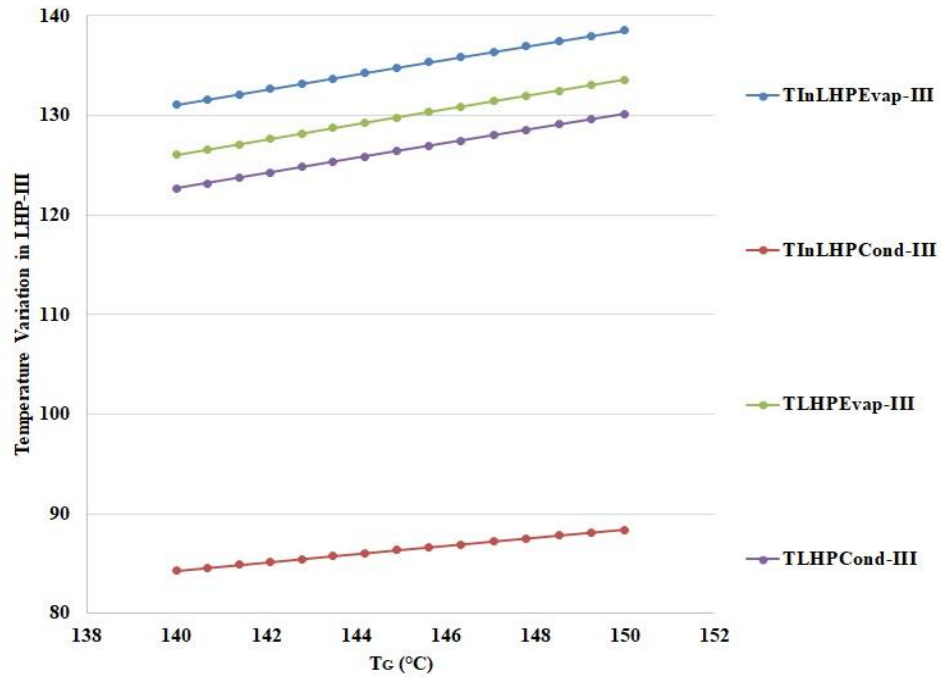


Fig 5.64: Temperature Variation in LHP-III with Generator Temperature

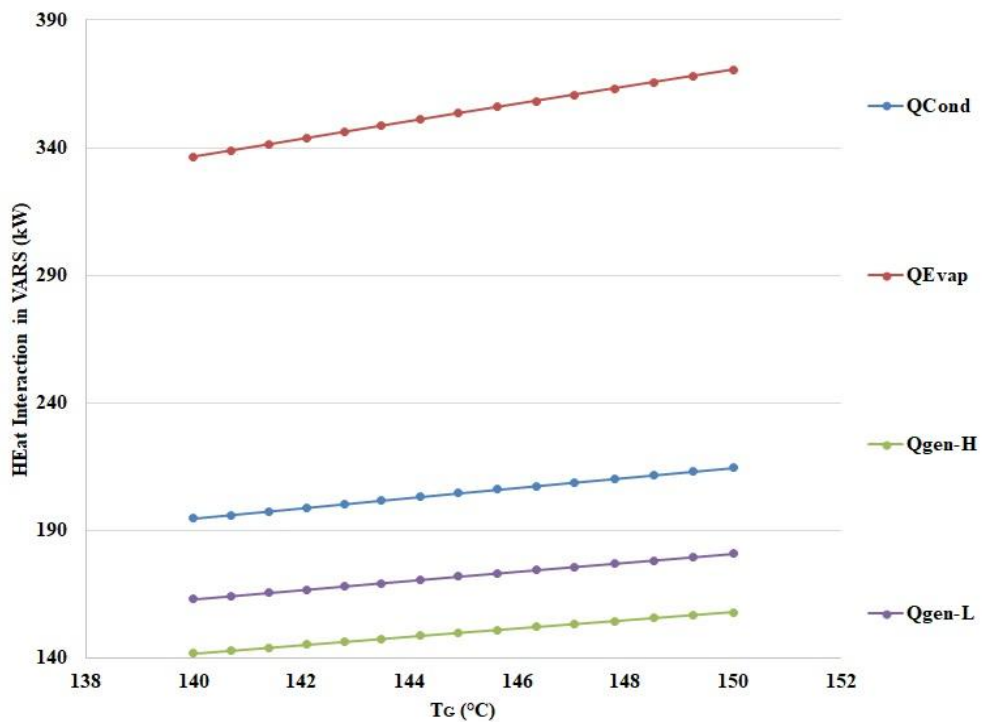


Fig 5.65: Heat Interaction in Double Effect Modification-II with Generator Temperature

Overall Percentage contribution to the Irreversibility in the VARS components is the same as it has been observed in Modification-I as shown in Fig 5.66.

Performance Improvement of Vapour Absorption System Using Loop Heat Pipes

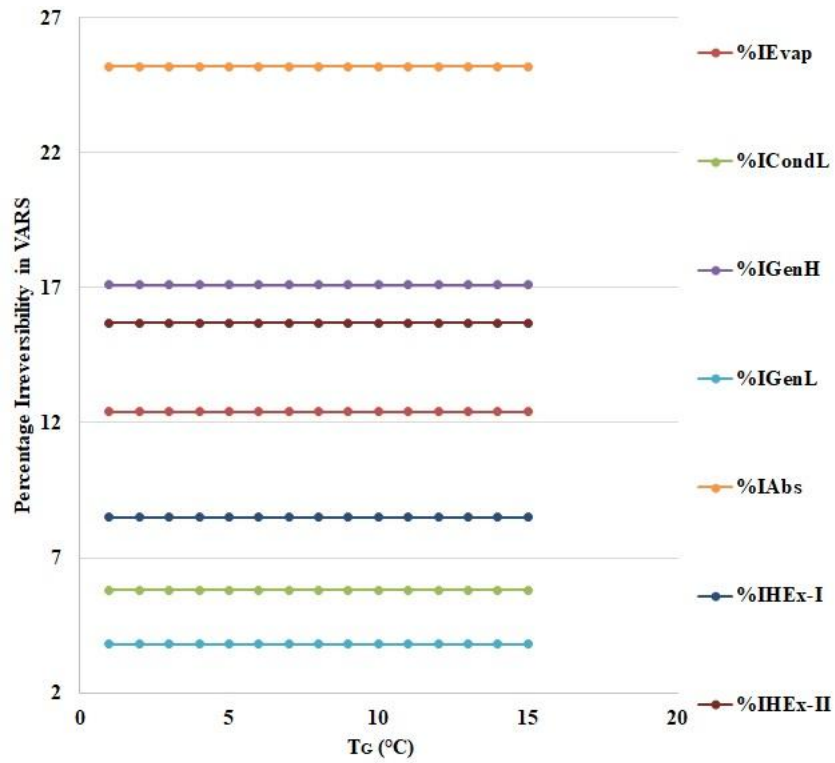


Fig 5.66: Percentage Irreversibility in Double Effect Modification-II Components with Generator Temperature

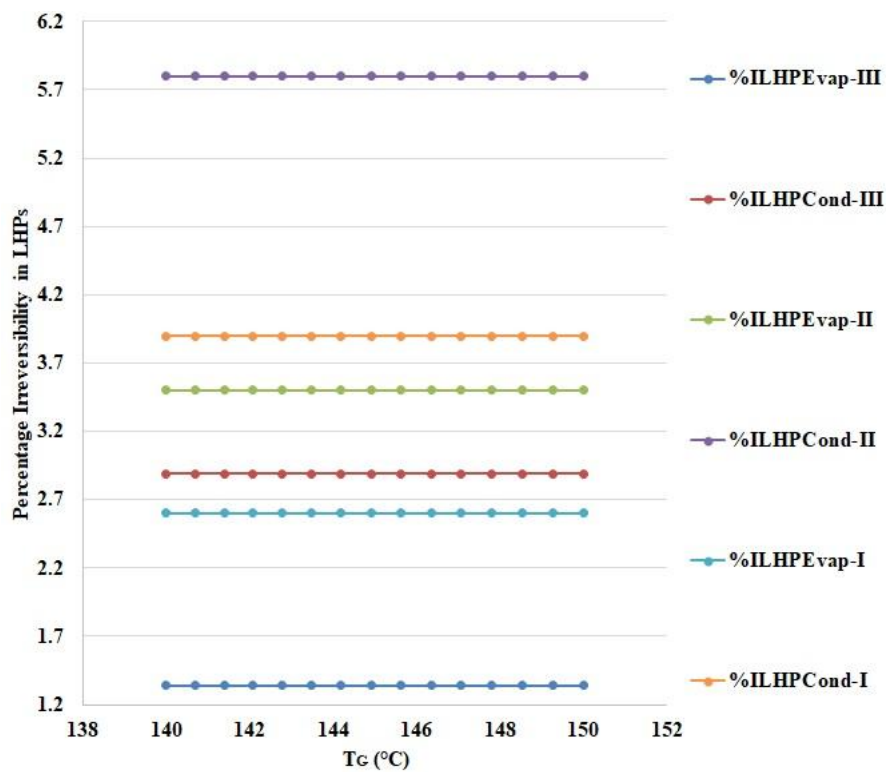


Fig 5.67: Percentage Irreversibility in LHP Components with Generator Temperature

As shown in Fig 5.67 the Percentage contribution of the LHP-III to the Irreversibility is the same as that of LHP in Modification-I. The contributions of LHP-I Evaporator

Performance Improvement of Vapour Absorption System Using Loop Heat Pipes

& Condenser are 2.6 % & 3.9 % respectively, whereas, for LHP-II Evaporator & Condenser are 3.5 % & 5.8 % respectively.

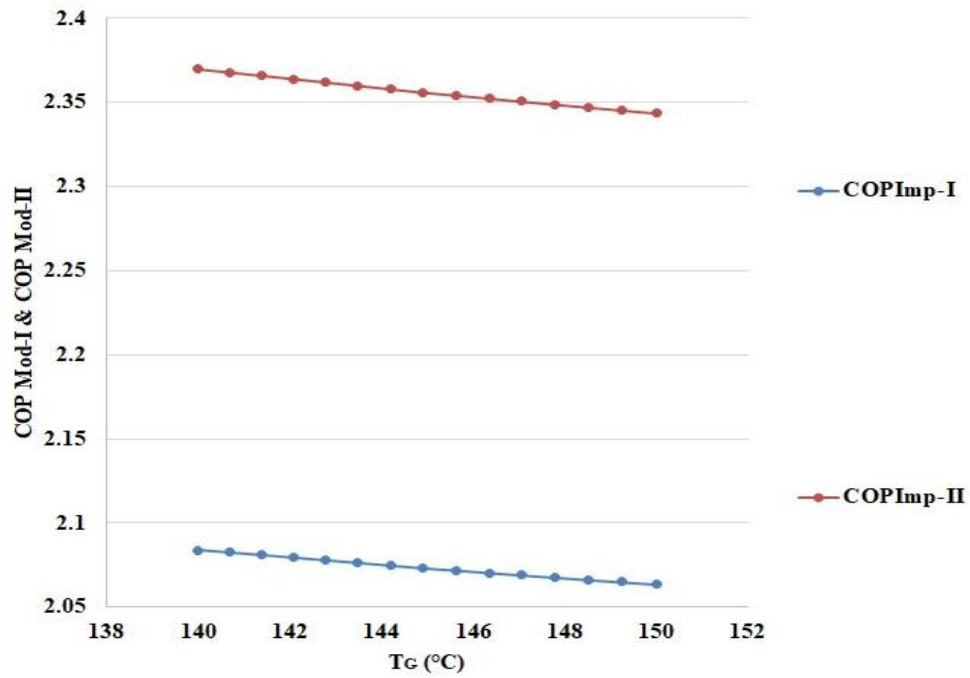


Fig 5.68: COP & Improved COP with Generator Temperature

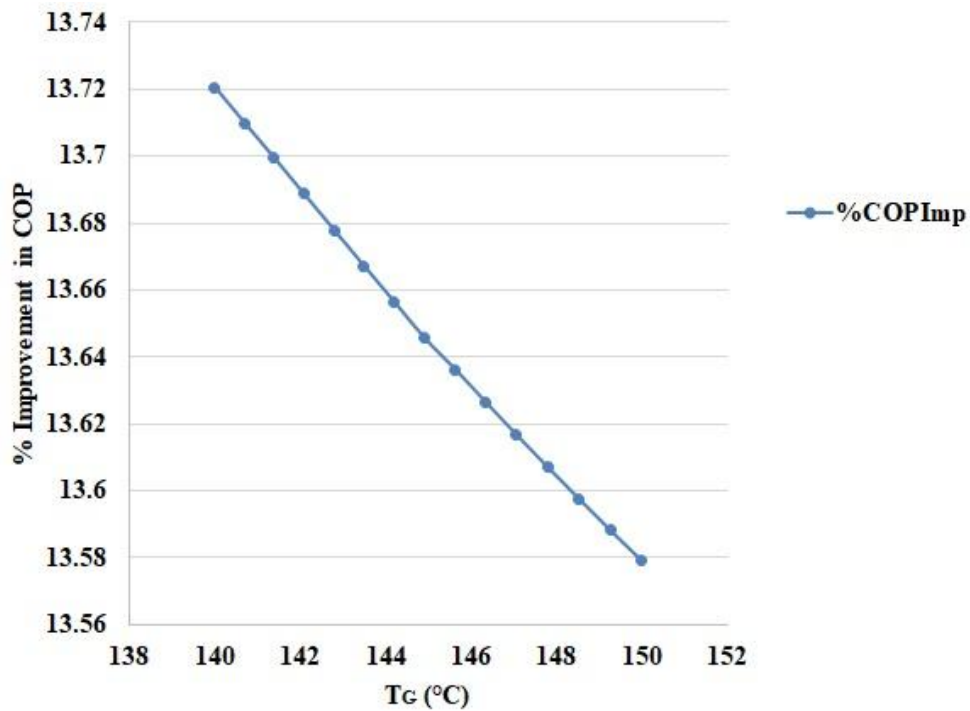


Fig 5.69: Percentage Improvement in COP with Generator Temperature

The COP of Modification-II has been observed to be 2.36 – 2.34 against the 2.08 - 2.07 COP of Modification-I as presented in Fig 5.68. It has also been presented that

the percentage improvement of Modification-I is around 13% for Modification-II in Fig 5.69.

The comparison of performance parameters of the Text, Published Literature & Proposed work has been tabulated in Table 5.9. It can be seen that for the input parameters the performance parameters of the proposed work are best for all the literature available.

Table 5.9: Comparison of Modified Double Effect VARS

Parameters	Herold et. al. (2016) ^[176]	Gomri et. al. (2016) ^[81]	Proposed Work	
			Modification-I	Modification-II
Mass Flow Rate of Mixture from Absorbent (kg/s)	1	1.73	1	1
Mass Flow Rate of Refrigerant in Evaporator (kg/s)	0.155	0.12702	0.155	0.155
Generator Temperature (°C)	140	130	140	140
Evaporator Temperature (°C)	5	5	5	5
Absorber Temperature	35	42.4	35	35
Q_{Evap} (kW)	370.4	300.000	370.4	370.4
Q_{Cond} (kW)	194.759	167.205	194.759	194.759
Q_{Gen-H} (kW)	297.5	252.407	179.5	179.5
COP	1.24	1.19	2.01	2.3
η_{II} (%)	32.37	32.85	53.84	61.23

Table 5.10 presents the comparison of Published Research work with Proposed works based on Irreversibility at 130 °C.

Table 5.10: Irreversibility in Double Effect Components

Parameters/ Irreversibility	Gomri et. al. (2017) ^[178]		Proposed Work			
	kW	%	Modification-I		Modification-II	
			kW	%	kW	%
I_{Evap}	6.3	13.6	5.98	12.4	5.98	12.4
I_{Gen-H}	8.718	18.8	8.24	17.1	8.24	17.1
I_{Gen-L}	1.97	4.26	1.833014	3.8	1.833014	3.8
I_{Cond-L}	2.98	6.42	2.8	5.8	2.8	5.8
I_{HEX-I}	4.11	8.87	4.1	8.5	-	-
I_{HEX-II}	7.56	16.31	7.57	15.7	-	-
I_{Abs}	0.2197	28.67	12.15	25.2	0.51	27.9
LHP-I	-	-	-	-	4.48606147	9.3
LHP-II	-	-	-	-	3.135419	6.5
LHP-III	-	-	2.04	4.23	2.04	4.23
Refrigeration Capacity (RC) (kW)	300		336.395			
Total Irreversibility (kW)	46.4		48.23722		46.2	

5.3.3. Combined Double Effect VARS & GPC

The GPC has been combined with the Double Effect VARS Modification-II through the LHP-IV. The performance parameters have been presented in this section. Fig 5.70 shows the comparison of the Peak GPC temperature, GPC exhaust Temperature, and the proposed Double Effect Modification-II System. The GPC Peak & Exhaust are at 927 -1227 °C & 299 – 360 °C temperature, whereas, the Modification-II Generator works at 140 -150 °C.

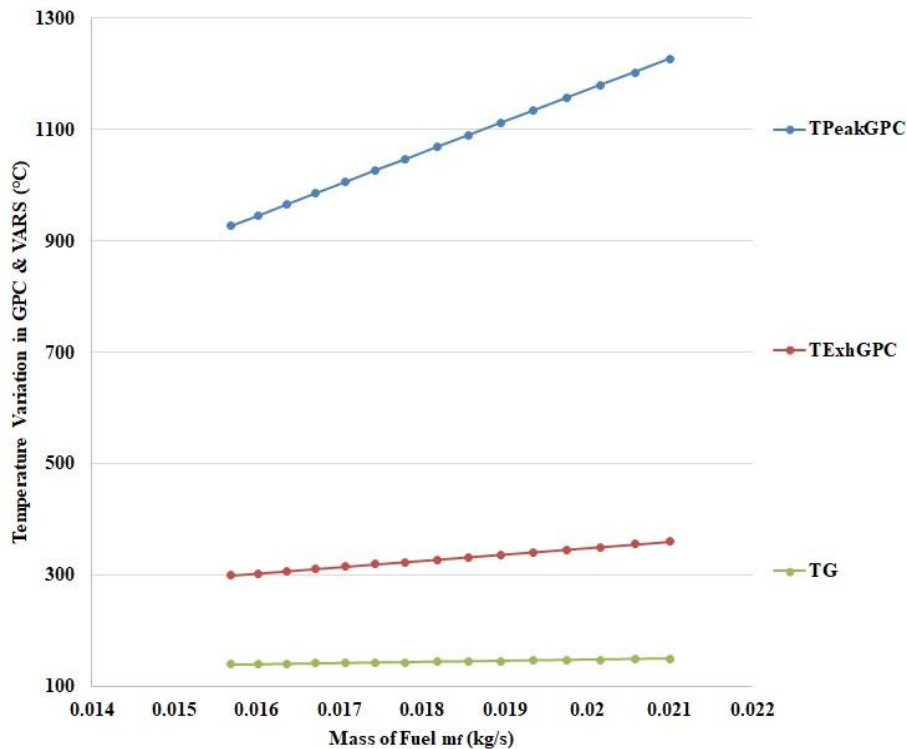


Fig 5.70: Temperatures of GPC and Generator Double Effect Modification-II with Mass of Fuel in GPC

Similarly, Fig. 5.72 shows the temperature variation in LHP-IV where the exhaust gases enter the LHP evaporator at 299 – 360 °C to release heat to the LHP to run the VARS. The LHP-IV evaporator works at 293 – 354 °C and the Condenser works at 288 – 348 °C, whereas, the generator operates at 140 – 150 °C, sufficient heat source temperature & heat are available to run the VARS System. Moreover, Fig 5.71 Presents the Heat Rejected and Exergy & Irreversibility associated with it. It can be seen that the Heat Rejected is 133.6 – 197.6 kW, the Exergy is 58.74 – 93.24 kW and the Irreversibility is 74.8 - 104.3 kW respectively.

Performance Improvement of Vapour Absorption System Using Loop Heat Pipes

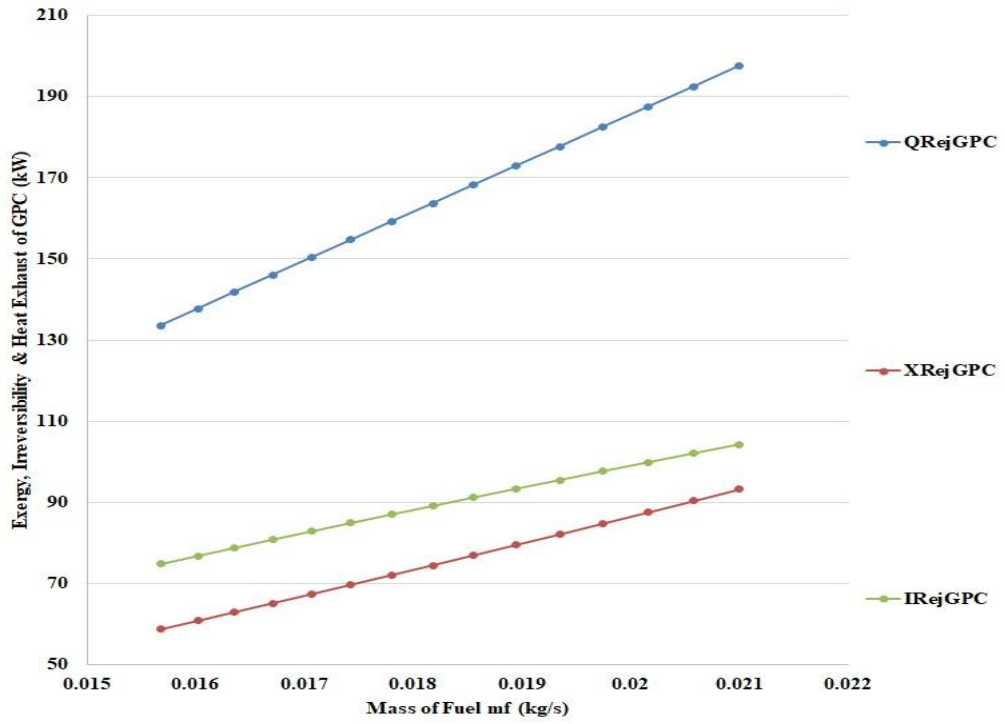


Fig 5.71: Exergy, Irreversibility, and Heat Rejected from GPC Exhaust Double Effect Modification-II with Mass of Fuel in GPC

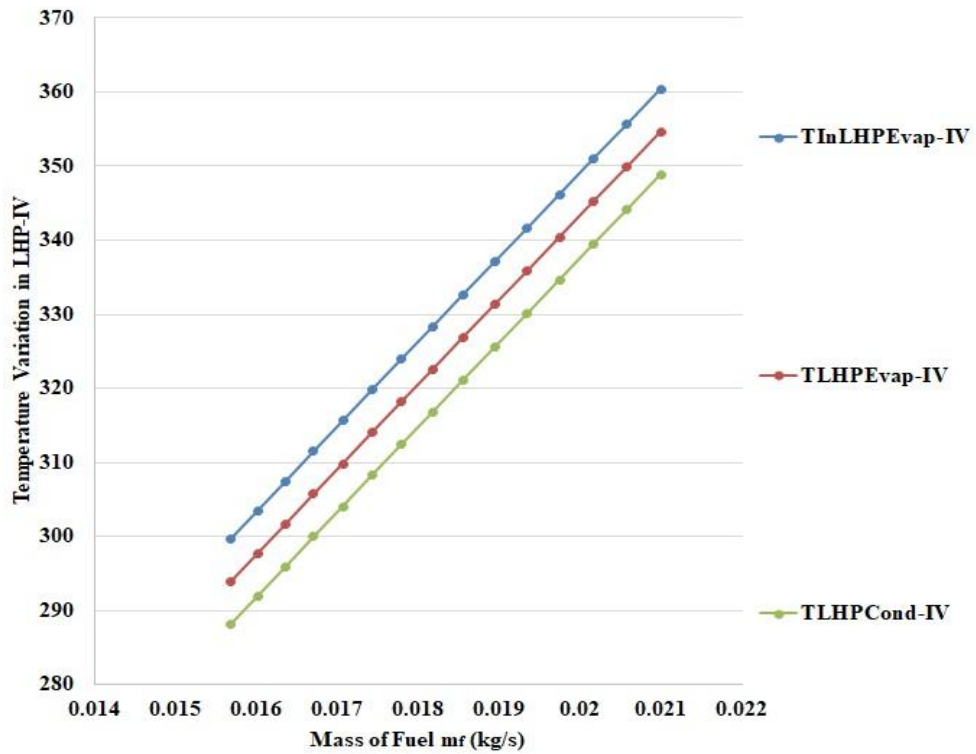


Fig 5.72: Temperatures of LHP-IV with Mass of Fuel in GPC

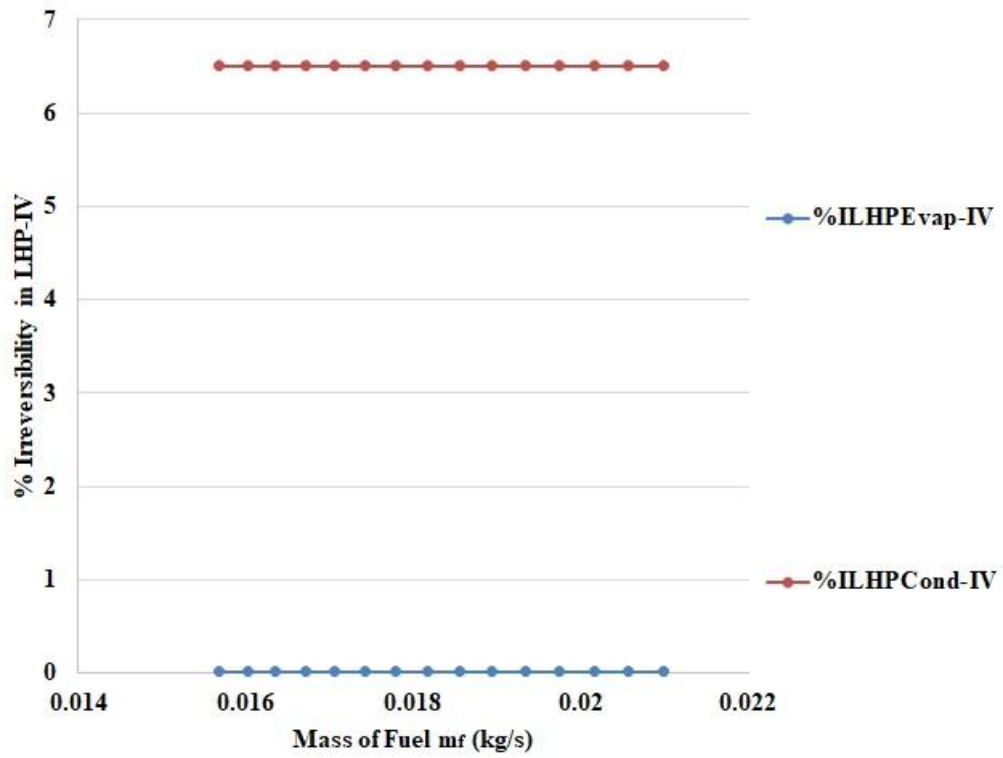


Fig 5.73: Percentage Irreversibility of LHP-IV with Mass of Fuel in GPC

Fig 5.73 presents the percentage contribution to the Irreversibility by LHP-IV to be 0.02 % & 6.5 % for Evaporator & Condenser respectively.

5.4. Modified Triple Effect VARS

Triple effect VARS utilizes higher temperature sources than the Double Effect System. It shows normally higher performance and higher heat utilization. This chapter presents the analysis of the enhancement & modification of the Triple Effect System. Various performance parameters are studied to assess the viability of the system at various input variables. Table 5.11 presents the input data used for the analysis of the Triple Effect System.

Table 5.11: Input Data for Triple Effect VARS Analysis

Sl. No.	Input Parameters	Data
1.	Peak Temperature, T_G	180 °C
2.	Evaporator Temperature, T_{Evap}	5°C
3.	Working Fluid	LiBr-H ₂ O
4.	Heat Exchanger Effectiveness, ϵ_{H-Ex}	0.5-0.7
5.	Condenser Temperature, T_{C-L}	30°C
6.	Mixture Mass Flow rate after absorber, m_2	1 kg/s
7.	Low Generator Temperature, T_{G-L}	80°C
8.	Medium Generator Temperature, T_{G-M}	130°C

5.4.1. Triple Effect VARS Modification-I (Ankit Dwivedi, et. al. 2018) ^[186]

High & Medium Condensers of the Series Triple Effect System have been replaced by LHP-II & I respectively to serve the purpose of Intra-Cycle Heat Exchange for Pre-heating the Mixture entering the High Generator & Supplying Lower Generators to Increase the overall COP of the system similar to the double effect system. Fig 5.74 is used to present the overall Temperature variation in the VARS at different components. It can be seen that the Mixture Enters the High Generator at 136-155 °C, whereas, the entry at Med Generator occurs at 69-79 °C and for Low Generator it

takes place at 65-73 °C. Furthermore, the Vapour Refrigerant exits the Low, Med & High Generator at 58 – 64 °C and 102 – 111 °C & 152 – 172 °C respectively. The refrigerant from Med & High Generator enters the LHP for intra-cycle heat exchange. The Mixture temperature entering the high generator of the unmodified system was 128.4 – 142.8 °C

Similarly, the high-temperature absorbent leaves the High, Med & Low Generator at temperatures 165 – 182 °C, 109 – 126 °C & 64 – 72 °C. Evaporator Temperature is 5 °C.

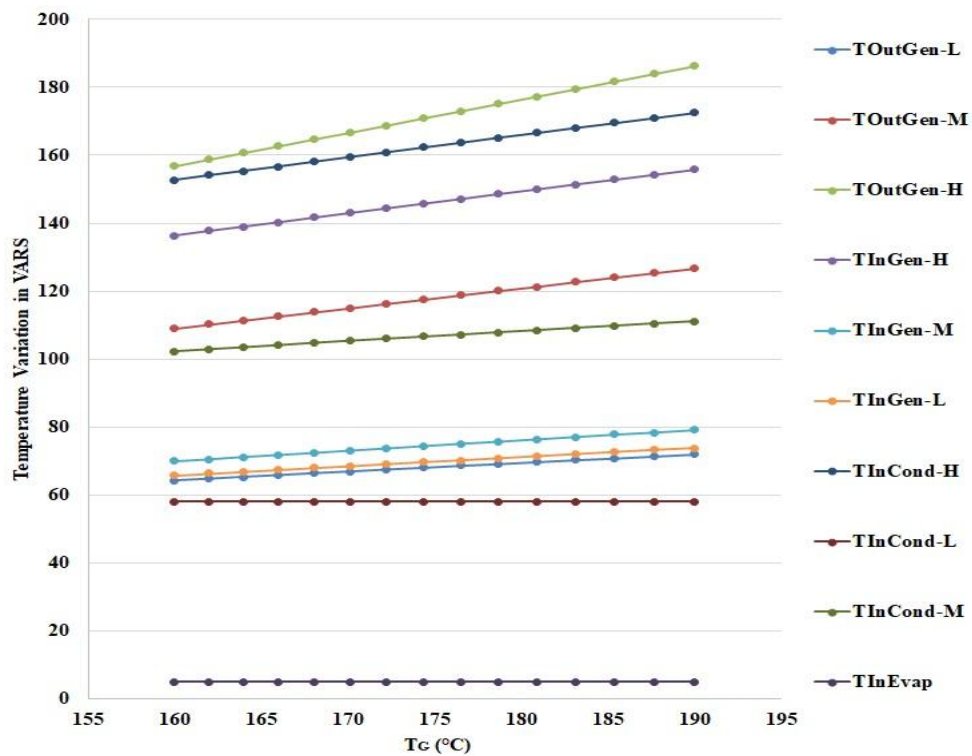


Fig 5.74: Temperature Variation in Triple Effect Modification-I with Generator Temperature

The 5.75 presents the Temperature variation in the HEx - I, II & III. The Mixture exits the HEx - I, II & III at 45 – 47 °C, 81.2 – 85.7 °C, and 128 – 142 °C. Similarly, the absorbent temperature entering the HEx - I, II & III are 64 – 72 °C, 109 – 126 °C & 160 – 190 °C.

Fig 5.76 presents the temperature variation in the LHP I & II components. The Evaporator & Condenser of LHP – I work at 97 – 106 °C & 93 – 102 °C, whereas, the Evaporator & Condenser of LHP – I function at 147 – 167 °C & 144 – 163 °C.

Performance Improvement of Vapour Absorption System Using Loop Heat Pipes

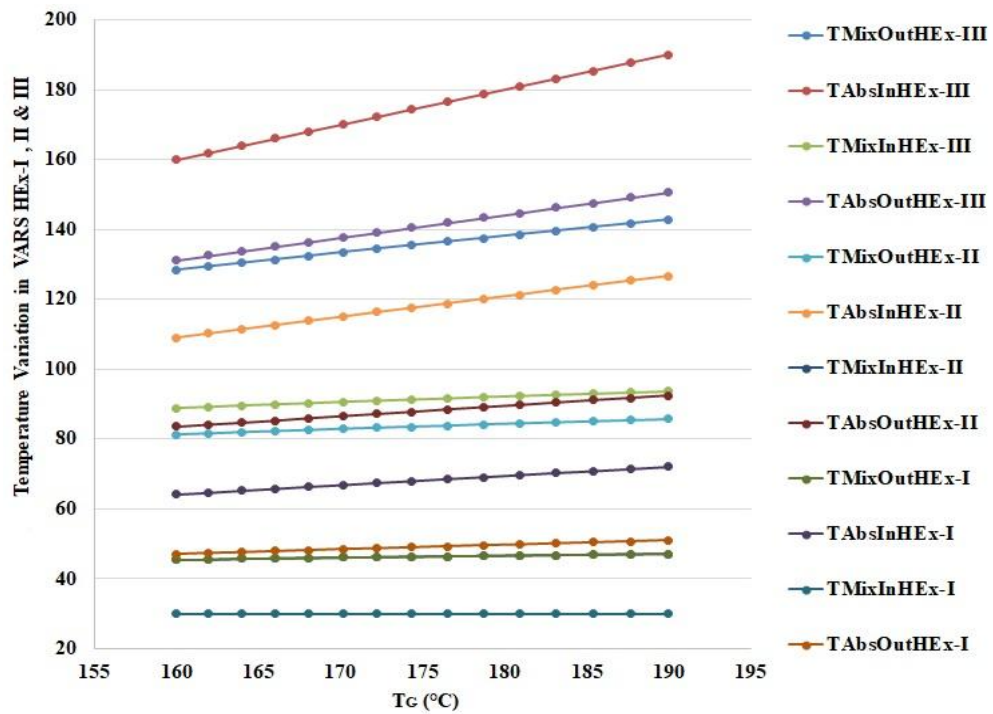


Fig 5.75: Temperature Variation in Triple Effect Modification-I Heat Exchangers with Generator Temperature

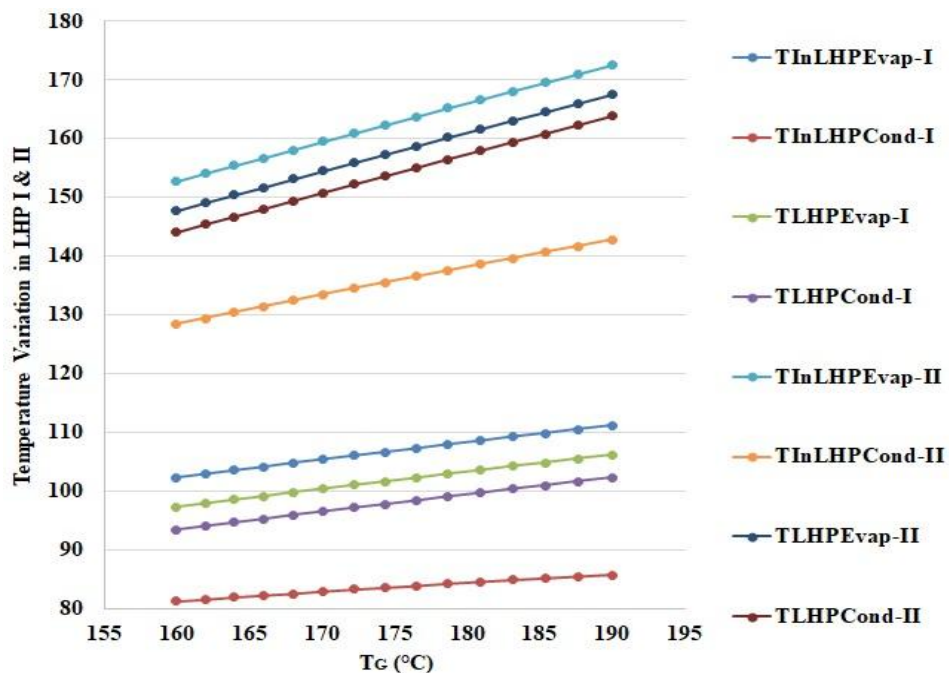


Fig 5.76: Temperature Variation in LHPs with Generator Temperature

Fig 5.77 shows the Heat Interaction in the VARS Components. The Heat input for Low, Med & High Generators are 22 – 46 kW, 30 – 58 kW & 58 – 99 kW. The Heat Input to the High Generator presented is the reduced requirement post the implementation on LHP – I & II. The heat extracted in the Evaporator for the

Performance Improvement of Vapour Absorption System Using Loop Heat Pipes

Refrigeration is 134 – 274 kW. Heat available for extraction by LHP – I & II are 44 – 95.6 kW & 69 – 135 kW respectively. The Heat Input to the Original System High Generator was 91.3 – 164 kW ^[176].

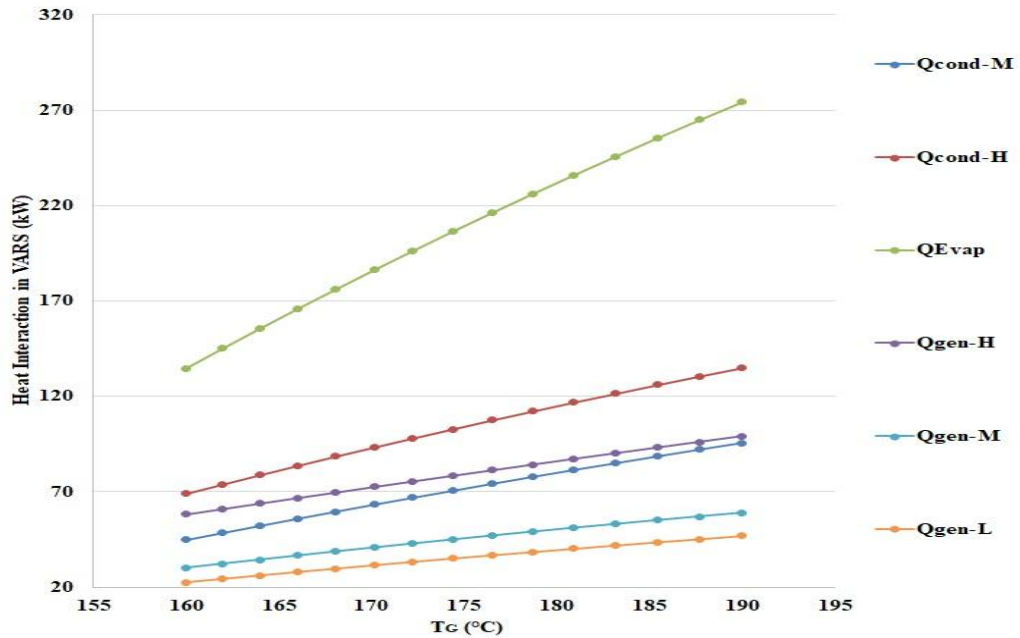


Fig 5.77: Heat Interaction in Triple Effect Modification-I with Generator Temperature

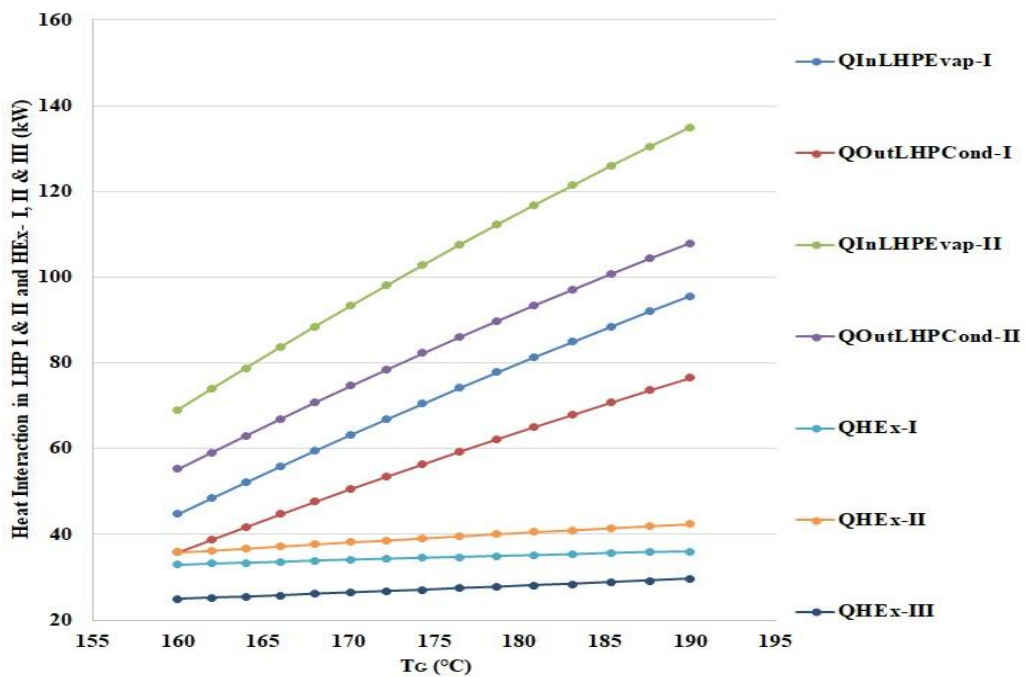


Fig 5.78: Heat Interaction in LHPs & HEX with Generator Temperature

Fig 5.78 explores the Heat interaction in LHP I & II and HEX – I, II & III. The Heat Extracted by the LHP – I & II available for delivery at the LHP Condenser can be

Performance Improvement of Vapour Absorption System Using Loop Heat Pipes

given as 35 – 76 kW & 55 – 107 kW respectively. Similarly, the Heat interaction in HEX – I, II & III has been observed as 32 – 35 kW, 35.8 – 42 kW & 25 – 29.6 kW.

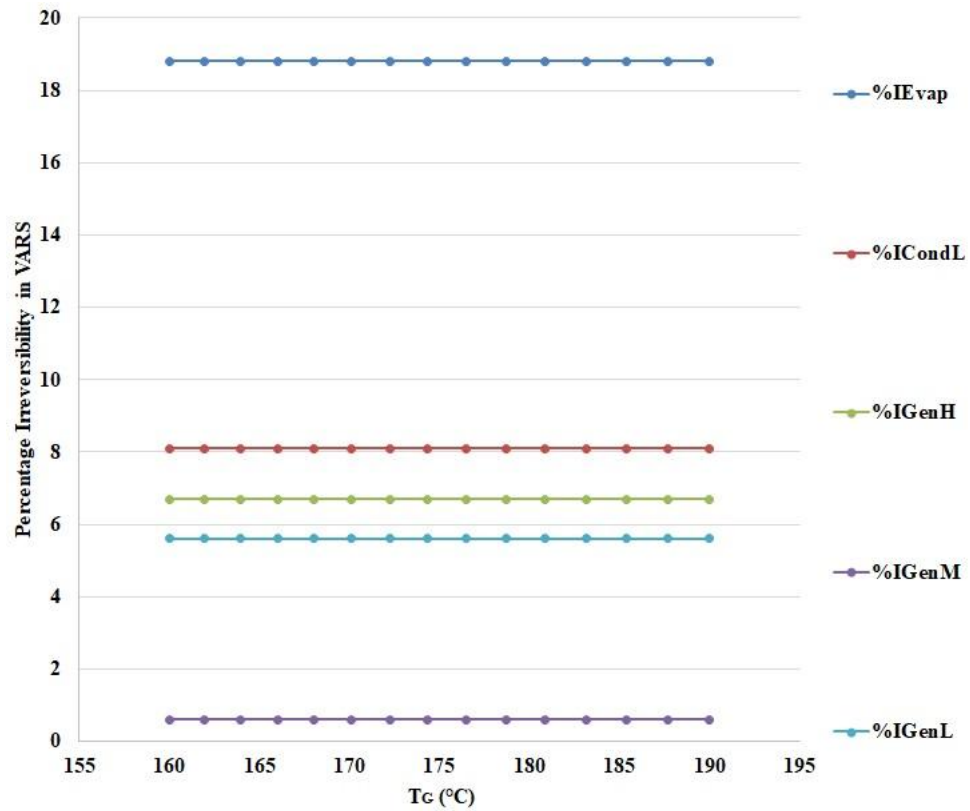


Fig 5.79: Percentage Irreversibility in Triple Effect Modification-I Components with Generator Temperature

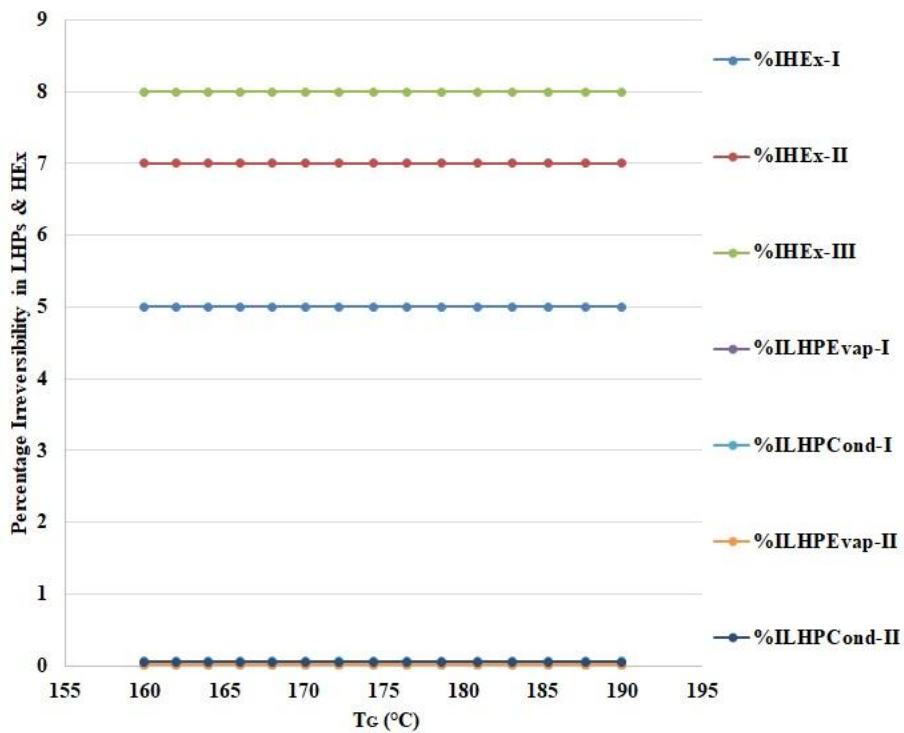


Fig 5.80: Percentage Irreversibility in LHP Components with Generator Temperature

Fig 5.79 & 5.80 present the percentage contribution to the overall Irreversibility by the various components in the Modification – I. It can be seen that the Percentage contribution to Irreversibility by Evaporator, Low, Med & High Generators are 18.8 %, 5.6 %, 0.6 % & 6.7 % respectively. Whereas, the Percentage contribution to Irreversibility by LHP – I & II Condenser & Evaporator can be given as 0.065 % & 0.02 % and 0.057 % & 0.015 % respectively. Similarly, the HEx – I, II & III contribute to the overall Irreversibility by 5, 7 & 8% respectively.

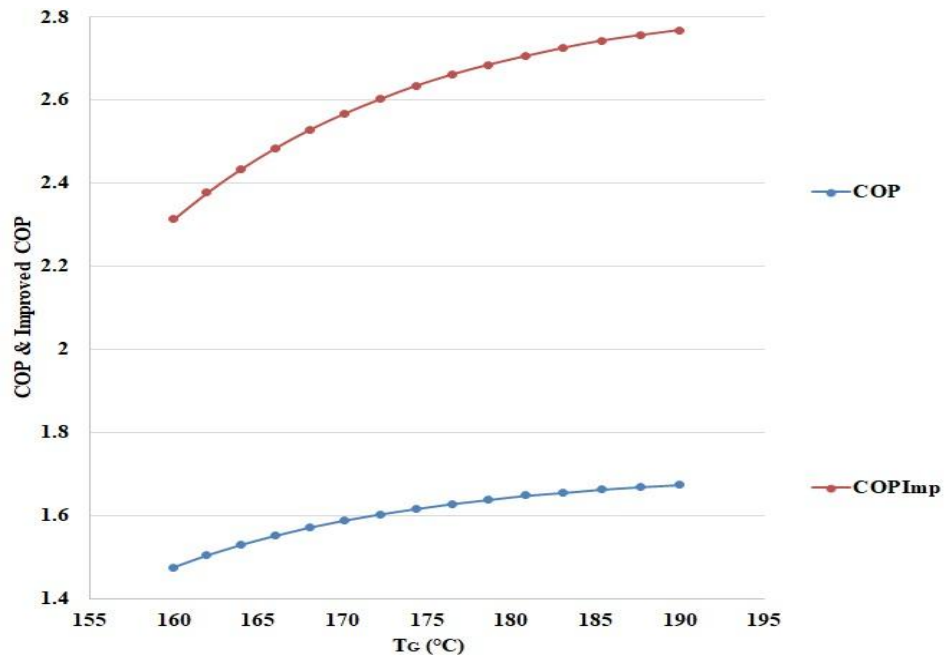


Fig 5.81: COP & Improved COP with Generator Temperature

Fig 5.81 & Fig 5.82 present the Improved COP & Percentage Improvement in the COP. It can be seen that the improved COP owing to the intra-cycle heat recovery is 2.3 – 2.7, whereas, the original COP was 1.47 – 1.67 ^[176]. The overall percentage increment can be observed as 58.8 – 65.3 %.

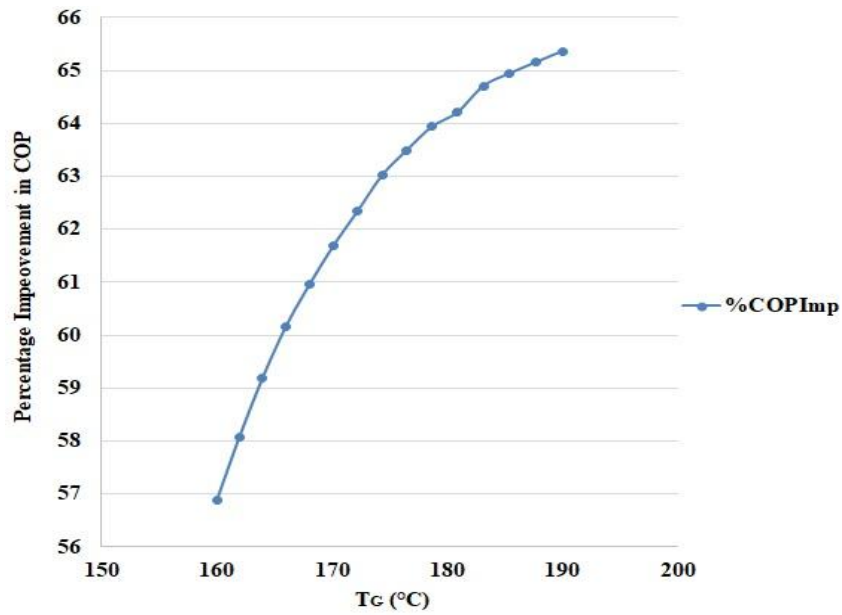


Fig 5.82: Percentage Improvement in COP with Generator Temperature

Fig 5.83, 5.84 & 5.85 present the mass flow taking place in the High, Medium & Low side segments of the VARS. The Mass Flow Rate of the Refrigerant Vapour out of the High Generator is 0.025 – 0.05 kg/s and the absorbent exiting the High Generator is 0.975 – 0.95 kg/s.

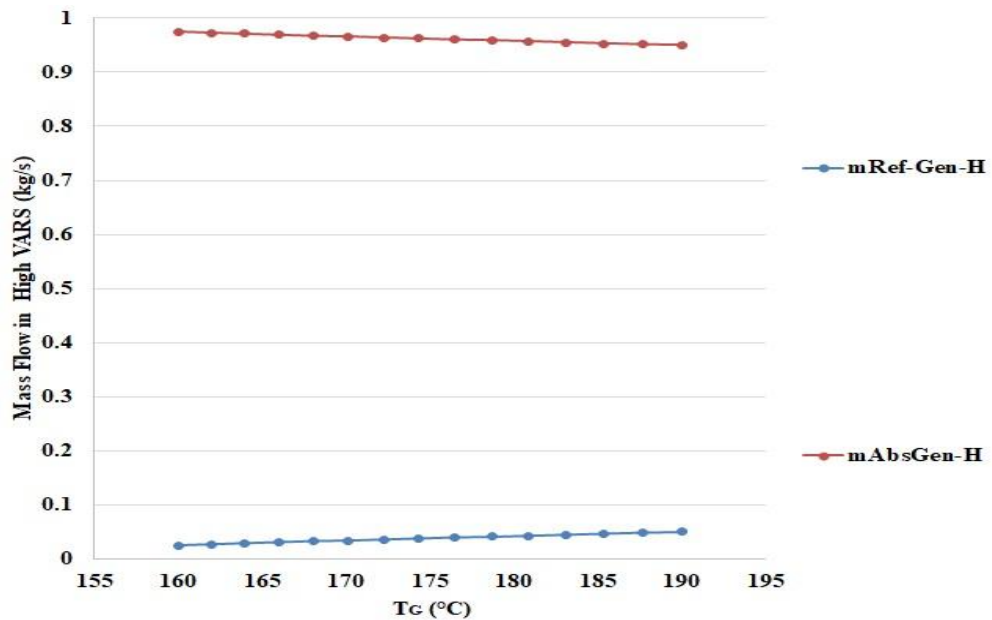


Fig 5.83: Mass Flow Rates in Triple Effect Modification-I High with Generator Temperature

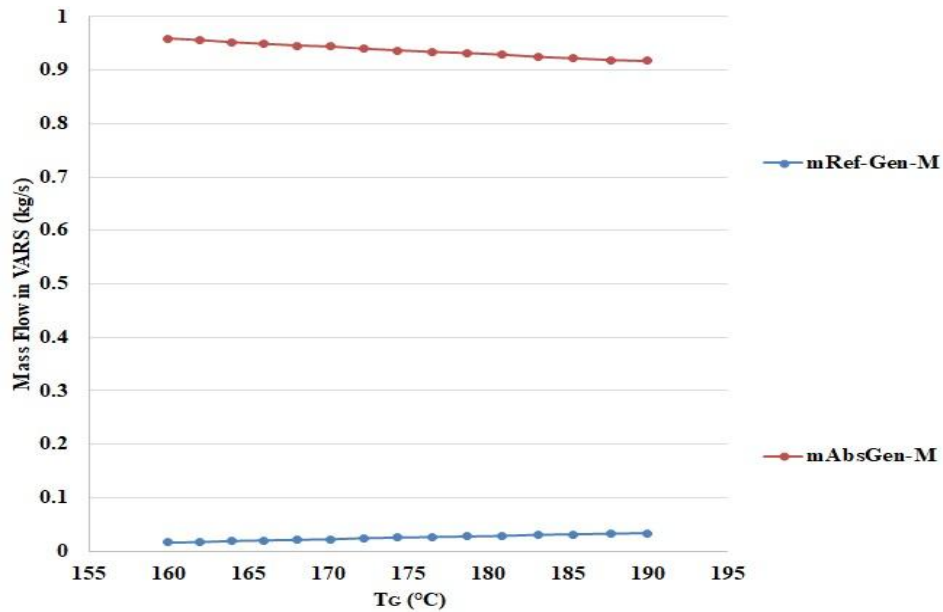


Fig 5.84: Mass Flow Rates in Triple Effect Modification-I Med with Generator Temperature

Similarly, Fig 5.84 shows the mass flow rate in Med VARS. The mass of vapour refrigerant leaving the medium generator is 0.016 – 0.033 kg/s & the mass flow rate of absorbent leaving the medium generator is 0.959 – 0.917 kg/s.

Moreover, Fig 5.85 in the low side of VARS. The mixture mass flow rate after the absorber is 1 kg/s. Also, the mass of vapour leaving the low generator is 0.015 – 0.032 kg/s. Mass of Absorbent leaving low generator 0.944 – 0.885 kg/s. The mass of refrigerant entering the evaporator is the summation of the refrigerant vapour exiting all the generators 0.056 – 0.115 kg/s.

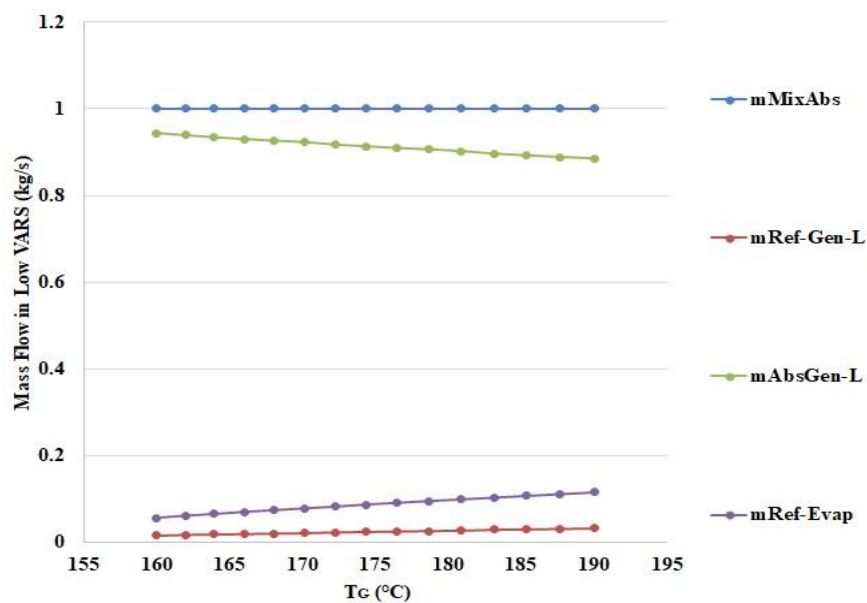


Fig 5.85: Mass Flow Rates in Triple Effect Modification-I Low with Generator Temperature

5.4.2. Triple Effect VARS Modification-II

The Heat Exchangers being used in the Modification-I have been replaced by the LHP- I, II & IV. The LHP – I & II have been designated as LHP- III & V respectively for this analysis. The analysis has been performed in the same manner as Modification-I. Fig 5.86 Presents the Temperature variation in the Triple Effect VARS Modification-II. Owing to the implementation of LHPs, the Temperature at the Inlet to the High Generator is increased from the Modification-I. It can be observed that the temperature is 140 – 160 °C.

Fig 5.87 shows that the inlet temperature of the Mixture to the LHP – V Condenser is 131 – 146 °C. Similarly, the inlet temperature of the Mixture to the LHP – III Condenser is 83 – 87 °C. An increase has been observed in the temperature owing to the replacement of HEx by the LHPs.

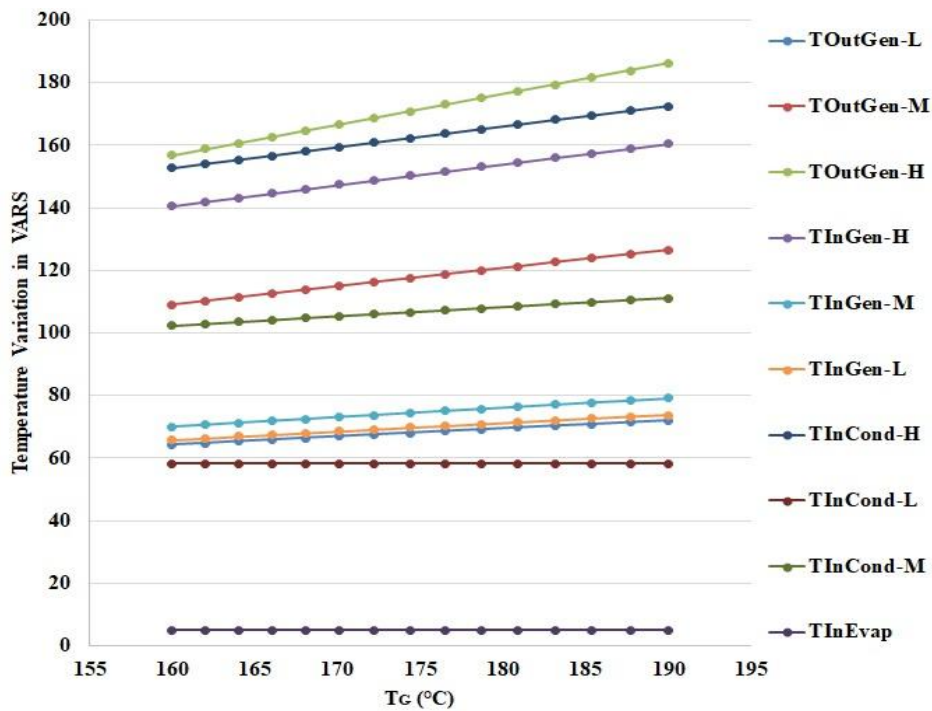


Fig 5.86: Temperature Variation in Triple Effect Modification-II with Generator Temperature

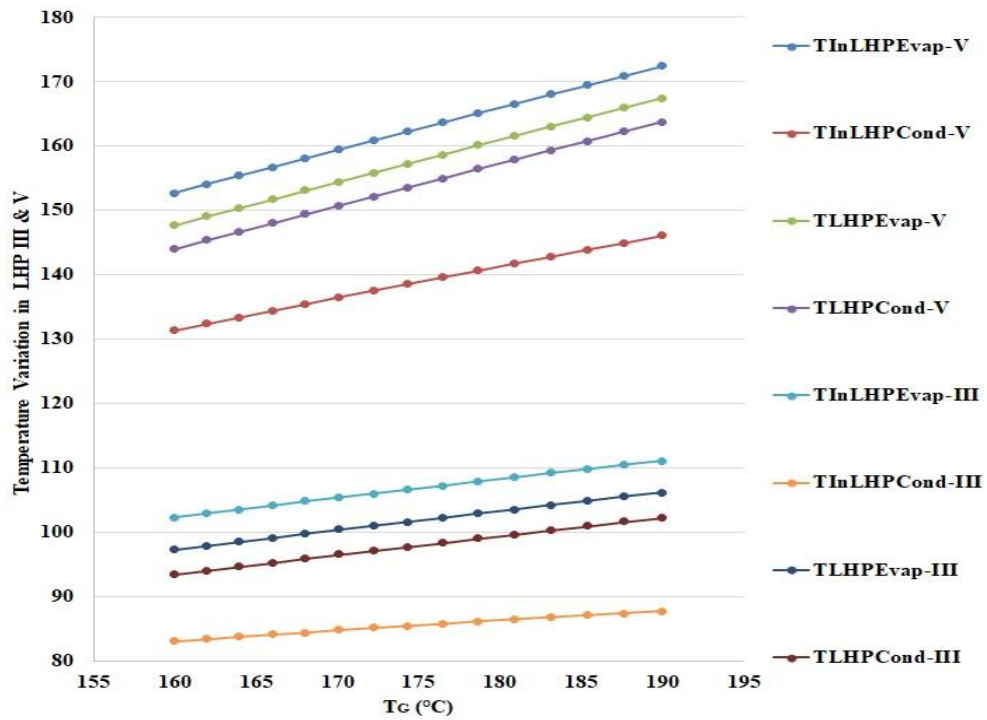


Fig 5.87: Temperature Variation in LHP-III & V with Generator Temperature

Fig 5.88 shows that the Inlet Temperature of the Absorbent to the LHP -IV evaporator is 160 – 190 °C and the outlet temperature of the Mixture from the LHP-IV Condenser is 131 – 146 °C. The LHP Evaporator & Condenser work at 138 – 153 °C & 136 – 151 °C.

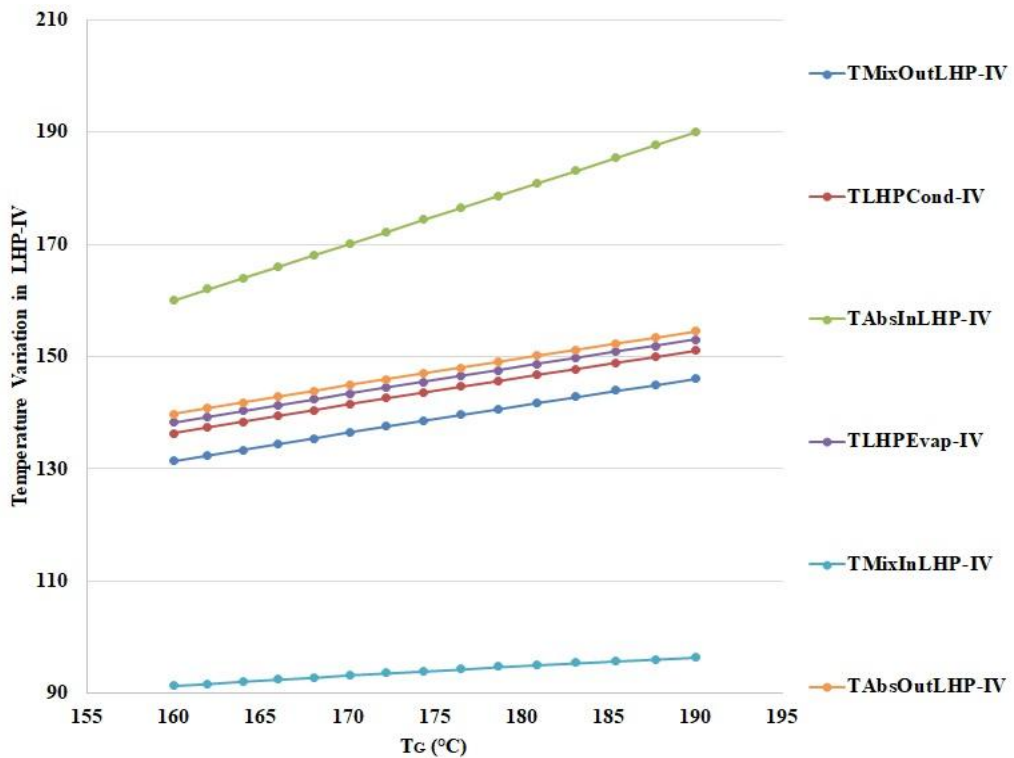


Fig 5.88: Temperature Variation in LHP-IV with Generator Temperature

Performance Improvement of Vapour Absorption System Using Loop Heat Pipes

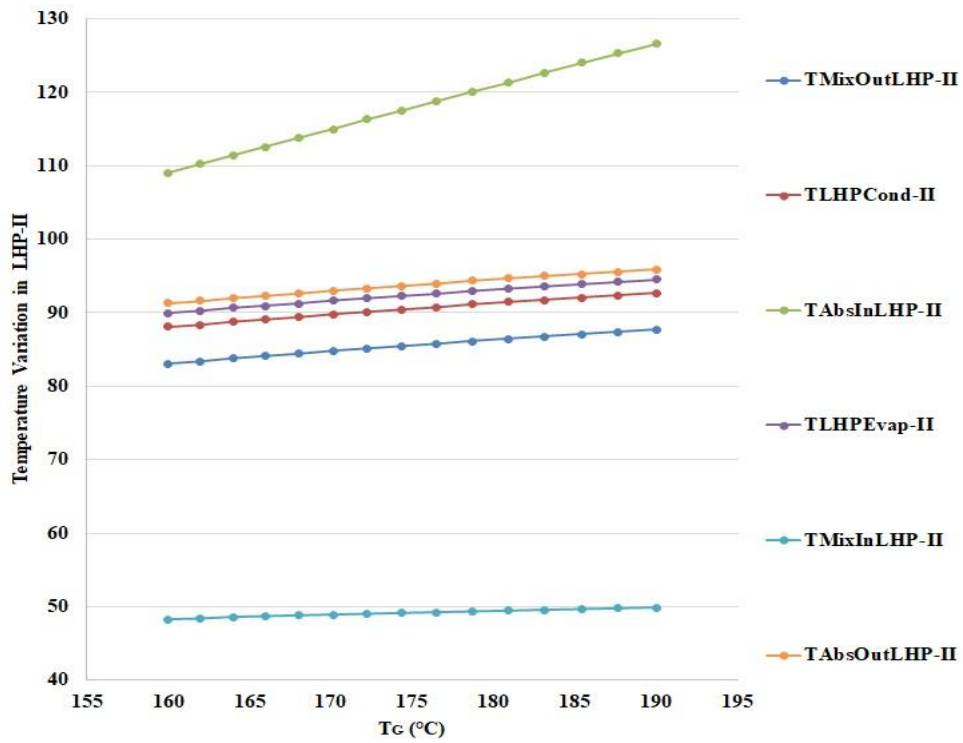


Fig 5.89: Temperature Variation in LHP-II with Generator Temperature

Furthermore, Fig 5.89 shows that the Inlet Temperature of the Absorbent to the LHP-II evaporator is 109 – 126 °C and the outlet temperature of the Mixture from the LHP-II Condenser is 83 – 87 °C. The LHP Evaporator & Condenser work at 90 – 94 °C & 88 – 92 °C.

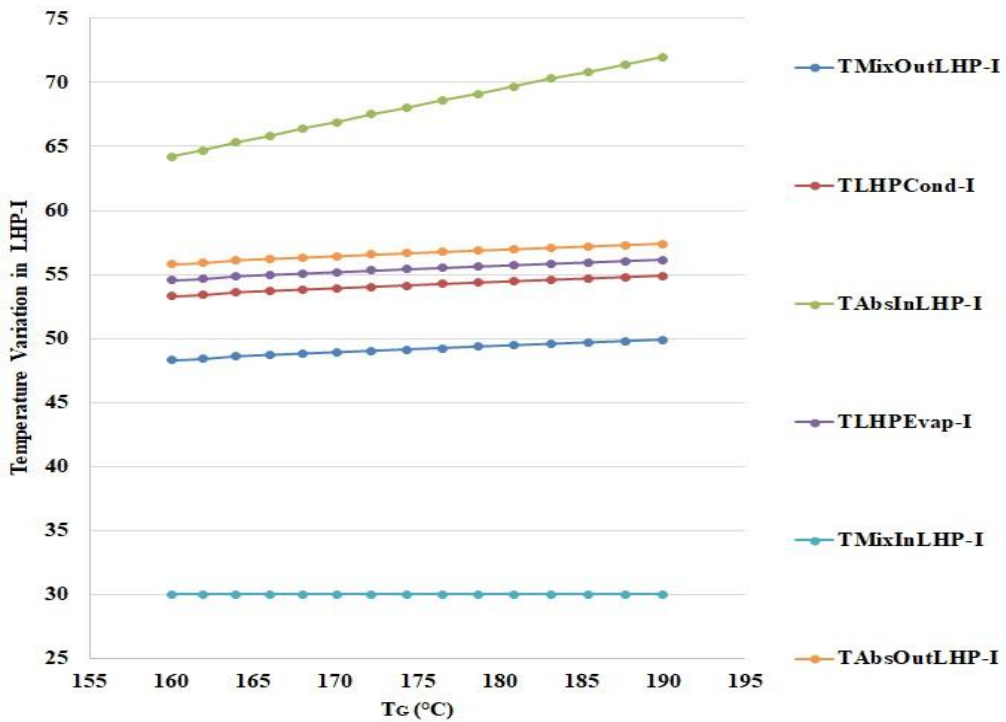


Fig 5.90: Temperature Variation in LHP-I with Generator Temperature

Performance Improvement of Vapour Absorption System Using Loop Heat Pipes

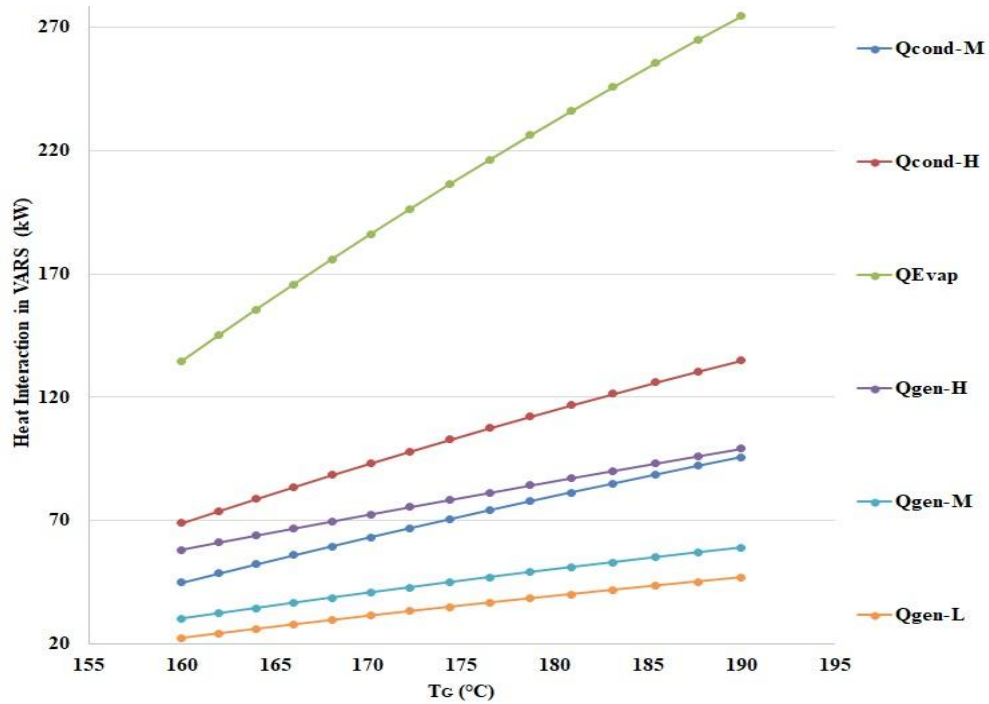


Fig 5.91: Heat Interaction in Triple Effect Modification-II with Generator Temperature

Moreover, Fig 5.90 shows that the Inlet Temperature of the Absorbent to the LHP - I evaporator is 64 – 72 °C and the outlet temperature of the Mixture from the LHP -I Condenser is 48 – 49 °C. The LHP Evaporator & Condenser work at 54 –56 °C & 53 – 54 °C.

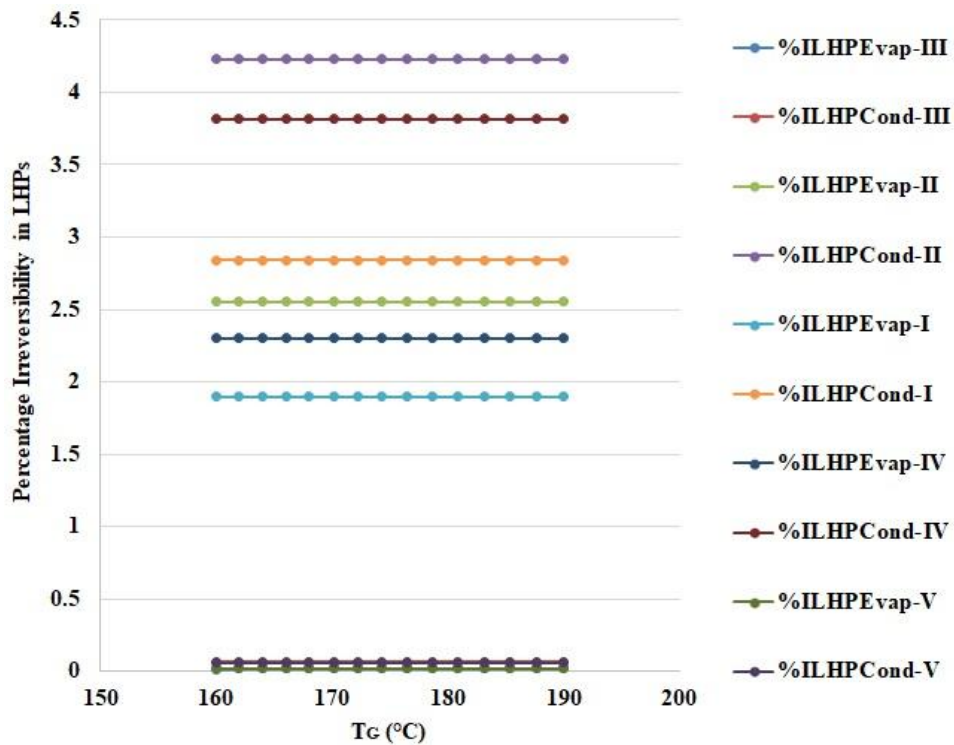


Fig 5.92: Percentage Irreversibility in LHPs Components with Generator Temperature

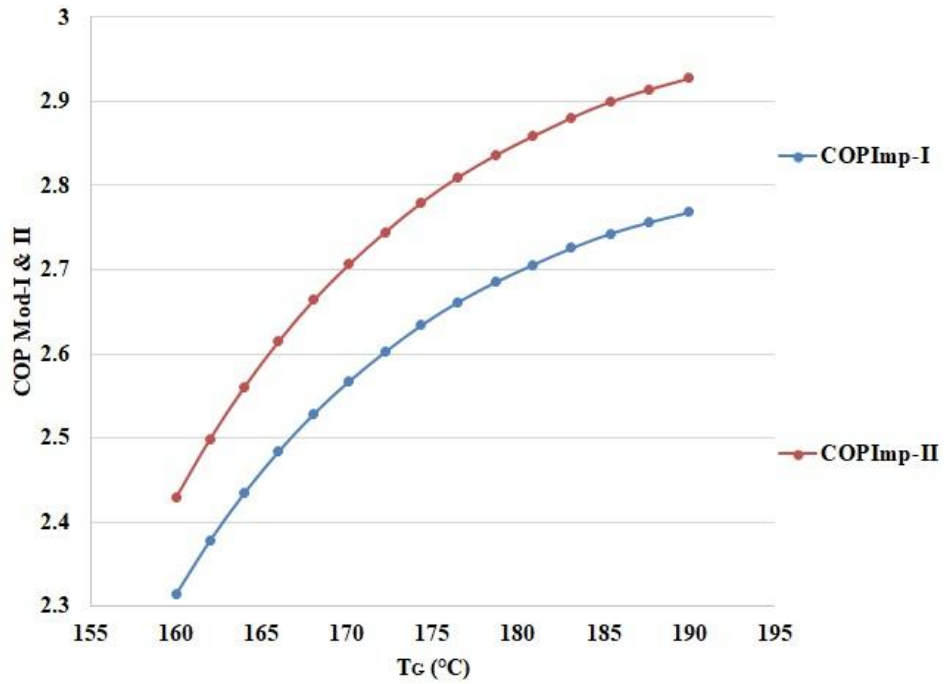


Fig 5.93: COP & Improved COP with Generator Temperature

Fig 5.91 presents that the heat requirement in the High Generator has reduced further to 55 – 93 kW for Modification-II from the 58 – 99 kW for Modification-I owing to the implementation of LHPs. Whereas, Fig 5.92 presents the percentage irreversibility contribution of LHP - I, II, III, IV & V. The LHP- I, II, III, IV & V Evaporator Contribute to 1.8%, 2.5%, 0.02%, 2.3 % & 0.019% respectively. Similarly, LHP- I, II, III, IV & V Condenser Contribute to 2.8 %, 4.2%, 0.065%, 3.81% & 0.06% respectively.

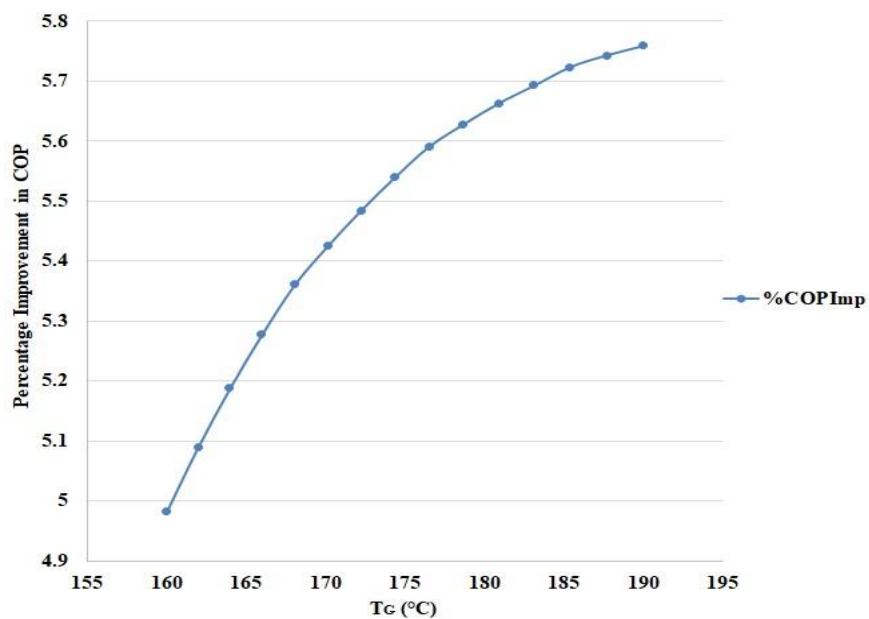


Fig 5.94: Percentage Improvement in COP with Generator Temperature

Moreover, Fig 5.93 & Fig 5.94 present a comparison of the COP for Modification-I & Modification-II. It can be seen that the COP for Modification-II is 2.4 – 2.9. The further percentage improvement in COP is around 5 % over the COP of Modification-I.

The comparison of the performance parameters of triple effect systems based on the Text, published research work & proposed work has been presented in Table 5.12. It can be seen that the proposed work has better performance than the Published work and text.

Table 5.12: Comparison of Modified Triple Effect

Parameters	Herold et. al. (2016) ^[176]	Solanki et. al. (2016) ^[84]	Proposed Work	
			Modification-I	Modification-II
Mass Flow Rate of Mixture from Absorbent (kg/s)	1	12.01	1	1
Mass Flow Rate of Refrigerant in Evaporator (kg/s)	0.107	1	0.107	0.107
Generator Temperature (°C)	185	185	185	185
Evaporator Temperature (°C)	5	7.2	5	5
Absorber Temperature (°C)	30	37.2	30	30
Q _{Evap} (kW)	274.4	2355	134.6	134.6
Q _{Cond-H} (kW)	126.021	-	126.021	126.021

Performance Improvement of Vapour Absorption System Using Loop Heat Pipes

$Q_{\text{Cond-M}}$ (kW)	88.5	-	88.5	88.5
$Q_{\text{Gen-H}}$ (kW)	163.9	1441	58.1704	55.4096
COP	1.276	1.63	2.74	2.9
η_{II}	34.03	29.64	53.4	56.05

Table 5.13 presents the comparison between the published work & proposed work based on the irreversibility experienced in the components at 185°C.

Table 5.13: Irreversibility in Triple Effect Components

Parameters/ Irreversibility	Solanki et. al. (2017) ^[178]		Proposed Work			
	kW	%	Modification-I		Modification-II	
			kW	%	kW	%
I_{Evap}	85.03	19.07	8.74	18.8	8.74	18.8
$I_{\text{Gen-H}}$	30.22	6.78	3.11	6.7	3.11	6.7
$I_{\text{Gen-M}}$	2.8	0.63	0.28	0.6	0.28	0.6
$I_{\text{Gen-L}}$	25.68	5.76	2.6	5.6	2.6	5.6
$I_{\text{Cond-L}}$	36.77	8.24	3.76	8.1	3.76	8.1
$I_{\text{HEX-I}}$	24.52	5.5	2.32	5	-	-
$I_{\text{HEX-II}}$	33.16	7.44	3.25	7	-	-
$I_{\text{HEX-III}}$	36.06	8.09	3.72	8	-	-
I_{Abs}	164.8	36.95	16.93	36.4	16.93	36.4
LHP-I	-	-	-	-	2.20	4.73
LHP-II	-	-	-	-	3.15	6.77
LHP-III	-	-	0.039	0.085	0.039	0.085

Performance Improvement of Vapour Absorption System Using Loop Heat Pipes

LHP-IV	-	-	-	-	2.84	6.11
LHP-V	-	-	0.037	0.08	0.037	0.08
Refrigeration Capacity (RC) (kW)	2355.7		255.4			
Total Irreversibility (kW)	445.97		46.5		43.7	

5.4.3. Combined Triple Effect VARS & GPC

The Modification-II has been connected with the GPC through LHP-VI. The Condenser side of the LHP is connected to the High Generator. Fig 5.95 exhibits the Temperature variation in the GPC & Generator Temperature of VARS. It can be seen that the Peak Temperature of GPC, Exhaust Temperature of GPC, and High Generator temperature of VARS are 927 – 1227 °C, 299.6 – 360.4 °C, and 160 – 190 °C.

Fig 5.96 presents the Temperature Variation in the LHP – VI. The LHP Evaporator & Condenser temperature attained are 293.8 – 354.6 °C & 288 – 348.8 °C.

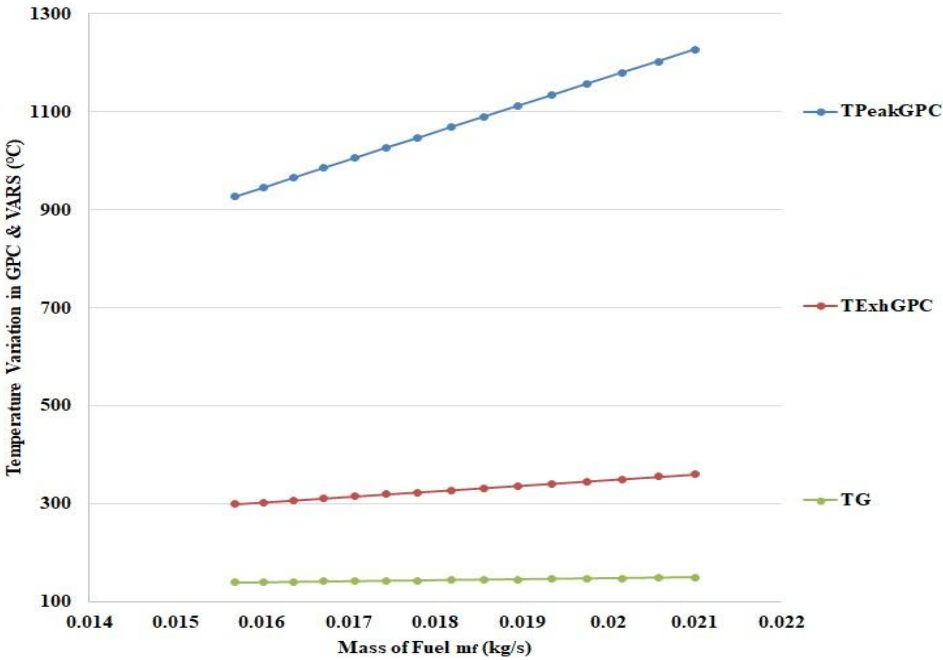


Fig 5.95: Temperatures of GPC and Generator Triple Effect Modification-II with Mass of Fuel in GPC

Performance Improvement of Vapour Absorption System Using Loop Heat Pipes

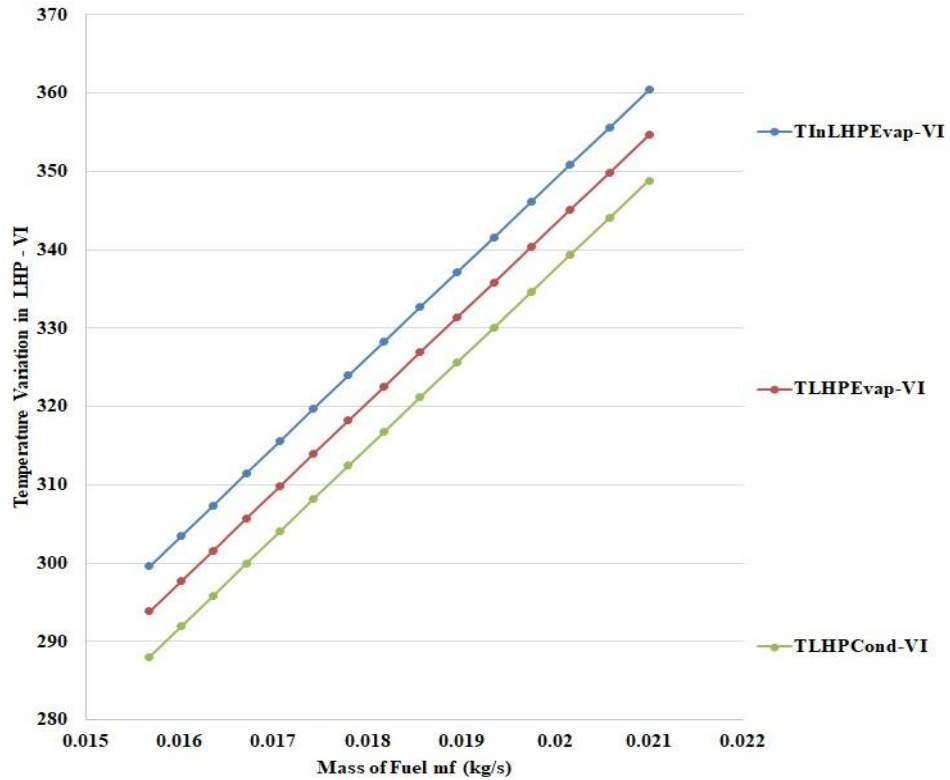


Fig 5.96: Temperatures of LHP-VI with Mass of Fuel in GPC

Fig 5.97 discusses the Contribution of the LHP-VI to the Irreversibility in the System. The LHP-VI Evaporator & Condenser contribute by 0.023 % & 6.305 %.

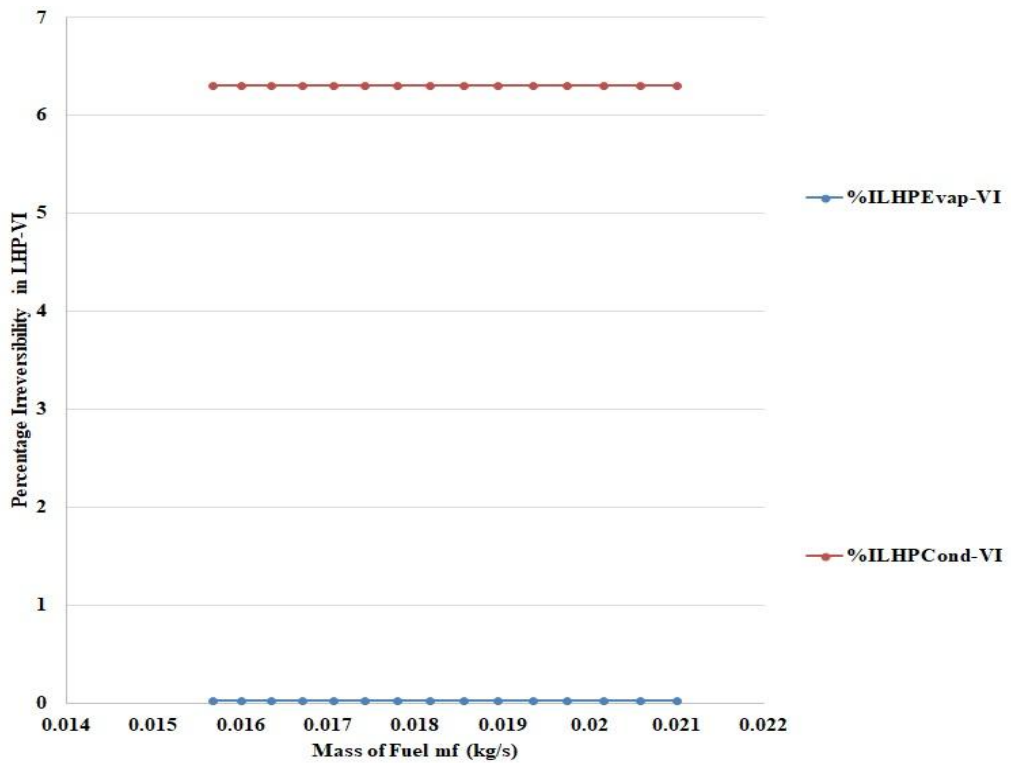


Fig 5.97: Percentage Irreversibility of LHP-VI with Mass of Fuel in GPC

Performance Improvement of Vapour Absorption System Using Loop Heat Pipes

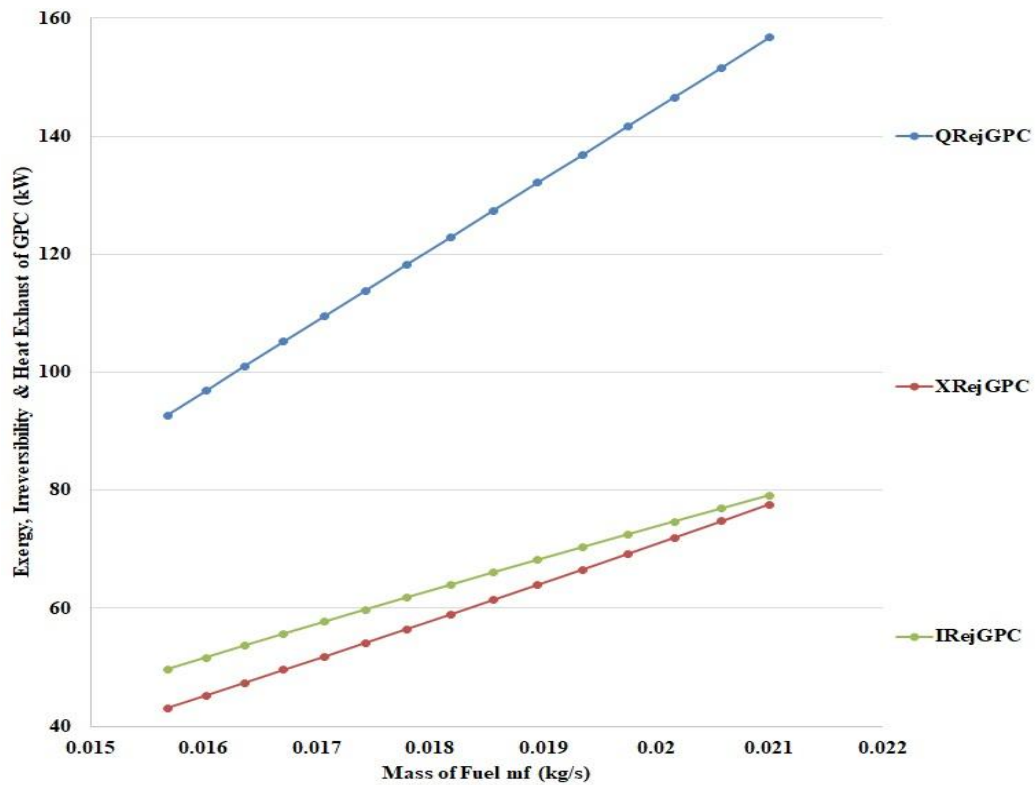


Fig 5.98: Exergy, Irreversibility, and Heat Rejected from GPC Exhaust Triple Effect Modification-II with Mass of Fuel in GPC

Fig 5.98 presents the Heat Rejected in Exhaust, Exergy & Irreversibility related to the system. It can be seen that the Heat, Exergy & Irreversibility are 92.71 – 156.7 kW, 43.06 – 77.57 kW & 49.65 – 79.11 kW respectively.

5.5. Modified Quadruple Effect VARS

This section presents the analysis of the Quadruple effect system performance which has been improved by the use of LHP. The Highest generator temperature (HG-II) has been varied from 180 – 205 °C. All the other performance parameters have been calculated and presented. Table 5.14 consists of the input variable for the basic analysis of the quadruple system.

Table 5.14: Input Variables for Quadruple Effect VARS Analysis

Sl. No.	Input Parameters	Data
1.	Peak Temperature, T_{G-H-II}	180 °C

2.	Evaporator Temperature, T_{Evap}	5 °C
3.	Working Fluid	LiBr-H ₂ O
4.	Heat Exchanger Effectiveness, $\epsilon_{\text{H-Ex}}$	0.7
5.	Condenser Temperature, $T_{\text{C-L}}$	30°C
6.	Mixture Mass Flow rate after absorber, m_2	1 kg/s
7.	Low Generator Temperature, $T_{\text{G-L}}$	65°C
8.	Medium Generator Temperature, $T_{\text{G-M}}$	100°C
9.	High Generator-I Temperature, $T_{\text{G-H-I}}$	130°C

5.5.1. Quadruple Effect VARS Modification-I

This section presents the Performance Evaluation of the Mod – I of Quadruple Effect System. The High-II, High-I, and Medium Condenser have been replaced by the LHP-III, II & I respectively for performing as the condenser and intra-cycle heat recovery devices. Similar to the systems presented in the previous sections, the objective of Increasing the COP has been studied.

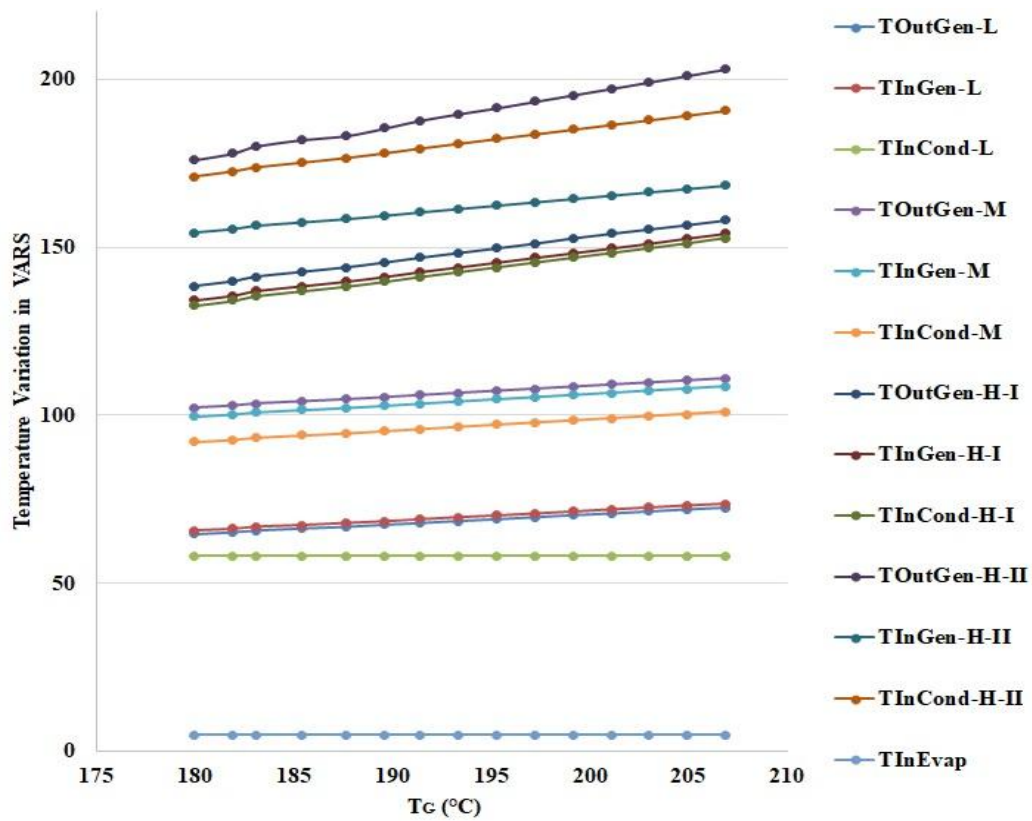


Fig 5.99: Temperature Variation in Quadruple Effect Modification-I with Generator Temperature

Fig 5.99 projects the results obtained for the Temperature variation in the Quadruple Effect Modification-I along with the varying High Generator – II Temperature. The Vapour Refrigerant leaves the Low, Medium, High -I and High -II generators at 58.1°C, 92.1 – 101 °C, 132.7 – 152.7 °C, and 171 – 190.7 °C respectively. Furthermore, the Absorbent exits the Low, Medium, High -I and High -II generators at 64.7 – 72.5 °C, 102.2 – 111 °C, 138.4 – 158.1 °C, and 176 – 203 °C respectively. The mixture enters the High Generator -II at 154.5 – 168.3 °C. The Mixture temperature entering the High Generator-II of the unmodified system was 143.7 – 156.7 °C

Performance Improvement of Vapour Absorption System Using Loop Heat Pipes

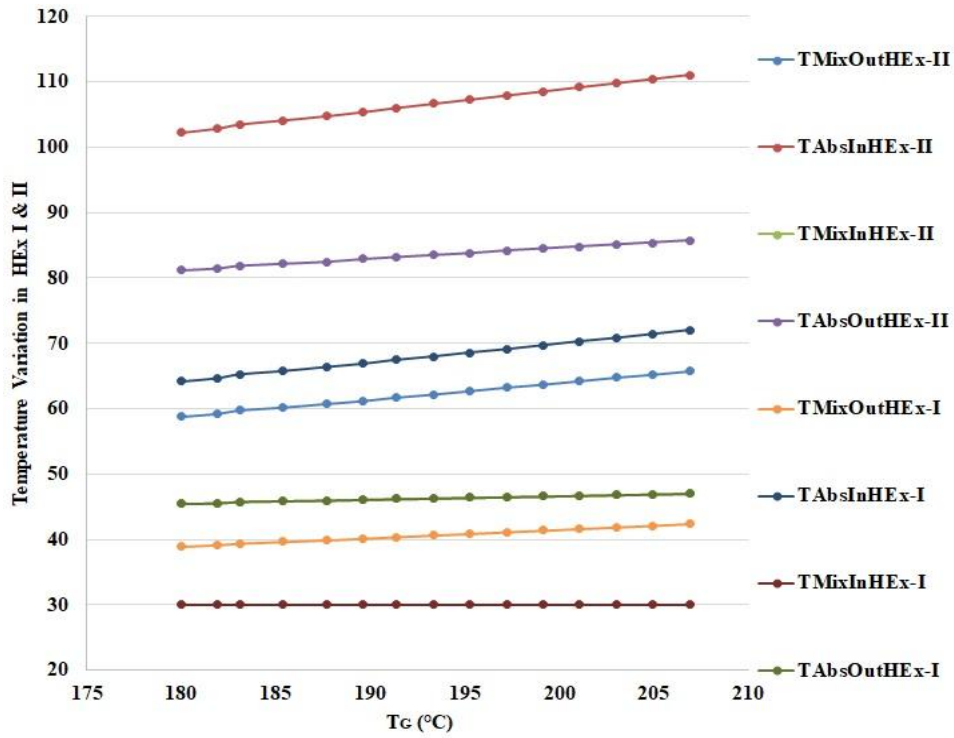


Fig 5.100: Temperature Variation in Quadruple Effect Modification-I Heat Exchangers I & II with Generator Temperature

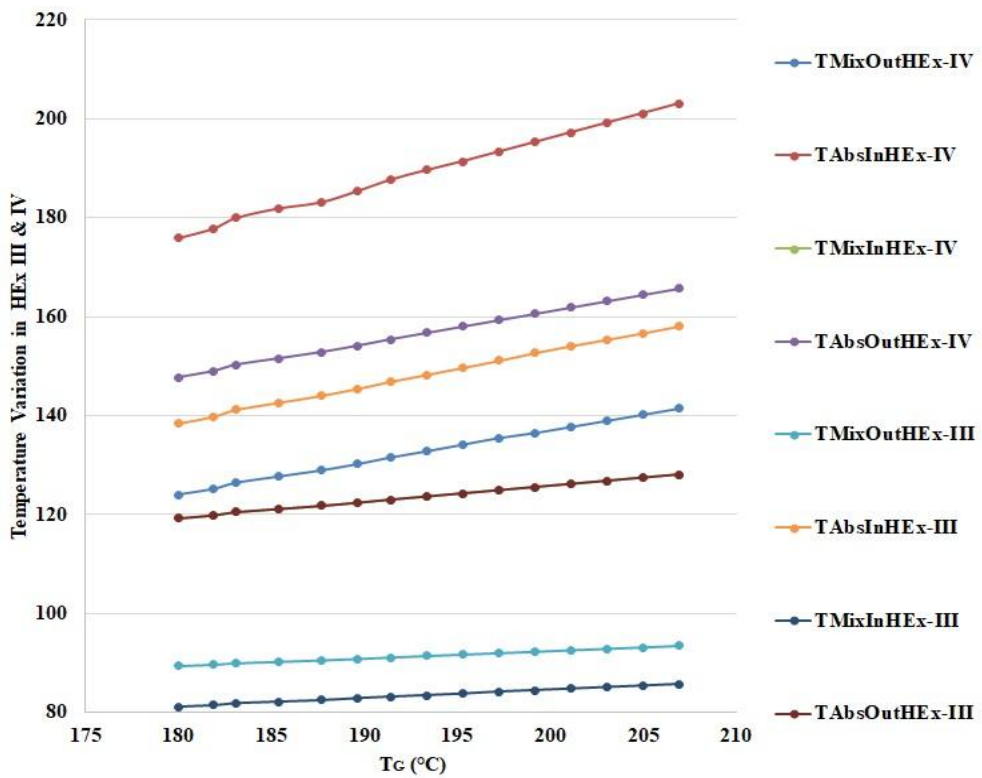


Fig 5.101: Temperature Variation in Quadruple Effect Modification-I Heat Exchangers III & IV with Generator Temperature

Fig 5.100 presents the temperature variation in the Heat Exchanger - I & II. It can be observed that the Exit of the HEx – I is the inlet of the HEx – II. The Mixture enters the HEx- I at 30 °C and exits at 38.8 – 42.4 °C, whereas the absorbent from the Low Generator enters the HEx – I at 64.2 – 72 °C and exits at 45.5 – 47 °C. The Absorbent from the Medium Generator enters the HEx – II at 102.2 – 111 °C and exits at 79.5 – 84 °C. Moreover, the Mixture exits the HEx - II at 58.7 – 68.7 °C.

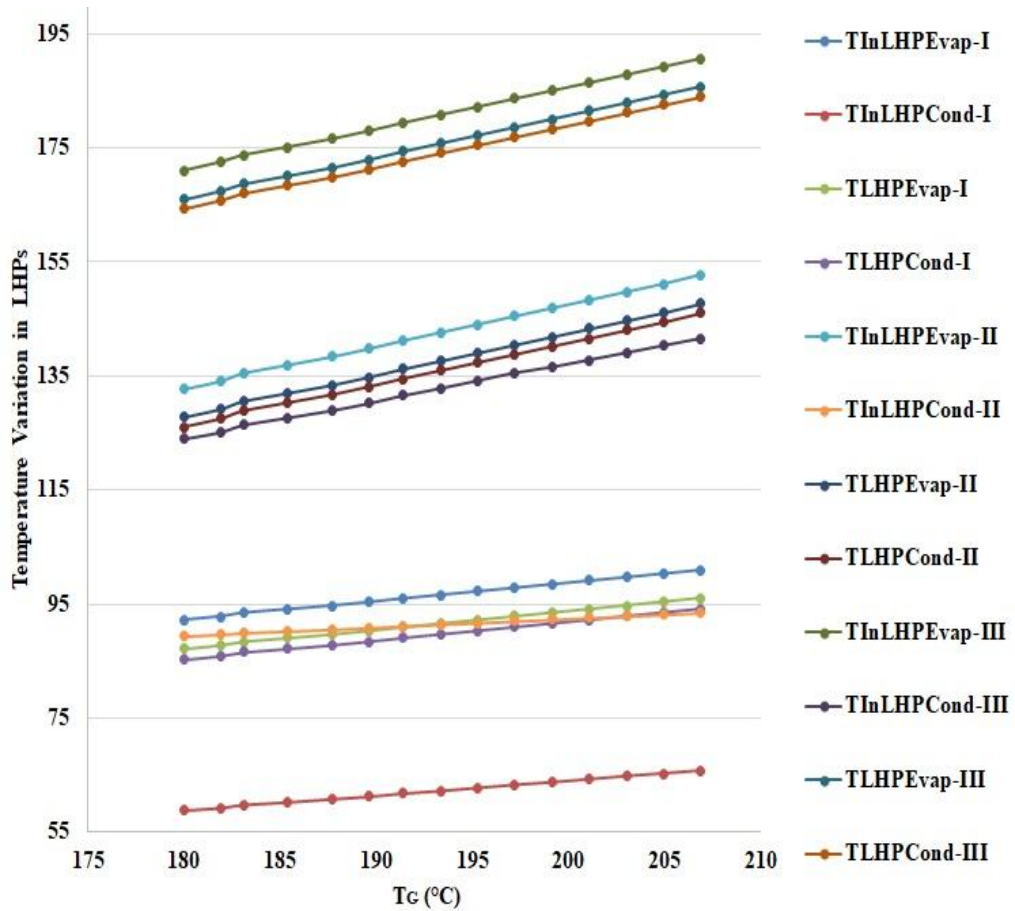


Fig 5.102: Temperature Variation in LHPs with Generator Temperature

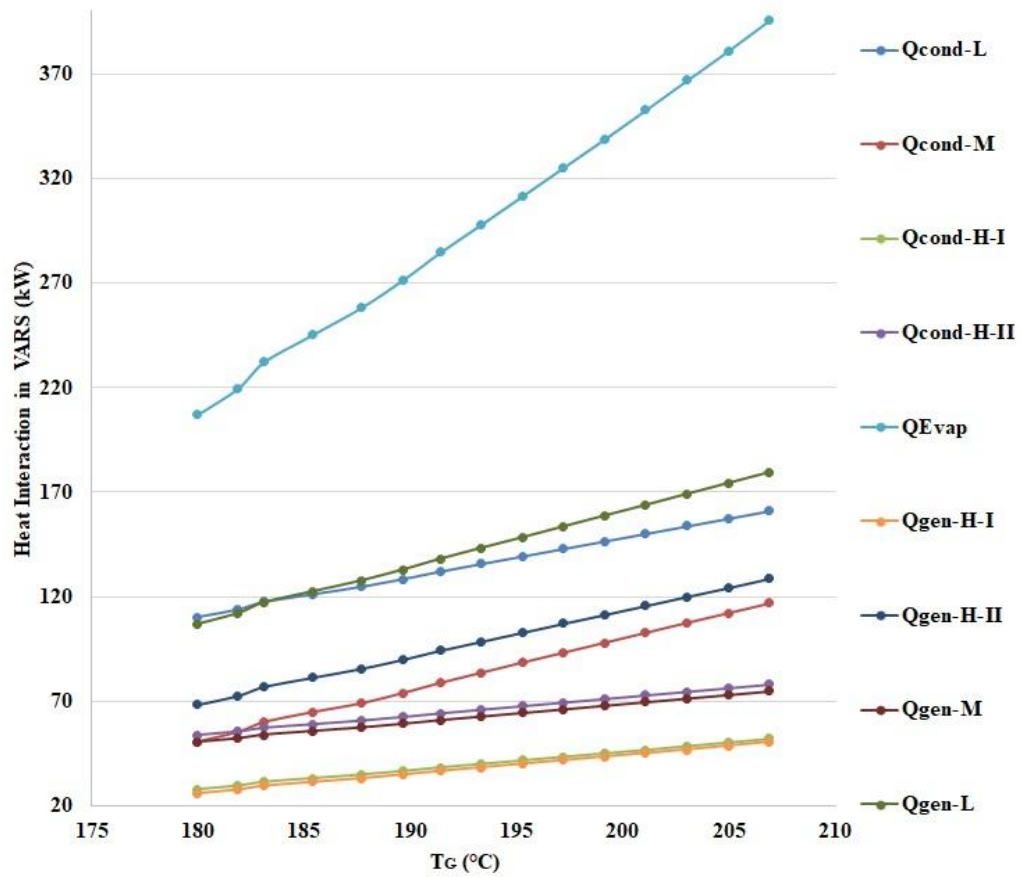


Fig 5.103: Heat Interaction in Quadruple Effect Modification-I with Generator Temperature

Similarly, Fig 5.101 shows the temperature variation in the Heat Exchanger – III & IV. The Exit of HEx – II is the inlet to the LHP - I and the Exit to the LHP – I is the inlet to the HEx – III. Similarly, the exit of the HEx-III is the inlet to LHP – II & the Exit of LHP-II is the inlet to the HEx – IV. The Mixture exiting the HEx – IV is further heated in the LHP – III and thereafter the Mixture enters the High Generator - II, thus making the system series quadruple effect system.

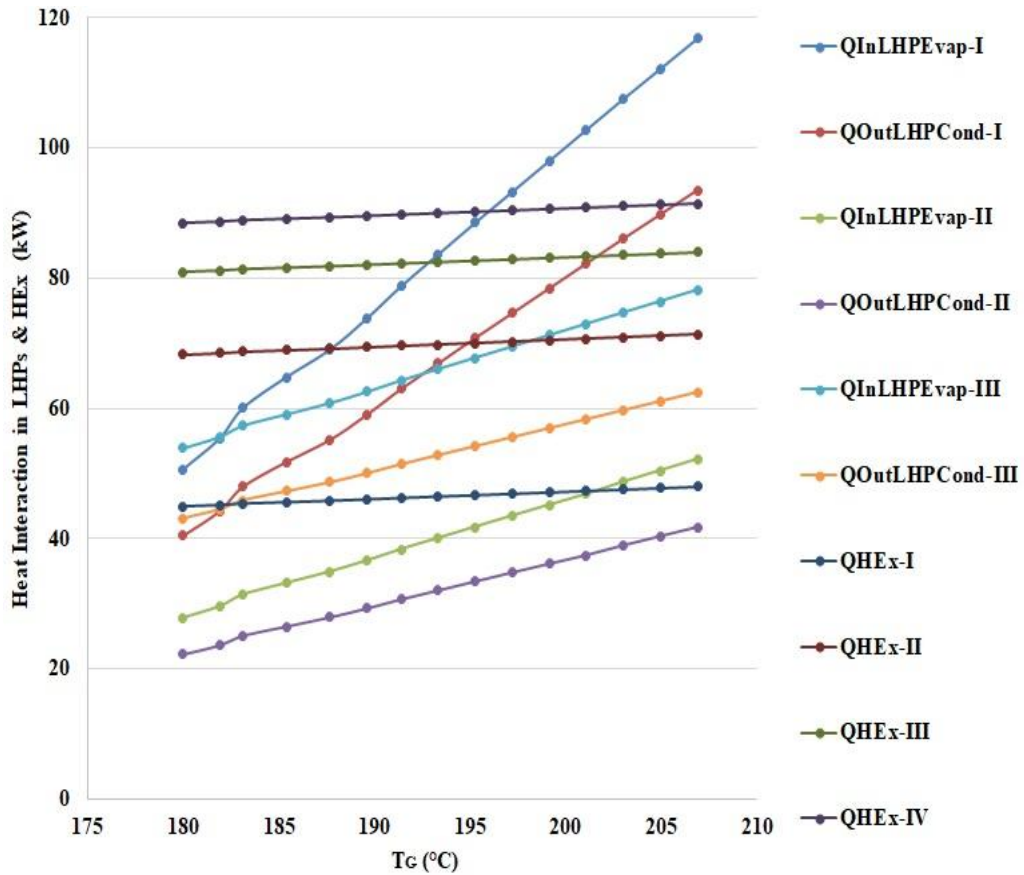


Fig 5.104: Heat Interaction in LHPs & HEX with Generator Temperature

The mixture enters the HEX – III at 81.2 – 85.7 °C and exits the HEX – III at 89.3 – 93.4 °C. Moreover, the Absorbent enters the HEX-III at 138.4 – 158.1 °C and exits at 119.2 – 128 °C. Similarly, the mixture inlet to the HEX – IV is at 119.2 – 128 °C, and the outlet to the HEX – IV is at 124 – 141.5 °C. Moreover, the Absorbent inlet to the HEX-IV is at 175.9 – 203 °C and the outlet is at 147.9 – 165.7 °C.

Furthermore, Fig 5.102 presents the Temperature variation in the LHP – I, II & III. It presents the temperature being attained at the Evaporators & Condensers of the LHPs owing to the vapour refrigerant. The Mixture Enters the LHP – I, II & III Condenser at 58.7 – 65.7 °C, 89.4 – 93.4 °C, and 124 – 147.7 °C respectively. Whereas, the Vapour Refrigerant enters the LHP - I, II & III Evaporator at 92.2 – 101 °C, 132.7 – 147.7 °C, and 171 – 190.7 °C. The Mixture leaves the LHP – I, II & III Condensers at 81.2 – 85.7 °C, 119.2 – 128 °C, and 154.4 – 168.3 °C. Consequently, the LHP- I, II & III Evaporator and Condenser Temperature attained are 87.1 – 96 °C, 127.7 – 147.7 °C & 166 – 185.7 °C and 85.2 – 94.11 °C, 126 – 146 °C & 164.3 – 184 °C respectively.

Performance Improvement of Vapour Absorption System Using Loop Heat Pipes

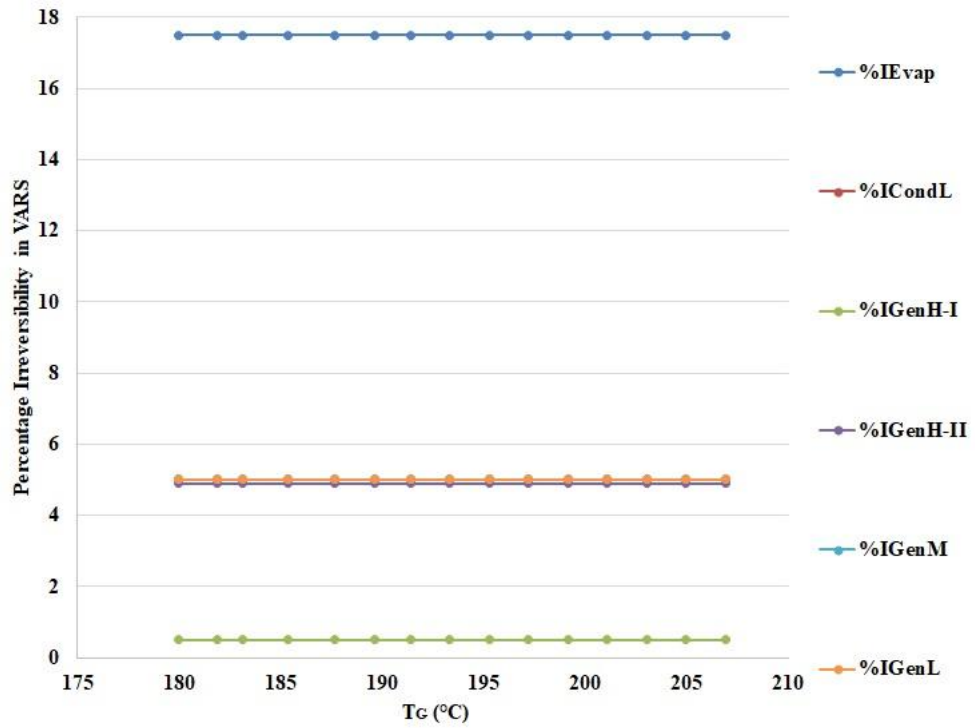


Fig 5.105: Percentage Irreversibility in Quadruple Effect Modification-I Components with Generator Temperature

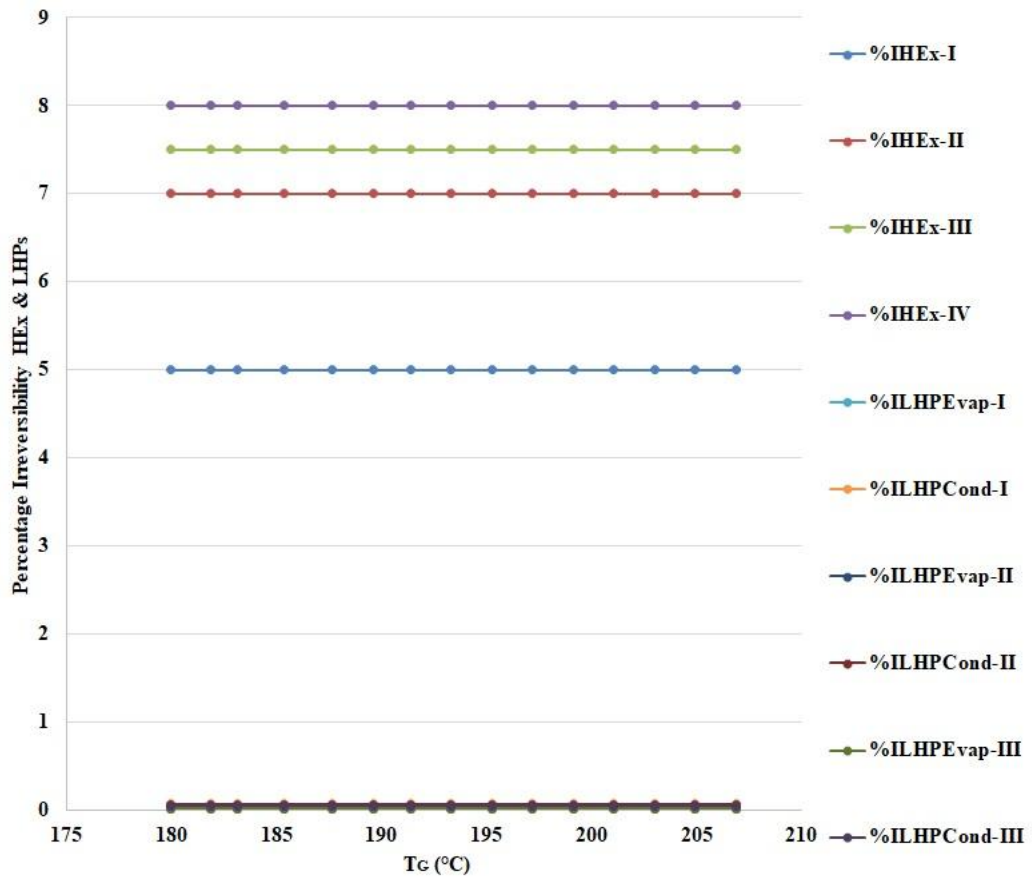


Fig 5.106: Percentage Irreversibility in LHP Components with Generator Temperature

The heat interaction in the VARS has been shown in Fig 5.103. It can be observed that the Heat Absorbed by the Evaporator is 207.2 – 395.6 kW. Also, the Heat Rejected in the Medium, High - I & High – II Condensers to the LHP – I, II & III are 50.6 – 116.8 kW, 27.82 - 52.2 kW & 54 – 78.1 kW respectively.

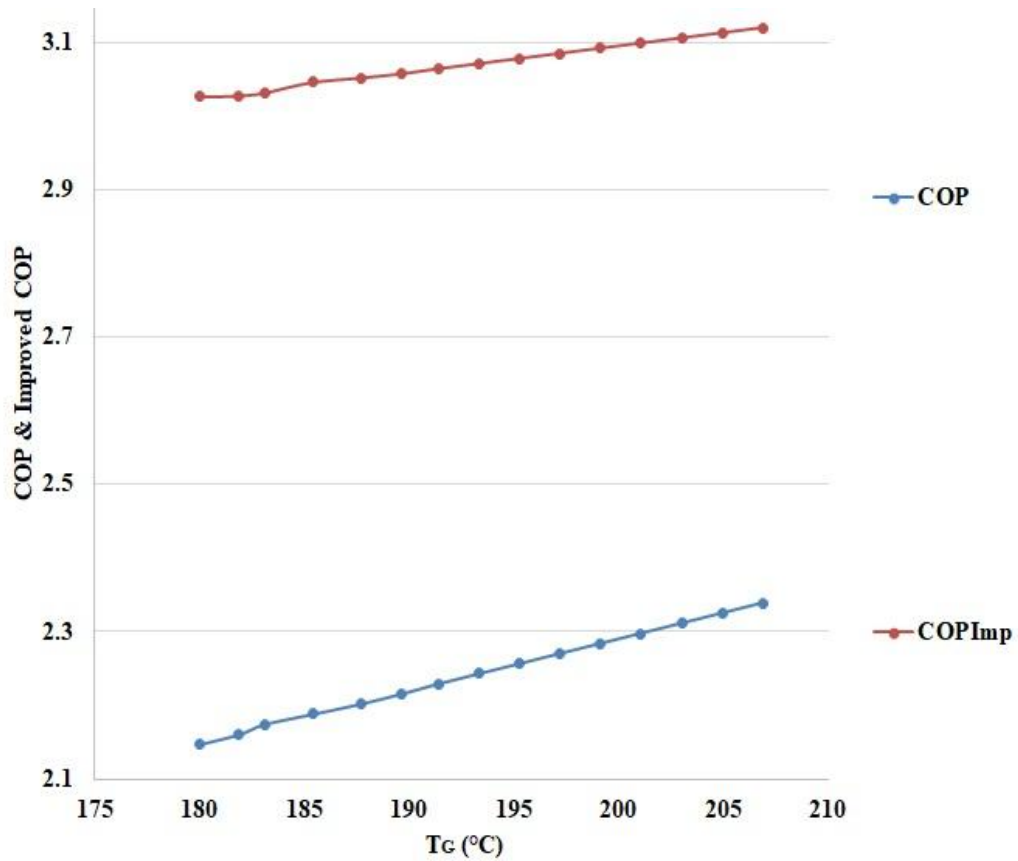


Fig 5.107: COP & Improved COP with Generator Temperature

Moreover, the Heat input to the Low, Medium, High – I & High – II Generators are 106.9 – 179.5 kW, 50.4 – 75 kW, 26 – 50.4 & 68.4 – 128.5 kW. Similarly, Fig 5.104 shows the Heat interaction in the LHP – I, II & III and HEx – I, II, III & IV. The heat interaction in the HEx – I, II, III & IV are 45 – 48 kW, 68.3 – 71.3 kW, 81 – 84 kW & 88.4 – 91.5 kW respectively. Moreover, the LHP – I, II & III Evaporator & Condenser extract 50.6 – 116.8 kW, 27.8 – 52.2 kW & 54 – 78.1 kW and 40.5 – 93.4 kW, 22.25 – 41.7 kW & 43.1 – 62.54 kW respectively. The Heat Input to the Original System High Generator -II was 96.5 – 169 kW.

Percentage Contribution to the Irreversibility of the system by the components of the VARS is presented in Fig 5.105. it has been calculated that the Evaporator, Condenser, High –I, High-II, Medium & Low Generators, and Low Condenser contribute approximately 17.5 %, 0.5 %, 4.89 %, 5 %, 5 %, and 5% to the total

irreversibility of the system. Similarly, the Percentage Irreversibility of the HEx – I, II, III & IV and for LHP – I, II & III have been discussed in Fig 5.106. It has been studied that for the HEx – I, II, III & IV the percentage contribution of irreversibility are 5%, 7%, 7.5% & 8%. Moreover, the LHP - I, II & III Evaporator & Condenser are 0.02 %, 0.015% & 0.013% and 0.065 % , 0.057 % & 0.046 % respectively.

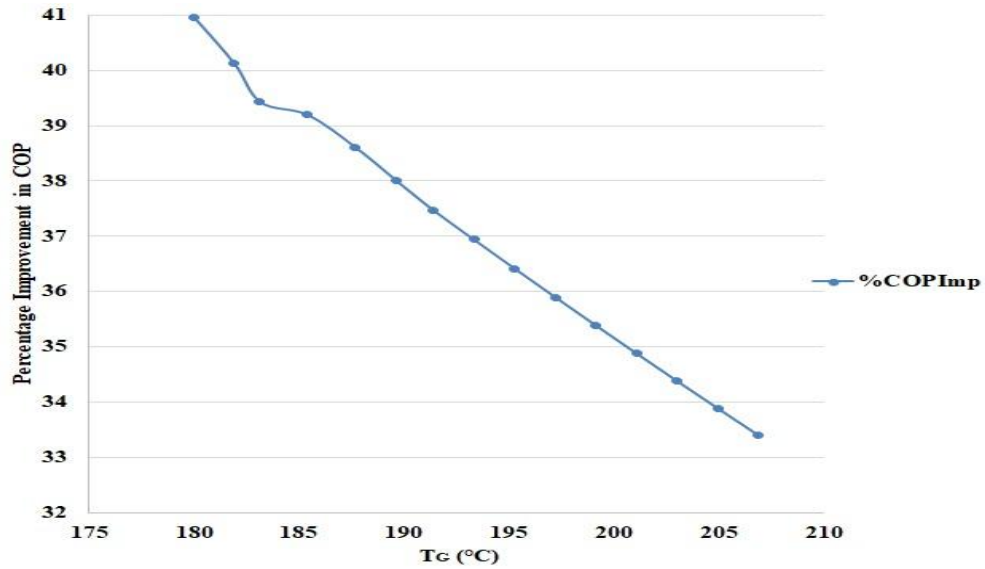


Fig 5.108: Percentage Improvement in COP with Generator Temperature

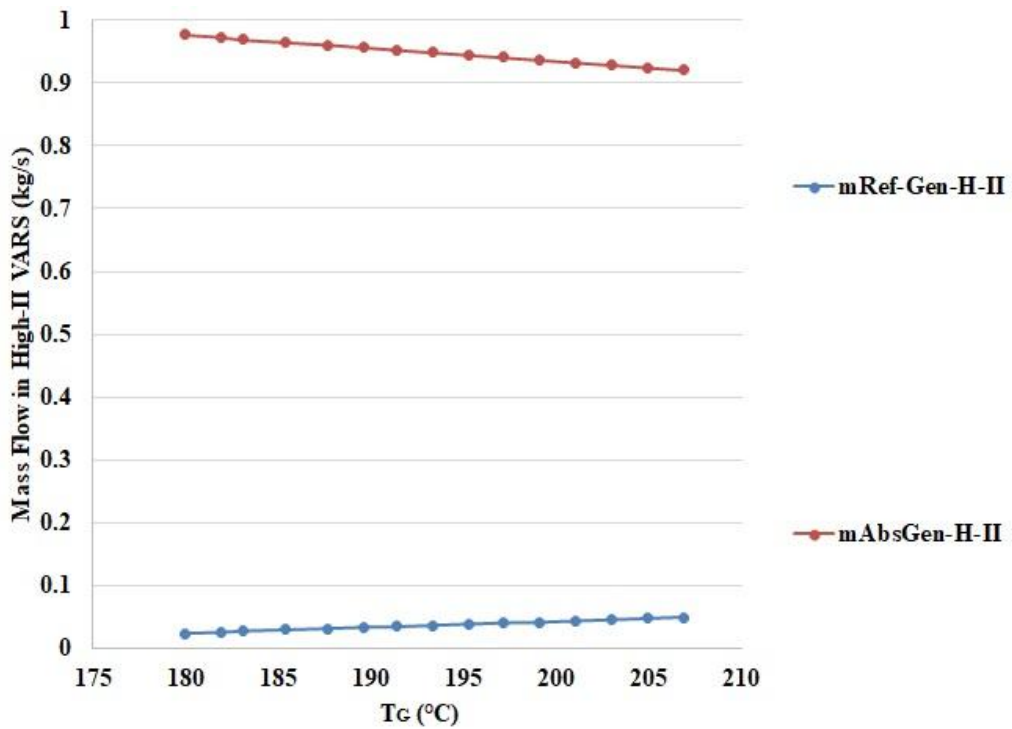


Fig 5.109: Mass Flow Rates in Quadruple Effect Modification-I High-II with Generator Temperature

The Improved COP & Percentage Improvement in the COP has been presented in Fig 5.107 & 5.108. The Original COP of the Quadruple Effect System was recorded as 2.14 – 2.3. Whereas, the COP obtained for the Modification-I was 3 – 3.1, which is an overall 41% - 33.4 % increment. It can be seen that the increase in COP and percentage increase in COP with the temperature rise is lesser for the Quadruple effect system when compared to the other lower effect systems.

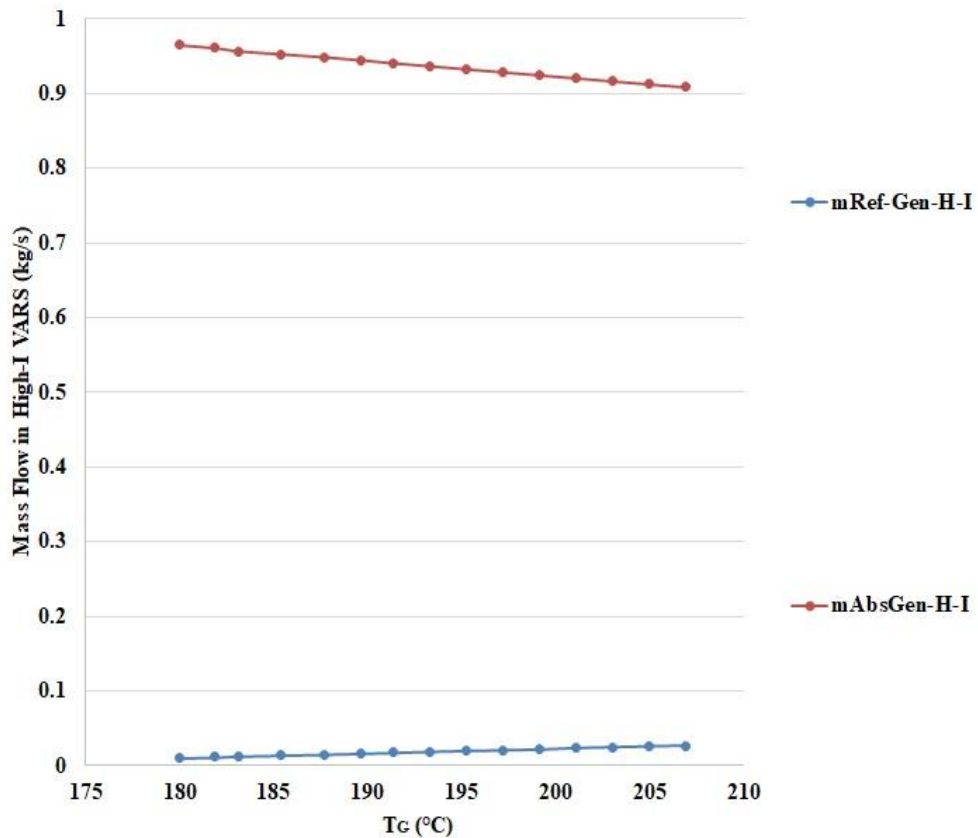


Fig 5.110: Mass Flow Rates in Quadruple Effect Modification-I High-I with Generator Temperature

The Mass Flow in the High-II, High-I, Medium, and Low generators are discussed from Fig 5.109 to 5.112. It has been mentioned that the Mass Flow rate of the Mixture from the Absorber is taken as 1kg/s. It can be observed from Fig 5.109 that the mass flow rate of Vapour Refrigerant leaving the High Generator –II is 0.023 – 0.05 kg/s, whereas, the Absorbent leaves at 0.97 – 0.951 kg/s. Furthermore, Fig 5.110 shows that the Vapour refrigerant leaves the High Generator – I at 0.01 – 0.027 kg/s and the absorbent leaves at 0.96 – 0.924 kg/s. Moreover, the vapour refrigerant leaves the Medium Generator at 0.02 – 0.03 kg/s and absorbent at 0.94 – 0.88 kg/s as shown in Fig 5.111. The lowest generator evaporates the refrigerant from the mixture

Performance Improvement of Vapour Absorption System Using Loop Heat Pipes

and exits it at 0.04 – 0.05 kg/s and the absorbent is finally transferred to the absorber at 0.9 – 0.83 kg/s. The total mass flow of refrigerant in the Evaporator for the generation of Refrigeration is 0.09 – 0.16 kg/s from Fig 5.112.

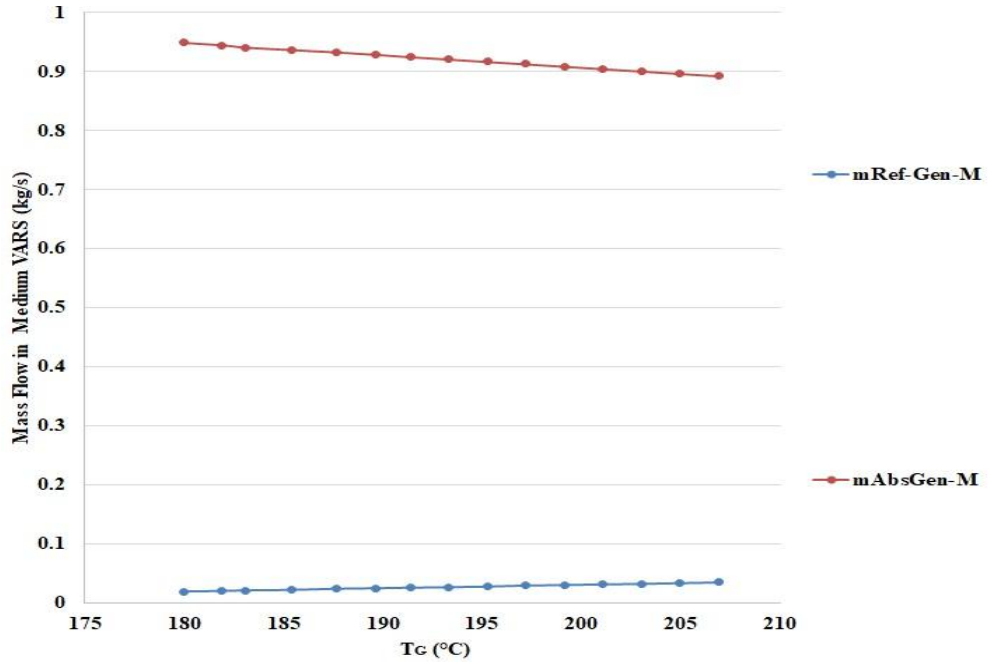


Fig 5.111: Mass Flow Rates in Quadruple Effect Modification-I Medium with Generator Temperature

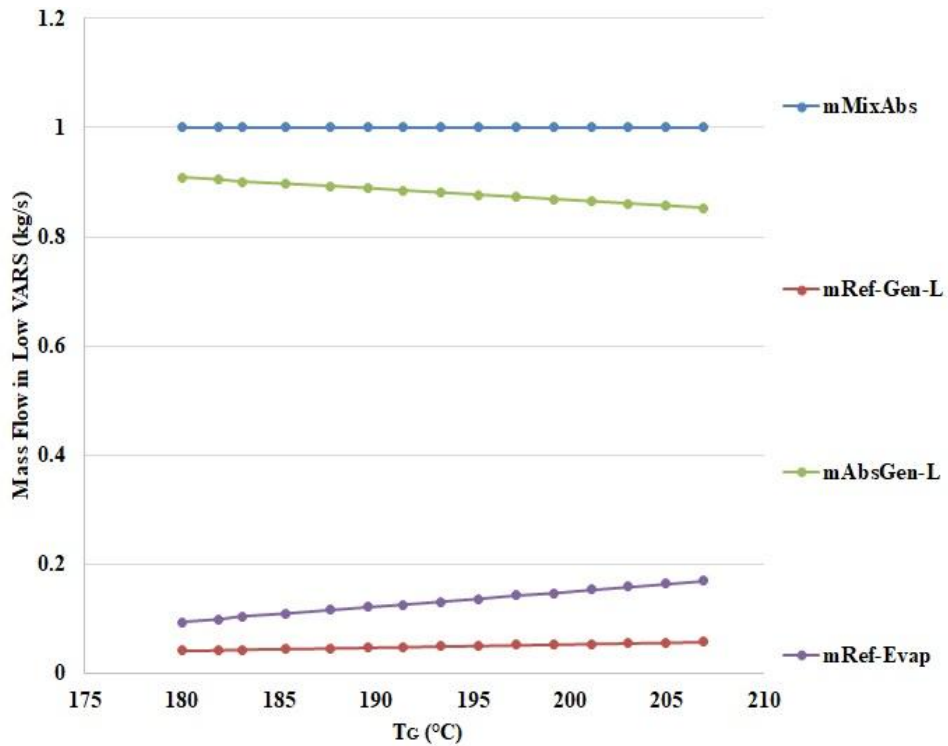


Fig 5.112: Mass Flow Rates in Quadruple Effect Modification-I Low with Generator Temperature

5.5.2. Quadruple Effect VARS Modification-II

The Quadruple Effect Modification-II has been obtained by Replacing HEx- I, II, III & IV with LHP - I, II, IV & VI in this system. The LHP-I, II & III have been designated as LHP – III, V & VII. The changes in the different states and improvements in COP have been studied in this section for Modification-II.

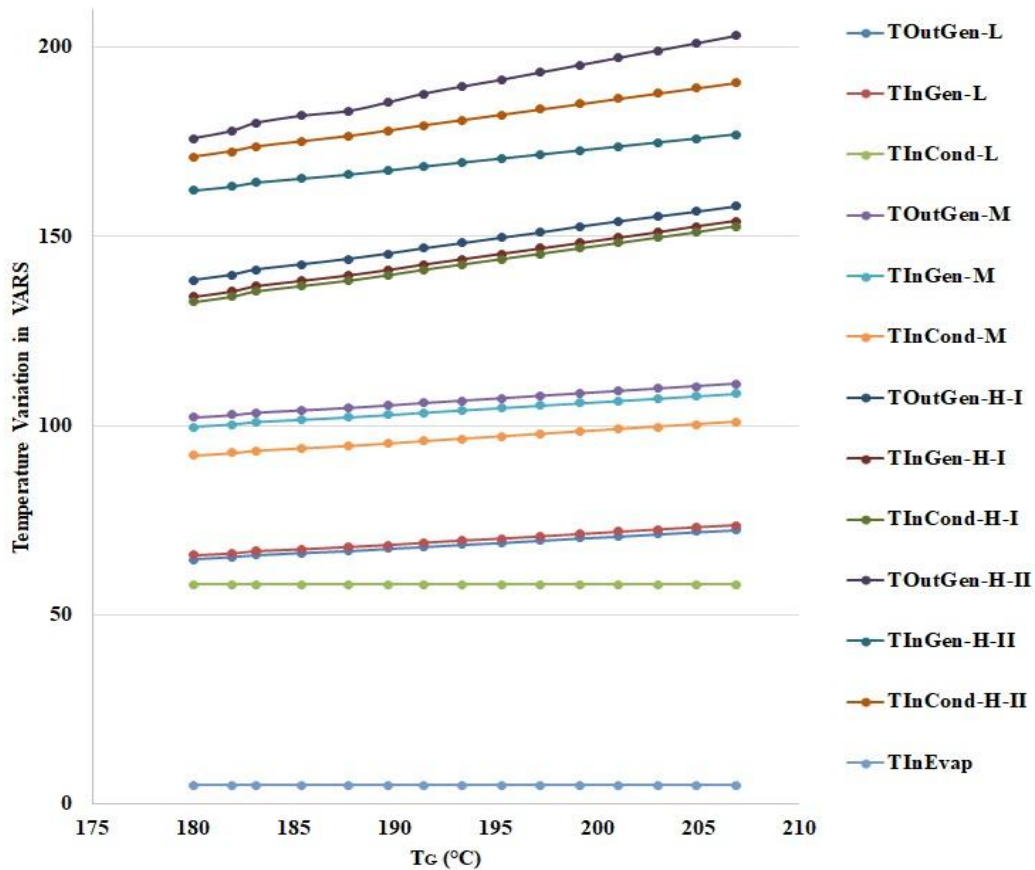


Fig 5.113: Temperature Variation in Quadruple Effect Modification-II with Generator Temperature

Fig 5.113 shows the temperature variation in the VARS. The input to the High Generator – II can be observed as 162.2 – 176.8 °C. Whereas, Fig 5.114 presents the Temperature variation in the LHP - III, V, VII. The Mixture enters the LHP –III, V & VII Condenser at 65.3 – 73 °C, and 99.3 – 103.8 °C & 137.8 – 157.2 °C respectively. The Mixture exits the LHP – III, V & VII Condenser at 83 – 87.6 °C, 109.2 – 114.2 °C & 162.2 – 176.8 °C respectively. All the LHPs are in series from Absorber to the High Generator-II. The LHP – III, V & VII Evaporator and Condenser Temperatures are the same as explained for Modification-I.

Similarly, Fig 5.115 presents the Temperature variation in the LHP-IV & VI. The Absorbent enters & leaves the LHP – IV and VI Evaporator at 138.3 – 158.1 °C & 119.2 – 128 °C and 175.9 – 203 °C & 147.7 – 165.7 °C respectively. Furthermore, Mixture inlet & outlet of the LHP – IV and VI Condenser are at 83 – 87.6 °C & 99.3 – 103.8 °C and 109.2 – 114 °C & 137.8 – 157.2 °C respectively. The LHP IV & VI Evaporator & Condenser Temperatures are 104.3 – 108.8 °C & 106.2 – 110.7°C and 114.69 – 164.15 °C & 137.8 – 157.2 °C respectively.

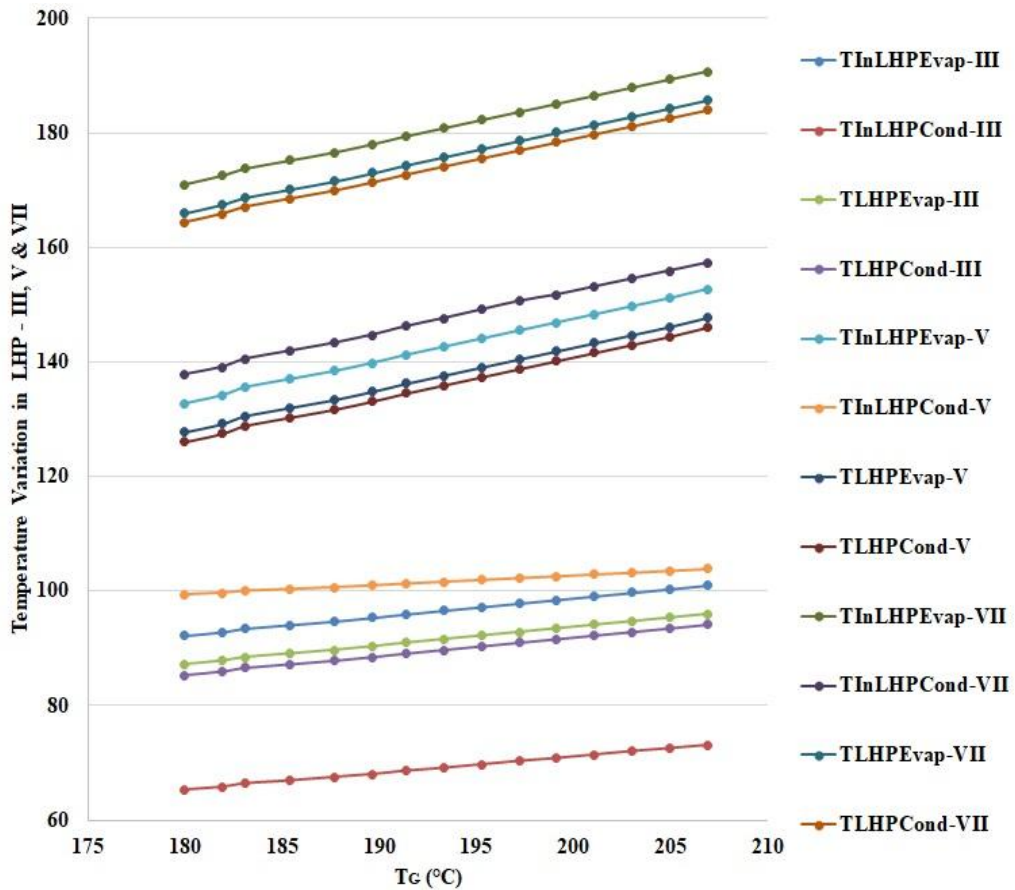


Fig 5.114: Temperature Variation in LHP-III, V & VII with Generator Temperature

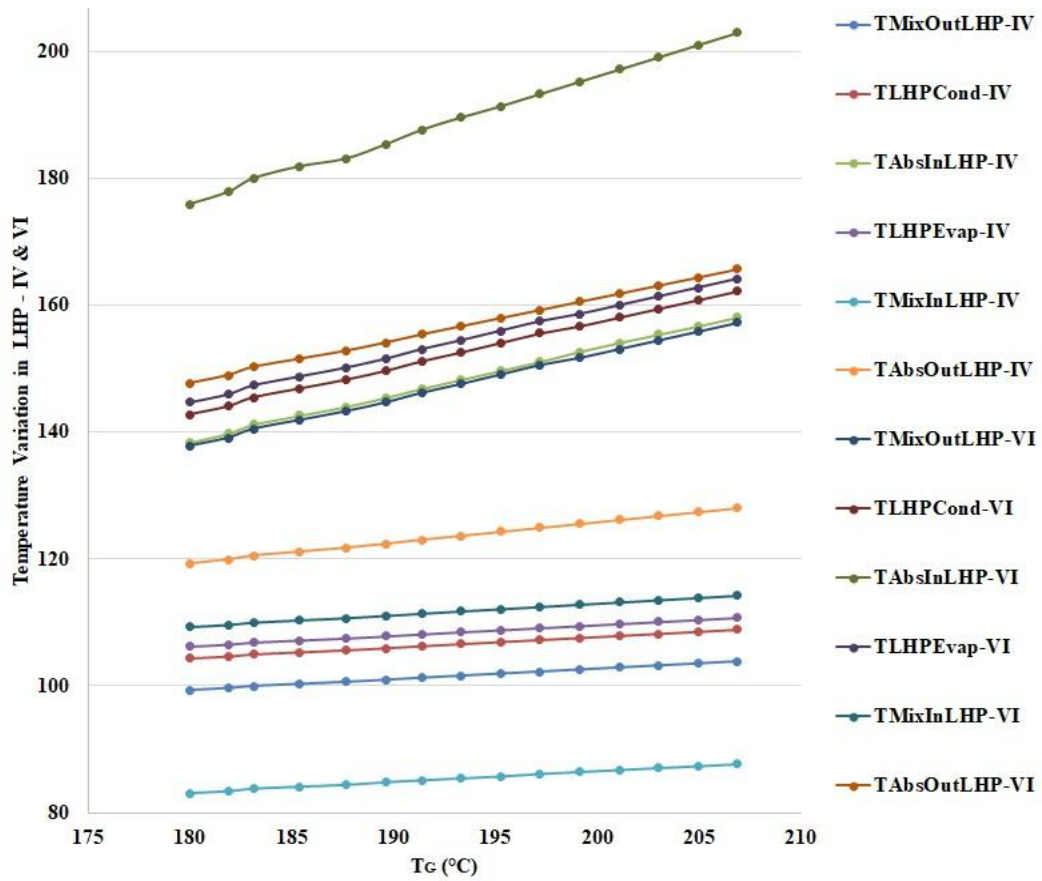


Fig 5.115: Temperature Variation in LHP-IV & VI with Generator Temperature

Furthermore, Fig 5.116 discusses the Temperature variation in the LHP-I & II. The Absorbent enters & leaves the LHP – I and II Evaporator at 64.2 – 72 °C & 48.2 – 49.8 °C and 102.2 – 111 °C & 83 – 87.6 °C respectively. Furthermore, the Mixture inlet & outlet of the LHP – I and II Condenser are at 30 °C & 43.2 – 47.1 °C and 48.2 – 49.8 °C & 65.3 – 73 °C respectively. The LHP I & II Evaporator & Condenser Temperatures are 49.4 – 53.3 °C & 48.2 – 52.1 °C and 72.1 – 82 °C & 70.3 – 78 °C respectively.

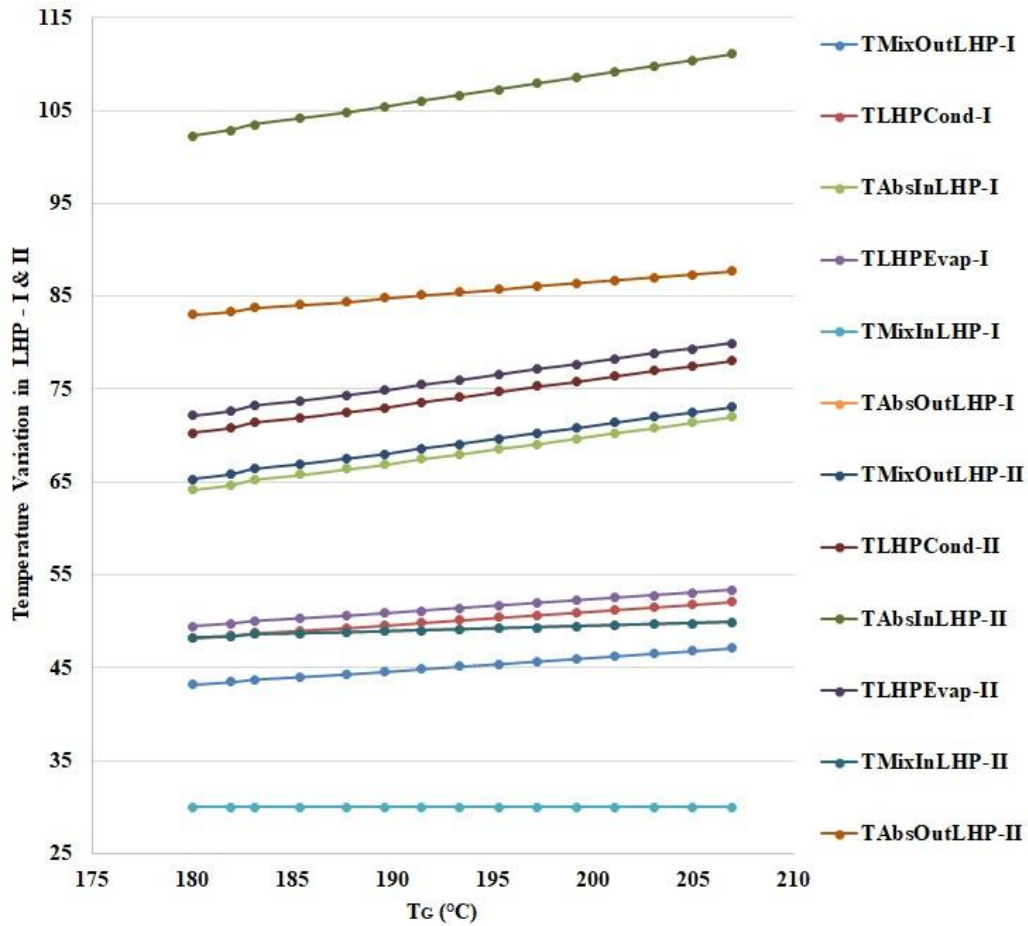


Fig 5.116: Temperature Variation in LHP- I & II with Generator Temperature

The Heat Input requirement has been reduced owing to the replacement of HEx from 68.4 - 128 kW to 64.1 – 122.2 kW as shown in Fig 5.117. This results in a further increase in the COP of the system. The Percentage Contribution of the LHP Components to the Irreversibility has been presented in Fig 5.118 & Fig 5.119. It can be seen that the Evaporator of LHP – I, II, III, IV, V, VI & VII is 1.7 %, 2.4%, 0.019%, 2.2 %, 0.014, 32.5% & 0.012% respectively. Moreover, for the Condenser of LHP – I, II, III, IV, V, VI & VII it has been observed to be 2.5 %, 3.9 %, 0.06%, 3.7 %, 0.05, 4.2 % & 0.04% respectively.

Performance Improvement of Vapour Absorption System Using Loop Heat Pipes

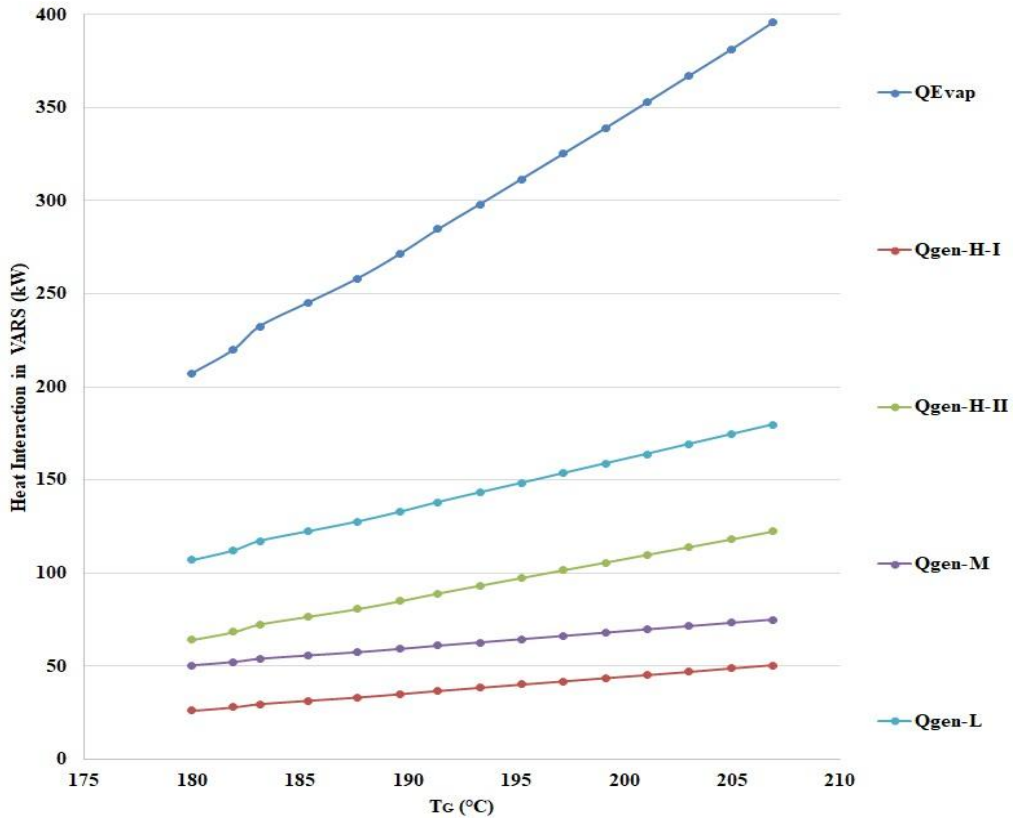


Fig 5.117: Heat Interaction in Quadruple Effect Modification-II with Generator Temperature

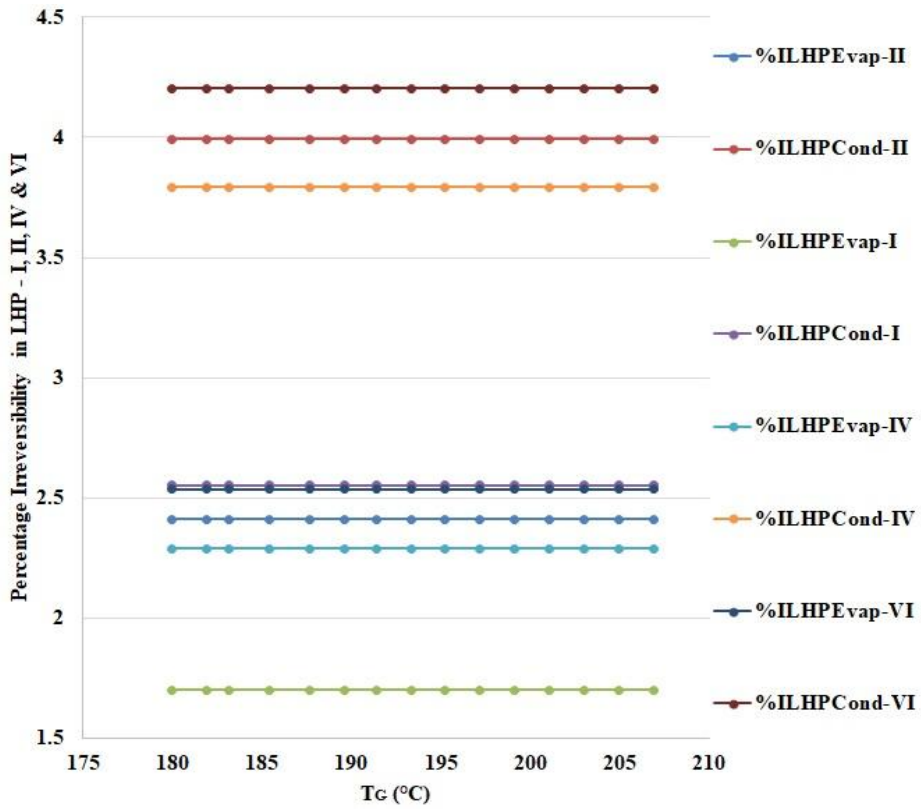


Fig 5.118: Percentage Irreversibility in LHP I, II, IV & VI Components with Generator Temperature

Performance Improvement of Vapour Absorption System Using Loop Heat Pipes

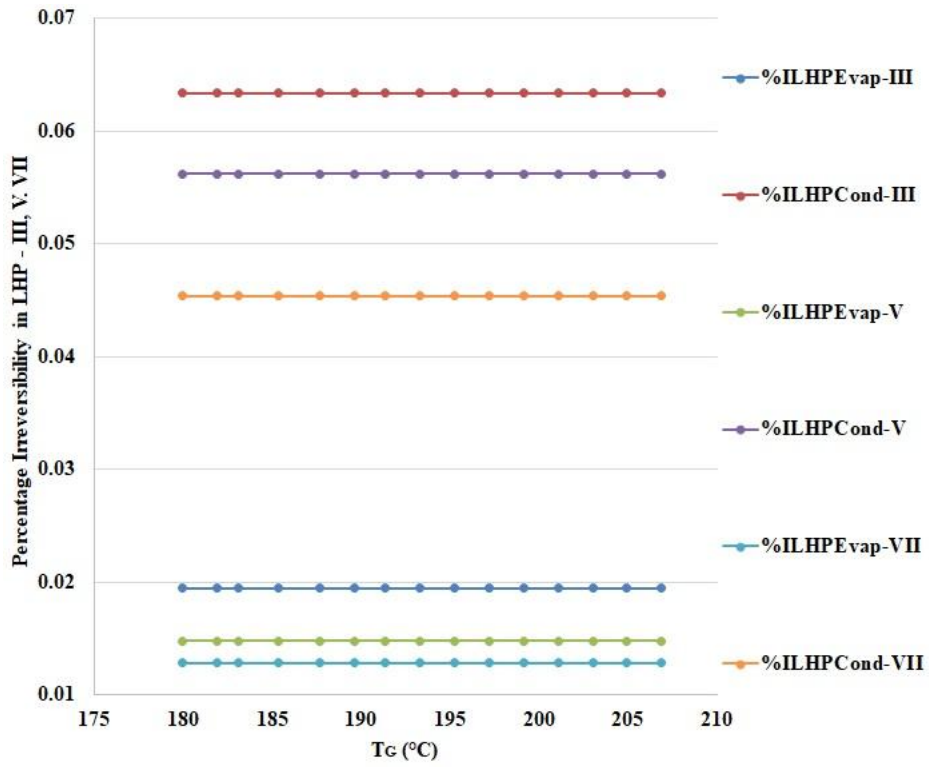


Fig 5.119: Percentage Irreversibility in LHP V, VI & VII Components with Generator Temperature

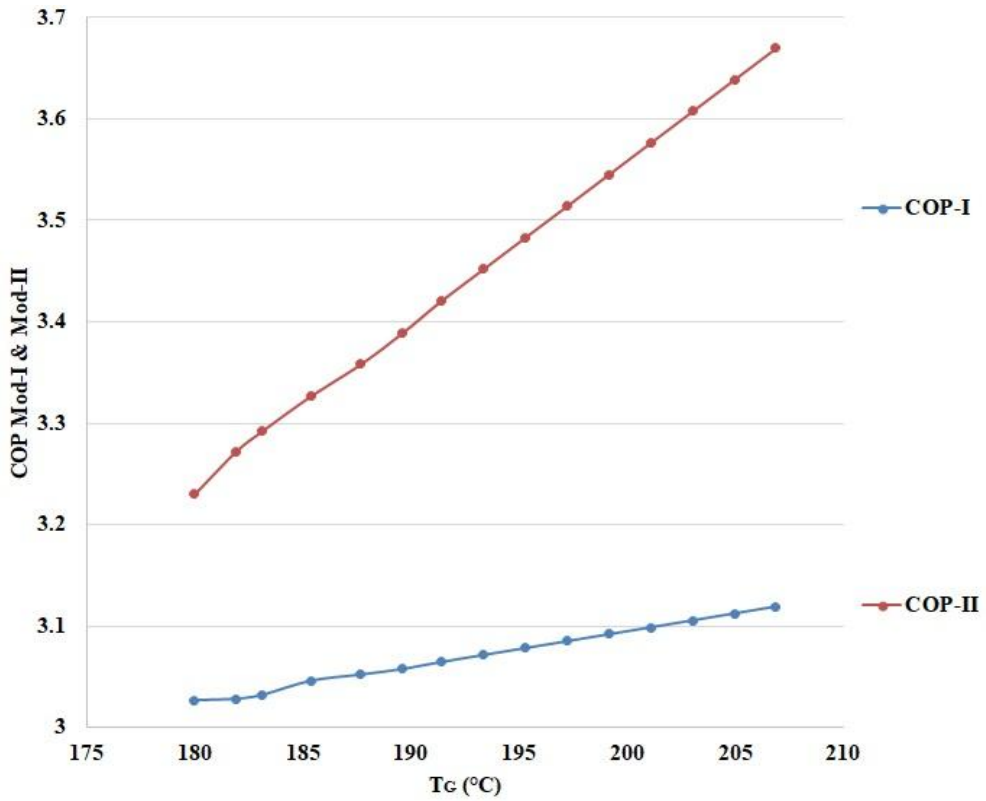


Fig 5.120: COP & Improved COP with Generator Temperature

The Increased COP of Modification-II & COP of Modification-I has been presented in Fig 5.121. The COP for Modification-II is 3.2 – 3.6 whereas for the Modification-I COP was 3 – 3.1. This is a total 6 % to 15% increase in the COP as presented in Fig 5.122.

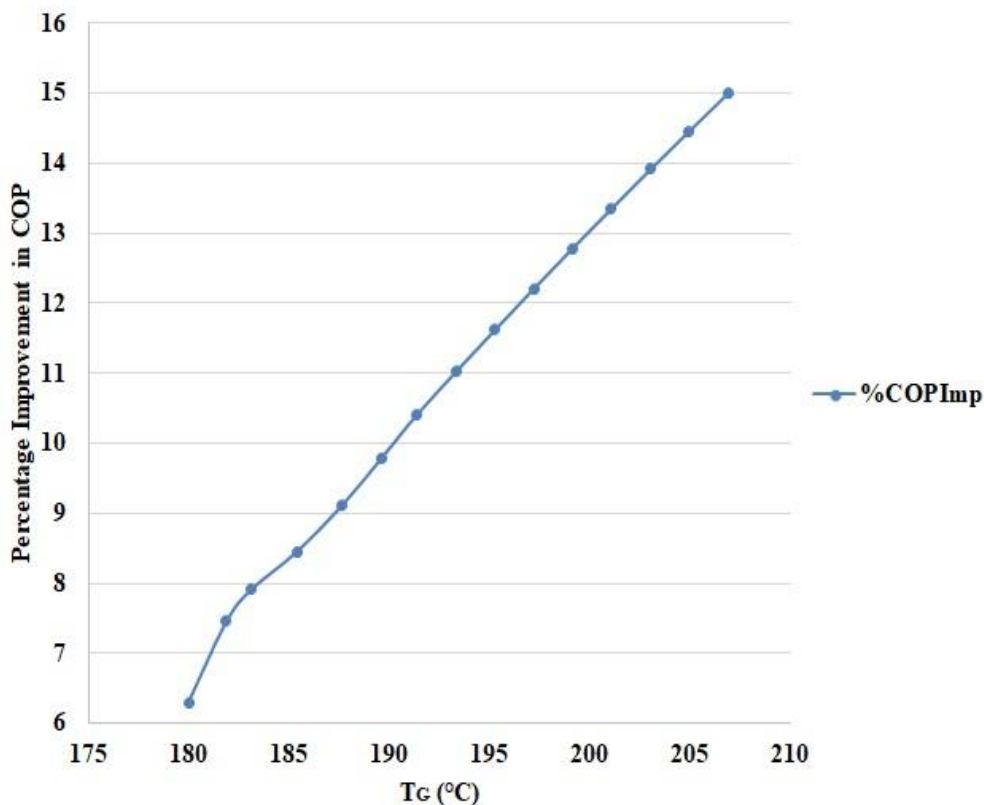


Fig 5.121: Percentage Improvement in COP with Generator Temperature

The Comparison of Performance Parameters of Quadruple Effects of the Proposed Work with Published work has been presented in Table 5.14. It can be seen that the performance of the proposed system is better than the published work under similar inputs.

Table 5.15: Comparison of Modified Quadruple Effect VARS

Parameters	Chaudhari et. al. (2019) [180]	Proposed Work	
		Modification-I	Modification-II
Mass Flow Rate of Mixture from Absorbent (kg/s)	10.7	1	1

Performance Improvement of Vapour Absorption System Using Loop Heat Pipes

Mass Flow Rate of Refrigerant in Evaporator (kg/s)	0.25	0.093	0.093
Generator Temperature (°C)	180	180	180
Evaporator Temperature (°C)	5	5	5
Absorber Temperature (°C)	30	30	30
Q_{Evap} (kW)	2385	207.2	207.2
$Q_{Cond-H-II}$ (kW)	-	54	54
$Q_{Evap-H-I}$ (kW)	-	27.8	27.8
Q_{Cond-M} (kW)	-	50.6	50.6
$Q_{Gen-H-II}$ (kW)	1047	68.4	64.1
COP	2.27	3.02	3.23
η_{II}	47.72	79.54	84.9

Table 5.15 presents the Irreversibility of the Proposed Work.

Table 5.16: Irreversibility in Quadruple Effect Components

Parameters/ Irreversibility	Proposed Work			
	Modification-I		Modification-II	
	kW	%	kW	%
I_{Evap}	5.7	17.5	5.7	17.5
$I_{Gen-H-II}$	1.59	4.89	1.59	4.89
$I_{Gen-H-I}$	0.163	0.5	0.163	0.5
I_{Gen-M}	1.63	5	1.63	5
I_{Gen-L}	1.63	5	1.63	5
I_{Cond-L}	1.63	5	3.76	8.1

Performance Improvement of Vapour Absorption System Using Loop Heat Pipes

I_{HEX-I}	1.63	5	-	-
I_{HEX-II}	2.28	7	-	-
$I_{HEX-III}$	2.4	7.5	-	-
I_{HEX-IV}	2.6	8	-	-
I_{Abs}	11.73	36	11.73	36
LHP-I	-	-	2.20	4.73
LHP-II	-	-	3.15	6.77
LHP-III	0.027	0.085	0.027	0.085
LHP-IV	-	-	2.84	6.11
LHP-V	0.023	0.072	0.023	0.072
LHP-VI	-	-		
LHP-VII	0.02	0.059	0.02	0.059
Refrigeration Capacity (RC) (kW)	207.02			
Total Irreversibility (kW)	32.6		31.8	

5.5.3. Combined Quadruple Effect VARS & GPC

The Quadruple Effect Mod – II has been connected with GPC through LHP – VIII which extracts the Heat from the GPC Exhaust and transfers the heat to the High Generator – II. Fig 5.122 projects the feasible number of the resent Modification-II system that could be operated in connection with GPC. It can be seen that the Number is 01. Similarly, Fig 5.123 presents the Temperature variation in the GPC & Generator Temperature of VARS. It can be seen that the Peak Temperature of GPC, Exhaust Temperature of GPC, and High Generator temperature of VARS are 927 – 1227 °C, 299.6 – 360.4 °C, and 180 – 205 °C.

Moreover, Fig 5.124 presents the Temperature Variation in the LHP – VIII. The LHP Evaporator & Condenser temperature attained are 293.8 – 354.6 °C & 288 – 348.8

°C. Fig 5.125 discusses the Contribution of the LHP-VI to the Irreversibility in the System. The LHP-VIII Evaporator & Condenser contribute by 0.02 % & 6.1 %.

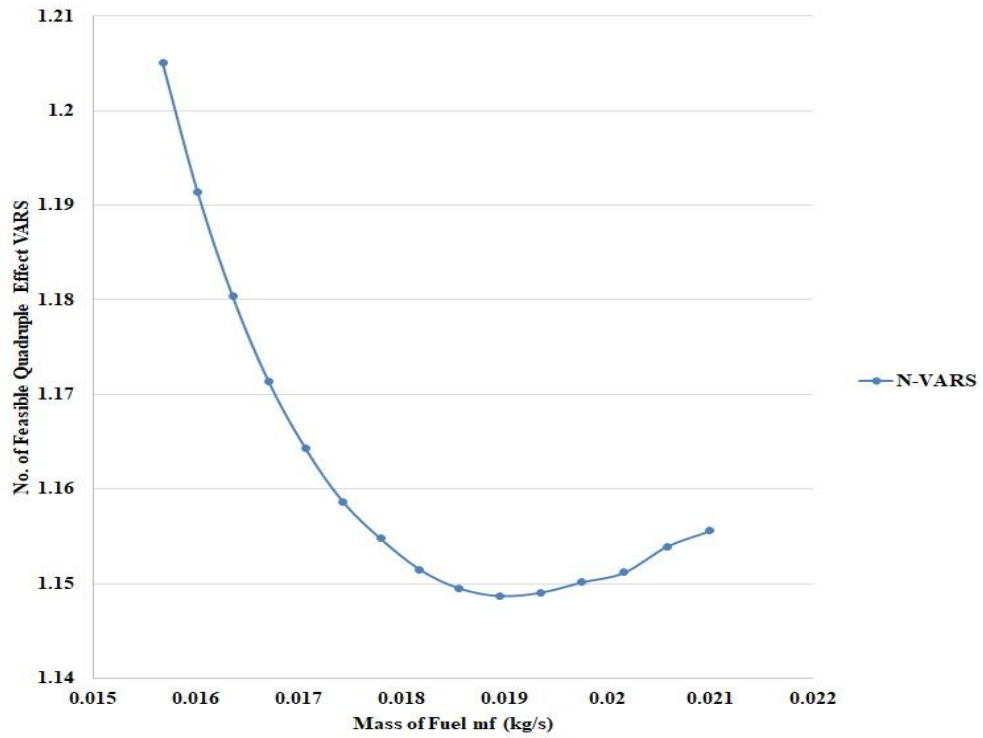


Fig 5.122: No. of Feasible Quadruple Effect Modification-II with Mass of Fuel in GPC

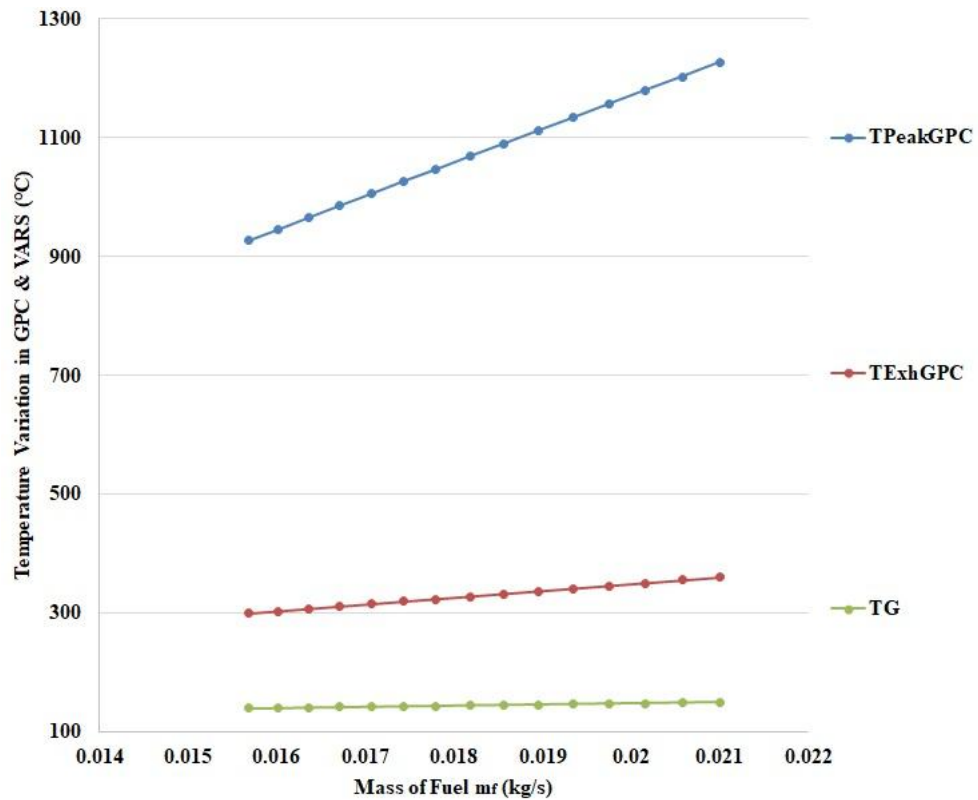


Fig 5.123: Temperatures of GPC and Generator Quadruple Effect Modification-II with Mass of Fuel in GPC

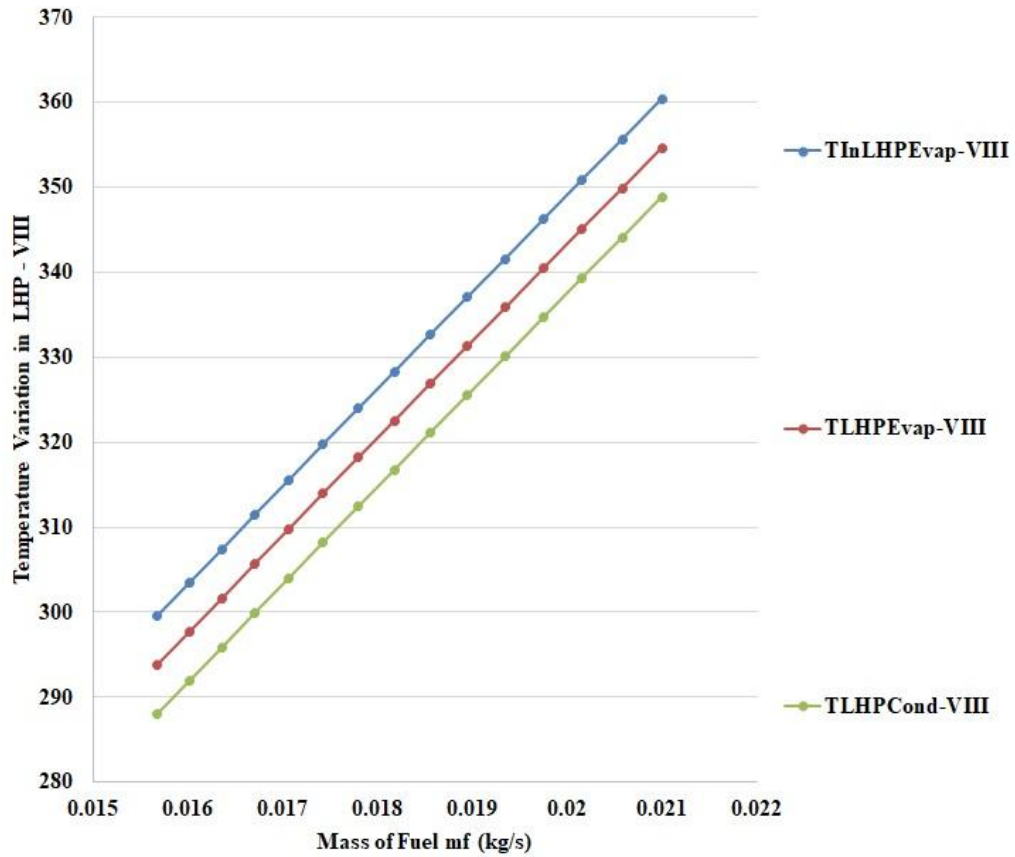


Fig 5.124: Temperatures of LHP-VIII with Mass of Fuel in GPC

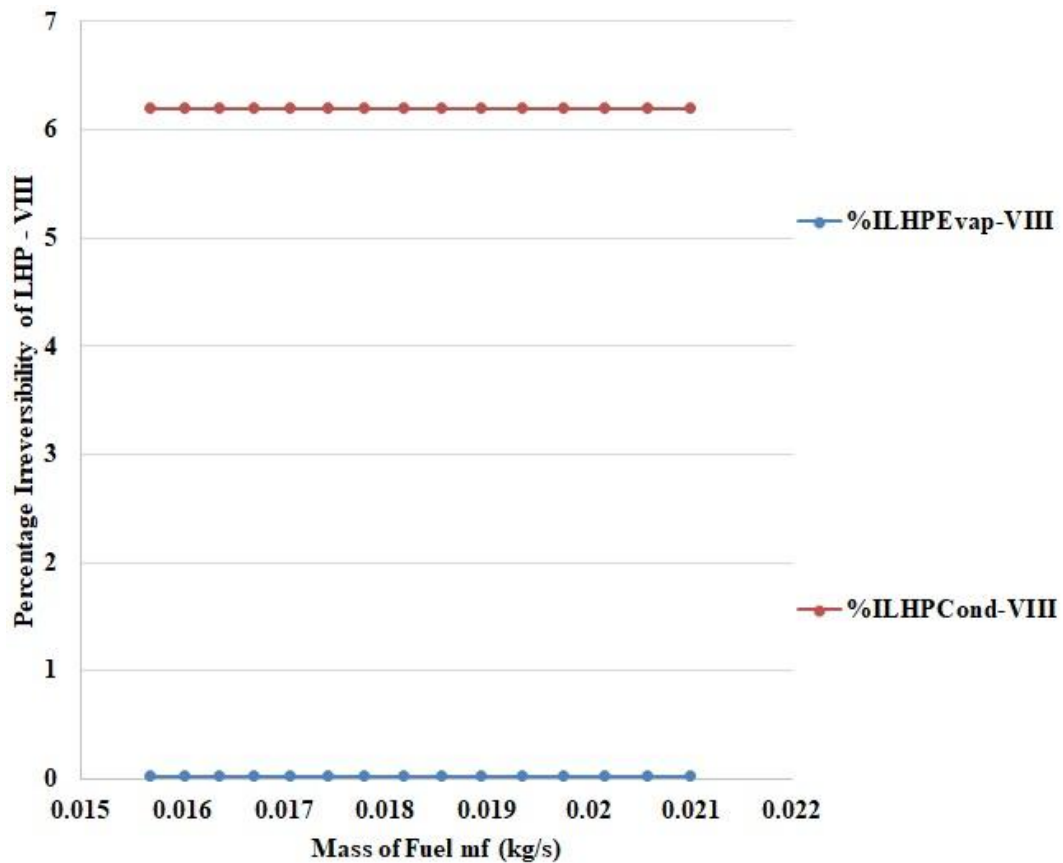


Fig 5.125: Percentage Irreversibility of LHP-VIII with Mass of Fuel in GPC

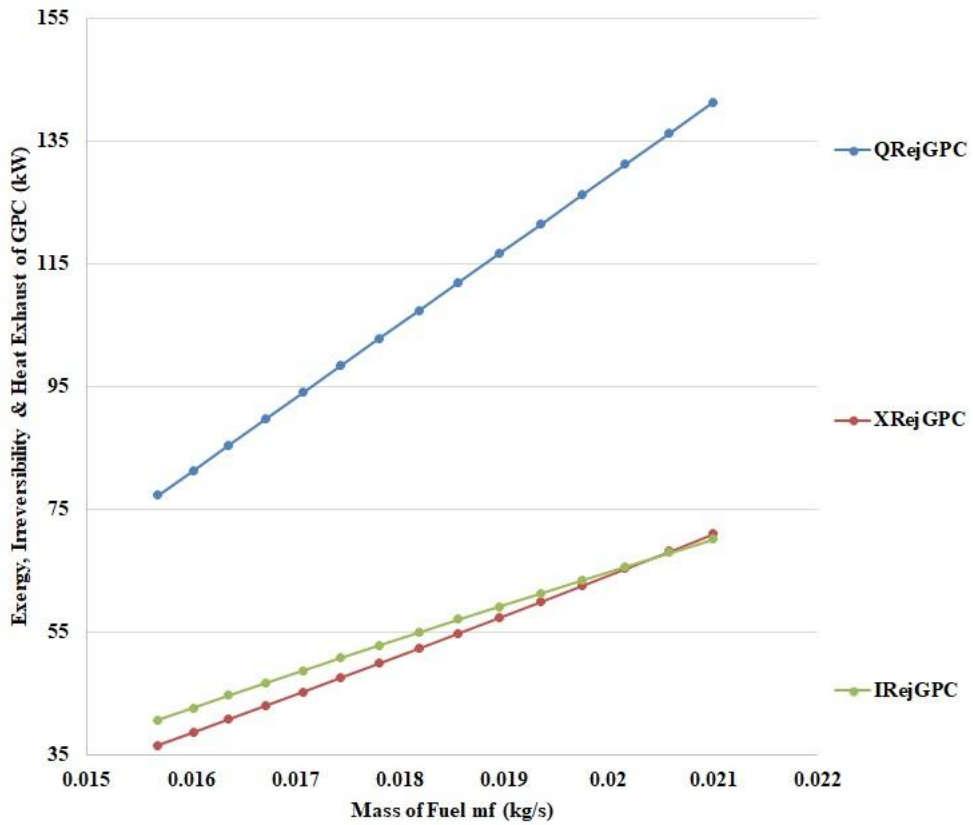


Fig 5.126: Exergy, Irreversibility, and Heat Rejected from GPC Exhaust Quadruple Effect Modification-II with Mass of Fuel in GPC

Fig 5.126 presents the Heat Rejected in Exhaust, Exergy & Irreversibility related to the system. It can be seen that the Heat, Exergy & Irreversibility are 77.3 – 141.3 kW, 35.58 – 71 kW & 40.72 – 70.19 kW respectively.

5.6: Combined ORC & GPC (Ankit Dwivedi, et. al. 2021) ^[189]

Software-based simulations have been prepared on an engineering equation solver based on the modeled equations of GPC, LHP & ORC. The Peak Temperature of the GPC (T_5), Condenser Pressure of ORC (P_9), and working fluids for LHP & ORC have been kept as the input variables for this research work. The input heat source that has been obtained for the Boiler of ORC is in the range of 400 K- 450 K (127 °C-177 °C) as a constant source owing to the condensation in the LHP. All 4 working fluids selected for this range are compatible. For the construction of such LHP, Silica, Copper, and Stainless Steel can be selected. Different performance parameters such as Net-Work Output of ORC (W_{NetR}), Exergy (X) & Irreversibility (I) of different components, Corresponding Efficiencies & Effectiveness of the Components (η & ϵ), and Mass Flow rates of the working fluids have been closely recorded and studied through different simulations and the results have been presented and explained in the following sections. Table 5.17 presents the Input variable for the ORC.

Table 5.17: Input Variables for ORC Analysis

Sl. No.	Input Parameters	Data
1.	Working Fluid	R124, R125, R134a, R152a, R290, R600
2.	Condenser & Boiler Effectiveness, ϵ	0.7
3.	Condenser Temperature, T_C	35 °C
4.	Pressure Ratio	5
5.	A/F Ratio	300
6.	Peak Temperature of GPC, T_5	1500K

5.6.1. Peak Temperature of GPC (T_5) as Input Variable:

The Peak Temperature (T_5) has been varied from 1400 K to 1800K. In Fig 5.127 and Fig 5.128 comparative study of Exergy and Irreversibility has been recorded for the

Condenser and Boiler of the ORC for 6 selected refrigerants. For the Condenser of ORC, it can be seen that the Irreversibility range from 10kW to 50 kW with R125 having the highest value, whereas, the top most Exergy results with R600 with a range from 40 kW to 130 kW.

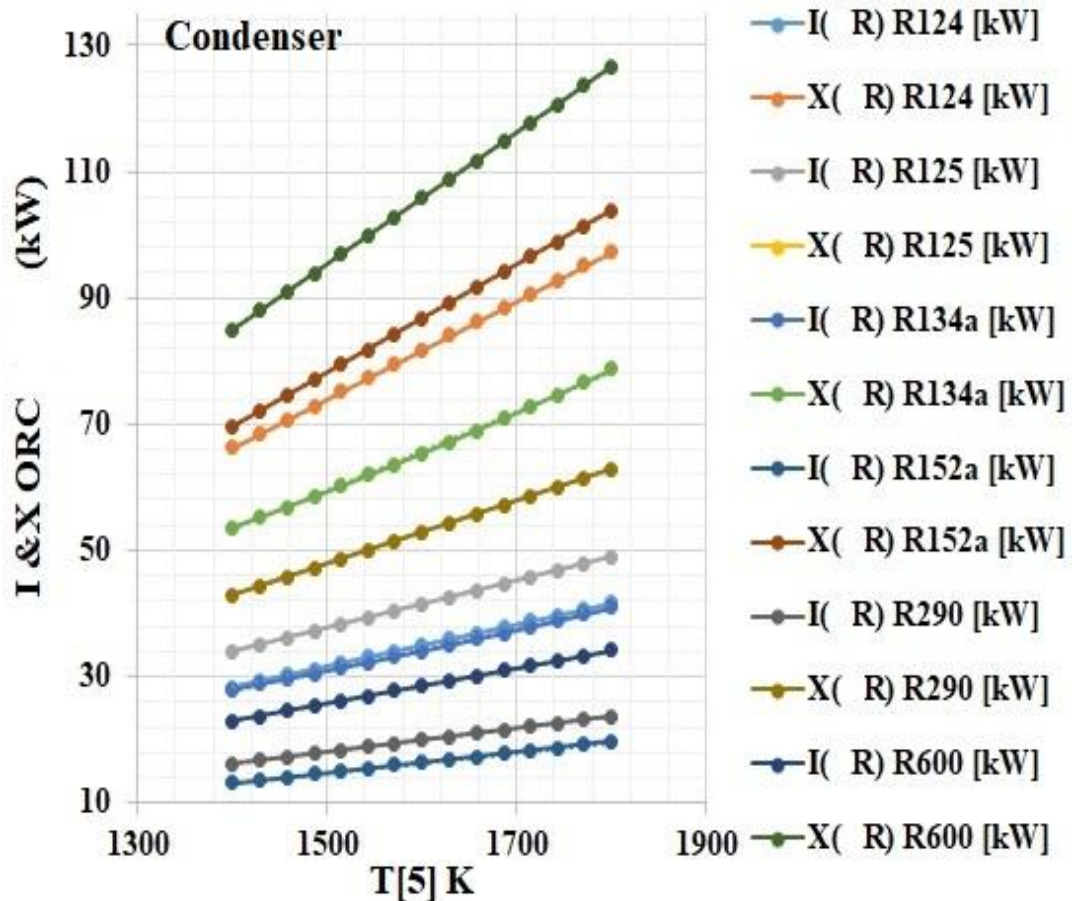


Fig 5.127: Irreversibility & Exergy associated with the Condenser of the ORC

The comparative study of Exergy and Irreversibility has been recorded for the Condenser and Boiler of the ORC for 6 selected refrigerants. It can be assessed that the Irreversibility of the Boiler for all the refrigerants lies within the range of 10kW to 30 kW. Moreover, R125 shows the maximum Irreversibility in the condenser whereas R600 has the lowest. The exergy of the condenser varies from a range of 40 kW to 190 kW. The highest Exergy has been observed for R125 whereas the lowest has been observed for R600.

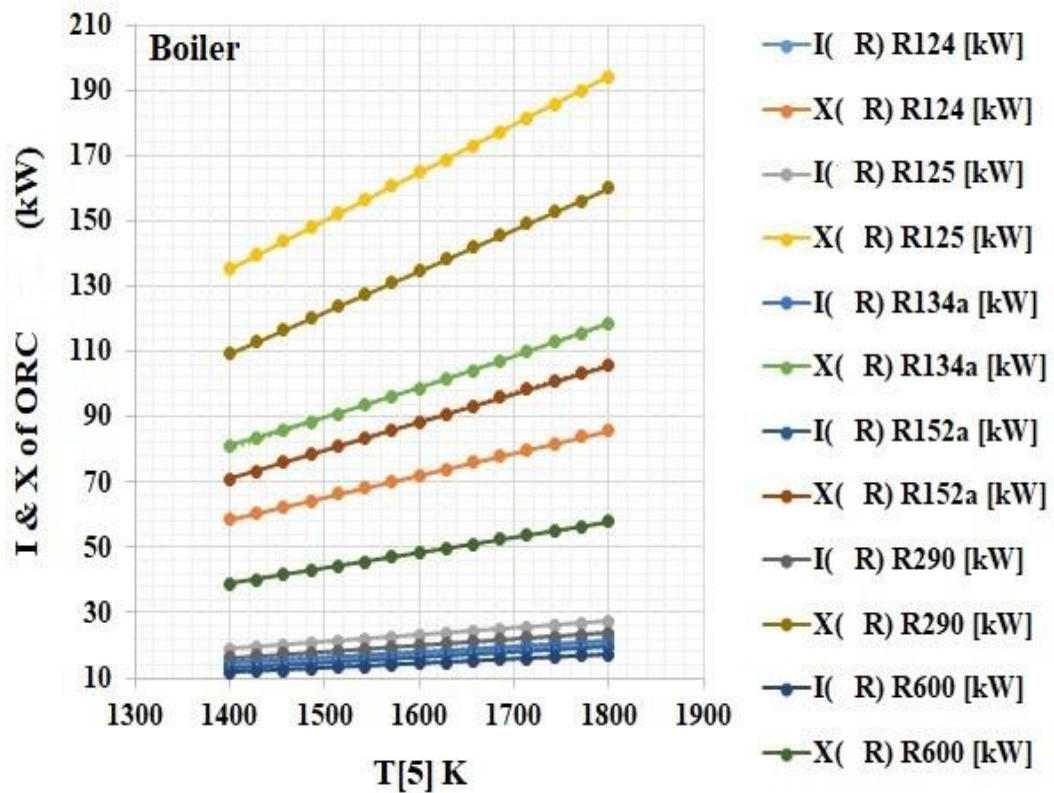


Fig 5. 128: Irreversibility & Exergy associated with the Boiler of the ORC

The following Fig 5.129 & Fig 5.130 represents the results of Exergy & Irreversibility associated with the LHP Condenser & Evaporator. It can be seen that the exergy is being transferred from the evaporator to the condenser with high effectiveness. Moreover, sufficient exergy is available at the condenser to transfer to the Boiler of the ORC to complete the connections. It can again be seen that R600 has generated the best possible results for the subject input variables.

In the Evaporator the range for Exergy is from 700 kW to 1150 (kW), whereas, the Irreversibility ranges from 150 kW to 350 kW. On the other hand, for the Condenser, the Exergy available varies from 550 kW to 900 kW and Irreversibility from 60 kW to 250 (kW).

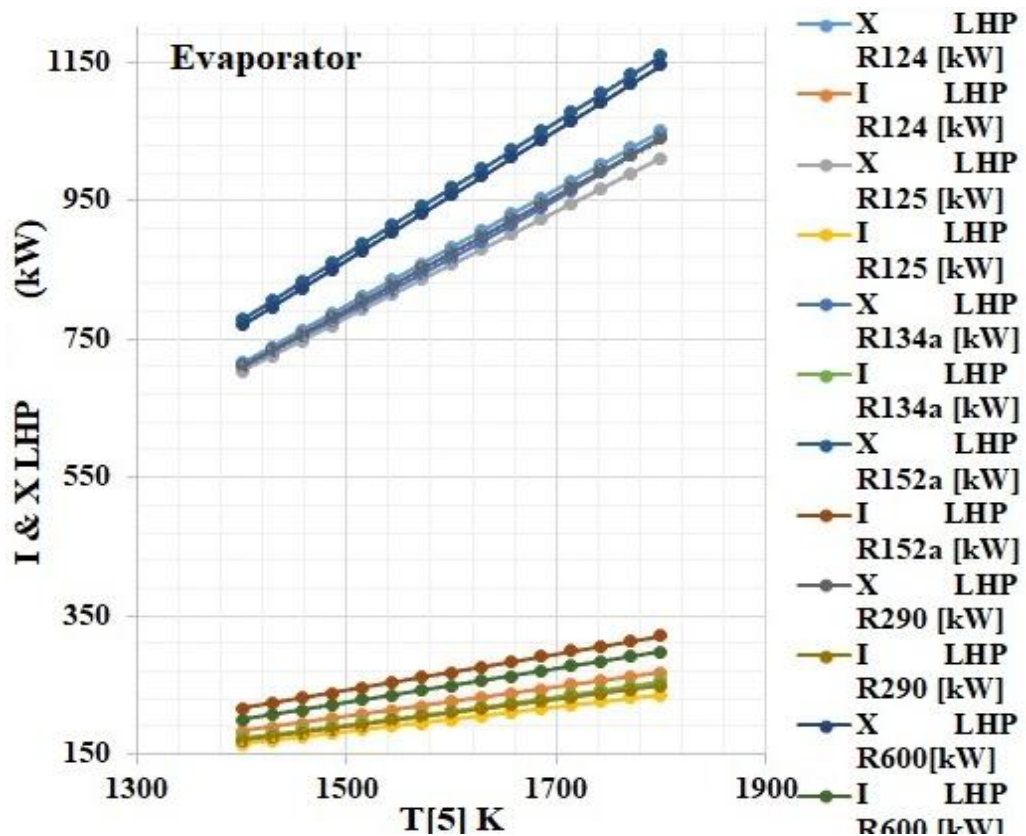


Fig 5.129: Irreversibility & Exergy associated with the Evaporator of the LHP

It can be seen that the LHP effectively with high efficiency interconnects the two cycles and high work output can be achieved with maximum waste heat utilization. Refrigerants being used for ORC can also be seen affecting the overall performance of the heat exchange taking place within the Condenser of the LHP. For R125, an exceptional ratio of transfer of Exergy from Evaporator to Condenser can be seen to have taken place.

The First Law & Second Law Efficiency for the ORC has been presented in Fig 5.131. The range for First Law Efficiency is from 25% to 32% with the maximum value for R125 whereas the Second Law Efficiency has the range of 73 % to 80% with R152a having maximum results.

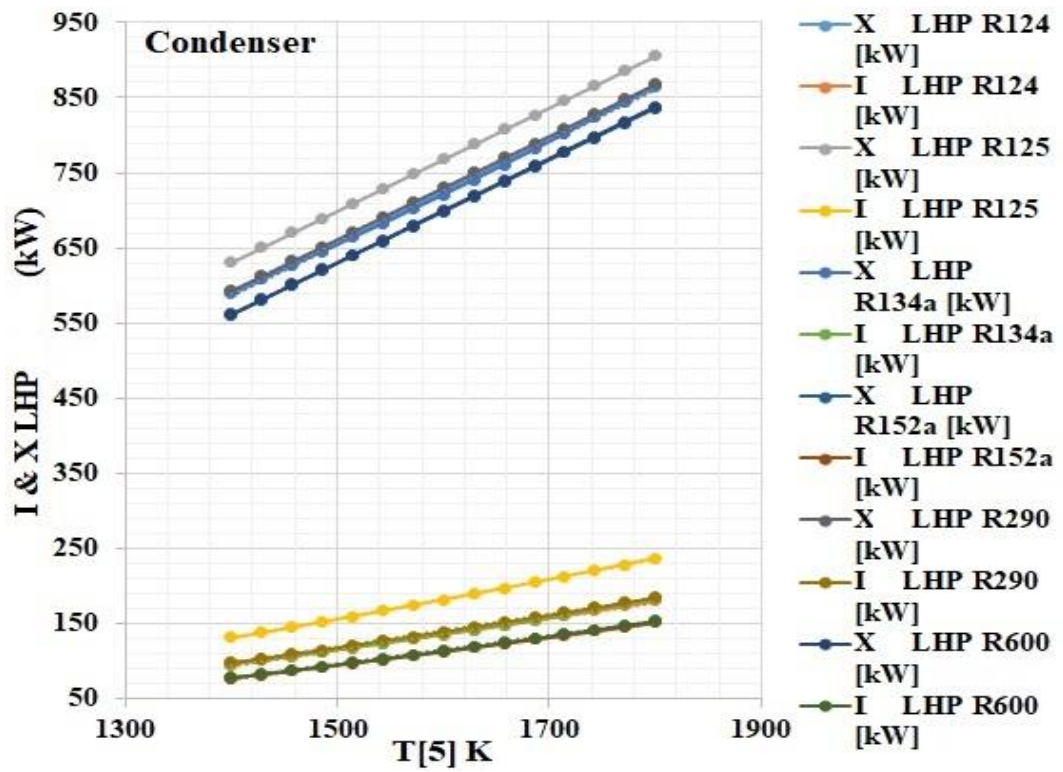


Fig 5.130: Irreversibility & Exergy associated with the Condenser of the LHP

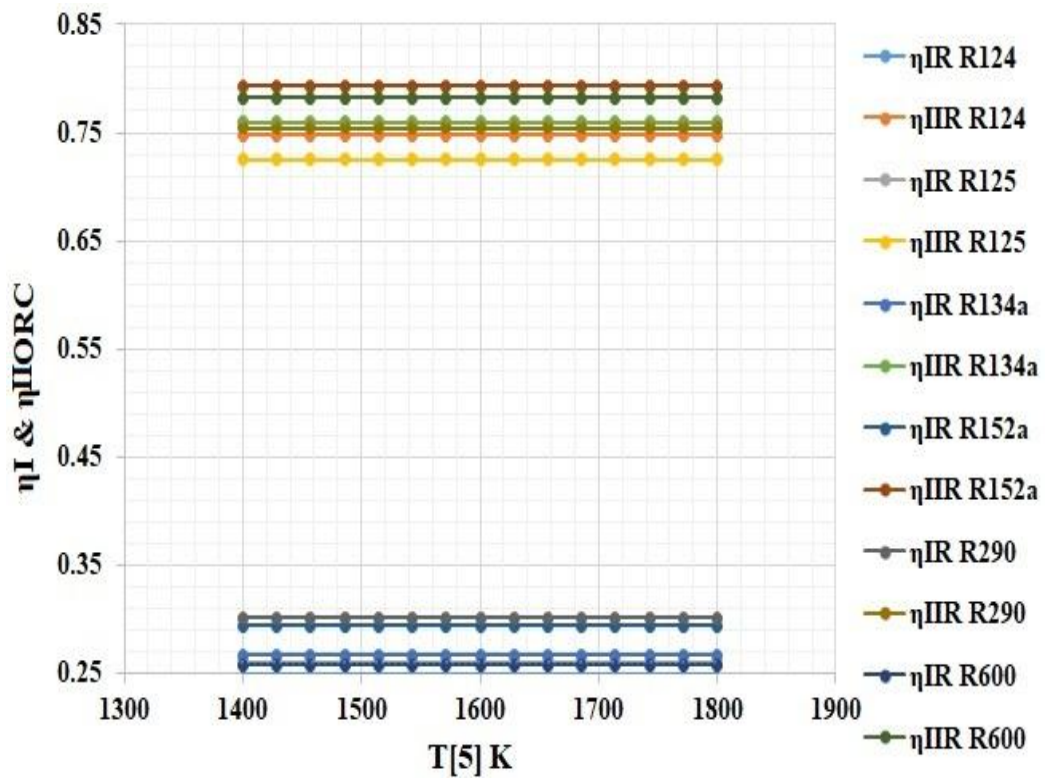


Fig 5.131: First & Second Law Efficiencies of the ORC

Subsequently, in Fig 5.132 Net-Work Output of the ORC can be observed. R600 & R124 have coinciding and the least results. For R290, the maximum net-work output has been obtained.

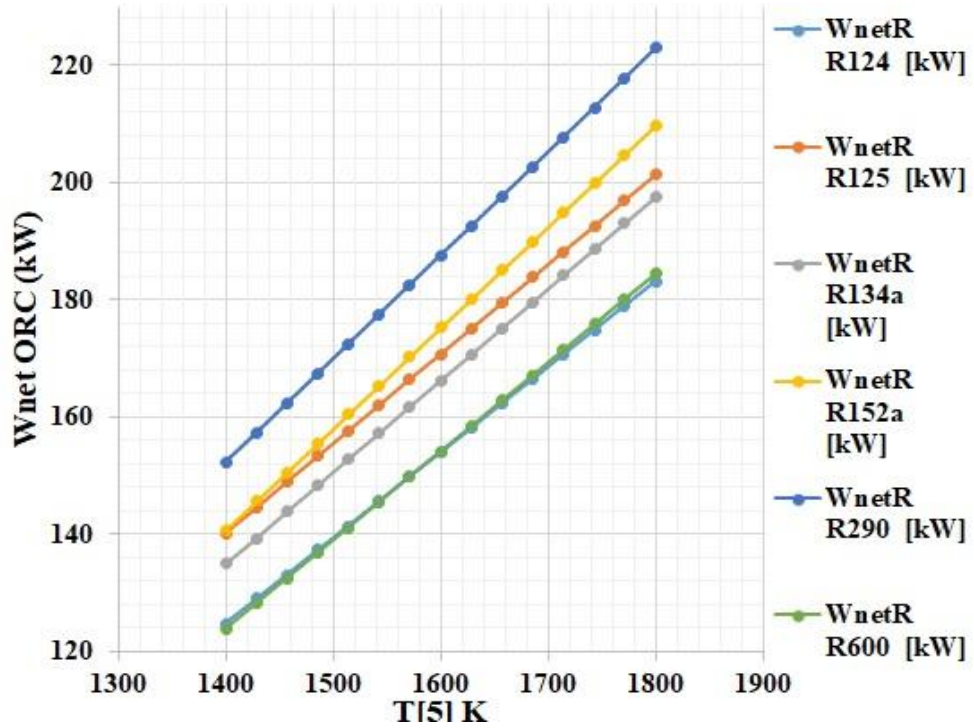


Fig 5.132: Net-Work Output of the ORC

In Fig 5.133 the Mass Flow rate inside the LHP and the ORC has been presented. It can be seen that requirement of the amount of working fluid in the LHP is quite less i.e., in the range of 0.3 kg/s to 0.5 kg/s when compared to the mass flow rate required for the ORC in which the range varies from 0.8 kg/s to 3.4kg/s for the subject input parameters.

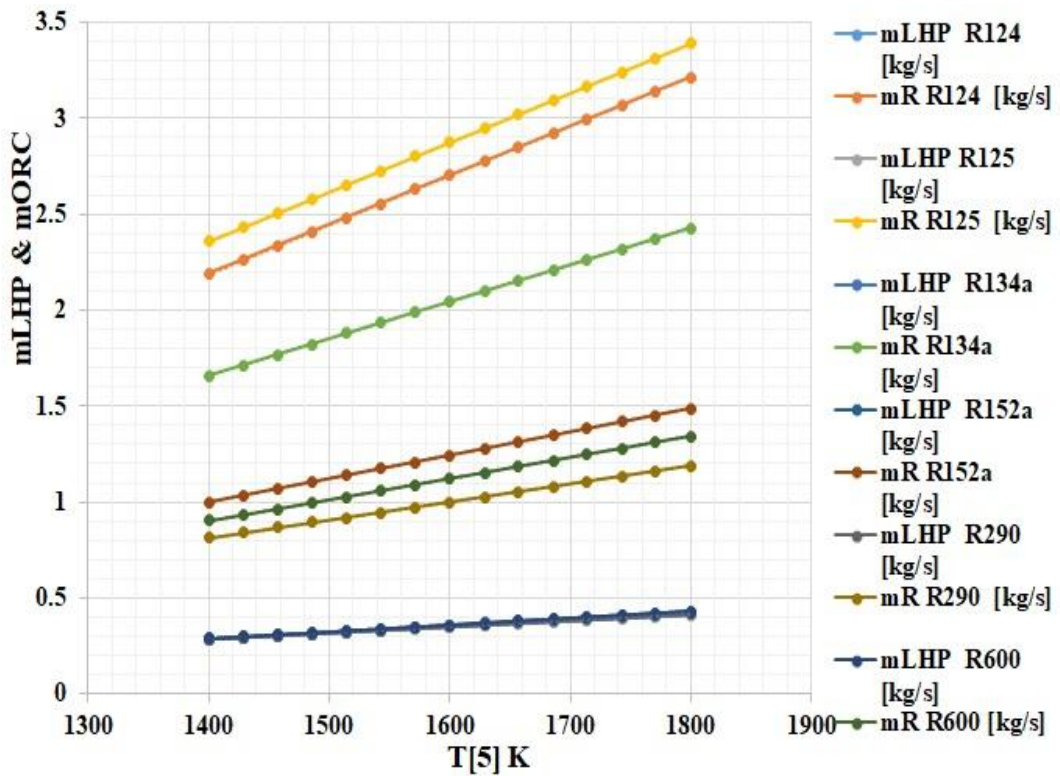


Fig 5.133: Mass Flow Rates in LHP & ORC

It can be seen that for the given input condition of Peak Temperature of GPC, Maximum Network Output in the ORC has been obtained for R290 and the Max First Law & Second Law Efficiency for R290 & R152a respectively. For the different components such as LHP, Boiler & Condenser maximum Exergy achieved is with R125, R152a, and R600& R125 respectively. It can also be seen that the Mass Flow of LHP is relatively lower than the ORC for the given condition. The overall Exergy transfer within the LHP is highly effective and efficient.

5.6.2. Condenser Pressure (P_9) of ORC as Input Variable:

The performance parameters have been studied for LHP & ORC by varying the Condenser Pressure of the ORC (P_9). It has been varied from 10 kPa to 100 kPa. Fig 5.134 shows the Irreversibility & Exergy in the condenser of the ORC. R125 isn't suitable for the pressure range as the value of the Exergy is extremely low. R600 has the maximum Exergy ranging from 65kW to 90kW. It can also be seen that the trend for other refrigerants is the same and parallel except R124 which has a zigzag trend ranging from 45 kW to 67.5 kW. Irreversibility also decreases with the range of

pressure for all the refrigerants. For R152a, the irreversibility can be seen to be the lowest and constant at 25 kW. Moreover, for R124 the irreversibility is maximum.

Fig 5.135 shows the Exergy of the boiler. Trends for all the refrigerants are similar and decreasing with maximum Exergy for R125 & ranging from 200 to 110 kW. The lowest Exergy value is associated with R600 ranging from 100 to 40 kW. Irreversibility data for all the refrigerants are coinciding and almost constant near 10 kW. Only R124 shows the zigzag trend.

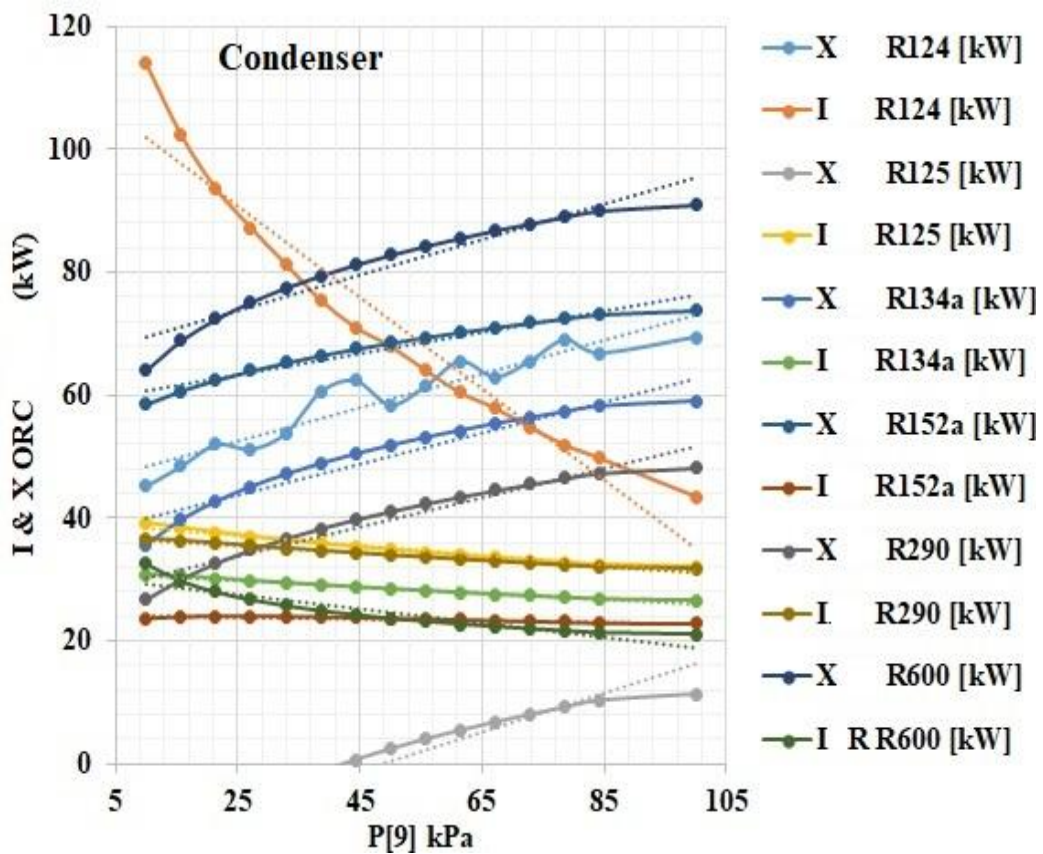


Fig 5.134: Irreversibility & Exergy associated with the Condenser of the ORC

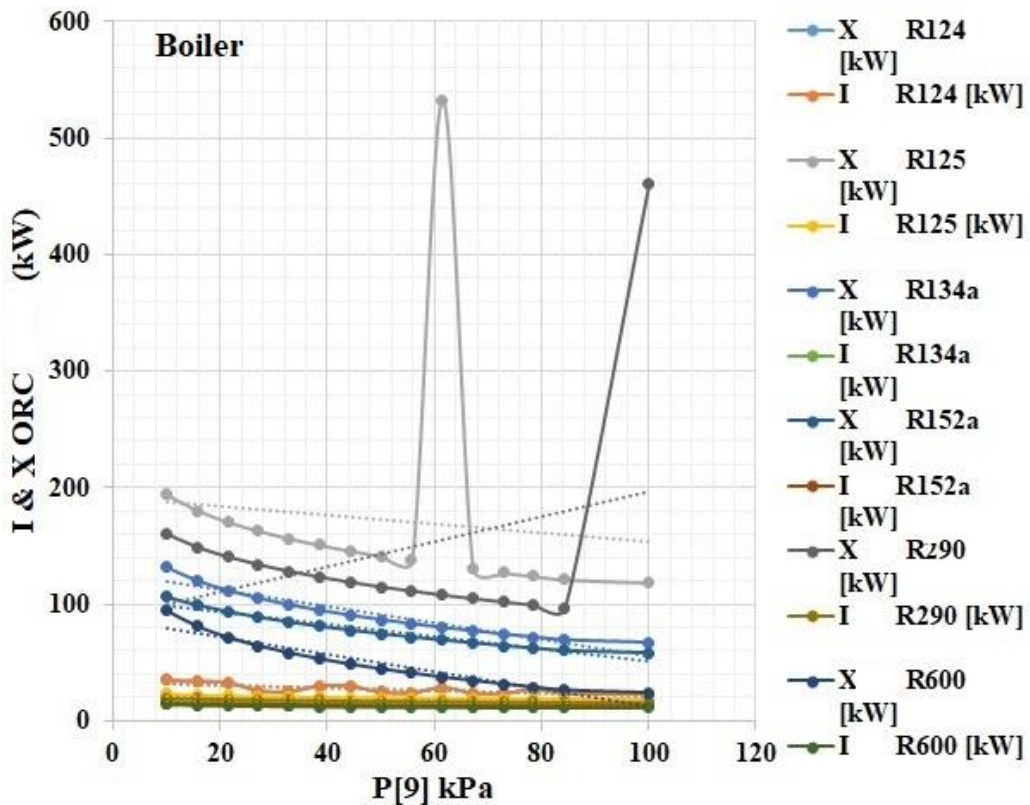


Fig 5.135: Irreversibility & Exergy associated with the Boiler of the ORC

Exergy & Irreversibility in the LHP has been studied in Fig 5.136 & 5.137. It can be seen from the Figures that for both the Evaporator and Condenser of the LHP, the values are quite distinct and have the same trends for Exergy and Irreversibility. It can also be seen that the values of the Exergy in the evaporator are constant except for R134a. Similarly, Irreversibility is constant except for R152a. The Evaporator Exergy has the range of 1000kW for R152a -700kW for R125 and Irreversibility has values varying from 380kW for R152a to 280 kW for R125.

The Condenser Exergy has values from 640 kW for R125 to 540 kW for R 152a and Irreversibility varies from 140 kW for R125 to 60 kW for 152a. The performance of the Evaporator & Condenser has been observed to be high and low for the same refrigerants.

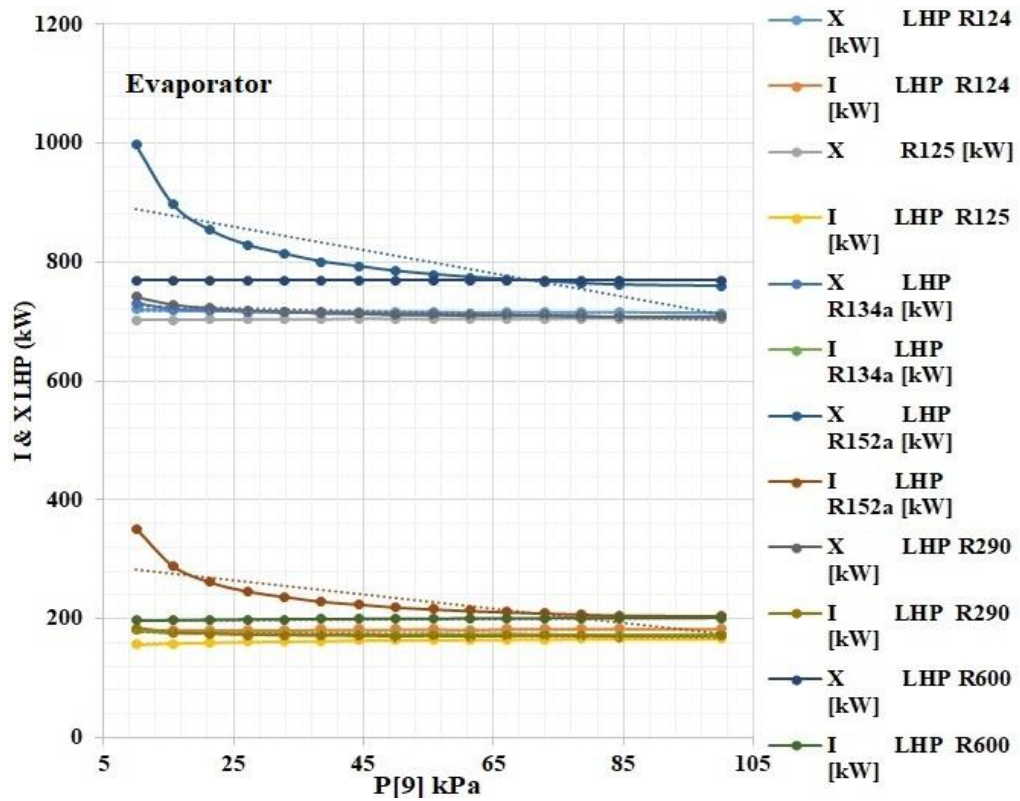


Fig 5.136: Irreversibility & Exergy associated with the Evaporator of the LHP

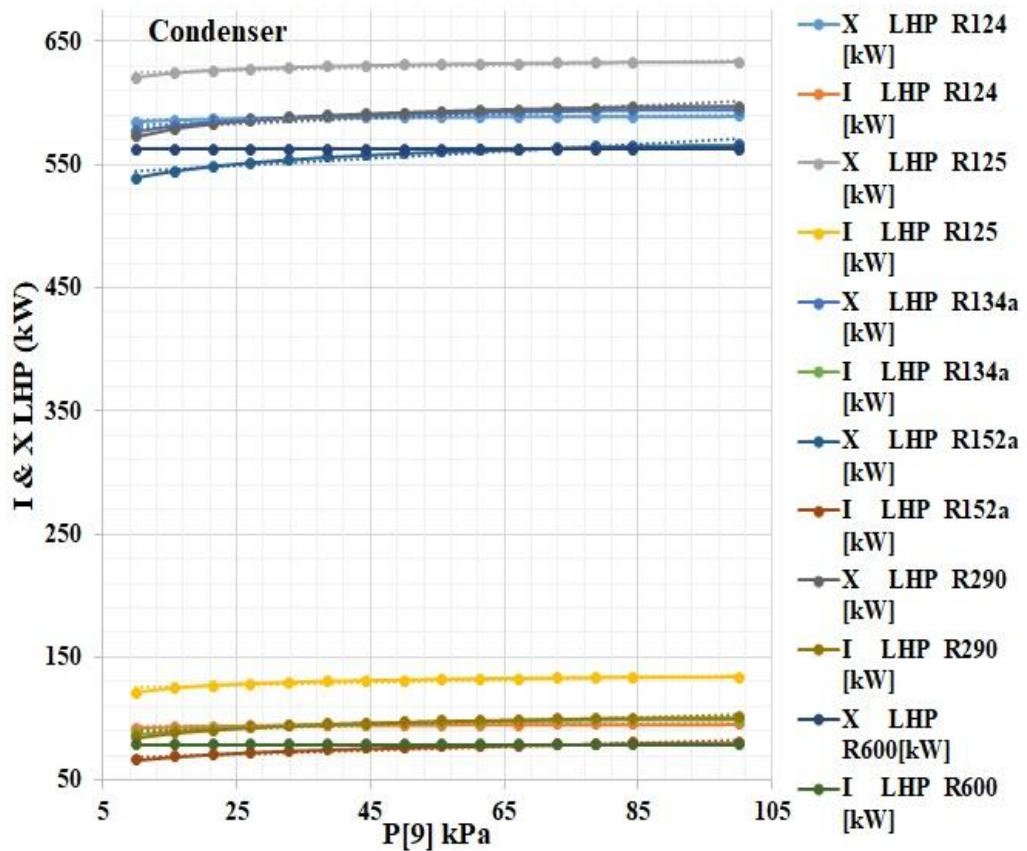


Fig 5.137: Irreversibility & Exergy associated with the Condenser of the LHP

In Fig 5.138 the First Law & Second Law Efficiencies are presented. It can be observed that the First Law Efficiency varies from 38% for R290 to 22% for R124. The trend for the first law efficiencies is as expected.

The Second Law Efficiency for the ORC ranges from 81% for 152a to 74% for R125. The results vary with every refrigerant and input variable. Brief disruptions can be observed for R125 & R290 hence it can't perform for the complete range.

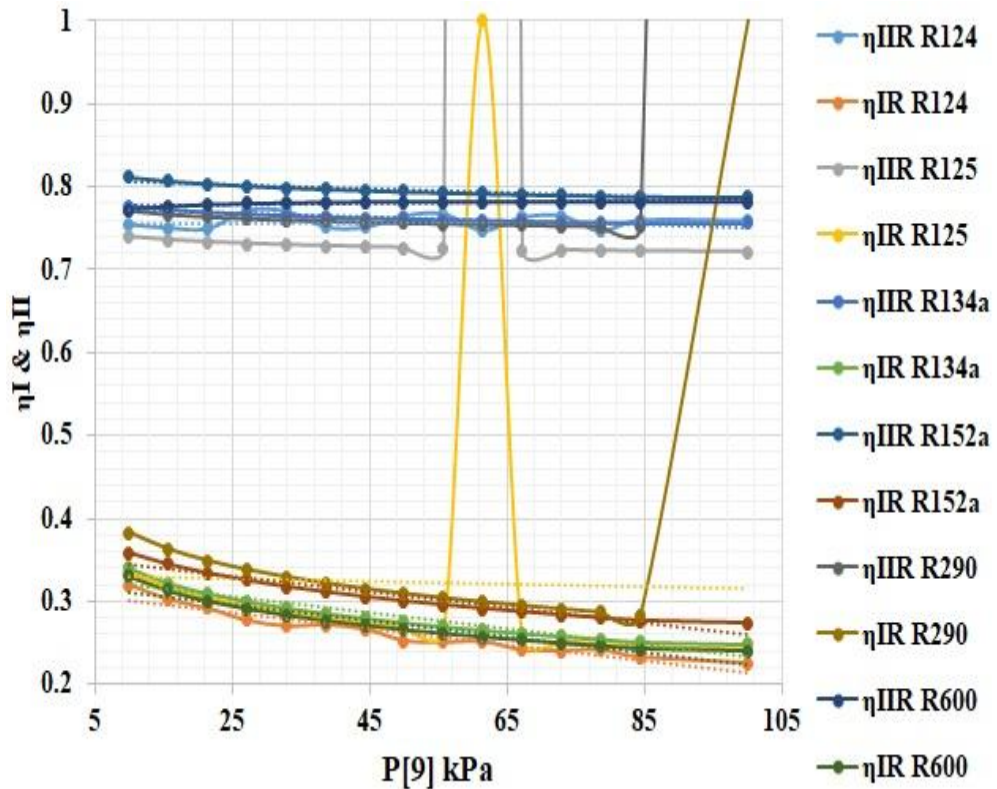


Fig 5.138: First & Second Law Efficiency of ORC with Condenser Pressure

Work out from Fig 5.139 can have been studied to be 190 kW for R290 to 110 kW for R600. R125 & R290 can't perform for the complete range. Brief disruptions can be observed.

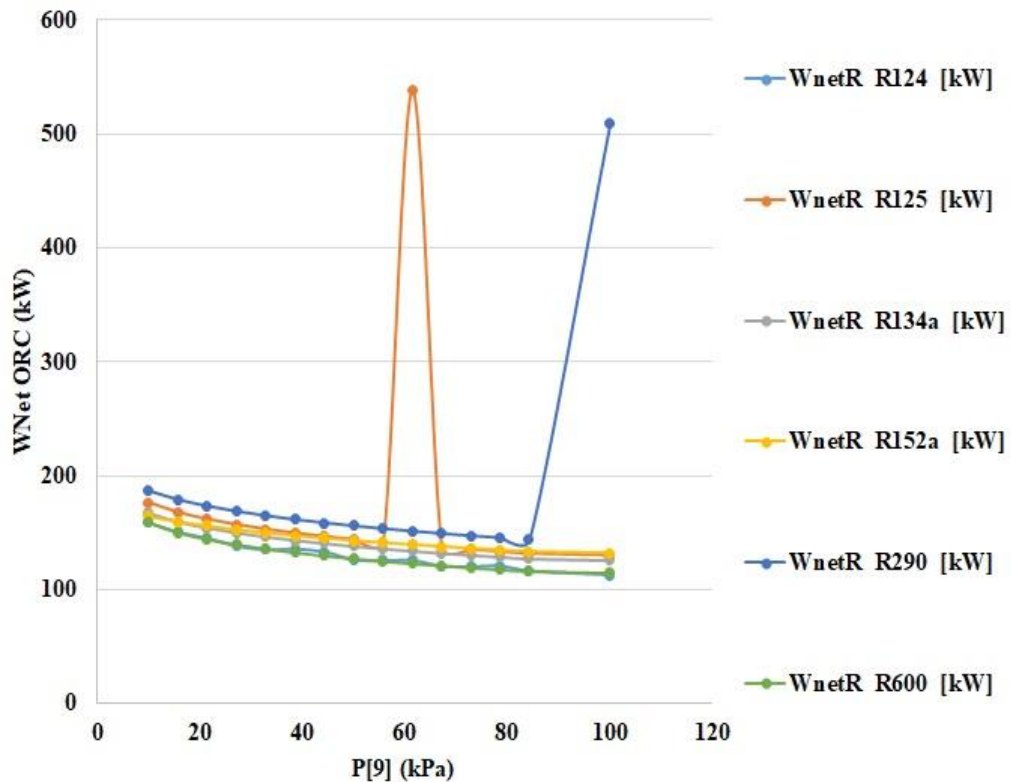


Fig 5.139: Work Output of ORC with P₉

5.6.3. Working Fluid of LHP as Input Variable:

In this segment results on the Mass Flow Rate of LHP & ORC have been presented varying the working fluid of the LHP, and the Condenser Pressure of the ORC. Following Fig 5.140 presents the results with Acetone as the working fluid in the LHP. It can be seen that for the 3 working fluids in the ORC namely R290, R600 & R152a the mass flow trend is parallel, increasing & in the same range 0.5 kg/s to 1.1 kg/s. For R134 the increasing trend from 1.3 to 2.5 kg/s is similar to R 125 from all other refrigerants. For R125 we get a continuously increasing trend from 1.9kg/s to 2.5 kg/s and for R124 the discontinuously increasing trend of in the range of 1.8 kg/s to 2.3 kg/s. The same trend in the ORC can be seen independent of the working fluid of the LHP.

In Fig 5.140 the mass flow rate for Acetone in the LHP varies from 1.5 kg/s with R125 in the bottom cycle to 3 kg/s with R152a as the fluid in the ORC. Moreover, we can see that with pressure increase in the boiler the required mass flow rate has a decreasing trend.

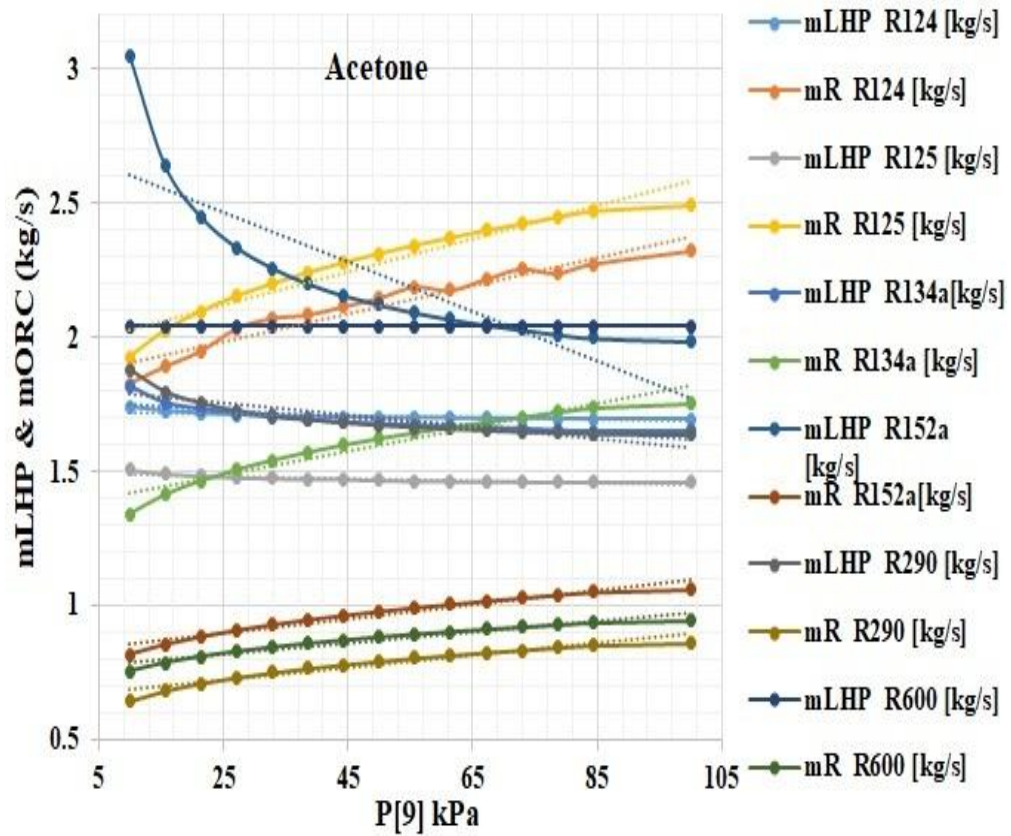


Fig 5.140: Mass Flow Rates in LHP & ORC with Acetone as LHP Fluid

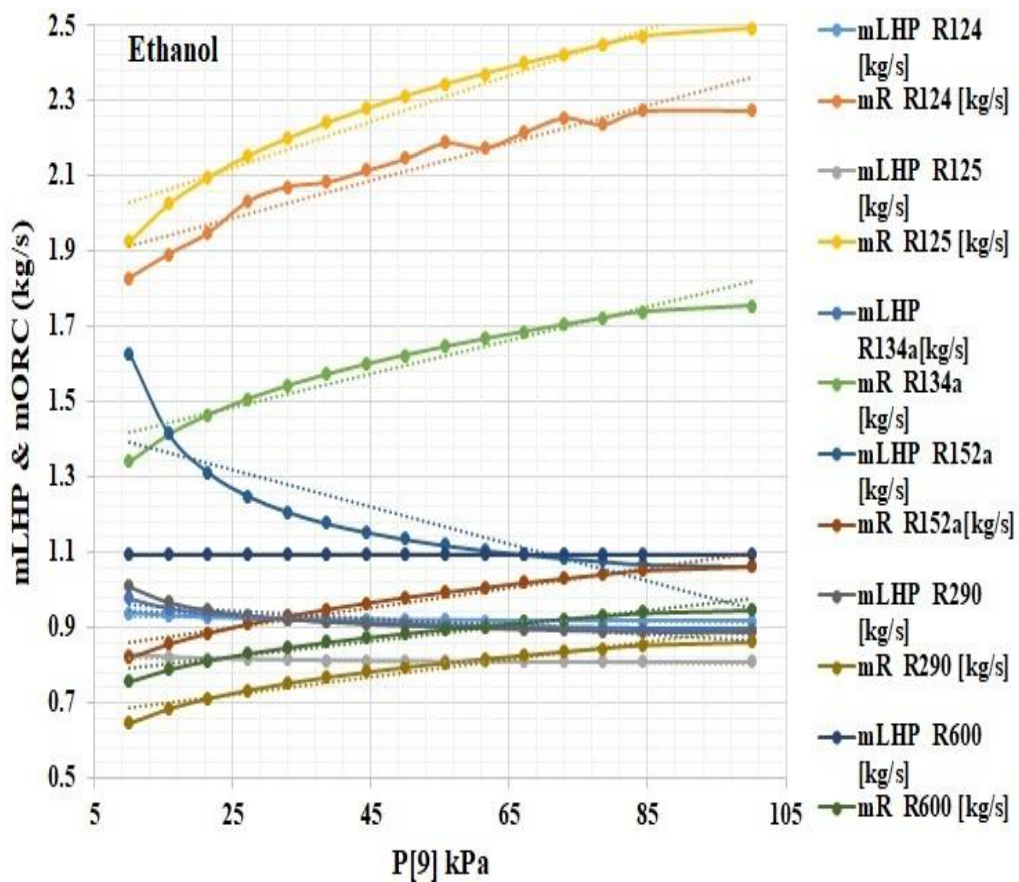


Fig 5.141: Mass Flow Rates in LHP & ORC with Ethanol as LHP Fluid

Whereas, in Fig 5.141, the results have been discussed for Ethanol in the LHP. The mass flow rate varies from 0.85kg/s for R125 and 1.65 kg/s for R152a. The trends are similar to the Acetone.

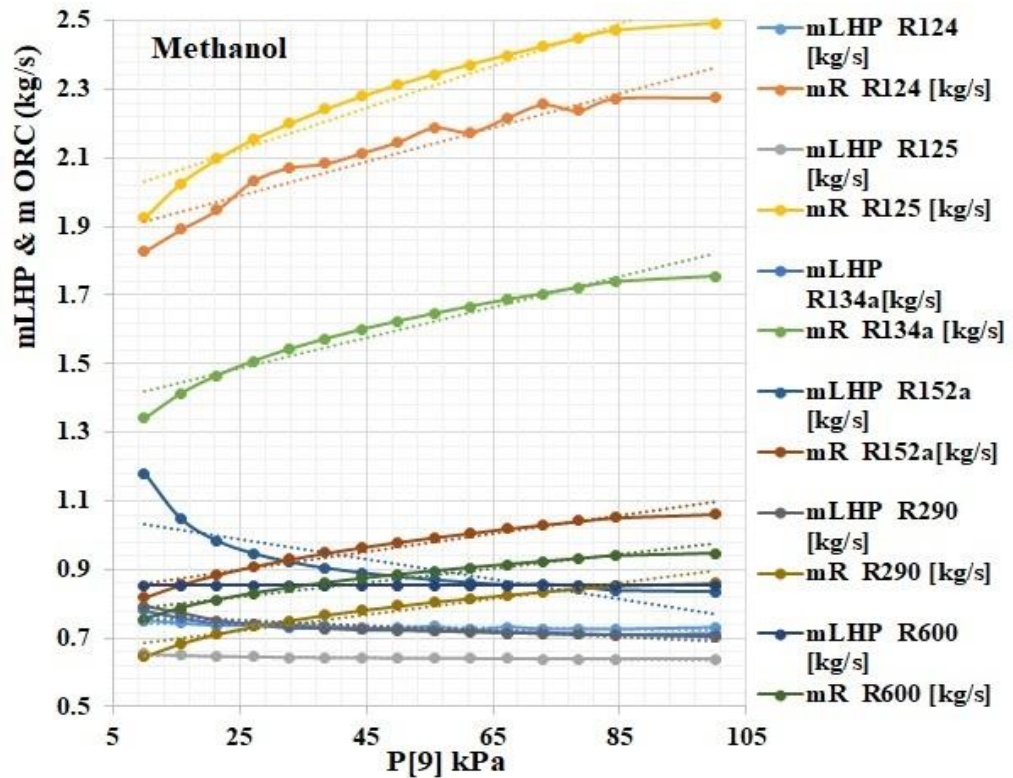


Fig 5.142: Mass Flow Rates in LHP & ORC with Methanol as LHP Fluid

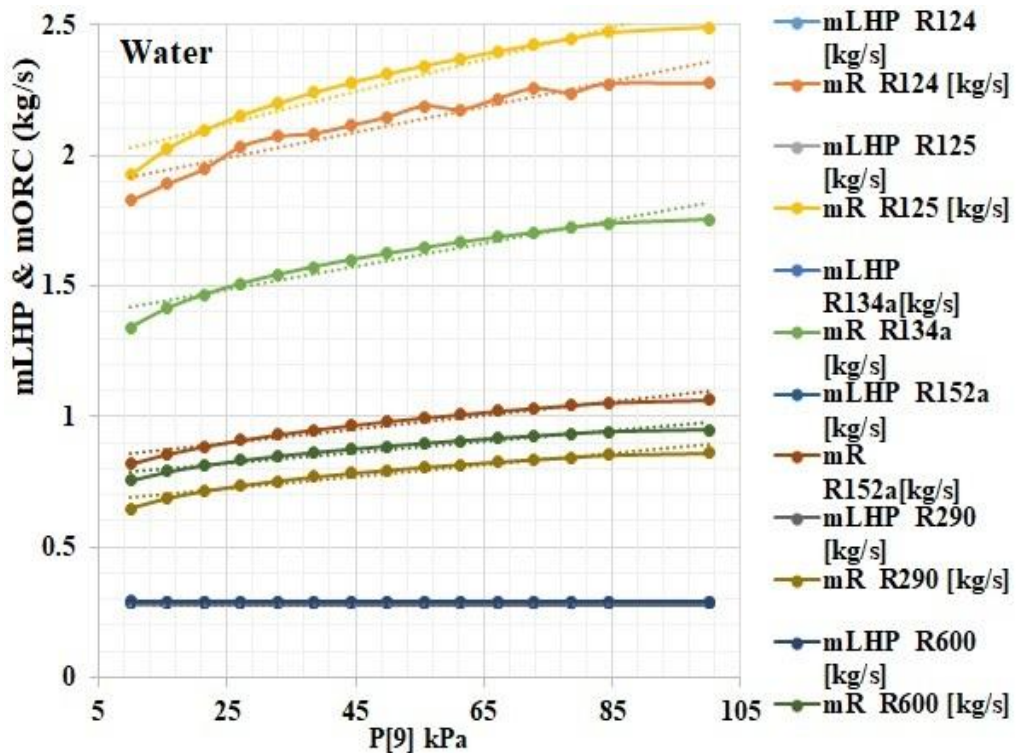


Fig 5.143: Mass Flow Rates in LHP & ORC with Water as LHP Fluid

In Fig 5.142 mass flow of Methanol can be seen to vary from 0.65 kg/s for R125 to 1.2 kg/s for R152a. The results can be seen to be constant and coinciding for all the refrigerants in the case of water in LHP in Fig 5.143. The mass flow rate can be seen to be 0.3kg/s.

5.7: Combined ERC & GPC (Ankit Dwivedi, et. al. 2021) ^[190]

The results obtained have been presented in this section. As input parameters the Boiler Pressure (P_{11}) of ERS has been varied from 500 kPa to 800 kPa, Peak Temperature of the GPC (T_5) from 600 K to 1000 K, 6 Eco-friendly Working Fluids for ERS, and 4 Working Fluids of the LHP Ex. have been used for the investigation. This section has been separated into 3 sub-sections which present the results based on T_5 (subsection-3.1), P_{11} (subsection-3.2) & Working Fluids in the LHP (subsection-3.3). These results have been presented for the different working fluids being used in the ERS. In sub-section 3.3, results based on 3 input variables namely ERC working fluid-LHP working fluid- P_{11} and ERC working fluid-LHP working fluid- T_5 respectively have been presented. The results have been emphasized for R718 for being the widely available and origin of Steam Jet Refrigeration System as well as all other ancient refrigeration systems and for R1224yd (Z) as it has 0 ODP & 0 GWP and is the most eco-friendly refrigerant of all the chosen refrigerants. By the end of this section, we will be able to assess the feasibility and best operating parameters for such a combined system. The dotted – discontinuous lines/curves may be neglected for they are mere projections. Table 5.18 presents the Input variable for the ERC.

Table 5.18: Input Variables for ERC Analysis

Sl. No.	Input Parameters	Data
1.	Evaporator Temperature, T_{Evap}	5 °C
2.	Working Fluid	R236ea, R1224yd(Z), R1233zd(E), R245fa, R365mfc, R718
3.	Condenser Effectiveness, ϵ_{Cond}	0.7
4.	Condenser Temperature, T_C	35 °C
5.	Flash Chamber Temperature, T_{16}	20 °C
6.	Peak Temperature of GPC, T_5	1000K

7.	A/F Ratio	300
-----------	-----------	-----

5.7.1. The Peak Temperature of GPC (T_5):

As the T_5 has been varied from 600K to 1000K, the effect of temperature available for heat transfer has been studied. In Fig 5.144 it can be observed that the Temperature available in the boiler of ERC varies from 380 K to 455 K. It can be reiterated that the critical temperatures of the Eco-friendly refrigerants chosen for the study are in the range of 380K – 450K as well. Hence, the boiler can be operated at high temperatures near critical points and low heat consumption for the cycle to work.

In Fig 5.145 refrigeration capacity obtained for the temperature range has been presented. It can be seen that owing to the critical temperature limits, all the ERC working fluids except R718 have been studied for the range of 600K to 800K and 800K - 1000K for R718. It can be seen R365mfc (i.e., 8.601kW to 10.35kW) & R1233zd (E) (i.e., 7.657kW to 11.05kW) provide consistent high values of the refrigeration capacities. R245fa & R1224yd (Z) (7.87kW-9.903kW) have coinciding values. With the temperature rise, it can be observed that the Refrigeration capacity also increases. For R718 the rise is the steepest from 6.835kW to 31.545kW.

The COP can be seen to be decreasing with the increase in temperature Fig 5.146. For R365mfc the value of COP has been noted to be the maximum from 0.2856 to 0.249. Whereas, for R718 the COP is more consistent and is in the range of 0.285 to 0.282.

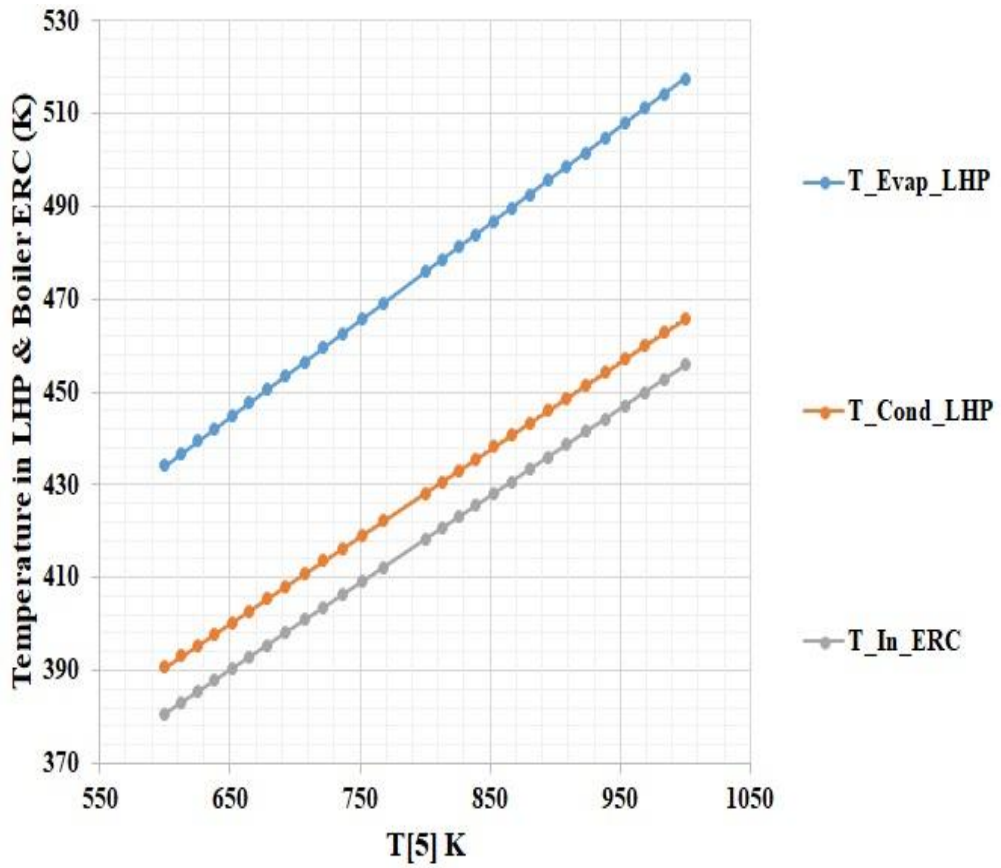


Fig 5.144: Temperature Profiles of the Components of Combined Cycle with T₅

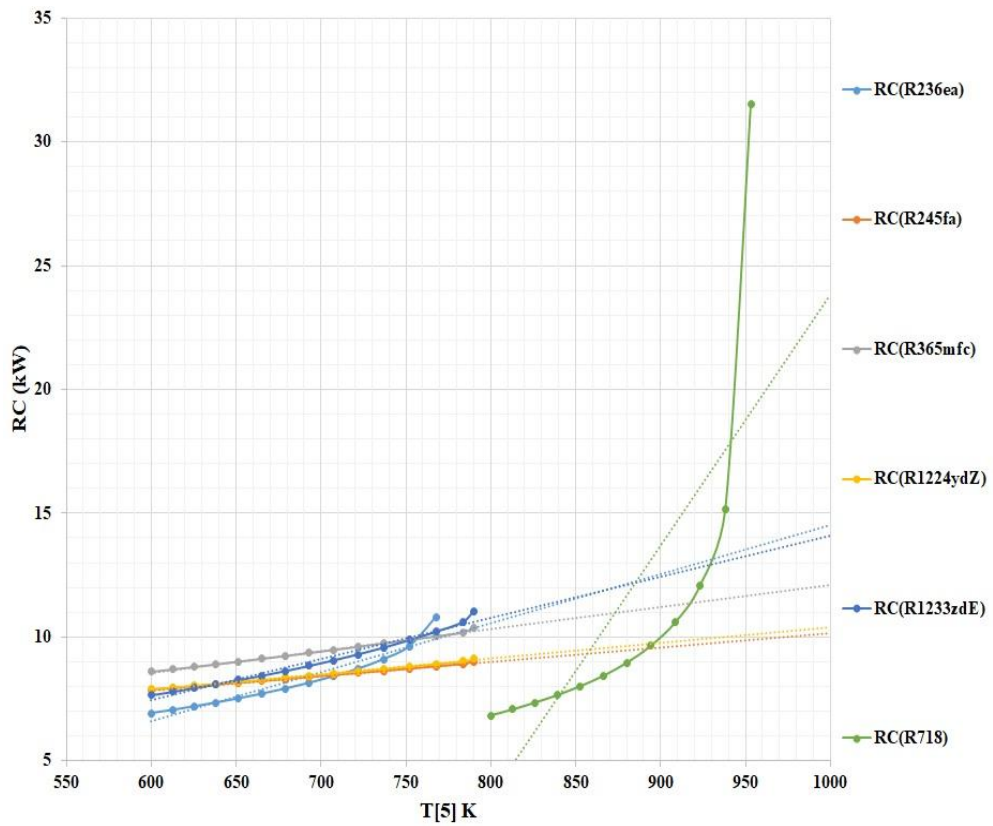


Fig 5.145: Refrigeration Capacity of the ERS with T₅

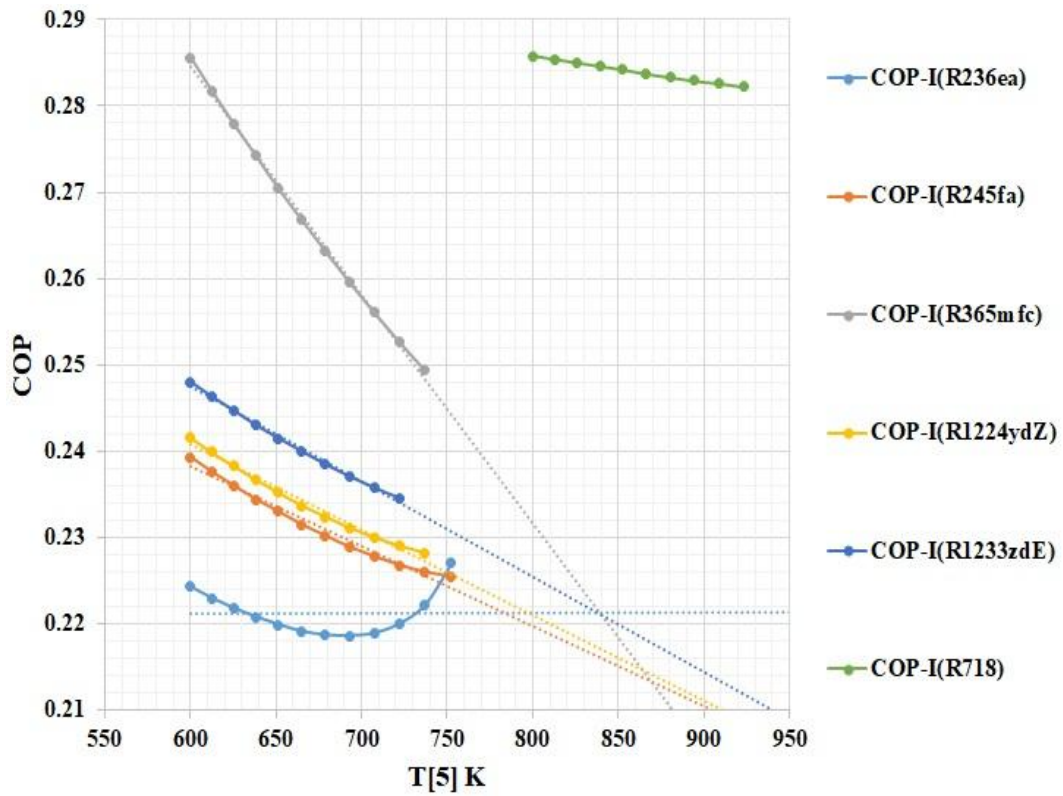


Fig 5.146: COP of the ERS with T_5

The main drawback of R718 being not able to run below 278 K. For R1224yd (Z) the value of COP is close and parallel with R245fa in the range of 0.241 to 0.225.

5.7.2. The Boiler Pressure of ERS (P_{11}):

Refrigeration capacity and COP have also been presented with the varying Boiler Pressure in Fig 5.147 & 5.148 respectively. Unlike the previous sub-section, all the refrigerants have been studied for the same range of pressure 500kPa to 800kPa. A continuous and gradual increase can be seen in the refrigeration capacity with the increase in pressure.

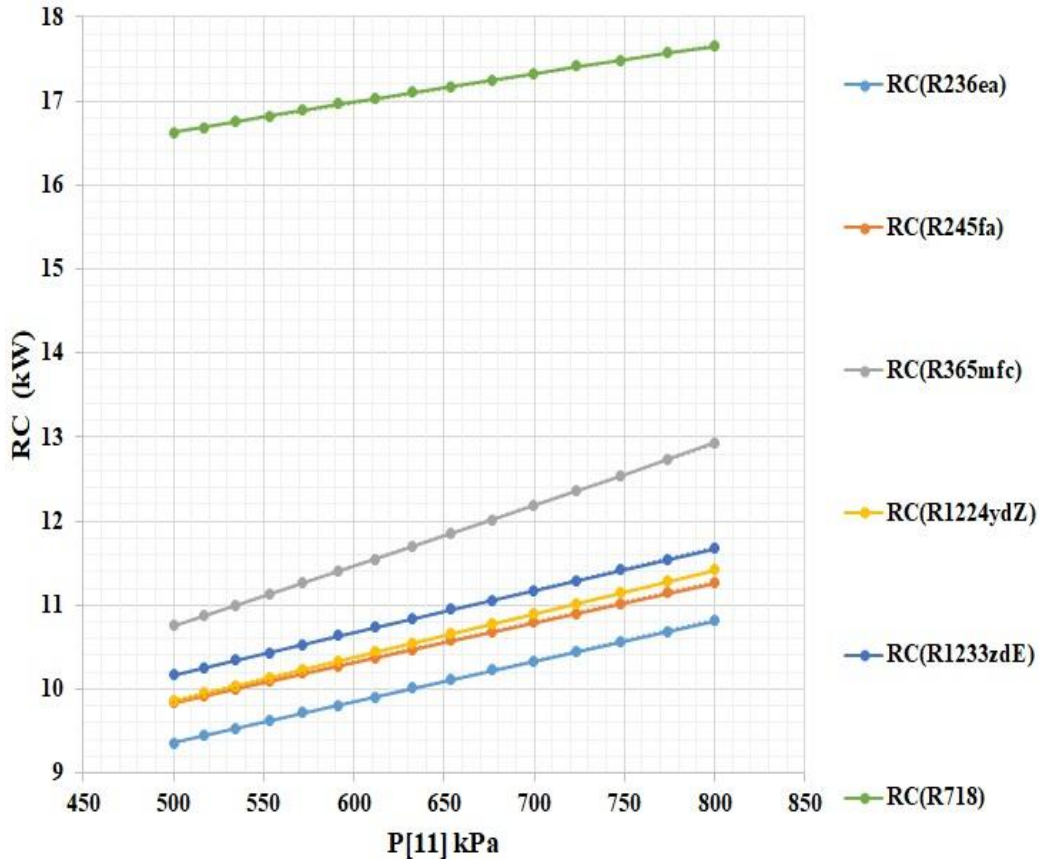


Fig 5.147: Refrigeration Capacity of the ERS with P₁₁

It can be seen in Fig 5.147 that for R718 the refrigeration capacity has been recorded as a maximum of 16.62 to 17.65 kW, whereas, for the refrigerants, R365mfc provides a cooling effect of 10.75 to 12.93 kW under the subject conditions. It must be mentioned that the R1224yd (Z) which has 0 GWP & 0 ODP in a system has recorded RC of 9.86 to 11.41 kW.

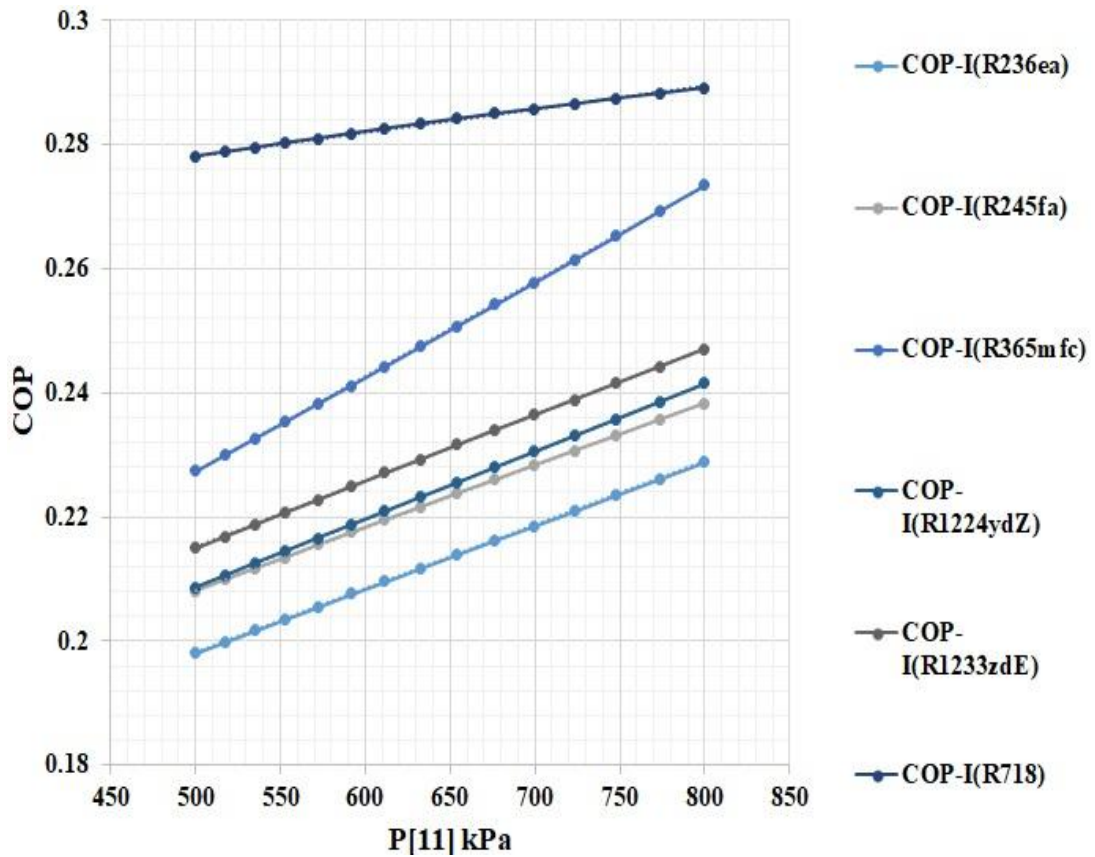


Fig 5.148: COP of the ERS with P₁₁

Fig 5.148 presents the data recorded for COP under the variable Boiler pressure. The COP can be seen gradually increasing with an increase in boiler pressure. R718, R365mfc & R1224yd (Z) have maximum COP of 0.289, 0.275 & 0.241 respectively.

5.7.3. Working fluids in the LHP:

Four easily available and eco-friendly working fluids have been selected for the LHP Ex. As mentioned in Section 2, the working fluids have defined working temperatures as well as suitable materials based on the corresponding thermo-physical properties. This section has focussed on the mass flow rate of the working fluids, availability of Heat at the inlet of LHP & ERC for all the working fluids subject to variable Peak Temperature of GPC, Peak Pressure of ERC, and different working fluids. Smaller the mass flow handling, Compacter the whole combined system. It can be seen that mass flow rate and Heat Input for LHP for all the refrigerants except R718 and R718 it's different. Moreover, as mentioned above the primary focus of this section is on R718 & R1224yd (Z), which has the potential of

providing the most compatible eco-friendly system subject to the variable Temperature & Pressure.

5.7.3.1. Acetone:

In Fig 5.149 to Fig 5.150, the results based on Acetone as LHP working fluid have been presented based on variable Pressure & Temperature. In Fig 5.149 the mass flow rate of refrigerants in the ERC is maximum for R1224yd (Z) (1.041kg/s) and least for R718 (0.097kg/s). The mass flow rate in the LHP for the R718 system is 0.639kg/s, whereas, for other refrigerants, it was recorded as 0.4635kg/s.

In Fig 5.150 heat inputs can be seen to be constant with varying Pressure. Input to the LHP can be seen to be carried away for transfer with R718 system is at 197.1 kW & for other refrigerants 155.9 kW. Whereas, the heat input to the ERC for R718 is 160.1kW & for other eco-friendly refrigerants is 142kW.

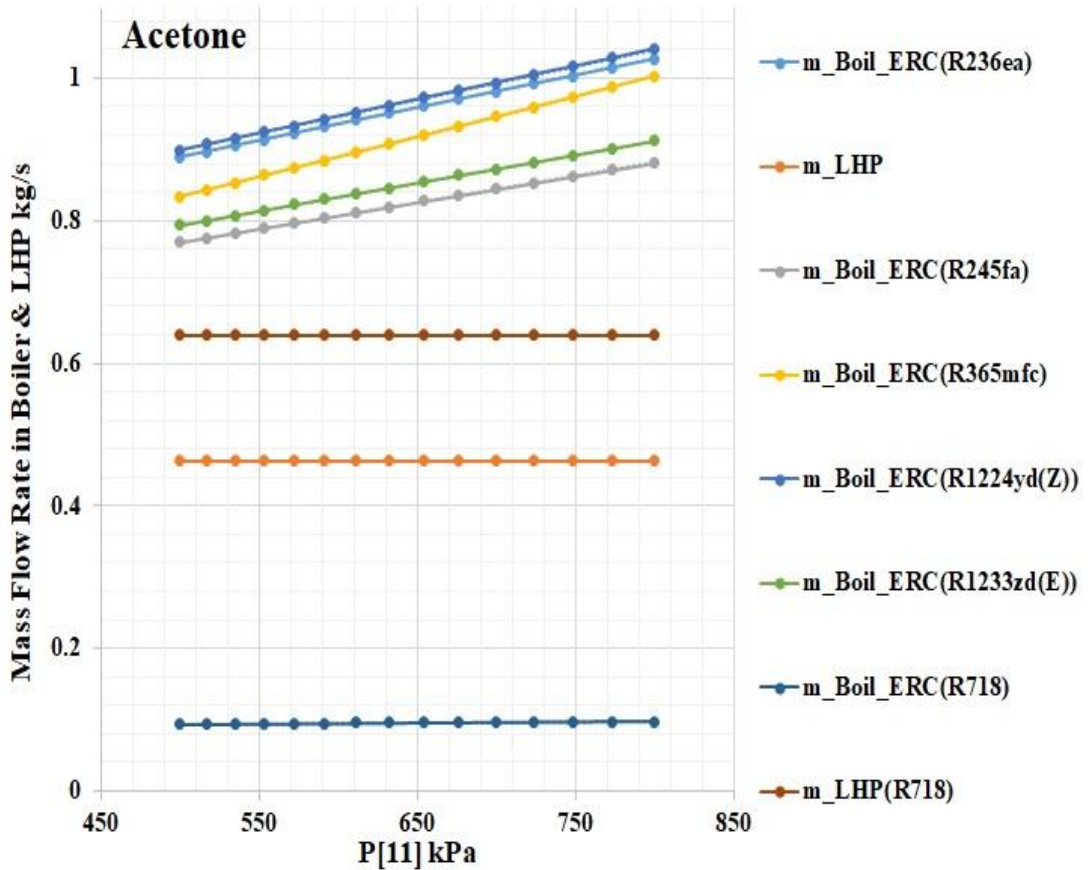


Fig 5.149: Mass Flow Rate of ERS & LHP with P₁₁ for Acetone

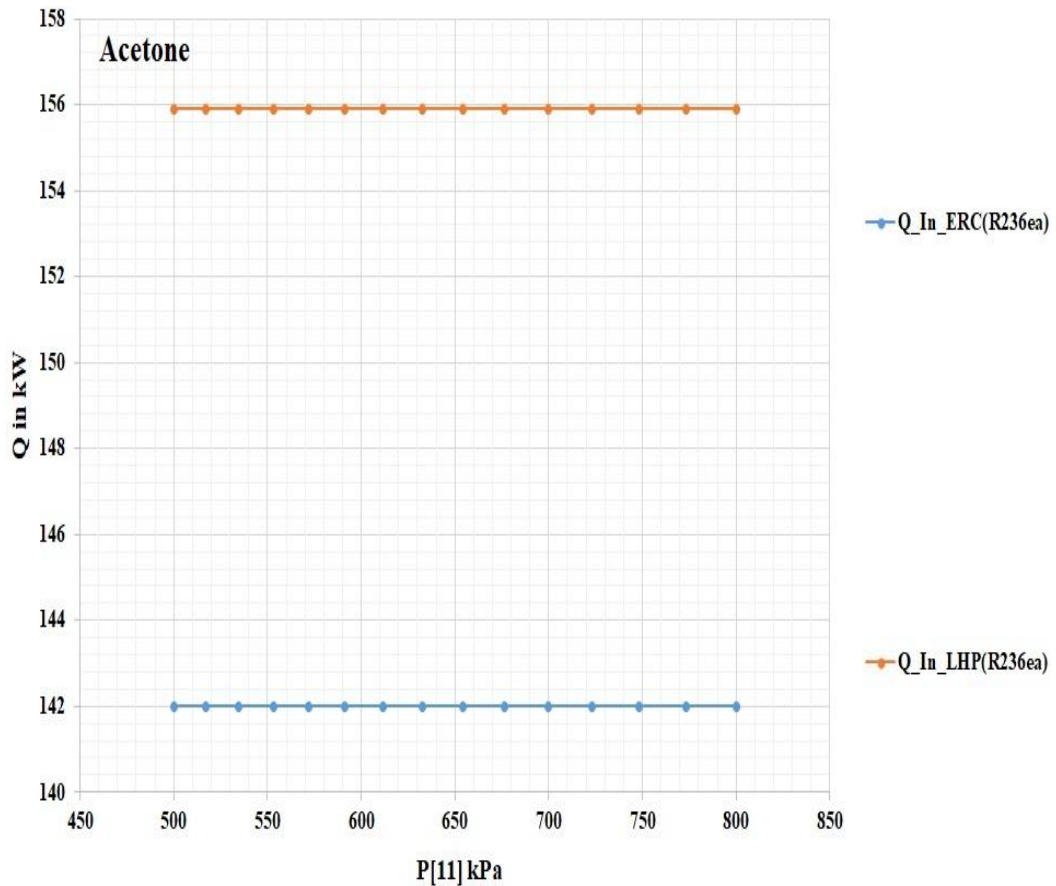


Fig 5.150: Heat Available as Input to ERC & LHP with P₁₁ for Acetone

The results for the analysis of Acetone are based on the Peak Temperature of GPC Fig 5.151 & Fig 5.152. From Fig 5.151 the maximum range of mass flow rate in ERC has been recorded as 0.821-1.283 kg/s for R236ea and for R1224yz (D) it has been recorded as 0.85-1.245 kg/s. For R718 the range of mass flow rate in ERC is 0.096-0.17 kg/s. The maximum mass flow rate range inside the LHP is recorded for R365mfc at 0.342-0.439 kg/s and for R1224yz (D) at 0.3401-0.498 kg/s. It can also be seen that for R 718 the LHP range of mass flow rate is 0.6396 - 1.321 kg/s.

The heat input range at ERC for R718 can be seen from Fig 5.152 as 160.1- 182.6 kW & for LHP it has been recorded as 197.1- 353.1 kW. Whereas, for other refrigerants, the range has been recorded as 123.8- 154.3 kW & 127.2- 181.5 kW respectively for ERC & LHP.

Performance Improvement of Vapour Absorption System Using Loop Heat Pipes

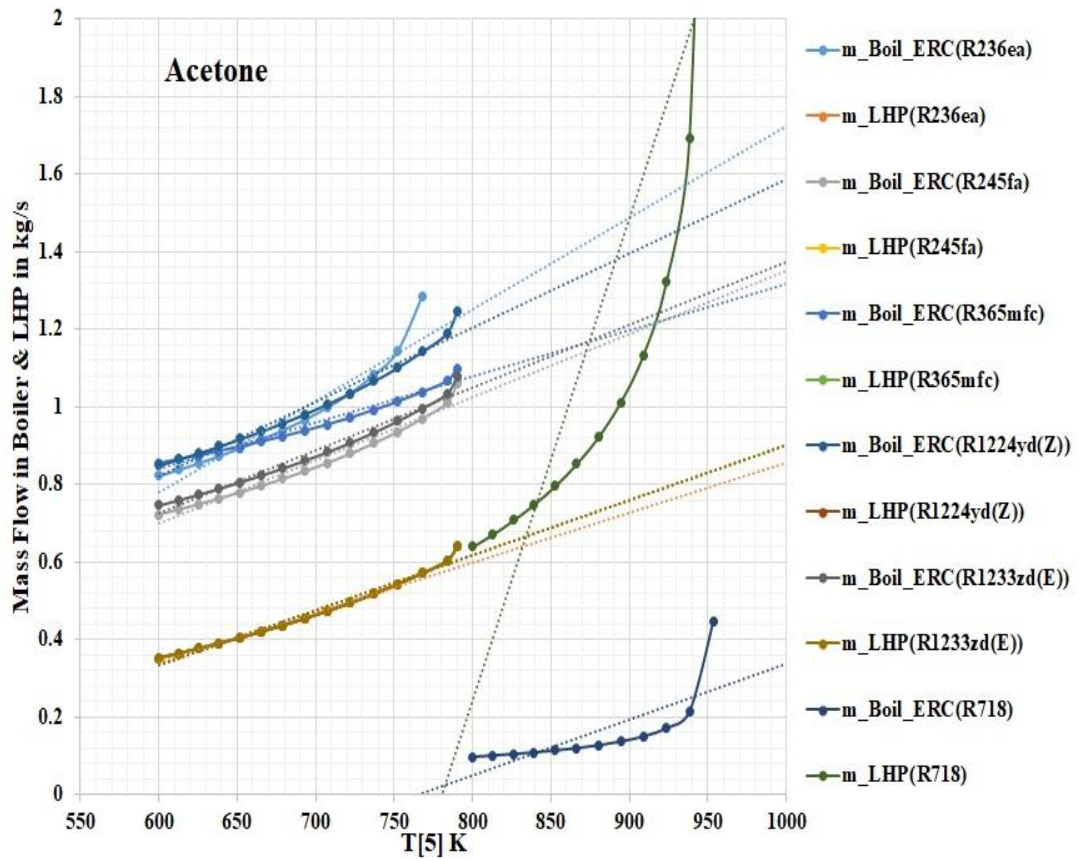


Fig 5.151: Mass Flow Rate of ERS & LHP with T₅ for Acetone

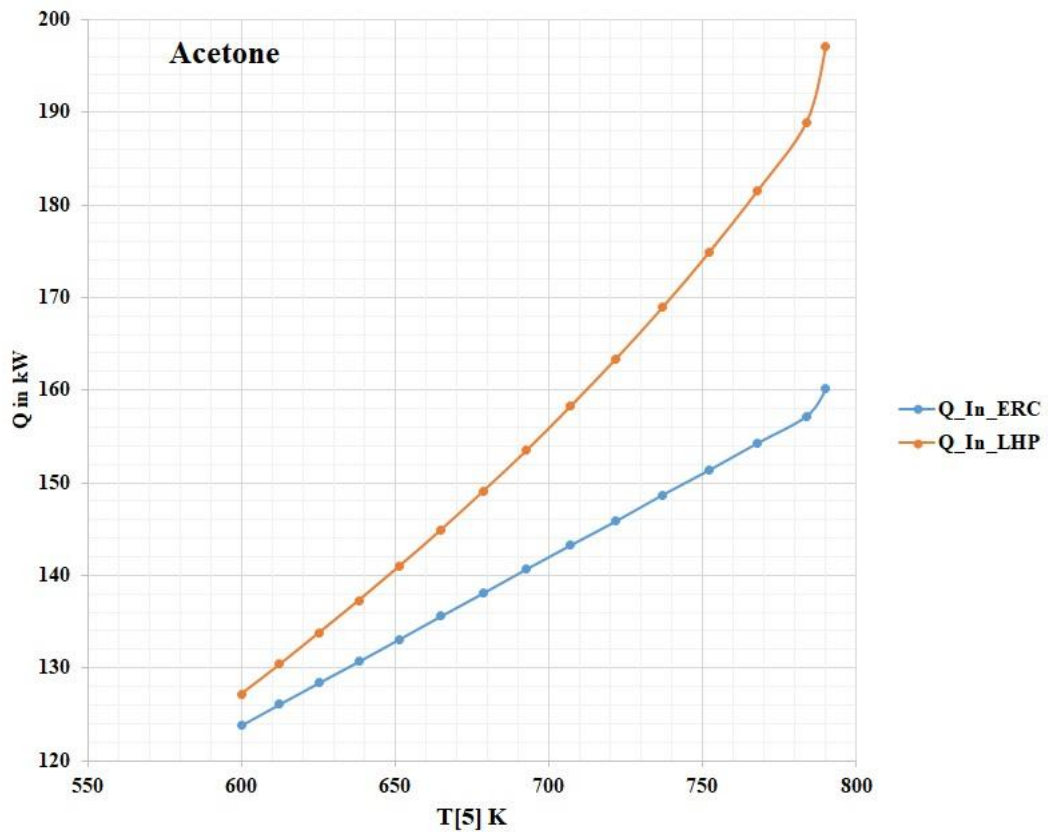


Fig 5.152: Heat Available as Input to ERS & LHP with T₅ for Acetone

5.7.3.2. Ethanol:

In Fig 5.153 & 5.154 the results of the analysis of Ethanol with variable pressure have been presented. It can be observed from Fig 14 that the maximum mass flow in ERC is for R1224yz (D) at 1.01 kg/s and the minimum is for R718 at 0.096 kg/s. Maximum mass flow in LHP for refrigerants is 0.244 kg/s and for R718 is at 0.342 kg/s.

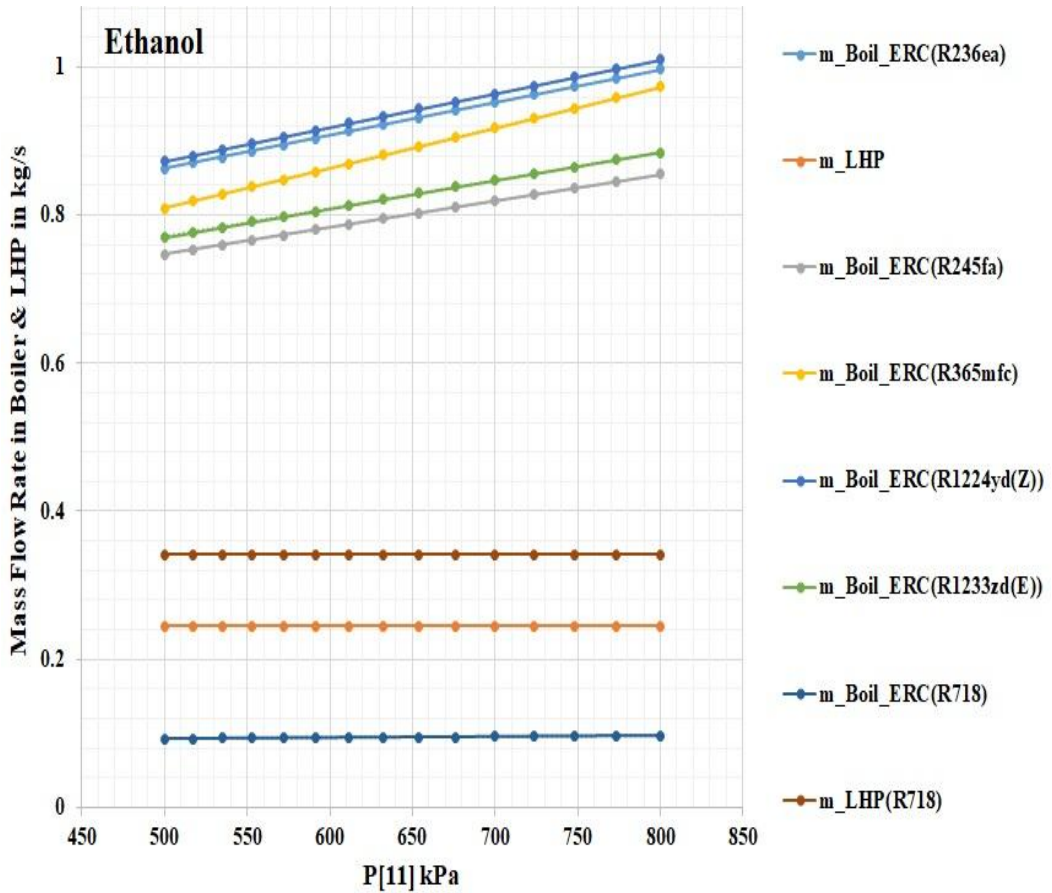


Fig 5.153: Mass Flow Rate of ERS & LHP with P_{11} for Ethanol

From Fig 5.154 it can be observed that heat input available at ERC & LHP for refrigerants are 142 kW & 155.9 kW. For R718 heat input available at ERC & LHP are 160.1kW & 194.4 kW.

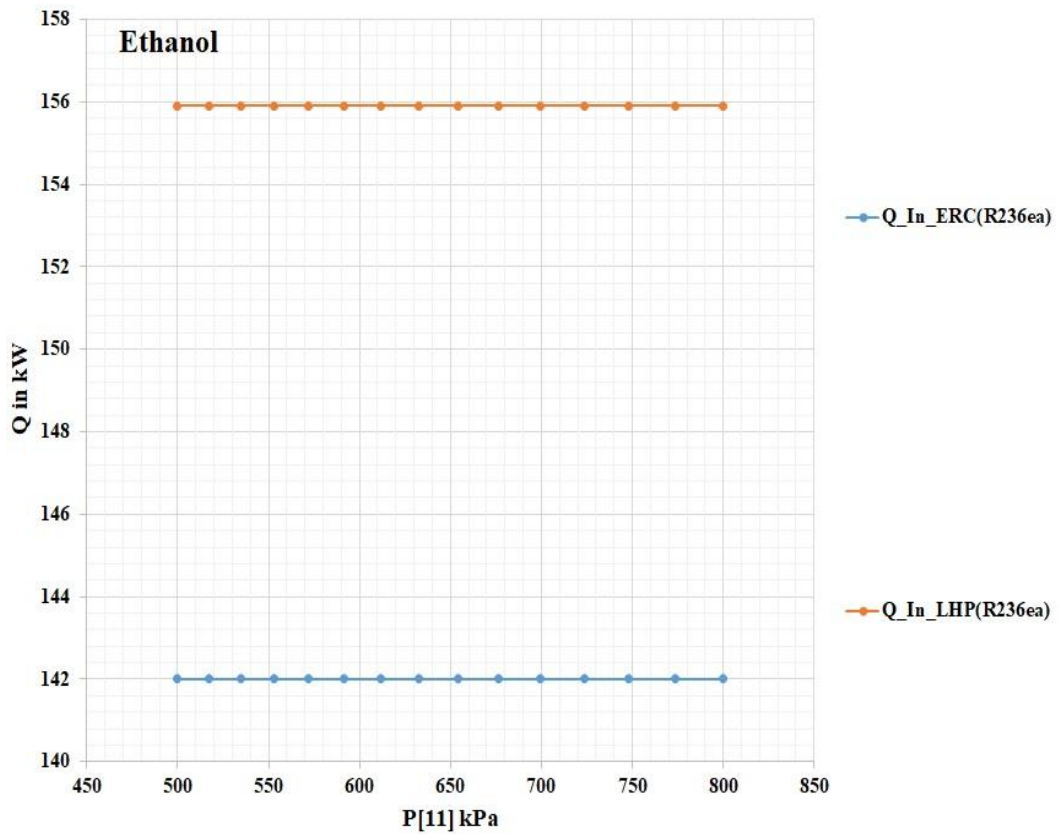


Fig 5.154: Heat Available as Input to ERC & LHP with P₁₁ for Ethanol

Similarly, the results of analysis based on the Peak Temperature have been reported in Fig 5.155 & 5.156. The range of Maximum mass flow rate in ERC from Fig 5.155 is for R1224yz (D) at 0.8321- 1.178 kg/s. The range of mass flow rate for LHP for R1224yz (D) is 0.1893 - 0.3261 kg/s. The range of mass flow rate in ERC & LHP for R718 can be observed as 0.09514 - 0.1877 kg/s & 0.3419 - 0.7967 kg/s respectively.

Furthermore, from Fig 5.156 it has been studied that the Heat input range available for ERC & LHP for refrigerants is 123.8 - 154.3 kW & 124.5 - 173.7 kW. Moreover, for R718 it has been observed for ERC & LHP are 160.1 - 185.4 kW & 194.4 - 388.9 kW

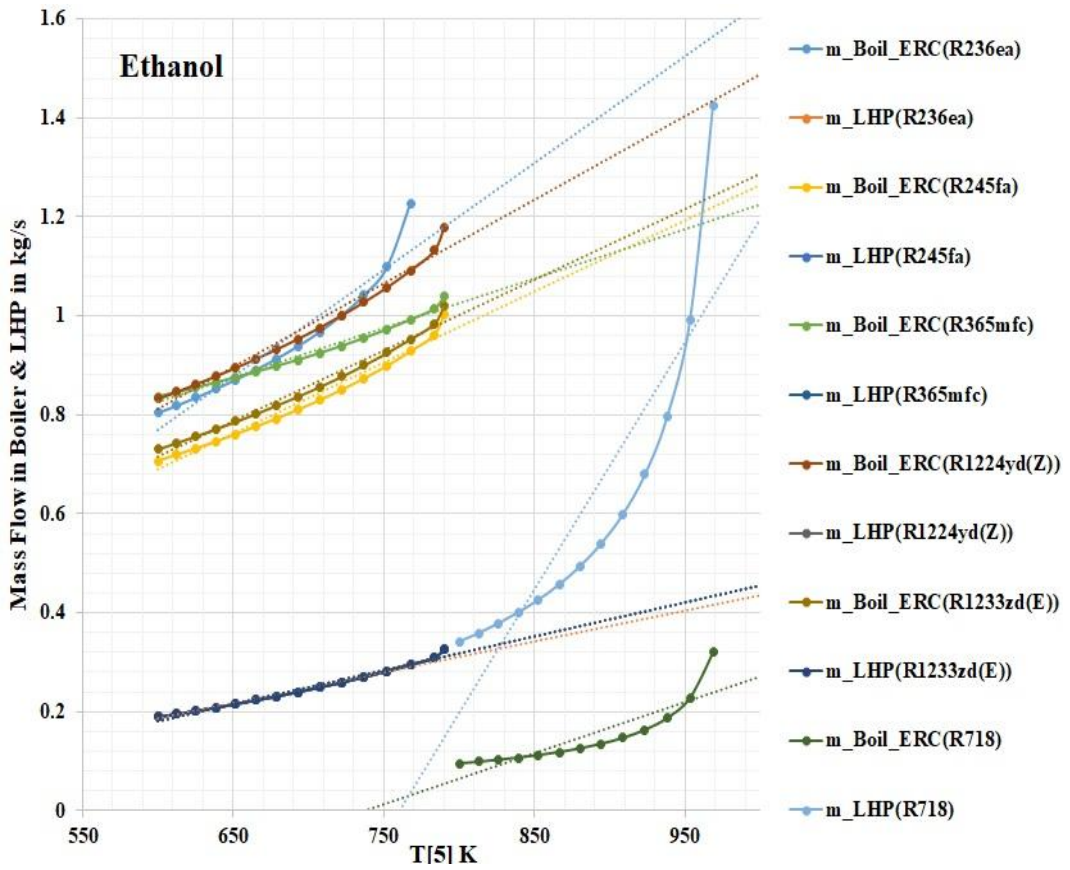


Fig 5.155: Mass Flow Rate of ERS & LHP with T_5 for Ethanol

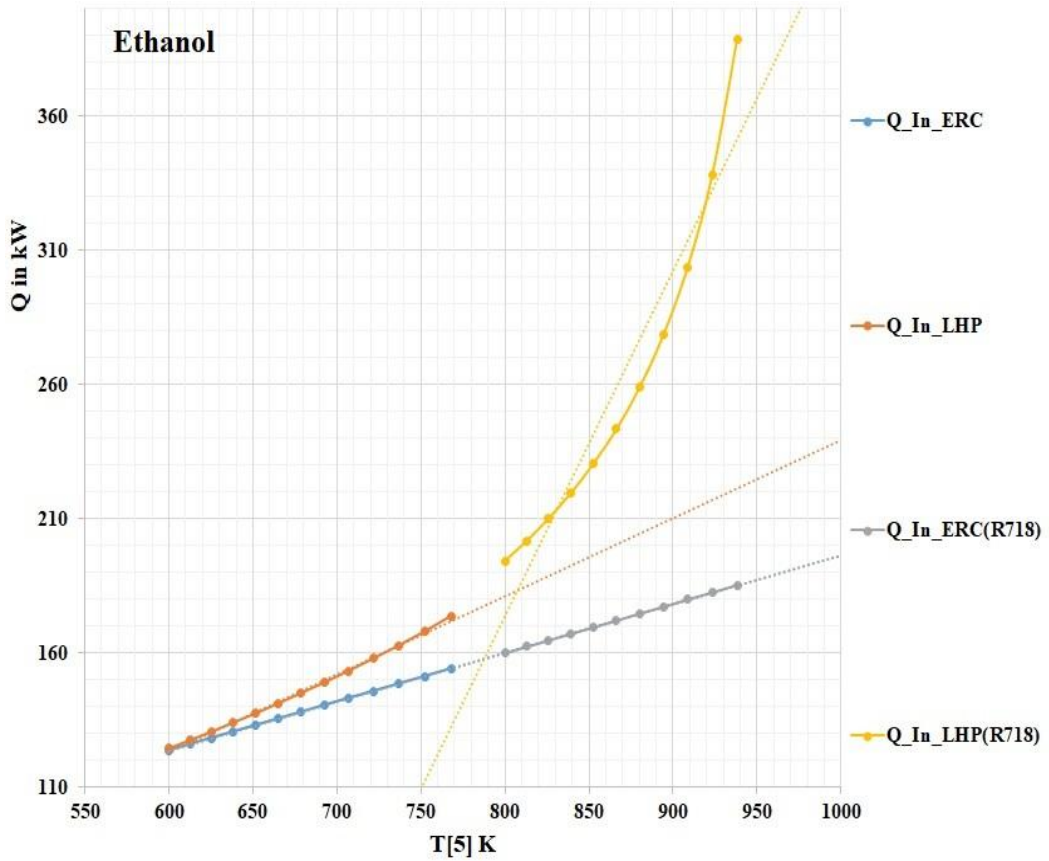


Fig 5.156: Heat Available as Input to ERS & LHP with T_5 for Ethanol

5.7.3.3. Methanol:

For methanol as well Maximum Mass flow for variable boiler pressure can be observed for R1224yz (D) as 1.023 Kg/s from Fig 5.157. For R718 the maximum mass flow rate is 0.09247 kg/s. The maximum mass flow rate for all the refrigerants has been recorded as 0.1968 kg/s and 0.2618 kg/s for R718.

From Fig 5.158 it has been studied that the Heat Input available for refrigerants at ERC & LHP is 142 kW & 153.2 kW respectively. Similarly, for R718 Heat Input available is 160.1 kW & 186.7 kW.

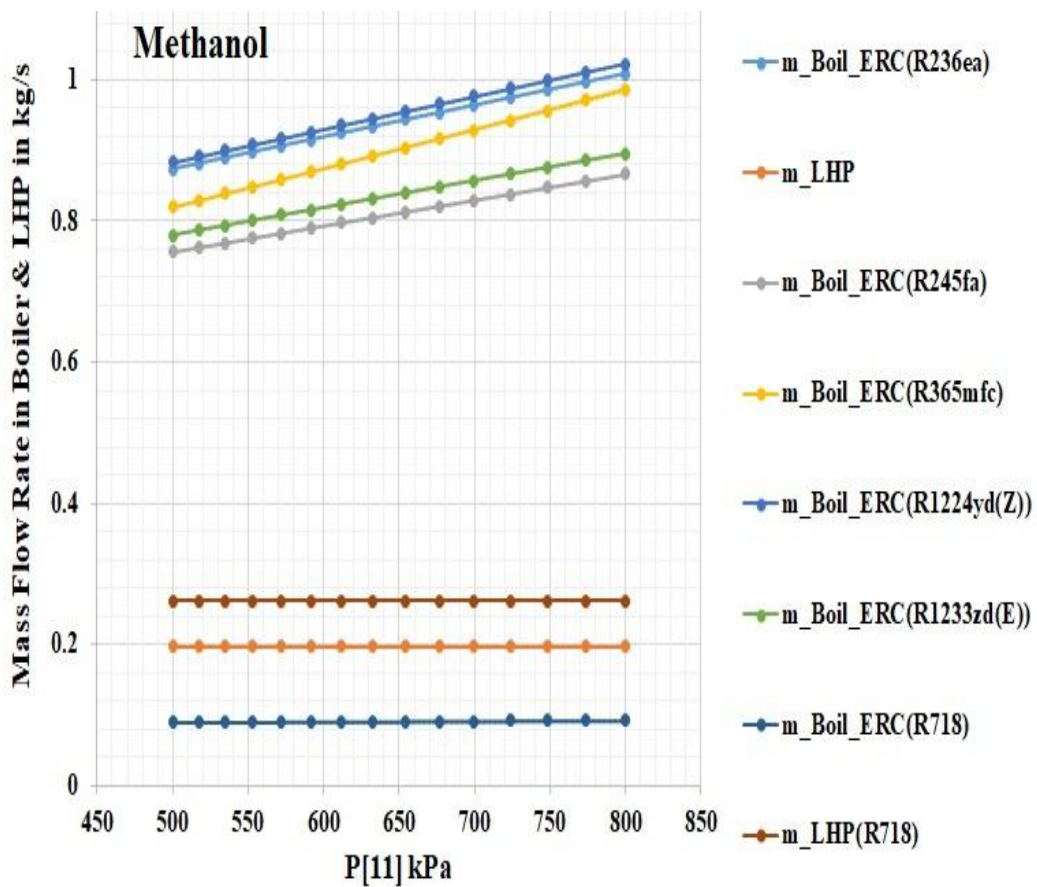


Fig 5.157: Mass Flow Rate of ERS & LHP with P₁₁ for Methanol

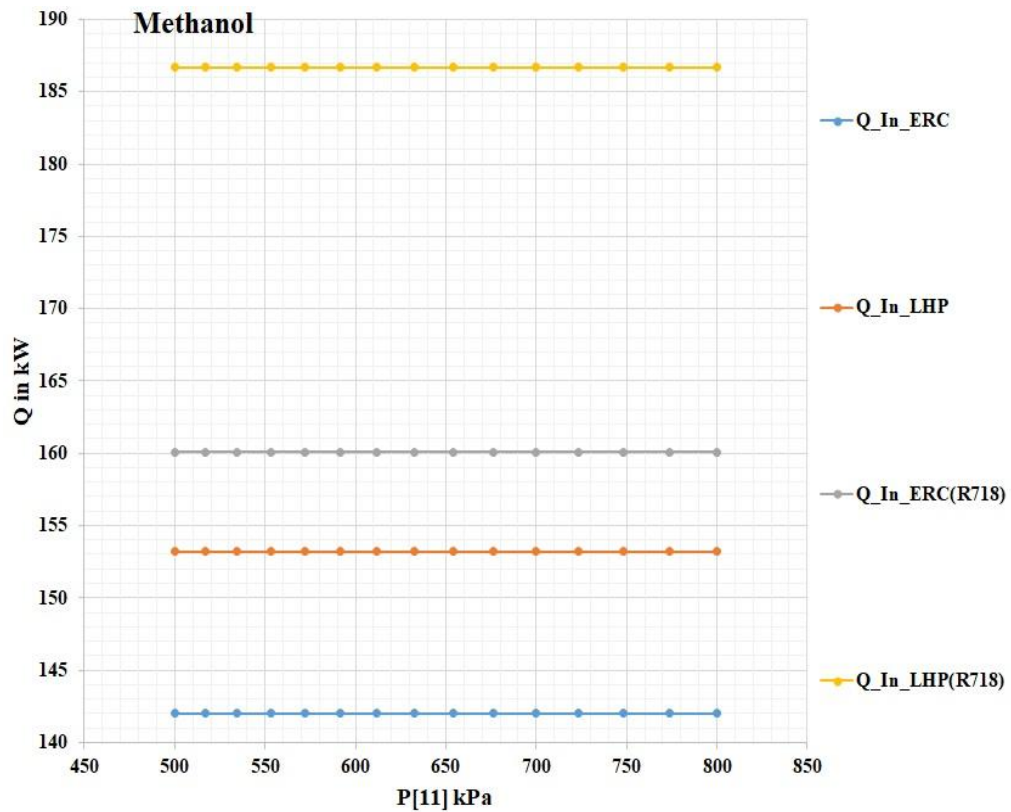


Fig 5.158: Heat Available as Input to ERS & LHP with P_{11} for Methanol

For the study based on the Peak GPC Temperature Fig 5.159 & 5.160 have been presented. It has been observed from Fig 5.159 that the range for maximum mass flow rate in ERC is for R236ea as 0.8109 - 1.239 kg/s. For R1224yz (D) the range has been observed to be 0.8389 - 1.186 kg/s. Moreover, mass flow rate range for LHP for R236ea & R1224yz (D) is 0.1512 - 0.2375 kg/s & 0.1512 - 0.2618 kg/s respectively. For R718 mass flow rate ranges for ERC & LHP are 0.09139- 0.1621 kg/s & 0.2618 - 0.5451 kg/s respectively.

The ranges of Input Heat available for ERC & LHP for Refrigerants are 123.8 - 154.3 kW & 125.5 - 175.3 kW respectively. Moreover, the R718 range of Heat Input Available for ERC & LHP is 160.1- 185.4 kW & 186.7 - 336 kW respectively in Fig 5.160.

Performance Improvement of Vapour Absorption System Using Loop Heat Pipes

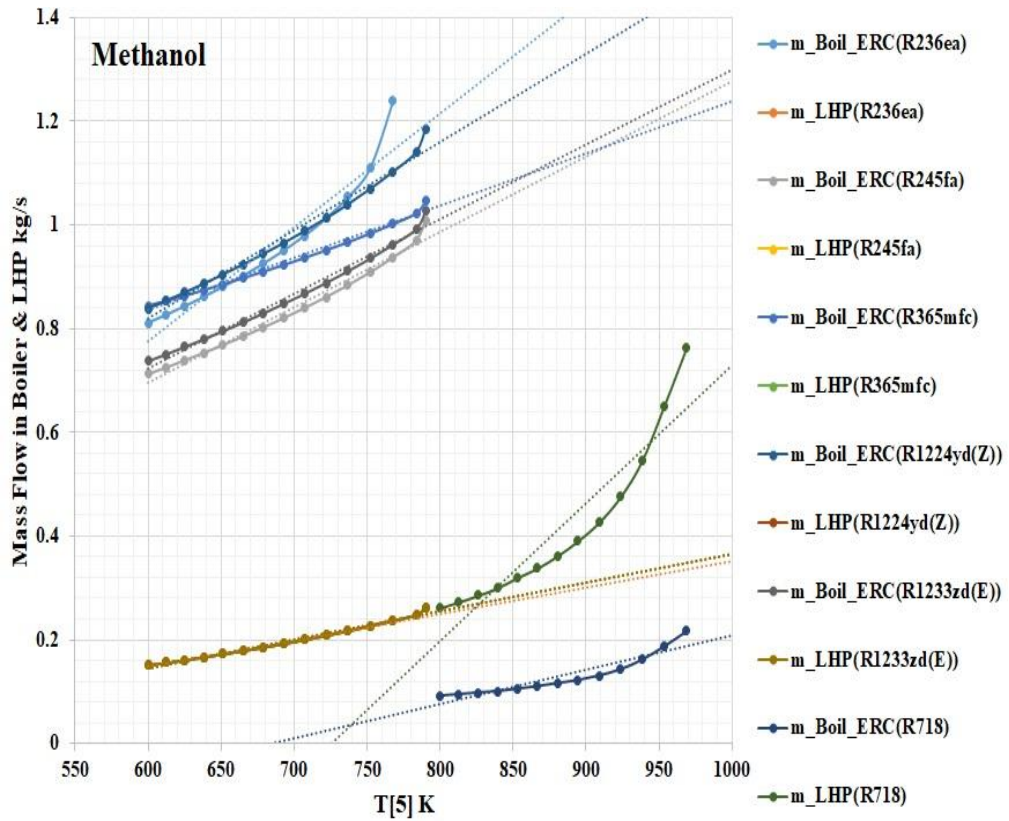


Fig 5.159: Mass Flow Rate of ERS & LHP with T_5 for Methanol

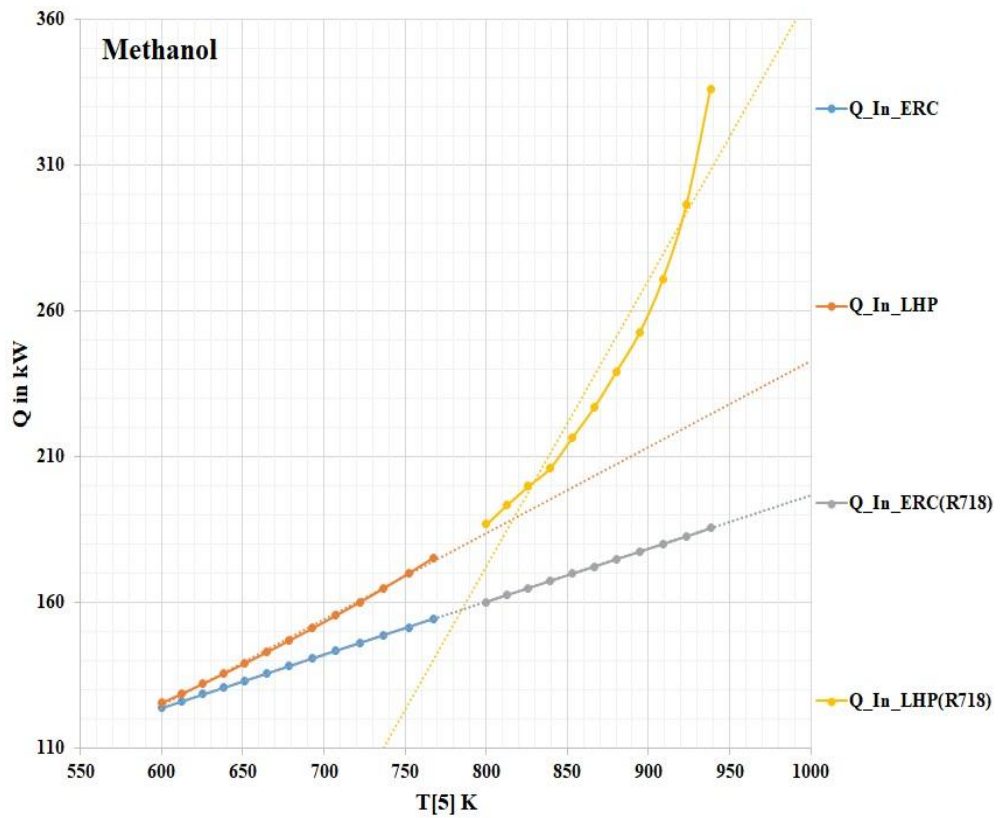


Fig 5.160: Heat Available as Input to ERS & LHP with T_5 for Methanol

5.7.3.4. Water:

In Fig 5.161 & 5.162 results for water in LHP have been presented for variable Boiler Pressure. In Fig 5.161, the Maximum mass flow rate in ERC has been required for R1224yz (D) as 0.8651 kg/s whereas, for R718 the value of the same rounds up to 0.07329 kg/s. Furthermore, the mass flow rate for the LHP for R1224yz (D) & R718 is 0.07071 kg/s & 0.08299 kg/s.

Heat Input available at ERC & LHP in Fig 5.162 for refrigerants is 129.5 kW & 142 kW, while, the heat available at ERC % LHP for R718 is 148 kW & 160.1 kW.

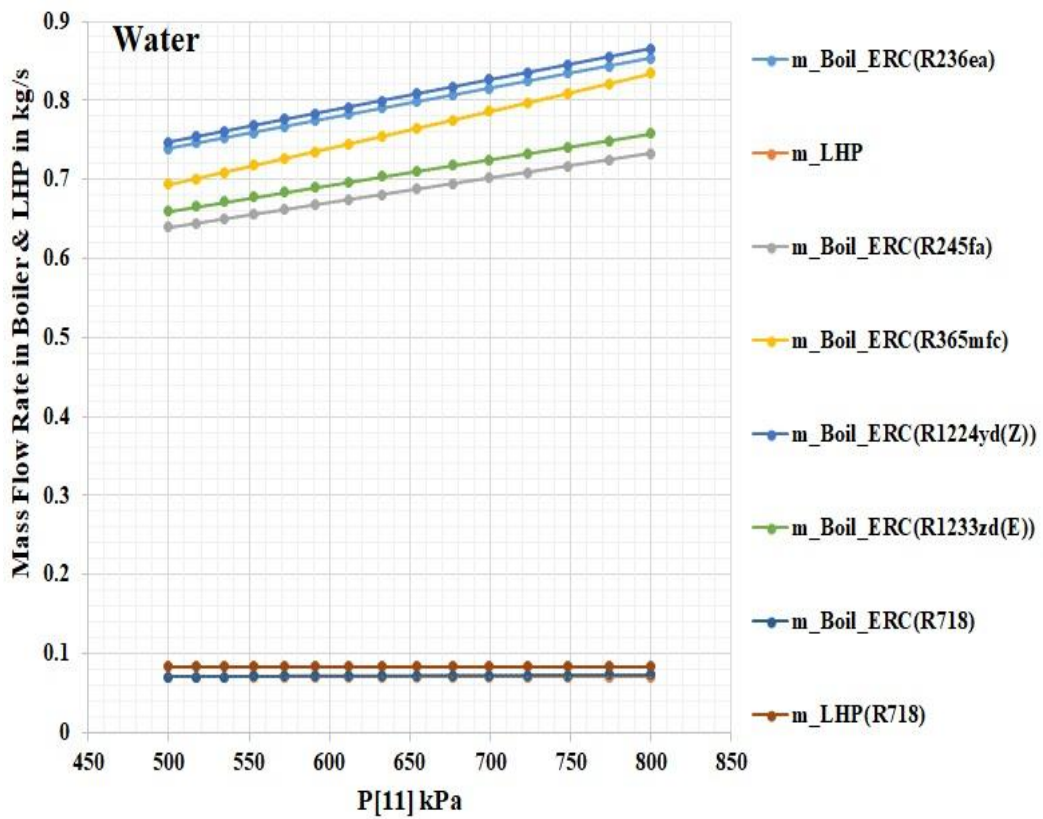


Fig 5.161: Mass Flow Rate of ERS & LHP with P₁₁ for Water

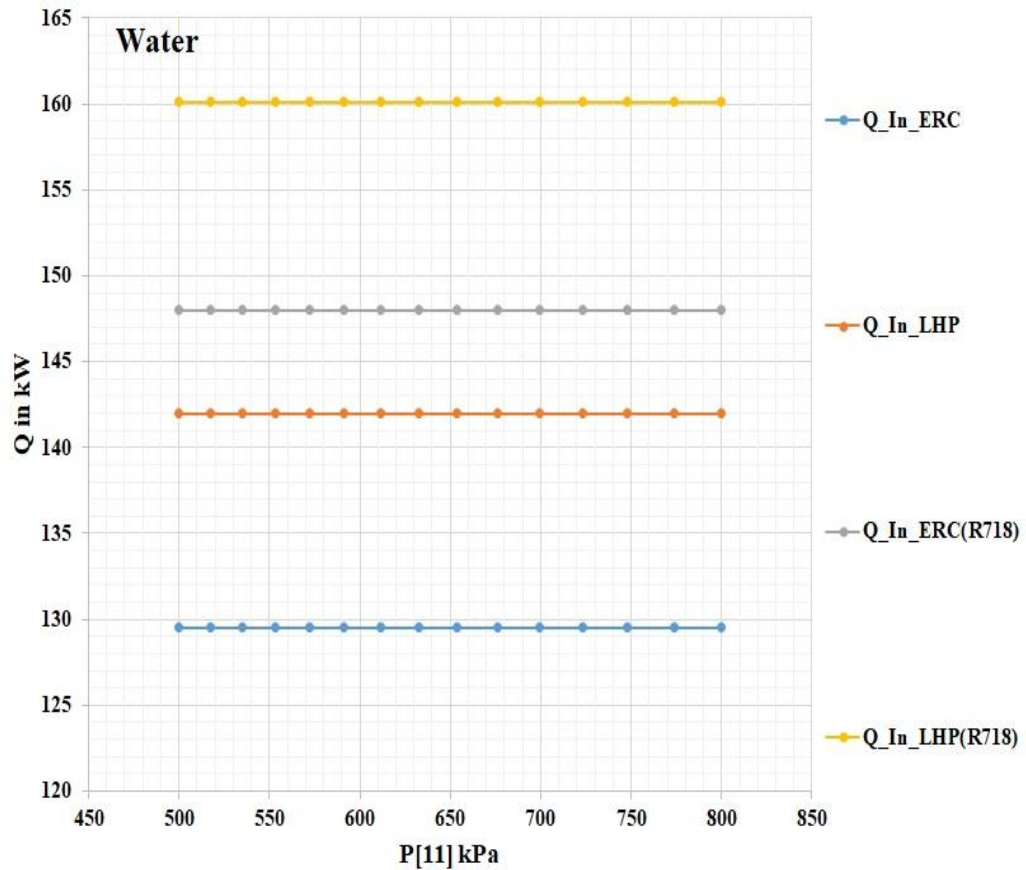


Fig 5.162: Heat Available as Input to ERS & LHP with P₁₁ for Water

Fig 5.163 & 5.164 present the study with variable temperature. In the Fig 5.163, the Range of mass flow rate in ERC & LHP for R1224yz(D) is 0.7475 - 0.9348 kg/s & 0.05957 - 0.08301 kg/s respectively, whereas, for R718 the range of mass flow rate 0.07244 - 0.0906 kg/s & 0.08299 - 0.1128 kg/s respectively.

From Fig 5.164, the heat input range available at the ERC & LHP for the refrigerants is 111.9 - 142 kW & 123.8 - 154.3 kW, whereas, for R718 it is 148 - 188.7 kW & 160.1 - 196.7 kW respectively.

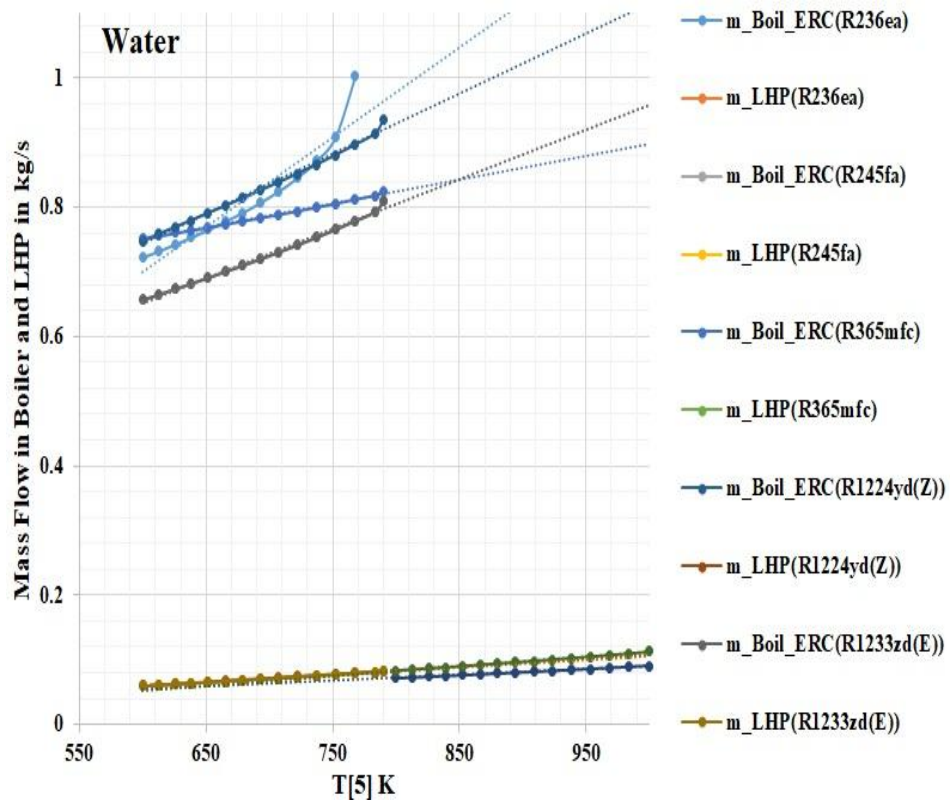


Fig 5.163: Mass Flow Rate of ERS & LHP with T_5 for Water

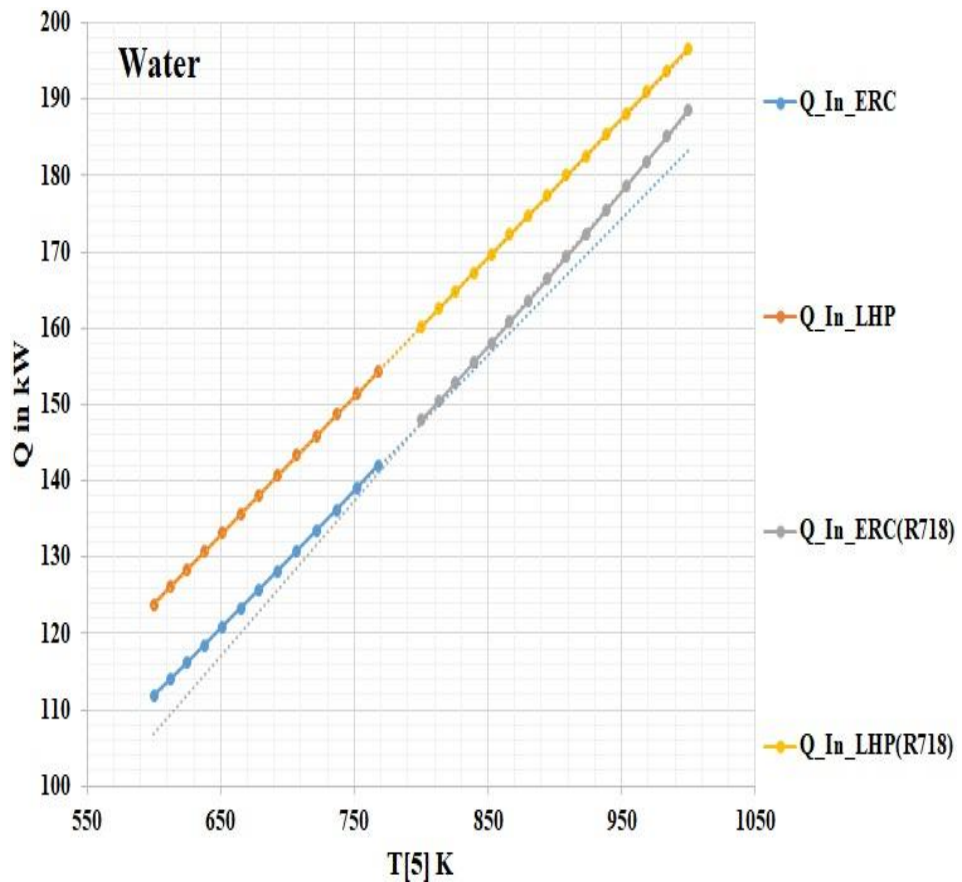


Fig 5.164: Heat Available as Input to ERS & LHP with T_5 for Water

5.8. The Patent- Refrigeration without Condenser-compressor

5.8.1. Background of the Invention:

It's become too usual a practice to develop and control the environment at a temperature below the available surrounding, from home to office, from prep school to high-end research facilities, every place has air-conditioners, refrigerators, desert coolers, etc. In the beginning, the cooling of water was done by the night being relatively cooler than the day, or the mud-pots were used to utilize the evaporative tendency of water because of which it has a temperature below the surrounding by 1 to 2 °C approx., or ice falling from the sky during the rains etc. After several advancements in processes Compression Systems work on naturally available substances water, ammonia, air, etc. The Freons were developed and Vapour Compression Refrigeration System (VCRS) came into existence and worked exquisitely for several years till environmental issues arose and further changes and developments were in demand. In the series of frequent developments, systems not consuming high-grade energy were also developed. One of the most popular systems has been the Vapour Absorption Refrigeration System (VARs), in which the main power consuming bulky part of the system i.e., the compressor, was removed from the system and the system works on low-grade energy leaving a huge opportunity behind for utilizing numerous waste heat sources with one drawback of performance inferior to that of VCR system creating incredible opportunities for extensive research experiments.

The system consumes very less work energy in the pump rest it works on low-grade energy supplied by the Generator. It's very clear that to improve the performance of the system, either supply of heat can be reduced or internal heat losses can be reduced. Devices such as heat exchangers, analyzers, rectifiers, dephlegmator, etc. to improve performance. At a temperature of around 100°C, strong refrigerant leaves the generator and condenses, followed by the expansion in the valve and providing a cooling effect in the evaporator, just similar to the VCRS. During condensation, heat is released into the surrounding. As a quick visualization of the amount of energy involved, for a simple water-lithium bromide system with absorber and condenser working at 40°C, chiller at 10°C, and the generator at 97°C for 1TR capacity, the

generator will require 4.6kW heat energy (Q_G), absorber (Q_A) and condenser (Q_C) will reject 4.35kW and 3.77kW heat respectively, with a COP of 0.77 majorly dependent on Q_G and RC. The power input to the pump is negligible. With the rise in RC and a decrease in Q_G , the first law COP will improve. Also, the second law COP will improve if heat losses are reduced.

The idea of a Refrigerating unit without the bulky compressor-condenser unit proposed is a modification brought to a Vapour Absorption System. This system will be very useful where waste heat is available if used in conjunction with the Power Plants, Industrial Processing Plants, or very effective with the solar heating systems. The bio-fuels can be used despite the lower calorific values when compared to petroleum.

5.8.2. Prior Art:

It has been proposed in the prior art to use heat pipes for cold storage purposes along with thermoelectric modules. The heat pipes in the prior art have been proposed to be used for the cooling of the electronic multi-chip module. In one prior art, a plurality of heat pipes was proposed to be used for air-conditioning applications. In prior arts, heat pipes have also been proposed to be used for cryogenics effects to obtain the superconductivity of the semiconductors. For vapour absorption refrigeration systems, in the prior art, a refrigeration plant working on a Water-Lithium Bromide system has been proposed. Cascading of vapour absorption refrigeration system has also been proposed in another prior art. In the prior art, multiple effects absorption systems have been proposed. A prior art proposed multiple temperature absorption refrigeration systems that produce lower temperatures.

5.8.3. Brief Description of Drawings:

In the accompanying drawings, the embodiment of the invention of Refrigeration without a Condenser-Compressor is explained. In these drawings:

Drawing 1 is the schematic diagram of the proposed invention, which consists of an addition of a loop heat pipe (LHP) **12** that acts as an evaporator-condenser. The weak mixture can be observed to be entering into the LHP **12** before going into the

generator. Also, strong refrigerant out of the generator gets condensed in LHP 12 only. The figure also shows the heat interactions, operating temperatures, and vital parts of the proposed invention.

Drawing 2 shows the arrangement of heat transfer between the mixture and the vapour flowing inside 4. The mixture in this arrangement absorbs heat being rejected during the condensation of the Heat Pipe working fluid.

Drawing 3 shows the LHP 12 supplying heat to generator 9. Heat is supplied inside the evaporator of Loop Heat Pipe 7 and having the condenser of the Loop Heat Pipe 4 connected to the generator 9. Two systems are connected through Loop Heat Pipe 12.

Drawing 4 explains the LHP 12 introduced in the refrigeration system. It has mainly four parts components 4, 5, 6 & 7. Component 4 is the condenser of the LHP 12 where the working fluid of LHP 12 (ammonia, water, ethanol, methanol, etc.) gets condensed, component 5 carries saturated or superheated vapour working fluid to the component 4 called vapour line, component 6 is called liquid line which transfers the condensed liquid working fluid to the component 7 where the liquid working fluid absorbs heat and gets vaporized and moves into 5. In 6 there are two sub-components 6-1 and 6-2 which ensure that only liquid enters 7.

Drawing 5 explains the compartments of component 7 along with the cross-section. 7-1 is defined to be the compensation chamber (CC) that stores the liquid working fluid and makes sure fluid for evaporation doesn't fall short. 7-2 is the vapour removal channel that clears the vapours after getting evaporated towards 5. 7-3 is the porous wick through which vapours move into 5 through 7-2. 7-4 is the part of the where the heat interaction takes place, and heat is supplied to the working fluid.

5.8.4. Refrigeration without Condenser-Compressor

The invention produces refrigeration without condenser and compressor units in the system. It's evident from the former developments that an absorber 2, a pump 3, a generator 9 & a valve 8, all together form a thermal compressor and replace the conventional compressor of Vapour Compression System. Other accessories (analyzer, rectifier, dephlegmator) can also be used as desired. Along with the

changes, refrigerants are also changed, two fluids have been used an absorbent and a refrigerant. As in Ammonia-Water, water is absorbent, while in Lithium Bromide-Water; Lithium Bromide is the absorbent, also an easily available fluid. Whereas in the proposed invention, the condenser is also replaced with an LHP **12**. The system can operate between temperature limits of 100-120 °C to sub-zero (-5,-10,-15°C, etc) temperatures depending on the requirements of the user. The system will need only heat for operation. The loop heat pipe/s **12** is used here especially to act as a condenser and as an intra-system heat exchanger, as it can remove heat and heat has to be removed from it and this removed heat can be used before generator **9**.

This induction also enhances the performance of the system on several thermodynamic grounds. The LHP/s in the system is/are used to condense the strong refrigerant, during the condensation, the fluid inside LHP such as water/ammonia/Ethanol, etc. which are very easily available fluids, get evaporated and this vapour is condensed by rejecting heat to the strong solution, preheating the mixture. This preheating decreases the heat-supplied requirements through the external sources, making it possible to be installed at locations where heat supplied from external sources isn't in high amounts. Chiller (evaporator) unit **1** is chosen, keeping the utility of the system in mind. Bare tube chillers to shell & tube type chillers can be used. Loop Heat Pipes **12** having coherent porous wicks can be used for high heat flux operations or more than one loop heat pipe **12** can be used for high heat flux operations. The bio-fuels having lesser Calorific Value compared to petroleum products can be used as external heat sources. Apart from this, solar energy and waste energy from plants can very well be used.

To describe the chain of events we must focus on the **Drawing 1** saturated vapour refrigerant exits the chiller (evaporator) **1** at **2'** and enters **2**, there it gets mixed with the absorbent liquid, Q_A is rejected and liquid is then pumped with **3** at **3'** to **4'**, through **4** where the mixture liquid is used to condense the saturated/superheated vapour flowing inside **4**, Q_{Cond} is exchanged. The condensed liquid in **4** moves into **5** and the mixture in this process gets heated up to **5'** and moves into a heat exchanger **11**, exiting **11** the heated mixture nearing the desorption temperature of the mixture at **6'** enters **9** where external source as mentioned above is used to heat the mixture and desorption takes place, the absorbent at high temperature at **7'**, rejecting heat in **11** is throttled at **8'** by **8** to **9'**, is fed back to the absorber. The refrigerant exiting **9** at **10'**,

is passed through **7** to get condensed, while the refrigerant gets condensed, Q_{Evap} is exchanged, the fluid in **7** gets vaporized and moves into the **5**, and through **5** it moves into **4**. The condensed liquid refrigerant at **11'** is then throttled in valve **10** to **1'** to produce refrigeration in the **1** and exits at **2'**. The heat input Q_{Gen} to the proposed invention is supplied through another loop heat pipe **12**. The process is evaporation and condensation inside **12**, so the heat transfer characteristics are improved, and heat utilization is increased, reducing the losses within the proposed invention.

Table 5.19 consists of the abbreviations used for the proposed invention. Along with the abbreviations, the operating temperatures as well as the heat interactions of the invention. The total heat intake of the invention is only in **9&1**. In a system with the condenser, the heat was also rejected to the surrounding which was avoidable and is avoided by the use of LHP **12**. The proposed invention utilizes intra-system heat for performance enhancement. Only unavoidable heat loss to surroundings in **2** remains. As the rejected heat is reduced, the global warming potential of the system also gets reduced. Also, reduction of the requirement of heat addition externally, unconventional energy sources such as solar energy and bio-fuels can be implemented, which in turn reduces the environmental pollution.

Table: 5.19: Abbreviations Used in the System-Patent

Terms	Abbreviations	Terms	Abbreviations
Refrigeration Effect	RE (kW)	Heat rejected in absorber	Q_A (kW)
Heat supplied in generator	Q_G (kW)	Heat rejected in condenser of LHP	Q_{Cond} (kW)
Heat absorbed in the evaporator of LHP	Q_{Evap} (kW)	Absorber Temperature in K	T_A (K)
Generator Temperature in K	T_G (K)	Evaporator Temperature in K	T_E (K)

5.8.5. Conclusions on The Patent

The proposed invention can produce refrigeration without a compressor and condenser in the system. The condenser is replaced by a loop heat pipe and the loop heat pipe acts as a heat exchanger as well. This intra-system heat exchange pre-heats the mixture before the generator reduces the requirement for external heat. This opens the opportunity for the invention to get installed at places where the heat source isn't rich. As the loop heat pipes can be flexibly arranged, the proposed invention as well is flexible in terms of arrangements. The invention can also work on the bio-fuels as it can work on fuels with low calorific value. Thus, a new less polluting method of refrigeration is developed. Also, the loop heat pipe is a device that is self-driven through capillary actions, it doesn't require any power input. The invention thus requires very little power input in a pump. Heat rejected remains only in the absorber, this also curbs global warming as well.

5.8.6. The Claims

I claim that;

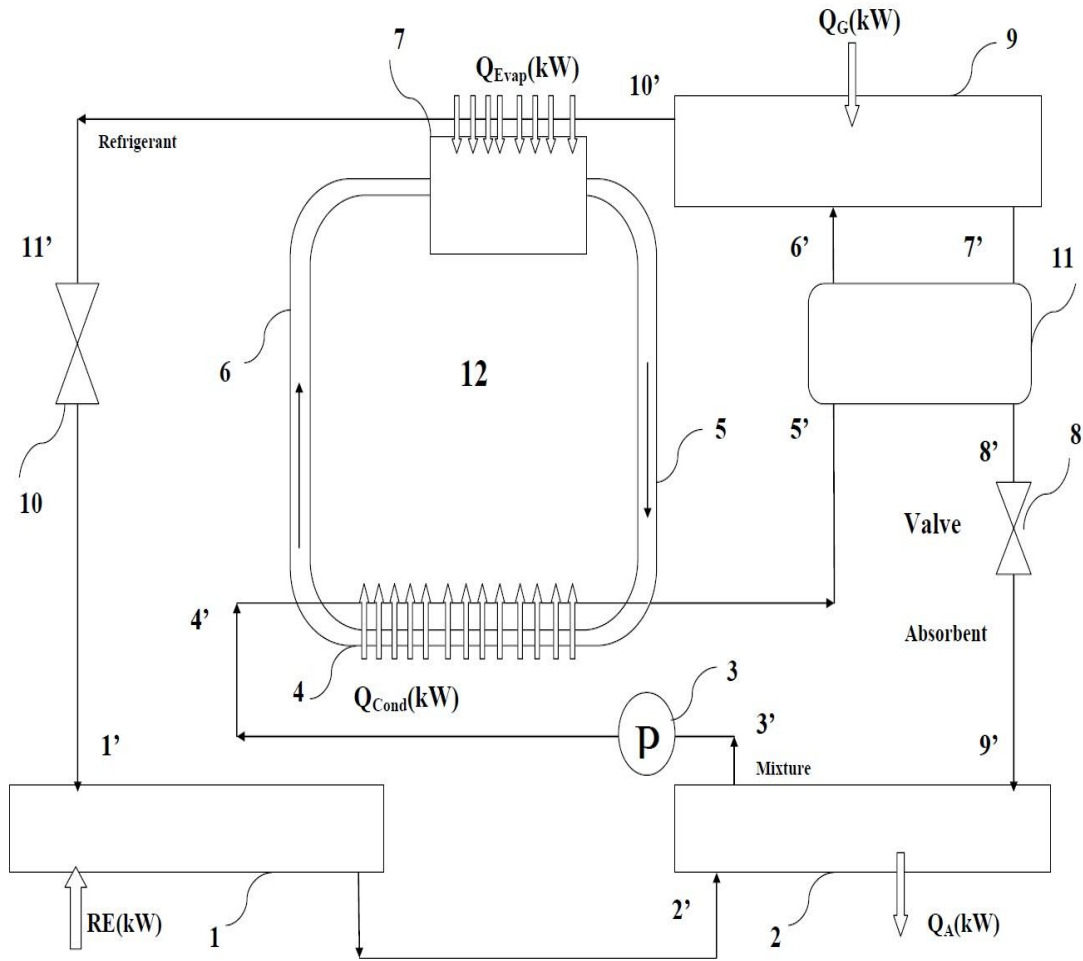
1. A refrigerator comprising of:
a chiller (evaporator) **1**, an absorber **2**, a generator **9**, and a two-loop heat pipe **12** operatively connected;
said loop heat pipe **12** exchanges heat with mixture leaving the absorber **2** and vapour refrigerant leaving generator **9**;
said evaporator **1**, absorber **2** generators **9** capable of working on well-defined and available temperatures following environmental requirements while connected to loop heat pipe **12**;
said loop heat pipe **12**, working as a superconductor of heat, also connects the external heat source to generator **9**, to supply heat to generator **9**.
2. A system as claimed in **claim 1** in which:
heat which was wasted by the condenser to the surrounding is now utilized by the incorporation of the loop heat pipe **12**;
the fluid inside the evaporator part of the loop heat pipe **7** is evaporated to condense the vapour refrigerant coming out of the generator **9**;

the thus generated vapour inside the loop heat pipe **12** is used to preheat the mixture coming out of the absorber **2**, by getting condensed inside the condenser part of the loop heat pipe **4**;

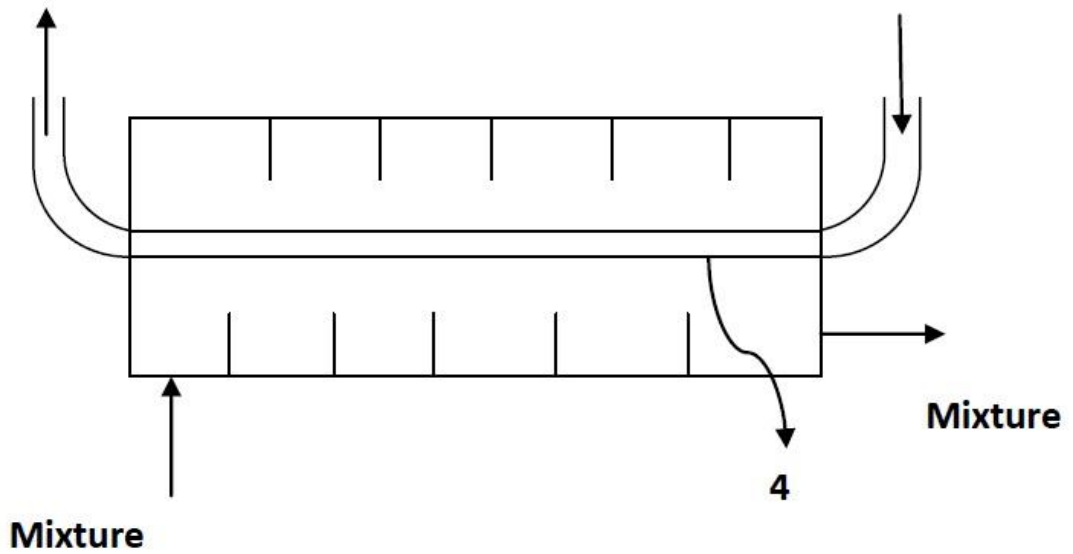
to supply the required heat for desorption the loop heat pipe **12** is connecting the heat source to generator **9**.

3. A system as claimed in **Claim 2** which:
requires lesser heat input from the external sources compared to another absorption system producing the same refrigeration effect and working under the same temperature ranges, with the same mixtures, without a loop heat pipe **12**;
is capable of using lesser calorific value bio-fuels with lesser heat input required, instead of polluting petroleum fuels.
4. The method of producing refrigeration as claimed in **Claim 2** utilizes the intra-cycle heat to reduce the heat input from outside sources and curb pollution and global warming.
5. A system as claimed in **Claim 2** in which loop heat pipe **12** is incorporated as a condenser and as well as a heat exchanger.
6. A system as claimed in **Claim 2** in which heat of condensation is rejected within the system itself.
7. A system as claimed in **claim 2** in which a loop heat pipe **9**, is used to connect two different systems, one where energy is abundantly available as waste heat, and the other where the waste energy is utilized to produce useful refrigeration; the benefit of loop heat pipe being a superconductor of heat is realized.

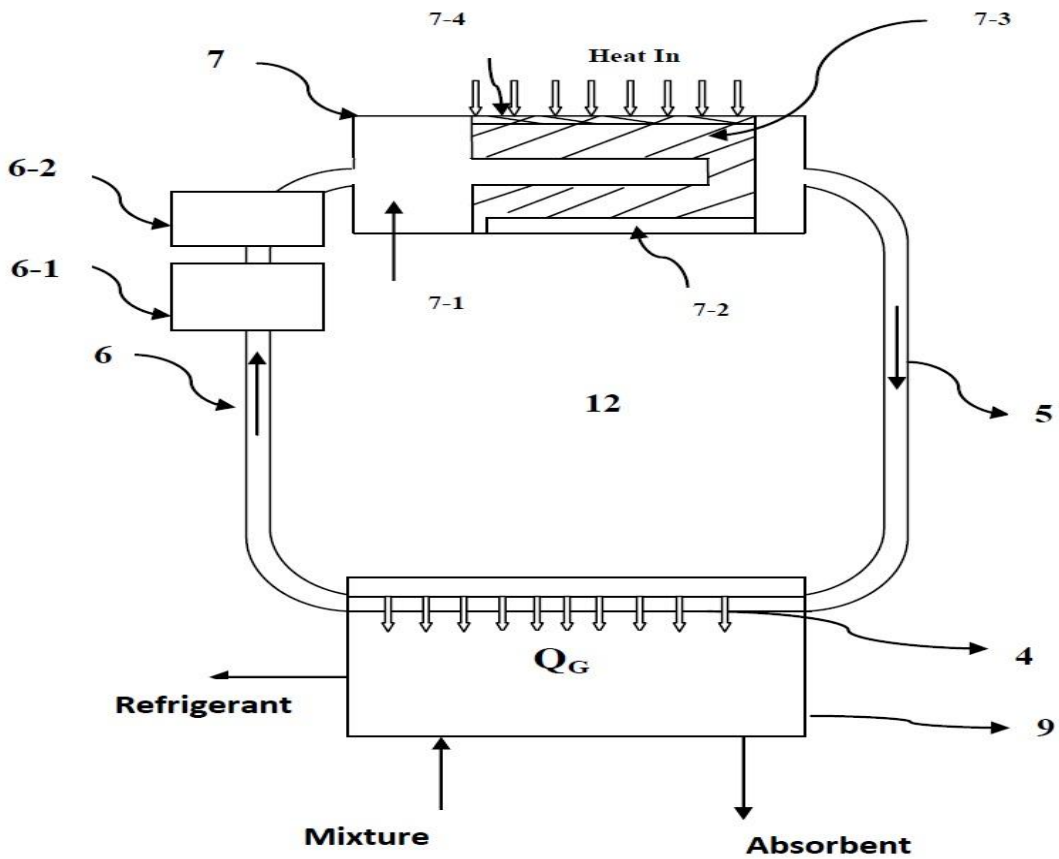
5.8.7. Drawings



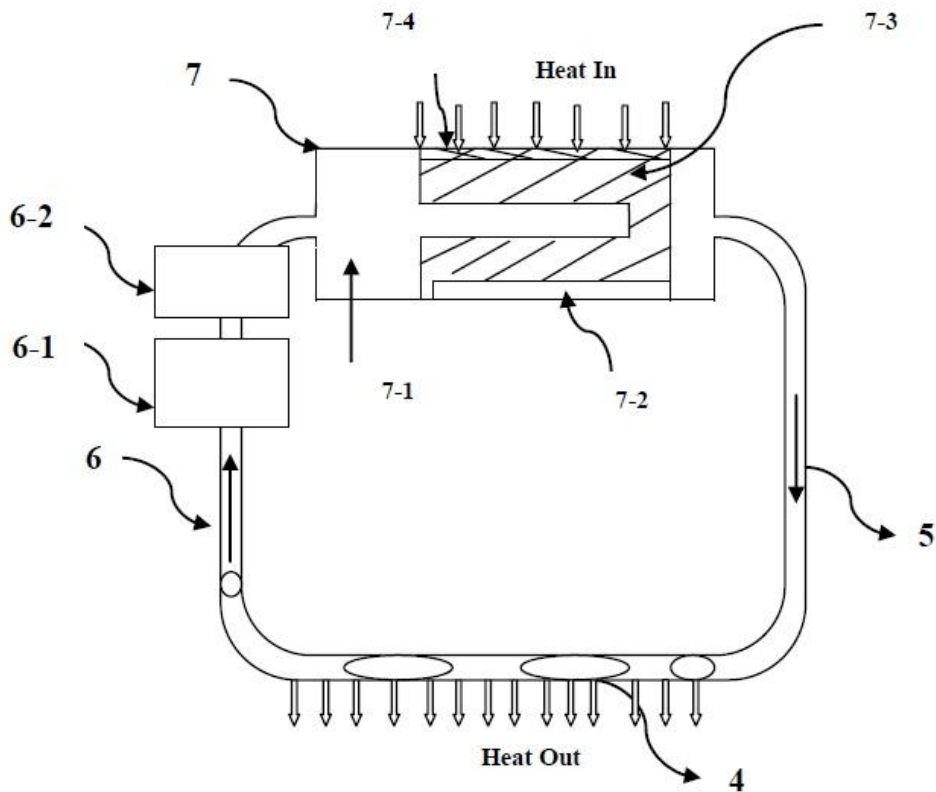
Drawing 1: Simple Single Effect System



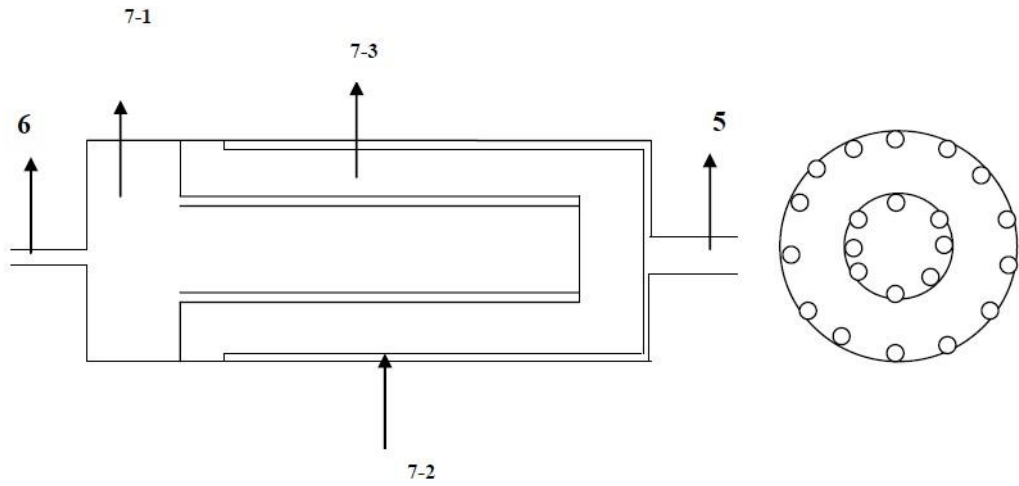
Drawing 2: Mixture Passing Through Condenser of LHP



Drawing 3: Simple Single Effect System



Drawing 4: A Loop Heat Pipe



Drawing 5: Cross-section of Evaporator of Loop Heat Pipe

5.9. Parameters of Loop Heat Pipes [69] [165]

Based on the heat inputs and heat transfer requirements, Table 5.20 contains the parameters of the design of the suitable LHP.

Table 5.20: Parameters of the LHP

Parameters	Data
Material	Copper
Outer Dia (cm)	54
Inner Dia (cm)	49.7 mm
Maximum Capacity	59.3 kW
Working Fluid	Water
Vessel Material	Copper, Nickel
Overall Effectiveness	0.5
Orientation	Gravity Assisted
Operating Temperature Range	Up to 180 – 200 °C
Wick	Various (140-180 °C), nickel felt (90 °C), mesh (90 °C), sintered copper (60 °C),
Capillary Height (cm)	156.8 (sintered copper)
Pore Radius (cm)	0.017 (nickel felt), 0.0009 (sintered copper)
Permeability (m ²)	6×10 ⁻¹⁰ (nickel felt), 1.74×10 ⁻¹² (sintered copper)
Porosity (%)	89 (nickel felt), 52 (sintered copper)

Table 5.21 presents the required number of LHPs which need to be applied in parallel to extract heat input for the usages.

Table 5.21: No. of Required LHPs to Replace Conventional Heat Exchangers

System	LHP	Capacity (kW)	Max Heat Load (kW)	Required No of LHPs
Single Effect VARS	LHP – I		3.3	1
	LHP – II		16.08	1
	LHP – III		9.81	1

Performance Improvement of Vapour Absorption System Using Loop Heat Pipes

Half Effect VARS	LHP – I	59.3	83.2	2
	LHP – II		79.3	2
	LHP – III		550	10
	LHP – IV		451	8 – 9
Double Effect VARS	LHP – I		41.7	1
	LHP – II		82.2	2
	LHP – III		214.6	4
	LHP – IV		159	3 – 4
Triple Effect VARS	LHP – I		35.9	1
	LHP – II		42.4	1
	LHP – III		95.6	2
	LHP – IV		29.6	1
	LHP – V		134.9	3
	LHP – VI		93.7	2 – 3
Quadruple Effect VARS	LHP – I		48	1
	LHP – II		71.3	2
	LHP – III	116.8	2	
	LHP – IV	84	2	
	LHP – V	52.2	1	
	LHP – VI	91.5	2	
	LHP – VII	78.17	2	
	LHP – VIII	122.2	3	
Combined ORC - GPC	LHP	250	5	
Combined ERC - GPC	LHP	250	5	

5.10. Assumption for the Analysis

To simplify the analysis and to obtain the results on various parameters, many suitable assumptions have been made in the analysis. This section defines the assumptions for the 04 Systems under consideration namely VARS, LHP, ORC & ERC.

5.10.1. Vapour Absorption Refrigeration Systems

The followings Assumptions have been taken from the analysis of the VARS:

- ❖ Refrigerant is saturated vapour at the exit from the evaporator.
- ❖ The specific enthalpy of the superheated refrigerant at the inlet of the condenser from the generator is equal to the specific enthalpy of the saturated refrigerant at the generator temperature.
- ❖ Solutions leaving the absorber and generator are saturated at the unit temperature.
- ❖ Absorber and generator pressures are equal to the evaporator and condenser respectively.
- ❖ Absorber Temperature is Equal to Condenser
- ❖ The solution entering the generator is at the generator pressure.

5.10.2. Loop Heat Pipes

The Assumptions taken for the LHP are as follows:

- ❖ The pipe wall temperature is equal to the temperature of the working fluid
- ❖ There is no heat loss in the vapour and liquid line
- ❖ The 1-D model is used to solve the energy balance equation.
- ❖ Wick is Fully saturated with Liquid
- ❖ Two-phase equilibrium in the reservoir exists
- ❖ Condensation occurs at temperature T_v ($T_c \approx T_v$)
- ❖ Laminar fully-developed flow in the vapour and liquid line
- ❖ The working medium flow inside the LHP is considered incompressible.

5.10.3. Organic Rankine Cycle

The analysis of the ORC has been performed on the following assumptions:

- ❖ Constant heat and cooling temperatures.
- ❖ An ambient temperature between 5 and 20 degrees Celsius.
- ❖ Inlet is equal to the outlet.
- ❖ No pressure drops in subsystem components.
- ❖ Adiabatic processes.
- ❖ No regard for Irreversibilities.
- ❖ 5-degree Celsius minimum pinch point i.e. thermal temperature 120 is only 115 degrees transferred or utilized.
- ❖ 0% lubricant in the working fluid.

5.10.3. Ejector Refrigeration System

The following main assumptions are taken for the analysis of the ERC:

- ❖ The pressure losses of the condenser, evaporator and connection pipeline of system components are neglected.
- ❖ In addition to the condenser and evaporator, there is no heat exchange between other parts of the system and the environment.
- ❖ The nozzle efficiency and diffuser efficiency of the ejector are given values.
- ❖ The throttling process is seen as an isenthalpic process.
- ❖ The sub cooling degree and evaporation and condensation temperature are known
- ❖ The pressure of two fluids into the suction chamber is the same as the given value, and the fluid in the ejector is the one-dimensional homogeneous flow

Chapter-6: Conclusions & Recommendations

The research investigation has been explained in Chapters- 3, 4 & 5 comprehensively with the objective of Improvement of Performance of Various Vapour Absorption Refrigeration Systems employing waste heat recovery through Loop Heat Pipes and studying of Combination of Organic Rankine Cycle & Ejector Refrigeration Cycle separately with Gas power Cycle using Loop Heat Pipes. It has been observed that the Use of LHP in place of Conventional Heat Exchangers has increased both the First Law Efficiency & Exergetic Efficiency of the Systems. The Overall Irreversibility corresponding to the Components & the systems gets reduced by the incorporation of the LHPs. The Investigation has been summarized and the Conclusions of the results obtained from EES-based Mathematical Modeling are, hereby, being presented in this Chapter.

6.1. Modified Single Effect LiBr - H₂O Vapour Absorption System:

The various performance parameters of the Single Effect VAR System such as Heat Input & Rejection, Refrigeration capacity, COP, Components-wise Percentage Contribution to the Irreversibility of the System, Temperature Variation and Improvement in the Modified System, etc. have been recorded against the variation in the Generator Temperature (100 – 110 °C). The investigations on the Modification of the Single Effect Systems are being concluded as follows:

- i.** The Refrigeration Capacity at 5 °C Evaporator temperature has been evaluated as 8.6 – 15.1 kW, whereas, the heat rejected into the LHP Evaporator replacing the condenser has been calculated as 9.13 – 16 kW for both Mod – I & II.
- ii.** The Heat Input to the Original System was 12.2 – 20.6 kW, whereas, it was recorded as 7.7 – 12.5 kW and 7.2 – 11.7 kW for Mod – I & Mod – II respectively.
- iii.** The Vapour refrigerant & Absorbent exit the generator at 85 – 95 °C & 90 – 100 °C respectively. The Mixture temperature entering the generator of the unmodified system was 65.5 – 66.9 °C, whereas, it has been calculated as approximately 70 – 80 °C & 72.5 – 82.5 °C for respectively.

- iv. The Heat input to the LHP Evaporator is 9.13 – 16.1 kW, whereas, 5.9 – 10.4 kW has been calculated to be available to be transferred to the Mixture for Preheating.
- v. The Percentage Irreversibility Contribution of the Evaporator, Generator, Condenser (replaced by LHP), Absorber & the Heat Exchanger are 8.92%, 39.3 %, 15.8 %, 27.9 % & 5.28 % respectively. Whereas, the LHP replacing the condenser in the Modification - I has shown to have lesser Irreversibility than the condenser as overall 7.08%, whereas, the LHP replacing the Heat Exchanger in Modification - II has been found to have only 3.4 % showing an overall decrement in the irreversibility.
- vi. Modification-I has presented a COP of 1.1 – 1.2 which is around a 65 % increment over the COP unmodified original single effect system as 0.7 – 0.73. Whereas, the COP of the Modification-II is 1.18 – 1.28 which is only a 6.5 % increment over the COP of Modification-I. It can be seen that the replacement of the Heat Exchanger by the LHP brings improvement but little. Also, the COP can be seen to be increasing with the Generator Temperature.
- vii. The Mixture Mass Flow rate from the absorber has been taken to be 0.05 kg/s, correspondingly, the mass of refrigerant & absorbent flow have been found to have increased from 0.0037 – 0.0065 kg/s and 0.0463 – 0.0435 kg/s respectively.
- viii. For the combined GPC & Modification-II, the Heat Available at the Exhaust of GPC is 187 – 251.4 whereas the associated Exergy & Irreversibility are 75.38-109.9 kW & 112.1-141.5 kW respectively.
- ix. The Percentage of Irreversibility Contribution to the LHP – III is approximately 16 %.
- x. Around 8-10 Single Effect VARS Modification-II can be operated with the GPC under the presented parameters.
- xi. Exergetic efficiency of the Single Effect Modification – I & II are 36.67 % & 38.66 % respectively against the 22.5 % for the Original System & 24 % for the Referred Literature.

6.2. Modified Half Effect LiBr - H₂O Vapour Absorption System:

The Half Effect System has been studied with the Varying Generator Temperature from 65 – 75 °C. The results of the investigation have been concluded as follows:

- i.** The Refrigeration Effect at 5 °C of Chiller temperature has been evaluated as 360.2 – 528.1 kW, whereas, the heat rejected into the LHP Evaporator replacing the Condenser has been calculated as 375.5 – 550.7 kW for both Modifications – I & II.
- ii.** The Heat Input to the Original System High & Low Generator was 435.56 – 630 kW & 339.9 – 488.9 kW respectively, whereas, the Heat Interaction in the High & Low Generators are approximately 332 - 478 kW & 236 – 337 kW and 313.5 – 451 kW & 217.1 – 309.9 kW respectively, for Modification – I & Modification – II respectively.
- iii.** The Vapour refrigerant & Absorbent exit the generator at 59.7 – 69.5 °C & 62 – 72 °C respectively. The Mixture temperature entering both the generators of the unmodified system was 40.5 – 43.5 °C, whereas, it has been calculated as approximately 47.8 – 57.8 °C & 51.1 – 59.1 °C for Modification – I & Modification – II respectively.
- iv.** The Heat input to the LHP Evaporator is 375.5 – 550.7 kW, whereas, 289.5 – 424.6 kW has been calculated to be available to be transferred to the Mixture for Preheating.
- v.** The Percentage Irreversibility Contribution of the Evaporator, Generator (I&II), Condenser (replaced by LHP), Absorber & the Heat Exchanger are 33.6%, 11.45 %, 7.5%, 44.7% & 1.2 % respectively. Whereas, the LHP replacing the condenser in the Modification - I has shown to have lesser Irreversibility than the condenser as overall 6.7 %, whereas, the LHPs replacing the Heat Exchangers have been found to have only 0.59 % & 0.69 % showing an overall decrement in the irreversibility.
- vi.** The Modification-I showed a COP of 0.63 – 0.64 is around a 60 % rise over the COP unmodified original Half effect system as 0.39 – 0.4. While the COP of the Modification-II is 0.67 – 0.69 which is only a 7 % rise over the COP of Modification-I. Consequent to the replacement of the Heat Exchanger by the LHP, the improvement is minute. The COP is seen to be increasing with the Generator Temperature.
- vii.** The Mixture Mass Flow rate from the low and high absorbers has been kept as 1 kg/s, correspondingly, the mass of refrigerant & absorbent flow in low and high generators have been found to have increased from 0.12-0.18 kg/s & 0.87 – 0.81

kg/s and 0.15-0.22 kg/s & 0.84 – 0.77 kg/s respectively. The mass flow rate of refrigerant in the evaporator is 0.15-0.22 kg/s.

- viii. For the combined GPC & Modification-II, the Heat Available at the Exhaust of GPC is 219.8 – 283 kW whereas the associated Exergy & Irreversibility are 82.73-117.2 kW & 137-166.5 kW respectively. Hence, as the mass flow rate of the GPC is increased from 1 kg/s to its normal operating mass flow rate, the GPC can easily be used for this system.
- ix. The Percentage of Irreversibility Contribution to the LHP – IV is approximately 6.1 %.
- x. Exergetic Efficiency of the Half Effect Modification – I & II are 38.52 % & 51.25 % respectively against the 24.07 % for the Original System & 37.37 % for the Referred Literature.

6.3. Modified Double Effect LiBr - H₂O Vapour Absorption System:

The Temperature of the High-Temperature Generator has been varied from 140-150 °C for the Double Effect VAR Systems. The analysis has the following conclusions:

- i. The Refrigeration at 5 °C Evaporator temperature has been evaluated as 336 – 370 kW, whereas, the heat rejected into the LHP Evaporator replacing the Condenser has been calculated as 194 – 214 kW for both Modifications – I & II.
- ii. The Heat Input to the Original System High & Low Generator was 268 – 297 kW & 163 – 181 kW respectively, whereas, the Heat Interaction in the High & Low Generators are approximately 161 – 179 kW & 163 – 180 kW and 142 – 158 kW & 153 – 169 kW respectively, for Modification – I & Modification – II respectively.
- iii. The Vapour Refrigerant & Absorbent exit the High and Low Generators at 131-138 °C & 137-146 °C and 56 - 58 °C & 74 – 78 °C respectively. The Mixture temperature entering both high & low generators of the unmodified system was 95– 102 °C, whereas, it has been calculated as approximately 107 – 114 °C and 118 – 126 °C for Mod – I & Mod – II respectively.
- iv. The Heat input to the LHP Evaporator replacing the Condenser is 194 – 214 kW, whereas, 155 – 171 kW has been calculated to be available to be transferred to the Mixture for Preheating.

- v. The Percentage Irreversibility Contribution of the Evaporator, High & Low Generators, Condenser (replaced by LHP), and the Heat Exchangers – I & II are 12.4%, 17.1 & 3.8 %, 5.8% and 8.5% & 15.7% respectively. Whereas, the LHP replacing the condenser in the Modification - I has shown to have lesser Irreversibility than the condenser as overall 4.23%, whereas, the LHPs replacing the Heat Exchangers I & II in Modification – II have been found to have 6.5 % & 9.3 % which presents an overall decrement in the irreversibility.
- vi. Modification-I has presented a COP of 2.08 – 2.06 which is around a 65 % increment over the COP unmodified original double effect system as 1.25 – 1.24. While the COP of the Modification-II is 2.37 – 2.34 which is only a 13 % increment over the COP of Modification-I. It can be seen that the replacement of the Heat Exchanger by the LHP brings improvement but little. Also, the COP can be seen to be decreasing with the Generator Temperature.
- vii. The Mixture Mass Flow rate from the absorber has been kept as 1 kg/s, correspondingly, the mass of refrigerant & absorbent flow in low and high generator have been found to have increased from 0.072 – 0.078 kg/s & 0.859 – 0.845 kg/s and 0.069 – 0.076 kg/s & 0.931 – 0.923kg/s respectively. The mass flow rate of refrigerant in the evaporator is 0.141- 0.155 kg/s.
- viii. For the combined GPC & Modification-II, the Heat Available at the Exhaust of GPC is 133.6 – 197.6 kW whereas the associated Exergy & Irreversibility are 58.74 – 93.24 kW & 58.74 – 93.24 kW respectively.
- ix. The Percentage of Irreversibility Contribution to the LHP – IV is approximately 6.52 %.
- x. Exergetic efficiency of the Double Effect Modification – I & II are 53.84 % & 61.23 % respectively against 32.37 % for the Original System & 32.85 % for the Referred Literature.

6.4. Modified Triple Effect LiBr - H₂O Vapour Absorption System:

The High Generator temperature has been varied from 160 – 190 °C. The followings are the conclusions:

- i. The Refrigeration at 5 °C Evaporator temperature has been evaluated as 134.6 – 274.4 kW, whereas, the heat rejected into the LHP Evaporators replacing the

Medium & High Condensers has been calculated as 44.8 – 95.6 kW & 69 – 135 kW for both Modification – I & II.

- ii. The Heat Input to the Original System High Generator was 91.3 – 164 kW, whereas, the Heat Interaction in the High Generator is approximately 58 – 99 kW and 55 – 93 kW respectively, for Modification – I & Modification – II respectively.
- iii. The Vapour refrigerant & Absorbent exit the High and Medium Generators at 152 – 172 °C & 165 – 182 °C and 102 – 111 °C & 109 – 126 °C respectively. The Mixture temperature entering the high generator of the unmodified system was 128.4 – 142.8 °C, whereas, it has been calculated as approximately 136-155 °C and 140.5 – 160.5 °C for Modification – I & Modification – II respectively.
- iv. The Heat input to the LHP Evaporator replacing Medium & High Condensers is 44 – 95.6 kW & 69 – 135 kW respectively, whereas, 35 – 76 kW & 55 – 107 kW has been calculated to be available to be transferred to the Mixture for Preheating.
- v. The Percentage Irreversibility Contribution of the Evaporator, High, Medium & Low Generators, Condenser (replaced by LHP), and the Heat Exchangers – I, II & III are 18.8 %, 6.7%, 0.6% & 5.6%, 8.1% and 5%, 7% & 8% respectively. Whereas, the LHPs replacing the Medium & High condenser in the Modification - I have shown to have lesser Irreversibility than the condensers as overall 0.085% & 0.072%, whereas, the LHPs replacing the Heat Exchangers I, II & III in Mod – II have been found to have 4.7 %, 6.7 & 6.1 % which presents an overall decrement in the irreversibility.
- vi. The Modification-I has attained the COP of 2.3 – 2.7 which is around 56 - 65 % increment against the COP unmodified original Triple effect system as 1.47 – 1.67. Whereas, the COP of the Modification-II is 2.4 – 2.9 which is only a 5% increment over the COP of Modification-I. It can be seen that the replacement of the Heat Exchanger by the LHP brings improvement but little. Also, the increase in COP can be seen to be decreasing with the Generator Temperature.
- vii. The Mixture Mass Flow rate from the absorber has been kept as 1 kg/s, correspondingly, the mass of refrigerant & absorbent flow in low, Medium and high generator have been found to have increased from 0.015 – 0.032 kg/s & 0.944 – 0.885 kg/s, 0.016 – 0.033 kg/s & 0.959 – 0.917 kg/s and 0.025 – 0.05

kg/s & 0.975 – 0.95 kg/s respectively. The mass flow rate of refrigerant in the evaporator is 0.056 – 0.115 kg/s.

- viii. For the combined GPC & Modification-II, the Heat Available at the Exhaust of GPC is 92.71 – 156.7 kW whereas the associated Exergy & Irreversibility are 43.06 – 77.57 kW & 49.65 – 79.11 kW respectively.
- ix. The Percentage of Irreversibility Contribution to the LHP – VI is approximately 6.3 %.
- x. Exergetic Efficiency of the Triple Effect Modification – I & II are 53.4 % & 56.05 % respectively against the 34.03 % for the Original System & 29.64 % for the Referred Literature.

6.5. Modified Quadruple Effect LiBr - H₂O Vapour Absorption System:

The Temperature of the Highest Generator (High Generator-II) has been varied from 180 – 205 °C, the conclusions of the study are as follows.

- i. The Refrigeration Capacity at 5 °C Evaporator temperature has been evaluated as 207.2 – 395.6 kW, whereas, the heat rejected into the LHP Evaporators replacing the Medium High-I & High-II Condensers has been calculated as 50.6 – 116.8 kW, 27.8 – 52.2 kW & 54 – 78.1 kW for both Modifications – I & II.
- ii. The Heat Input to the Original System High Generator -II was 96.5 – 169 kW, whereas, the Heat Interaction in the High Generator is approximately 68.4 – 128.5 kW and 64 – 122.2 kW respectively, for Modification – I & Modification – II respectively.
- iii. The Vapour refrigerant the High-II, High-I and Medium Generators at 171 – 190.7 °C & 132.7 – 152.7 °C and 102 – 111 °C & 92.1 – 101 °C respectively. The Mixture temperature entering the High Generator-II of the unmodified system was 150.1 – 169.5 °C, whereas, it has been calculated as approximately 154.4 – 168.3 °C and 162.2 – 176.8 °C for Modification – I & Modification – II respectively.
- iv. The Heat input to the LHP Evaporator replacing Medium, High - I & High - II Condensers is 50.6 – 116.8 kW, 27.8 – 52.2 kW & 54 – 78.1 kW respectively, whereas, 40.5 – 93.4 kW, 22.2 – 52.2 kW & 43.1 – 62.5 kW has been calculated

to be available to be transferred to the Mixture for Preheating at LHP Condensers.

- v. The Percentage Irreversibility Contribution of the Evaporator, High – II, High – I, Medium & Low Generators, Condenser (replaced by LHP), and the Heat Exchangers – I, II, III & IV are 17.5%, 4.89%, 0.5%, 5% & 5%, 5% and 5, 7, 7.5 & 8% respectively. Whereas, the LHPs replacing the Medium, High – I & II condensers in the Modification - I have shown to have lesser Irreversibility than the condensers as overall 0.085% & 0.072%, 0.059% whereas, the LHPs replacing the Heat Exchangers I, II, III & IV in Mod – II have been found to have 4.2%, 6.4%, 6.08% & 6.7 % which presents an overall decrement in the irreversibility.
- vi. The Modification-I has COP of 3 – 3.1 which is around 41 – 33.4 % increment against the COP unmodified original Quadruple effect system as 2.14– 2.3. Whereas, the COP of the Modification-II is 3.23 – 3.67 which is only a 6 – 15 % increment over the COP of Modification-I. It can be seen that the replacement of the Heat Exchanger by the LHP brings improvement but little. Also, the increase in COP can be seen to be decreasing with the Generator Temperature.
- vii. The Mixture Mass Flow rate from the absorber has been kept as 1 kg/s, correspondingly, the mass of refrigerant & absorbent flow in High – II, High-I low and medium generator have been found to have increased from 0.023 – 0.05 kg/s & 0.97 – 0.951 kg/s, 0.01 – 0.027 kg/s & 0.96 – 0.924 kg/s, 0.02 – 0.03 kg/s & 0.94 – 0.88 kg/s and 0.04 – 0.05 kg/s & 0.9 – 0.83 kg/s respectively. The mass flow rate of refrigerant in the evaporator is 0.09 – 0.16 kg/s.
- viii. For the combined GPC & Modification-II, the Heat Available at the Exhaust of GPC is 77.3 – 141.3 kW whereas the associated Exergy & Irreversibility are 35.58 – 71 kW & 40.72 – 70.19 kW respectively.
- ix. The Percentage of Irreversibility Contribution to the LHP – VIII is approximately 6.22 %.
- x. Exergetic Efficiency of the Quadruple Effect Modification – I & II are 79.54 % & 84.9 % respectively against 47.72 % for the Referred Literature.

6.6. Combined Organic Rankine Cycle with Gas Power Cycle:

It can be observed from the temperature profiles observed during the operations of the combined system that the temperatures available at the Condenser side of the LHP, the ORC also can be run super-critically, in turn, increasing its efficiency. The superconductor nature of the LHP Ex can be very effectively utilized in running a highly efficient system. Furthermore, the following numerical conclusions can be presented from the Investigation done in this research work:

- i.** The temperature source available for the ORC boiler is at 400-450K for which all the working fluids of the LHP seem to be compatible and show continuous performances.
- ii.** Silica, Stainless Steel & Copper can be chosen as materials for the LHP being compatible for all.
- iii.** Work output for the ORC at Peak Operating Temperature 1500K can be observed to be 170kW for R290 and 165 kW for R290 at 65 kPa Condenser Pressure.
- iv.** The Maximum First Law Efficiency for the ORC has been recorded at 30% for R290 across the Peak Temperature and 32% at 65 kPa Condenser Pressure.
- v.** The Maximum Second Law Efficiency for the ORC has been presented to be 75% for R290 & 82 % for R152a across the Peak Temperature and 80% for R132a & 78% for R290 at 65 kPa Condenser Pressure.
- vi.** Mass flow rate for working fluids in ORC can be observed to be in the range of 0.5kg/s & 0.35kg/s in LHP for R290-Water. All other Combinations result in more mass handling per unit of work output. Hence, multiple LHP Ex Pipes will be used for the operation of the Combined Cycle.
- vii.** Irreversibility associated with the components studied is in the range of 80kW.

For the Steel plants and Power Plants where low-grade energy is abundant, such a system can either be used to run either a centralized plant or separate systems as the total heat rejection from the Plants can be transferred through multiple LHPs depending upon the exhaust temperature of the GPC. As mentioned earlier Waste heat which is a great cause of thermal pollution and Global warming can be utilized

at higher temperatures and with substantial flexibility in such a Novel Combined Cycle. Hence, the research works offer an Eco-friendly system that works on a low heat source.

6.7. Combined Ejector Refrigeration Cycle with Gas Power Cycle:

The results obtained based on various Input parameters have been discussed, especially for R718 & R1224yz (D) (i.e., 0 ODP & 0 GDP). It has also been observed that the Temperature that can be made available for heat transfer with varying the Peak Temperature of GPC can be near or beyond the critical temperature of the eco-friendly refrigerants hence reducing the overall requirement of heat input. Hence, making the combined cycle highly attractive for industrial & eco-friendly usage. Moreover, the followings are the quantitative conclusions of the research investigation.

- i.** The temperature available at the ERC Boiler Input is in the range of 380 K to 455K which is very close to and above the Critical Temperature of the New Eco-Friendly Refrigerants.
- ii.** The Maximum Refrigeration capacity for variable Peak GPC Temperature conditions for R365mfc, R1224yd (Z) & R718 has been recorded as 10.35kW, 9.903kW & 31.545kW respectively, increasing with the temperature.
- iii.** Furthermore, the Maximum COP for variable Peak GPC Temperature Condition for R365mfc, R1224yd (Z) & R718 has been observed to be 0.2856, 0.241 & 0.285 respectively, showing a downwards trend with increasing temperature.
- iv.** Whereas, Peak Boiler Pressure Maximum Refrigeration Effect has been calculated for R365mfc, R1224yd (Z) & R718 at 12.93, 11.41 & 17.65 increasing with the pressure.
- v.** The COP under the variable pressure condition for R365mfc, R1224yd (Z) & R718 is 0.275, 0.241 & 0.289.
- vi.** For Water as working fluids of the LHP, the least Mass Flow Rate in ERC & LHP for R1224yd (Z) & R718 has been 0.8651 kg/s & 0.07329 kg/s and 0.07071 kg/s & 0.08299 kg/s respectively.

- vii.** Moreover, for Acetone as the working fluid of the LHP, Heat Input Available has been maximum at ERC & LHP for R1224yd (Z) & R718 is 142 kW & 160.1kW and 155.9 kW & 197.1 kW respectively, for variable pressure conditions.
- viii.** For Variable Peak GPC temperature condition for Water as working fluids of the LHP, the least Mass Flow Rate in ERC & LHP for R1224yd (Z) & R718 has been 0.747 kg/s & 0.072 kg/s and 0.0595 kg/s & 0.08299 kg/s respectively.
- ix.** Moreover, for Acetone as working fluids of the LHP, Heat Input Available has been maximum at ERC & LHP for R1224yd (Z) & R718 is 154.3 kW & 182.6kW and 181.5 kW & 363.1 kW respectively, for variable pressure conditions.

It can be observed that the combination of 1224yd (Z) (ERC)-Water (LHP) as a compact, eco-friendly & industrially viable combined system can be presented.

6.8. Scope for Future Research & Development Work:

This research work has focused on the various aforementioned LiBr - H₂O VAR Systems in which intra – cycle heat recovery using Loop Heat Pipes has been objectified for improvement of overall performance, reduction in size, and enhancement in the flexibility. Similar Comprehensive analysis for VAR system with pairs such as NH₃ – H₂O, LiCl - H₂O, CaCl₂ – H₂O, NH₃ – LiNO₃ & NH₃ – NaSCN, etc. and other triple fluid VAR Systems. Similarly, a comprehensive customized Heat Pipe Designing can be performed for the various systems being considered as per requirements. Moreover, experimental setups can be built to obtain results for the same.

Similarly, for the Combined ORC-GPC systems as well, the experimental analysis should be performed for final implementation on an industrial basis. The industrial application of these systems pre-requisites the successful design of high heat flux LHP HEx which has not been covered in detail. The LHP has very little Pressure & Temperature drops within its system providing the combined system with the advantage of a constant heat source at relatively high temperatures.

Furthermore, for the Combined ERC-GPC, further experimental work may be initiated on this novel system to obtain a low-cost, eco-friendly Industrial refrigeration system that can be used for the storage of different sensitive items as well as for comfort usages. Studies on customization of the LHP must also be taken up for heavy industrial applications similarly.

References

- [1]W. Chun, Y. H. Kang, H. Y. Kwak, and Y. S. Lee, “An experimental study of the utilization of heat pipes for solar water heaters,” *Applied Thermal Engineering*, vol. 19, no. 8, pp. 807–817, Aug. 1999, doi: 10.1016/S1359-4311(98)00096-9.
- [2]H. M. S. Hussein, M. A. Mohamad, and A. S. El-Asfour, “Optimization of a wickless heat pipe at plate solar collector,” *Energy Conversion*, p. 13, 1999.
- [3]S. A. Said and B. A. Akash, “Experimental performance of a heat pipe,” *International Communications in Heat and Mass Transfer*, vol. 26, no. 5, pp. 679–684, Jul. 1999, doi: 10.1016/S0735-1933(99)00054-8.
- [4]H. Khalkhali, A. Faghri, and Z. J. Zuo, “Entropy generation in a heat pipe system,” *Applied Thermal Engineering*, vol. 19, no. 10, pp. 1027–1043, Oct. 1999, doi: 10.1016/S1359-4311(98)00089-1.
- [5]S. H. Noie-Baghban and G. R. Majideian, “Waste heat recovery using heat pipe heat exchanger (HPHE) for surgery rooms in hospitals,” *Applied Thermal Engineering*, vol. 20, no. 14, pp. 1271–1282, Oct. 2000, doi: 10.1016/S1359-4311(99)00092-7.
- [6]H. F. Smirnov and B. V. Kosoy, “Refrigerating heat pipes,” *Applied Thermal Engineering*, vol. 21, no. 6, pp. 631–641, Apr. 2001, doi: 10.1016/S1359-4311(00)00085-5.
- [7]E. Mathioulakis and V. Belessiotis, “A new heat-pipe type solar domestic hot water system,” *Solar Energy*, vol. 72, no. 1, pp. 13–20, Jan. 2002, doi: 10.1016/S0038-092X(01)00088-3.
- [8]F. Yang, X. Yuan, and G. Lin, “Waste heat recovery using heat pipe heat exchanger for heating automobile using exhaust gas,” *Applied Thermal Engineering*, vol. 23, no. 3, pp. 367–372, Feb. 2003, doi: 10.1016/S1359-4311(02)00190-4.
- [9]Z. Ling, “A study on the new separate heat pipe refrigerator and heat pump,” *Applied Thermal Engineering*, vol. 24, no. 17–18, pp. 2737–2745, Dec. 2004, doi: 10.1016/j.applthermaleng.2004.04.002.

- [10]L. L. Vasiliev, "Heat pipes in modern heat exchangers," *Applied Thermal Engineering*, vol. 25, no. 1, pp. 1–19, Jan. 2005, doi: 10.1016/j.applthermaleng.2003.12.004.
- [11]Yu. F. Maydanik, M. A. Chernysheva, and V. G. Pastukhov, "Review: Loop heat pipes with flat evaporators," *Applied Thermal Engineering*, vol. 67, no. 1–2, pp. 294–307, Jun. 2014, doi: 10.1016/j.applthermaleng.2014.03.041.
- [12]K. Wang, J. Y. Wu, Z. Z. Xia, S. L. Li, and R. Z. Wang, "Design and performance prediction of a novel double heat pipes type adsorption chiller for fishing boats," *Renewable Energy*, vol. 33, no. 4, pp. 780–790, Apr. 2008, doi: 10.1016/j.renene.2007.04.023.
- [13]S. Launay, V. Sartre, and J. Bonjour, "Parametric analysis of loop heat pipe operation: a literature review," *International Journal of Thermal Sciences*, vol. 46, no. 7, pp. 621–636, Jul. 2007, doi: 10.1016/j.ijthermalsci.2006.11.007.
- [14]F. Korn Project Report 2008 MVK160 *Heat and Mass Transport* May 07, 2008, Lund, Sweden
- [15]K. N. Shukla, "Thermo-fluid dynamics of Loop Heat Pipe operation," *International Communications in Heat and Mass Transfer*, vol. 35, no. 8, pp. 916–920, Oct. 2008, doi: 10.1016/j.icheatmasstransfer.2008.04.020.
- [16]H. Nagano, H. Nagai, F. Fukuyoshi, and H. Ogawa, "Study on Thermal Performances of a Small Loop Heat Pipe," *JTST*, vol. 3, no. 2, pp. 355–367, 2008, doi: 10.1299/jtst.3.355.
- [17]S. Launay, V. Sartre, and J. Bonjour, "Analytical Model for Characterization of Loop Heat Pipes," *Journal of Thermophysics and Heat Transfer*, vol. 22, no. 4, pp. 623–631, Oct. 2008, doi: 10.2514/1.37439.
- [18]M. Hamdan and E. Elnajjar, "Thermodynamic analytical model of a loop heat pipe," *Heat Mass Transfer*, vol. 46, no. 2, pp. 167–173, Dec. 2009, doi: 10.1007/s00231-009-0555-0.

- [19]G. P. Celata, M. Cumo, and M. Furrer, "Experimental tests of a stainless steel loop heat pipe with flat evaporator," *Experimental Thermal and Fluid Science*, vol. 34, no. 7, pp. 866–878, Oct. 2010, doi: 10.1016/j.expthermflusci.2010.02.001.
- [20]J. Li, D. Wang, and G. P. Peterson, "Experimental studies on a high performance compact loop heat pipe with a square flat evaporator," *Applied Thermal Engineering*, vol. 30, no. 6–7, pp. 741–752, May 2010, doi: 10.1016/j.applthermaleng.2009.12.004.
- [21]G. B. Ribeiro, J. R. Barbosa, and A. T. Prata, "Mini-channel evaporator/heat pipe assembly for a chip cooling vapour compression refrigeration system," *International Journal of Refrigeration*, vol. 33, no. 7, pp. 1402–1412, Nov. 2010, doi: 10.1016/j.ijrefrig.2010.05.010.
- [22]R. Khodabandeh and R. Furberg, "Heat transfer, flow regime and instability of a nano- and micro-porous structure evaporator in a two-phase thermosyphon loop," *International Journal of Thermal Sciences*, vol. 49, no. 7, pp. 1183–1192, Jul. 2010, doi: 10.1016/j.ijthermalsci.2010.01.016.
- [23]Yeunyongkul, Pracha; Sakulchangsatjatai, Phrut; and Ghajar, Afshin J., "Experimental Investigation of Closed Loop Oscillating Heat Pipe as the Condenser for Vapour Compression Refrigeration" (2010). *International Refrigeration and Air Conditioning Conference*. Paper 1007. <http://docs.lib.purdue.edu/iracc/1007>
- [24]B. M. Ziapour and M. Tavakoli, "Performance study on a diffusion absorption refrigeration heat pipe cycle," *International Journal of Thermal Sciences*, vol. 50, no. 4, pp. 592–598, Apr. 2011, doi: 10.1016/j.ijthermalsci.2010.10.014.
- [25]Z. S. Lu, L. W. Wang, and R. Z. Wang, "Experimental analysis of an adsorption refrigerator with mass and heat-pipe heat recovery process," *Energy Conversion and Management*, vol. 53, no. 1, pp. 291–297, Jan. 2012, doi: 10.1016/j.enconman.2011.09.009.
- [26]J. Choi, M. Jeong, J. Yoo, and M. Seo, "A new CPU cooler design based on an active cooling heatsink combined with heat pipes," *Applied Thermal Engineering*, vol. 44, pp. 50–56, Nov. 2012, doi: 10.1016/j.applthermaleng.2012.03.027.

- [27]Y. Hu, J. Cheng, W. Zhang, R. Shirakashi, and S. Wang, “Thermal performance enhancement of grooved heat pipes with inner surface treatment,” *International Journal of Heat and Mass Transfer*, vol. 67, pp. 416–419, Dec. 2013, doi: 10.1016/j.ijheatmasstransfer.2013.08.035.
- [28]R. Senthilkumar, S. Prabhu, and M. Cheralathan, “Experimental investigation on carbon nano tubes coated brass rectangular extended surfaces,” *Applied Thermal Engineering*, vol. 50, no. 1, pp. 1361–1368, Jan. 2013, doi: 10.1016/j.applthermaleng.2012.05.040.
- [29]M. C. Page, M. J. Brooks, L. W. Roberts, and C. Bemont, “Modeling and Experimental Validation of a Loop Heat Pipe,” *R & D Journal of the South African Institution of Mechanical Engineering*, ISSN: 2309-8988, 2013, 29, 26-35.
- [30]D. A. Baitule and P. R. Pachghare, “EXPERIMENTAL ANALYSIS OF CLOSED LOOP PULSATING HEAT PIPE WITH VARIABLE FILLING,” p. 9, 2013.
- [31]Y.-C. Chiang, W.-C. Kuo, C.-C. Ho, and J.-J. Chieh, “Experimental study on thermal performances of heat pipes for air-conditioning systems influenced by magnetic nanofluids, external fields, and micro wicks,” *International Journal of Refrigeration*, vol. 43, pp. 62–70, Jul. 2014, doi: 10.1016/j.ijrefrig.2014.04.007.
- [32]M.A.Anwar, D.P.Kamble, and Dr. P.S. Utgikar, “Experimental Study of Thermal Performance of Heat Pipe With Boron Nitride/Water Nanofluid,” *IJSRE*, vol. 2, no. 11, pp. 2485–2492, Nov. 2014.
- [33]J.-S. Chen and J.-H. Chou, “Cooling performance of flat plate heat pipes with different liquid filling ratios,” *International Journal of Heat and Mass Transfer*, vol. 77, pp. 874–882, Oct. 2014, doi: 10.1016/j.ijheatmasstransfer.2014.06.029.
- [34]O. A. Alawi, N. A. C. Sidik, H. A. Mohammed, and S. Syahrullail, “Fluid flow and heat transfer characteristics of nanofluids in heat pipes: A review,” *International Communications in Heat and Mass Transfer*, vol. 56, pp. 50–62, Aug. 2014, doi: 10.1016/j.icheatmasstransfer.2014.04.014.

- [35]K. Nithyanandam and R. Pitchumani, “Design of a latent thermal energy storage system with embedded heat pipes,” *Applied Energy*, vol. 126, pp. 266–280, Aug. 2014, doi: 10.1016/j.apenergy.2014.03.025.
- [36]A. Khalifa, L. Tan, A. Date, and A. Akbarzadeh, “A numerical and experimental study of solidification around axially finned heat pipes for high temperature latent heat thermal energy storage units,” *Applied Thermal Engineering*, vol. 70, no. 1, pp. 609–619, Sep. 2014, doi: 10.1016/j.applthermaleng.2014.05.080.
- [37]J. Xu, L. Zhang, H. Xu, J. Zhong, and J. Xuan, “Experimental investigation and visual observation of loop heat pipes with two-layer composite wicks,” *International Journal of Heat and Mass Transfer*, vol. 72, pp. 378–387, May 2014, doi: 10.1016/j.ijheatmasstransfer.2014.01.016.
- [38]Y. Jiao, G. Xia, and W. Wang, “Transient and isothermal characteristics of a particular heat pipe,” *International Communications in Heat and Mass Transfer*, vol. 54, pp. 42–47, May 2014, doi: 10.1016/j.icheatmasstransfer.2014.03.011.
- [39]M. Ghajar and J. Darabi, “Evaporative heat transfer analysis of a micro loop heat pipe with rectangular grooves,” *International Journal of Thermal Sciences*, vol. 79, pp. 51–59, May 2014, doi: 10.1016/j.ijthermalsci.2013.12.014.
- [40]L. Jiang *et al.*, “Design and fabrication of sintered wick for miniature cylindrical heat pipe,” *Transactions of Nonferrous Metals Society of China*, vol. 24, no. 1, pp. 292–301, Jan. 2014, doi: 10.1016/S1003-6326(14)63060-0.
- [41]A. Khalifa, L. Tan, A. Date, and A. Akbarzadeh, “Performance of suspended finned heat pipes in high-temperature latent heat thermal energy storage,” *Applied Thermal Engineering*, vol. 81, pp. 242–252, Apr. 2015, doi: 10.1016/j.applthermaleng.2015.02.030.
- [42]M. Ebrahimi, M. B. Shafii, and M. A. Bijarchi, “Experimental investigation of the thermal management of flat-plate closed-loop pulsating heat pipes with interconnecting channels,” *Applied Thermal Engineering*, vol. 90, pp. 838–847, Nov. 2015, doi: 10.1016/j.applthermaleng.2015.07.040.

- [43]K. V. Paiva and M. B. H. Mantelli, "Wire-plate and sintered hybrid heat pipes: Model and experiments," *International Journal of Thermal Sciences*, vol. 93, pp. 36–51, Jul. 2015, doi: 10.1016/j.ijthermalsci.2015.01.037.
- [44]B. Siedel, V. Sartre, and F. Lefèvre, "Literature review: Steady-state modeling of loop heat pipes," *Applied Thermal Engineering*, vol. 75, pp. 709–723, Jan. 2015, doi: 10.1016/j.applthermaleng.2014.10.030.
- [45]P. Meisel, M. Jobst, W. Lippmann, and A. Hurtado, "Design and manufacture of ceramic heat pipes for high temperature applications," *Applied Thermal Engineering*, vol. 75, pp. 692–699, Jan. 2015, doi: 10.1016/j.applthermaleng.2014.10.051.
- [46]G. Spinato, N. Borhani, B. P. d'Entremont, and J. R. Thome, "Time-strip visualization and thermo-hydrodynamics in a Closed Loop Pulsating Heat Pipe," *Applied Thermal Engineering*, vol. 78, pp. 364–372, Mar. 2015, doi: 10.1016/j.applthermaleng.2014.12.045.
- [47]S. De Schampheleire, K. De Kerpel, T. Deruyter, P. De Jaeger, and M. De Paepe, "Experimental study of small diameter fibres as wick material for capillary-driven heat pipes," *Applied Thermal Engineering*, vol. 78, pp. 258–267, Mar. 2015, doi: 10.1016/j.applthermaleng.2014.12.027.
- [48]Z. Sun, Z. Zhang, and C. Duan, "The applicability of the wall implanted with heat pipes in winter of China," *Energy and Buildings*, vol. 104, pp. 36–46, Oct. 2015, doi: 10.1016/j.enbuild.2015.06.082.
- [49]M. Ghanbarpour, N. Nikkam, R. Khodabandeh, and M. S. Toprak, "Thermal performance of inclined screen mesh heat pipes using silver nanofluids," *International Communications in Heat and Mass Transfer*, vol. 67, pp. 14–20, Oct. 2015, doi: 10.1016/j.icheatmasstransfer.2015.06.009.
- [50]S. Tiari and S. Qiu, "Three-dimensional simulation of high temperature latent heat thermal energy storage system assisted by finned heat pipes," *Energy Conversion and Management*, vol. 105, pp. 260–271, Nov. 2015, doi: 10.1016/j.enconman.2015.08.004.

- [51]L. Bai, L. Zhang, G. Lin, J. He, and D. Wen, “Development of cryogenic loop heat pipes: A review and comparative analysis,” *Applied Thermal Engineering*, vol. 89, pp. 180–191, Oct. 2015, doi: 10.1016/j.applthermaleng.2015.06.010.
- [52]M. V. Oro and E. Bazzo, “Flat heat pipes for potential application in fuel cell cooling,” *Applied Thermal Engineering*, vol. 90, pp. 848–857, Nov. 2015, doi: 10.1016/j.applthermaleng.2015.07.055.
- [53]C. Yan, W. Shi, X. Li, and S. Wang, “A seasonal cold storage system based on separate type heat pipe for sustainable building cooling,” *Renewable Energy*, vol. 85, pp. 880–889, Jan. 2016, doi: 10.1016/j.renene.2015.07.023.
- [54]Z. Wang, X. Zhang, Z. Li, and M. Luo, “Analysis on energy efficiency of an integrated heat pipe system in data centers,” *Applied Thermal Engineering*, vol. 90, pp. 937–944, Nov. 2015, doi: 10.1016/j.applthermaleng.2015.07.078.
- [55]H. Tian, Z. He, and Z. Li, “A combined cooling solution for high heat density data centers using multi-stage heat pipe loops,” *Energy and Buildings*, vol. 94, pp. 177–188, May 2015, doi: 10.1016/j.enbuild.2015.03.002.
- [56]Shigeki Hirasawa, Tsuyoshi Kawanami, and Katsuaki Shirai, “Heat Transfer and Flow Analysis in Loop Heat Pipe with Multiple Evaporators Using Network Model,” *JMEA*, vol. 6, no. 7, Jul. 2016, doi: 10.17265/2159-5275/2016.07.001.
- [57]S. Föste, B. Schiebler, F. Giovannetti, G. Rockendorf, and S. Jack, “Butane Heat Pipes for Stagnation Temperature Reduction of Solar Thermal Collectors,” *Energy Procedia*, vol. 91, pp. 35–41, Jun. 2016, doi: 10.1016/j.egypro.2016.06.168.
- [58]I. Setyawan, I. Ibnu Hakim, and N. Putra, “Experimental study on a hybrid loop heat pipe,” *MATEC Web Conf.*, vol. 101, p. 03011, 2017, doi: 10.1051/mateconf/201710103011.
- [59]Y. Taamneh, “Thermal analysis of gas turbine disk integrated with rotating heat pipes,” *Case Studies in Thermal Engineering*, vol. 10, pp. 335–342, Sep. 2017, doi: 10.1016/j.csite.2017.09.002.

- [60]N. Hack, S. Unz, and M. Beckmann, “Ceramic Heat Pipes for High Temperature Application,” *Energy Procedia*, vol. 120, pp. 140–148, Aug. 2017, doi: 10.1016/j.egypro.2017.07.147.
- [61]H. M. Lee and H.-Y. Li, “A mathematical model for estimation of the maximum heat transfer capacity of tubular heat pipes,” *Energy Procedia*, vol. 142, pp. 3908–3913, Dec. 2017, doi: 10.1016/j.egypro.2017.12.295.
- [62]K. Yang, Y. Mao, Z. Cong, and X. Zhang, “Experimental research of novel aluminium-ammonia heat pipes,” *Procedia Engineering*, vol. 205, pp. 3923–3930, 2017, doi: 10.1016/j.proeng.2017.10.032.
- [63]S. Nakkaew *et al.*, “Application of the heat pipe to enhance the performance of the vapour compression refrigeration system,” *Case Studies in Thermal Engineering*, vol. 15, p. 100531, Nov. 2019, doi: 10.1016/j.csite.2019.100531.
- [64]V. Guichet and H. Jouhara, “Condensation, evaporation and boiling of falling films in wickless heat pipes (two-phase closed thermosyphons): A critical review of correlations,” *International Journal of Thermofluids*, vol. 1–2, p. 100001, Feb. 2020, doi: 10.1016/j.ijft.2019.100001.
- [65]D. Gai, Y. Yin, and C. Chen, “Investigation of instability on loop heat pipe with flat evaporator,” *IOP Conf. Ser.: Earth Environ. Sci.*, vol. 467, p. 012024, Apr. 2020, doi: 10.1088/1755-1315/467/1/012024.
- [66]D. Gai, J. Sun, C. Chen, and T. Chen, “Hysteresis phenomena in flat-type loop heat pipe,” *Therm sci*, vol. 25, no. 4 Part A, pp. 2539–2547, 2021, doi: 10.2298/TSCII191010166D.
- [67]L. Martvoňová, M. Malcho, and J. Jandačka, “Increase the efficiency of the fireplace insert with loop heat pipe,” *MATEC Web Conf.*, vol. 328, p. 04002, 2020, doi: 10.1051/mateconf/202032804002.
- [68]A. Anikivi, R. Naik, and K. R. Narasihma, “Investigation of copper-water loop heat pipe for different filling ratios,” *IOP Conf. Ser.: Mater. Sci. Eng.*, vol. 872, p. 012070, Jun. 2020, doi: 10.1088/1757-899X/872/1/012070.

- [69]T. Mallikharjuna Rao and S. Srinivasa Rao, "Steam condensation by heat pipes," *J. Phys. Conf.Ser.*, vol. 1473, p. 012028, Feb. 2020, doi: 10.1088/1742-6596/1473/1/012028.
- [70]H. Mbulu, Y. Laonual, and S. Wongwises, "Experimental study on the thermal performance of a battery thermal management system using heat pipes," *Case Studies in Thermal Engineering*, vol. 26, p. 101029, Aug. 2021, doi: 10.1016/j.csite.2021.101029.
- [71]V. Buz and K. Goncharov, "Loop heat pipe dynamics modeling and analysis," *IOP Conf. Ser.: Mater. Sci. Eng.*, vol. 1139, no. 1, p. 012011, Apr. 2021, doi: 10.1088/1757-899X/1139/1/012011.
- [72]P. Nemeč and J. Hužvár, "Mathematical Calculation OF Total Heat Powerofthe Sodium Heat Pipe," p. 6.
- [73]R. Oinuma and F. R. Best, "Fundamental Study of Heat Pipe Design for High Heat Flux Source," p. 22.
- [74]J. Ku , L. Ottenstein, M. Kobel, P. Rogers and T. Kaya, "Temperature Oscillations in Loop Heat Pipe Operation" International University, Strasburg, France.
- [75]D.-W. Sun, "Comparison of the performances of NH₃-H₂O, NH₃-LiNO₃ and NH₃-NaSCN absorption refrigeration systems," p. 12.
- [76]I. Horuz, "A comparison between ammonia-water and water-lithium bromide solutions in vapour absorption refrigeration systems," *International Communications in Heat and Mass Transfer*, vol. 25, no. 5, pp. 711–721, Jul. 1998, doi: 10.1016/S0735-1933(98)00058-X.
- [77]M. M. Talbi and B. Agnew, "Exergy analysis: an absorption refrigerator using lithium bromide and water as the working fluids," *Applied Thermal Engineering*, p. 12, 2000.
- [78]R. D. Misra, P. K. Sahoo, S. Sahoo, and A. Gupta, "Thermoeconomic optimization of a single effect water/LiBr vapour absorption refrigeration system,"

International Journal of Refrigeration, vol. 26, no. 2, pp. 158–169, Mar. 2003, doi: 10.1016/S0140-7007(02)00086-5.

[79]S. A. Adewusi and S. M. Zubair, “Second law based thermodynamic analysis of ammonia–water absorption systems,” *Energy Conversion and Management*, vol. 45, no. 15–16, pp. 2355–2369, Sep. 2004, doi: 10.1016/j.enconman.2003.11.020.

[80]S. Arivazhagan, R. Saravanan, and S. Renganarayanan, “Experimental studies on HFC based two-stage half effect vapour absorption cooling system,” *Applied Thermal Engineering*, vol. 26, no. 14–15, pp. 1455–1462, Oct. 2006, doi: 10.1016/j.applthermaleng.2005.12.014.

[81]R. Gomri and R. Hakimi, “Second law analysis of double effect vapour absorption cooler system,” *Energy Conversion and Management*, vol. 49, no. 11, pp. 3343–3348, Nov. 2008, doi: 10.1016/j.enconman.2007.09.033.

[82]A. Khaliq and R. Kumar, “Exergy analysis of double effect vapour absorption refrigeration system,” *Int. J. Energy Res.*, vol. 32, no. 2, pp. 161–174, Feb. 2008, doi: 10.1002/er.1356.

[83]R. Gomri, “Second law comparison of single effect and double effect vapour absorption refrigeration systems,” *Energy Conversion and Management*, vol. 50, no. 5, pp. 1279–1287, May 2009, doi: 10.1016/j.enconman.2009.01.019.

[84]S. C. Kaushik and A. Arora, “Energy and exergy analysis of single effect and series flow double effect water–lithium bromide absorption refrigeration systems,” *International Journal of Refrigeration*, vol. 32, no. 6, pp. 1247–1258, Sep. 2009, doi: 10.1016/j.ijrefrig.2009.01.017.

[85]B. H. Gebreslassie, M. Medrano, and D. Boer, “Exergy analysis of multi-effect water–LiBr absorption systems: From half to triple effect,” *Renewable Energy*, vol. 35, no. 8, pp. 1773–1782, Aug. 2010, doi: 10.1016/j.renene.2010.01.009.

[86]B. K. Agrawal and M. N. Karimi, “Thermodynamic performance assessment of a novel waste heat based triple effect refrigeration cycle,” *International Journal of Refrigeration*, vol. 35, no. 6, pp. 1647–1656, Sep. 2012, doi: 10.1016/j.ijrefrig.2012.05.020.

[87]L. G. Farshi, C. A. Infante Ferreira, S. M. S. Mahmoudi, and M. A. Rosen, "First and second law analysis of ammonia/salt absorption refrigeration systems," *International Journal of Refrigeration*, vol. 40, pp. 111–121, Apr. 2014, doi: 10.1016/j.ijrefrig.2013.11.006.

[88]G. Sachdeva and R. Bilash, "Thermodynamic Analysis of a Vapour Absorption System Using Modified Gouy-Stodola Equation," vol. 8, no. 12, p. 6, 2014.

[89]P. Rajkumar, R. Shankar, and T. Srinivas, "Exergy Analyses of LiBr-Water Double Solar Vapour Absorption Refrigeration System Coupled Using Condenser," vol. 10, p. 5, 2015.

[90]Department of Mechanical Engineering, Mehran University of Engineering and Technology, Jamshoro *et al.*, "Thermodynamic Analysis of Combined Vapour Compression and Vapour Absorption Refrigeration System," *Mehran Univ. res. j. eng. technol.*, vol. 36, no. 3, pp. 733–740, Jul. 2017, doi: 10.22581/muet1982.1703.27.

[91]R. S. Mishra, "Comparison of thermal performances of single effect, double effect and triple effect LiBr-H₂O absorption system cascaded with vapour compression refrigeration systems using ecofriendly refrigerants," *Int. J. Res. Eng. Innov.*, vol. 2, no. 6, p. 12, 2018.

[92]R. S. Mishra, "Thermodynamic performance evaluation of triple effect H₂O - Li/Br vapour absorption systems using multi cascading of vapour compression cycles for ultra-low temperature applications," *Int. J. Res. Eng. Innov.*, vol. 03, no. 06, pp. 475–508, 2019, doi: 10.36037/IJREI.2019.3613.

[93]R. S. Mishra, "Thermodynamic performance evaluation of triple effect H₂O - Li/Br vapour absorption systems using multi cascading of vapour compression cycles for ultra-low temperature applications," *Int. J. Res. Eng. Innov.*, vol. 03, no. 06, pp. 475–508, 2019, doi: 10.36037/IJREI.2019.3613.

[94]R. S. Mishra, "Thermal performance of multi cascaded vapour compression NH₃H₂O absorption systems for ultra-low temperature applications," *Int. J. Res. Eng. Innov.*, vol. 04, no. 01, pp. 39–55, 2020, doi: 10.36037/IJREI.2020.4104.

- [95]R. S. Mishra, "Performance evaluation of single effect Li/Br-H₂O vapour absorption systems using multi cascading of vapour compression cycles for ultra-low temperature applications," *Int. J. Res. Eng. Innov.*, vol. 04, no. 01, pp. 08–38, 2020, doi: 10.36037/IJREI.2020.4103.
- [96]R. S. Mishra, "Performance evaluation of triple effect Li/Br-H₂O vapour absorption refrigeration system with three cascaded vapour compression refrigeration systems using HFO refrigerants for ultra-low temperature applications," *Int. J. Res. Eng. Innov.*, vol. 4, no. 6, p. 5, 2020, doi: <https://doi.org/10.36037/IJREI.2020.4606>.
- [97]R. S. Mishra, "Performance evaluation of double effect Li/Br-H₂O vapour absorption refrigeration system with three cascaded vapour compression refrigeration systems using HFO refrigerants for ultra-low temperature applications," *Int. J. Res. Eng. Innov.*, vol. 5, no. 1, pp. 20–28, doi: <https://doi.org/10.36037/IJREI.2021.5103>.
- [98]R. S. Mishra, "Performance evaluation of single effect Li/Br-H₂O vapour absorption refrigeration system with three cascaded vapour compression refrigeration systems using HFO refrigerants for ultra-low temperature applications," *Int. J. Res. Eng. Innov.*, vol. 5, no. I, pp. 1–9, doi: <https://doi.org/10.36037/IJREI.2021.5101>.
- [99] R. S. Mishra, "Thermal performance evaluation of half effect Li/Br-H₂O vapour absorption refrigeration system with single & multi cascaded vapour compression refrigeration systems using HFO refrigerants for replacing HFC-134a," *Int. J. Res. Eng. Innov.*, vol. 5, no. 1, pp. 29–41, doi: <https://doi.org/10.36037/IJREI.2021.5104>.
- [100]S. D. Ali, M. S. Mahdi, and J. Abdulateef, "Thermodynamic Analysis of Solar Absorption Cooling System," *ARFMTS*, vol. 60, no. 2, pp. 233–246, Aug. 2019.
- [101] S. Hanriot, P. Brito, C. Maia, and A. Rêgo, "Analysis of working parameters for an ammonia-water absorption refrigeration system powered by automotive exhaust gas," *Case Studies in Thermal Engineering*, vol. 13, p. 100406, Mar. 2019, doi: 10.1016/j.csite.2019.100406.
- [102]S. Mohtaram, M. Omid, J. Lin, H. Sun, and W. Chen, "Exergy analysis of a multi mixture working fluid absorption refrigeration cycle," *Case Studies in Thermal Engineering*, vol. 15, p. 100540, Nov. 2019, doi: 10.1016/j.csite.2019.100540.

- [103] S. S. Alrwashdeh and H. Ammari, "Life cycle cost analysis of two different refrigeration systems powered by solar energy," *Case Studies in Thermal Engineering*, vol. 16, p. 100559, Dec. 2019, doi: 10.1016/j.csite.2019.100559.
- [104] N. Kurtulmuş, "Energy and exergy analysis of a vapour absorption refrigeration system in an intercity bus application," *Journal of Thermal Engineering*, pp. 355–371, Jun. 2019, doi: 10.18186/thermal.583316.
- [105] S. Sharifi, F. Nozad Heravi, R. Shirmohammadi, R. Ghasempour, F. Petrakopoulou, and L. M. Romeo, "Comprehensive thermodynamic and operational optimization of a solar-assisted LiBr/water absorption refrigeration system," *Energy Reports*, vol. 6, pp. 2309–2323, Nov. 2020, doi: 10.1016/j.egyr.2020.08.013.
- [106] B. Han, W. Li, M. Li, L. Liu, and J. Song, "Study on LiBr/H₂O absorption cooling system based on enhanced geothermal system for data center," *Energy Reports*, vol. 6, pp. 1090–1098, Dec. 2020, doi: 10.1016/j.egyr.2020.11.072.
- [107] W. I. Mazyan, A. Ahmadi, H. Ahmed, and M. Hoorfar, "Increasing the COP of a refrigeration cycle in natural gas liquefaction process using refrigerant blends of Propane-NH₃, Propane-SO₂ and Propane-CO₂," *Heliyon*, vol. 6, no. 8, p. e04750, Aug. 2020, doi: 10.1016/j.heliyon.2020.e04750.
- [108] T. Toppi, M. Aprile, and M. Motta, "Self-adapting double and triple-lift absorption cycles for low-grade heat driven cooling," *International Journal of Refrigeration*, vol. 113, pp. 206–218, May 2020, doi: 10.1016/j.ijrefrig.2020.01.009.
- [109] B. Huirem and P. K. Sahoo, "Thermodynamic Modeling and Performance Optimization of a Solar-Assisted Vapour Absorption Refrigeration System (SAVARS)," *Int. J. Air-Cond. Ref.*, vol. 28, no. 01, p. 2050006, Mar. 2020, doi: 10.1142/S2010132520500066.
- [110] Y. Gong, L. Yang, Z. Lu, L. Wang, and H. Li, "Thermodynamic performance assessment of ammonia/ionic liquid based half-effect absorption refrigeration cycle," *Case Studies in Thermal Engineering*, vol. 25, p. 100924, Jun. 2021, doi: 10.1016/j.csite.2021.100924.

- [111] F. Ahmed and W. A. Khan, "Efficiency enhancement of an air-conditioner utilizing nanofluids: An experimental study," *Energy Reports*, vol. 7, pp. 575–583, Nov. 2021, doi: 10.1016/j.egy.2021.01.023.
- [112] D. Raut, A. K. Tiwari, and V. R. Kalamkar, "Theoretical design of solar-powered vapour absorption refrigeration system coupled with latent heat energy storage," *IOP Conf. Ser.: Mater. Sci. Eng.*, vol. 1146, no. 1, p. 012026, May 2021, doi: 10.1088/1757-899X/1146/1/012026.
- [113] C. Vasilescu, D. Hera and C.I. Ferreira, "Model for double-effect absorption refrigeration cycle"
- [114] J. M. Abdulateef, M. A. Alghoul, R. Sirwan, A. Zaharim, and K. Sopian, "Second Law Thermodynamic Analysis of a Solar Single-Stage Absorption Refrigeration System," p. 6.
- [115] V. Srikanth, B. Raja Narendra, and Dr. AVSSKS Gupta, "Thermodynamic analysis of vapour absorption refrigeration system using solar energy," *IJLTET*, vol. 7, no. 4, 2016, doi: 10.21172/1.74.003.
- [116] P. Nemeč and M. Malcho, "Distribution of heat flux by working fluid in loop heat pipe," *EPJ Web of Conferences*, vol. 114, p. 02081, 2016, doi: 10.1051/epjconf/201611402081.
- [117] J. M. Abdulateef, K. Sopian, M. A. Alghoul, and M. Y. Sulaiman, "Review on solar-driven ejector refrigeration technologies," *Renewable and Sustainable Energy Reviews*, vol. 13, no. 6–7, pp. 1338–1349, Aug. 2009, doi: 10.1016/j.rser.2008.08.012.
- [118] A. Dahmani, Z. Aidoun, and N. Galanis, "On the Performance of Ejector Refrigeration Systems," in *RECENT ADVANCES in ENERGY & ENVIRONMENT*, Feb. 2010, p. 6.
- [119] Reddick, Christopher; Mercadier, Yves; and Ouzzane, Mohamed, "Experimental Study Of An Ejector Refrigeration System" (2012). *International Refrigeration and Air Conditioning Conference*. Paper 1176. <http://docs.lib.purdue.edu/iracc/1176>

- [120] D. Buyadgie, O. Buyadgie, O. Drakhnia, S. Artemenko, and A. Chamchine, "Solar Cooling Technologies Using Ejector Refrigeration System," *Energy Procedia*, vol. 30, pp. 912–920, 2012, doi: 10.1016/j.egypro.2012.11.103.
- [121] G. A. Untea, A. Dobrovicescu, L. Grosu, and E. C. Mladin, "ENERGY AND EXERGY ANALYSIS OF AN EJECTOR REFRIGERATION SYSTEM," *U.P.B. Sci. Bull., Series D*, vol. 75, no. 4, p. 16, 2013.
- [122] D. A. Pounds, J. M. Dong, P. Cheng, and H. B. Ma, "Experimental investigation and theoretical analysis of an ejector refrigeration system," *International Journal of Thermal Sciences*, vol. 67, pp. 200–209, May 2013, doi: 10.1016/j.ijthermalsci.2012.11.001.
- [123] H.-F. Zheng, X.-W. Fan, F. Wang, and G.-J. Tian, "Solar ejector refrigerant system in China's residential buildings," *Therm sci*, vol. 18, no. 5, pp. 1643–1647, 2014, doi: 10.2298/TSCI1405643Z.
- [124] F. Memet and A. Preda, "An analysis of the performance of an ejector refrigeration cycle working with R134a," *IOP Conf. Ser.: Mater. Sci. Eng.*, vol. 95, p. 012035, Nov. 2015, doi: 10.1088/1757-899X/95/1/012035.
- [125] M. Ebadollahi, H. Rostamzadeh, H Ghaebi, M Amidpour, F Rostamian, and H. Abioghli, "Energy analysis and performance evaluation of a novel multi-evaporator ejector refrigeration cycle (ERC)" *Journal of Energy Management and Technology (JEMT)* Vol. 1, Issue 2, p.38, 2018, doi: 10.22109/jemt.2017.90023.1022
- [126] R. S. Mishra, A. Dwivedi, and S. Ahmad, "A thermodynamic analysis of ejector type vapour refrigeration system using eco-friendly refrigerants," *IJREI*, vol. 1, no. 3, pp. 40–48, 2017.
- [127] C. Seçkin, "İki Fazlı Ejektör Kullanan Ejektörlü Soğutma Çevriminin Analizi," *SAÜ Fen Bilimleri Enstitüsü Dergisi*, pp. 1–1, Apr. 2018, doi: 10.16984/saufenbilder.290819.
- [128] B. Eh, F. S, and A. B, "Exergy Analysis for Brayton and Inverse Brayton Cycles with Steam Injection," *J Appl Mech Eng*, vol. 06, no. 06, 2017, doi: 10.4172/2168-9873.1000292.

- [129] Y. Fang, S. Croquer, S. Poncet, Z. Aidoun, and Y. Bartosiewicz, “Drop-in replacement in a R134 ejector refrigeration cycle by HFO refrigerants,” *International Journal of Refrigeration*, vol. 77, pp. 87–98, May 2017, doi: 10.1016/j.ijrefrig.2017.02.028.
- [130] Besagni Giorgio, Croci Lorenzo, and Nesa Riccardo, “A screening of low-gwp refrigerant for ejector refrigeration,” *Chemical Engineering Transactions*, vol. 70, pp. 1291–1296, 2018, doi: 10.3303/CET1870216.
- [131] L. R. Reddy, “Numerical Investigation of Ejectors for Ejector Refrigeration System,” *International Journal of Innovative Science and Research Technology*, vol. 3, no. 5, p. 7, 2018.
- [132] S. Taslimi Taleghani, M. Sorin, and S. Poncet, “Analysis and Optimization of Exergy Flows inside a Transcritical CO₂ Ejector for Refrigeration, Air Conditioning and Heat Pump Cycles,” *Energies*, vol. 12, no. 9, p. 1686, May 2019, doi: 10.3390/en12091686.
- [133] J. Liu, “Performance Improvement Potential Analysis of a Booster-Assisted Ejector Refrigeration System,” *IEEE Access*, vol. 7, pp. 58533–58540, 2019, doi: 10.1109/ACCESS.2019.2912076.
- [134] V. Kumar and G. Sachdeva, “Experimental investigation of an ejector refrigeration system using R-134a,” *J. Phys.: Conf. Ser.*, vol. 1240, p. 012168, Jul. 2019, doi: 10.1088/1742-6596/1240/1/012168.
- [135] X. Zhang, S. Deng, L. Zhao, W. Su, and W. Xu, “Performance Analysis on a Power and Ejector-Refrigeration System and the Involved Ejector,” *Front. Energy Res.*, vol. 7, p. 117, Oct. 2019, doi: 10.3389/fenrg.2019.00117.
- [136] K. B. Shovon, T. Kim, and K. H. Dong, “Analysis of thermo-fluid dynamics in the heat exchanger of an ejector refrigeration system,” p. 3.
- [137] N. Suvarnakuta, K. Pianthong, T. Sriveerakul, and W. Seehanam, “Performance analysis of a two-stage ejector in an ejector refrigeration system using computational fluid dynamics,” *Engineering Applications of Computational Fluid Mechanics*, vol. 14, no. 1, pp. 669–682, Jan. 2020, doi: 10.1080/19942060.2020.1756913.

- [138] R. S. Mishra, “Thermodynamic performances of ejector refrigeration systems (ERS) using low GWP ecofriendly HFO refrigerants,” *IJREI*, vol. 4, no. 5, pp. 236–240, 2020, doi: <https://doi.org/10.36037/IJREI.2020.4501>.
- [139] G. Besagni, L. Croci, N. Cristiani, G. R. Guédon, and F. Inzoli, “Refrigerant selection for ejector refrigeration systems: a multiscale evaluation,” *E3S Web Conf.*, vol. 197, p. 10011, 2020, doi: [10.1051/e3sconf/202019710011](https://doi.org/10.1051/e3sconf/202019710011).
- [140] V. Kiseev and O. Sazhin, “Loop Heat Pipes with a Steam Jet Pump,” *J Eng Phys Thermophy*, vol. 93, no. 3, pp. 700–709, May 2020, doi: [10.1007/s10891-020-02169-6](https://doi.org/10.1007/s10891-020-02169-6).
- [141] T. Miao, Z. Fang, L. Feng, and Y. Peng, “A small shipborne desalination plant based on the principle of loop heat pipe,” *E3S Web Conf.*, vol. 165, p. 01003, 2020, doi: [10.1051/e3sconf/202016501003](https://doi.org/10.1051/e3sconf/202016501003).
- [142] M. Bencharif, H. Nesreddine, S. C. Perez, S. Poncet, and S. Zid, “The benefit of droplet injection on the performance of an ejector refrigeration cycle working with R245fa,” *International Journal of Refrigeration*, vol. 113, pp. 276–287, May 2020, doi: [10.1016/j.ijrefrig.2020.01.020](https://doi.org/10.1016/j.ijrefrig.2020.01.020).
- [143] A. K. S. Al-Sayyab, J. Navarro-Esbrí, V. M. Soto-Francés, and A. Mota-Babiloni, “Conventional and Advanced Exergoeconomic Analysis of a Compound Ejector-Heat Pump for Simultaneous Cooling and Heating,” *Energies*, vol. 14, no. 12, p. 3511, Jun. 2021, doi: [10.3390/en14123511](https://doi.org/10.3390/en14123511).
- [144] B. Sharma, G. Sachdeva, and V. Kumar, “Exergy analysis of heat assisted ejector refrigeration system using R1234yf,” *IOP Conf. Ser.: Mater. Sci. Eng.*, vol. 1104, no. 1, p. 012035, Mar. 2021, doi: [10.1088/1757-899X/1104/1/012035](https://doi.org/10.1088/1757-899X/1104/1/012035).
- [145] S. Li, Y. Liu, Y. Liu, and J. Zhang, “Performance comparison of ejectors in ejector-based refrigeration cycles with R1234yf, R1234ze(E) and R134a,” *Environ Sci Pollut Res*, Jun. 2021, doi: [10.1007/s11356-021-14626-7](https://doi.org/10.1007/s11356-021-14626-7).
- [146] B.-J. Huang, H. H. Huang, T. L. Liang, P. E. Yang, and S. S. Hu, “A method of fast quality control inspection of loop heat pipe,” *IOP Conf. Ser.: Mater. Sci. Eng.*, vol. 1139, no. 1, p. 012004, Apr. 2021, doi: [10.1088/1757-899X/1139/1/012004](https://doi.org/10.1088/1757-899X/1139/1/012004).

- [147] S. K. Verma, S. Kumar, and G. Sachdeva, "A review on exergy analysis of ejector refrigeration system," *IOP Conf. Ser.: Mater. Sci. Eng.*, vol. 1104, no. 1, p. 012026, Mar. 2021, doi: 10.1088/1757-899X/1104/1/012026.
- [148] Y. Devarajan, B. Nagappan, G. Subbiah, and E. Kariappan, "Experimental investigation on solar-powered ejector refrigeration system integrated with different concentrators," *Environ Sci Pollut Res*, vol. 28, no. 13, pp. 16298–16307, Apr. 2021, doi: 10.1007/s11356-020-12248-z.
- [149] L. Vasiliev, M. Marengo, C. Ferrandi, S. Zinna, and V. Maziuk, "Advanced Design of a 'Low-cost' Loop Heat Pipe," Jul. 2009, pp. 2009-01–2519. doi: 10.4271/2009-01-2519.
- [150] A. Borsukiewicz-Gozdur, "Pumping work in the organic Rankine cycle," *Applied Thermal Engineering*, vol. 51, no. 1–2, pp. 781–786, Mar. 2013, doi: 10.1016/j.applthermaleng.2012.10.033.
- [151] M. Preißinger, F. Heberle, and D. Brüggemann, "Advanced Organic Rankine Cycle for geothermal application," *Int. J. Low-Carbon Tech.*, vol. 8, no. suppl 1, pp. i62–i68, Jul. 2013, doi: 10.1093/ijlct/ctt021.
- [152] S. Lecompte, S. Lemmens, A. Verbruggen, M. van den Broek, and M. De Paepe, "Thermo-economic Comparison of Advanced Organic Rankine Cycles," *Energy Procedia*, vol. 61, pp. 71–74, 2014, doi: 10.1016/j.egypro.2014.11.909.
- [153] D. Ziviani *et al.*, "ORCSIM: A GENERALIZED ORGANIC RANKINE CYCLE SIMULATION TOOL," p. 11, 2015.
- [154] T. Wenzel, P. Smith Schneider, and C. Seppi Bresolin, "Thermodynamic Analysis and Simulation of an Organic Rankine Cycle," presented at the 16th Brazilian Congress of Thermal Sciences and Engineering, 2016. doi: 10.26678/ABCM.ENCIT2016.CIT2016-0264.
- [155] F. H. Amsyari and T. H. Ariwibowo, "Perancangan Numerik Turbin Radial untuk Sistem Organic Rankine Cycle," Mar. 2016, p. 7.

- [156] F. Alshammari, M. Usman, and A. Pesyridis, “Expanders for Organic Rankine Cycle Technology,” in *Organic Rankine Cycle Technology for Heat Recovery*, E. Wang, Ed. InTech, 2018. doi: 10.5772/intechopen.78720.
- [157] D. I. Karabarin and S. A. Mihailenko, “Features Design of Organic Rankine Cycle,” *Journal of Siberian Federal University. Engineering & Technologies*, pp. 733–745, Sep. 2019, doi: 10.17516/1999-494X-0173.
- [158] G. L. Liu, J. L. Xu, and S. Cao, “Investigation of exergy efficiency of organic Rankine cycle,” *IOP Conf. Ser.: Earth Environ. Sci.*, vol. 354, p. 012050, Oct. 2019, doi: 10.1088/1755-1315/354/1/012050.
- [159] A. Mariani, B. Morrone, and A. Unich, “Bottoming Organic Rankine Cycles for Passenger Cars,” *IJES*, vol. 63, no. 2–4, pp. 404–408, Jun. 2019, doi: 10.18280/ti-ijes.632-442.
- [160] H. M. D. P. Herath, M. A. Wijewardane, R. A. C. P. Ranasinghe, and J. G. A. S. Jayasekera, “Working fluid selection of Organic Rankine Cycles,” *Energy Reports*, vol. 6, pp. 680–686, Dec. 2020, doi: 10.1016/j.egy.2020.11.150.
- [161] J. Bull, J. M. Buick, and J. Radulovic, “Heat Exchanger Sizing for Organic Rankine Cycle,” *Energies*, vol. 13, no. 14, p. 3615, Jul. 2020, doi: 10.3390/en13143615.
- [162] R. Touaibi, H. Koten, and O. Boydak, “Parametric Study of an Organic Rankine Cycle Using Different Fluids,” *Emerg Sci J*, vol. 4, no. 2, pp. 122–128, Apr. 2020, doi: 10.28991/esj-2020-01216.
- [163] S. Saadon and S. Md Saiful Islam, “A Recent Review in Performance of Organic Rankine Cycle (ORC),” in *Organic Rankine Cycles for Waste Heat Recovery - Analysis and Applications*, S. Lasala, Ed. IntechOpen, 2020. doi: 10.5772/intechopen.89763.
- [164] B. Zohuri, “Heat Pipe Design and Technology A Practical Approach” CRC Press, Taylor & Francis Group, ISBN: 978-1-4398-4523-3, 2011.
- [165] D. A. Reay and P. A. Kew, *Heat pipes*, 5. ed., Transferred to digital print. Amsterdam Heidelberg: Butterworth-Heinemann, 2010.

[166] <https://nptel.ac.in/courses/112/105/112105129/>

[167] <https://www.ee.co.za/article/organic-rankine-cycle-waste-heat-recovery.html>

[168] <https://www.engineeringenotes.com/mechanical-engineering/refrigeration/vapour-absorption-refrigeration-system-with-diagram-refrigeration/50659>

[169] http://www.ecourses.ou.edu/cgi-bin/ebook.cgi?topic=th&chap_sec=09.1&page=theory

[170] http://www.ertc.od.ua/en/about_ert_en.html

[171] Z. Zhang and L. Tian, “Effect of Suction Nozzle Pressure Drop on the Performance of an Ejector-Expansion Transcritical CO₂ Refrigeration Cycle,” *Entropy*, vol. 16, no. 8, pp. 4309–4321, Aug. 2014, doi: 10.3390/e16084309.

[172] http://www.ecourses.ou.edu/cgi-bin/ebook.cgi?topic=th&chap_sec=09.1&page=theory

[173] <https://www.nuclear-power.com/nuclear-engineering/thermodynamics/thermodynamic-cycles/brayton-cycle-gas-turbine-engine/brayton-cycle-pv-ts-diagram/>

[174] <https://basicmechanicalengineering.com/gas-turbine-power-plant-with-regeneration-reheat-intercooling/>

[175] C.P. Arora, “Refrigeration and Air Conditioning”, Tata McGraw-Hill Publishing Company Limited, Delhi, Third Edition, 2009.

[176] K. E. Herold, R. Radermacher, and S. A. Klein, *Absorption Chillers and Heat Pumps*, SECOND. 6000 Broken Sound Parkway NW, Suite 300 Boca Raton, FL 33487-2742: CRC Press Taylor & Francis Group, 2016.

[177] I. Dincer and T. A. H. Ratlamwala, *Integrated Absorption Refrigeration Systems*. Cham: Springer International Publishing, 2016. doi: 10.1007/978-3-319-33658-9.

- [178] B. Modi, A. Mudgal, and B. Patel, “Energy and Exergy Investigation of Small Capacity Single Effect Lithium Bromide Absorption Refrigeration System,” *Energy Procedia*, vol. 109, pp. 203–210, Mar. 2017, doi: 10.1016/j.egypro.2017.03.040.
- [179] A. Solanki and Y. Pal, “Energy and exergy evaluation of triple-effect H₂O/LiBr absorption cooling system,” *Int. J. Ambient Energy*, pp. 1–12, Nov. 2020, doi: 10.1080/01430750.2020.1831598.
- [180] S. R. Chaudhari, A. R. Chavan and S. S. Naik, “Energy analysis of quadruple effect series flow vapour absorption system” *International Journal of Engineering Research and Application*, ISSN: 2248-9622 Vol. 9, Issue 4 (Series -II) April 2019, pp 01-10, DOI: 10.9790/9622- 0904020110
- [181] Rabi KARAALI, “EXERGY ANALYSIS OF HALF-EFFECT ABSORPTION COOLING CYCLES,” *Int. J. Eng. Sci. Res. Technol.*, vol. 5, no. 9, pp. 405–411, 2016, doi: 10.5281/zenodo.154222.

Publications

Published Journal Articles:

- [182] A. Dwivedi and R. S. Mishra, “Optimization of Vapour Absorption System Using Heat Pipes,” *Int. J. Res. Appl. Sci. Eng. Technol.*, ISSN 2321-9653, vol. V, no. VIII, pp. 634–639, Aug. 2017, DOI: 10.22214/ijraset.2017.8092.
- [183] A. Dwivedi and R. S. Mishra, “Performance Enhancement of Simple Vapour Absorption System Using Loop Heat Pipes,” *Int. J. Res. Appl. Sci. Eng. Technol.*, ISSN 2321-9653, vol. 6, no. 1, pp. 865–873, Jan. 2018, DOI: 10.22214/ijraset.2018.1131.
- [184] A. Dwivedi and R. S. Mishra, “Study of Performance Enhancement of Half Effect Vapour Absorption System Using Loop Heat Pipes,” *Int. J. Res. Appl. Sci. Eng. Technol.*, ISSN 2321-9653, vol. 6, no. 1, pp. 1147–1156, Jan. 2018, DOI: 10.22214/ijraset.2018.1174.
- [185] A. Dwivedi and R. S. Mishra, “Performance Enhancement Analysis of Double Effect Vapour Absorption System Using Loop Heat Pipes,” *Int. J. Res. Appl. Sci. Eng. Technol.*, ISSN 2321-9653, vol. 6, no. 1, pp. 1523–1533, Jan. 2018, DOI: 10.22214/ijraset.2018.1234.

[186] A. Dwivedi and R. S. Mishra, "Study of Improvement in the Performance of Triple Effect Vapour Absorption System Using Loop Heat Pipes," *Int. J. Res. Appl. Sci. Eng. Technol.*, ISSN 2321-9653, vol. 6, no. 1, pp. 3160–3172, Jan. 2018, DOI: 10.22214/ijraset.2018.1438.

[187] A. Dwivedi and R. S. Mishra, "Comparative Study of Improvements in Multiple Effect Vapour Absorption Systems using Loop Heat Pipes," *Int. J. Res. Appl. Sci. Eng. Technol.*, ISSN 2321-9653, vol. 7, no. 12, pp. 1029–1041, Dec. 2019, DOI: 10.22214/ijraset.2019.12162.

[188] A. Dwivedi and R. S. Mishra, "Thermodynamic Analysis of Heat Pipe Using Ammonia, Water and Ethanol with a View to Being Used in Refrigeration," *Int. J. Adv. Res. Innov.*, ISSN 2347 - 3258, vol. 3, no. 3, pp. 498–502, 2015.

[189] A. Dwivedi and R. S. Mishra, "Analysis of Organic Rankine Cycle with Waste Heat Recovery from Gas Power Plant using Loop Heat Pipes," *J. Mech. Eng. Res. Dev.*, ISSN 1024-1752, vol. 44, no.9, pp. 265-285, 2021.

[190] A. Dwivedi and R. S. Mishra, "A Parametric Study of Eco-Friendly Refrigeration with Waste Heat Recovery from Gas Power Plants using Loop Heat Pipe," *J. Mech. Eng. Res. Dev.*, ISSN 1024-1752, vol.44, no.9, pp.286-310, 2021.

Articles Presented International Conference:

[191] A. Dwivedi, R. S. Mishra, and S. Ahmad, "A thermodynamic analysis of ejector type vapour refrigeration system using eco-friendly refrigerants," *Int. J. Res. Eng. Innov.*, ISSN 2456-6934, vol. I, no. 2, pp. 40–48, 2017.

[192] A. Dwivedi and R. S. Mishra, "Methods for improving thermal performances of vapour absorption system using heat pipes," *Int. J. Res. Eng. Innov.*, ISSN 2456-6934, vol. I, no. 3, pp. 118–125, 2017.

Curriculum Vitae (CV)

Ankit Dwivedi, IOFS ✉ ankitdwivedi.iofs@gmail.com Delhi Technological University, Delhi, IN
➤ <u>PROFILE SUMMARY:</u>
<ul style="list-style-type: none">• An Indian Civil Servant & Research Scholar in search of diversification of the Core Profile.• Over 3 Years' Experience in Academics as a Teaching Assistant & Research Scholar.• Over 5.5 Years' Experience in Diverse Industrial Management and R&D Profiles in the Manufacturing & Development of Weapons as an Officer in the Middle Management.• Very acquainted with the Functioning of Government setups, Vendor Development & Selection, Tendering, Contracts, Procurement, Bid Management, General Human Resource Management & Administration, Product Research & Development etc and the Legal Background & Implications.
➤ <u>EDUCATIONAL QUALIFICATIONS:</u>
<ul style="list-style-type: none">• M. Tech in Thermal Engineering, Delhi Technological University (Formerly DCE), Delhi-110042, 2013-15, 67.5%.• B. Tech in Mechanical Engineering, JSS Academy of Technical Education, NOIDA, UP-201301, 2008-12, 64.6%.
➤ <u>CERTIFICATIONS:</u>
<ul style="list-style-type: none">• Lead Auditor Training Course EMS (ISO 14001:2015), VEXIL, July'17.• Lead Auditor Training Course QMS (ISO 9001:2015), VEXIL, July'17.• Management Development Programme, IIM, Kashipur, Apr'17-May'17.• Technical Module Certificate, DIAT, Pune, Jan'17 – Mar'17.
➤ <u>WORK EXPERIENCE:</u>
<ul style="list-style-type: none">• Serving in the Indian Ordnance Factories Service (IOFS) (Indian Central Civil Service – Gr. A), under the Department of Defence Production, Ministry of Defence, Government of India through UPSC-Engineering Service Exam'15 since Aug'16.<ul style="list-style-type: none">i. Training Module (From Aug'16 to Sep'17). Posted at Gun & Shell Factory, Cossipore, Kolkata (GSF).ii. Mechanical Maintenance, Civil Maintenance, Procurement of Spares & Procurement of Civil Works at GSF (From Nov'17 to Sep'18).iii. Cyber Security Officer at GSF (From July'18 to Date).iv. Production Management of Guns & Barrels at GSF (From Oct '18 to Mar'19).

- v. Industrial Safety & Disaster Management at GSF (From Apr'19 to Sep'20).
- vi. Project Officer of R&D Projects of Mortar Weapons at GSF (From Sep'19 to Date).
- vii. Procurement of Plant & Machinery, Procurement of Civil Works, Bid Management, and Project Officer of Ordnance Weapon Systems R&D Projects at GSF (From Oct'20 to Date).
- Full-Time Research Scholarship- cum-Teaching at DTU, Delhi (From Aug'15 to July'16).
- Conducted B. Tech classes in M. Tech as a Teaching Assistant at DTU, Delhi (From Aug'13 to July'15).

➤ **PROJECTS:**

❖ **Ph.D. PROJECTS:**

- Thesis on Use of Loop Heat Pipes in Vapour Absorption Refrigeration System

❖ **M. TECH PROJECTS:**

- Thesis on Use of Heat Pipes in Vapour Compression Refrigeration System

❖ **B. TECH PROJECTS:**

- Thesis on Knowledge Process Outsourcing